ZEBRAFISH AS A MODEL FOR PHARMACOLOGICAL AND TOXICOLOGICAL RESEARCH

EDITED BY: Carla Denise Bonan and Anna Siebel
PUBLISHED IN: Frontiers in Pharmacology

frontiers Research Topics

ISSN 1664-8714
ISBN 978-2-88976-987-2
DOI 10.3389/978-2-88976-987-2

About Frontiers

Frontiers is more than just an open-access publisher of scholarly articles: it is a pioneering approach to the world of academia, radically improving the way scholarly research is managed. The grand vision of Frontiers is a world where all people have an equal opportunity to seek, share and generate knowledge. Frontiers provides immediate and permanent online open access to all its publications, but this alone is not enough to realize our grand goals.

Frontiers Journal Series

The Frontiers Journal Series is a multi-tier and interdisciplinary set of open-access, online journals, promising a paradigm shift from the current review, selection and dissemination processes in academic publishing. All Frontiers journals are driven by researchers for researchers; therefore, they constitute a service to the scholarly community. At the same time, the Frontiers Journal Series operates on a revolutionary invention, the tiered publishing system, initially addressing specific communities of scholars, and gradually climbing up to broader public understanding, thus serving the interests of the lay society, too.

Dedication to Quality

Each Frontiers article is a landmark of the highest quality, thanks to genuinely collaborative interactions between authors and review editors, who include some of the world's best academicians. Research must be certified by peers before entering a stream of knowledge that may eventually reach the public - and shape society; therefore, Frontiers only applies the most rigorous and unbiased reviews.
Frontiers revolutionizes research publishing by freely delivering the most outstanding research, evaluated with no bias from both the academic and social point of view. By applying the most advanced information technologies, Frontiers is catapulting scholarly publishing into a new generation.

What are Frontiers Research Topics?

Frontiers Research Topics are very popular trademarks of the Frontiers Journals Series: they are collections of at least ten articles, all centered on a particular subject. With their unique mix of varied contributions from Original Research to Review Articles, Frontiers Research Topics unify the most influential researchers, the latest key findings and historical advances in a hot research area! Find out more on how to host your own Frontiers Research Topic or contribute to one as an author by contacting the Frontiers Editorial Office: frontiersin.org/about/contact

ZEBRAFISH AS A MODEL FOR PHARMACOLOGICAL AND TOXICOLOGICAL RESEARCH

Topic Editors:
Carla Denise Bonan, Pontifical Catholic University of Rio Grande do Sul, Brazil
Anna Siebel, Federal University of Rio Grande, Brazil

Citation: Bonan, C. D., Siebel, A., eds. (2022). Zebrafish as a Model for Pharmacological and Toxicological Research. Lausanne: Frontiers Media SA. doi: 10.3389/978-2-88976-987-2

Table of Contents

frontiers | Frontiers in Pharmacology

TYPE Editorial
PUBLISHED 08 August 2022
DOI 10.3389/fphar.2022.976970

OPEN ACCESS

EDITED AND REVIEWED BY
Heike Wulff,
University of California, Davis,
United States

*CORRESPONDENCE
Carla Denise Bonan,
carladbonan@gmail.com,
cbonan@pucrs.br

SPECIALTY SECTION
This article was submitted to Experimental Pharmacology and Drug Discovery,
a section of the journal
Frontiers in Pharmacology

RECEIVED 24 June 2022
ACCEPTED 27 June 2022
PUBLISHED 08 August 2022

CITATION
Bonan CD and Siebel AM (2022), Editorial: Zebrafish as a model for pharmacological and toxicological research.
Front. Pharmacol. 13:976970.
doi: 10.3389/fphar.2022.976970

Editorial: Zebrafish as a model for pharmacological and toxicological research

Carla Denise Bonan[1]* and Anna Maria Siebel[2]

[1]Laboratório de Neuroquímica e Psicofarmacologia, Programa de Pós-Graduação em Biologia Celular e Molecular, Escola de Ciências da Saúde e da Vida, Pontifícia Universidade Católica do Rio Grande do Sul, Porto Alegre, RS, Brazil, [2]Instituto de Ciências Biológicas, Universidade Federal do Rio Grande-FURG, Rio Grande, Brazil

KEYWORDS

drug discovery, toxicity, behavior, development, high-throughput screening

Editorial on the Research Topic
Zebrafish as a Model for Pharmacological and Toxicological Research

Zebrafish (*Danio rerio*) is a small freshwater teleost widely used as an *in vivo* vertebrate model system for biomedical research. This species has a fully sequenced genome, high fecundity, external and rapid development, optical transparency during the developmental period, several physiological similarities with humans, and endophenotypes similar to human diseases (Kimmel et al., 1995; Howe et al., 2013; Kalueff et al., 2013). The research employing zebrafish embryos and larvae can provide massive knowledge about pharmacological and toxicological effects in high throughput drug screening (Petersen et al., 2022). In addition, the complex behavioral repertoire of adult zebrafish, its sensitivity to drugs, and the ability to respond to them similarly to humans support their utility for pharmacological and toxicological research (Rico et al., 2011; Zanandrea et al., 2020).

The use of pharmacological and toxicological approaches to different developmental stages of zebrafish is relevant to deepen the knowledge of drugs and toxicants' mechanisms. Therefore, this Research Topic aimed to collect studies that exploit the zebrafish model as a tool for pharmacological and toxicological research. After the joint efforts of the journal, editors, reviewers, and contributors, a total of fourteen high-quality articles were published. So, we prepared a detailed summary for these fourteen articles as follows.

Alijevic et al. investigated the neuropharmacological *in vitro* and *in vivo* effects of three alkaloids—nicotine, cotinine, and anatabine. Natural nicotinic alkaloids induced an anxiolytic-like behavior, and this effect depends on the activation of nAChRs and regulation of other neurotransmitter systems, such as noradrenergic and dopaminergic systems. Organic cation transporters (OCTs) facilitate the transport of cations and other compounds between extracellular fluids and cells. Gould et al. characterized *in vivo* uptake to the brain and the high-affinity brain membrane binding of the mammalian OCT blocker 1-1′-diethyl-2,2′cyanine iodide (decynium-

22) in zebrafish. Obtained data showed that D-22 can reach the zebrafish brain and induce anxiolytic effects, decreasing anti-predator dorsal camouflaging. Monoamine oxidases (MAO) catalyze the oxidative deamination of a variety of monoamines, promoting a critical role in neuromodulation. Jaka et al. demonstrated the anxiolytic-like effects of natural MAO inhibitors on novel environment-induced anxiety in zebrafish. Vossen et al. showed for the first time that male zebrafish showed more severe behavioral impairments than females when exposed to ethanol, showing the importance of clearly including sex and time course as factors in behavioral experiments with adult zebrafish.

Ciclosporin A is a powerful immunosuppressant widely used in clinics. Wan et al. observed that ciclosporin A promoted cardiac toxicity in zebrafish larvae, which may be related to an up-regulation of Wnt signaling and oxidative stress.

Pesticides contaminate aquatic systems, which may impact non-target organisms such as fish. Zaluski et al. demonstrated changes in survival, hatching, and morphological parameters after acute exposure to atrazine and diuron commercial formulations in zebrafish embryos and larvae. These findings highlight the relevance of additional studies on the sublethal effects of these compounds, as well as the comparison of commercial formulas vs. isolated active ingredients. Chackal et al. demonstrated that nanoplastics and the Flame Retardant BDE-47, detected in the aquatic environment, promote cumulative metabolic disruption in zebrafish larvae and that co-exposure exacerbates this effect. These data raised concerns about the influence of these compounds in aquatic systems and on human health.

Related to the visual system, nerve growth factor (NGF) is a neurotrophin with an important role in ocular homeostasis. Cocchiaro et al. investigated the expression of NGF receptors in adult zebrafish retina and showed that intravitreal (IV) administration of rhNGF can increase zebrafish retinal regeneration in this model. In a review article, Cohen et al. discussed the role of estrogenic and thyroidogenic signaling in the modulation of the development and function of the visual system.

Regarding neurological disorders, Milder et al. developed a method to achieve a more robust screening of anti-seizure drugs using a seizure model in zebrafish. The findings can help us connect physiological and behavioral responses to anti-seizure drugs and better assess anti-seizure drug efficacy. Doyle and Croll discussed the Parkinson's disease models developed in zebrafish and the benefits and advantages of this species in comparison to other animal models.

Kim et al. performed a screen of 1,403 bioactive small molecule compounds using transgenic larval zebrafish, characterized by dopamine neuron loss. The study showed, by the combination of *in vivo* imaging-based screen and bioinformatic analysis, an approach for identifying hit-to-lead candidates and unknown pathways and targets involved in dopamine neuron protection. Bedrossiantz et al. demonstrate that zebrafish, as a poikilothermic animal, is a suitable model to investigate binge-like methamphetamine neurotoxicity without hyperthermia as a confounding effect.

Finally, Winter et al. tested a combination of *in silico* analysis of clinical data with *in vivo* assessment of CRISPR/Cas9-mediated mutation in zebrafish crispant. The study showed evidence of the role of three genes in cardiovascular development and function, as well as the potential effect of loss of gene function on organ system pathophysiology.

In conclusion, this Research Topic has provided new experimental data and updated reviews. Wonderfully, this Research Topic advanced the understanding and updated insights on zebrafish as a model for translational pharmacology and toxicology.

Author contributions

CB: Conceptualization, methodology, writing-original draft, preparation, writing-review, and editing. AS: Conceptualization, methodology, writing-original draft, preparation.

Acknowledgments

We would like to thank all the authors for submitting their manuscripts and the reviewers and editors for their contribution to this topic.

Conflict of interest

The authors declare that the research was conducted in the absence of any commercial or financial relationships that could be construed as a potential conflict of interest.

Publisher's note

References

Howe, K., Clark, M. D., Torroja, C. F., Torrance, J., Berthelot, C., Muffato, M., et al. (2013). The zebrafish reference genome sequence and its relationship to the human genome. *Nature* 496 (7446), 498–503. Erratum in: Nature. 2014 Jan 9; 505(7482):248. doi:10.1038/nature12111

Kalueff, A. V., Gebhardt, M., Stewart, A. M., Cachat, J. M., Brimmer, M., Chawla, J. S., et al. (2013). Towards a comprehensive catalog of zebrafish behavior 1.0 and beyond. *Zebrafish* 10 (1), 70–86. doi:10.1089/zeb.2012.0861

Kimmel, C. B., Ballard, W. W., Kimmel, S. R., Ullmann, B., and Schilling, T. F. (1995). Stages of embryonic development of the zebrafish. *Dev. Dyn.* 203 (3), 253–310. doi:10.1002/aja.1002030302

Petersen, B. D., Bertoncello, K. T., and Bonan, C. D. (2022). Standardizing zebrafish behavioral paradigms across life stages: an effort towards translational pharmacology. *Front. Pharmacol.* 13, 833227. doi:10.3389/fphar.2022.833227

Rico, E. P., Rosemberg, D. B., Seibt, K. J., Capiotti, K. M., Da Silva, R. S., and Bonan, C. D. (2011). Zebrafish neurotransmitter systems as potential pharmacological and toxicological targets. *Neurotoxicol. Teratol.* 33 (6), 608–617. doi:10.1016/j.ntt.2011.07.007

Zanandrea, R., Bonan, C. D., and Campos, M. M. (2020). Zebrafish as a model for inflammation and drug discovery. *Drug Discov. Today* 25 (12), 2201–2211. doi:10.1016/j.drudis.2020.09.036

frontiers in Pharmacology

ORIGINAL RESEARCH
published: 13 May 2021
doi: 10.3389/fphar.2021.669370

Effects of Natural Monoamine Oxidase Inhibitors on Anxiety-Like Behavior in Zebrafish

Oihane Jaka[1†], Iñaki Iturria[1†], Marco van der Toorn[2], Jorge Hurtado de Mendoza[3], Diogo A. R. S. Latino[2], Ainhoa Alzualde[1], Manuel C. Peitsch[2], Julia Hoeng[2] and Kyoko Koshibu[2]**

[1]Biobide, Gipuzkoa Scientific and Technological Park, San Sebastian, Spain, [2]PMI R&D, Philip Morris Products S.A., Quai Jeanrenaud 5, Neuchâtel, Switzerland, [3]Gestión de Recursos e Innovación S.L. (Grilab) C/ Américo Castro 94, Madrid, Spain

Monoamine oxidases (MAO) are a valuable class of mitochondrial enzymes with a critical role in neuromodulation. In this study, we investigated the effect of natural MAO inhibitors on novel environment-induced anxiety by using the zebrafish novel tank test (NTT). Because zebrafish spend more time at the bottom of the tank when they are anxious, anxiolytic compounds increase the time zebrafish spend at the top of the tank and vice versa. Using this paradigm, we found that harmane, norharmane, and 1,2,3,4-tetrahydroisoquinoline (TIQ) induce anxiolytic-like effects in zebrafish, causing them to spend more time at the top of the test tank and less time at the bottom. 2,3,6-trimethyl-1,4-naphtoquinone (TMN) induced an interesting mix of both anxiolytic- and anxiogenic-like effects during the first and second halves of the test, respectively. TIQ was unique in having no observable effect on general movement. Similarly, a reference MAO inhibitor clorgyline—but not pargyline—increased the time spent at the top in a concentration-dependent manner. We also demonstrated that the brain bioavailability of these compounds are high based on the *ex vivo* bioavailability assay and in silico prediction models, which support the notion that the observed effects on anxiety-like behavior in zebrafish were most likely due to the direct effect of these compounds in the brain. This study is the first investigation to demonstrate the anxiolytic-like effects of MAO inhibitors on novel environment-induced anxiety in zebrafish.

Keywords: alkaloids, harmane, norharmane, anxiety, zebrafish, monoamine oxidase, 1,2,3,4-tetrahydroisoquinoline, 2,3,6-trimethyl-1,4- naphtoquinone

OPEN ACCESS

Edited by:
Banasri Hazra, Jadavpur University, India

Reviewed by:
Hoon Kim, Sunchon National University, South Korea
Gary Ivan Stafford, University of Pretoria, South Africa

***Correspondence:**
Manuel C. Peitsch
manuel.peitsch@pmi.com
Kyoko Koshibu
kyoko_koshibu@yahoo.com

†*These authors share first authorship*

Specialty section:
This article was submitted to Ethnopharmacology, a section of the journal Frontiers in Pharmacology

Received: *18 February 2021*
Accepted: *28 April 2021*
Published: *13 May 2021*

Citation:
Jaka O, Iturria I, van der Toorn M, Hurtado de Mendoza J, Latino DARS, Alzualde A, Peitsch MC, Hoeng J and Koshibu K (2021) Effects of Natural Monoamine Oxidase Inhibitors on Anxiety-Like Behavior in Zebrafish. Front. Pharmacol. 12:669370. doi: 10.3389/fphar.2021.669370

INTRODUCTION

Historically, plants have been a rich source of nutrients and chemical ingredients that help maintain physical and mental health for centuries (Perry and Perry, 2018). Scientific interests in these natural sources of health benefits have been steadily rising, where, for example, investigations on "herbal medicine" alone sored from approximately 2,000 publications in 2010 to almost 5,000 publications in 2020 reported on PubMed (accessed Feb 15, 2021). In some cases, active ingredients in plants have been identified and investigated for specific health benefits (Perry and Perry, 2018). Monoamine oxidase (MAO) inhibitors are a class of one such naturally occurring compounds that have been clinically developed as an antidepressant and as a treatment for social anxiety and Parkinson's disease (Youdim et al., 2006; Finberg and Rabey, 2016; Menkes et al., 2016; Tipton, 2018; Sabri and Saber-Ayad, 2020). Monoamine oxidase is a widely distributed mitochondrial enzyme with high levels of expression in the brain as well as gastro-intestinal and hepatic tissues (Fowler et al., 2003; Finberg

and Rabey, 2016). Two isoenzymes of MAO – MAO-A and MAO-B – are present in most mammalian tissues and can be differentiated by their substrate specificities, inhibitor sensitivities, and tissue localizations (Shih et al., 1999; Tipton, 2018). The enzyme catalyzes the oxidative deamination of a variety of monoamines, both endogenous and exogenous. It has major roles in metabolizing neurotransmitters, including serotonin, histamine, dopamine, noradrenaline, and adrenaline, and in detoxifying a large variety of endogenous and exogenous amines (Dos Santos Passos et al., 2014; Finberg and Rabey, 2016; Edmondson and Binda, 2018).

In nature, various plants or plant extracts, such as a chewing nut *Areca catechu* L. (Arecaceae) and a popular curry or tea component *Curcuma longa* L. (Zingiberaceae), have been identified to suppress MAO activity and induce anti-depressant-like effects (Vina et al., 2012). Similarly, the leaves of *Ginkgo biloba* L. (Ginkgoaceae) have been suggested to restore the striatal dopamine levels in rodent models of Parkinson's disease through the regulation of MAO, although the antioxidant property of *G. Biloba* probably also contributed to the observed effects (Pardon et al., 2000; Ahmad et al., 2005). In addition, MAO inhibiting β-carbolines in *Coffea* (Rubiaceae) – more commonly known as coffee – have been suggested to induce neuroprotection against Parkinson's disease (Herraiz and Chaparro, 2006). The effect of β-carbolines and other MAO inhibitors on anxiety, in contrast, seems to be rather complex, with early findings reporting anxiogenic effect in rhesus monkeys and humans (Schweri et al., 1982; Skolnick et al., 1984; Crawley et al., 1985), but withdrawing from MAO inhibitor treatments has been associated with anxiety (Dilsaver, 1994). In addition, MAO inhibitors seem to induce anxiolytic effect in specific types of anxiety, such as social phobia (Liebowitz et al., 1993; Schneier, 2001).

In this study, we aimed to understand the effect of natural MAO inhibitors on another behavioral phenomenon, novel environment-induced anxiety, in a relatively high throughput behavioral paradigm–the zebrafish novel tank test (NTT). During the past few decades, zebrafish have emerged as a model vertebrate organism for analyzing complex molecular and cellular interactions *in vivo* (Eliceiri et al., 2011; Stewart et al., 2012; Stewart and Kalueff, 2012; Pickart and Klee, 2014). Their usefulness as an animal model for neurobehavioral research has been recognized, and mounting evidence suggests the suitability of zebrafish for modeling various aspects of anxiety-related states (Stewart et al., 2012; Khan et al., 2017b; Kysil et al., 2017). The NTT takes advantage of the innate behavior of zebrafish to dive and dwell at the bottom of a body of water to avoid danger or stress. It is a relatively high-throughput behavioral test with some translational relevance to humans (Levin et al., 2007; Papke et al., 2012; Stewart et al., 2012). For example, anxiolytic drugs, such as diazepam and buspirone, have been shown to induce anxiolytic-like efficacy in this zebrafish behavioral paradigm (Levin et al., 2007; Bencan and Levin, 2008; Bencan et al., 2009; Stewart et al., 2012). Using this zebrafish model, three alkaloids (harmane, norharmane, 1,2,3,4-tetrahydroisoquinoline (TIQ)), and 2,3,6-trimethyl-1,4-naphtoquinone (TMN), previously identified to be present in, for example, solanaceous and rubiaceous plants (Boulton et al., 1988; Herraiz and Chaparro, 2006), were investigated in order to understand their potential efficacy in modulating anxiety-like behavior in animals. Buspirone, a clinically approved anxiolytic drug, was also tested to confirm the validity of the NTT. Harmane, norharmane, and TIQ were selected due to previous reports suggesting their role in regulating depression or anxiety in rodents and/or in humans (Pepplinkhuizen et al., 1996; Verheij et al., 1997; Aricioglu and Altunbas, 2003; Farzin and Mansouri, 2006; Smith et al., 2013; Antkiewicz-Michaluk et al., 2014; Mozdzen et al., 2014; Dos Santos et al., 2016; Khan et al., 2017a; Piechowska et al., 2019). Harmane and norharmane are the most abundant β-carbolines found in numerous plants and food stuffs (Herraiz, 2004, 2007; Piechowska et al., 2019). Passifloraceae flowers of plants belonging to this family (e.g., passion fruit) have been found to contain 126 ± 27 ng/g dry matter (d.m.) harmane and 68.3 ± 5.3 ng/g d.m. norharmane, as well as in herbal medicines, such as Evodiae Fructus (a.k.a., wu zhu yu; 0.63 ± 0.13 μg/g harmane and 8.24 ± 0.13 μg/g norharmane) and *Tribulus terrestris* (a.k.a., puncture vine; 44 μg/g d.m for both to 99.5 ± 13.2 ng/g and 131 ± 11 ng/g, respectively) (Tsuchiya et al., 1999; Pfau and Skog, 2004; Piechowska et al., 2019). In food, harmane and norharmane are found in, for example, brewed coffee (335 ± 105 ng/g and 1430 ± 540 ng/g ground coffee, respectively), soy sauce (187.6 ± 21.9 μg/L and 44.0 ± 10.6 μg/L, respectively), well-done cooked meat (26.4 ± 8.05 ng/g and 82.3 ± 64.8 ng/g, respectively) – but not in raw or medium cooked meat –, and raisins (6–644 ng/g and 2–120 ng/g, respectively) (Herraiz, 2004; Pfau and Skog, 2004; Herraiz, 2007). β-carbolines are reversible competitive inhibitors of MAO. In addition to its potent inhibitory activity particularly against MAO A, harmane has been reported to act on serotonin, opiate, dopamine, imidazole, benzodiazepine receptors as well as acetylcholinesterase and butyrylcholinesterase (Arib et al., 2010; Khan et al., 2017a). Norharmane inhibits both MAO A and B and also has been suggested to act on other targets similar to harman, such as serotonine, benzodiazepine, and opiate receptors (Pepplinkhuizen et al., 1996).

TIQ is an isoquinoline derivative found in foods with a high 2-phenylethylamine content, such as white wine (1.7 ± 0.8 ng/g), cheese (15.0 ± 2.2 ng/g), and cocoa (0.8 ± 0.3 to 1.1 ± 0.8 ng/g), and have been detected in rat and human brains (Makino et al., 1988). Isoquinoline alkaloids are a large family of phytochemicals found in plant families, such as Papaveraceae, Berberidaceae, and Ranunculaceae, and have been used in folk medicine as, for example, digestive stimulant, immune stimulant, muscle relaxant, analgesic, sedative, and anti-inflammatory (Khan and Suresh Kumar, 2015). Less information is available about TIQ, but it has been reported to reversibly inhibit MAO-A and B and acts as an anti-depressant in rodents (Thull et al., 1995; Antkiewicz-Michaluk et al., 2014; Mozdzen et al., 2014). It is an interesting compound, because it forms a basic chemical unit for numerous other natural isoquinolines and for drugs for relaxation, such as

tubocurarine, and anti-depressants, such as diclofensine (Cherpillod and Omer, 1981; Exley et al., 2005).

Lastly, TMN was selected to understand a novel anxiolytic-like property of this compound that has been previously identified to be a MAO inhibitor isolated from a tobacco plant (Mostert et al., 2016). TMN is a derivative of naphthalene. Naphthoquinones are secondary metabolites derived from primary metabolites – carbohydrates, amino acids and lipids – that are present in various organisms, such as plants (e.g. Ebenaceae), fungi (e.g. *Fusarium* spp.), lichens (e.g. *Cetraria* spp.), algae (*Landsburgia quercifolia*), and in actinomycetes (*Streptomyces* spp.) (Babula et al., 2009; Pinho et al., 2012). One of more well-known members of this chemical class include vitamin K (Coelho Cerqueira et al., 2011; Pinho et al., 2012). The biological effects of naphthoquinones are wide and include neuroprotection, cardioprotection, and hepatoprotection as well as anti-inflammatory and anti-microbial activities (Aminin and Polonik, 2020). Thus, this chemical family is increasingly considered as a source of drug development (Babula et al., 2009; Pinho et al., 2012; Aminin and Polonik, 2020). It has been reported that TMN, a minor component of flue-cured tobacco leaves and smoke, is a reversible competitive inhibitor of MAO-A and MAO-B that exhibits protective properties against MPTP toxicity in mice (Castagnoli et al., 2001; Coelho Cerqueira et al., 2011). To our knowledge, the present study is the first to examine the effects of TIQ and TMN on anxiety-like behavior in a non-clinical animal model.

Furthermore, to support the validity of our behavioral findings, we demonstrated that these natural MAO inhibitors indeed reach the brain by using the *ex vivo* bioavailability assay and in silico blood brain barrier models.

MATERIALS AND METHODS

Animals

Wild-type zebrafish (*Danio rerio*; strain AB) were bred and housed at Biobide (San Sebastián, Gipuzkoa, Spain) in accordance with standard procedures (Zebrafish Information Network) as described previously (Alzualde et al., 2018; Quevedo et al., 2019). In brief, the fish were maintained in a 300-L aquarium with a maximum of 1,000 fish per tank. The system water was maintained at 28.5°C, pH 7–7.8, 500–800 μS conductivity, and 80–100% oxygen and continuously filtered. The system water condition was monitored daily and regulated. The fish were kept under a 14-/10 h light/dark cycle (light on at 7:30 am). Adult fish were fed ground dry pellets (Gemma Micro 300; Sketting Zebrafish, Westbrook, ME, United States) and live food (artemia; Catvis B.V., 's-Hertogenbosch, Netherlands) once a day. All behavioral experiments were performed on adult male and female zebrafish (approximately 36–52 weeks post fertilization) in accordance with European standards of animal welfare in animal use for scientific purposes (2010/63/EU), compiled with national regulations for the care of experimental animals, and were approved as described in national regulations (RD 53/2013) by local and regional committees: PRO-AE-SS-121 and PRO-AE-SS-134.

Chemicals

Harmane (CAS No. 486–84–0), norharmane (CAS No. 244–63–3), 1,2,3,4-tetrahydroisoquinoline (TIQ; CAS No. 91–21–4), clorgyline hydrochloride (CAS No. 17780–75–5), and pargyline hydrochloride (CAS No. 306–07–0) were purchased from Sigma-Aldrich® (St. Louis, MO, United States of America). 2,3,6-trimethyl-1,4-naphtoquinone (TMN; CAS No. 20490–42–0) was purchased from Enamine Ltd. (Kyiv, Ukraine). Buspirone hydrochloride (CAS No. 33386–08–2) was purchased from Tocris Bioscience (Bio-Techne®, Minneapolis, MN, United States). The chemical structures of compounds are shown in **Figure 1A**.

Zebrafish NTT

Adult male and female wild-type zebrafish were treated with the compounds for 20 min in a final volume of 50 ml in a 250-ml treatment beaker, one fish at a time. The treatment concentrations were determined by first testing the compounds at 30 mg/L. If the fish tolerated the concentration in the treatment beaker for 20 min, then higher concentrations were tested. If not, the concentration was reduced until no obvious signs of tolerability problems (e.g., seizure-like tail or body movement) were observed. The test concentrations for the NTT were as follows: harmane (1, 3, and 10 mg/L; equivalent to 5, 17, and 55 μM), norharmane (0.3, 1, and 3 mg/L; equivalent to 2, 6, and 18 μM), TIQ (10, 30, and 100 mg/L; equivalent to 75, 226, and 752 μM), TMN (3, 10, and 30 mg/L; equivalent to 15, 50, and 150 μM), clorgyline (10, 30, and 100 mg/L; equivalent to 32, 97, and 324 μM), pargyline (10, 30, and 100 mg/L; equivalent to 51, 153, and 510 μM), and buspirone (10, 30, and 100 mg/L; equivalent to 26, 78, and 259 μM).

Following compound treatment in a 250 ml beaker, the fish were briefly rinsed in fresh system water, and then immediately transferred to a trapezoidal tank (14.6 cm height x 5.5 cm width x 27.9 cm top length and x 23.6 cm bottom length) filled with 1.5 L system water (**Figure 1B**). The behavior of the fish was monitored for the next 5 min by using the Noldus EthoVision XT system (Wageningen, Netherlands), with the camera placed approximately 1 m from the test tank (**Figure 1C**). The water-filled part of the tank (11.5 cm height) was virtually divided into top, center, and bottom (**Figure 1B**). The average time spent at the top and bottom portions of the tank was analyzed to determine the anxiety-like behavior of fish. The average total distance traveled and freezing time (as defined by a complete cessation of movement except for gills and eyes (Kalueff et al., 2013)) were calculated to determine the effects of the compounds on the general behavior of fish. The analyses were conducted in 1-min time bins to demonstrate the change in their behavior overtime. Any fish that stayed immobile for longer than 200 s out of a total of 5 min test period were considered as an outlier as they were generally >2 standard deviations away from the mean and excluded from all analysis. One fish from 10 mg/L harmane, one fish from 3 mg/L norharmane, one fish from 100 mg/L TIQ, two fish from 10 mg/L TMN, five fish from 30 mg/L TMN, four fish from 30 mg/L clorgyline, six fish from 100 mg/L clorgyline, and three fish from 100 mg/L buspirone were removed from the final analysis as their behavior was uninterpretable. There was no

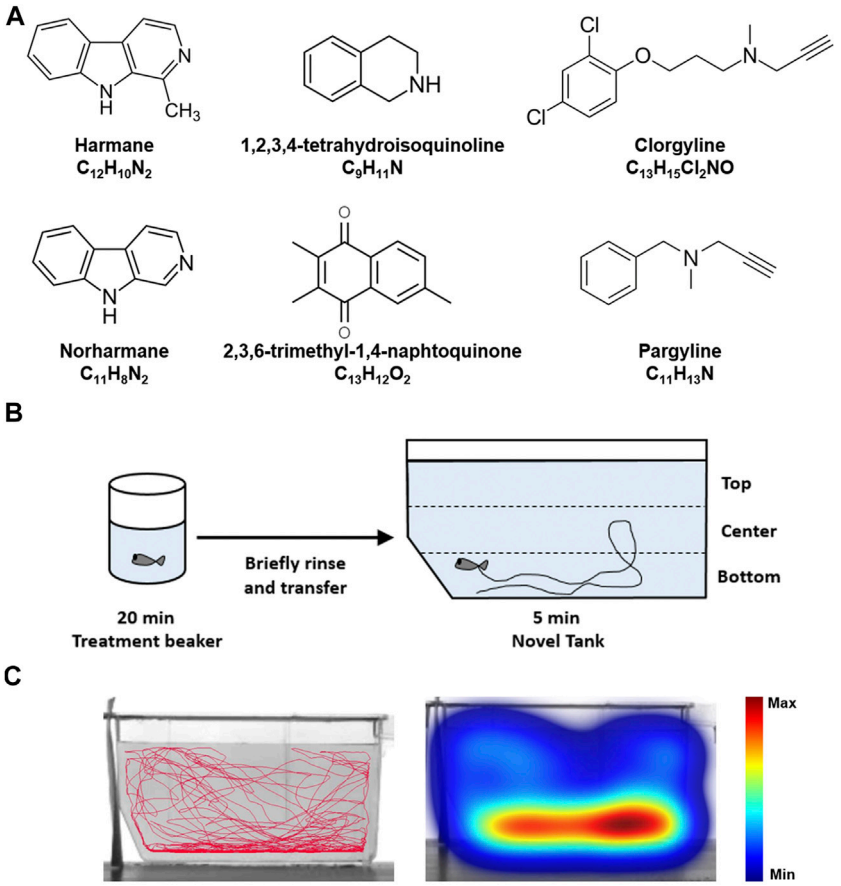

FIGURE 1 | Zebrafish NTT experimental paradigm **(A)** The chemical structures of the test compounds–harmane, norharmane, TMN, TIQ, clorgyline, and pargyline–are shown **(B)** Zebrafish are placed in a treatment beaker with respective compounds for 20 min, briefly rinsed in system water, and then monitored in a novel tank for 5 min. The time spent at the top and bottom one third of the tank were then analyzed **(C)** A representative trace and heatmap of the swimming activity is presented for a vehicle control. The heatmap shows the minimum (dark blue) to maximum (dark red) amount of time a fish spent in each pixel. Abbreviations: NTT = novel tank test.

sex-dependent effect on these abnormally long bouts of freezing. Relatively high number of zebrafish that showed freezing for the highest concentrations of TMN, clorgyline, and buspirone, suggested that the respective concentrations were at the borderline of tolerability. The experimenters were blind to the test conditions. A minimum of 12 fish (6 females and 6 males) per condition were used for the study.

Monoamine Oxidase Assay

The two-step bioluminescent assay (MAO-Glo™ Assay Systems; Promega, Madison, WI, United States) was performed in Nunc white, 96-well, flat-bottom assay plates (Life Technologies Europe B.V., Zug, Switzerland) as described previously (Van Der Toorn et al., 2019). Fluostar Omega 96 Microplate reader (BMG LABTECH GmbH, Ortenberg, Germany) was used to measure the luminescent signal and to determine the IC_{50} (half maximal inhibitory concentration). Z' scores were between 0.75 and 0.86 for both MAO A and B assays. The constant (Km) of MAO A was 17.1 and 2.6 μM for MAO B. The substrate concentrations (S) were 20 μM for MAO A assay and 3 μM for MAO B. The Ki values referred in the discussion were calculated accordingly to the following formula: $Ki = IC_{50}/\left(1 + \frac{Km}{S}\right)$.

Brain Dissection

Four fish (2 male and 2 female) per test condition were exposed to 3 mg/L harmane, 3 mg/L norharmane, 30 mg/L TMN, 100 mg/L TIQ, 100 mg/L clorgyline, or 100 mg/L pargyline. The selected concentrations were either the highest effective concentration or the highest tested concentration to optimize the chance of compound detection in the brain. Immediately after the 20 min compound treatment, the zebrafish were rinsed briefly to remove excessive compound on their body and euthanized with 250 mg/L tricaine (CAS No. 886–86–2; Sigma). The fish were decapitated at the level of the gills by using a surgical knife. The head was turned dorsal side down, and, soft tissue was removed from the ventral side of the skull using two forceps until the base of the skull was exposed. The skull was broken open, and the bone from the ventral side of the brain was removed. The brain was then placed in a microcentrifuge tube, weighed, snap-frozen in liquid nitrogen, and stored at −80°C until the analysis.

Bioavailability Assay

Briefly, on the day of analysis, the brain samples were defrosted, resuspended in a methanol solution (2:1 [v/v] methanol:MilliQ water), and homogenized with vigorous agitation and ultrasonication (5 min each). The homogenate was centrifuged at 15,000 x rpm for 10 min, and the supernatant was analyzed by using a UPLC-Q Exactive Orbitrap-HRMS system (Thermo Fisher Scientific™, Bremen, Germany) for all compounds except for TMN, which was analyzed by gas chromatography/mass spectrometry (GC/MS) system. Chromatographic separation was achieved on a Synergi™ 4-µm Hydro-RP 80 Å, L.C. Column (250 × 4.6 mm; Phenomenex Inc., Torrance, CA, United States) with 0.1% formic acid in water (mobile phase A) and 0.1% formic acid in acetonitrile (mobile phase B). A gradient method at a 500 µL/min flow rate was applied as follows: 1) 5% B for 1 min and 2) increase to 95% B over 7 min and hold for 2 min. The injection volume was 5 µL. The mass spectrometer was operated in electrospray positive mode (ESI; Thermo Fisher Scientific), while data acquisition was performed by using the parallel reaction monitoring (PRM) and full scan modes. The source settings were set as follows: sheath gas flow rate = 60 psi; aux gas flow rate = 20 arbitrary units; spray voltage = 3.5 kV; capillary temperature = 280°C; and sweep gas flow rate = 1. The full scan mode parameters were set as follows: resolution = 35,000 FWHM at 200 m/z; AGC target = 1E6; maximum injection time = 110 ms; and scan range = 100–350 m/z. The chromatographic and Orbitrap MS parameters for PRM analysis were the same as those in the full scan mode, except for: AGC target = 2E5; maximum IT = 60 ms; and resolution = 17,500 FWHM at 200 m/z. The XCalibur™ v4.0.27.19 software (Thermo Fisher Scientific) and TraceFinder™ v4.1 Forensic (Thermo Fisher Scientific, San José, CA, United States) were used for system control and data processing, respectively. The Q Exactive 2.8 SP 1 software (Thermo Fisher Scientific) was used to control the mass spectrometer.

For TMN, the Agilent GC/MS system (Agilent, Santa Clara, CA, United States) was used, because it is an apolar aromatic compound that could not be ionized for the detection by the UPLC-Q Exactive Orbitrap-HRMS system. The Agilent GC/MS system consisted of Agilent 3800 GC coupled to an Agilent Ion Trap 2200 MS/MS operated in electron impact ionization mode. The GC system was equipped with an electronic pressure control and an isothermal injector. One µL of cleaned extract was injected on a DB-5 column (30 m × 0.25 mm × 0.25 µm) using splitless injection mode. The injection temperature was set at 250°C. The GC temperature program was 60°C, hold 2 min, ramp 30°C/min to 120°C, ramp 10°C/min to 240°C, ramp 30°C/min to 300°C, and hold 5 min. Helium was used as carrier gas with a flow rate of 1.2 ml/min. The MS was employed in Multiple Reaction Monitoring mode. The ion source, ion trap, and interface temperatures were set at 200, 200, and 280°C. The results were quantified using Agilent MS Workstation software (v6.9.3). Recoveries of compounds were within 80–120%.

In Silico Blood–Brain Barrier Permeability Prediction

The Ligand Express (Cyclica; Toronto, Ontario, Canada), admetSAR, and Biovia ADMET Blood Brain Barrier Model (Dassault 545 Systémes, Vélizy-Villacoublay, France) were used to predict the BBB permeability of the compounds. Ligand Express® is a cloud-based platform that screens small-molecule drugs against repositories of structurally characterized proteins or "proteomes" to determine polypharmacological profiles. In terms of BBB permeability prediction, the system implements a classification model based on machine learning methods using a compiled BBB dataset of 1335 BBB-permeable and 360 BBB-impermeable compounds. The Anatomical Therapeutic Chemical Classification was used to filter out compounds that have an ambiguous status regarding their passage through the BBB or were not strictly CNS-active. In addition, 45 molecules that are known to cross the BBB and 91 P-glycoprotein substrates on the BBB impermeable set were included (Seelig, 1998; Adenot and Lahana, 2004; Shen et al., 2010).

The admetSAR (v2.0) server was developed as a comprehensive source and free tool for *in silico* prediction of chemical absorption, distribution, metabolism, excretion, and toxicity (ADMET) properties on the basis of structure–activity relationships (Cheng et al., 2012; Yang et al., 2019). More than 40 predictive models are implemented in admetSAR for *in silico* filtering of new chemical ADMET properties. These models are trained by state-of-the-art machine learning methods. The BBB model was developed by using a similar dataset as that used by Ligand Express®, derived mainly from the work of Shen et al. which included 1839 compounds (1438 BBB-permeable and 401 BBB-impermeable compounds) (Shen et al., 2010). Because both of these platforms gave almost identical BBB penetration probability values for all compounds, only the results from Ligand Express® are shown in **Table 1**. Values equal to or close to 1 indicate compounds with a high probability of BBB penetration.

Lastly, the Biovia ADMET Blood Brain Barrier Model was used to predict the BBB penetration of a molecule, defined as the ratio of concentrations (brain concentration/blood concentration) after oral administration, and to report the predicted penetration as well as a classification of penetration level. The model combines a confidence ellipse in the Polar surface area and LogP descriptor space, derived from over 800 orally administered compounds classified as CNS therapeutics with a robust regression model based on 120 compounds with measured penetration to predict Log (Brain Blood (BB)) penetration values for those molecules falling within the confidence ellipse (Egan et al., 2000). The model predicts the BB permeation level based on the categories "very high" (BB ratio >5:1), "high" (between 1:1 and 5:1), "medium" (between 0.3:1 and 1:1), "low" (<0.3:1), and "undefined" (outside the 99% confidence range ellipse). This translates into the regression model prediction values of Log (BB) > 0.7 for "very high", 0 < Log (BB) < 0.7 for "high", −0.52 < Log (BB) < 0 for "medium", and Log (BB) < −0.52 for "low". No prediction was made for compounds outside the 95% confidence ellipsoids.

Statistics

The behavioral findings were analyzed in 1 min bins using two-way repeated measures ANOVA with Dunnett *post hoc* analysis. The analyses were conducted by using GraphPad Prism v8.2.1 (GraphPad Software, San Diego, CA, United States).

TABLE 1 | Summary of MAO activities and BBB permeability prediction.

Compounds	MW (g/mol)	MAO a IC_{50} (μM)[a]	MAO B IC_{50} (μM)[a]	BBB Ligand Express®	Log (BB) Biovia ADMET[b]
Harmane	182	0.05 ± 0.03	>100	0.955	High
Norharmane	168	1.05 ± 0.36	9.27 ± 5.8	0.990	High
TIQ	133	33.04 ± 7.56	50.25 ± 9.99	0.996	High
TMN	200	1.14 ± 0.74	7.14 ± 2.29	0.912	High
Clorgyline	272	0.01 ± 0.01	3.93 ± 1.00	1.000	Very high
Pargyline	159	1.84 ± 0.79	1.07 ± 0.48	1.000	Very high

[a]*Data are presented in mean ± SEM.*

[b]*Low < -0.52; medium = -0.52 to 0; high = 0 to 0.7; very high = > 0.7.*

Abbreviations: ADMET = absorption, distribution, metabolism, excretion, and toxicity; BB = blood brain; BBB = blood-brain barrier; MAO = monoamine oxidase; MW = molecular weight; TIQ = 1.2,3,4-tetrahydroisoquinoline; TMN = 2,3,6-trimethyl-1,4-naphthoquinone.

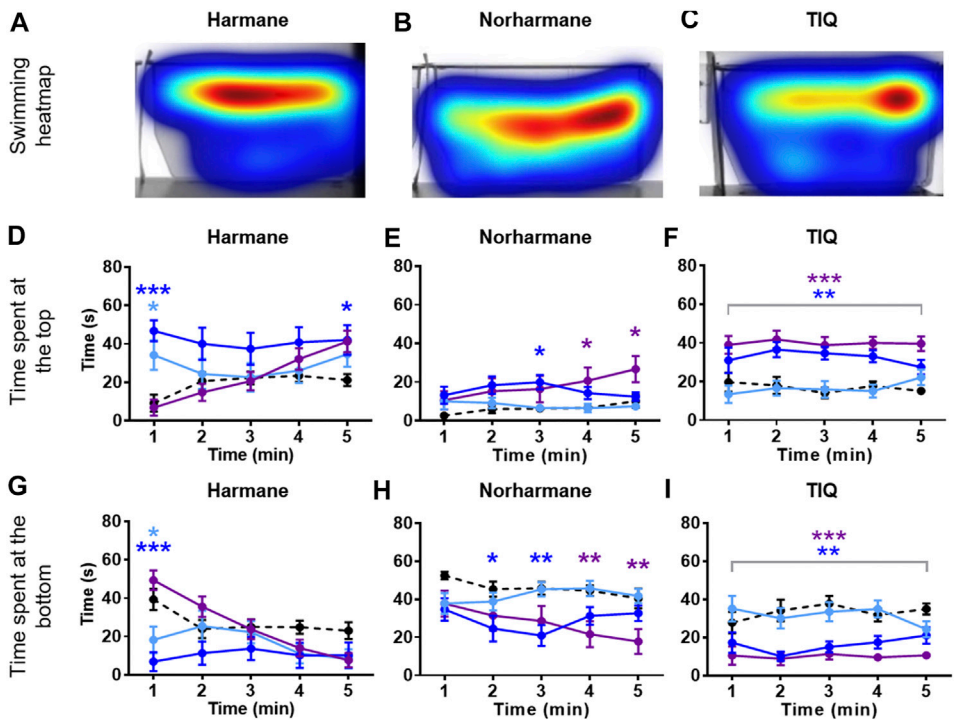

FIGURE 2 | NTT results for harmane, norharmane, and TIQ. Representative heatmaps for **(A)** harmane (3 mg/L) **(B)** norharmane (3 mg/L), and **(C)** TIQ (100 mg/L) during the NTT for one zebrafish per compound are shown. The heatmaps show the minimum (dark blue) to maximum (dark red) amount of time a fish spent in each pixel. Time spent at the top and the bottom of the tank are quantified for **(D and G)** harmane (1, 3, and 10 mg/L), **(E and H)** norharmane (0.3, 1, and 3 mg/L), and **(F and I)** TIQ (10, 30, and 100 mg/L). All compounds show anxiolytic-like effects at at least one of the concentrations and time point. Black dashed line = vehicle control; light blue = lowest concentration; blue = middle concentration; purple = highest concentration. The sample size was 12 except for 10 mg/L harmane, control group for norharmane, 3 mg/L norharmane, and 100 mg/L TIQ, which were $n = 11$. Data are expressed as mean ± SEM. *$p < 0.05$; **$p < 0.01$; ***$p < 0.001$; Abbreviations: NTT = novel tank test; TIQ = 1.2,3,4-tetrahydroisoquinoline.

RESULTS

Effects of the Compounds on Zebrafish NTT Response

Zebrafish were placed in an NTT tank immediately after being exposed to the system water containing one of the four natural MAO inhibitors (harmane, norharmane, TIQ, or TMN) or reference compounds (clorgyline or pargyline) for 20 min (**Figure 1B**). Interestingly, all four compounds induced a distinct behavioral profile in the zebrafish (**Figures 2**, **3**; **Supplementary Figure S1** in **Supplementary Material S1**). There was a significant treatment effect by harmane ($F(3, 43) = 5.311$, $p = 0.020$ (top); $F(3,43) = 4.047$, $p = 0.013$ (bottom)). The lowest two concentrations of harmane (1 and 3 mg/L) increased the time spent at the top and decreased the time spent at the bottom during the first minute of the 5 min test ($p < 0.05$ for 1 mg/L; $p < 0.001$ for 3 mg/L), while the highest concentration (10 mg/L) had no effect (**Figures 2A,D,G**; treatment x time effect:

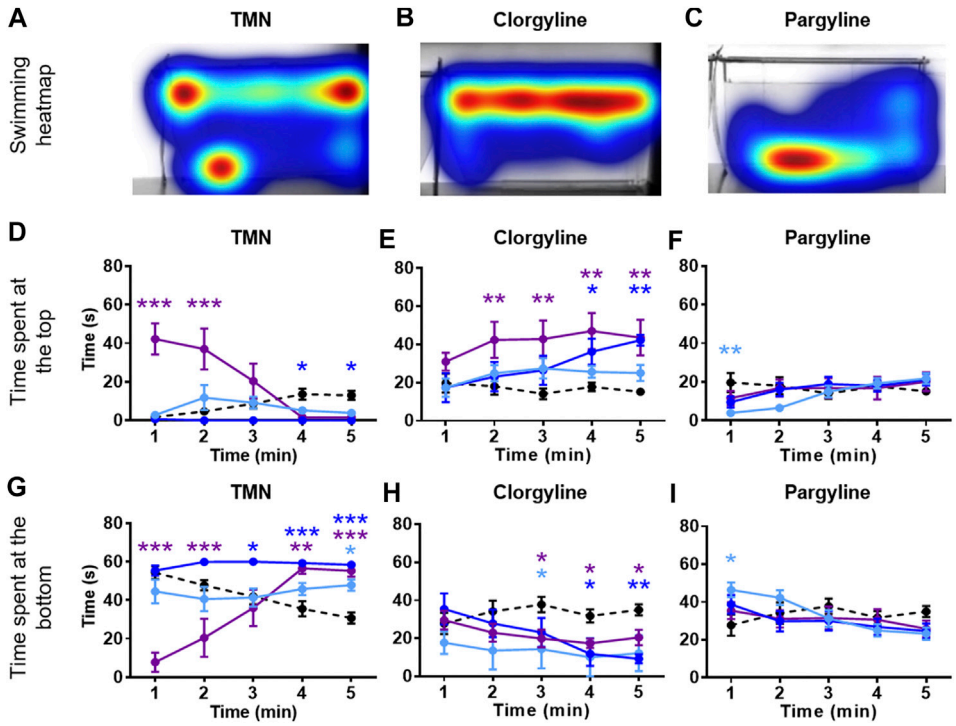

FIGURE 3 | NTT results for TMN, clorgyline, and pargyline. Representative heatmaps for **(A)** TMN (30 mg/L) **(B)** clorgyline (100 mg/L), and **(C)** pargyline (10 mg/L) during the NTT for one zebrafish per compound are shown. The heatmaps show the minimum (dark blue) to maximum (dark red) amount of time a fish spent in each pixel. Time spent at the top and the bottom of the tank are quantified for **(D and G)** TMN (3, 10, and 30 mg/L), **(E and H)** clorgyline (10, 30, and 100 mg/L), and **(F and I)** pargyline (10, 30, and 100 mg/L). All compounds show anxiolytic-like effects at at least one of the concentrations and time point. Black dashed line = vehicle control; light blue = lowest concentration; blue = middle concentration; purple = highest concentration. The sample size was 12 except for control group for TMN ($n = 11$), 3 mg/L TMN ($n = 9$), 10 mg/L and 30 mg/L TMN ($n = 7$), 30 mg/L Clorgyline ($n = 8$), and 100 mg/L Clorgyline (n = 6). Data are expressed as mean ± SEM. $^{*}p < 0.05$; $^{**}p < 0.01$; $^{***}p < 0.001$; Abbreviations: NTT = novel tank test; TMN = 2,3,6-trimethyl-1,4-naphthoquinone.

F (12, 172) = 3.534, $p = 0.0001$ (top), F (12, 172) = 3.822, $p < 0.0001$ (bottom)). For norharmane, the highest concentration (3 mg/L) increased the time spent at the top and decreased the time spent at the bottom during the last 2 min of the test ($p < 0.05$ for top; $p < 0.01$ for bottom), while the middle concentration (1 mg/L) had a significant effect between 2 and 3 min of the test, particularly for the time spent at the bottom ($p < 0.05$ at 2 min; $p < 0.01$ at 3 min) (**Figures 2B,E,H**; treatment x time effect: F (12, 168) = 2.612, $p = 0.0032$ (top), F (12, 168) = 2.357, $p = 0.0080$ (bottom)). The lowest concentration (0.3 mg/L) had no effect. TIQ had a significant treatment effect also, where the highest two concentrations of TIQ (30 and 100 mg/L) generally increased and decreased the time spent at the top and bottom, respectively ($p < 0.01$ for 30 mg/L; $p < 0.001$ for 100 mg/L), while the lowest concentration had no effect **(Figures 2C,F,I**; F (3, 43) = 14.89, $p < 0.0001$ (top), F (3, 43) = 11.73, $p < 0.0001$). There was no time-dependent treatment effect. TMN induced a mix of both anxiolytic- and anxiogenic-like behaviors at the highest concentration tested (30 mg/L) (**Figures 3A,D,G**; treatment effect: F (3,30) = 8.746, $p = 0.0003$ (top); F (3, 30) = 7.128, $p = 0.0009$; treatment x time effect: F (12, 120) = 11.99, $p < 0.0001$ (top), F (12, 120) = 15.44, $p < 0.0001$ (bottom)). It increased the time spent at the top and decreased the time spent at the bottom during the first 2 min of the test ($p < 0.001$). In contrast, the fish spent more time at the bottom ($p < 0.001$) and had the tendency to spend less time at the top during the last 2 min of the test. The middle concentration (10 mg/L) of TMN induced only an anxiogenic-like effect during the last couple of minutes of the test ($p < 0.05$ for top; $p < 0.001$ for bottom).

Zebrafish treated with the two reference compounds, clorgyline and pargyline, also behaved quite differently from each other and from those treated with the natural MAO inhibitors. Clorgyline, in general, showed a concentration-dependent anxiolytic-like effect, with the highest concentration (100 mg/L) increasing the time spent at the top for almost the entire test period ($p < 0.01$), the middle concentration (30 mg/L) significantly increasing it only during the last 2 min ($p < 0.05$), and the lowest concentration (10 mg/L) having no effect (**Figures 3B,E**; treatment effect: F (3,34) = 4.864, $p = 0.0064$; treatment x time effect: F (12, 135) = 2.269, $p = 0.0118$). A corresponding reduction in the time spent at the bottom was evident, but the concentration-dependency was less prominent (**Figure 3H**; treatment effect: F (3, 34) = 3.225, $p = 0.0345$; treatment x time effect: F (12, 135) = 2.230, $p = 0.0135$). Pargyline was the only compound to show only an anxiogenic-like effect, but only for the first 1 min of the test at the lowest concentration tested (10 mg/L; $p < 0.01$ (top); $p < 0.05$ (bottom)) (**Figures 3C,F,I**; treatment x time effect: F (12, 176) = 3.520, $p = 0.0001$ (top); F

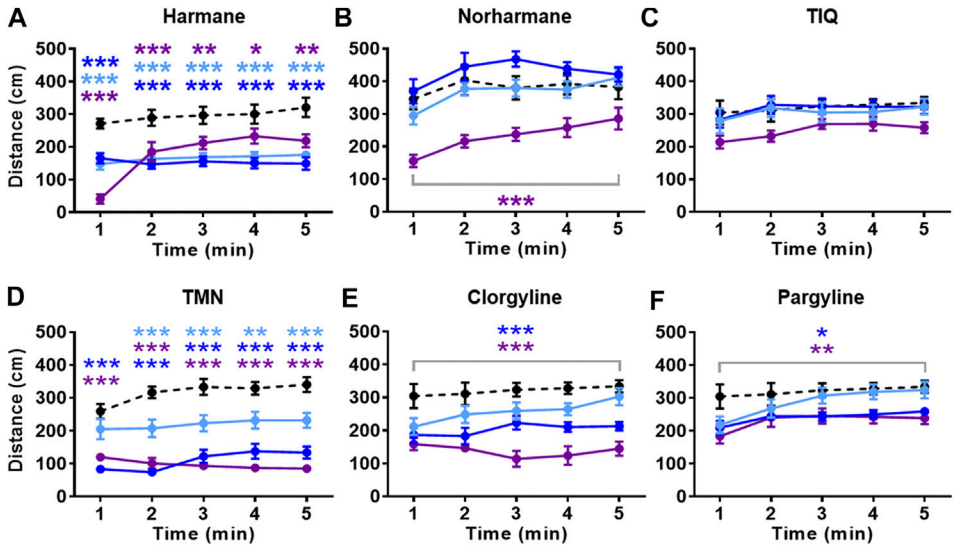

FIGURE 4 | Effects of MAO inhibitors on total distance traveled. Total distance traveled during the NTT is presented for **(A)** harmane (1, 3, and 10 mg/L) **(B)** norharmane (0.3, 1, and 3 mg/L) **(C)** TIQ (10, 30, and 100 mg/L) **(D)** TMN (3, 10, and 30 mg/L) **(E)** clorgyline (10, 30, and 100 mg/L), and **(F)** pargyline (10, 30, and 100 mg/L). Black dashed line = vehicle control; light blue = lowest concentration; blue = middle concentration; purple = highest concentration. The sample size is detailed in the legends for **Figures 3**, **4**. Data are expressed as mean ± SEM. $^{*}p < 0.05$; $^{**}p < 0.01$; $^{***}p < 0.001$. Abbreviations: NTT = novel tank test; TIQ = 1.2,3,4-tetrahydroisoquinoline; TMN = 2,3,6-trimethyl-1,4-naphthoquinone.

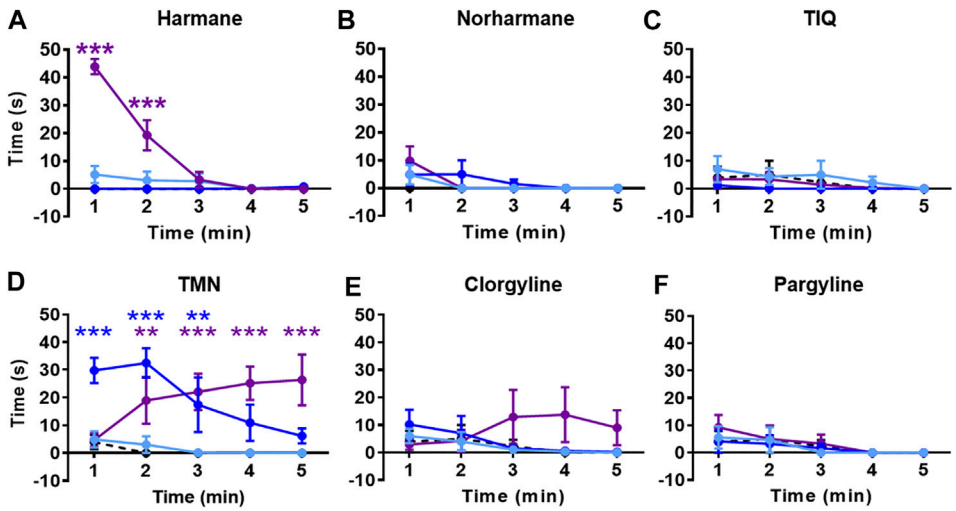

FIGURE 5 | Effects of MAO inhibitors on freezing time. Total freezing time during the NTT is presented for **(A)** harmane (1, 3, and 10 mg/L) **(B)** norharmane (0.3, 1, and 3 mg/L) **(C)** TIQ (10, 30, and 100 mg/L) **(D)** TMN (3, 10, and 30 mg/L) **(E)** clorgyline (10, 30, and 100 mg/L), and **(F)** pargyline (10, 30, and 100 mg/L). Black dashed line = vehicle control; light blue = lowest concentration; blue = middle concentration; purple = highest concentration. The sample size is detailed in the legends for **Figures 3**, **4**. Data are expressed as mean ± SEM. $^{**}p < 0.01$; $^{***}p < 0.001$. Abbreviations: NTT = novel tank test; TIQ = 1.2,3,4-tetrahydroisoquinoline; TMN = 2,3,6-trimethyl-1,4-naphthoquinone.

(12, 176) = 3.400, $p = 0.0002$ (bottom)). It is worthy to note that buspirone, a clinical anxiolytic drug for general anxiety, induced a significant treatment effect in this paradigm (**Supplementary Figure S2** in **Supplementary Material S1**; treatment effect: F (3, 70) = 27.25, $p < 0.0001$ (top); F (3, 70) = 16.34, $p < 0.0001$ (bottom); time x treatment effect: F (12, 280) = 3.838, $p < 0.0001$ (top); F (12, 280) = 4.030, $p < 0.0001$ (bottom)). This finding supports the validity of the zebrafish NTT to detect an anxiolytic-like drugs.

All compounds except TIQ significantly affected the general activity, measured by total distance traveled (**Figure 4**). The total distance traveled was significantly reduced by all concentrations of harmane and TMN, the highest concentration of norharmane, and the two highest concentrations of clorgyline and pargyline

throughout the test period (treatment effect for harmane: F (3, 43) = 16.81, $p < 0.0001$; for norharmane: F (3, 42) = 11.56, $p < 0.0001$; for TMN: F (3, 30) = 36.21, $p < 0.0001$; for clorgyline: F (3, 34) = 12.64, $p < 0.0001$; for pargyline: F (3, 44) = 4.656, $p = 0.0065$; treatment x time effect for harmane: F (12, 172) = 8.170, $p < 0.0001$; for TMN: F (12, 120) = 2.501, $p = 0.0058$). In addition, the highest concentration of harmane increased the freezing time during the first 2 min of the test ($p < 0.0001$) (**Figure 5A**; treatment effect: F (3, 43) = 23.94, $p < 0.0001$; treatment x time effect: F (12, 172) = 35.38, $p < 0.0001$). TMN increased the freezing time for the two highest concentrations (F (3, 30) = 15.50, $p < 0.0001$). The effect of the middle concentration was significant during the first 3 min ($p < 0.01$), while the effect of the highest concentration was significant from 1 min onward ($p < 0.001$) (**Figure 5D**; treatment x time effect: F (12, 120) = 4.920, $p < 0.0001$). Other compounds had no effect on the freezing response. The effects of the compounds on the total distance traveled and freezing time did not seem to parallel the anxiolytic- or anxiogenic-like effects of the respective compounds. Thus, it is not likely that any changes in the observed general movement had a direct association with the anxiolytic- or anxiogenic-like effects of the compounds.

Monoamine Oxidase Inhibition

All compounds were tested for their efficacy to inhibit MAO-A and MAO-B by MAO assays *in vitro*. Of the four alkaloids, harmane was the most potent and selective MAO-A inhibitor in our assay (IC_{50} = 0.05 ± 0.03 and >100 μM for MAO-A and MAO-B, respectively) (**Table 1**). In fact, harmane was as potent as clorgyline in inhibiting MAO-A and showed greater MAO-A selectivity than clorgyline with >2,000-fold greater selectivity over MAO-B in contrast to the approximately 400-fold greater selectivity of clorgyline. Norharmane and TMN were approximately 100-fold less potent, and TIQ was 400-fold less potent than harmane (MAO-A IC_{50} = 1.05 ± 0.36 for norharmane, 1.14 ± 0.74 for TMN, and 20.88 ± 2.97 for TIQ). These three compounds did not show selectivity between MAO-A and MAO-B. The potency and lack of selectivity of norharmane and TMN most closely resembled those of pargyline.

Blood–Brain Barrier Penetration

To understand whether the MAO inhibitors in the present study have good BBB penetrability, two qualitative classification models for predicting the probability of BBB penetration (Ligand Express® and admetSAR) and one quantitative regression model for predicting the Log (BB) compound penetration values (Biovia ADMET) were used. Both the Ligand Express® and admetSAR models predicted all compounds to have good BBB penetrability, as indicated by a probability close to 1 (**Table 1**). The predicted Log (BB) values for all compounds were in the high (0–0.7) or very high (>0.7) range. To confirm the predicted BBB penetration values, the concentrations of the compounds in brain were tested in bioavailability assay. All compounds were detected at high concentrations in the zebrafish brain (**Table 2**). Harmane and TIQ levels, in particular were approximately 10-fold higher than the rest of compounds tested. The observed concentrations for other compounds were within the expected level (1 ng/mg brain tissue), assuming that the brain density is approximately the same as that of water (Weisenburger and Vaziri, 2018).

DISCUSSION

MAO inhibitors have been previously reported to ameliorate depression and specific types of anxiety (Sabri and Saber-Ayad, 2020). In this study, we detected anxiolytic-like effects of four natural MAO inhibitors – harmane, norharmane, TMN, and TIQ – in novel-environment-induced anxiety by using the zebrafish NTT. The observed effects were most likely due to a direct regulation of brain function as all tested compounds showed a high level of brain bioavailability and predicted blood-brain-barrier permeability. The anxiolytic-like effect of harmane is in agreement with previous reports indicating reduction in anxiety-related behaviors in, for example, elevated plus maze in rodents (Aricioglu and Altunbas, 2003; Khan et al., 2017a). Such effect of norharmane has been speculated (Pepplinkhuizen et al., 1996), but it has not been reported. There have been no previous reports regarding the anxiolytic-like effect of TIQ or TMN. We believe that this is the first time that the anxiolytic-like effect of these compounds for this particular type of anxiety, as predicted in this zebrafish model, is reported. There are several different types of anxiety recognized in *Diagnostic and Statistical Manual of Mental Disorders* by American Psychiatric Association, including, for example generalized anxiety disorder, panic disorder, social anxiety disorder, and agoraphobia (Leahy et al., 2012; Salum et al., 2013; Park and Kim, 2020). The zebrafish NTT may most closely mimic agoraphobia, a type of panic disorder characterized by symptoms of anxiety in situations where the person perceives their environment to be unsafe with no easy way to escape. In this paradigm, a zebrafish fears the potential threat of predator in a new environment, and dives to the bottom of the tank, avoiding the potential danger. This behavior is interpreted as an anxiety-like response.

Classically, MAO inhibitors have been considered as a treatment of panic disorders with agoraphobia, but their use was rather restricted due to the risk of, for example, hypertension (Tyrer and Shawcross, 1988; Vina et al., 2012; Sabri and Saber-Ayad, 2020). The alkaloids in this study, however, belong to the reversible type of MAO inhibitors, which have been favored due to reduced side effects (Buller, 1995; Herraiz and Chaparro, 2005; Wasik et al., 2014). It is worthy to note that three out of four test compounds also reduced the total distance travelled at the concentrations that showed anxiolytic-like effect in zebrafish. TIQ was the only compound that showed a steady anxiolytic-like effect throughout the test period without affecting the general movement of the fish. The reason for the observed difference may be difficult to interpret purely on the basis of MAO-A or -B activities. For example, TIQ was the weakest MAO-A/B inhibitor *in vitro*, yet it induced the most steady anxiolytic-like effect during the behavioral test. Its brain bioavailability and blood-brain barrier permeability probability were similar to harmane. One alternative explanation is that these naturally occurring compounds have other molecular targets in addition to MAO.

TABLE 2 | Summary of compound bioavailability in fish brain.

Compounds	Brain Analytes	Relative brain level per 1 mg/L compound[a,b] (ng/mg tissue)	Log (BB) Biovia ADMET
Harmane	Harmane	10.64 ± 2.36	0.188
Norharmane	Norharmane	2.81 ± 1.52	0.101
TIQ	TIQ	11.47 ± 1.07	0.089
TMN	TMN	1.08 ± 0.33	0.268
Clorgyline	Clorgyline	3.92 ± 1.85	1.053
Pargyline	Pargyline	0.92 ± 0.37	0.750

[a]*Data are presented in mean ± SEM.*

[b]*Relative compound level in the brain per 1 mg/L compound was calculated by assuming a linear relationship between compound concentration and BBB penetration.*

Abbreviations: ADMET = absorption, distribution, metabolism, excretion, and toxicity; BB = blood brain; TIQ = 1,2,3,4-tetrahydroisoquinoline; TMN = 2,3,6-trimethyl-1,4-naphthoquinone.

For example, previous reports suggest that harmane and norharmane can also bind benzodiazepine receptor binding albeit at high concentrations (Muller et al., 1981). We have also observed serotonin receptor and norepinephrine transporter binding activities for harmane and norharmane in the 10 μM range in a pilot study *in vitro* (data not shown). Thus, it is possible that the anxiolytic-like effect of TIQ may be mediated by other molecules in addition to MAO.

It is worth noting that in the present study, clorgyline induced anxiolytic-like effect while pargyline did not. This finding supports and confirms previous reports indicating that the MAO A inhibitor clorgyline more effectively regulates mood and anxiety than the MAO B inhibitor pargyline (Tyrer and Shawcross, 1988). In support of this behavioral finding, we found that, in fact, clorgyline inhibits MAO A approximately 400-fold stronger than MAO B, which is similar to previous reports by others suggesting approximately 1000-fold selectivity (Ramsay et al., 2020). The *in vitro* inhibitory activity of pargyline was less straight forward to interpret, where we detected similar IC_{50} values – thus, similar Ki values (0.85 μM for MAO A and 0.50 μM) – for MAO A and B. This is in line with the previous observation by Fisar et al. (2010), showing 1.4-fold difference between the Ki values of MAO-A and MAO-B by using MAO from crude pig brain mitochondrial fractions (Fisar et al., 2010). Interestingly, it has been shown that assay conditions (e.g., preincubation time) can affect the apparent selectivity of pargyline (Fowler et al., 1982; Ramsay et al., 2020). For example, with the direct assay without substrate preincubation with pargyline, the Ki values were 15 μM for MAO A and 1.8 μM for MAO B (Fowler et al., 1982; Ramsay et al., 2020), yielding a mere 8-fold difference which cannot be considered as a selectivity. In contrast, recent studies performed by Oh et al. (2020) and Takao et al. (2019) observed >100-fold and 21-fold differences in Ki values of MAO-A and MAO-B, respectively, by using recombinant human MAO-A and MAO-B enzymes (Oh et al., 2020) (Takao et al., 2019). One could speculate that additional differences in, for example, pargyline batch or salt form, substrate type, MAO enzyme type or source, and enzymatic reaction condition may have contributed to the slightly different MAO selectivity observed for pargyline in the present study and by others. This new pharmacological insight suggests that perhaps, previous conclusion that the lack of anxiolytic-like effect by pargyline is due solely to the lack of MAO A inhibitory activity may be over simplistic and should be interpreted with caution. The MAO inhibitory potency and selectivity of the other four compounds tested in this study – harmane, norharmane, TIQ, and TMN – were within the range of previous reports substrate (Thull et al., 1995; Herraiz and Chaparro, 2005; Dos Santos Passos et al., 2014; Wiart, 2014). Of these compounds, harmane was the only MAO A selective inhibitor, while norharmane, TIQ, and TMN showed no selectivity between MAO A and B in the present study and in previous reports (Thull et al., 1995; Herraiz and Chaparro, 2005; Coelho Cerqueira et al., 2011; Dos Santos Passos et al., 2014). Because TIQ, TMN, and norharmane were non-selective MAO inhibitor similar to pargyline, it is possible that the anxiolytic-like effect observed for TIQ, TMN, and norharmane may be partially induced by other molecular targets in addition to MAO.

In conclusion, anxiety disorders are among the most common psychiatric disorders that affect all groups of the general population. The current available treatments have unwanted side effects, such as excessive sedation, cognitive impairment, ataxia, aggression, sexual dysfunction, tolerance and dependence (Vina et al., 2012). In this study, we have shown that MAO-inhibiting compounds that are naturally present in plants can induce anxiolytic-like effects in zebrafish. TIQ, in particular, showed a promising neurobehavioral profile, inducing steady anxiolytic-like effect without affecting the general movement. The current findings highlight the importance of investigating natural compounds as alternative herbal remedies for anxiety and support the usefulness of zebrafish as an experimental tool to screen for anxiolytic-like compounds.

DATA AVAILABILITY STATEMENT

The raw data supporting the conclusion of this article will be made available by the authors, without undue reservation.

ETHICS STATEMENT

The animal study was reviewed and approved by the European standards of animal welfare in animal use for scientific purposes (2010/63/EU), compiled with national regulations for the care of experimental animals, and were approved as described in national

regulations (RD 53/2013) by local and regional committees: PRO-AE-SS-121 and PRO-AE-SS-134.

AUTHOR CONTRIBUTIONS

OJ, II, and AA designed, conducted, and analyzed the zebrafish experiment. JM designed, conducted, and analyzed the bioavailability assay. MT designed, conducted, and analyzed the MAO assay and managed the compound library. DL conducted in silico BBB modeling. MCP, and JH critically reviewed the manuscript for important intellectual content. KK initiated, designed, and analyzed the experiments and wrote the manuscript. All authors approved the final version to be published and declare that all data were generated in-house and that no paper mill and other ways of manipulating research materials were used.

FUNDING

This work was funded solely by Philip Morris International.

ACKNOWLEDGMENTS

We thank Stefan Frentzel, Wenhao Xia, and Karsta Luettich for the insightful scientific discussions.

SUPPLEMENTARY MATERIAL

The Supplementary Material for this article can be found online at: https://www.frontiersin.org/articles/10.3389/fphar.2021.669370/full#supplementary-material

REFERENCES

Adenot, M., and Lahana, R. (2004). Blood-brain Barrier Permeation Models: Discriminating between Potential CNS and Non-CNS Drugs Including P-Glycoprotein Substrates. *J. Chem. Inf. Comput. Sci.* 44, 239–248. doi:10.1021/ci034205d

Ahmad, M., Saleem, S., Ahmad, A. S., Yousuf, S., Ansari, M. A., Khan, M. B., et al. (2005). Ginkgo Biloba Affords Dose-dependent Protection against 6-Hydroxydopamine-Induced Parkinsonism in Rats: Neurobehavioural, Neurochemical and Immunohistochemical Evidences. *J. Neurochem.* 93, 94–104. doi:10.1111/j.1471-4159.2005.03000.x

Alzualde, A., Behl, M., Sipes, N. S., Hsieh, J.-H., Alday, A., Tice, R. R., et al. (2018). Toxicity Profiling of Flame Retardants in Zebrafish Embryos Using a Battery of Assays for Developmental Toxicity, Neurotoxicity, Cardiotoxicity and Hepatotoxicity toward Human Relevance. *Neurotoxicology and Teratolog.* 70, 40–50. doi:10.1016/j.ntt.2018.10.002

Aminin, D., and Polonik, S. (2020). 1,4-Naphthoquinones: Some Biological Properties and Application. *Chem. Pharm. Bull.* 68, 46–57. doi:10.1248/cpb.c19-00911

Antkiewicz-Michaluk, L., Wąsik, A., Możdżeń, E., Romańska, I., and Michaluk, J. (2014). Antidepressant-like Effect of Tetrahydroisoquinoline Amines in the Animal Model of Depressive Disorder Induced by Repeated Administration of a Low Dose of Reserpine: Behavioral and Neurochemical Studies in the Rat. *Neurotox Res.* 26, 85–98. doi:10.1007/s12640-013-9454-8

Arib, O., Rat, P., Molimard, R., Chait, A., Faure, P., and De Beaurepaire, R. (2010). Electrophysiological Characterization of Harmane-Induced Activation of Mesolimbic Dopamine Neurons. *Eur. J. Pharmacol.* 629, 47–52. doi:10.1016/j.ejphar.2009.12.012

Aricioglu, F., and Altunbas, H. (2003). Harmane Induces Anxiolysis and Antidepressant-like Effects in Rats. *Ann. N.Y Acad. Sci.* 1009, 196–201. doi:10.1196/annals.1304.024

Babula, P., Adam, V., Havel, L., and Kizek, R. (2009). Noteworthy Secondary Metabolites Naphthoquinones - Their Occurrence, Pharmacological Properties and Analysis. *Curr. Pharm. Anal.* 5, 47–68. doi:10.2174/157341209787314936

Bencan, Z., and Levin, E. D. (2008). The Role of α7 and α4β2 Nicotinic Receptors in the Nicotine-Induced Anxiolytic Effect in Zebrafish. *Physiol. Behav.* 95, 408–412. doi:10.1016/j.physbeh.2008.07.009

Bencan, Z., Sledge, D., and Levin, E. D. (2009). Buspirone, Chlordiazepoxide and Diazepam Effects in a Zebrafish Model of Anxiety. *Pharmacol. Biochem. Behav.* 94, 75–80. doi:10.1016/j.pbb.2009.07.009

Boulton, A., Yu, P. H., and Tipton, K. F. (1988). Biogenic Amine Adducts, Monoamine Oxidase Inhibitors, and Smoking. *Lancet.* 331, 114–115. doi:10.1016/s0140-6736(88)90308-x

Buller, R. (1995). Reversible Inhibitors of Monoamine Oxidase A in Anxiety Disorders. *Clin. Neuropharmacology.* 18, S38–S44. doi:10.1097/00002826-199518002-00006

Castagnoli, K. P., Steyn, S. J., Petzer, J. P., Van Der Schyf, C. J., and Castagnoli, N., Jr. (2001). Neuroprotection in the MPTP Parkinsonian C57BL/6 Mouse Model by a Compound Isolated from Tobacco. *Chem. Res. Toxicol.* 14, 523–527. doi:10.1021/tx000224v

Cheng, F., Li, W., Zhou, Y., Shen, J., Wu, Z., Liu, G., et al. (2012). admetSAR: a Comprehensive Source and Free Tool for Assessment of Chemical ADMET Properties. *J. Chem. Inf. Model.* 52, 3099–3105. doi:10.1021/ci300367a

Cherpillod, C., and Omer, L. M. O. (1981). A Controlled Trial with Diclofensine, a New Psychoactive Drug, in the Treatment of Depression. *J. Int. Med. Res.* 9, 324–329. doi:10.1177/030006058100900505

Coelho Cerqueira, E., Netz, P. A., Diniz, C., Petry Do Canto, V., and Follmer, C. (2011). Molecular Insights into Human Monoamine Oxidase (MAO) Inhibition by 1,4-naphthoquinone: Evidences for Menadione (Vitamin K3) Acting as a Competitive and Reversible Inhibitor of MAO. *Bioorg. Med. Chem.* 19, 7416–7424. doi:10.1016/j.bmc.2011.10.049

Crawley, J., Ninan, P., Pickar, D., Chrousos, G., Linnoila, M., Skolnick, P., et al. (1985). Neuropharmacological Antagonism of the Beta-Carboline-Induced "anxiety" Response in Rhesus Monkeys. *J. Neurosci.* 5, 477–485. doi:10.1523/jneurosci.05-02-00477.1985

Dilsaver, S. C. (1994). Withdrawal Phenomena Associated with Antidepressant and Antipsychotic Agents. *Drug Saf.* 10, 103–114. doi:10.2165/00002018-199410020-00002

Dos Santos Passos, C. D. S., Simoes-Pires, C., Henriques, A., Cuendet, M., Carrupt, P.-A., and Christen, P. (2014). "Alkaloids as Inhibitors of Monoamine Oxidases and Their Role in the Central Nervous System," in *Studies in Ñatural Products Chemistry*. Editor F. Atta-Ur-Rahman (Oxford, UK: Elsevier), 123–144. doi:10.1016/b978-0-444-63430-6.00004-7

Dos Santos, R. G., Osório, F. L., Crippa, J. A. S., and Hallak, J. E. C. (2016). Antidepressive and Anxiolytic Effects of Ayahuasca: a Systematic Literature Review of Animal and Human Studies. *Rev. Bras. Psiquiatr.* 38, 65–72. doi:10.1590/1516-4446-2015-1701

Edmondson, D. E., and Binda, C. (2018). Monoamine Oxidases. *Subcell Biochem.* 87, 117–139. doi:10.1007/978-981-10-7757-9_5

Egan, W. J., Merz, K. M., Jr., and Baldwin, J. J. (2000). Prediction of Drug Absorption Using Multivariate Statistics. *J. Med. Chem.* 43, 3867–3877. doi:10.1021/jm000292e

Eliceiri, B. P., Gonzalez, A. M., and Baird, A. (2011). Zebrafish Model of the Blood-Brain Barrier: Morphological and Permeability Studies. *Methods Mol. Biol.* 686, 371–378. doi:10.1007/978-1-60761-938-3_18

Exley, R., Iturriaga-Vásquez, P., Lukas, R. J., Sher, E., Cassels, B. K., and Bermudez, I. (2005). Evaluation of Benzyltetrahydroisoquinolines as Ligands for Neuronal Nicotinic Acetylcholine Receptors. *Br. J. Pharmacol.* 146, 15–24. doi:10.1038/sj.bjp.0706307

Farzin, D., and Mansouri, N. (2006). Antidepressant-like Effect of Harmane and Other β-carbolines in the Mouse Forced Swim Test. *Eur. Neuropsychopharmacol.* 16, 324–328. doi:10.1016/j.euroneuro.2005.08.005

Finberg, J. P., and Rabey, J. M. (2016). Inhibitors of MAO-A and MAO-B in Psychiatry and Neurology. *Front. Pharmacol.* 7, 340. doi:10.3389/fphar.2016.00340

Fisar, Z., Hroudová, J., and Raboch, J. (2010). Inhibition of Monoamine Oxidase Activity by Antidepressants and Mood Stabilizers. *Neuro Endocrinol. Lett.* 31, 645–656.

Fowler, C. J., Mantle, T. J., and Tipton, K. F. (1982). The Nature of the Inhibition of Rat Liver Monoamine Oxidase Types A and B by the Acetylenic Inhibitors Clorgyline, L-Deprenyl and Pargyline. *Biochem. Pharmacol.* 31, 3555–3561. doi:10.1016/0006-2952(82)90575-5

Fowler, J. S., Logan, J., Wang, G.-J., Franceschi, D., Volkow, N. D., Telang, F., et al. (2003). Monoamine Oxidase A Imaging in Peripheral Organs in Healthy Human Subjects. *Synapse*. 49, 178–187. doi:10.1002/syn.10231

Herraiz, T. (2004). Relative Exposure to Beta-Carbolines Norharman and Harman from Foods and Tobacco Smoke. *Food Addit Contam.* 21, 1041–1050. doi:10.1080/02652030400019844

Herraiz, T. (2007). Identification and Occurrence of β-Carboline Alkaloids in Raisins and Inhibition of Monoamine Oxidase (MAO). *J. Agric. Food Chem.* 55, 8534–8540. doi:10.1021/jf0719151

Herraiz, T., and Chaparro, C. (2005). Human Monoamine Oxidase Is Inhibited by Tobacco Smoke: β-carboline Alkaloids Act as Potent and Reversible Inhibitors. *Biochem. Biophysical Res. Commun.* 326, 378–386. doi:10.1016/j.bbrc.2004.11.033

Herraiz, T., and Chaparro, C. (2006). Human Monoamine Oxidase Enzyme Inhibition by Coffee and β-carbolines Norharman and Harman Isolated from Coffee. *Life Sci.* 78, 795–802. doi:10.1016/j.lfs.2005.05.074

Kalueff, A. V., Gebhardt, M., Stewart, A. M., Cachat, J. M., Brimmer, M., Chawla, J. S., et al. (2013). Towards a Comprehensive Catalog of Zebrafish Behavior 1.0 and beyond. *Zebrafish*. 10, 70–86. doi:10.1089/zeb.2012.0861

Khan, A. Y., and Suresh Kumar, G. (2015). Natural Isoquinoline Alkaloids: Binding Aspects to Functional Proteins, Serum Albumins, Hemoglobin, and Lysozyme. *Biophys. Rev.* 7, 407–420. doi:10.1007/s12551-015-0183-5

Khan, H., Patel, S., and Kamal, M. A. (2017a). Pharmacological and Toxicological Profile of Harmane-Beta-Carboline Alkaloid: Friend or Foe. *Curr. Drug Metab.* 18, 853–857. doi:10.2174/1389200218666170607100947

Khan, K. M., Collier, A. D., Meshalkina, D. A., Kysil, E. V., Khatsko, S. L., Kolesnikova, T., et al. (2017b). Zebrafish Models in Neuropsychopharmacology and CNS Drug Discovery. *Br. J. Pharmacol.* 174, 1925–1944. doi:10.1111/bph.13754

Kysil, E. V., Meshalkina, D. A., Frick, E. E., Echevarria, D. J., Rosemberg, D. B., Maximino, C., et al. (2017). Comparative Analyses of Zebrafish Anxiety-like Behavior Using Conflict-Based Novelty Tests. *Zebrafish*. 14, 197–208. doi:10.1089/zeb.2016.1415

Leahy, R. L, Holland, S. J. F., and Mcginn, L. K. (2012). *Treatment Plans and Intereventions for Depression and Anxiety Disorders*. New York, NY: The Guilford Press.

Levin, E. D., Bencan, Z., and Cerutti, D. T. (2007). Anxiolytic Effects of Nicotine in Zebrafish. *Physiol. Behav.* 90, 54–58. doi:10.1016/j.physbeh.2006.08.026

Liebowitz, M. R., Schneier, F., Gitow, A., and Feerick, J. (1993). Reversible Monoamine Oxidase-A Inhibitors in Social Phobia. *Clin. Neuropharmacol* 16 (Suppl. 2), S83–S88.

Makino, Y., Ohta, S., Tachikawa, O., and Hirobe, M. (1988). Presence of Tetrahydroisoquinoline and 1-Methyl-Tetrahydro-Isoquinoline in Foods: Compounds Related to Parkinson's Disease. *Life Sci.* 43, 373–378. doi:10.1016/0024-3205(88)90115-4

Menkes, D., Bosanac, P., and Castle, D. (2016). MAOIs - Does the Evidence Warrant Their Resurrection?. *Australas. Psychiatry*. 24, 371–373. doi:10.1177/1039856216634824

Mostert, S., Petzer, A., and Petzer, J. P. (2016). Evaluation of Natural and Synthetic 1,4-naphthoquinones as Inhibitors of Monoamine Oxidase. *Chem. Biol. Drug Des.* 87, 737–746. doi:10.1111/cbdd.12708

Mozdzen, E., Papp, M., Gruca, P., Wasik, A., Romanska, I., Michaluk, J., et al. (2014). 1,2,3,4-Tetrahydroisoquinoline Produces an Antidepressant-like Effect in the Forced Swim Test and Chronic Mild Stress Model of Depression in the Rat: Neurochemical Correlates. *Eur. J. Pharmacol.* 729, 107–115. doi:10.1016/j.ejphar.2014.01.075

Müller, W. E., Fehske, K. J., Borbe, H. O., Wollert, U., Nanz, C., and Rommelspacher, H. (1981). On the Neuropharmacology of Harmane and Other β-carbolines. *Pharmacol. Biochem. Behav.* 14, 693–699. doi:10.1016/0091-3057(81)90133-7

Oh, J. M., Rangarajan, T. M., Chaudhary, R., Singh, R. P., Singh, M., Singh, R. P., et al. (2020). Novel Class of Chalcone Oxime Ethers as Potent Monoamine Oxidase-B and Acetylcholinesterase Inhibitors. *Molecules*. 25, 2356. doi:10.3390/molecules25102356

Papke, R. L., Ono, F., Stokes, C., Urban, J. M., and Boyd, R. T. (2012). The Nicotinic Acetylcholine Receptors of Zebrafish and an Evaluation of Pharmacological Tools Used for Their Study. *Biochem. Pharmacol.* 84, 352–365. doi:10.1016/j.bcp.2012.04.022

Pardon, M.-C., Joubert, C., Perez-Diaz, F., Christen, Y., Launay, J.-M., and Cohen-Salmon, C. (2000). *In vivo* regulation of Cerebral Monoamine Oxidase Activity in Senescent Controls and Chronically Stressed Mice by Long-Term Treatment with Ginkgo Biloba Extrac3t (EGb 761). *Mech. Ageing Develop.* 113, 157–168. doi:10.1016/s0047-6374(99)00107-4

Park, S.-C., and Kim, Y.-K. (2020). Anxiety Disorders in the DSM-5: Changes, Controversies, and Future Directions. *Adv. Exp. Med. Biol.* 1191, 187–196. doi:10.1007/978-981-32-9705-0_12

Pepplinkhuizen, L., Fekkes, D., and Timmerman, L. (1996). Norharman and Anxiety Disorders. *Acta Neuropsychiatr.* 8, 93–95. doi:10.1017/s0924270800036991

Perry, N., and Perry, E. (2018). *Botanical Brain Balms*. China: Filbert Press.

Pfau, W., and Skog, K. (2004). Exposure to β-carbolines Norharman and Harman. *J. Chromatogr. B.* 802, 115–126. doi:10.1016/j.jchromb.2003.10.044

Pickart, M. A., and Klee, E. W. (2014). Zebrafish Approaches Enhance the Translational Research Tackle Box. *Translational Res.* 163, 65–78. doi:10.1016/j.trsl.2013.10.007

Piechowska, P., Zawirska-Wojtasiak, R., and Mildner-Szkudlarz, S. (2019). Bioactive Beta-Carbolines in Food: A Review. *Nutrients*. 11, 814. doi:10.3390/nu11040814

Pinho, B. R., Sousa, C., Oliveira, J. M. A., Valentão, P., and Andrade, P. B. (2012). "Naphthoquinones' Biological Activities and Toxicological Effects," in *Bioactive Compounds: Type, Biological Activities and Health Effects*. Editors A. Bitterlich and S. Fischl (New York, NY: Nova Science Publishers), 181–218.

Quevedo, C., Behl, M., Ryan, K., Paules, R. S., Alday, A., Muriana, A., et al. (2019). Detection and Prioritization of Developmentally Neurotoxic And/or Neurotoxic Compounds Using Zebrafish. *Toxicol. Sci.* 168, 225–240. doi:10.1093/toxsci/kfy291

Ramsay, R. R., Basile, L., Maniquet, A., Hagenow, S., Pappalardo, M., Saija, M. C., et al. (2020). Parameters for Irreversible Inactivation of Monoamine Oxidase. *Molecules*. 25, 5908. doi:10.3390/molecules25245908

Sabri, M. A., and Saber-Ayad, M. M. (2020). "MAO Inhibitors," in *StatPearls* (FL: Treasure Island).

Salum, G. A., Desousa, D. A., Rosario, M. C. d., Pine, D. S., and Manfro, G. G. (2013). Pediatric Anxiety Disorders: from Neuroscience to Evidence-Based Clinical Practice. *Rev. Bras. Psiquiatr.* 35 (Suppl. 1), S03–S21. doi:10.1590/1516-4446-2013-s108

Schneier, F. R. (2001). Treatment of Social Phobia with Antidepressants, *J. Clin. Psychiatry*. 62 (Suppl. 1), 43–48. doi:10.4088/jcp.v62n0511

Schweri, M., Cain, M., Cook, J., Paul, S., and Skolnick, P. (1982). Blockade of 3-Carbomethoxy-β-Carboline Induced Seizures by Diazepam and the Benzodiazepine Antagonists, Ro 15-1788 and CGS 8216. *Pharmacol. Biochem. Behav.* 17, 457–460. doi:10.1016/0091-3057(82)90304-5

Seelig, A. (1998). A General Pattern for Substrate Recognition by P-Glycoprotein. *Eur. J. Biochem.* 251, 252–261. doi:10.1046/j.1432-1327.1998.2510252.x

Shen, J., Cheng, F., Xu, Y., Li, W., and Tang, Y. (2010). Estimation of ADME Properties with Substructure Pattern Recognition. *J. Chem. Inf. Model.* 50, 1034–1041. doi:10.1021/ci100104j

Shih, J. C., Chen, K., and Ridd, M. J. (1999). Monoamine Oxidase: from Genes to Behavior. *Annu. Rev. Neurosci.* 22, 197–217. doi:10.1146/annurev.neuro.22.1.197

Skolnick, P., Crawley, J. N., Glowa, J. R., and Paul, S. M. (1984). Beta-Carboline-Induced Anxiety States. *Psychopathology*. 17 (Suppl. 3), 52–60. doi:10.1159/000284131

Smith, K. L., Ford, G. K., Jessop, D. S., and Finn, D. P. (2013). Behavioural, Neurochemical and Neuroendocrine Effects of the Endogenous β-carboline Harmane in Fear-Conditioned Rats. *J. Psychopharmacol.* 27, 162–170. doi:10.1177/0269881112460108

Stewart, A., Gaikwad, S., Kyzar, E., Green, J., Roth, A., and Kalueff, A. V. (2012). Modeling Anxiety Using Adult Zebrafish: a Conceptual Review. *Neuropharmacology*. 62, 135–143. doi:10.1016/j.neuropharm.2011.07.037

Stewart, A. M., and Kalueff, A. V. (2012). The Developing Utility of Zebrafish Models for Cognitive Enhancers Research. *Curr. Neuropharmacol.* 10, 263–271. doi:10.2174/157015912803217323

Takao, K., Endo, S., Nagai, J., Kamauchi, H., Takemura, Y., Uesawa, Y., et al. (2019). 2-Styrylchromone Derivatives as Potent and Selective Monoamine Oxidase B Inhibitors. *Bioorg. Chem.* 92, 103285. doi:10.1016/j.bioorg.2019.103285

Thull, U., Kneubühler, S., Gaillard, P., Carrupt, P.-A., Testa, B., Altomare, C., et al. (1995). Inhibition of Monoamine Oxidase by Isoquinoline Derivatives. *Biochem. Pharmacol.* 50, 869–877. doi:10.1016/0006-2952(95)00220-t

Tipton, K. F. (2018). 90 Years of Monoamine Oxidase: Some Progress and Some Confusion. *J. Neural Transm.* 125, 1519–1551. doi:10.1007/s00702-018-1881-5

Tsuchiya, H., Shimizu, H., and Iinuma, M. (1999). Beta-Carboline Alkaloids in Crude Drugs. *Chem. Pharm. Bull.* 47, 440–443. doi:10.1248/cpb.47.440

Tyrer, P., and Shawcross, C. (1988). Monoamine Oxidase Inhibitors in Anxiety Disorders. *J. Psychiatr. Res.* 22 (Suppl. 1), 87–98. doi:10.1016/0022-3956(88)90070-2

Van Der Toorn, M., Koshibu, K., Schlage, W. K., Majeed, S., Pospisil, P., Hoeng, J., et al. (2019). Comparison of Monoamine Oxidase Inhibition by Cigarettes and Modified Risk Tobacco Products. *Toxicol. Rep.* 6, 1206–1215. doi:10.1016/j.toxrep.2019.11.008

Verheij, R., Timmerman, L., Passchier, J., Fekkes, D., and Pepplinkhuizen, L. (1997). Trait Anxiety, Coping with Stress, and Norharman. *Psychol. Rep.* 80, 51–59. doi:10.2466/pr0.1997.80.1.51

Vina, D., Serra, S., Lamela, M., and Delogu, G. (2012). Herbal Natural Products as a Source of Monoamine Oxidase Inhibitors: a Review. *Curr. Top. Med. Chem.* 12, 2131–2144. doi:10.2174/156802612805219996

Wasik, A., Mozdzen, E., Michaluk, J., Romanska, I., and Antkiewicz-Michaluk, L. (2014). 1-Methyl-1,2,3,4-tetrahydroisoquinoline, an Endogenous Neuroprotectant and MAO Inhibitor with Antidepressant-like Properties in the Rat. *Neurotox Res.* 25, 323–334. doi:10.1007/s12640-013-9425-0

Weisenburger, S., and Vaziri, A. (2018). A Guide to Emerging Technologies for Large-Scale and Whole-Brain Optical Imaging of Neuronal Activity. *Annu. Rev. Neurosci.* 41, 431–452. doi:10.1146/annurev-neuro-072116-031458

Wiart, C. (2014). "Phenolics," in *Lead Compounds from Medicinal Plants for the Treatment of Neurodegenerative Diseases* (Oxford, UK: Academic Press), 285–374. doi:10.1016/b978-0-12-398373-2.00003-0

Yang, H., Lou, C., Sun, L., Li, J., Cai, Y., Wang, Z., et al. (2019). admetSAR 2.0: Web-Service for Prediction and Optimization of Chemical ADMET Properties. *Bioinformatics*. 35, 1067–1069. doi:10.1093/bioinformatics/bty707

Youdim, M. B. H., Edmondson, D., and Tipton, K. F. (2006). The Therapeutic Potential of Monoamine Oxidase Inhibitors. *Nat. Rev. Neurosci.* 7, 295–309. doi:10.1038/nrn1883

Conflict of Interest: MT, DL, MCP, JH, and KK are employed by Philip Morris International. OJ, II, and AA are employed by Biobide and JM is employed by Grilab. Philip Morris International employed Biobide's and Grilab's services for zebrafish research and the bioavailability assay, respectively.

frontiers in Pharmacology

ORIGINAL RESEARCH
published: 12 November 2021
doi: 10.3389/fphar.2021.747991

Cyclosporine A Induces Cardiac Developmental Toxicity in Zebrafish by Up-Regulation of Wnt Signaling and Oxidative Stress

Mengqi Wan[1], Ling Huang[2], Jieping Liu[2], Fasheng Liu[2], Guilan Chen[2], Huiwen Ni[2], Guanghua Xiong[2], Xinjun Liao[2], Huiqiang Lu[2], Juhua Xiao[3], Qiang Tao[1]* and Zigang Cao[2]**

[1]Department of General Surgery, The Affiliated Children's Hospital of Nanchang University, Nanchang, China, [2]Jiangxi Engineering Laboratory of Zebrafish Modeling and Drug Screening for Human Diseases, Jiangxi Key Laboratory of Developmental Biology of Organs, College of Life Sciences, Jinggangshan University, Ji'an, China, [3]Department of Ultrasound, Jiangxi Provincial Maternal and Child Health Hospital, Nanchang, China

OPEN ACCESS

Edited by:
Anna Siebel,
Universidade Comunitária da Região de Chapecó, Brazil

Reviewed by:
Matheus Marcon,
Universidade Federal do Triângulo Mineiro, Brazil
Jan Willem Van Der Laan,
Medicines Evaluation Board, Netherlands

***Correspondence:**
Zigang Cao
zigangcao@126.com
Qiang Tao
taoqiang_2008@126.com
Juhua Xiao
xjh1230@163.com

Specialty section:
This article was submitted to Predictive Toxicology, a section of the journal Frontiers in Pharmacology

Received: 27 July 2021
Accepted: 22 October 2021
Published: 12 November 2021

Citation:
Wan M, Huang L, Liu J, Liu F, Chen G, Ni H, Xiong G, Liao X, Lu H, Xiao J, Tao Q and Cao Z (2021) Cyclosporine A Induces Cardiac Developmental Toxicity in Zebrafish by Up-Regulation of Wnt Signaling and Oxidative Stress. Front. Pharmacol. 12:747991. doi: 10.3389/fphar.2021.747991

Due to the widely application of Cyclosporine A (CsA) as an immunosuppressant in clinic, it is necessary to study its potential toxicity. Therefore, we used zebrafish as a model animal to evaluate the toxicity of CsA on embryonic development. Exposure of zebrafish embryos to CsA at concentrations of 5 mg/L, 10 mg/L, and 15 mg/L from 12 hpf to 72 hpf resulted in abnormal embryonic development, including cardiac malformation, pericardial edema, decreased heart rate, decreased blood flow velocity, deposition at yolk sac, shortened body length, and increased distance between venous sinus and arterial bulb (SV-BA). The expression of genes related to cardiac development was disordered, and the apoptotic genes were up-regulated. Oxidative stress level was up-regulated and accumulated in pericardium in a dose-dependent manner. Astaxanthin (ATX) treatment could significantly alleviate zebrafish heart defects. CsA induced up-regulation of Wnt signaling in zebrafish, and IWR-1, an inhibitor of Wnt signaling pathway, could effectively rescue the heart defects induced by CsA. Together, our study indicated that CsA induced cardiac developmental toxicity in zebrafish larvae through up-regulating oxidative stress and Wnt signaling, contributing to a more comprehensive evaluation of the safety of the drug.

Keywords: cyclosporine a, cardiac toxicity, oxidative stress, wnt signaling, apoptosis

INTRODUCTION

CsA, a lipophilic cyclic polypeptide isolated from the fungus tolypocladium inflatum, is a powerful immunosuppressant. CsA inhibits the proliferation of T cells by inhibiting the activation of calcineurin (Matsuda and Koyasu, 2000; Beauchesne et al., 2007). It is widely used in the prevention of immune rejection of organ transplantation and the treatment of T cell related autoimmune diseases (Damiano et al., 2015). Although CsA has no bone marrow toxicity of other immunosuppressants, its own toxicity also hinders the research and application. The most common is that CsA causes nephrotoxicity. In addition, CsA can also cause a series of toxic and side effects such as hepatotoxicity and neurotoxicity (Thomas and Gordon, 1986), and a series of changes in the cardiovascular system such as endothelial cell injury and inhibition of angiogenesis (Woywodt et al., 2003; Nacev et al., 2011; Kim et al., 2020). At present, CsA is not only used as immunosuppressant, but also used as a cardiac protectant in clinic. For example, CsA can

improve cardiac dysfunction caused by sepsis via inhibiting calcineurin (Liu et al., 2017), and inhibit the mitochondrial permeability transition pore (MPTP) in the treatment of ischemic heart disease (Hausenloy et al., 2012). Related studies have shown that CsA has cardiotoxicity (Ozkan et al., 2012), but the specific mechanism is unknown. The cardiovascular side effects of CsA greatly limit its clinical application and research.

Zebrafish, a complex organism with highly conserved organ systems and metabolic pathways, is a commonly used toxicological biological model at present. Zebrafish is small in size, economical and easy to feed. The embryo develops *in vitro*, and the main organ systems are formed at about 72 hpf (Horzmann and Freeman, 2018), which greatly shorten the cycle of drug toxicity screening and make the process more convenient. Zebrafish is particularly suitable for cardiotoxicity studies and does not rely entirely on the functional cardiovascular system as compared to embryo models in mice and chickens. Zebrafish embryos can obtain oxygen through passive diffusion, so they can survive even with severe heart defects (Stainier, 2001). The acquisition of zebrafish transgenic lines is easier than other animal models, and the transgenic fish lines labeled with fluorescent protein can more intuitively observe a series of effects of drugs on the development of zebrafish (Bambino and Chu, 2017). More importantly, the zebrafish genome sequence is highly homologous to the human genome sequence (Howe et al., 2013), so zebrafish is an ideal biological model to simulate cardiovascular, immunological, neurological and other toxic effects in an increasingly wide range of applications.

The heart is one of the earliest organs to develop in vertebrates. The development of cardiomyocyte progenitor cells and endocardial progenitor cells is the characteristic of the beginning of heart development. The pool of cardiomyocyte progenitor cells (atrium and ventricle) located in the marginal areas of both sides of the embryo migrate to the midline and fuse to form a cardiac disc structure in the midline. After a series of differentiation and torsion in 24 hpf, the S-shaped linear lumen with circulatory function is formed (Wu et al., 2020), which is divided into atrium and ventricle. At 48 hpf, the heart begins to revolve, and the right ventricle and left atrium are formed. The heart cavity expands and begins to form cardiac circulation (Bakkers, 2011). The heart, one of the most important organs to maintain the body function, carries gas and nutrients to various tissues and organs through the blood circulation. Serious heart defects can affect the growth and development of human or animal and even threaten life. Unlike mouse and chicken cardiovascular models, zebrafish embryos can obtain oxygen through passive diffusion, so they can survive for 7 days even with severe heart defects. In addition, almost all the tools available for studying the cardiovascular system in other model systems can also be used in zebrafish models (Stainier, 2001; Sarmah and Marrs, 2016). Therefore, zebrafish as an animal model to study cardiac developmental toxicity has brought great convenience to this study.

In this study, CsA was used to intervene the embryonic development of Tg (my17: GFP) transgenic zebrafish, and cardiac developmental toxicity was observed in zebrafish treated with different concentrations of CsA. The expression of genes related to heart development was disturbed, and the level of oxidative stress was increased accordingly. Astaxanillin intervention could effectively rescue CsA induced cardiotoxicity in zebrafish. In addition, CsA induced the up-regulation of Wnt signaling, and Wnt signaling inhibitors significantly reduced the cardiotoxicity. Therefore, our study showed that CsA was cardiotoxic, which was achieved by up-regulating the Wnt signaling pathway.

METHODS AND MATERIALS

Reagents and Materials

CsA was purchased from Chengdu Deste Biotechnology Co., Ltd. (ChengDu, China) (CAS No.59865-13-3; >98% Assay), and the drug was dissolved in DMSO. Trizol reagent, reverse transcription kit and qPCR kit were purchased from Takara (DaLian, China) and Transgen Biotech (BeiJing, China) respectively. Superoxide dismutase (SOD), malondialdehyde (MDA) and reactive oxygen species (ROS) detection reagents were purchased from Nanjing Jiancheng Bioengineering Institute (Nanjing, China). IWR-1 was purchased from MedchemExpress (New Jersey,United States) (CAS: 1127442-82-3).

Experimental Animals

Tg(my17:GFP) and Tg(kdrl:mCherry) transgenic strains, and AB strains were purchased from China Zebrafish Resource Center. The zebrafish used were kept at 28°C, 14 h of light, and 10 h of dark under constant temperature conditions. The water for culturing the zebrafish had a pH of 7.0 and a conductivity of 500 μS/cm. The live brine shrimp were fed once at 9 a.m and 2 p.m daily. On the night before spawning, the male and female fish were placed in the mating tank at a ratio of 1:1, and the embryos the next day were collected. The collected embryos were cultured with 1% methyl blue for 10 h and abnormal and dead embryos were removed under the microscop. Healthy embryos at the same developmental stage were randomly assigned to six-well plates with 20 embryos per well. The embryos were cultured in a medium containing 0.003% PTU (Sigma, United States) to inhibit the growth of pigment.

Chemical Treatment

Healthy embryos at the same developmental stage were randomly assigned to six-well plates with 20 embryos per well. CsA was dissolved in DMSO. 5 ml of 0.003% PTU culture medium is added to each well, so that the final concentration of CsA is 5 mg/L, 10 mg/L, 15 mg/L. Zebrafish embryos were treated with CsA at concentration of 0, 5, 10 and 15 mg/L from 12 hpf to 72 hpf respectively, and cultured in an incubator at a constant temperature of 28°C. The control group was treated with DMSO only. CsA and PTU were replaced for 3 consecutive days, and the experiment was repeated three times.

The sensibility test of zebrafish embryos exposed to CsA at different stages of cardiac development was performed as previously described (Cao et al., 2020). Healthy zebrafish embryos were randomly distributed into a six-well plate, with

20 in each well. The final concentration of the CsA treatment group was 10 mg/L, 15 mg/L, and the control group was only treated with DMSO, and the time of first dosing include 0 hpf, 12 hpf, 15.5 hpf, 19 hpf, and 48 hpf, and the effects of zebrafish exposure to CsA on the morphology and function of the heart were observed at 72 hpf.

For resuced experiment, Tg (my17: GFP) was treated with 5 mg/L, 10 mg/L, 15 mg/L CsA and 0.18 mg/L astaxanthin from 12 hpf to 72 hpf, and placed in a incubator at 28°C. Drugs were changed daily. Larva were photographed with Leica M205FA. The CsA treatment group, PTU treatment group and 0.18 mg/L astaxanthin treatment group were taken as controls. Wnt signaling pathway was activated by 15 mg/L CsA and 10 nmol Wnt signaling pathway inhibitor. The 15 mg/L CsA treatment group, the PTU treatment group and the 10 nmol inhibitor treatment group were taken as controls. The results were photographed with Leica M205FA.

Quantification of Cardiac Morphology and Function

Heart morphology and function of zebrafish in each group were recorded and analyzed. The heart rate of zebrafish at 72 hpf was calculated. The heart morphology of zebrafish at 72 hpf was photographed under fluorescence and white light by Zeiss Discovery 20 microscope. The Zesis Discovery 20 system was used to calculate the pericardial area, yolk sac area, body length (length from head to tail) and the distance from cardiac venous sinus to cardiac artery bulb (SV-BA). Each group measured 15 pieces and repeated the experiment for 3 times.

mRNA Level Analysis

Zebrafish were treated with CsA for 72 h, 40 juveniles were taken from each group to extract total RNA, and 1 μg total RNA was used for reverse transcription (Takara). The cDNA obtained was used for qPCR experiments on the ABI Step One Plus RT-PCR system (Applied Biosystem, CA, United States), and the experiments were repeated for 3 times. The expression of cardiac related developmental genes (GATA4, Nkx2.5, vmhc, kl2a), apoptotic related genes (p53, mdm2, bax) and Wnt signaling pathway related genes (β-catenin, lef1, axin2) were analyzed, and $2^{-\triangle\triangle Ct}$ formula was used to calculate the results. Primers were obtained from Thermo Fisher.

Histological Analysis

Embryos treated with CsA for 72 h were collected, washed 3 times with PBS, fixed overnight in 4% PFA at 4°C, embedded in paraffin, and made into 7 um sections, which were dewaxed with xylene, dehydrated with alcohol, stained with hematoxylin and eosin, and finally sealed with neutral resin. The images of zebrafish heart section were observed and collected under light microscope.

Acridine Orange Staining

Acriridine orange (AO) is a nucleic acid dye with unique spectral properties, which can penetrate and specifically label apoptotic cells, and emit green fluorescence (Liu et al., 2021). Zebrafish embryos at 72 hpf were washed three times in embryo culture medium, treated with 4 mg/L AO and were incubated for 30 min in the dark. Then the embryo were washed three times with culture medium, anesthetized with 0.16% tricaine, and fixed in a confocal dish with 1% low solubility agarose. Images were collected using Zeiss Microscale (Discovery, V20). The experiment was repeated for 3 times.

Analysis of Indicators Related to Oxidative Stress

60 Juvenile zebrafish at 72 hpf were collected in each group, and washed by PBS for 3 times, 5 min each time. Total protein of each group was extracted with 0.9% normal saline, and oxidative stress indicators such as superoxide dismutase (SOD) and malondialdehyde (MDA) were detected. The absorbance was measured using the SpectraMax® iD3 Multi Mode. Embryos were stained with ROS in dark for 30 min at 72 h after drug treatment and pictures were taken using Zeiss Microscale (Discovery, V20).

Statistical Analysis

The control group and different experimental groups were statistically analyzed by one-way ANOVA and *t* test. All data were expressed as mean ± standard deviation, and $^{*}p < 0.05$, $^{**}p < 0.01$ and $^{***}p < 0.001$ indicated that the data were statistically significant. The F values and the df (degrees of freedom) are listed in **Table 1**.

RESULTS

Cyclosporine A Induced Cardiac Development Defects in Zebrafish

CsA is an immunosuppressant widely used in clinic. To study the toxic effects of CsA, zebrafish embryos were treated with different

TABLE 1 | The statistical data of F, degrees of freedom.

Fig	Descriptions	F Value	Df (degrees of freedom)
Figure 1	Pericardial area	259.4	59
	SV-BA distance	71.34	59
	Body length	21.67	55
	Yolk propotion	23.42	53
	Heart rate	257.6	55
Figure 2	Cardiac related developmental genes	2.751	35
Figure 3	Pericardial area at different time periods	76.550	175
	SV-BA distance at different time periods	73.805	174
Figure 4	Apoptotic related genes	36.979	26
Figure 5	SOD	143.9	11
	MDA	1017	11
Figure 6	Pericardial area	119	19
	SV-BA distance	76.5	19
	Body length	35.05	19
	Yolk propotion	16.52	19
	Heart rate	36.86	59
Figure 7	Wnt signal pathway related genes	8.608	35

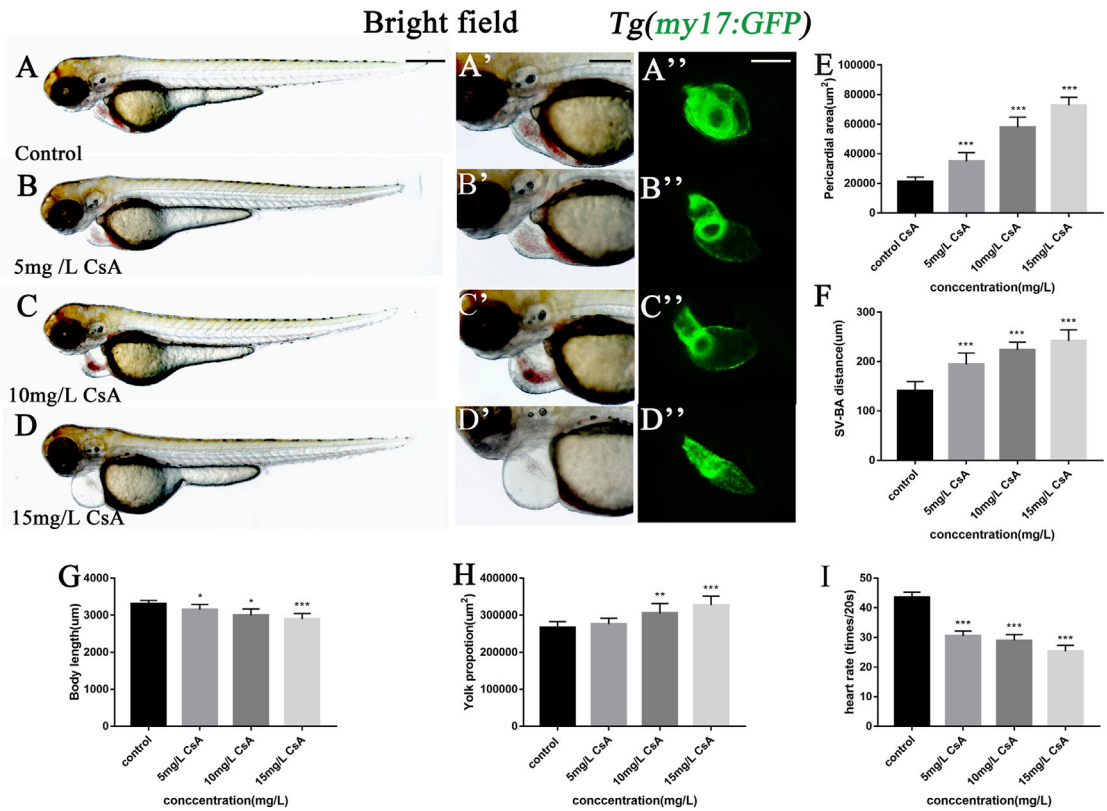

FIGURE 1 | Exposure to CsA induced cardiac developmental toxicity in zebrafish embryos. **(A-D)** Tg (my17: GFP) transgenic lines were exposed to 5 mg/L, 10 mg/L, and 15 mg/L CsA from 12 hpf to 72 hpf **(E)** The pericardial area of juvenile zebrafish at 72 hpf exposed to 5 mg/L, 10 mg/L, and 15 mg/L CsA. (n = 15. Compared with control: $^{*}p < 0.05$, $^{***}p < 0.001$, mean ± S. D). **(F)** The distance of SV-BA of juvenile zebrafish at 72 hpf exposed to 5 mg/L, 10 mg/L, and 15 mg/L CsA (n = 15. Compared with control:$^{***}p < 0.001$, mean ± S. D). SV: sinus vein; BA: artery bulb; scale: 100 mm. **(G)** The body lenth of juvenile zebrafish at 72 hpf exposed to 5 mg/L, 10 mg/L, and 15 mg/L CsA (n = 15. Compared with control: $^{***}p < 0.001$, mean ± S. D). **(H)** Yolk sac area of zebrafish embryos at 72 hpf exposed to 5 mg/L, 10 mg/L, and 15 mg/L CsA (n = 15. Compared with control: $^{*}p < 0.05$, mean ± S. D) **(I)** The heart rate of juvenile zebrafish at 72 hpf exposed to 5 mg/L, 10 mg/L, and 15 mg/L CsA (n = 15. Compared with control:$^{***}p < 0.001$, mean ± SD).Scale bars:500 μm **(A-D)**, 100 μm **(A-D)**.

concentrations of CsA, and the heart rate, body length, yolk sac area and pericardium area of zebrafish at 72 hpf were recorded. It was found that compared with the control group (3,309 ± 92.85), embryonic body length was significantly shorter in 5 mg/L (3,153 ± 142.8,$p < 0.001$), 10 mg/L (2,998 ± 172,$p < 0.001$) and 15 mg/L (2,899 ± 146.7, $p < 0.001$) groups (**Figures 1A–D,G**)and blood stasis appeared in the yolk sac (**Figure 1A-D**). Compared with the control group, 10 mg/L and 15 mg/L groups have obvious absorption delays (**Figure 1H**). Heart rate was significantly lower than that of the control group, especially the 15 mg/L (25.36 ± 1.985, $p < 0.001$) group (**Figure 1I**). Pericardial edema worsened and was most significant at 10 mg/L (21184 ± 3,102, $p < 0.001$) and 15 mg/L (72680 ± 5,518, $p < 0.001$) (**Figure 1A-D,E**). The phenotypes induced by cyclosporin A including shorter body lengths, decreased heart rate, delayed absorption of yolk sac, and pericardial edema, showed obvious concentration dependence. It is worth noting that, compared with the control group, with the increase of CsA concentration, the atria and ventricles of zebrafish gradually separated, and the SV-AV distance gradually increased (**Figure 1A-D,F**). 5 mg/L (194.4 ± 23.05, $p < 0.001$), 10 mg/L (223.8 ± 15.86, $p < 0.001$) and 15 mg/L (241.8 ± 22.56, $p < 0.001$) have significant differences compared with the control group (140.8 ± 18.62).

The results of hematoxylin-eosin (HE) staining showed the toxic effects of CsA on cardiac development at the histological level (**Figure 2A-D**). In addition, the mRNA expressions of GATA4, Nkx2.5, vmhc and klf2a related to cardiac development were disturbed after CsA treatment (**Figure 2E**). We exposed the Tg(kdrl:mCherry) and Tg(my17:GFP) double-transgenic zebrafish embryos to 15 mg/L CsA and found that the cardiomyocytes in the drug treated group were significantly separated from the endocardia compared with the control group (**Figure 2F**). These results indicated that CsA had toxic effects on the heart development of zebrafish embryos.

Cyclosporine A Initiated Cardiac Dysplasia During Precardiac Mesoderm Formation

To further investigate the role of CsA in heart development, zebrafish embryos treated with 10 mg/L and 15 mg/L in different time periods, and found that at 0 hpf, there was almost no cardiac

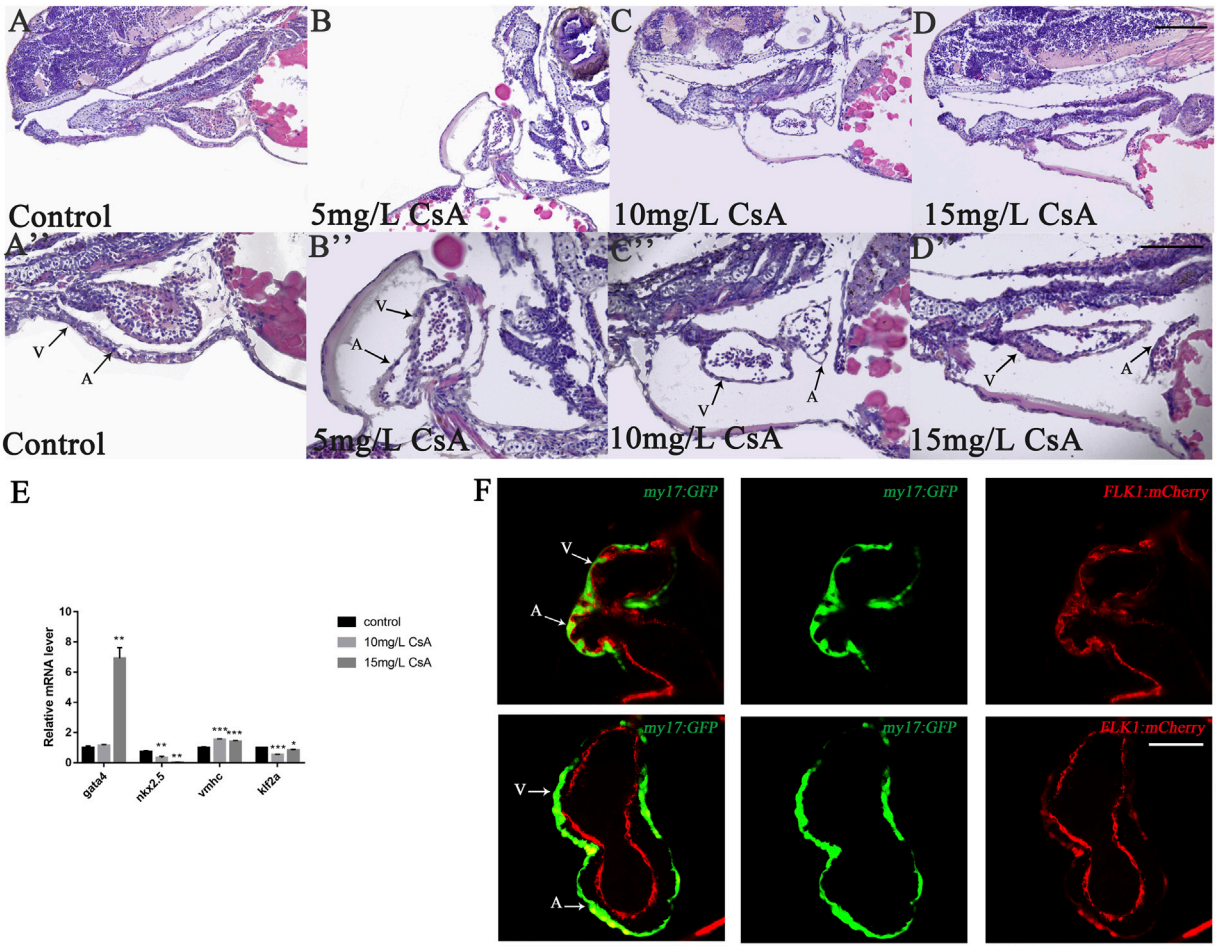

FIGURE 2 | CsA exposure induced cardiac development defects. **(A-D)** HE staining of heart of zebrafish at 72 hpf exposed to 5 mg/L, 10 mg/L, and 15 mg/L CsA. Magnification: ×200 (top), ×400 (bottom); the black arrows indicated the atria and ventricles; A: atria and V: ventricles **(E)** The mRNA levels of heart-related genes in the control group and the 15 mg/L CsA exposure group (Compared with control: $^{*}p < 0.05$, $^{**}p < 0.01$, $^{***}p < 0.001$, mean ± S. D). **(F)** Confocal images of the cardiac region of the dual transgenic lines Tg (my17: GFP) and Tg (flk1: mCherry) in the control and treatment groups. 50 μm **(A-D)**, 25 μm **(A-D)**, 50 μm **(F)**.

injury in embryos (**Figure 3A**), while at 12 hpf, zebrafish treated with 15 mg/L CsA showed pericardial edema (**Figure 3B**). However, the heart injury was less severe than at other time periods. In addition, the pericardial edema increased gradually with the prolongation of treatment time, and the distance between the venous sinus and the bulb of artery also increased gradually (**Figures 3A–G**). These results suggested that CsA might initiate cardiac dysplasia during precardiac mesodermal formation (12 hpf).

Cyclosporine A Induced Apoptosis of Embryonic Cardiomyocytes in Zebrafish

To study whether CsA induced cardiac development defects by inducing apoptosis of cardiomyocytes, we collected juvenile zebrafish treated with CsA for 72 h and stained them with AO to detect the expression of apoptosis related genes. The results showed that the number of apoptotic cardiomyocytes (green label) increased with increasing drug exposure concentration (**Figures 4A–D**). qPCR results showed that after CsA treatment, pro-apoptotic gene bax, p53 and mdm2 were significantly up-regulated compared with the control group (**Figure 4E**). These results suggested that CsA induced apoptosis of zebrafish cardiomyocytes.

The Oxidative Stress Response Induced by Cyclosporine A Was Concentrated in the Heart Region

Oxidative stress plays an important role in physiological and pathological changes of all aerobic organisms (Li et al., 2016). To study the mechanism of CsA induced cardiotoxicity in zebrafish, oxidative stress level after CsA treatment was reflected by detecting ROS and MDA content, and SOD activity. The results of ROS staining showed that oxidative stress response accumulated in the heart and head of zebrafish, and the fluorescence intensity of ROS staining gradually increased with the increase of CsA concentration (**Figure 5A-D**). SOD activity

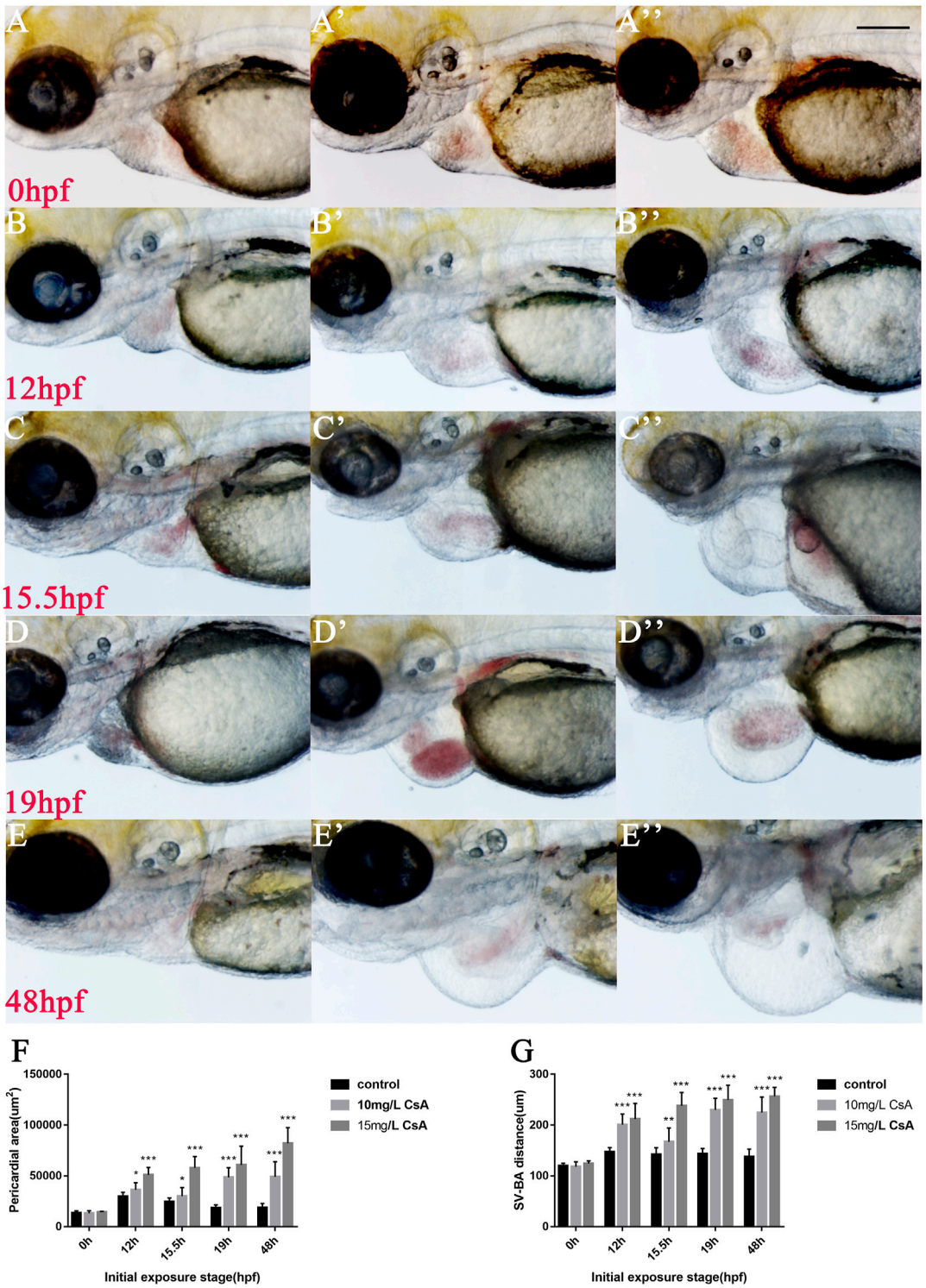

FIGURE 3 | Cardiac developmental defects in zebrafish embryos induced by CsA exposure at different time periods. **(A-E)** The images of cardiac development in zebrafish embryos at 0, 12, 15.5, 19 and 48 hpf exposed to 10 mg/L and 15 mg/L CsA. **(F)** Statistical chart of pericardial area of zebrafish embryos at 0, 12, 15.5, 19 and 48 hpf exposed to CsA (Compared with control: $^{**}p < 0.01$, $^{***}p < 0.001$, mean ± S. D) **(G)** Statistical chart of the distance of SV-BA of juvenile zebrafish at 0, 12, 15.5, 19 and 48 hpf exposed to CsA (Compared with control: $^{**}p < 0.01$, $^{***}p < 0.001$, mean ± S. D). Scale bars:100 μm **(A-E)**.

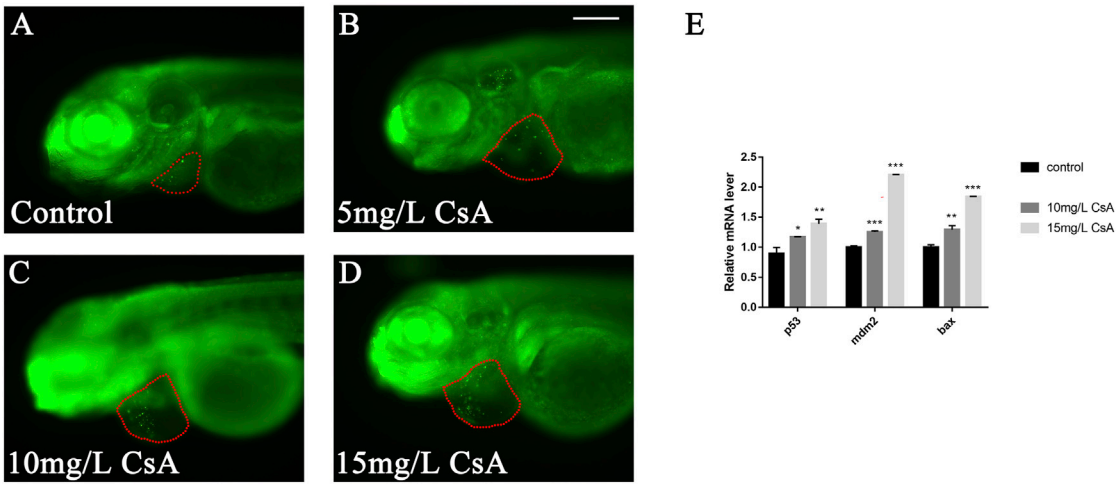

FIGURE 4 | CsA-induced apoptosis of zebrafish cardiomyocytes. **(A-D)** AO staining of heart of zebrafish embryos at 72 hpf exposed to 5 mg/L, 10 mg/L, and 15 mg/L CsA. The red dotted line indicated the heart area, and the green fluorescent dots indicated apoptotic cells. **(E)** mRNA levels of apoptotic and anti-apoptotic genes in control group and 10 mg/L CsA treated group (Compared with control: $^{*}p < 0.05$, $^{**}p < 0.01$, $^{***}p < 0.001$, mean ± S. D). Scale bars: 100 μm **(A-D)**.

test showed that compared to control group (5.204 ± 0.043), SOD activity in 5 mg/L (3.713 ± 0.191,$p < 0.01$), 10 mg/L (4.136 ± 0.023, $p < 0.001$) and 15 mg/L (3.041 ± 0.173, $p < 0.01$) significantly decreased. MDA content in 5 mg/L (0.747 ± 0.015,$p < 0.001$), 10 mg/L (1.135 ± 0.014, $p < 0.001$) and 15 mg/L (0.717 ± 0.036, $p < 0.001$) was significantly up-regulated compared to control group (0.056 ± 0.025, $p < 0.001$) (**Figures 5E,F**). The results of SOD and MDA were also consistent with the results of ROS staining (**Figure 5A-D**). Then we used astaxanthin (ATX) (an antioxidant) to rescue CsA-induced cardiotoxicity in zebrafish. Compared with the control group and the zebrafish without astaxanthin treatment, the heart rates of astaxanthin rescued group (31.27 ± 2.52, $p > 0.05$) have little difference from that of the control group (32.67 ± 1.915) (**Figure 6J**), and the pericardial edema was significantly reduced (**Figure 6A-D,F**). The dose-response curve showed that astaxanthin could effectively reduce pericardial edema in zebrafish (**Figure 6K**). The SV-AV distance had little difference between rescued group (150.3 ± 8.277,$p > 0.05$) and control group (143.5 ± 9.972,$p > 0.05$) and the symptoms of atrial and ventricular separation were reduced (**Figure 6G**). And the fluorescence intensity of ROS staining decreased significantly (**Figure 6E**). Therefore, it could be inferred that oxidative stress played a role in CsA induced cardiac dysplasia.

Cyclosporine A Induced Abnormal Heart Development in Zebrafish by Up-Regulating Wnt Signaling

The up-regulated expression of Wnt signaling can be observed in many cardiovascular diseases, and Wnt signal plays an important role in many cardiovascular pathological changes (Foulquier et al., 2018). To investigate whether Wnt signaling is involved in CsA induced cardiac dysplasia, we detected the expression of Wnt signaling-associated genes β-catenin, lef1 and axin2, and the results showed that the expression of these three genes was significantly up-regulated after CsA treatment, especially β-catenin (**Figure 7A**). This suggested that the abnormal cardiac development induced by CsA might be related to Wnt signaling. To further verify this result, we treated zebrafish with IWR-1, a Wnt signaling inhibitor, and CsA. At 72 hpf, IWR-1 significantly rescued CsA-induced cardiac dysplasia compared with the zebrafish treated without IWR-1 (**Figure 7B-C**). The results of ROS staining in IWR-1 rescued group were not significantly different from those in 15 mg/L CsA-treated group (**Figures 7D,E**), suggesting that CsA-induced cardiac developmental toxicity in zebrafish might be caused by the combination of up-regulation of oxidative stress level and up-regulation of Wnt signaling in zebrafish heart.

DISCUSSION

Recently, zebrafish has been widely used in environmental toxicology, pathological toxicology and embryonic developmental toxicology. Many studies have confirmed that zebrafish larva have the transparency to directly evaluate drug toxicity *in vivo*, and the toxicity characteristics are similar to those of mammals, such as hepatotoxicity, cardiotoxicity and neurotoxicity (Cao et al., 2020; Wang et al., 2020; Xiong et al., 2020). CsA is an immunosuppressant widely used clinically and is also accompanied by a series of side effects such as liver toxicity, neurotoxicity and vascular toxicity. However, little is known about its effects on embryonic development Therefore, we used zebrafish to evaluate CsA toxic effects and the related mechanisms. The results showed that CsA could induce developmental toxicity and cardiotoxicity in

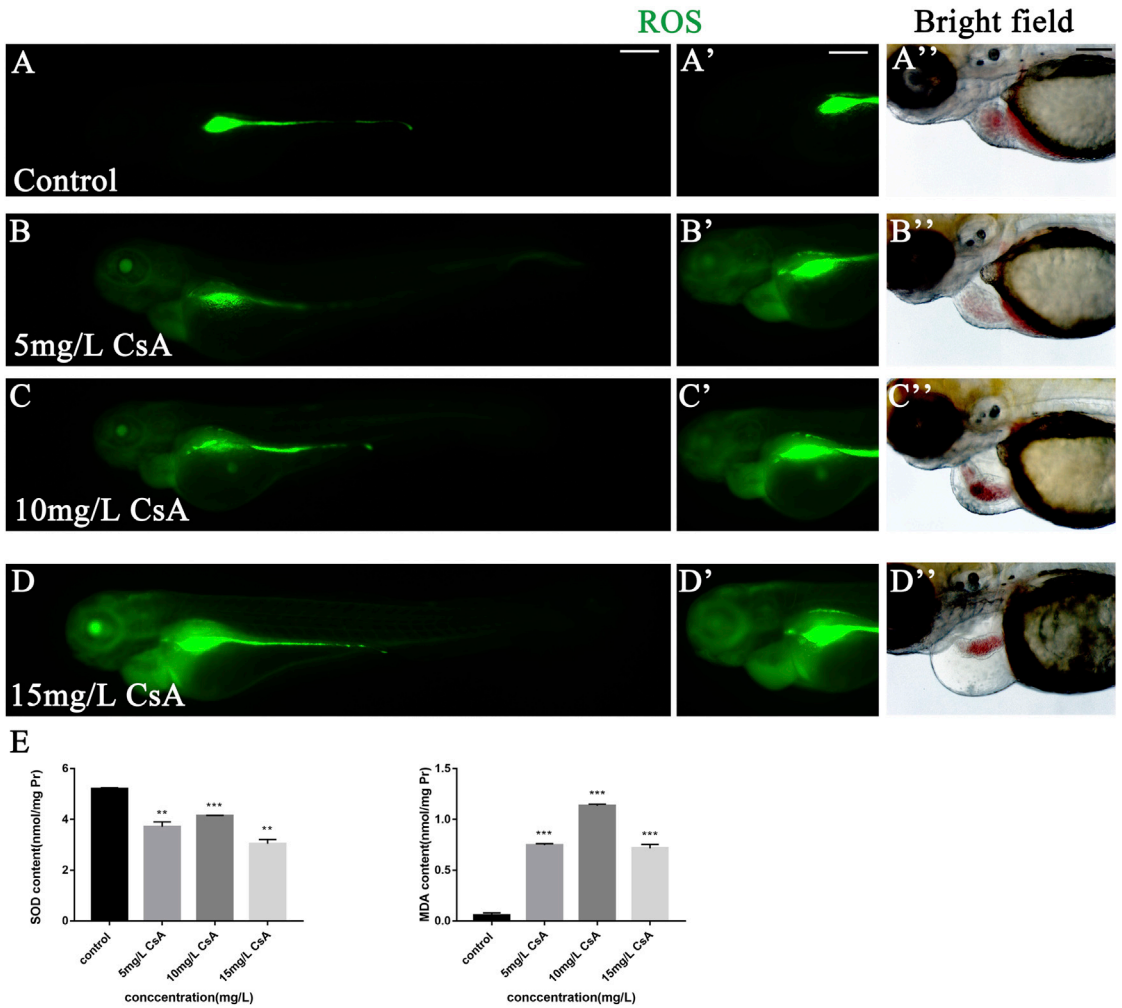

FIGURE 5 | The accumulation of oxidative stress in zebrafish induced by CsA. **(A-D)** ROS staining of heart of zebrafish embryos at 72 hpf exposed to 5 mg/L, 10 mg/L, and 15 mg/L CsA. The ROS staining was green. **(E)** The SOD activity and MDA content of zebrafish at 72 hpf exposed to 5 mg/L, 10 mg/L, and 15 mg/L CsA (Compared with control: $^{**}p < 0.01$, $^{***}p < 0.001$, mean ± S. D). Scale bars:100 μm **(A-D)**.

zebrafish larvae. Further studies suggested that generation of ROS and activation of wnt signaling pathway might be the underlying mechanism of cardiotoxicity induced by CsA. However, an important question about the human relevance of the concentrations used in the zebrafish assay still need to be investigated.

To study the underlying mechanism of cardiac developmental toxicity induced by CsA, expression levels of genes correlated with cardiac development, and apoptosis were detected by qPCR. GATA4 is one of the earliest developing transcription factors during heart development, and its up-regulated expression can promote the differentiation of embryonic stem cells into heart (Grepin et al., 1997). Nkx2.5 regulates cardiac tube elongation and has different effects on the number of ventricular and atrial cells (Targoff et al., 2008). Gata4 and NKX2.5 play an important role in the differentiation, maturation and homeostasis of cardiomyocytes. The deficiency of Gata4 leads to failure of heart tube formation in mice, and the targeted destruction of Nkx2.5 leads to abnormal heart morphology (Schlesinger et al., 2011). Activation of the both is essential in stretch-induced cardiomyocyte hypertrophy (Valimaki et al., 2017). Klf2a is a major endocardial blood flow response gene, and its expression enables endocardial cells (EDCs) to coupling mechanical transduction to valve morphology by activating a series of downstream target genes (Steed et al., 2016). Ventricular myosin heavy chain (Vmhc), expressed primarily in the ventricle, can be used to distinguish between two types of cardiac precursors at an early stage before the formation of cardiac catheters (Yelon et al., 1999). Our results showed that CsA treatment led to disruption in the expression of the above heart-related transcriptional genes and upregulation of apoptotic gene bax, p53 and mdm2.

Oxidative stress is one of reasons for toxicity caused by drug. The imbalance between the production of ROS and the

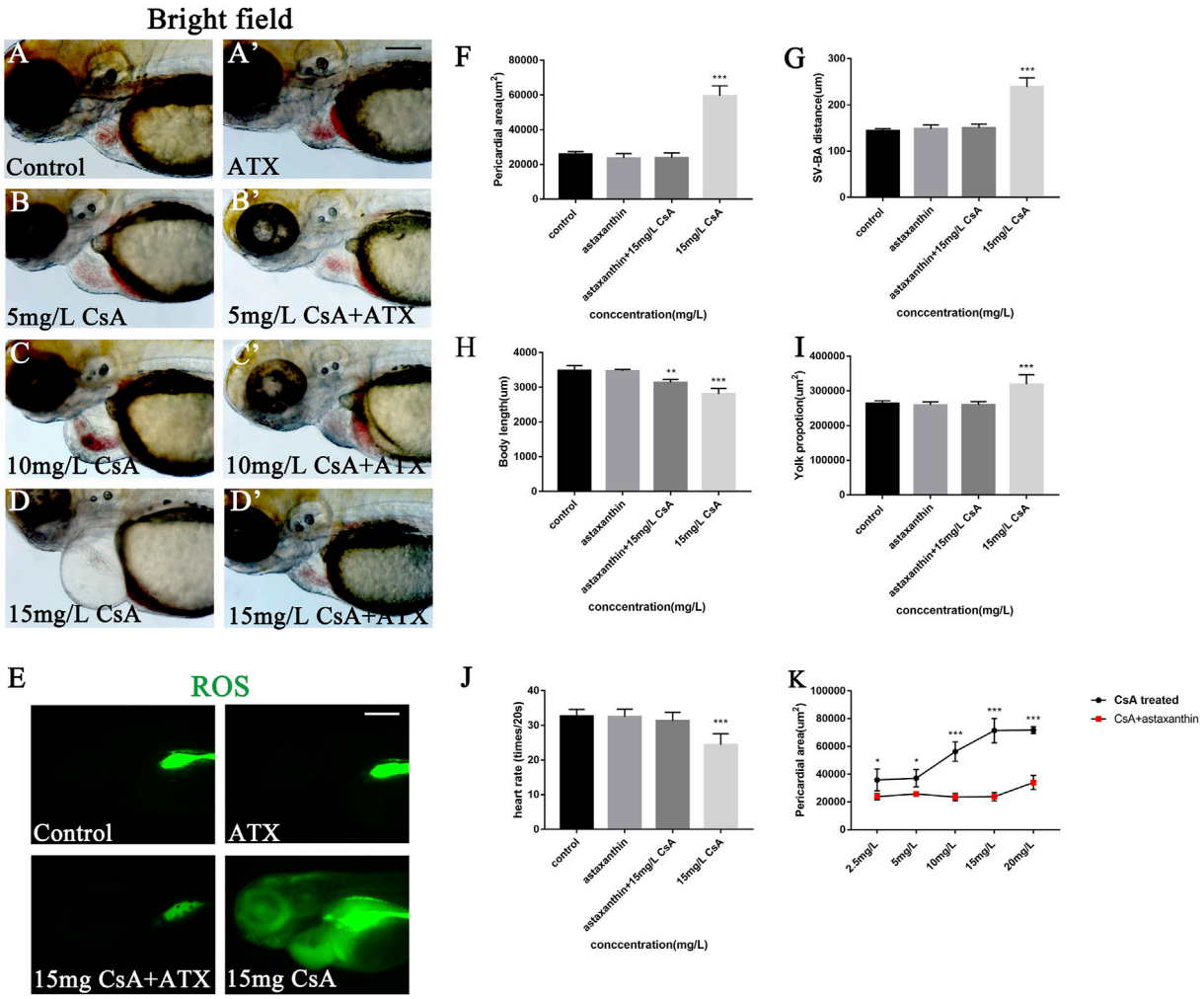

FIGURE 6 | ATX rescued the cardiac developmental toxicity induced by CsA. **(A-D)** ATX rescued cardiac defects in 72 hpf zebrafish exposed to CsA at 5 mg/L, 10 mg/L, 15 mg/L. **(E)** ATX rescued ROS staining of 72 hpf zebrafish exposed to CsA. **(F)** ATX relived pericardial area of 72 hpf zebrafish exposed to CsA (n = 15. Compared with control: $^{*}p < 0.05$, $^{***}p < 0.001$, mean ± S. D). **(G)** ATX rescued the distance of SV-BA of 72 hpf zebrafish exposed to CsA (n = 15. Compared with control: $^{***}p < 0.001$, mean ± S. D). SV: sinus vein; BA: artery bulb; scale: 100 mm **(H)** ATX rescued the body length of 72 hpf zebrafish exposed to CsA (n = 15. Compared with control: $^{***}p < 0.001$, mean ± S. D). **(I)** ATX rescued yolk sac area of 72 hpf zebrafish exposed to CsA (n = 15. Compared with control: $^{*}p < 0.05$, mean ± S. D). **(J)** ATX rescued the heart rate of 72 hpf zebrafish exposed to CsA (n = 15. Compared with control: $^{***}p < 0.001$, mean ± S. D). **(K)** dose-response curve. Scale bars:100 μm **(A-H)**.

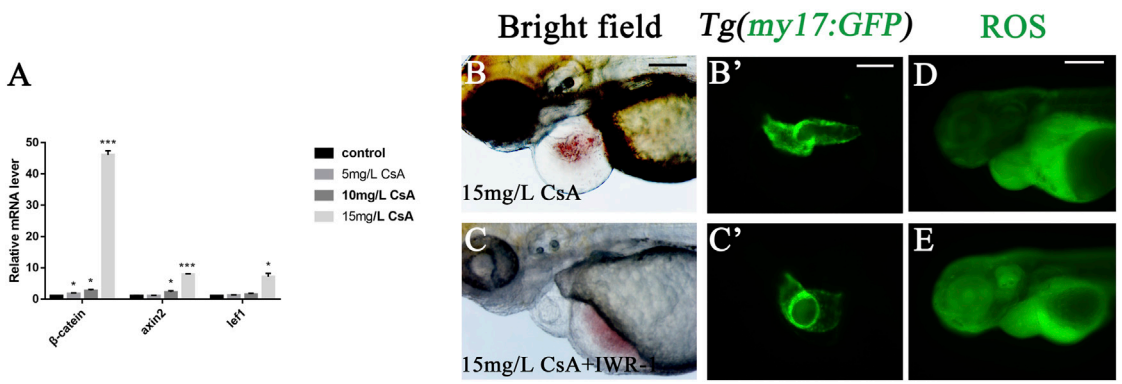

FIGURE 7 | IWR-1 rescued cardiac development defects induced by CsA exposure. **(A)** The up-regulation of β-catenin, lef1 and axin2 in the heart of 72 hpf zebrafish exposed to 15 mg/L CsA (Compared with control:$^{*}p < 0.05$, $^{**}p < 0.01$, mean ± SD). **(B-C)** IWR-1 rescued heart defects in 72 hpf zebrafish exposed to CsA at 15 mg/L. **(D-E)** IWR-1 rescued ROS staining in 72 hpf zebrafish exposed to CsA at 15 mg/L. Scale bars:100 μm (**B-E**).

endogenous antioxidant defense system results in oxidative stress (van der Pol et al., 2019). Malondialdehyde (MDA) and superoxide dismutase (SOD) are important indicators of oxidative stress. MDA is a product of the peroxidation of polyunsaturated fatty acids, which can interact with DNA and proteins to induce mutations or atherosclerosis (Del Rio et al., 2005). SOD is an ubiquitous antioxidant enzyme that catalyzes the conversion of superoxide hydrogen ion radical (O2-) to hydrogen peroxide (H2O2) (Sakamoto and Imai, 2017). Excessive accumulation of ROS can lead to a variety of cardiovascular diseases, such as endothelial dysfunction and, atherosclerosis (Victor et al., 2009; Chistiakov et al., 2018), and it has been shown that the accumulation of ROS has a toxic effect on the heart development of zebrafish (Cao et al., 2020; Meng et al., 2020). Our experimental results showed that with the increase of CsA concentration, the accumulation of ROS in the pericardium of juvenile zebrafish gradually increased and SOD activity gradually decreased, while MDA content significantly increased. This suggested that CsA caused oxidative stress accumination in zebrafish. Astaxanthin (ATX) is a kind of lutein carotenoid with strong antioxidant, anti-inflammatory and anti-apoptotic activities (Brotosudarmo et al., 2020). Studies by Cun Dong Fan and his colleagues have shown that ATX can improve heart defects by eliminating reactive oxygen species (ROS) and inhibiting oxidative damage to inhibit homocysteine (Hcy)–induced cardiotoxicity (Fan et al., 2017). Here, ATX was used to interfere with CsA induced zebrafish cardiotoxicity, and the results showed that ATX had a significant inhibitory effect on CsA-induced cardiotoxicity, and the ROS level in ATX group was significantly decreased. This provided further evidence that the cardiotoxicity of CsA to zebrafish might be caused by oxidative stress.

Wnt signaling is a secreted glycoprotein that regulates cell proliferation, survival, and behavior in both vertebrates and invertebrates. Wnt/β-catenin is the most studied signaling pathway. In the absence of Wnt signaling, β-catenin is phosphorylated or degraded in the cytoplasm. When Wnt signaling is activated, β-catenin accumulates in the nucleus (Moon, 2005). The Wnt/β-catenin signaling pathway is involved in the formation of the right ventricle in zebrafish and plays an important role in the proliferation and regeneration of mature cardiomyocytes (Fan et al., 2018). Therefore, the expression of Wnt signaling-associated genes β-catenin, lef1 and axin2 was detected, and the results showed that the expression of these three genes was significantly up-regulated after CsA treatment, especially β-catenin. Wnt signal inhibitor IWR-1 could alleviate the heart defects caused by CsA, but there was no significant difference in ROS staining between the IWR-1 rescue group and the CsA-exposed group only. This suggested that zebrafish heart malformation might be induced by both the up-regulation of ROS and the activation of Wnt signaling. In conclusion, CsA can induce cardiac developmental toxicity in zebrafish larvae. Our results show that CsA exposure caused pericardial edema, body length shortened, and yolk sac absorption delayed. Moreover, CsA induced generation of ROS and apoptosis of cardiomyocytes, and activated Wnt signaling. These results indicate that CsA may induce zebrafish cardiotoxicity by generation of oxidative stress (ROS) and activation of Wnt signaling. Our findings will be helpful to understanding CsA-induced caidiac developmental toxicity and the underlying mechanism, and provide reference for new treatment and prevention methods for the side effects of clinical use of CsA and new evidence of the influence of CsA exposure on aquatic organisms.

DATA AVAILABILITY STATEMENT

The original contributions presented in the study are included in the article/Supplementary Material, further inquiries can be directed to the corresponding authors.

ETHICS STATEMENT

The animal study was reviewed and approved by Institutional Animal Care and Use Committee protocols from Jinggangshan University.

AUTHOR CONTRIBUTIONS

ZC, MW, QT, and JX designed experiment; MW and ZC. wrote the manuscript; MW. performed all of experiments; HL, JL, FL, HN, GX, XJ, HL, JX, QT, and ZC analyzed data.

FUNDING

This work was supported by the National Natural Science Foundation (81860282, 31900597), Natural Science Foundation Project of Jiangxi Province (20192ACB21013) and Jiangxi Province's major academic and technical leaders training plan for young talents (20204BCJL23043).

REFERENCES

Bakkers, J. (2011). Zebrafish as a Model to Study Cardiac Development and Human Cardiac Disease. *Cardiovasc. Res.* 91 (2), 279–288. doi:10.1093/cvr/cvr098

Bambino, K., and Chu, J. (2017). Zebrafish in Toxicology and Environmental Health. *Curr. Top. Dev. Biol.* 124, 331–367. doi:10.1016/bs.ctdb.2016.10.007

Beauchesne, P. R., Chung, N. S., and Wasan, K. M. (2007). Cyclosporine A: a Review of Current Oral and Intravenous Delivery Systems. *Drug Dev. Ind. Pharm.* 33 (3), 211–220. doi:10.1080/03639040601155665

Brotosudarmo, T. H. P., Limantara, L., Setiyono, E., and Heriyanto, D. S. (2020). Structures of Astaxanthin and Their Consequences for Therapeutic Application. *Int. J. Food Sci.* 2020, 2156582. doi:10.1155/2020/2156582

Cao, Z., Huang, Y., Xiao, J., Cao, H., Peng, Y., Chen, Z., et al. (2020). Exposure to Diclofop-Methyl Induces Cardiac Developmental Toxicity in Zebrafish Embryos. *Environ. Pollut.* 259, 113926. doi:10.1016/j.envpol.2020.113926

Chistiakov, D. A., Shkurat, T. P., Melnichenko, A. A., Grechko, A. V., and Orekhov, A. N. (2018). The Role of Mitochondrial Dysfunction in Cardiovascular Disease: a Brief Review. *Ann. Med.* 50 (2), 121–127. doi:10.1080/07853890.2017.1417631

Damiano, S., Ciarcia, R., Montagnaro, S., Pagnini, U., Garofano, T., Capasso, G., et al. (2015). Prevention of Nephrotoxicity Induced by Cyclosporine-A: Role of Antioxidants. *J. Cel Biochem* 116 (3), 364–369. doi:10.1002/jcb.25022

Del Rio, D., Stewart, A. J., and Pellegrini, N. (2005). A Review of Recent Studies on Malondialdehyde as Toxic Molecule and Biological Marker of Oxidative Stress. *Nutr. Metab. Cardiovasc. Dis.* 15 (4), 316–328. doi:10.1016/j.numecd.2005.05.003

Fan, C. D., Sun, J. Y., Fu, X. T., Hou, Y. J., Li, Y., Yang, M. F., et al. (2017). Astaxanthin Attenuates Homocysteine-Induced Cardiotoxicity *In Vitro* and *In Vivo* by Inhibiting Mitochondrial Dysfunction and Oxidative Damage. *Front. Physiol.* 8, 1041. doi:10.3389/fphys.2017.01041

Fan, Y., Ho, B. X., Pang, J. K. S., Pek, N. M. Q., Hor, J. H., Ng, S. Y., et al. (2018). Wnt/β-Catenin-Mediated Signaling Re-Activates Proliferation of Matured Cardiomyocytes. *Stem Cel Res Ther* 9 (1), 338. doi:10.1186/s13287-018-1086-8

Foulquier, S., Daskalopoulos, E. P., Lluri, G., Hermans, K. C. M., Deb, A., and Blankesteijn, W. M. (2018). WNT Signaling in Cardiac and Vascular Disease. *Pharmacol. Rev.* 70 (1), 68–141. doi:10.1124/pr.117.013896

Grépin, C., Nemer, G., and Nemer, M. (1997). Enhanced Cardiogenesis in Embryonic Stem Cells Overexpressing the GATA-4 Transcription Factor. *Development* 124 (12), 2387–2395. doi:10.1242/dev.124.12.2387

Hausenloy, D. J., Boston-Griffiths, E. A., and Yellon, D. M. (2012). Cyclosporin A and Cardioprotection: From Investigative Tool to Therapeutic Agent. *Br. J. Pharmacol.* 165 (5), 1235–1245. doi:10.1111/j.1476-5381.2011.01700.x

Horzmann, K. A., and Freeman, J. L. (2018). Making Waves: New Developments in Toxicology with the Zebrafish. *Toxicol. Sci.* 163 (1), 5–12. doi:10.1093/toxsci/kfy044

Howe, K., Clark, M. D., Torroja, C. F., Torrance, J., Berthelot, C., Muffato, M., et al. (2013). The Zebrafish Reference Genome Sequence and its Relationship to the Human Genome. *Nature* 496 (7446), 498–503. doi:10.1038/nature12111

Kim, H. J., Yoo, J. H., Choi, Y., Joo, J. Y., Lee, J. Y., and Kim, H. J. (2020). Assessing the Effects of Cyclosporine A on the Osteoblastogenesis, Osteoclastogenesis, and Angiogenesis Mediated by Human Periodontal Ligament Stem Cells. *J. Periodontol.* 91 (6), 836–848. doi:10.1002/JPER.19-0168

Li, R., Jia, Z., and Trush, M. A. (2016). Defining ROS in Biology and Medicine. *React. Oxyg Species (Apex)* 1 (1), 9–21. doi:10.20455/ros.2016.803

Liu, J., Chen, D., Liu, X., and Liu, Z. (2017). Cyclosporine A Attenuates Cardiac Dysfunction Induced by Sepsis via Inhibiting Calcineurin and Activating AMPK Signaling. *Mol. Med. Rep.* 15 (6), 3739–3746. doi:10.3892/mmr.2017.6421

Liu, L., Wu, F. Y., Zhu, C. Y., Zou, H. Y., Kong, R. Q., Ma, Y. K., et al. (2021). Involvement of Dopamine Signaling Pathway in Neurodevelopmental Toxicity Induced by Isoniazid in Zebrafish. *Chemosphere* 265, 129109. doi:10.1016/j.chemosphere.2020.129109

Matsuda, S., and Koyasu, S. (2000). Mechanisms of Action of Cyclosporine. *Immunopharmacology* 47 (2-3), 119–125. doi:10.1016/s0162-3109(00)00192-2

Meng, Y., Zhong, K., Xiao, J., Huang, Y., Wei, Y., Tang, L., et al. (2020). Exposure to Pyrimethanil Induces Developmental Toxicity and Cardiotoxicity in Zebrafish. *Chemosphere* 255, 126889. doi:10.1016/j.chemosphere.2020.126889

Moon, R. T. (2005). Wnt/Beta-Catenin Pathway. *Sci. STKE* 2005 (271), cm1. doi:10.1126/stke.2712005cm1

Nacev, B. A., Low, W. K., Huang, Z., Su, T. T., Su, Z., Alkuraya, H., et al. (2011). A Calcineurin-Independent Mechanism of Angiogenesis Inhibition by a Nonimmunosuppressive Cyclosporin A Analog. *J. Pharmacol. Exp. Ther.* 338 (2), 466–475. doi:10.1124/jpet.111.180851

Ozkan, G., Ulusoy, S., Alkanat, M., Orem, A., Akcan, B., Ersöz, S., et al. (2012). Antiapoptotic and Antioxidant Effects of GSPE in Preventing Cyclosporine A-Induced Cardiotoxicity. *Ren. Fail.* 34 (4), 460–466. doi:10.3109/0886022X.2012.656563

Sakamoto, T., and Imai, H. (2017). Hydrogen Peroxide Produced by Superoxide Dismutase SOD-2 Activates Sperm in *Caenorhabditis E. J. Biol. Chem.* 292 (36), 14804–14813. doi:10.1074/jbc.M117.788901

Sarmah, S., and Marrs, J. A. (2016). Zebrafish as a Vertebrate Model System to Evaluate Effects of Environmental Toxicants on Cardiac Development and Function. *Int. J. Mol. Sci.* 17 (12), 2123. doi:10.3390/ijms17122123

Schlesinger, J., Schueler, M., Grunert, M., Fischer, J. J., Zhang, Q., Krueger, T., et al. (2011). The Cardiac Transcription Network Modulated by Gata4, Mef2a, Nkx2.5, Srf, Histone Modifications, and microRNAs. *Plos Genet.* 7 (2), e1001313. doi:10.1371/journal.pgen.1001313

Stainier, D. Y. (2001). Zebrafish Genetics and Vertebrate Heart Formation. *Nat. Rev. Genet.* 2 (1), 39–48. doi:10.1038/35047564

Steed, E., Faggianelli, N., Roth, S., Ramspacher, C., Concordet, J. P., and Vermot, J. (2016). klf2a Couples Mechanotransduction and Zebrafish Valve Morphogenesis through Fibronectin Synthesis. *Nat. Commun.* 7, 11646. doi:10.1038/ncomms11646

Targoff, K. L., Schell, T., and Yelon, D. (2008). Nkx Genes Regulate Heart Tube Extension and Exert Differential Effects on Ventricular and Atrial Cell Number. *Dev. Biol.* 322 (2), 314–321. doi:10.1016/j.ydbio.2008.07.037

Thomas, S. E., and Gordon, D. S. (1986). Cyclosporine. *South. Med. J.* 79 (2), 205–214. doi:10.1097/00007611-198602000-00017

Välimäki, M. J., Tölli, M. A., Kinnunen, S. M., Aro, J., Serpi, R., Pohjolainen, L., et al. (2017). Discovery of Small Molecules Targeting the Synergy of Cardiac Transcription Factors GATA4 and NKX2-5. *J. Med. Chem.* 60 (18), 7781–7798. doi:10.1021/acs.jmedchem.7b00816

van der Pol, A., van Gilst, W. H., Voors, A. A., and van der Meer, P. (2019). Treating Oxidative Stress in Heart Failure: Past, Present and Future. *Eur. J. Heart Fail.* 21 (4), 425–435. doi:10.1002/ejhf.1320

Victor, V. M., Apostolova, N., Herance, R., Hernandez-Mijares, A., and Rocha, M. (2009). Oxidative Stress and Mitochondrial Dysfunction in Atherosclerosis: Mitochondria-Targeted Antioxidants as Potential Therapy. *Curr. Med. Chem.* 16 (35), 4654–4667. doi:10.2174/092986709789878265

Wang, H., Meng, Z., Liu, F., Zhou, L., Su, M., Meng, Y., et al. (2020). Characterization of Boscalid-Induced Oxidative Stress and Neurodevelopmental Toxicity in Zebrafish Embryos. *Chemosphere* 238, 124753. doi:10.1016/j.chemosphere.2019.124753

Woywodt, A., Schroeder, M., Mengel, M., Schwarz, A., Gwinner, W., Haller, H., et al. (2003). Circulating Endothelial Cells Are a Novel Marker of Cyclosporine-Induced Endothelial Damage. *Hypertension* 41 (3 Pt 2), 720–723. doi:10.1161/01.HYP.0000052948.64125.AB

Wu, R., Chen, H., Chang, N., Xu, Y., Jiao, J., and Zhang, H. (2020). Unlocking the Drug Potential of the Bryostatin Family: Recent Advances in Product Synthesis and Biomedical Applications. *Chemistry* 26 (6), 1166–1195. doi:10.1002/chem.201903128

Xiong, G., Deng, Y., Liao, X., Zhang, J., Cheng, B., Cao, Z., et al. (2020). Graphene Oxide Nanoparticles Induce Hepatic Dysfunction through the Regulation of Innate Immune Signaling in Zebrafish (*Danio R*). *Nanotoxicology* 14 (5), 667–682. doi:10.1080/17435390.2020.1735552

Yelon, D., Horne, S. A., and Stainier, D. Y. (1999). Restricted Expression of Cardiac Myosin Genes Reveals Regulated Aspects of Heart Tube Assembly in Zebrafish. *Dev. Biol.* 214 (1), 23–37. doi:10.1006/dbio.1999.9406

Conflict of Interest: The authors declare that the research was conducted in the absence of any commercial or financial relationships that could be construed as a potential conflict of interest.

frontiers in Pharmacology

ORIGINAL RESEARCH
published: 22 November 2021
doi: 10.3389/fphar.2021.770319

A Zebrafish Model of Neurotoxicity by Binge-Like Methamphetamine Exposure

*Juliette Bedrossiantz[1], Marina Bellot[2], Pol Dominguez-García[2], Melissa Faria[1], Eva Prats[3], Cristian Gómez-Canela[2], Raul López-Arnau[4], Elena Escubedo[4] and Demetrio Raldúa[1]**

[1]Institute for Environmental Assessment and Water Research (IDAEA-CSIC), Barcelona, Spain, [2]Department of Analytical and Applied Chemistry (Chromatography Section), School of Engineering, Institut Químic de Sarrià-Universitat Ramon Llull, Barcelona, Spain, [3]Research and Development Center (CID-CSIC), Barcelona, Spain, [4]Department of Pharmacology, Toxicology and Therapeutic Chemistry, Pharmacology Section and Institute of Biomedicine (IBUB), Faculty of Pharmacy, University of Barcelona, Barcelona, Spain

Hyperthermia is a common confounding factor for assessing the neurotoxic effects of methamphetamine (METH) in mammalian models. The development of new models of methamphetamine neurotoxicity using vertebrate poikilothermic animals should allow to overcome this problem. The aim of the present study was to develop a zebrafish model of neurotoxicity by binge-like methamphetamine exposure. After an initial testing at 20 and 40 mg/L for 48 h, the later METH concentration was selected for developing the model and the effects on the brain monoaminergic profile, locomotor, anxiety-like and social behaviors as well as on the expression of key genes of the catecholaminergic system were determined. A concentration- and time-dependent decrease in the brain levels of dopamine (DA), norepinephrine (NE) and serotonin (5-HT) was found in METH-exposed fish. A significant hyperactivity was found during the first hour of exposure, followed 3 h after by a positive geotaxis and negative scototaxis in the novel tank and in the light/dark paradigm, respectively. Moreover, the behavioral phenotype in the treated fish was consistent with social isolation. At transcriptional level, *th1* and *slc18a2* (*vmat2*) exhibited a significant increase after 3 h of exposure, whereas the expression of *gfap*, a marker of astroglial response to neuronal injury, was strongly increased after 48 h exposure. However, no evidences of oxidative stress were found in the brain of the treated fish. Altogether, this study demonstrates the suitability of the adult zebrafish as a model of METH-induced neurotoxicity and provides more information about the biochemical and behavioral consequences of METH abuse.

Keywords: methamphetamine neurotoxicity, zebrafish model, behavior, neurochemicals, gene expression

OPEN ACCESS

Edited by:
Carla Denise Bonan, Pontifical Catholic University of Rio Grande do Sul, Brazil

Reviewed by:
Vania Loro, Federal University of Santa Maria, Brazil
Eduardo Rico, Universidade do Extremo Sul Catarinense, Brazil

****Correspondence:***
Demetrio Raldúa
drpqam@cid.csic.es

Specialty section:
This article was submitted to Predictive Toxicology, a section of the journal Frontiers in Pharmacology

Received: *03 September 2021*
Accepted: *08 November 2021*
Published: *22 November 2021*

Citation:
Bedrossiantz J, Bellot M, Dominguez-García P, Faria M, Prats E, Gómez-Canela C, López-Arnau R, Escubedo E and Raldúa D (2021) A Zebrafish Model of Neurotoxicity by Binge-Like Methamphetamine Exposure. Front. Pharmacol. 12:770319. doi: 10.3389/fphar.2021.770319

INTRODUCTION

Methamphetamine (METH) is a highly addictive psychostimulant drug affecting both the dopaminergic and serotonergic systems in the central nervous system (CNS) (Kobeissy et al., 2012). Some of the effects of METH related with CNS-stimulation include euphoria, increased alertness, aggressiveness, intensified emotions and altered self-esteem (Davidson et al., 2001). Some METH abusers binge on the drug for days in order to prolong euphoria (Shabani et al., 2019). METH binge is characterized by the administration of large doses of this drug, at short inter-dose durations

(every 2 h), over several days (typically 1–3 days). This abuse pattern results in nearly steady-state plasma levels of METH during most of the binge period (Davidson et al., 2001; Shabani et al., 2019). Acute and chronic exposure to toxic doses of METH induces unpleasant CNS symptoms such as anxiety, depression, hallucinations, psychosis, and seizures, as well as uncontrollable hyperthermia (Davidson et al., 2001; Darke et al., 2008). Whereas central dopaminergic system seems to mediate the changes in mood, excitation level and motor movement, serotonergic system may also contribute to the METH-related mood changes, psychosis, and aggressiveness (Albertson et al., 1999).

The neurotoxic effects of the METH binge administration regime, with constant high levels of METH in the CNS, have been extensively investigated (Shin et al., 2021). In fact, it is widely known that METH is able to induce the release of monoamine neurotransmitters [dopamine (DA), serotonin (5-HT), and norepinephrine (NE)] from nerve endings (Sulzer et al., 1995; Jones et al., 1998; Sitte et al., 1998; Fleckenstein et al., 2009). The mechanism apparently involves the initial redistribution of these neurotransmitters to the cytoplasm from the synaptic vesicles via the vesicular monoamine transporter 2 (VMAT2) and then the reverse transport of neurotransmitters into the synapses via specific plasma membrane transporters (DAT, NET, SERT) (Kish, 2008). The released DA will react with molecular oxygen to form quinones and semiquinones, as well as reactive oxygen species (ROS), finally resulting in oxidative stress generation and injury in dopaminergic terminals (Kita et al., 2009). Neurotoxic effects after high doses of METH in rodents include, therefore, long-lasting depletion in the striatal content of DA and its metabolites (Ricaurte et al., 1982), decrease in tyrosine hydroxylase (TH) activity (Ellison et al., 1978), and loss of DATs (Escubedo et al., 1998), a marker of terminal integrity. The persistent loss of DA axons in mice striatum induced by METH has been correlated with DA cell body loss in the substantia nigra pars compacta (SNpc) (Granado et al., 2011; Ares-Santos et al., 2012). However, the mechanisms underlying METH-induced striatal neurotoxicity are complex and still being investigated (Pubill et al., 2003, 2005). Moreover, the hyperthermia associated to acute toxic dosing of METH has been related with changes in the neurochemical profile, oxidative stress and neurodegeneration (reviewed at Davidson et al., 2001). Therefore, hyperthermia is an important confounding factor for understanding of the specific neurotoxic effects induced by METH. Consequently, this leads us to believe that new animal models of METH neurotoxicity could provide interesting new insights.

Zebrafish is an emerging model for studying complex brain disorders, covering the major human neuropsychiatric and neurotoxic syndromes (Kalueff et al., 2014; Stewart et al., 2014). This poikilotherm organism exhibits an overall nervous system organization and neurotransmitter systems similar to humans, responding also in a similar fashion to most of the neurotropic drugs used in human pharmacology. As a result, zebrafish has emerged as a new and powerful model species in translational neuroscience, including in the study of drug abuse-related phenotypes (Stewart et al., 2011; Neelkantan et al., 2013; Kolesnikova et al., 2019, 2021). Although a few studies have analyzed some effects of METH in adult zebrafish (Jiang et al., 2016; Mi et al., 2016; Zhu et al., 2017), most of them were focused on METH addiction and not in assessing neurotoxicity. The development of a model of METH neurotoxicity in this poikilotherm organism should be extremely useful for deciphering the direct effects of METH without the confounding factor of hyperthermia.

In this study adult zebrafish were continuously exposed to 20 or 40 mg/L METH for 48 h in order to achieve high and constant METH levels in CNS, as it is attained in the binge rodent models. Effects on motor activity, anxiety-like behavior, and social behavior have been thoroughly analyzed, as well as changes in the monoaminergic profile and gene expression in the brain of the fish at 3 and 48 h after exposure. Finally, the presence of oxidative stress in the whole brain of the fish was also analyzed after 48 h exposure.

MATERIALS AND METHODS

Animals and Housing

Adult wild-type zebrafish (standard length: 3.5–4.0 cm; weight: 0.62–0.67 g) were obtained from Exopet (Madrid, Spain) and maintained into a recirculating zebrafish system (Aquaneering Inc., San Diego, United States) at the Research and Development Center zebrafish facilities (CID-CSIC) for 2 months before starting the exposures. Fish were housed in 2.8 L tanks (density: 20 fish/tank) with fish water [reverse-osmosis purified water containing 90 mg/L Instant Ocean® (Aquarium Systems, Sarrebourg, France), 0.58 mM $CaSO_4 \cdot 2H_2O$, and 0.59 mM $NaHCO_3$] under a 12L:12D photoperiod. The main parameters of the fish water in the housing facilities were: temperature: 28 ± 1°C; pH: 7.6–8.0; conductivity: 700–800 μS/cm; hardness: 120–130 mg/L. Fish were fed twice a day with flake food (TetraMin, Tetra, Germany). All procedures were approved by the Institutional Animal Care and Use Committees at the CID-CSIC (OH 1032/2020) and conducted in accordance with the institutional guidelines under a license from the local government (agreement number 9027).

Chemicals and Material

Crystalline solid standards of L-tyrosine (Tyr), dopamine hydrochloride (DA), 3,4-dihydroxyphenylacetic acid (DOPAC), homovanillic acid (HVA), L-tryptophan (Trp), 5-hydroxy-L-tryptophan (5-HTP) and serotonin hydrochloride (5-HT) were purchased from Sigma-Aldrich (St. Louis, MO, United States). 3-methoxytyramine hydrochloride (3-MT) was obtained from Merck (Darmstadt, Germany), norepinephrine (NE) was supplied by Tocris Bioscience (Ellisville, United States) and 5-hydroxyindoleacetic acid (5-HIAA) was provided by Toronto Research Chemicals (TRC, Toronto, Canada). Labelled neurotransmitters standards such as 5-HT-d4 HCl, 5-HTP-d4, DOPAC-d5, Trp-1–13C, L-dopa-d3, 5-HIAA-d5 and DL-NE-d6 HCl were obtained from Toronto Research Chemicals (TRC, Toronto, Canada), whereas DA-1,1,2,2-d4 HCl was provided from Merck (Darmstadt, Germany) and 3-MT-d4 HCl from Sigma-Aldrich (St. Louis, MO, United States).

METH hydrochloride was generously provided by Prof. J. Camarasa, Faculty of Pharmacy at University of Barcelona (Spain).

Acetonitrile (ACN) and methanol (MeOH) LC-MS grade were purchased from VWR Chemicals Prolabo (Leuven, Belgium). Formic acid (FA) was provided by Fischer Scientific (Loughborough, United Kingdom), while dimethyl sulfoxide (DMSO), ammonium formate and sodium bicarbonate ($NaHCO_3$) were supplied by Sigma-Aldrich (St. Louis, MO, United States). Ultra-pure water was daily obtained through Millipore Milli-Q purification system (Millipore, Bedford, MA, United States).

Stock solutions of all labeled and unlabeled compounds were prepared at 1 mg/ml in MeOH, DMSO or ultra-pure water depending on their solubility. Standard solutions of unlabeled neurotransmitters as well as the mixture of labeled standards (ISM) used as internal standard were prepared at the desired concentration in starting mobile phase solvent.

Working solutions of METH were prepared at 20 and 40 mg/L in fish water (pH 8).

Stability of Methamphetamine in Water

Working solutions of 20 mg/L (C_1) and 40 mg/L (C_2) METH were freshly prepared from solid METH by dissolving it in fish water (pH 8). Fish water was used as control solution (C_0). Solutions (500 ml) were introduced in beakers and kept in an incubation chamber (POL-EKO APARATURA Climatic chamber KK350, Poland) set to 28.5°C and 12 h light: 12 h dark photoperiod. Sample aliquots (C_0, C_1 and C_2) were picked at 0, 24 and 48 h. Standards of 5, 10, 15, 30, 50 mg/L of METH were used to obtain a calibration line.

Water samples were analyzed using an Acquity UPLC® H-class system coupled to fluorescence detector (Waters, MA). METH elution was achieved in a gradient mode with a BEH C18 column (100 mm × 2.1 mm, 1.7 μm) maintained at 35°C. The mobile phase consisted of H_2O with 0.1% of FA (solvent A), and acetonitrile (solvent B). The gradient started at 5% of B and increased to 15% B in 1.5 min. Then, solvent B increased to 20% in 4 min, and held for 1 min. Finally, initial conditions were restored in 0.5 min, and held for 3 min resulting in a total run time of 10 min.

Aliquots of 10 μl were injected in both standards and samples, using a flow rate of 200 μl min^{-1}. The fluorescence detector excitation/emission wavelengths were 256 and 288 nm. Chromatographic data acquisition and processing were performed using Empower 2 software (Waters, Milford, MA, United States).

Experimental Procedure

In order to build a METH acute neurotoxicity model in adult zebrafish, the first step was to determine the METH concentration with strongest effects on neurobehavior and neurochemicals profile, but without evidences of systemic toxicity (Experiment 1). Three METH concentrations, 20, 40 and 80 mg/L, were selected for an initial range-finding test, as this range of METH concentrations has been already used in drinking water in some rodent models (Shabani et al., 2016). The highest concentration, 80 mg/L METH, was discarded, as this concentration exhibited a 100% of lethality in only 24 h in the range-finding test. No lethality, however, was found with 20 and 40 mg/L after 48 h exposure. **Supplementary Figure S1** shows the experimental design of the two types of experiments performed in this study. Working solutions of 20 and 40 mg/L METH were directly prepared in fish water (pH 8) the day of the experiment. Adult zebrafish (≈50:50 male:female ratio) were randomly selected from the CID-CSIC facilities and exposed for 48 h to 20 or 40 mg/L METH, at 28.5°C and 12L:12D photoperiod. Control fish were maintained in fish water under identical conditions. Experiments were conducted in duplicate or triplicate, in glass tanks containing 500 ml of water with three fish in each. Experimental solutions were renewed at 24 h, 30 min after the first feeding of the day. Tanks were kept in an incubation chamber (POL-EKO APARATURA Climatic chamber KK350, Poland) set to 28.5°C and 12L:12D photoperiod. Fish were euthanized by inducing hypothermic shock in ice-chilled water (2–4°C) and brains for neurotransmitters, gene expression and oxidative stress were immediately dissected and individually stored at −80°C for further analysis.

Behavioral Testing

Behavioral testing was performed in an isolated behavior room (27–28°C) between 10:00 and 17:00 h. Animals (≈50:50 male: female ratio) were transferred to the behavior room 1 hour before testing began, for acclimation. All fish used in this study were experimentally naïve and the testing was performed in a blind manner. In order to avoid the potential interference of any conspecific alarm cues, water of the experimental tank was changed after each trial.

Locomotor activity was determined after placing shoals of six fish into an experimental tank containing fish water (control group) or 40 mg/L METH (treated group) and video-recorded for 180 min. Two independent trials were conducted (n = 12). The distance moved and the percentage of time spent in hypermobility state [when the software detects changes in more than 70% of the pixels identified as the during at least 150 consecutive frames (≥5 s)] by each fish of the shoal was analyzed using Ethovision XT 13.0 social interaction module.

The Novel Tank Test (NTT), used to assess geotaxis (preference for the bottom of the tank), freezing and erratic movements of fish, was performed using an experimental setup previously described (Faria et al., 2018). Videos from each trial were analyzed by Ethovision XT 13.0 (Noldus, Wageningen, Netherlands). First, the front of the tank was divided into two equal virtual zones, top and bottom, and the distance travelled at the top and at the bottom (cm), the time spent in the top (s), latency to top (s), and entrances to the top were determined. Freezing behavior was defined as immobility (identified by the software, when less than 3% mobility) combined with increased opercular movements (visually identified by the observer), for at least 5 s. Additional details are provided in **Supplementary Methods**.

The Dark-Light Test (DLT), used to determine scototaxis (preference for the dark background) of the fish, was performed using an experimental setup previously described

(Faria et al., 2019). Each trial was video-recorded with a GigE camera mounted on the top of the experimental tank. The recorded videos were analyzed by Ethovision XT 13.0, and the time spent in the white zone (s), number of transitions to the white zone and the latency to enter to the white zone (s) were determined. Additional details are provided in **Supplementary Methods**.

The shoaling test, used to assess social and anxiety-like behaviors, was performed using an experimental setup previously described (Green et al., 2012) Two independent trials were performed, with a shoal size of nine fish per experimental group in each (n = 18). Groups of nine zebrafish from the control and METH groups were video-recorded for 6 min in our novel tank (**Supplementary Methods**), and analyzed using Ethovision XT 13.0 social interaction module. This automated method permits us to detect and track every fish in the group and measure the distance moved and inter-fish distances continuously in order to assess shoal density or the shoaling tendency of each individual. The total distance (cm) as well as the average interfish distance (cm), farthest neighbor distance (cm) and nearest neighbor distance (cm) were calculated.

Finally, the social preference test was adapted from the protocol described by (Carreño Gutiérrez et al., 2019). A single fish was transferred to an experimental tank (20 cm length, 20 cm width, 25 cm height) containing 5 L. The single focal fish was allowed to interact with a stimulus compartment–a fish's shoal placed into the one-side extern housing tank, or with the non-stimulus compartment–a one-side extern empty housing tank. The focal fish was recorded 6 min (AVI video format, 30 fps) with the uEye Cockpit software (version 4.90; Imaging Development Systems, Germany) controlling the GigE cameras (UI-5240CP-NIR-GL, Imaging Development Systems, Germany) placed in front of the testing tanks. The recorded videos were analyzed with Ethovision XT 13.0 (Noldus, Wageningen, the Netherlands). First, the central experimental arena was divided into three equal size virtual zones: empty, center and conspecific (**Supplementary Figure S2**). The time spent (s) and the distance moved (cm) by the focal fish, was recorded in each arena.

Analysis of Neurochemicals by LC-MS/MS

The profile of monoaminergic neurochemicals was determined in the whole brain of controls and fish exposed for 3 and 48 h to 20 and 40 mg/L METH. Extraction of monoamine neurochemicals from zebrafish brain was mainly based in the methodology described by Mayol-Cabré et al. (2020). This extraction procedure required working at 4°C during all the process due to the high degradation of target NTs compounds. Briefly, each zebrafish whole brain was introduced in an Eppendorf tube with 300 µl of cold extractant solvent (90:10 ACN/H_2O + 1% FA), 50 µl of the ISM solution and three stainless steel beads (3 mm diameter), and were homogenized and grounded using a bead mill homogenizer (TissueLyser LT, Quiagen, Hilden, Germany) programmed at 50 osc/min for 90 s. The supernatant was transferred to a new Eppendorf tube, centrifuged for 20 min at 13,500 rpm in a cold room (4°C), filtered through 0.22 µm nylon filters (Scharlab, Barcelona, Spain) and kept in chromatographic vials at −80°C until the analysis. **Supplementary Figure S3** summarizes the zebrafish brain extraction procedure with five different stages and subsequent LC-MS/MS analysis.

LC-MS/MS analysis was performed using an Acquity UPLC® H-Class liquid chromatograph (Waters, Milford, MA, United States) coupled to a triple quadrupole mass spectrometer (Xevo, TQ-S micro, Waters, United States) and equipped with an electrospray ionization source (ESI) able to measure the neurotransmitters under positive electrospray ionization. An Acquity UPLC BEH Amide column (150 mm × 2.1 mm ID, particle size 1.7 µm) provided with an Acquity UPLC BEH Amide pre-column (5 mm × 2.1 mm ID, particle size 1.7 µm) (Waters, Milford, MA, United States) was employed. Column operated at a flow rate of 0.25 ml min^{-1} at 30°C. Aliquots of 10 µl of standard and/or samples were injected at 10 ± 5°C. Mobile phase consisted in Milli-Q water and acetonitrile (H_2O: ACN) (95:5) containing 100 mM ammonium formate at pH 3.0 (solvent A) and H_2O:ACN (15:85) containing 30 mM ammonium formate at pH 3.0 (solvent B). pH was adjusted to 3 with FA 80%. The LC gradient used for the chromatographic separation started at 100% B, decreased at 80% B in 4 min, and held for 1 min. From 5 to 7 min, B was increased to 100%. Finally, initial conditions were accomplished in 3 min, resulting in a 10 min total run time. Desolvation gas (N_2) flow was set to 900 L h^{-1}, whereas cone gas (N_2) flow was performed at 150 L h^{-1}. Source temperature was set at 100°C and a capillary voltage of 2.0 kV was applied. Desolvation temperature was 350°C. Acquisition was performed in SRM mode, using the most intense fragment as the quantifier ion, and the second most intense as the qualifier ion. Data were acquired and processed using MassLynx® Software v 4.1 (Waters, Manchester, United Kingdom).

Analysis of Methamphetamine Levels in Brain

Brains of fish exposed to 40 mg/L METH for 3 or 48 h, were extracted by using the same protocol already described for neurochemicals. Extracts were evaporated to dryness under a gentle stream of nitrogen (N_2) in a sample concentrator (Techne®, Staffordshire, United Kingdom) and reconstituted with 300 µl of ultra-pure water.

For the analysis of METH in the reconstituted extracts, an Acquity UPLC BEH C18 column (100 mm × 2.1 mm ID, particle size 1.7 µm) provided with an Acquity UPLC BEH C18 pre-column (5 mm × 2.1 mm ID, particle size 1.7 µm) (Waters, Milford, MA, United States) were employed. Elution was performed using a binary mobile phase of MilliQ water with 0.1% FA (A) and acetonitrile (B) in a gradient mode at 0.2 ml/min. The gradient started at 5% B, and held for 0.5 min. Then, it was increased to 30% B in 5.5 min, and held for 1 min. Finally, initial conditions were reached in 1.5 min, and held for 2 min, resulting in a total run time of 10 min. Autosampler injection volume was set at 10 µl, and the samples were maintained at 4°C during the injection sequence. MS conditions were similar to the described for neurochemicals.

Quality Assurance of Neurotransmitters, Methamphetamine in Brain and Methamphetamine in Water Studies

Extractant solvent (ACN:H_2O 90:10 + 1% FA) was used to prepare the calibration standards. Linearity was performed over a concentration range from 0.005 to 1 mg/L, using six calibration points. ISM was used as internal labeled standards for extraction and analytical quality control. Target compounds were quantified by internal calibration, except for HVA that was determined using external calibration. The validation of the method was checked with the recovery studies selecting seven replicates, using zebrafish brain samples spiked at 250 ng (QCs) with the neurochemical standard mixture and the ISM. In addition, the matrix effect (ME) was calculated comparing slopes between standard calibration line and matrix calibration line. Instrumental detection limits (IDLs) were determined using the lowest concentration standard solution at 0.005 mg/L that yielded a S/N ratio equal to 3. Method detection limits (MDLs) were calculated using QCs that also produced a S/N ratio equal to 3. Moreover, intra-day precision was assessed by three consecutive injections of 1 mg/L standard solution, while inter-day precision was determined by measuring the same standard solution on four different days. The analysis of solvent blanks showed no carryover effect during the LC-MS/MS analysis in all neurochemicals.

In the study of the levels of METH in zebrafish brain, standards of 0.5 to 1,000 µg/L were prepared in water and used to check linearity. Instrumental detection limits (IDLs) were determined using the 0.5 µg/L standard. Inter-day and intra-day precision was determined by measuring the standard solution of 50 µg/L.

For the study of METH stability in water, standards of 5, 10, 15, 30, and 50 mg/L of METH were used to check the calibration range. External calibration was used for METH determination in the stability study. Instrumental detection limits (IDLs) were determined using the lowest concentration standard solution at 5 mg/L. Intra-day precision was determined by measuring a standard of 5 mg/L three times the same day, and inter-day precision was determined by measuring standard solution of 10 mg/L on three different continuous days.

Real-Time Polymerase Chain Reaction

Total RNA was extracted from the brain of zebrafish control and exposed to 40 mg/L METH for 3, 24, and 48 h, using Trizol Reagent (Invitrogen Life Technologies, Carlsbad, CA). RNA quality and concentration were determined on a NanoDrop ND-8000 spectrophotometer (NanoDrop Technologies). First strand cDNA was synthesized from 1 µg of total RNA previously treated with DNaseI (Ambion, Austin, TX), using First Strand cDNA synthesis Kit (Roche Diagnostics, Mannheim, Germany) and oligo(dT) according to manufacturer's instructions.

Real Time qRT-PCR was performed in a LightCycler® 480 Real-Time PCR System with SYBR Green PCR Master Mix (Roche Diagnostics, Mannheim, Germany). Cycling parameters: 95°C for 15 min and 45 cycles of 95°C, 10 s and 60°C, 30 s. A dissociation curve analysis was added to ensure the specificity of the reaction. Eight biological replicates were assayed for each treatment, and three technical replicates were run for each sample.

Primer sequences for the selected genes [tyrosine hydroxylases 1 and 2 (*th1, th2*), dopamine transporter (*dat* or *slc6a3*), vesicular monoamine transporter (*vmat2* or *slc18a2*), dopamine-β-hydroxylase (*dbh*), and glial fibrillary acidic protein (*gfap*)] are listed in **Supplementary Table S1**. Specificity of primers was previously confirmed by the presence of a single peak in the melting curves of PCR reactions.

The mRNA expression of each target gene was normalized to the housekeeping *ppia2* as reference gene. Relative quantification of mRNA abundance for the selected genes among treatments with respect to the control group were calculated following the ΔΔCt method (Livak and Schmittgen, 2001) deriving fold-change ratios from these values.

Lipid Peroxidation Determination

Lipid peroxidation was determined in the brain of zebrafish exposed 48 h to METH, by quantifying the levels of malondialdehyde (MDA) according to Faria et al. (2019). Pools of three brains were homogenized at a proportion of 50 mg/ml (tissue weight/buffer volume), in ice cold 0.1 M phosphate buffer with 150 mM KCl and 0.1 mM ethylenediamine-tetraacetic acid, disodium, salt, dihydrate (EDTA) and 0.01% BHT. The brain homogenates were then incubated with 5 mM 1-methyl-2-phenylindole prepared in acetonitrile:methanol (3:1 v/v), 5.55% of HCl at 45°C, for 40 min. Following incubation, absorbance was read at 586 nm and MDA content in each sample was extrapolated from a standard curve of 1,1,3,3-tetramethoxypropane (TMP) treated under similar conditions as samples. The final results were normalized by mg of tissue ww (wet weight) corresponding to each sample and expressed as pmol/mg.

Data Analysis

Data were analyzed with IBM SPSS v26, and plotted with GraphPad Prism 9.02 for Windows (GraphPad software Inc., La Jolla, CA). Normality was assessed using Shapiro-Wilk test. One-way ANOVA followed by Dunnett's or Tukey's multiple comparison test was used to test differences between normally distributed groups, whereas the Kruskal-Wallis test followed by a pairwise comparison using the Bonferroni correction was used to test differences between groups that did not meet parametric assumptions.

RESULTS

Stability of Methamphetamine in Fish Water

Supplementary Table S2 shows the measured concentrations and the stability of METH in fish water in our experimental conditions. The measured concentrations, 20.66 ± 0.02 and 40.05 ± 0.11 mg/L, were very close to the nominal values tested in this study, 20 and 40 mg/L. Moreover, no significant degradation of METH with time was found for both 20 mg/L

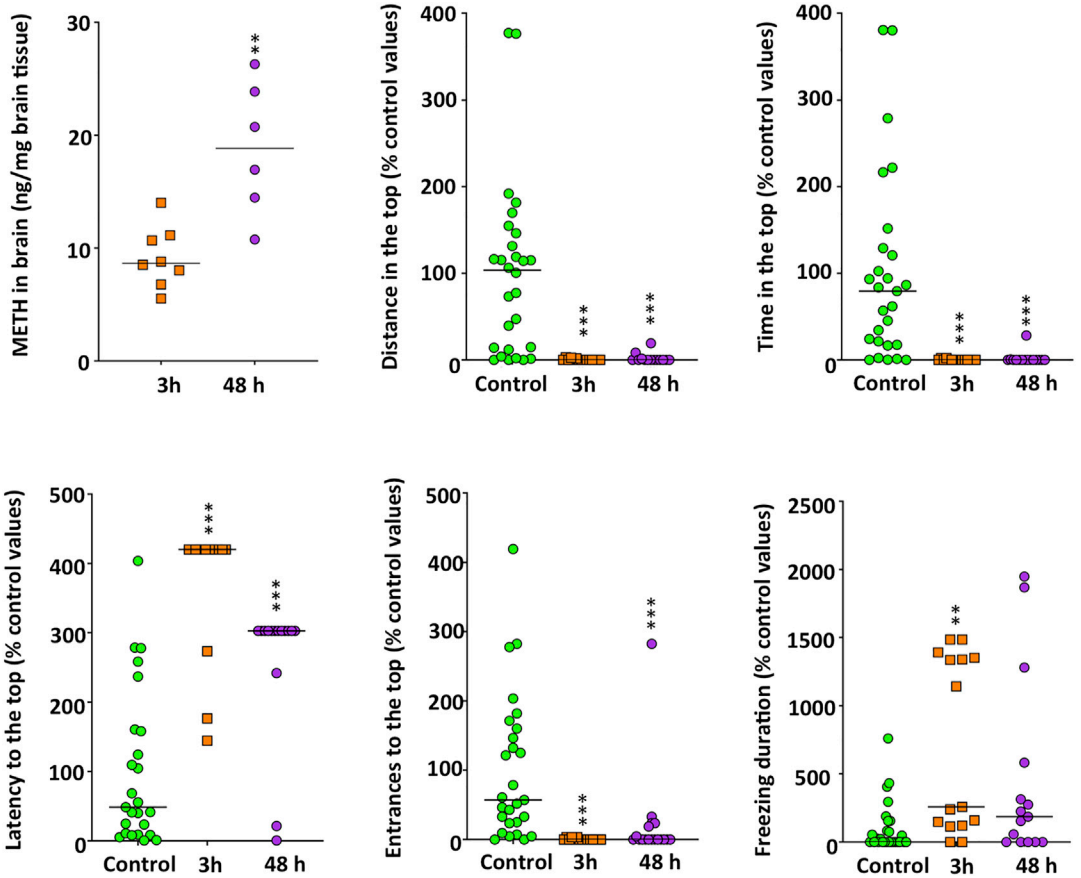

FIGURE 1 | Time-dependent increase in methamphetamine brain levels in adult zebrafish waterborne exposed to 40 mg/L methamphetamine (METH) for 3 and 48 h and anxiety-like behavior, assessed in standard 6-min novel tank test (NTT) of zebrafish exposed to the same concentration and times. Data from each experiment were normalized to the corresponding control values. The combined data is reported as scatter plot with the median (n = 6–8 for METH levels in the brain and n = 14–15 for the NTT results), $^{**}p < 0.01$, $^{***}p < 0.001$; Student's t-test for METH levels in brain and Kruskal Wallis test with Bonferroni correction for NTT endpoints. Data from two independent experiments.

($H_{(2)}$ = 0.605, p = 0.739) and 40 mg/L ($H_{(2)}$ = 4.356, p = 0.113) concentrations. Finally, no signal was observed in fish water control samples, proving that there was no cross-contamination.

Determining the Methamphetamine Concentration to Build the Acute Neurotoxicity Model

The NTT paradigm was used to determine the effects on anxiety-like behavior (**Supplementary Figure S4**) in animals treated with the 20 and 40 mg/L METH 48 h after exposure. Both concentrations of METH induced an anxiety-like state characterized by positive geotaxis, with a significant decrease in the time spent in the top of the tank ($H_{(2)}$ = 19.030, p = 0.00007), the distance moved in this zone ($H_{(2)}$ = 23.027, p = 9.99 × 10^{-6}) and the number of entrances to the top ($H_{(2)}$ = 25.295, p = 3.21 × 10^{-6}). Moreover, the latency to enter to the top increased in the treated animals ($H_{(2)}$ = 28.631, p = 6.07 × 10^{-7}). No differences between the fish exposed to 20 and 40 mg/L METH were found in any of the parameters measured in the NTT (p > 0.05 when results were adjusted by the Bonferroni correction).

When the neurochemical profile of the control and treated fish was determined (**Supplementary Figure S5**), the main effect of METH was a significant decrease in the levels of the monoaminergic neurotransmitters DA ($F_{(2,28)}$ = 57.523, p = 1.21 × 10^{-10}), NE ($F_{(2,28)}$ = 115.191, p = 3.08 × 10^{-14}) and 5-HT ($F_{(2,28)}$ = 50.063, p = 5.67 × 10^{-10}). However, no differences between the fish exposed to 20 and 40 mg/L METH were found in the levels of these three neurotransmitters (p > 0.05; one-way ANOVA followed by Tukey's multiple comparison test). Whereas the levels of the DA metabolite, DOPAC, were also significantly decreased by both METH concentrations (($H_{(2)}$ = 15.164, p = 0.00051), only 40 mg/L METH was able to decrease the levels of 3-MT ($H_{(2)}$ = 10.827, p = 0.0044), HVA ($H_{(2)}$ = 11.069, p = 0.0039), as well as the DA precursor tyrosine ($H_{(2)}$ = 8.526, p = 0.014).

These results show that although 20 and 40 mg/L METH induce similar effects, the effect of 40 mg/L METH is stronger and more evident than 20 mg/L METH in most of the assessed

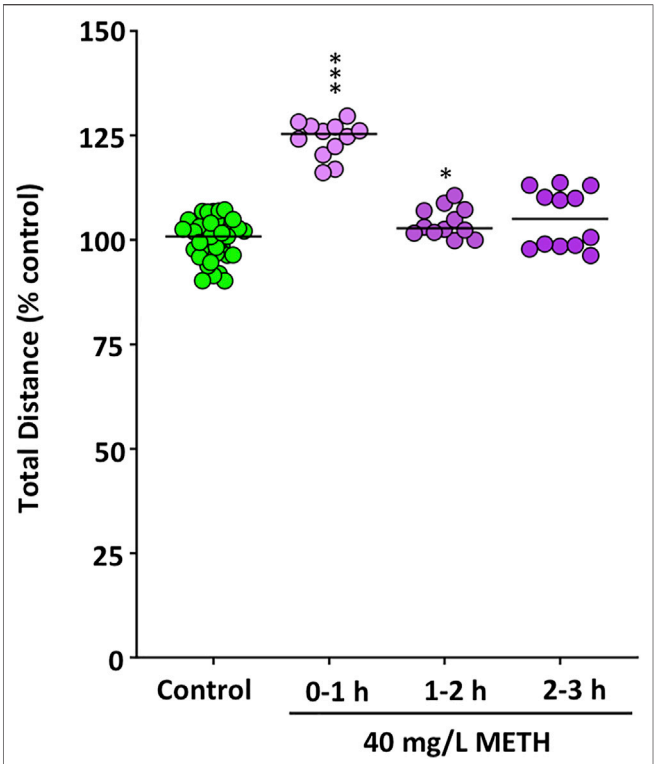

FIGURE 2 | Increased motor activity in fish waterborne exposed to 40 mg/L methamphetamine. The total distance (m) moved during the first hour of the exposure for control fish and exposed fish was measured for each individual fish in shoals of six animals. Data reported as scatter plot with the median ($n = 12$), ***$p < 0.001$; Student's *t*-test. Data from two independent experiments.

endpoints. Therefore, this concentration was selected for the further analysis of the neurotoxic effects (Experiment 2).

Time-dependent Increase in Methamphetamine Brain Levels

Concentration of METH in the brain of fish exposed to 40 mg/L METH increased significantly with time ($t_{(12)}$ = -4.150, p = 0.0013), with levels of 9.19 ± 0.95 and 18.84 ± 2.40 ng/mg brain tissue for 3 and 48 h exposures, respectively (**Figure 1**).

Behavioral Effects of Methamphetamine

First of all, the effect of METH on the locomotor activity of the control and METH (40 mg/L)-treated fish was determined per hour during the first 3 h of exposure by measuring both the distance moved and the percentage of time they spent in hypermobility state. As zebrafish is a very social animal, even the short social isolation of testing each fish individually could result in a mild stressful stimulus. Therefore, in order to avoid the potential confounding factor of the social isolation, the locomotor activity was determined in shoals of six fish. As **Figure 2** shows, during the first hour of exposure, METH induced hyperactivity, with the exposed fish moving a significant higher distance than controls ($t_{(22)}$ = -11.573, $p = 7.95 \times 10^{-11}$). Moreover, the percentage of time spent in hypermobility state by the exposed fish (*Mdn* = 59.2%) was significantly higher than that of control fish (*Mdn* = 18.6%) [$U(N_{control} = 12, N_{treated} = 12) = 132.000$, z = 3.464, p = 0.0002]. During the second hour of exposure, the distance moved by the treated fish was still higher than that of controls, although the significance of the differences was lower ($t_{(22)} = -2.663$, $p = 0.014$), whereas the time spent in hypermobility state by METH-exposed fish (*Mdn* = 57.8%) was also significantly higher than that for control fish (*Mdn* = 21.5%) [$U(N_{control} = 12, N_{treated} = 12) = 138.000$, z = 3.811, $p = 0.00002$]. Finally, although no statistical differences in locomotor activity were found between control and treated fish during the third hour of exposure [$U(N_{control} = 12, N_{treated} = 12) = 101.000$, z = 1.674, p = 0.094], hypermobility state in the exposed fish (*Mdn* = 57.5%) was still significantly higher that that in the control fish (*Mdn* = 22.5%) [$U(N_{control} = 12, N_{treated} = 12) = 122.000$, z = 2.887, p = 0.0029]. Distance moved in the locomotor assay was also analyzed during the last 6 min of the assay, in order to be able to directly compare locomotor activity in this assay with that in other behavioral 6-min assays also performed after 3 h exposure. In contrast with the results of total distance moved during the 2–3 h period, distance moved by the exposed fish during the last 6-min of the assay (*Mdn* = 977.04 cm) was significantly higher than that for the control (*Mdn* = 900.52 cm) %) [$U(N_{control} = 12, N_{treated} = 12) = 127.000$, z = 3.175, p = 0.00086].

In order to better understand the progression of the neurotoxic effects of METH in adult zebrafish, the behavioral effects in animals exposed for 3 and 48 h were analyzed. When the effect of 40 mg/L METH was assessed in the NTT (**Figure 1** and **Supplementary Figure S6**), Kruskal-Wallis analysis showed a significant hypolocomotion ($H(2) = 37.762$, $p = 6.31 \times 10^{-9}$), a positive geotaxis, characterized by a decrease in the time spent in the top of the experimental tank ($H_{(2)} = 35.964$, $p = 1.55 \times 10^{-8}$), in the distance moved in this zone ($H_{(2)} = 32.272$, $p = 9.82 \times 10^{-8}$), and in the number of entrances to this zone ($H_{(2)} = 36.527$, $p = 1.17 \times 10^{-8}$). METH-treated fish also exhibited a significant increase in the latency to enter for the first time to the top of the tank ($H_{(2)} = 17.264$, $p = 0.00018$). No differences were found in the effect of METH at 3 and 48 h for any of the parameters measured in the NTT when results were adjusted by the Bonferroni correction ($p > 0.8$). However, a significant effect of the exposure time was found for the freezing time ($H_{(2)} = 13.120$, $p = 0.0014$). Whereas the freezing time significantly increased 3 h after exposure ($p = 0.0012$), no differences with the control values were found after 48 h ($p = 0.16$). METH had no effect on erratic movements at any time.

The anxiety-like behavior was also assessed by using the DLT (**Figure 3**). In this experimental paradigm treated fish exhibited a negative scototaxis ($H_{(2)} = 9.557$, $p = 0.0084$), increasing their preference by the white background. Results of the Bonferroni post hoc test indicated that only after 48 h of exposure the treated fish spent significantly more time on the white background (p = 0.0071). Moreover, whereas the number of entrances to the white zone significantly decreased in METH-treated fish ($H_{(2)} = 21.768$, $p = 0.000019$), the average duration of each visit to this zone was significantly longer ($H_{(2)} = 13.478$, $p = 0.0012$). Results of the Bonferroni post hoc test did not show significant differences

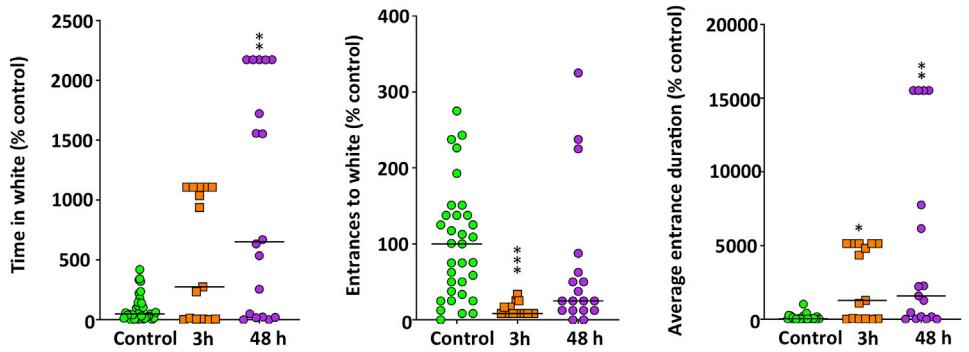

FIGURE 3 | Anxiety-like behavior, assessed in standard 6-min dark-light test (DLT), in adult zebrafish waterborne exposed to 40 mg/L methamphetamine (METH) for 3 and 48 h. Data from each experiment were normalized to the corresponding control values. The combined data is reported as scatter plot with the median (n = 15–18), $^{*}p < 0.05$, $^{**}p < 0.01$, $^{***}p < 0.001$; Kruskal Wallis test with Bonferroni correction. Data from two independent experiments.

between the two times analyzed for any of the endpoints in the DLT paradigm ($p > 0.5$).

Finally, in order to assess the effects of the acute exposure to METH on the social behavior, two experimental paradigms were used. The first one, the shoaling test (**Figure 4A**), showed significantly higher average interfish distance ($H_{(2)}$ = 53.261, $p = 2.72 \times 10^{-12}$), farthest interfish distance ($H_{(2)}$ = 52.504, $p = 3.97 \times 10^{-12}$) and nearest interfish distance ($H_{(2)}$ = 52.762, $p = 3.49 \times 10^{-12}$) in the METH-treated fish, a behavioral phenotype consistent with social isolation. No time effect was found by using the Bonferroni post hoc test ($p > 0.5$). Moreover, when the effect of METH on the total distance moved for each fish was measured in this test, a significant effect was found ($H_{(2)}$ = 30.612, $p = 2.52 \times 10^{-7}$). As **Supplementary Figure S6** shows, the mobility of the fish in this test was significantly reduced 48 h after exposure ($p = 1.56 \times 10^{-7}$), but not 3 h after exposure ($p > 0.5$). The second paradigm used for assessing the effects on social behavior was the social preference test (**Figure 4B**). Results from this paradigm show a significant decrease in both the time that the treated fish spent in the zone closest to the conspecifics ($F_{(2,74)}$ = 14.497, $p = 4.87 \times 10^{-6}$) and the distance moved in this zone ($F_{(2,73)}$ = 13.461, p = 0.00001). These results are consistent with the social isolation phenotype suggested by the shoaling test results. Results of the Tukey's Honest Significant Difference (HSD) post hoc test did not show significant differences between the two times analyzed ($p > 0.5$).

Methamphetamine Decreases Monoaminergic Neurotransmitters

Figure 5 shows the main changes in the monoaminergic neurochemicals profile occurring in the brain of zebrafish exposed for 3 and 48 h to 40 mg/L METH. First of all, a significant decrease was found in DA ($F_{(2,35)}$ = 55.503, $p = 1.39 \times 10^{-11}$), NE ($F_{(2,34)}$ = 66.932, $p = 1.62 \times 10^{-12}$) and 5-HT levels ($F_{(2,35)}$ = 33.209, $p = 8.21 \times 10^{-9}$), the three most relevant monoaminergic neurotransmitters. Results of the Tukey's HSD test showed that the effect of METH on these neurotransmitters was time-dependent, with the maximum effect after 48 h of exposure (p = 0.00016 for DA, $p = 2.04 \times 10^{-7}$ for NE and p = 0.016 for 5-HT). Interestingly, the effect of METH on the dopaminergic system was not restricted to DA, as a significant decrease was also observed in the precursor tyrosine ($H_{(2)}$ = 9.621, p = 0.008) as well as in the main metabolites of this neurotransmitter, including DOPAC ($H^{(2)}$ = 8.240, p = 0.016), 3-MT ($H_{(2)}$ = 8.202, p = 0.017) and HVA ($H_{(2)}$ = 12.378, p = 0.002). Although the levels of these neurochemicals exhibited a general trend to decrease with time, results of the Bonferroni post hoc test only showed significant differences for those animals exposed for 48 h respect to the control fish (p = 0.006 for tyrosine, p = 0.016 for DOPAC, p = 0.013 for 3-MT and p = 0.001 for HVA). Regarding 5-HIAA, the degradation product of 5-HT, no differences with the control were found ($p > 0.05$).

Effects of Methamphetamine on Gene Expression

First, the expression of five genes involved in the synthesis (*th1*, *th2*, *dbh*) and transport (*slc6a3, slc18a2*) of catecholaminergic neurotransmitters were analyzed in the brain of zebrafish control and exposed to 40 mg/L METH for 3, 24, and 48 h. **Figure 6** shows a significant effect of exposure time to METH on the expression levels for *th1* ($F_{(3,44)}$ = 5.660, p = 0.002), *th2* ($F_{(3,44)}$ = 6.684, p = 0.001), *dbh* ($F_{(3,28)}$ = 11.180, $p = 5.36 \times 10^{-5}$), and *slc18a2* ($F_{(3,44)}$ = 4.990, p = 0.005), but not for *slc6a3* ($H_{(3)}$ = 4.838, p = 0.184). *th1* and *slc18a2* exhibited an early response to METH, increasing their levels significantly (p = 0.004) after only 3 h of exposure. The levels of *th1* remained increased at 24 h (p = 0.022), returning to the control values 48 h after exposure (p = 0.844). In contrast with *th1* and *slc18a2*, the expression of *th2* and *dbh* was altered by METH at the end of the exposure. Whereas the levels of *th2* significantly decreased (p = 0.019) at 48 h after exposure, the levels of *dbh* increased (p = 0.004).

The expression of *gfap* was also analyzed (**Figure 6**), as this gene is a classical marker of neuroinflammation. The exposure time to METH had a significant effect on *gfap* expression ($F_{(3,44)}$ = 6.534, p = 0.001), with the levels of this transcript strongly increased after 48 h of exposure (p = 0.0003).

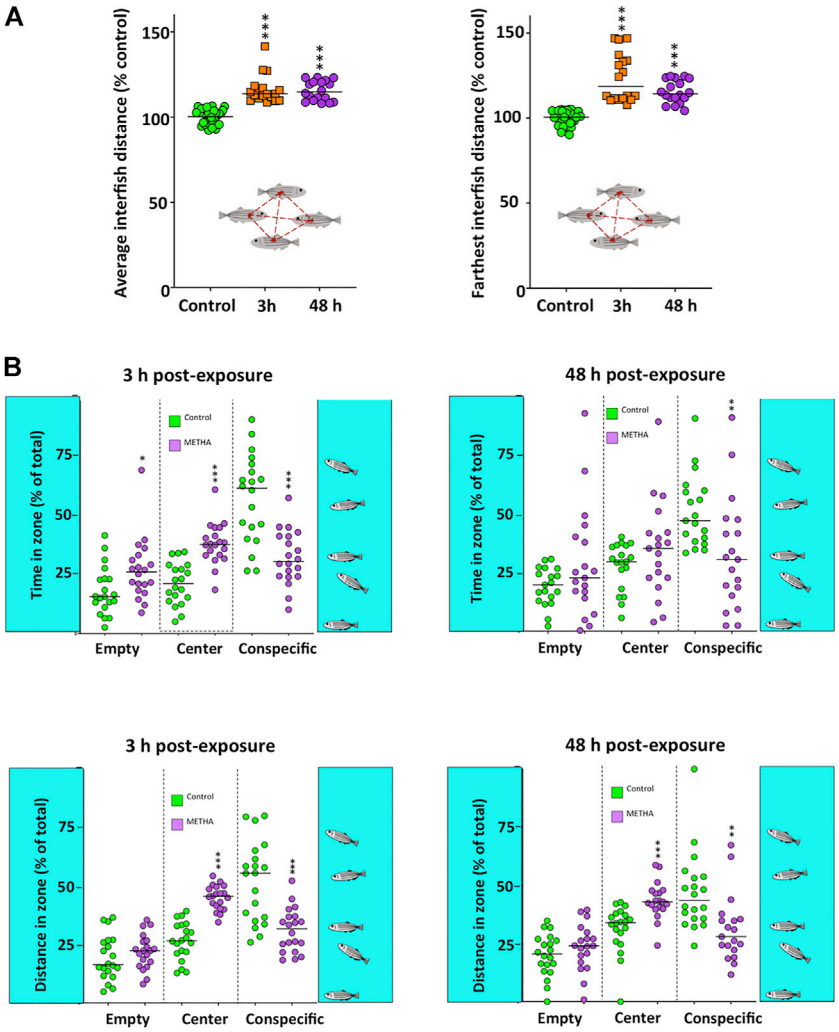

FIGURE 4 | Social behavior in adult zebrafish waterborne exposed to 40 mg/L methamphetamine (METH) for 3 and 48 h. **(A)** Shoaling test results, including the average and the farthest interfish distances. **(B)** Social preference test results, including time and distance of the fish in each of the three virtual zones of the experimental tank: empty, center and conspecific. Data from each experiment were normalized to the corresponding control values. The combined data is reported as scatter plot with the median (n = 18 for shoaling test and n = 17–20 for social preference test), $^{*}p < 0.05$, $^{**}p < 0.01$, $^{***}p < 0.001$; one-way ANOVA with Dunnett's multiple comparison test (Social Preference Test data) or Kruskal Wallis test with Bonferroni correction (Shoaling test data). Data from two independent experiments.

Effects of Methamphetamine on Lipid Peroxidation

No differences in lipid peroxidation levels in the brain were found between control and fish exposed for 48 h to 40 mg/L METH [15.78 ± 0.95 vs 13.49 ± 0.73 pmol MDA/mg ww for control (n = 10) and METH-exposed (n = 9) fish, respectively; $t_{(17)} = 1.216$, p = 0.066; Data from three independent experiments].

DISCUSSION

Zebrafish has become a relevant vertebrate model species in neurophenotyping neuroactive compounds and abuse drugs (Neelkantan et al., 2013; Kyzar and Kalueff, 2016). However, although a few recent studies have analyzed some of the addictive effects of METH in adult zebrafish (Mi et al., 2016; Zhu et al., 2017), information on the neurotoxic effects of the acute exposure to this stimulant drug is currently missing. One interesting potential advantage of using zebrafish for modeling methamphetamine neurotoxicity is that, as this animal is a vertebrate poikilotherm, it should be possible to perform mechanistic studies without the confounding factor of hyperthermia (Xie et al., 2000). In this study we have continuously exposed adult zebrafish to a METH dose of 40 mg/L for 48 h, and the effects on the brain monoaminergic profile, locomotor, anxiety-like and social behaviors as well as on the expression of key genes of the catecholaminergic system have been determined.

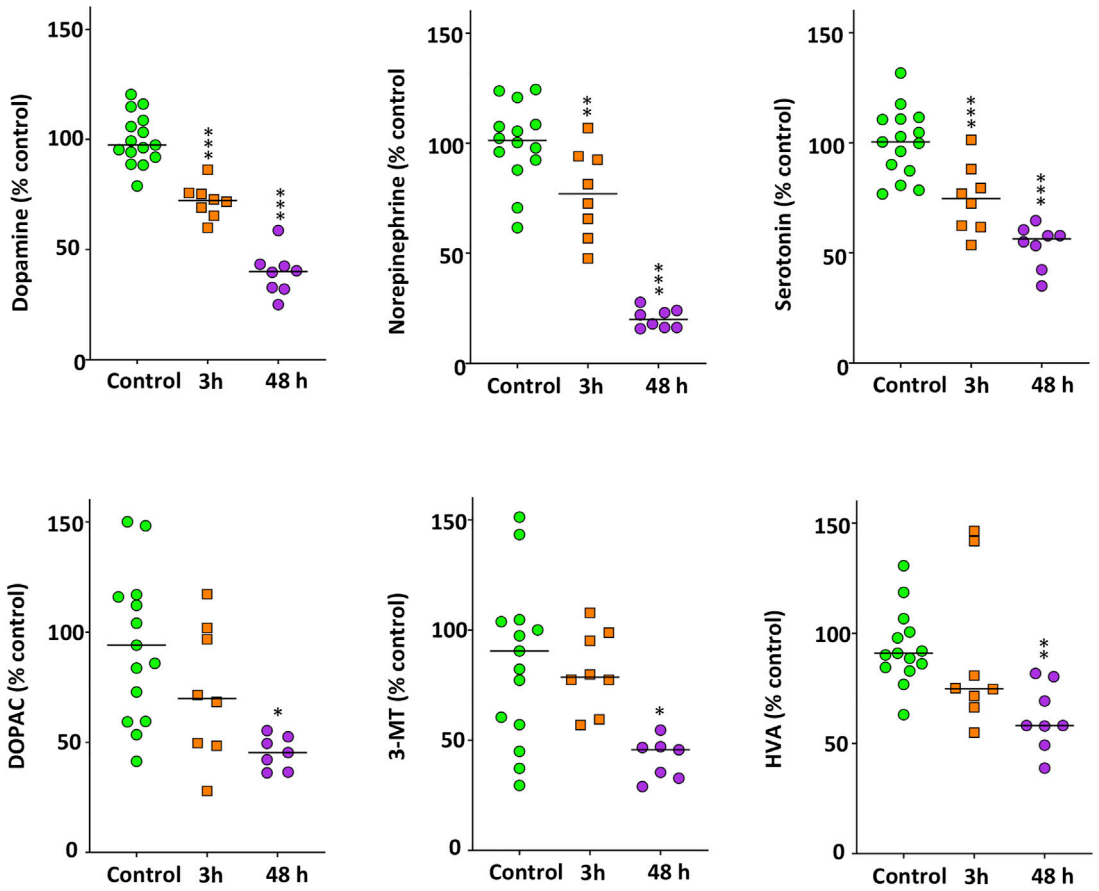

FIGURE 5 | Significant decrease in the monoaminergic neurotransmitters and other neurochemicals in the brain of zebrafish waterborne exposed to 40 mg/L methamphetamine for 3 and 48 h. In each experiment, levels of each neurochemical were normalized to the corresponding control values. For each neurochemical, the combined data is reported as scatter plot with the median (n = 7–8 for 3 h exposure and n = 15–16 for 48 h exposure), *p < 0.05, **p < 0.01, ***p < 0.001; one-way ANOVA with Dunnett's multiple comparison test (dopamine, norepinephrine, serotonin) or Kruskal Wallis test with Bonferroni correction (DOPAC, 3-MT, HVA). Data from two independent experiments.

METH levels determined in the brain of chronic human consumers are in the range 0.24–56.6 ng/mg brain tissue, and the distribution among the different brain areas seems quite homogeneous (Wilson et al., 1996; Kalasinsky et al., 2001; Moszczynska et al., 2004). Similarly, in rodents, METH levels determined in different brain areas after a binge of METH (5 injections of 12.5 mg/kg every 4 h) were about 8 ng/mg brain tissue (Danaceau et al., 2007). However, other authors reported higher METH levels (≈30 ng/mg brain tissue) in the whole brain of rats after similar dosing schedule (four to five injections of 11.5–15 mg/kg every 2–6 h interval) (Alburges et al., 1990; Gygi et al., 1996) (Alburger et al., 1990; Gygi et al., 1996). In our study, the average METH concentration in the brain of fish after 48 h of exposure to 40 mg/L METH was 18.8 ng/mg brain tissue, which is in the range of the described in human and rodent models. Peak plasma concentration of METH has been reported to occur as early as 3–5 h after dosing (Kalasinsky et al., 2001), which should be reflected in an early increase in brain levels of this drug. In this study, the average brain levels of METH 3 h after exposure were 9.19 ng/mg brain tissue suggesting a rapid increase in METH plasmatic levels, explaining some of the behavioral and neurochemical changes found at this time.

In mammalian models, after an initial release of DA and 5-HT, acute high doses of METH causes damage to dopaminergic and serotonergic axon terminals in the brain. As a result, a decrease in the DA and 5-HT in the brain is commonly used as a neurochemical marker of METH neurotoxicity (Yu et al., 2015). Similarly, a concentration- and time-dependent decrease in the levels of DA, NE and 5-HT were found in the brain of the treated fish. Moreover, the levels of the DA metabolites DOPAC, 3-MT and HVA also decreased after 48 h exposure to 40 mg/L METH, an effect probably related with the decreased DA levels, although it is not possible to discard the potential involvement of the monoamineoxidase (MAO) activity inhibition (Egashira and Yamanaka, 1993; Xie et al., 2000; Escubedo et al., 2011).

The observed changes in the neurochemical profile in the brain of the treated fish are consistent with the observed changes in behavior. First of all, the fact that fish exhibited a significant hyperactivity during the first hour of exposure to 40 mg/L METH,

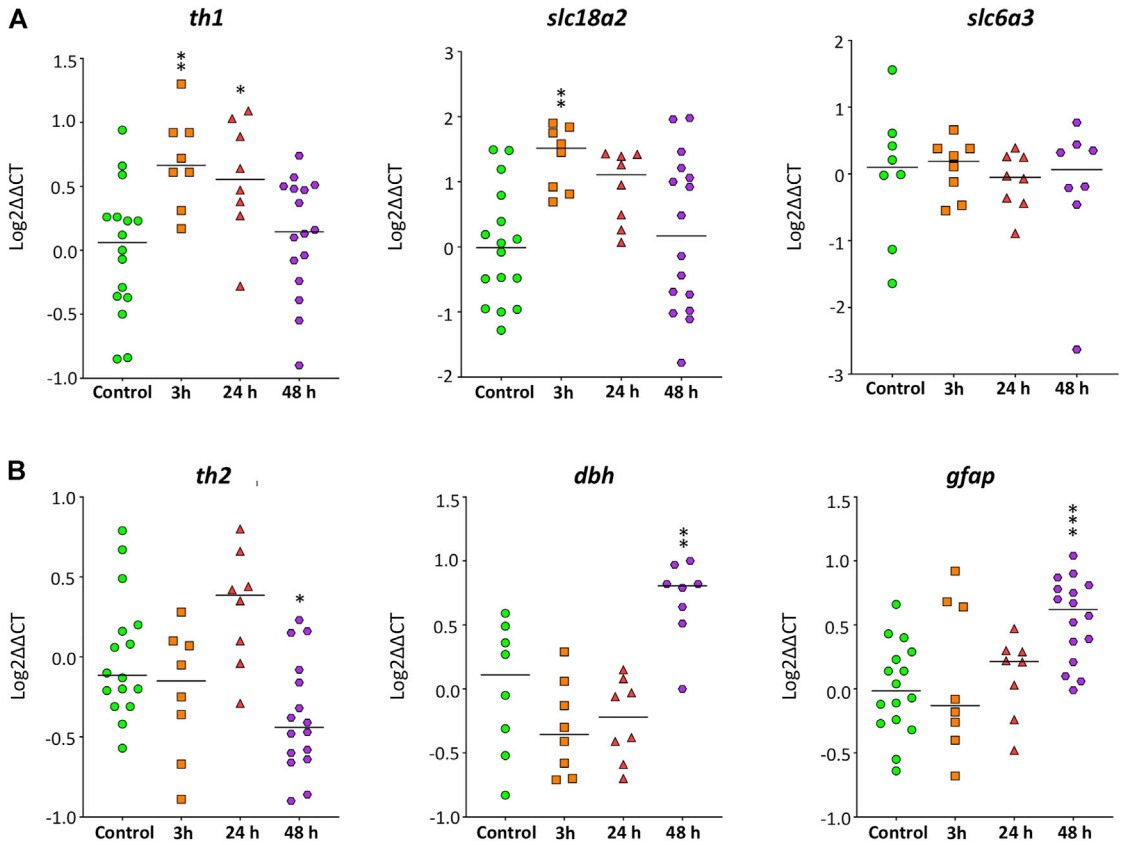

FIGURE 6 | Time-course of the expression of genes involved in the synthesis and transport of catecholamines and neuroinflammation in zebrafish brain after waterborne exposure to 40 mg/l methamphetamine. **(A)** Expression of *th1* and *slc18a2,* but nor *slc6a3* exhibits an early response to methamphetamine. **(B)** Expression of *th2*, *dbh* and *gfap* exhibits a late response. Data reported as scatter plot with the median. $^{*}p < 0.05$, $^{**}p < 0.01$; one-way ANOVA with Dunnett's multiple comparison test (*th1*, *th2*, *dbh*, *slc18a2*) or Kruskal Wallis test with Bonferroni correction (*slc6a3*, *gfap*). Data from two to three independent experiments (n = 8–16 for *th1*, *th2* and *gfap* and n = 8 for *slc18a2*, *dbh* and *slc6a3*).

and then the activity returned to the control values strongly suggest that after the initial release of DA, the levels of this neurotransmitter decline very fast. However, the similar distance moved by the control and treated fish in the locomotor activity assay by the end of the 3 h exposure period contrast with the highly significant decrease in mobility observed in the exposed fish during the 6 min of the NTT performed immediately after the 3 h exposure (**Supplementary Figure S3**). The important differences in the design of both behavioral assays might by behind the differences in the results. In the locomotor activity assay shoals of six fish are placed into experimental tanks and video-recorded for 180 min. Under these conditions, fish do not have stressful stimuli such as handling induced stress, novelty or social isolation. In the NTT, however, fish are transferred from the exposure tank (handling induced stress) to the observation tank (stress induced by a novel environment) individually (stress associate to social isolation). Interestingly, in the shoaling test, an assay where the fish is exposed to the stress associated with handling and the novel environment, but not to social isolation, no effects on mobility were observed 3 h after exposure, a result consistent with that obtained in the locomotor assay, another test performed on shoals. This result suggests that the interaction of METH with social isolation, a stressful stimulus in highly social species like zebrafish, is the behind of the observed differences in the mobility between the locomotor and NTT assays. In rodents and zebrafish, stressors have been shown to potentiate the effects of drugs on locomotor activity (Arias et al., 2010; Tran et al., 2016), but the effect of the interactions between neuroactive drugs and stressors on locomotor activity is generally difficult to interpret (Tran and Gerlai, 2016).

In this study METH-treated fish exhibited a significant effect on the anxiety-like behavior, spending more time on the bottom of the tank (positive geotaxis) and increasing the preference for the white background (negative scototaxis) compared to the corresponding controls. Positive geotaxis, with decreased time and distance in the top of the tank, has been previously reported in adult zebrafish acutely water-exposed to 5–10 mg/L D-amphetamine (Kyzar et al., 2013) and 2 mg/L METH (Mi et al., 2016).

Anxiety-like behaviors have been positively correlated with brain serotonin levels in the novel tank test, whereas this correlation is negative in the light/dark test (Maximino et al., 2016). For instance, when 5-HT levels were decreased with para-chlorophenylalanine (PCPA) in the brain of adult zebrafish,

animals exhibited positive geotaxis (increased time on the bottom) and negative scototaxis (decreased time on the dark background) (Maximino et al., 2013). These results are similar to the situation in zebrafish exposed to METH in the present study, with decreased brain levels of serotonin, positive geotaxis and negative scototaxis, strongly suggesting that the effects of METH on the anxiety-like behavior are mediated by the decrease in brain 5-HT.

In this study, METH-treated fish also exhibited impaired social behavior in both the shoaling test and the social preference test. This result is consistent with a number of studies with rats and monkeys, where the acute and chronic exposure to METH results in social withdrawal (reviewed in Homer et al., 2008). In humans, changes in social behavior also associated with METH abuse have been explained by impairments in social-cognitive function (Homer et al., 2008).

Expression of *slc18a2*, the gene encoding the vesicular monoamine transporter 2 (VMAT2), was upregulated after only 3 h of exposure, a finding suggesting a rapid inhibition of VMAT2 activity in the exposed fish. VMAT2 is one of the molecular targets of amphetamine and its derivatives. It's well known that the disruption of VMAT activity in mammalian models by genetic knockdown or by chemical inhibitors results in a significant decrease in brain monoaminergic neurotransmitters. Interestingly, the brain of *Vmat2* heterzygous mutant zebrafish also showed decreased levels of the monoaminergic neurotransmitters DA, NE and 5-HT, as well as some of their metabolites. Moreover, these mutants displayed altered anxiety-like behavior, with positive geotaxis and negative scototaxis (Wang et al., 2016). Although VMAT2 activity has not been determined in this study, the similarity between the neurochemical and behavioral phenotypes of the *Vmat2* mutants and the METH-treated fish suggests that VMAT inhibition plays also an essential role in the neurotoxic effects of METH in adult zebrafish.

Information about the effects on gene expression of METH and other amphetamine derivatives in zebrafish brain is very scarce. An early and transient upregulation *th1*, gene encoding the rate-limiting enzyme in the synthesis of catecholamines, has been found in fish acutely exposed to METH in this study. Acute exposure to METH has also been reported to induce a transient early overexpression of this gene in specific nuclei of rodent brain (Shishido et al., 1997; Ferrucci et al., 2007; Braun et al., 2011). Moreover, in the only study that to our knowledge has analyzed the effect of D-amphetamine on tyrosine hydroxylase transcription in fish (*Carassius auratus*), an early up-regulation was also found in the expression levels of this gene at the telencephalon (Volkoff, 2013). Interestingly, the tyrosine hydroxylase gene regulated by METH in this fish species is homologous to zebrafish *th1* (**Supplementary Figure S7**), the gene exhibiting an early upregulation by METH in our study. Treatment with high doses of METH induces a significant increase in PKCδ expression in the striatum, an effect resulting in a significant inhibition of TH activity by phosphorylation at Ser40 (Dunkley et al., 2004). The observed upregulation in *th* mRNA expression after high doses of METH might be a mechanism trying to counteract this inhibition in TH activity.

In contrast with the early increase in the expression of *th1* found in the brain of METH-exposed fish in this study, *th2* was found to be significant downregulated. Interestingly, *th2*, but not *th1*, was reduced in the telencephalon of zebrafish exposed to cocaine (Darland et al., 2012), an illicit drug also targeting dopaminergic system. Moreover, mild oxidative stress has been reported to induce a clear decrease in *th2*, but not in *th1* expression in zebrafish (Priyadarshini et al., 2013). Whereas we have not been able to detect oxidative stress in the whole brain of the exposed fish, it is not possible to discard the generation of oxidative stress at specific areas enriched in dopaminergic terminals. Therefore, the downregulation of *th2* found in the brain after 48 h of exposure to METH is probably a much more sensitive marker of oxidative stress at specific brain areas (Priyadarshini et al., 2013) than the LPO levels on the whole brain.

Whereas a persistent loss of DA transporter (DAT) in the cortex and caudate-putamen is one of the neurodegenerative changes observed in the brain of human addicts (Cadet and Krasnova, 2009), no differences in the expression on *slc6a3*, the gene encoding DAT, have been found in the brain of the exposed fish at any of the selected times. However, effects of METH at the protein and transcript levels are often different. For instance, METH challenges induced a significant decrease in DAT (protein) levels in the midbrain of rats, with no effect on *slc6a3* (transcript) levels (Krasnova et al., 2011). No differences in the expression of *slc6a3* were either found in the brain of METH conditioned preference place rats (Hensleigh and Pritchard, 2014).

Glial fibrillary acid protein (GFAP) is commonly used as an index of astroglial response to neuronal injury. In rodent models, METH exposure led to an up-regulation of GFAP, both at transcript and protein levels (Sriram et al., 2002, 2006; Shen et al., 2011; Robson et al., 2014). Therefore, the up-regulation in *gfap* expression observed in the brain of zebrafish after 48 h exposure to 40 mg/L METH is consistent with the effect of this drug on mammalian models.

Despite the early upregulation of *th1* and *slc18a2* expression observed in the brain of the METH-exposed fish, DA levels significantly decreased between the 3 and 48 h of exposure to 40 mg/L METH, a result suggesting a quick turnover rate for the recently synthesized TH and VMAT2 proteins induced by METH. However, other potential explanations to the absence of recovery of DA levels include a specific effect of METH on mRNA translation, post-translational modifications (Zhu et al., 2016) of TH and VMAT2 or a high rate of impairment of dopaminergic terminals by the end of the exposure period, as suggested by the significant increase in *gfap* expression, counteracting any potential increase in DA synthesis resulting from the early increase in *th1* expression.

Finally, an unexpected finding in this study has been that the brain of the exposed fish had levels of lipid peroxidation similar to those of controls. METH neurotoxicity has been reported to depend on the formation of DA quinones and superoxide radicals within the nerve terminals. Moreover, it is known that METH decreases the levels of reduced glutathione (GSH) and saturates the capacity of the antioxidant defense system, increasing lipid peroxidation in the dopaminergic neurons (Cadet and Krasnova, 2009). The most suitable

explanation to the absence of evidences of oxidative stress in this study is that oxidative stress is produced at the dopaminergic terminals, but the lipid peroxidation analysis has been performed on the whole brain. In this context, the increase in oxidative stress at very restricted locations would be diluted and non-detected when the whole brain is analyzed, as in our study. On the other hand, a number of studies support that the adult zebrafish brain exhibits an antioxidant defense system with high capacity. For instance, no lipid peroxidation was recently found in a zebrafish model for acute acrylamide neurotoxicity, despite the brain exhibited a total depletion of glutathione levels and a severely impaired thioredoxin system (Raldúa et al., 2020). No lipid peroxidation was either found in the brain of zebrafish treated with paraquat at concentrations inducing 30–40% lethality, although the exposure to this herbicide resulted in a decrease in the superoxide dismutase (SOD) activity, catalase activity and GSH content (Anand et al., 2021). However, in our study, only lipid peroxidation has been determined as indicator of oxidative stress, and the evaluation of the effects on the different components of the antioxidant defense system were out of the scope of the study. Moreover, another explanation for the lack of oxidative stress evidenced in our study could be related to the non-hyperthermic response in adult zebrafish since there are several mechanisms by which hyperthermia may enhance METH-induced neurotoxicity to DA terminals. It is known that METH-induced hyperthermia directly increases ROS formation in rats and mice striatum and cause an increase in ROS-induced gene expression (Cadet and Brannock, 1997; Imam et al., 2001; Krasnova et al., 2001; Cadet et al., 2007); for review see (Bowyer and Hanig, 2014). In fact, hyperthermia alone produces equivalent increases in genes up-regulated by ROS in some brain regions (Bowyer et al., 2013).

To sum up, data presented in this manuscript support the suitability of the adult zebrafish model for studying the neurotoxic effects of a binge-like methamphetamine exposure without to potential confounding factor of hyperthermia. Interestingly, the absence of oxidative stress in the phenotype of the brain of METH-treated fish has allowed to identify some relevant components of METH neurotoxicity that are oxidative stress-independent, such as the observed behavioral effects, the reduction of monoamines content, the effects on *th1, th2 and slc18a2* expression, as well as an astroglial response. However, further studies are needed in order to evaluate the presence of oxidative stress in the dopaminergic terminals and the different components of the antioxidant defense system of the exposed fish.

DATA AVAILABILITY STATEMENT

The raw data supporting the conclusions of this article will be made available by the authors, without undue reservation.

ETHICS STATEMENT

The animal study was reviewed and approved by Institutional Animal Care and Use Committees at the CID-CSIC (OH 1032/2020) and conducted in accordance with the institutional guidelines under a license from the local government (agreement number 9027).

AUTHOR CONTRIBUTIONS

JB, PD-G, MF and EP performed all the exposure experiments; JB, and PD-G performed all the behavioral analysis; MF performed the biochemical analysis; MB, PD-G, and CG-C performed the analysis of METH stability, neurochemical analysis and METH brain levels; EP, and JB performed the gene expression analysis; DR, RL-A, and EE were involved in the conception, design and interpretation of the data; DR wrote the manuscript with the input of CG-C, RL-A and EE.

FUNDING

This work was supported by Grants PID2020-113371RB-C21 and PID2019-109390RB-I00 funded by MCIN/AEI/ 10.13039/501100011033 and by ERDF A way of making Europe, as well as by Grant CEX2018-000794-S funded by MCIN/AEI/ 10.13039/501100011033. Moreover, J.B. was supported by Grant PRE2018-083513 funded by MCIN/AEI/10.13039/501100011033 and by ESF Investing in your future. The work was also partially supported by the Catalan Government through the network of recognized research groups (2017 SGR_902 (DR, EP) and 2017SGR979 (RL-A, EE)).

SUPPLEMENTARY MATERIAL

The Supplementary Material for this article can be found online at: https://www.frontiersin.org/articles/10.3389/fphar.2021.770319/full#supplementary-material

REFERENCES

Albertson, T. E., Derlet, R. W., and Van Hoozen, B. E. (1999). Methamphetamine and the Expanding Complications of Amphetamines. *West. J. Med.* 170, 214–219. Available at:/pmc/articles/PMC1305551/?report=abstract. (Accessed July 18, 2021).

Alburges, M. E., Hanson, G. R., and Gibb, J. W. (1990). Role of Methamphetamine Metabolism in the Development of CNS Tolerance the Drug. *Invest. Clín*, 165–176.

Anand, S. K., Sahu, M. R., and Mondal, A. C. (2021). Bacopaside-I Alleviates the Detrimental Effects of Acute Paraquat Intoxication in the Adult Zebrafish Brain. *Neurochem. Res.* 46, 3059–3074. doi:10.1007/s11064-021-03416-9

Ares-Santos, S., Granado, N., Oliva, I., O'Shea, E., Martin, E. D., Colado, M. I., et al. (2012). Dopamine D(1) Receptor Deletion Strongly Reduces Neurotoxic Effects of Methamphetamine. *Neurobiol. Dis.* 45, 810–820. doi:10.1016/j.nbd.2011.11.005

Arias, C., Solari, A. C., Mlewski, E. C., Miller, S., Haymal, B., Spear, N. E., et al. (2010). Social Isolation and Stress Related Hormones Modulate the Stimulating

Effect of Ethanol in Preweanling Rats. *Behav. Brain Res.* 211, 64–70. doi:10.1016/j.bbr.2010.03.010

Bowyer, J. F., and Hanig, J. P. (2014). Amphetamine- and Methamphetamine-Induced Hyperthermia: Implications of the Effects Produced in Brain Vasculature and Peripheral Organs to Forebrain Neurotoxicity. *Temperature (Austin)* 1, 172–182. doi:10.4161/23328940.2014.982049

Bowyer, J. F., Patterson, T. A., Saini, U. T., Hanig, J. P., Thomas, M., Camacho, L., et al. (2013). Comparison of the Global Gene Expression of Choroid Plexus and Meninges and Associated Vasculature under Control Conditions and after Pronounced Hyperthermia or Amphetamine Toxicity. *BMC Genomics* 14, 147. doi:10.1186/1471-2164-14-147

Braun, A. A., Herring, N. R., Schaefer, T. L., Hemmerle, A. M., Dickerson, J. W., Seroogy, K. B., et al. (2011). Neurotoxic (+)-methamphetamine Treatment in Rats Increases Brain-Derived Neurotrophic Factor and Tropomyosin Receptor Kinase B Expression in Multiple Brain Regions. *Neuroscience* 184, 164–171. doi:10.1016/j.neuroscience.2011.03.045

Cadet, J. L., and Brannock, C. (1997). Free Radicals and the Pathobiology of Brain Dopamine Systems. *Neurochem. Int.* 32, 117–131. doi:10.1016/S0197-0186(97)00031-4

Cadet, J. L., Krasnova, I. N., Jayanthi, S., and Lyles, J. (2007). Neurotoxicity of Substituted Amphetamines: Molecular and Cellular Mechanisms. *Neurotox. Res.* 11, 183–202. doi:10.1007/BF03033567

Cadet, J. L., and Krasnova, I. N. (2009). Molecular Bases of Methamphetamine-Induced Neurodegeneration. *Int. Rev. Neurobiol.* 88, 101–119. doi:10.1016/S0074-7742(09)88005-7

Carreño Gutiérrez, H., Colanesi, S., Cooper, B., Reichmann, F., Young, A. M. J., Kelsh, R. N., et al. (2019). Endothelin Neurotransmitter Signalling Controls Zebrafish Social Behaviour. *Sci. Rep.* 9, 3040. doi:10.1038/s41598-019-39907-7

Danaceau, J. P., Deering, C. E., Day, J. E., Smeal, S. J., Johnson-Davis, K. L., Fleckenstein, A. E., et al. (2007). Persistence of Tolerance to Methamphetamine-Induced Monoamine Deficits. *Eur. J. Pharmacol.* 559, 46–54. doi:10.1016/j.ejphar.2006.11.045

Darke, S., Kaye, S., McKetin, R., and Duflou, J. (2008). Major Physical and Psychological Harms of Methamphetamine Use. *Drug Alcohol. Rev.* 27, 253–262. doi:10.1080/09595230801923702

Darland, T., Mauch, J. T., Meier, E. M., Hagan, S. J., Dowling, J. E., and Darland, D. C. (2012). Sulpiride, but Not SCH23390, Modifies Cocaine-Induced Conditioned Place Preference and Expression of Tyrosine Hydroxylase and Elongation Factor 1α in Zebrafish. *Pharmacol. Biochem. Behav.* 103, 157–167. doi:10.1016/j.pbb.2012.07.017

Davidson, C., Gow, A. J., Lee, T. H., and Ellinwood, E. H. (2001). Methamphetamine Neurotoxicity: Necrotic and Apoptotic Mechanisms and Relevance to Human Abuse and Treatment. *Brain Res. Brain Res. Rev.* 36, 1–22. doi:10.1016/S0165-0173(01)00054-6

Dunkley, P. R., Bobrovskaya, L., Graham, M. E., Von Nagy-Felsobuki, E. I., and Dickson, P. W. (2004). Tyrosine Hydroxylase Phosphorylation: Regulation and Consequences. *J. Neurochem.* 91, 1025–1043. doi:10.1111/j.1471-4159.2004.02797.x

Egashira, T., and Yamanaka, Y. (1993). Changes in Monoamine Oxidase Activity in Mouse Brain Associated with D-Methamphetamine Dependence and Withdrawal. *Biochem. Pharmacol.* 46, 609–614. doi:10.1016/0006-2952(93)90545-8

Ellison, G., Eison, M. S., Huberman, H. S., and Daniel, F. (1978). Long-Term Changes in Dopaminergic Innervation of Caudate Nucleus after Continuous Amphetamine Administration. *Science* 201, 276–278. doi:10.1126/science.26975

Escubedo, E., Abad, S., Torres, I., Camarasa, J., and Pubill, D. (2011). Comparative Neurochemical Profile of 3,4-methylenedioxymethamphetamine and its Metabolite Alpha-Methyldopamine on Key Targets of MDMA Neurotoxicity. *Neurochem. Int.* 58, 92–101. doi:10.1016/j.neuint.2010.11.001

Escubedo, E., Guitart, L., Sureda, F. X., Jiménez, A., Pubill, D., Pallàs, M., et al. (1998). Microgliosis and Down-Regulation of Adenosine Transporter Induced by Methamphetamine in Rats. *Brain Res.* 814, 120–126. doi:10.1016/S0006-8993(98)01065-8

Faria, M., Valls, A., Prats, E., Bedrossiantz, J., Orozco, M., Porta, J. M., et al. (2019). Further Characterization of the Zebrafish Model of Acrylamide Acute Neurotoxicity: Gait Abnormalities and Oxidative Stress. *Sci. Rep.* 9, 7075. doi:10.1038/s41598-019-43647-z

Faria, M., Ziv, T., Gómez-Canela, C., Ben-Lulu, S., Prats, E., Novoa-Luna, K. A., et al. (2018). Acrylamide Acute Neurotoxicity in Adult Zebrafish. *Sci. Rep.* 8, 7918. doi:10.1038/s41598-018-26343-2

Ferrucci, M., Busceti, C. L., Nori, S. L., Lazzeri, G., Bovolin, P., Falleni, A., et al. (2007). Methamphetamine Induces Ectopic Expression of Tyrosine Hydroxylase and Increases Noradrenaline Levels within the Cerebellar Cortex. *Neuroscience* 149, 871–884. doi:10.1016/j.neuroscience.2007.07.057

Fleckenstein, A. E., Volz, T. J., and Hanson, G. R. (2009). Psychostimulant-induced Alterations in Vesicular Monoamine Transporter-2 Function: Neurotoxic and Therapeutic Implications. *Neuropharmacology* 56, 133–138. doi:10.1016/j.neuropharm.2008.07.002

Granado, N., Ares-Santos, S., Oliva, I., O'Shea, E., Martin, E. D., Colado, M. I., et al. (2011). Dopamine D2-Receptor Knockout Mice Are Protected against Dopaminergic Neurotoxicity Induced by Methamphetamine or MDMA. *Neurobiol. Dis.* 42, 391–403. doi:10.1016/j.nbd.2011.01.033

Green, J., Collins, C., Kyzar, E. J., Pham, M., Roth, A., Gaikwad, S., et al. (2012). Automated High-Throughput Neurophenotyping of Zebrafish Social Behavior. *J. Neurosci. Methods* 210, 266–271. doi:10.1016/j.jneumeth.2012.07.017

Gygi, M. P., Gygi, S. P., Johnson, M., Wilkins, D. G., Gibb, J. W., and Hanson, G. R. (1996). Mechanisms for Tolerance to Methamphetamine Effects. *Neuropharmacology* 35, 751–757. doi:10.1016/0028-3908(96)84647-8

Hensleigh, E., and Pritchard, L. M. (2014). The Effect of Early Environmental Manipulation on Locomotor Sensitivity and Methamphetamine Conditioned Place Preference Reward. *Behav. Brain Res.* 268, 66–71. doi:10.1016/j.bbr.2014.03.045

Homer, B. D., Solomon, T. M., Moeller, R. W., Mascia, A., DeRaleau, L., and Halkitis, P. N. (2008). Methamphetamine Abuse and Impairment of Social Functioning: A Review of the Underlying Neurophysiological Causes and Behavioral Implications. *Psychol. Bull.* 134, 301–310. doi:10.1037/0033-2909.134.2.301

Imam, S. Z., El-Yazal, J., Newport, G. D., Itzhak, Y., Cadet, J. L., Slikker, W., et al. (2001). Methamphetamine-induced Dopaminergic Neurotoxicity: Role of Peroxynitrite and Neuroprotective Role of Antioxidants and Peroxynitrite Decomposition Catalysts. *Ann. N Y Acad. Sci.* 939, 366–380. doi:10.1111/j.1749-6632.2001.tb03646.x

Jiang, M., Chen, Y., Li, C., Peng, Q., Fang, M., Liu, W., et al. (2016). Inhibiting Effects of Rhynchophylline on Zebrafish Methamphetamine Dependence Are Associated with Amelioration of Neurotransmitters Content and Down-Regulation of TH and NR2B Expression. *Prog. Neuropsychopharmacol. Biol. Psychiatry* 68, 31–43. doi:10.1016/j.pnpbp.2016.03.004

Jones, S. R., Gainetdinov, R. R., Wightman, R. M., and Caron, M. G. (1998). Mechanisms of Amphetamine Action Revealed in Mice Lacking the Dopamine Transporter. *J. Neurosci.* 18, 1979–1986. doi:10.1523/jneurosci.18-06-01979.1998

Kalasinsky, K. S., Bosy, T. Z., Schmunk, G. A., Reiber, G., Anthony, R. M., Furukawa, Y., et al. (2001). Regional Distribution of Methamphetamine in Autopsied Brain of Chronic Human Methamphetamine Users. *Forensic Sci. Int.* 116, 163–169. doi:10.1016/S0379-0738(00)00368-6

Kalueff, A. V., Stewart, A. M., and Gerlai, R. (2014). Zebrafish as an Emerging Model for Studying Complex Brain Disorders. *Trends Pharmacol. Sci.* 35, 63–75. doi:10.1016/j.tips.2013.12.002

Kish, S. J. (2008). Pharmacologic Mechanisms of crystal Meth. *CMAJ* 178, 1679–1682. doi:10.1503/cmaj.071675

Kita, T., Miyazaki, I., Asanuma, M., Takeshima, M., and Wagner, G. C. (2009). Dopamine-Induced Behavioral Changes and Oxidative Stress in Methamphetamine-Induced Neurotoxicity. *Int. Rev. Neurobiol.* 88, 43–64. doi:10.1016/S0074-7742(09)88003-3

Kobeissy, F. H., Mitzelfelt, J. D., Fishman, I., Morgan, D., Gaskins, R., Zhang, Z., et al. (2012). Methods in Drug Abuse Models: Comparison of Different Models of Methamphetamine Paradigms. *Methods Mol. Biol.* 829, 269–278. doi:10.1007/978-1-61779-458-2_17

Kolesnikova, T. O., Khatsko, S. L., Eltsov, O. S., Shevyrin, V. A., and Kalueff, A. V. (2019). When Fish Take a bath: Psychopharmacological Characterization of the Effects of a Synthetic Cathinone bath Salt 'flakka' on Adult Zebrafish. *Neurotoxicol. Teratol.* 73, 15–21. doi:10.1016/j.ntt.2019.02.001

Kolesnikova, T. O., Shevyrin, V. A., Eltsov, O. S., Khatsko, S. L., Demin, K. A., Galstyan, D. S., et al. (2021). Psychopharmacological Characterization of an Emerging Drug of Abuse, a Synthetic Opioid U-47700, in Adult Zebrafish. *Brain Res. Bull.* 167, 48–55. doi:10.1016/j.brainresbull.2020.11.017

Krasnova, I. N., Ladenheim, B., Hodges, A. B., Volkow, N. D., and Cadet, J. L. (2011). Chronic Methamphetamine Administration Causes Differential Regulation of Transcription Factors in the Rat Midbrain. *PLoS One* 6, e19179. doi:10.1371/journal.pone.0019179

Krasnova, I. N., Ladenheim, B., Jayanthi, S., Oyler, J., Moran, T. H., Huestis, M. A., et al. (2001). Amphetamine-induced Toxicity in Dopamine Terminals in CD-1 and C57BL/6J Mice: Complex Roles for Oxygen-Based Species and Temperature Regulation. *Neuroscience* 107, 265–274. doi:10.1016/S0306-4522(01)00351-7

Kyzar, E., Stewart, A. M., Landsman, S., Collins, C., Gebhardt, M., Robinson, K., et al. (2013). Behavioral Effects of Bidirectional Modulators of Brain Monoamines Reserpine and D-Amphetamine in Zebrafish. *Brain Res.* 1527, 108–116. doi:10.1016/j.brainres.2013.06.033

Kyzar, E. J., and Kalueff, A. V. (2016). Exploring Hallucinogen Pharmacology and Psychedelic Medicine with Zebrafish Models. *Zebrafish* 13, 379–390. doi:10.1089/zeb.2016.1251

Livak, K. J., and Schmittgen, T. D. (2001). Analysis of Relative Gene Expression Data Using Real-Time Quantitative PCR and the 2(-Delta Delta C(T)) Method. *METHODS* 25, 402–408. doi:10.1006/meth.2001.1262

Maximino, C., Puty, B., Benzecry, R., Araújo, J., Lima, M. G., de Jesus Oliveira Batista, E., et al. (2013). Role of Serotonin in Zebrafish (*Danio rerio*) Anxiety: Relationship with Serotonin Levels and Effect of Buspirone, WAY 100635, SB 224289, Fluoxetine and Para-Chlorophenylalanine (pCPA) in Two Behavioral Models. *Neuropharmacology* 71, 83–97. doi:10.1016/j.neuropharm.2013.03.006

Maximino, C., P. Costa, B., and G. Lima, M. M. (2016). A Review of Monoaminergic Neuropsychopharmacology in Zebrafish, 6 Years Later: Towards Paradoxes and Their Solution. *Cpsp* 5, 96–138. doi:10.2174/2211556005666160527105104

Mayol-Cabré, M., Prats, E., Raldúa, D., and Gómez-Canela, C. (2020). Characterization of Monoaminergic Neurochemicals in the Different Brain Regions of Adult Zebrafish. *Sci. Total Environ.* 745, 141205. doi:10.1016/j.scitotenv.2020.141205

Mi, G., Gao, Y., Yan, H., Jin, X., Ye, E., Liu, S., et al. (2016). l-Scoulerine Attenuates Behavioural Changes Induced by Methamphetamine in Zebrafish and Mice. *Behav. Brain Res.* 298, 97–104. doi:10.1016/j.bbr.2015.09.039

Moszczynska, A., Fitzmaurice, P., Ang, L., Kalasinsky, K. S., Schmunk, G. A., Peretti, F. J., et al. (2004). Why Is Parkinsonism Not a Feature of Human Methamphetamine Users? *Brain* 127, 363–370. doi:10.1093/brain/awh046

Neelkantan, N., Mikhaylova, A., Stewart, A. M., Arnold, R., Gjeloshi, V., Kondaveeti, D., et al. (2013). Perspectives on Zebrafish Models of Hallucinogenic Drugs and Related Psychotropic Compounds. *ACS Chem. Neurosci.* 4, 1137–1150. doi:10.1021/cn400090q

Priyadarshini, M., Orosco, L. A., and Panula, P. J. (2013). Oxidative Stress and Regulation of Pink1 in Zebrafish (*Danio rerio*). *PLoS One* 8, e81851. doi:10.1371/journal.pone.0081851

Pubill, D., Canudas, A. M., Pallàs, M., Camins, A., Camarasa, J., and Escubedo, E. (2003). Different Glial Response to Methamphetamine- and Methylenedioxymethamphetamine-Induced Neurotoxicity. *Naunyn. Schmiedebergs. Arch. Pharmacol.* 367, 490–499. doi:10.1007/s00210-003-0747-y

Pubill, D., Chipana, C., Camins, A., Pallàs, M., Camarasa, J., and Escubedo, E. (2005). Free Radical Production Induced by Methamphetamine in Rat Striatal Synaptosomes. *Toxicol. Appl. Pharmacol.* 204, 57–68. doi:10.1016/j.taap.2004.08.008

Raldúa, D., Casado, M., Prats, E., Faria, M., Puig-Castellví, F., Pérez, Y., et al. (2020). Targeting Redox Metabolism: the Perfect Storm Induced by Acrylamide Poisoning in the Brain. *Sci. Rep.* 10, 312. doi:10.1038/s41598-019-57142-y

Ricaurte, G. A., Guillery, R. W., Seiden, L. S., Schuster, C. R., and Moore, R. Y. (1982). Dopamine Nerve Terminal Degeneration Produced by High Doses of Methylamphetamine in the Rat Brain. *Brain Res.* 235, 93–103. doi:10.1016/0006-8993(82)90198-6

Robson, M. J., Turner, R. C., Naser, Z. J., McCurdy, C. R., O'Callaghan, J. P., Huber, J. D., et al. (2014). SN79, a Sigma Receptor Antagonist, Attenuates Methamphetamine-Induced Astrogliosis through a Blockade of OSMR/gp130 Signaling and STAT3 Phosphorylation. *Exp. Neurol.* 254, 180–189. doi:10.1016/j.expneurol.2014.01.020

Shabani, S., Houlton, S. K., Hellmuth, L., Mojica, E., Mootz, J. R., Zhu, Z., et al. (2016). A Mouse Model for Binge-Level Methamphetamine Use. *Front. Neurosci.* 10, 493. doi:10.3389/fnins.2016.00493

Shabani, S., Schmidt, B., Ghimire, B., Houlton, S. K., Hellmuth, L., Mojica, E., et al. (2019). Depression-like Symptoms of Withdrawal in a Genetic Mouse Model of Binge Methamphetamine Intake. *Genes Brain Behav.* 18, e12533. doi:10.1111/gbb.12533

Shen, H., Luo, Y., Yu, S. J., and Wang, Y. (2011). Enhanced Neurodegeneration after a High Dose of Methamphetamine in Adenosine A3 Receptor Null Mutant Mice. *Neuroscience* 194, 170–180. doi:10.1016/j.neuroscience.2011.08.013

Shin, E. J., Jeong, J. H., Hwang, Y., Sharma, N., Dang, D. K., Nguyen, B. T., et al. (2021). Methamphetamine-induced Dopaminergic Neurotoxicity as a Model of Parkinson's Disease. *Arch. Pharm. Res.* 44, 668–688. doi:10.1007/s12272-021-01341-7

Shishido, T., Watanabe, Y., Matsuoka, I., Nakanishi, H., and Niwa, S. (1997). Acute Methamphetamine Administration Increases Tyrosine Hydroxylase mRNA Levels in the Rat Locus Coeruleus. *Brain Res. Mol. Brain Res.* 52, 146–150. doi:10.1016/S0169-328X(97)00266-0

Sitte, H. H., Huck, S., Reither, H., Boehm, S., Singer, E. A., and Pifl, C. (1998). Carrier-mediated Release, Transport Rates, and Charge Transfer Induced by Amphetamine, Tyramine, and Dopamine in Mammalian Cells Transfected with the Human Dopamine Transporter. *J. Neurochem.* 71, 1289–1297. doi:10.1046/j.1471-4159.1998.71031289.x

Sriram, K., Benkovic, S. A., Miller, D. B., and O'Callaghan, J. P. (2002). Obesity Exacerbates Chemically Induced Neurodegeneration. *Neuroscience* 115, 1335–1346. doi:10.1016/S0306-4522(02)00306-8

Sriram, K., Miller, D. B., and O'Callaghan, J. P. (2006). Minocycline Attenuates Microglial Activation but Fails to Mitigate Striatal Dopaminergic Neurotoxicity: Role of Tumor Necrosis Factor-Alpha. *J. Neurochem.* 96, 706–718. doi:10.1111/j.1471-4159.2005.03566.x

Stewart, A., Wong, K., Cachat, J., Gaikwad, S., Kyzar, E., Wu, N., et al. (2011). Zebrafish Models to Study Drug Abuse-Related Phenotypes. *Rev. Neurosci.* 22, 95–105. doi:10.1515/RNS.2011.011

Stewart, A. M., Braubach, O., Spitsbergen, J., Gerlai, R., and Kalueff, A. V. (2014). Zebrafish Models for Translational Neuroscience Research: From Tank to Bedside. *Trends Neurosci.* 37, 264–278. doi:10.1016/j.tins.2014.02.011

Sulzer, D., Chen, T. K., Lau, Y. Y., Kristensen, H., Rayport, S., and Ewing, A. (1995). Amphetamine Redistributes Dopamine from Synaptic Vesicles to the Cytosol and Promotes Reverse Transport. *J. Neurosci.* 15, 4102–4108. doi:10.1523/jneurosci.15-05-04102.1995

Tran, S., Nowicki, M., Fulcher, N., Chatterjee, D., and Gerlai, R. (2016). Interaction between Handling Induced Stress and Anxiolytic Effects of Ethanol in Zebrafish: A Behavioral and Neurochemical Analysis. *Behav. Brain Res.* 298, 278–285. doi:10.1016/j.bbr.2015.10.061

Tran, S., and Gerlai, R. (2016). The Novel Tank Test: Handling Stress and the Context Specific Psychopharmacology of Anxiety. *Cpsp* 5, 169–179. doi:10.2174/2211556005666160519144414

Volkoff, H. (2013). The Effects of Amphetamine Injections on Feeding Behavior and the Brain Expression of Orexin, CART, Tyrosine Hydroxylase (TH) and Thyrotropin Releasing Hormone (TRH) in Goldfish (*Carassius auratus*). *Fish. Physiol. Biochem.* 39, 979–991. doi:10.1007/s10695-012-9756-4

Wang, Y., Li, S., Liu, W., Wang, F., Hu, L. F., Zhong, Z. M., et al. (2016). Vesicular Monoamine Transporter 2 (Vmat2) Knockdown Elicits Anxiety-like Behavior in Zebrafish. *Biochem. Biophys. Res. Commun.* 470, 792–797. doi:10.1016/j.bbrc.2016.01.079

Wilson, J. M., Kalasinsky, K. S., Levey, A. I., Bergeron, C., Reiber, G., Anthony, R. M., et al. (1996). Striatal Dopamine Nerve Terminal Markers in Human, Chronic Methamphetamine Users. *Nat. Med.* 2, 699–703. doi:10.1038/nm0696-699

Xie, T., McCann, U. D., Kim, S., Yuan, J., and Ricaurte, G. A. (2000). Effect of Temperature on Dopamine Transporter Function and Intracellular Accumulation of Methamphetamine: Implications for Methamphetamine-Induced Dopaminergic Neurotoxicity. *J. Neurosci.* 20, 7838–7845. doi:10.1523/jneurosci.20-20-07838.2000

Yu, S., Zhu, L., Shen, Q., Bai, X., and Di, X. (2015). Recent Advances in Methamphetamine Neurotoxicity Mechanisms and its Molecular Pathophysiology. *Behav. Neurol.* 2015, 1–11. doi:10.1155/2015/103969

Zhu, C., Liu, W., Luo, C., Liu, Y., Li, C., Fang, M., et al. (2017). Inhibiting Effects of Rhynchophylline on Methamphetamine-dependent Zebrafish Are Related with the Expression of Tyrosine Hydroxylase (TH). *Fitoterapia* 117, 47–51. doi:10.1016/j.fitote.2017.01.001

Zhu, L., Li, J., Dong, N., Guan, F., Liu, Y., Ma, D., et al. (2016). MRNA Changes in Nucleus Accumbens Related to Methamphetamine Addiction in Mice. *Sci. Rep.* 6, 36993. doi:10.1038/srep36993

Conflict of Interest: The authors declare that the research was conducted in the absence of any commercial or financial relationships that could be construed as a potential conflict of interest.

Publisher's Note: All claims expressed in this article are solely those of the authors and do not necessarily represent those of their affiliated organizations, or those of the publisher, the editors and the reviewers. Any product that may be evaluated in this article, or claim that may be made by its manufacturer, is not guaranteed or endorsed by the publisher.

frontiers in Pharmacology

ORIGINAL RESEARCH
published: 16 February 2022
doi: 10.3389/fphar.2022.822111

Metabolic Consequences of Developmental Exposure to Polystyrene Nanoplastics, the Flame Retardant BDE-47 and Their Combination in Zebrafish

*Raphaël Chackal[1†], Tyler Eng[1†], Emille M. Rodrigues[2], Sara Matthews[3], Florence Pagé-Lariviére[4], Stephanie Avery-Gomm[4], Elvis Genbo Xu[5], Nathalie Tufenkji[3], Eva Hemmer[2] and Jan A. Mennigen[1]**

[1]Department of Biology, University of Ottawa, Ottawa, ON, Canada, [2]Department of Chemistry and Biomolecular Sciences, University of Ottawa, Ottawa, ON, Canada, [3]Department of Chemical Engineering, McGill University, Montréal, QC, Canada, [4]National Wildlife Research Center, Environment and Climate Change Canada, Ottawa, ON, Canada, [5]Department of Biology, University of Southern Denmark, Odense, Denmark

OPEN ACCESS

Edited by:
Anna Siebel,
Universidade Comunitária da Região de Chapecó, Brazil

Reviewed by:
Ricieri Mocelin,
Universidade Federal da Fronteira Sul, Brazil
Frederick E. Williams,
University of Toledo, United States

***Correspondence:**
Jan A. Mennigen
jan.mennigen@uottawa.ca

[†]These authors have contributed equally to this work

Specialty section:
This article was submitted to Predictive Toxicology, a section of the journal Frontiers in Pharmacology

Received: 25 November 2021
Accepted: 17 January 2022
Published: 16 February 2022

Citation:
Chackal R, Eng T, Rodrigues EM, Matthews S, Pagé-Lariviére F, Avery-Gomm S, Xu EG, Tufenkji N, Hemmer E and Mennigen JA (2022) Metabolic Consequences of Developmental Exposure to Polystyrene Nanoplastics, the Flame Retardant BDE-47 and Their Combination in Zebrafish. Front. Pharmacol. 13:822111. doi: 10.3389/fphar.2022.822111

Single-use plastic production is higher now than ever before. Much of this plastic is released into aquatic environments, where it is eventually weathered into smaller nanoscale plastics. In addition to potential direct biological effects, nanoplastics may also modulate the biological effects of hydrophobic persistent organic legacy contaminants (POPs) that absorb to their surfaces. In this study, we test the hypothesis that developmental exposure (0–7 dpf) of zebrafish to the emerging contaminant polystyrene (PS) nanoplastics (⌀100 nm; 2.5 or 25 ppb), or to environmental levels of the legacy contaminant and flame retardant 2,2′,4,4′-Tetrabromodiphenyl ether (BDE-47; 10 ppt), disrupt organismal energy metabolism. We also test the hypothesis that co-exposure leads to increased metabolic disruption. The uptake of nanoplastics in developing zebrafish was validated using fluorescence microscopy. To address metabolic consequences at the organismal and molecular level, metabolic phenotyping assays and metabolic gene expression analysis were used. Both PS and BDE-47 affected organismal metabolism alone and in combination. Individually, PS and BDE-47 exposure increased feeding and oxygen consumption rates. PS exposure also elicited complex effects on locomotor behaviour with increased long-distance and decreased short-distance movements. Co-exposure of PS and BDE-47 significantly increased feeding and oxygen consumption rates compared to control and individual compounds alone, suggesting additive or synergistic effects on energy balance, which was further supported by reduced neutral lipid reserves. Conversely, molecular gene expression data pointed to a negative interaction, as co-exposure of high PS generally abolished the induction of gene expression in response to BDE-47. Our results demonstrate that co-exposure to emerging nanoplastic contaminants and legacy contaminants results in cumulative metabolic disruption in early development in a fish model relevant to eco- and human toxicology.

Keywords: brominated flame retardants, legacy contaminants, nanoplastics, emerging contaminant, energy metabolism, gene expression, cumulative effects

1 INTRODUCTION

As the rapidly increasing production of plastic overwhelms the world's ability to efficiently manage its disposal, plastic pollution has quickly become one of the most pressing environmental issues. Since 2013, the global annual production of plastic has exceeded 300 million tonnes (Mt) with rates reaching as high as 368 Mt in 2019 (www.plasticseurope.org). Due to their durability, low recycling rates and poor waste management, a significant portion of the plastic produced worldwide enters and persists in marine and, to a lesser degree, freshwater aquatic ecosystems (Barnes et al., 2009; Lebreton et al., 2017). It has been estimated that between 4.8 and 12.7 MT of plastic infiltrate oceans every year from coastal populations worldwide (Lebreton et al., 2017). In freshwater samples from the Western Lake Superior, estuary and harbour samples averaged 54,000 plastic particles/km^2, followed by open water samples averaging 38,000 particles/km^2 and then nearshore samples averaging 28,000 particles/km^2 (Hendrickson et al., 2018).

Once released into aquatic systems, plastics are exposed to varying weathering conditions; factors such as water turbulence, erosion and intense sunlight exposure degrade large plastic fragments into increasingly smaller particles on the micro- and nanosized scales (Ter Halle et al., 2017). Nanoplastics are small plastic particles that exhibit characteristics distinct from microplastics (Gigault et al., 2021). Polystyrene (PS) plastics are among the most abundant plastics detected in aquatic ecosystems. A study of microplastic pollution in the Bohai Sea, a model chosen because it is almost entirely enclosed by land and thus exhibits limited self-cleaning abilities, found PS to be the third most abundant plastic particle after polyethene and polypropylene (Zhang et al., 2017). In another study, water samples obtained from the coastlines of the Canterbury region of New Zealand showed that PS made up 55% of all particles identified (Clunies-Ross et al., 2016).

While the hazards associated with macro- and microplastics to aquatic organisms are relatively well characterized, the bioaccumulation and toxicity of nanoplastics are only beginning to be considered even though they could potentially be more hazardous (Koelmans et al., 2015b; Mitrano et al., 2021). Thus far, several studies have shown that nanoplastics can transport through the food web (Mattsson et al., 2017), translocate between organs in the body (Farrell and Nelson, 2013) and transfer from mothers to offspring (Pitt et al., 2018). The potential of PS nanoplastic particles to bioconcentrate through dietary exposure was established in a study exploring the accumulation of fluorescent particles in the food chain (Chae et al., 2018). The study involved phytoplankton *Chlamydomonas reinhardtii* (a producer), zooplankton *Daphnia magna* (primary consumer), *Oryzias sinensis* (secondary consumer) and dark chub *Zacco temmincki* (tertiary consumer). Although only the phytoplankton was exposed to 50 mg/L of PS nanoplastics, microscopic observations demonstrated that PS nanoplastic particles were present in digestive organs of the primary, secondary, and tertiary consumers. The accumulated nanoplastic further penetrated fish embryos and was detected in their yolk sac (Chae et al., 2018). The concern for plastic particles to reach higher trophic levels extends to humans (Farrell and Nelson, 2013; Watts et al., 2014). A study examining human colectomy specimens in long-time coastal residents found on average 28.1 particles/g tissue (Ibrahim et al., 2021). Microplastics were detected in human stool in the order of 2 microplastic particles/g (Schwabl et al., 2019). A recent study estimated that globally, on average, humans may ingest 0.1–5 g of microplastics weekly through various exposure pathways (Senathirajah et al., 2021). While less information on human tissue levels is currently available for nanoplastics, these studies reveal that nanoplastics may, in addition to ecotoxicological concerns, also pose a direct risk to human health (Revel et al., 2018). In addition to the possibility to elicit biological effects independently, nanoplastics such as PS have been shown to interact with persistent organic pollutants (POP) (Lee et al., 2014) like BDE-47 (Xu et al., 2019; Sun et al., 2021). Such interactions have raised the question of potential vector or sequestering effects of nanoplastic with regard to POPs, which may promote bioaccumulation of POPs on the one hand or limit their bioavailability on the other. Thus, the investigation of the combined biological effects of nanoplastic and POP mixtures in freshwater fish is warranted.

2,2′,4,4′-Tetrabromodiphenyl ether (BDE-47), a Polybrominated Diphenyl Ether (PBDE) is one example of a legacy POP with an absorption capacity that is particularly high for PS compared to other microplastics (Xu et al., 2019). Historically used in PBDE mixtures as a flame retardant in materials including polyurethane and firefighting foam, BDE-47 has been voluntarily phased out in Europe since 2003 and in the U.S. since 2004. However, due to its chemical inertness and physicochemical properties including a high octanol-water partition coefficient (K_{OW}) of 6.57, significant amounts of the world's water, terrestrial land, and most animals and humans contain traces of BDE-47: In United Kingdom and United States freshwater lakes, average ΣBDE water sample concentrations largely dominated by BDE-47 were reported in the pg/L range (Streets et al., 2006; Yang et al., 2014). BDE-47 is also the predominant BDE species in Great Lake top predator fish, which after peaking at ~150 ng/g in 2000 have declined to concentrations <50 ng/g in 2015 (Zhou et al., 2019). BDE-47 is also of concern to humans, who are exposed via water, food and atmosphere (Webster et al., 2005). Concentrations of BDE-47 in humans in North America are approximately 35 ng/g of lipid (Hites, 2004). In addition to its propensity to bioconcentrate and biomagnify (Kamel et al., 2012), BDE-47 is transferred to offspring *via* egg deposition in fish (Wen et al., 2015) and placental transfer and lactation in mammals (Mazdai et al., 2003; Frederiksen et al., 2010; Koenig et al., 2012). These data highlight concerns regarding consequences of developmental BDE-47 exposure in multiple species (Mohammed, 2013).

Among the biological effects of both PS nanoplastics and BDE-47 exposure, evidence points to energy metabolism as a common endpoint. In fish, PS nanoplastics have been reported to affect morphometric parameters such as body weight, behaviours relevant to organismal energy balance such as feed-intake, interfere with intestinal nutrient absorption (Jovanović, 2017), dysregulate glucose and lipid metabolism (Cedervall et al., 2012; Brun et al., 2019), and reduce

mitochondrial function (Trevisan et al., 2019). Similar effects on energy metabolism are emerging from studies in mammalian systems (Yee et al., 2021). In fish, BDE-47 has been demonstrated to reduce body weight (Torres et al., 2013), induce motor deficits (Chen et al., 2012) and disrupt mitochondrial biogenesis, dynamics and function (Zhuang et al., 2020). Effects of BDE-47 on energy metabolism are corroborated by epidemiological and rodent model studies, which support a role for developmental BDE-47 exposure in the etiology of diabetes and associated perturbations in glucose and lipid metabolism (McIntyre et al., 2015; Zhang et al., 2016; Wang D et al., 2018).

Taking advantage of the high-throughput zebrafish model relevant to eco- and human toxicology (Dai et al., 2014; Garcia et al., 2016; Bambino and Chu, 2017), early development (Kimmel et al., 1995) and metabolic disease (Seth et al., 2013; Benchoula et al., 2019), we here test the hypothesis that (I) acute developmental exposure to PS or environmental levels of BDE-47 alone disrupts larval energy metabolism and (II) their mixture will exacerbate metabolic disruption.

2 MATERIALS AND METHODS

2.1 Validation of PS Nanoplastic Uptake by Fluorescence Microscopy

To validate bioaccumulation of PS nanoparticles in wildtype TU strain zebrafish, eleutheroembryos were either left unexposed (n = 3) or exposed to Firefli Fluorescent Green labelled 100 nm ⌀ PS nanoplastics (Catalogue # G100, Thermo-Fisher Scientific, Ottawa, ON, Canada) at concentrations of 2.5 (n = 3) and 25 ppm (n = 3) in a glass Petri dish containing 25 ml of RO salt-dosed (Instant Ocean, PetSmart, Ottawa, ON, Canada) University of Ottawa Aquatics Facility system water (pH = 7.4, conductivity = μS) maintained at 28°C and from 0–7 days post fertilization (dpf) under a 12:12 L:D photoperiod. Prior to experimental use, particles were dialyzed to remove free dye and additives from the PS nanoparticle formulation as previously described (Pikuda et al., 2019; Xu et al., 2019). Zebrafish were euthanized with tricaine at 7 dpf, fixed in 4% PFA at 4°C o/n and then transferred to 80% ethanol. Whole zebrafish were placed on a glass slide and imaged using a custom-built microscope (IMA Upconversion by PhotonEtc, Montreal, QC, Canada) equipped with an inverted optical microscope (Nikon Eclipse Ti-U), a broadband camera for color imaging, a Princeton Instruments ProEM EMCCD camera for detection of visible emission, a Nikon halogen lamp (IntensiLight 100 W) with a single band FITC filter cube for 490 nm light excitation and 509 nm emission, collected epifluorescently, to screen for PS nanoplastic-emitted fluorescence at the University of Ottawa. To assess tissue-specific PS uptake, adult zebrafish were exposed to fluorescently labelled PS for a period of 4 days in a separate experiment, and tissues processed and analyzed at the Advanced Bioimaging Facility at McGill University as described in **Supplementary Figure S1**.

2.2 Developmental Exposure of Zebrafish (eleuthero)embryos to PS, BDE-47 and Their Combination

To assess metabolic consequences of developmental exposure to PS nanoplastics, BDE-47 and their combination, wildtype TU embryos from multiple breeding pairs were pooled and subsequently randomly divided into 6 treatment groups (n = 50 embryos/Petri dish) and exposed to prepared stocks of DMSO vehicle control (<0.001% v/v), dialyzed (Xu et al., 2019), unlabelled 100 nm ⌀ PS nanoplastics (Catalogue # 5010A, Thermo-Fisher Scientific) at 2.5 (low) or 25 ppm (high), 10 ppt analytical grade >97% purity BDE-47 (Catalogue # 91,834 Sigma-Aldrich, Oakville, ON Canada), or their combinations from 0–7 dpf under 12:12 L:D photoperiod in a static, single pulse exposure (**Figure 1**). All groups were exposed in glass Petri dishes filled with 25 ml of University of Ottawa Aquatic Facility RO-distilled and salt-dosed 28°C system water. In absence of available direct measurements of nanoplastic concentration in natural aquatic environments (Koelmans et al., 2015a), nanoplastic concentrations were based on reported freshwater microplastic ranges (Lu et al., 2021). Multiple cohorts were exposed to obtain necessary sample numbers for three replicate assays for each organismal endpoint measured during the exposure period (**Figure 1**). Sample sizes were determined a priori based on previous studies reporting metabolic disruption following developmental contaminant exposures in zebrafish larvae in our lab (Tu et al., 2019; Martínez et al., 2020). To avoid contamination or contaminant transfer between cohorts, a three-step treatment process was used. Following manual cleaning with soap and deionized water, the equipment was dried with paper towels and rinsed with hexane. Finally, dishes were rinsed with acetone, dried and cleaned with molecular grade distilled water. All experimental protocols were approved by the University of Ottawa's Animal Care and Veterinary Service (BL-2786). While following recommended parameter guidelines (water quality, photoperiod, temperature) specified in OECD guidelines for test number 210—Fish, Early-life stage Toxicity test (https://doi.org/10.1787/9789264203785-en), our experimental design deviates from the recommended exposure duration for zebrafish. Thus, while start of exposure occurs prior to blastodisc cleavage, our experimental duration (0-7 dpf) is, while in line with previous contaminant exposures preceding beginning sexual differentiation (Tu et al., 2019), shorter than the recommended zebrafish exposure duration 0–30 dpf.

2.3 Assessment of the Organismal-Level Metabolic Phenotype

2.3.1 Morphometric Parameters

Body length and lateral surface area of eleutheroembryos (5 dpf) were quantified by an investigator blind to the treatment groups on ImageJ using images captured with a stereomicroscope (Nikon SMZ 1500) and the Lumenera Infinity 2 camera and Infinity

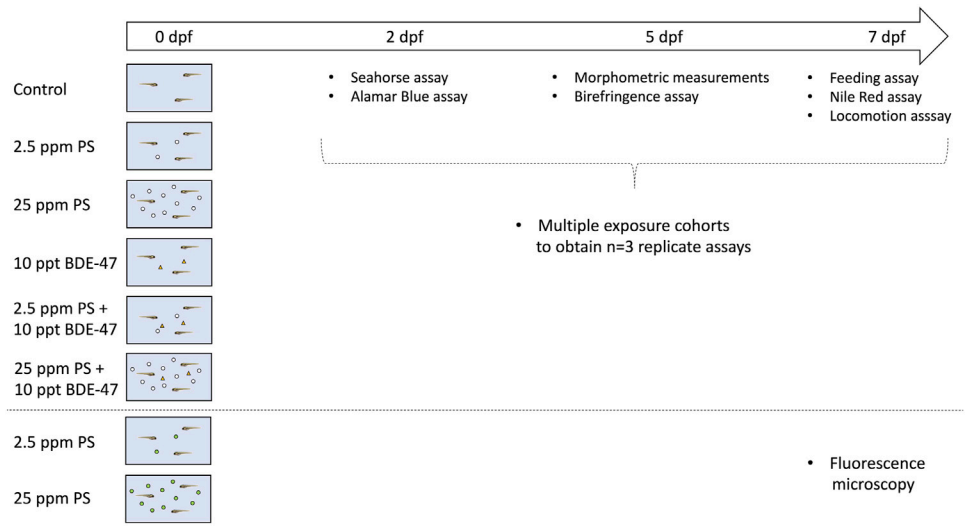

FIGURE 1 | Schematic representation of the experimental design.

Capture software (Teledyne Lumenera, Ottawa, ON, Canada) as previously described (Martínez et al., 2020). A subset of the same specimens was subsequently used to assess myofilament organization using a birefringence assay as previously described (Berger et al., 2012; Smith et al., 2013; Martínez et al., 2020). Briefly, following bright-field microscopy imaging, a subsequent picture of the eleutheroembryos was taken immediately afterward using two perpendicularly placed 77 mm circular polarizing lenses (MC CPL 77 mm, AmazonBasics, Seattle, United States) to visualize and image birefringence created from the diffraction of polarised light through the pseudo-crystalline array of the muscle sarcomeres. Care was taken to maintain eleutheroembryo position between images. Birefringence intensity was analyzed using ImageJ and normalized to the whole-body area of the larvae. A total of three cohorts were analyzed reaching a total n = 20–23 per treatment group for length and surface area measurements and a subset of n = 12–19 per treatment group for birefringence assay measurements. The difference in sample size in the birefringence assay is due to removal of larvae imaged in curved positioning prior to analysis, as these result in strongly reduced birefringence readings.

2.3.2 Feeding Behaviour

Food consumption was quantified by feeding zebrafish (7 dpf) with food labelled with a lipophilic fluorescent dye as described previously (Tu et al., 2019; Martínez et al., 2020). Briefly, 30 µL of 4-Di-10-ASP (4-(4-(Didecylamino)styryl)-N-Methylpyridinium iodide) (Thermo-Fisher Scientific) were dissolved in 1.47 ml of analytical grade acetone and mixed with 300 mg of G75 zebrafish feed (Skretting, Stavanger, Norway). The feed was allowed to saturate, covered by tinfoil and then dried under the fumehood in a glass Petri dish for 48 h at RT. Each group of treated zebrafish was fed with excess labelled food and allowed to feed for 1 h in a dark incubator at 27°C. One control group received unlabelled food under the same conditions to assess background fluorescence. After 1 h, fish were anesthetized with tricaine to suspend feeding. An n = 9 larvae were collected and pooled as replicate in a microcentrifuge tube, and n = 12 pooled replicates were collected per treatment group. Using a micropipette, the water was carefully removed, and larvae were washed repeatedly and finally resuspended in 300 µL of molecular biology grade water. Each pooled replicate was then homogenized using a Pellet Pestle™ homogenizer (Thermo-Fisher Scientific). 250 µL of homogenate was then placed into individual wells of a 96-well Nunc™ Microplate™ (Thermo-Fisher, Scientific) and plates analyzed for fluorescence emission using the SpectraMax Gemini fluorometer (Molecular Devices, Sunnyvale, CA, United States). The excitation wavelength used was 485 nm and the measured emission wavelength was 530 nm. The average background fluorescence values were subtracted from measured values and obtained measurements normalized to average control group values to depict fold-change. A total of three cohorts were analyzed reaching a combined sample size of n = 12 per treatment group.

2.3.3 Neutral Lipid Storage

Neutral lipid deposition was measured in 7 dpf larvae using Nile Red (9-Diethylamino-5H-benzo [alpha]phenoxazine-5-one, Sigma-Aldrich), a lipophilic fluorescent stain (Jones et al., 2008; Minchin and Rawls, 2017). Nile red stock was diluted in analytical grade acetone to a concentration of 500 µg/ml. This was then diluted 1:100 in system water and larvae were maintained in 10 ml of this solution for 30 min in the dark at 27°C. Larvae were then rinsed twice in system water and anesthetized with tricaine. Each larva was imaged under a fluorescent stereomicroscope with a super high-pressure mercury lamp (Nikon SMZ 1500). Images were captured with a Lumenera Infinity 2 camera using a Texas Red filter and processed using the Infinity Capture software (Teledyne Lumenera, Ottawa, ON, Canada). All images were

taken at the same exposure settings and magnification. Fluorescence was quantified using ImageJ and Nile red stains were normalized to the lateral body area of the fish. A total of three cohorts were analyzed reaching a combined sample size of $n = 18–22$ per treatment group. All images were renamed prior to analysis to assure the experimenter was blind to specific treatment groups during analysis.

2.3.4 Oxidative Metabolism

2.3.4.1 Oxygen Consumption Rate Measurement

The baseline oxygen consumption rate was assessed in 2 dpf eleutheroembryos using a Seahorse Xf24 Analyzer (Agilent, Mississauga, ON, Canada) as previously described (Tu et al., 2019). Briefly, eleutheroembryos were rinsed in Aquatic Facility system water and individually transferred into a 24-well Islet capture plate (#101122–100, Agilent) in 500 µL Aquatic Facility system water using a micropipette. Each well was then sealed using a mesh. Cartridges were prepared 24 h in advance and allowed to equilibrate with calibration solution in a 27°C incubator o/n. A total of three cohorts were analyzed reaching a combined sample size of n = 7-9 per treatment group.

2.3.4.2 Oxidative Metabolism-Dependent Energy Expenditure Assay

Cumulative oxygen metabolism-dependent energy expenditure was assessed over a 24 h in 2 dpf eleutheroembryos using the Alamar Blue assay, which is dependent on a NADH-, NADPH-based reduction of Alamar Blue (resazurin) and has been described as proxy to quantify zebrafish oxidative metabolism (Renquist et al., 2013; Williams and Renquist, 2016; Reid et al., 2018). Briefly, eleutheroemberyos from each treatment group were transferred to a solution made up of 0.3 ml Alamarblue Cell Viability Reagent (Thermo-Fisher Scientific), 3.0 ml of 4 mM $NaHCO_3$ (aq), 0.03 ml DMSO, and 26.67 ml of system water. Individual eleutheroembryos were then captured in 200 µL of this solution using a micropipette and dispensed into a 96-well plate. The plate was incubated at 27°C in the dark incubator until reading. Two blank wells not containing eleutheroembryos were also prepared for each group and used to acquire the background readings for a 24 h incubation of solution alone. Each plate was then placed in a fluorometer (Molecular Devices) to measure NADH/NADPH emission at 590 nm following excitation at 530 nm. Readings were normalized by subtraction of background readings and obtained values normalized to group values to depict fold-change. A total of three cohorts were analyzed reaching a combined sample size of n = 33–47 per treatment group.

2.3.5 Light-Dark Locomotion Assay

The locomotion behavior of 7 dpf zebrafish larvae was assessed at baseline and under different lighting conditions. To achieve this, larvae from each group were placed into individual wells of a 96-well plate with 250 µL of Aquatic Facility system water. The plate was then placed into the ZebraBox Larvae and Embryos Monitor (ViewPoint Behavior Technology, Montréal, QC, Canada) where the larvae were allowed to acclimatize to the full intensity light for 30 min to reduce sampling stress. The larvae were then exposed to instantaneous 100% light/dark intensity changes with the following pattern (times in min, L, light, D, darkness): 20L-5D-5L-5D-5L-5D-5L. The Viewpoint Zebralab v3 quantization software was used to track the individual's movements and to perform the automated behavioral analysis to obtain the movement time and distance of a given larvae within three defined movement ranges [inactivity (<3 mm/s), short-(3–6 mm/s), and long- (6 mm/s) movements] analyzed for each minute. Speed was calculated by dividing distance by time values. Data were analyzed separately for baseline, light and dark conditions.

2.4 Gene Expression

Samples were homogenized using a sonicator and total RNA extracted using the Trizol method. Total RNA purity and quantity were determined using a Nanodrop ™ (Thermo-Fisher Scientific) as previously described (Tu et al., 2019; Martínez et al., 2020). Using an input of 1 µg RNA, cDNA was then generated using Superscript II kit (Thermo-Fisher Scientific) according to the manufacturer's instructions. Controls omitting template (no template control) and reverse transcriptase (no RT control) were included in subsequent *realtime* RT-PCR assays using SSo Advanced Universal SYBR Green reagents (Bio-Rad, Montréal, QC, Canada). Briefly, relative gene expression was quantified using a two-step protocol on a CFX96 machine (Bio-Rad). Using pooled cDNA, 1:2 serial dilutions were pipetted to generate standard curves which were run in duplicates along with samples for each specific run. The individual reaction volume was 20 µL consisting of 10 µL 2x SSo Advanced Universal SYBR Green Master Mix (BioRad), 1 µL of 10 µM forward and reverse primers and 1 µL of cDNA template. Primer sequences, gene accession numbers and specific annealing temperatures (Tm) are reported in **Table 1**. For all gene expression assays, efficiencies between 90 and 100% and R^2 values exceeding 0.98 were considered acceptable. Reactions were monitored for single product by generating dissociation curves following each run. The specificity of reactions had previously been confirmed by sequencing (Tu et al., 2019; Martínez et al., 2020). Gene expression was normalized using the NORMAgene approach (Heckmann et al., 2011) and expressed as fold-change of control group values.

2.5 Statistical Analysis

All data were analyzed using SPSS Version 27 and visualized using GraphPad Prism Version 8.0. Data were tested for normality and homoscedasticity using Shapiro-Wilk and Levene's tests, respectively. In cases where data did not meet ANOVA criteria, standard transformations were used to improve normality and homoscedasticity of data. Univariate ANOVAs were used to assess significant effects of either treatment at a significance level of $p < 0.05$. In all cases cohorts were analyzed on individual plates and run as a fixed factor. Thus, the experimental design does not allow to dissociate (biological) cohort and

TABLE 1 | Primer sequences and annealing temperatures used in real-time RT-PCR assay for energy metabolism related gene targets.

Gene	NCBI Genbank ID	FW primer sequence	RV primer sequence	Tm (°C)
apoa1a	NM_131128.1	GAAGGCCTTCGAGTCCAACA	TCTGTGCCGAATGTGGTCCTC	55
apoba	XM_689735.9	AGCTGAAGAACGCACTCTCC	GAACTTCAGGGCCGCATCTA	57
insa	NM_131056.1	TAAGCACTAACCCAGGCACA	GATTTAGGAGGAAGGAAACC	59
insb	NM_001039064.1	ACTCTTCACAGACTCTGCTC	ACAGATGCTGGGATGGAGAA	59
pck	NM_214751.1	GCACGGAGTGTTTGTAGGG	GGTCTCGGTTCAGTTCACG	56
pomca	NM_181438.3	GCCCCTGAACAGATAGAGCC	CTCGTTATTTGCCAGCTCGC	54
pomcb	NM_001083051.1	TCCATCGAGCTCCAAAACCC	ACATTTTACGGTCTGCGT	54

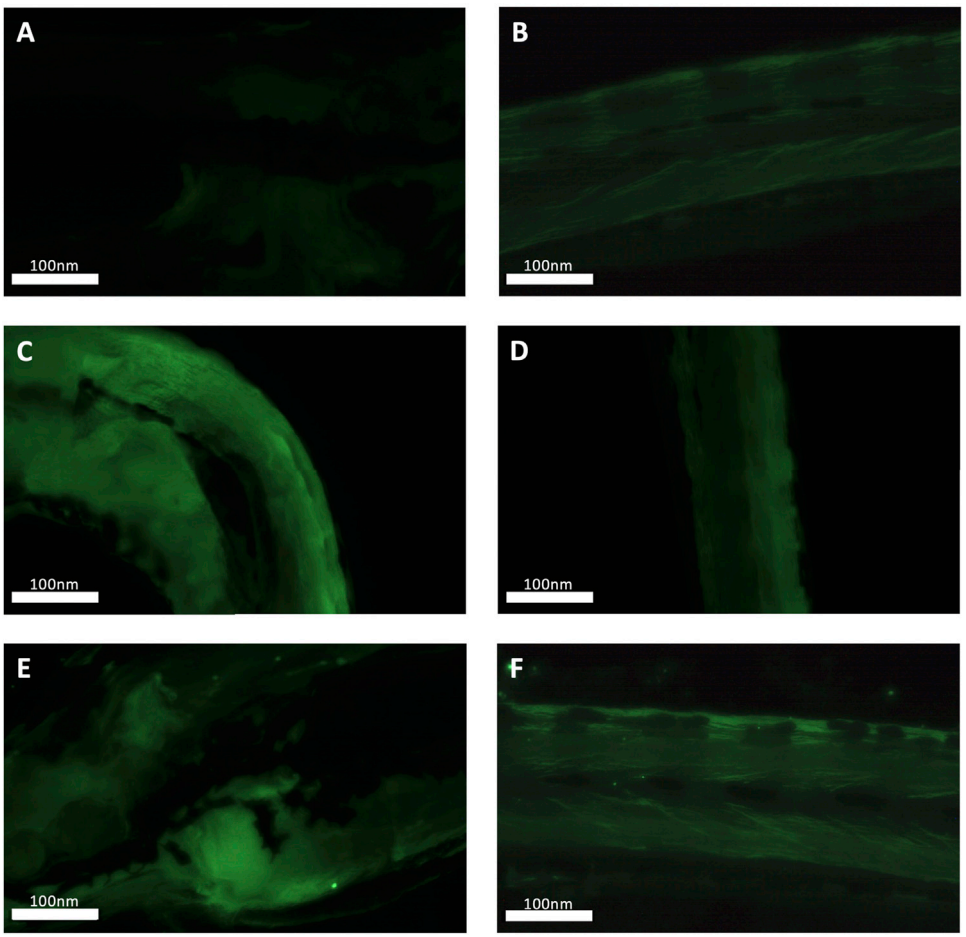

FIGURE 2 | Fluorescence microscopy-based validation of nanoplastic uptake in control, 2.5 and 25 ppm fluorescent polystyrene nanoplastic particle exposed zebrafish. Representative head and tail images of control **(A,B)**, low PS **(C,D)** and high PS exposure group **(E,F)** 7 dpf zebrafish larvae are shown.

(technical) plate effects. Significant differences in omnibus tests were resolved using Tukey's post-hoc test at a significance level of $p < 0.05$. For repeated measurement data, the same between-subject factor (treatment) as above were used in analysis, in addition to within-subject factor (time). Significant between-subject and within-subject treatment effects and their interactions were assessed at a significance level of $p < 0.05$. In cases where the sphericity assumption was violated, as assessed using Mauchly's W test, appropriate corrections (Greenhouse-Geisser or Huynh-Feldt) were used to assess significance of effects according to epsilon-based criteria as recommended (Girden, 1992).

3 RESULTS

3.1 Nanoplastics Bioaccumulate in Zebrafish (eleuthero)embryos

A qualitative increase in fluorescence signal was consistently observed in the PS nanoplastic exposed groups compared to

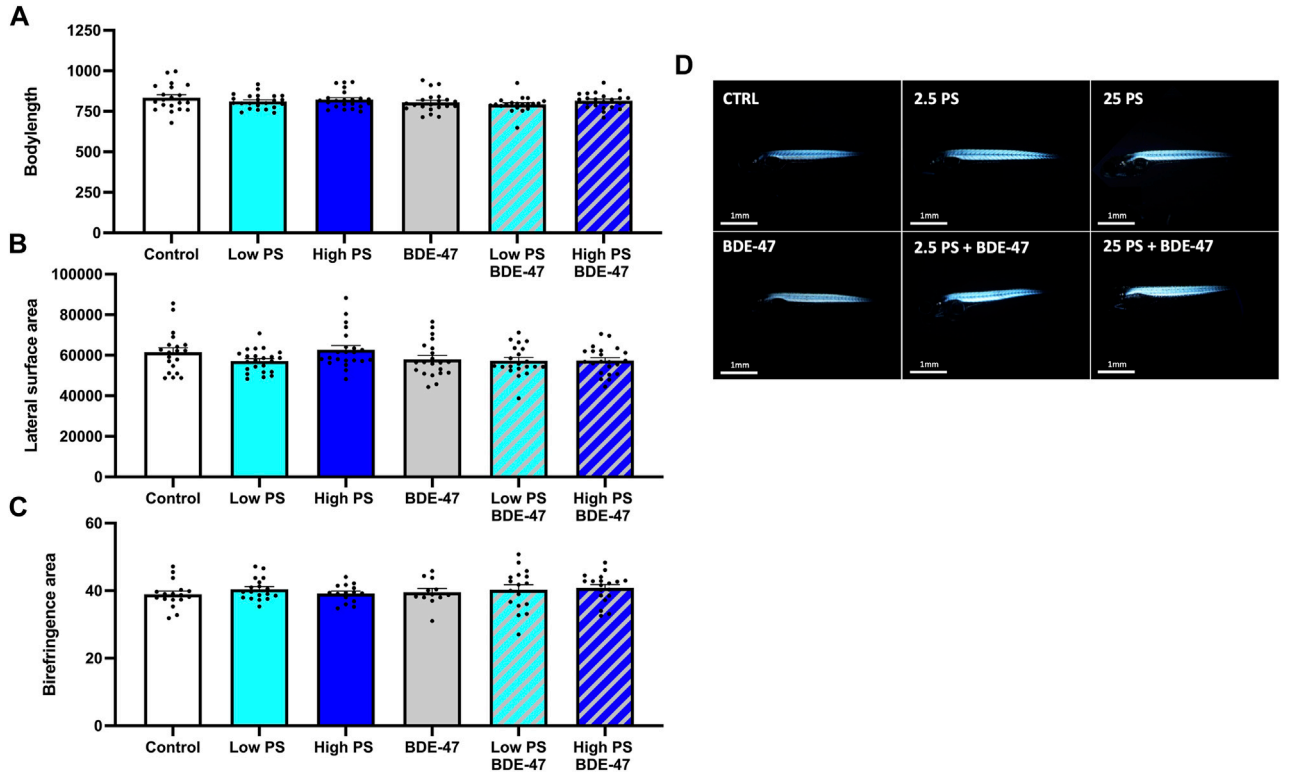

FIGURE 3 | Morphometric indices of 7 dpf zebrafish larvae exposed to vehicle control, 2.5 ppm PS, 25 ppm PS, 10 ppt BDE-47 or their combinations: Body length **(A)**, lateral surface area **(B)** and birefringent lateral somite area **(C)**. Individual measurements and average data +S.E.M. from $n = 3$ replicate assays with combined $n = 20–23$ **(A,B)** and $n = 12–19$ **(C)** per treatment group are presented. Representative images of birefringence measurements of laterally positioned zebrafish are presented **(D)**. Data were analyzed using a one-way ANOVA with a significance cut-off of $p < 0.05$.

the control group in the anterior part of eleutheroembryos containing the yolk sac and digestive tract, but not the caudal part containing skeletal muscle tissue (**Figure 2**).

3.2 Exposure to PS Nanoplastics, BDE-47 or Their Combination has Minimal Effects on Larval Growth

Treatment did not significantly affect body length (df = 5; F = 1.698; $p = 0.141$; **Figure 3A**). Treatment effect size (η2p) and observed power were 0.071 and 0.569, respectively. A significant cohort effect (df = 2; F = 34.937; $p < 0.001$) and significant interaction between cohort and treatment effect (df = 10; F = 2.037; $p = 0.036$) were observed. Treatment significantly affected lateral surface area (df = 5; F = 2.557; $p = 0.031$; **Figure 3B**). Treatment effect size (η2p) and observed power were 0.103 and 0.775, respectively. However, post-hoc analysis was unable to resolve differences between treatment groups. A significant cohort effect (df = 2; F = 26.008; $p < 0.001$) was observed. Muscle sarcomere-dependent birefringence was not affected by treatment (df = 5; F = 0.778; $p = 0.561$; **Figure 3C**). Treatment effect size (η2p) and observed power were 0.047 and 0.269, respectively. A significant cohort effect (df = 2; F = 17.711; $p < 0.001$) was observed. Representative images showing birefringence in each group are shown in **Figure 3D**.

3.2 PS Nanoplastics Alone and in Combination With BDE-47 Increase Larval Food Consumption

Treatment significantly affected food consumption in 7 dpf larvae (df = 5; F = 35.256; $p < 0.001$; **Figure 4A**). The effect size (η2p) and observed power of the treatment were 0.766 and 1, respectively. A significant cohort effect (df = 2; F = 10.443; $p < 0.001$) was observed. Post-hoc analysis of the treatment effect revealed that PS exposure at both low and high concentrations alone and in co-exposure with BDE-47 significantly increased food consumption compared to control. Both low and high PS + BDE-47 co-exposures also significantly increased food consumption compared to BDE-47 exposure alone.

3.3 Co-Exposure to High PS Nanoplastic and BDE-47 Significantly Reduce Larval Neutral Lipid Stores

Treatment significantly affected neutral lipid storage in zebrafish larvae (df = 5; F = 11.274; $p < 0.001$; **Figures 4B,C**). The effect size (η2p) and observed power of the treatment were 0.34 and 1, respectively. Post-hoc analysis revealed a significant reduction of neutral lipid storage in zebrafish co-exposed to high PS + BDE-47

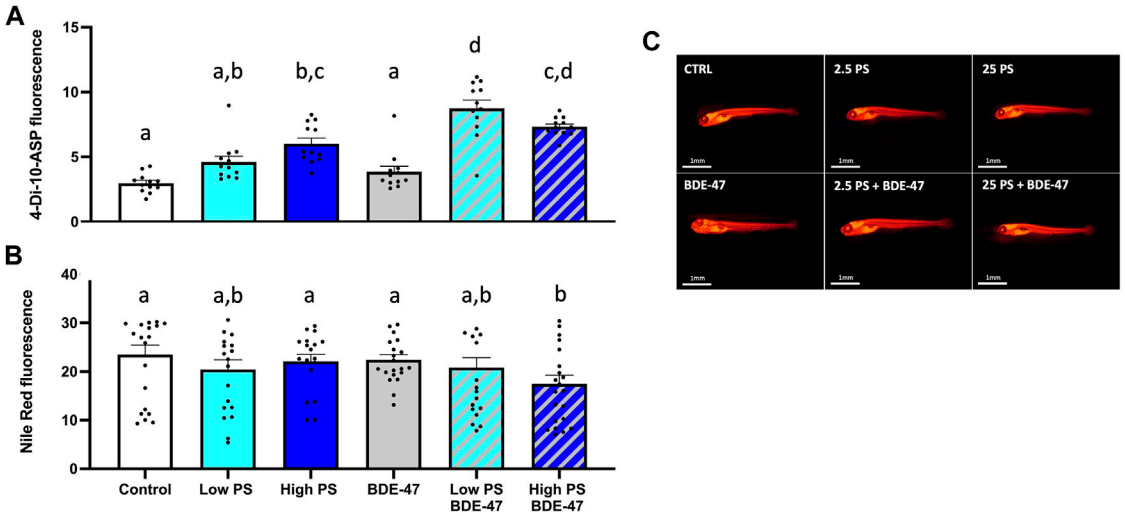

FIGURE 4 | Feed-intake **(A)** and neutral lipid deposition **(B)** of 7 dpf zebrafish larvae exposed to vehicle control, 2.5 ppm PS, 25 ppm PS, 10 ppt BDE-47 or their combinations. Individual measurements and average data +S.E.M. from $n = 3$ replicate assays with a combined $n = 12$ **(A)** and $n = 18–22$ **(B)** per treatment group are presented. Representative images of Nile Red based neutral lipid staining are shown **(C)**. Data were analyzed using a one-way ANOVA with a significance cut-off of $p < 0.05$. Different letters indicate significant differences between groups as analyzed by Tukey's post-hoc test.

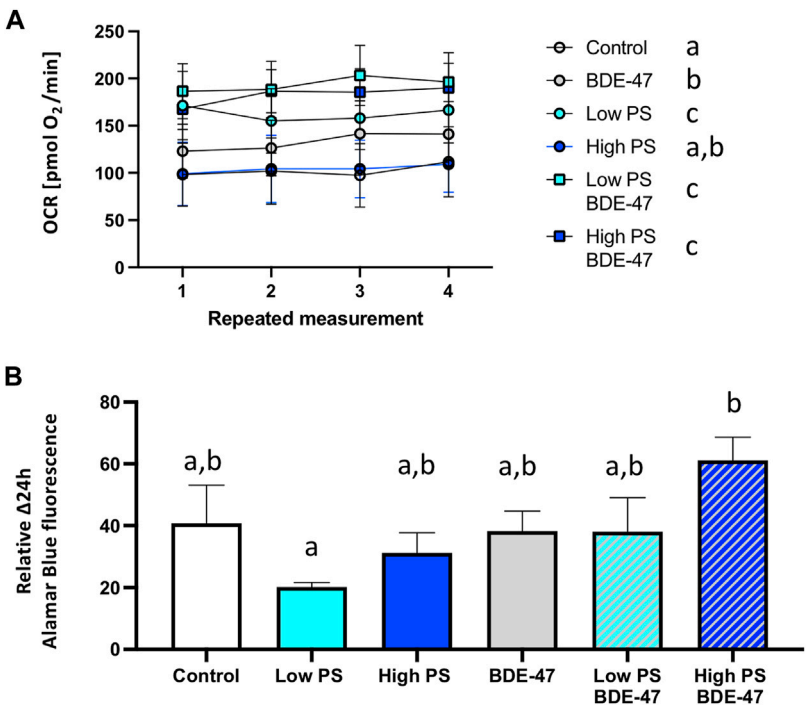

FIGURE 5 | Oxygen consumption rate **(A)** and 24 h oxygen metabolism-dependent energy expenditure of 2 dpf zebrafish eleutheroembryos exposed to vehicle control, 2.5 ppm PS, 25 ppm PS, 10 ppt BDE-47 or their combinations **(B)**. Average oxygen consumption rates +S.E.M. from $n = 3$ replicate assays for each group with a combined $n = 7–9$ per treatment group are presented **(A)**. Average repeated measurements of 24 h oxygen metabolism-dependent energy expenditures +S.E.M. from $n = 3$ replicate assays for each group with an $n = 33–47$ per treatment group are presented **(B)**. Data were analyzed using a one-way repeated measurement ANOVA **(A)** and one-way ANOVA **(B)** measurement with a significance cut-off of $p < 0.05$. Different letters indicate significant differences between groups as analyzed by Tukey's post-hoc test.

TABLE 2 | Repeated measurement ANOVA analyses of treatment effects on locomotion assay endpoints. Effect sizes and observed power are reported. Bold font indicates significance at a $p < 0.05$ threshold.

Locomotion endpoint	Baseline	Dark	Light
Total movement counts	**df = 5 F = 2.641 p = 0.024**	**df = 5 F = 2.509 p = 0.031**	df = 5 F = 2.246 p = 0.050
	η2p = 0.47 Power = 0.80	*η2p = 0.44 Power = 0.78*	*η2p = 0.40 Power = 0.73*
Total movement duration	df = 5 F = 0.896 p = 0.485	df = 5 F = 0.765 p = 0.575	df = 5 F = 1.828 p = 0.108
	η2p = 0.16 Power = 0.32	*η2p = 0.14 Power = 0.27*	*η2p = 0.33 Power = 0.62*
Total movement distance	**df = 5 F = 2.509 p = 0.031**	df = 5 F = 1.747 p = 0.124	df = 5 F = 0.461 p = 0.805
	η2p = 0.44 Power = 0.78	*η2p = 0.31 Power = 0.60*	*η2p = 0.08 Power = 0.17*
Total movement speed	**df = 5 F = 3.216 p = 0.008**	**df = 5 F = 9.623 p = 0.001**	df = 5 F = 1.090 p = 0.366
	η2p = 0.57 Power = 0.89	*η2p = 0.15 Power = 1.00*	*η2p = 0.20 Power = 0.39*
Short movement counts	**df = 5 F = 2.898 p = 0.014**	**df = 5 F = 3.479 p = 0.005**	**df = 5 F = 2.465 p = 0.044**
	η2p = 0.05 Power = 0.84	*η2p = 0.06 Power = 0.91*	*η2p = 0.04 Power = 0.77*
Short movement duration	**df = 5 F = 3.161 p = 0.009**	**df = 5 F = 13.41 p = 0.001**	**df = 5 F = 6.236 p = 0.001**
	η2p = 0.06 Power = 0.88	*η2p = 0.20 Power = 1.00*	*η2p = 0.10 Power = 1.00*
Short movement distance	**df = 5 F = 4.411 p = 0.001**	**df = 5 F = 14.39 p = 0.001**	**df = 5 F = 7.163 p = 0.001**
	η2p = 0.08 Power = 0.97	*η2p = 0.21 Power = 1.00*	*η2p = 0.12 Power = 1.00*
Short movement speed	**df = 5 F = 6.876 p = 0.001**	**df = 5 F = 5.081 p = 0.001**	**df = 5 F = 4.081 p = 0.001**
	η2p = 0.12 Power = 1.00	*η2p = 0.09 Power = 0.98*	*η2p = 0.07 Power = 0.95*
Long movement counts	**df = 5 F = 2.259 p = 0.049**	df = 5 F = 1.727 p = 0.129	df = 5 F = 2.090 p = 0.067
	η2p = 0.04 Power = 0.73	*η2p = 0.03 Power = 0.59*	*η2p = 0.04 Power = 0.69*
Long movement duration	**df = 5 F = 2.270 p = 0.048**	**df = 5 F = 4.721 p = 0.001**	df = 5 F = 0.996 p = 0.421
	η2p = 0.04 Power = 0.73	*η2p = 0.08 Power = 0.98*	*η2p = 0.02 Power = 0.35*
Long movement distance	**df = 5 F = 4.929 p = 0.001**	**df = 5 F = 6.123 p = 0.001**	df = 5 F = 1.495 p = 0.191
	η2p = 0.08 Power = 0.98	*η2p = 0.10 Power = 1.00*	*η2p = 0.03 Power = 0.52*
Long movement speed	**df = 5 F = 3.654 p = 0.003**	df = 5 F = 1.398 p = 0.255	df = 5 F = 0.709 p = 0.617
	η2p = 0.07 Power = 0.93	*η2p = 0.03 Power = 0.49*	*η2p = 0.01 Power = 0.26*

compared to control. A significant cohort effect (df = 2; F = 58.57; $p < 0.001$) was observed.

3.4 PS and BDE-47 Exposure and Their Combination Significantly Increase Oxygen Consumption Rates

Treatment significantly affected oxygen consumption in 2 dpf zebrafish (df = 5; F = 142.6; p=<0.001; **Figure 5A**). The effect size (η2p) and observed power of the treatment were 0.965 and 1.0, respectively. Post-hoc analysis revealed that all treatments except 25 ppm PS significantly increased oxygen consumption rate (OCR) compared to controls. Irrespective of the PS concentration used, co-exposure groups exhibited increased OCR compared to BDE-47 exposed fish alone. In the high PS + BDE-47 co-exposure group, this increase was also significant compared to the high PS exposure alone. No significant cohort effect (df = 3; F = 2.765 $p < 0.059$) was observed. Treatment significantly affected 24 h oxidative metabolism related energy expenditure in 2 dpf zebrafish as quantified using the Alamar Blue assay (df = 5; F = 2.918; $p = 0.014$; **Figure 5B**). The effect size (η2p) and observed power of the treatment were 0.06 and 0.847, respectively. Post-hoc analysis revealed a significantly increased oxidative metabolism related energy expenditure in eleutheroembryos exposed to high PS + BDE-47 compared to elutheroembryos exposed to low PS alone. No significant cohort effect (df = 2; F = 1.331; $p < 0.266$) was observed.

3.5 Locomotor Assay

Several indices of locomotion were affected by treatment under baseline conditions in zebrafish larvae (**Table 2**). Cohort effects are reported in **Table 3**. Counts of total movement observations were significantly reduced in zebrafish larvae co-exposed to high PS + BDE-47 compared to control ($p < 0.05$; **Figure 6A**). While total movement duration did not exhibit significant differences between treatment groups (**Figure 6B**), total distance covered (**Figure 6C**) and total movement speed (**Figure 6D**) were significantly affected by treatment. However, post-hoc analysis revealed that no treatment group exhibited significant differences from the control group. When analyzing parameters under specific lighting conditions, zebrafish larvae under dark conditions exhibited specific responses to treatment both for total movement counts (**Figure 6A**) and total movement speed (**Figure 6D**). However, only total movement speed in low and high PS exposure groups revealed significant increases compared to control group ($p < 0.05$; **Figure 6D**).

Indices of short movement were affected by treatment in zebrafish larvae under baseline conditions (**Table 2**). Counts of short movement were significantly decreased in zebrafish co-exposed to high PS and BDE-47 compared to control ($p < 0.05$; **Figure 7A**). While significant effects of treatment on short movement duration could not be resolved by post-hoc analysis (**Figure 7B**), short movement distance (**Figure 7C**) and short movement speed (**Figure 7D**) exhibited significant reductions in low and high PS compared to control ($p < 0.05$; **Figure 7C**) and in all treatment groups except for high PS + BDE-47 compared to control ($p < 0.05$; **Figure 7D**), respectively. All measured short distance parameters were also significantly affected by treatment when analyzing dark and light conditions (**Table 2**). In dark conditions, short movement counts were significantly reduced in larvae exposed to high PS + BDE-47 compared to control ($p <$

TABLE 3 | Cohort effects in repeated measurement ANOVA analyses on locomotion assay endpoints. Bold font indicates significance at a $p < 0.05$ threshold.

Locomotion endpoint	Baseline	Dark	Light
Total movement counts	**df = 2 F = 5.013 p = 0.007**	df = 2 F = 0.870 p = 0.420	df = 2 F = 0.637 p = 0.529
Total movement duration	**df = 2 F = 4.462 p = 0.012**	df = 2 F = 0.120 p = 0.887	df = 2 F = 0.61 p = 0.941
Total movement distance	**df = 2 F = 10.10 p = 0.001**	**df = 2 F = 6.358 p = 0.002**	**df = 2 F = 5.871 p = 0.003**
Total movement speed	**df = 2 F = 6.287 p = 0.002**	**df = 2 F = 22.63 p = 0.001**	df = 2 F = 1.169 p = 0.312
Short movement counts	**df = 2 F = 4.578 p = 0.011**	df = 2 F = 1.013 p = 0.365	df = 2 F = 0.999 p = 0.370
Short movement duration	**df = 2 F = 1.763 p = 0.174**	**df = 2 F = 10.63 p = 0.001**	**df = 2 F = 8.238 p = 0.001**
Short movement distance	df = 2 F = 2.620 p = 0.075	**df = 2 F = 12.105 p = 0.001**	**df = 2 F = 9.279 p = 0.001**
Short movement speed	**df = 2 F = 4.058 p = 0.018**	df = 2 F = 2.596 p = 0.077	**df = 2 F = 3.525 p = 0.031**
Long movement counts	**df = 2 F = 5.141 p = 0.006**	df = 2 F = 1.100 p = 0.335	df = 2 F = 0.618 p = 0.540
Long movement duration	**df = 2 F = 7.918 p = 0.001**	**df = 2 F = 7.074 p = 0.001**	**df = 2 F = 8.923 p = 0.001**
Long movement distance	**df = 2 F = 12.283 p = 0.001**	**df = 2 F = 14.594 p = 0.001**	**df = 2 F = 11.56 p = 0.001**
Long movement speed	**df = 2 F = 13.72 p = 0.001**	**df = 2 F = 13.79 p = 0.001**	df = 2 F = 1.959 p = 0.143

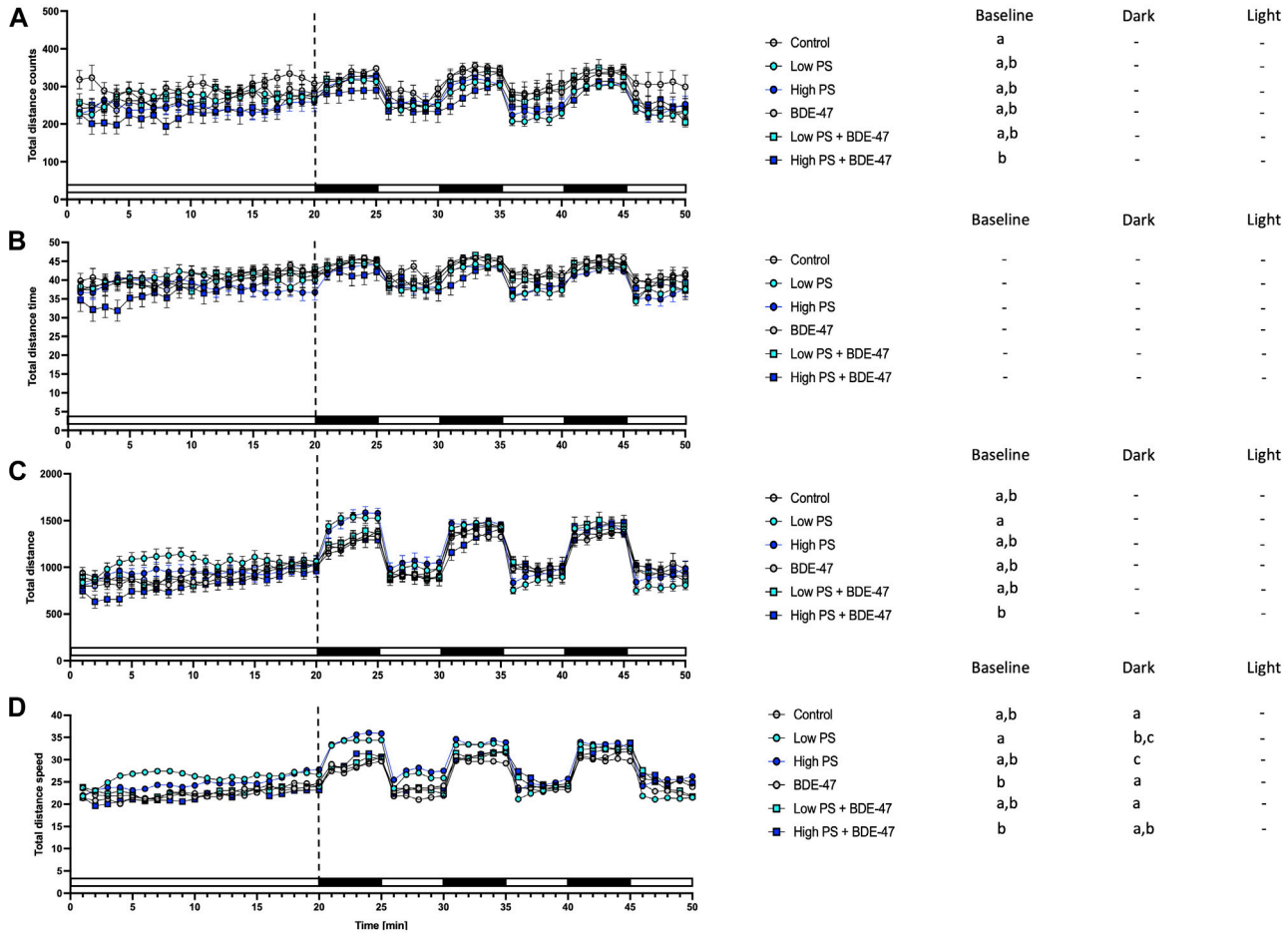

FIGURE 6 | Total movement parameters from 7 dpf zebrafish larvae locomotion assays ($n = 3$) with a total $n = 48$ per treatment group consisting of exposures to vehicle control, 2.5 ppm PS, 25 ppm PS, 10 ppt BDE-47 or their combinations. All measurements over the 50 min assays were binned in 1 min units, with 20 min baseline followed by 3 cycles of 5 min dark light alterations. Average total counts of movement events +/− S.E.M. **(A)**, average duration of total movement events +/− S.E.M in s **(B)**, Distance of total movement events +/− S.E.M in mm **(C)**, Average speed +/− S.E.M of total movements in mm/s **(D)**. Data were analyzed using separate one-way repeated measurement ANOVAs for baseline, dark, and light conditions. Significant treatment effects ($p < 0.05$) are shown in **Table 2**, and specific post-hoc analysis results are depicted next to the graphs for all parameters. Different letters indicate significant differences between groups as analyzed by Tukey's post-hoc test ($p < 0.05$).

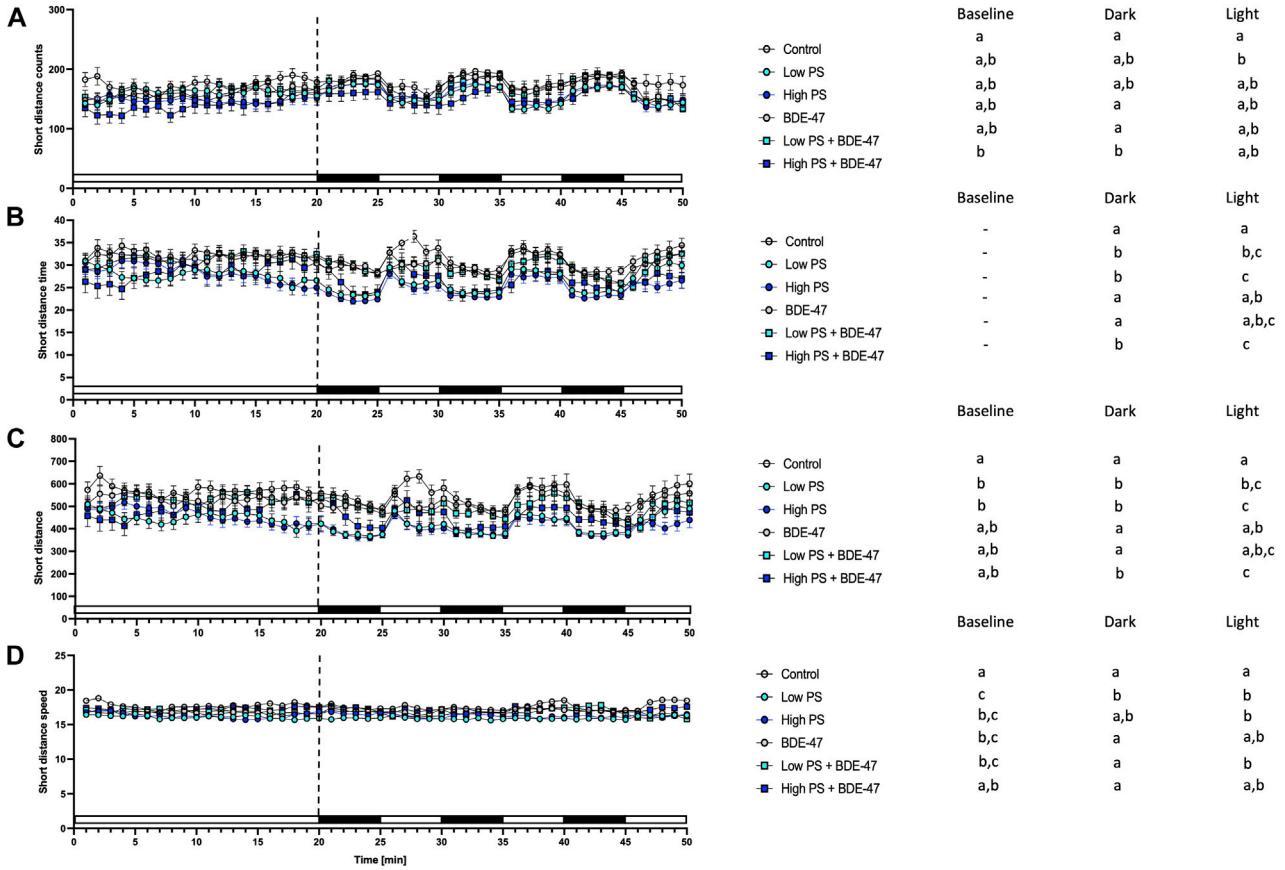

FIGURE 7 | Short movement parameters from 7 dpf zebrafish larvae locomotion assays ($n = 3$) with a total $n = 48$ for each treatment groups. All measurements over the 50 min assays were binned in 1 min units, with 20 min baseline followed by 3 cycles of 5 min dark light alterations. Average short counts of movement events +/− S.E.M. **(A)**, average duration of total movement events +/− S.E.M in s **(B)**, Distance of short movement events +/− S.E.M in mm **(C)**, Average speed +/− S.E.M of short movements in mm/s **(D)**. Data were analyzed using separate one-way repeated measurement ANOVAs for baseline, dark, and light conditions. Significant treatment effects ($p < 0.05$) are shown in **Table 1**, and specific post-hoc analysis results are depicted next to the graphs for all parameters. Different letters indicate significant differences between groups as analyzed by Tukey's post-hoc test ($p < 0.05$).

0.05; **Figure 7A**). Short movement distance covered in low PS, high PS and high PS + BDE-47 was significantly less compared to control ($p < 0.05$; **Figure 7C**), while short movement speed was significantly reduced by low PS exposure compared to control ($p < 0.05$; **Figure 7D**) under dark conditions. In light conditions, short movement counts were significantly reduced in the low PS exposure group compared to control ($p < 0.05$; **Figure 7A**), while short movement duration and distance were significantly lower in low PS, high PS and high PS + BDE-47 exposed groups compared to control ($p < 0.05$; **Figures 7B,C**). Under light conditions short movement speed was slower in low PS, high PS and low PS + BDE-47 exposed groups compared to control ($p < 0.05$; **Figure 7D**).

Indices of short movement were affected by treatment in zebrafish larvae under baseline conditions (**Table 2**). Under baseline conditions, counts of long distance movement were significantly decreased in high PS + BDE-47 exposed larvae compared to control ($p < 0.05$; **Figure 8A**). Conversely low PS exposed larvae covered larger distances with long movement at greater speed compared to control larvae ($p < 0.05$; **Figures 8C,D**). Under dark conditions, low and high PS exposure increased duration and distance of long movements compared to controls ($p < 0.05$; **Figures 8B,C**).

3.6 Gene Expression

Relative transcript abundance of *apoa1a* was significantly affected by treatment (df = 5; F = 3.936; $p = 0.0138$; **Figure 9A**). The effect size (η2p) and observed power of the treatment were 0.52 and 0.86, respectively. However, Tukey's post-hoc analysis was unable to discern differences in *apoa1a* transcript abundance between specific treatment groups. Relative transcript abundance of *apoba* was significantly affected by treatment (df = 5; F = 4.786; $p = 0.0059$; **Figure 9B**). The effect size (η2p) and observed power of the treatment were 0.57 and 0.92, respectively. Tukey's post-hoc analysis revealed a significant increase of *apoa1a* transcripts in BDE-47 exposed zebrafish compared to control and BDE-47 co-exposed with high PS nanoplastics ($p < 0.05$). While relative

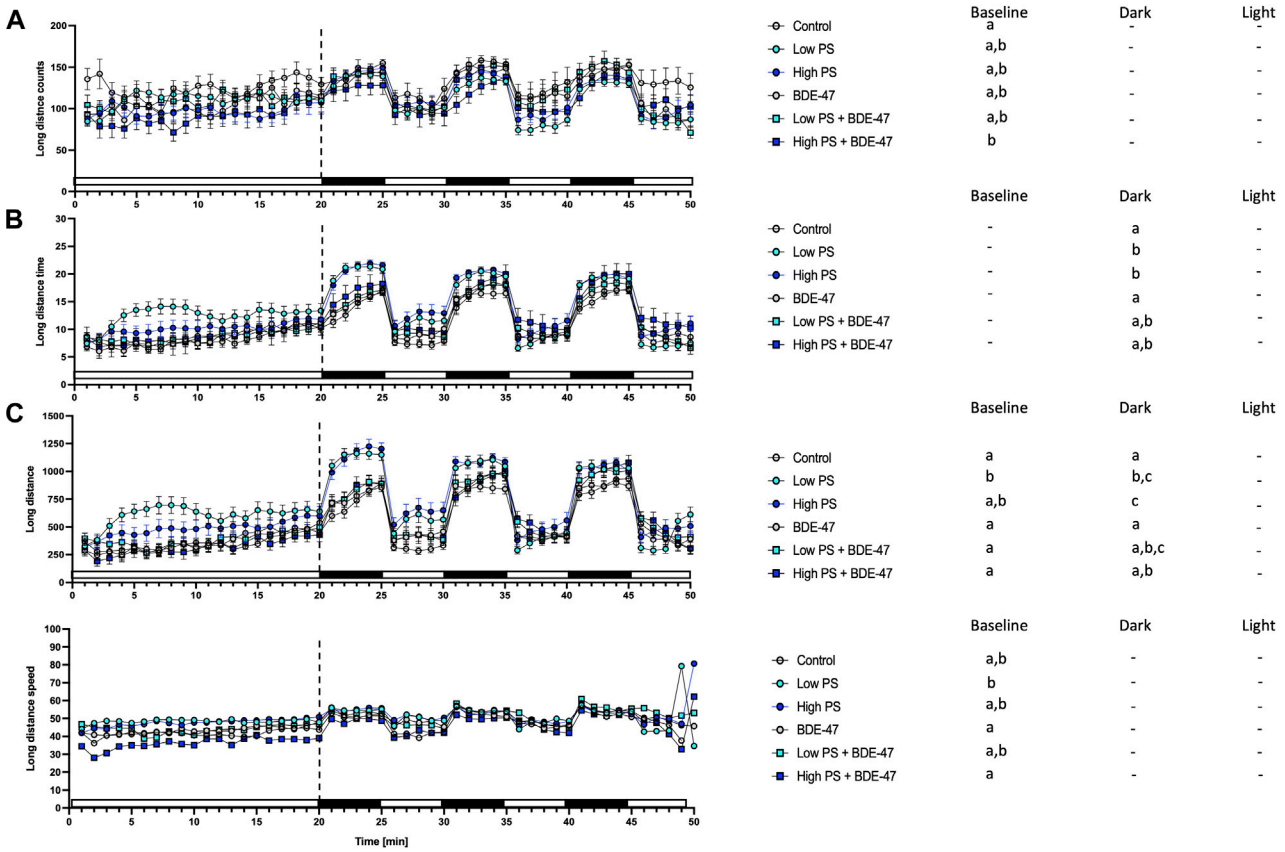

FIGURE 8 | Long movement parameters from 7 dpf zebrafish larvae locomotion assays ($n = 3$) with a total $n = 48$ for each treatment group consisting of exposures to vehicle control, 2.5 ppm PS, 25 ppm PS, 10 ppt BDE-47 or their combinations. All measurements over the 50 min assays were binned in 1 min units, with 20 min baseline followed by 3 cycles of 5 min dark light alterations. Average long counts of movement events +/– S.E.M. **(A)**, average duration of total movement events +/– S.E.M in s **(B)**, Distance of long movement events +/– S.E.M in mm **(C)**, Average speed +/– S.E.M of long movements in mm/s **(D)**. Data were analyzed using separate one-way repeated measurement ANOVAs for baseline, dark, and light conditions. Different letters indicate significant differences between groups as analyzed by Tukey's post-hoc test ($p < 0.05$).

transcript abundance of *insa* was not significantly affected by treatment (df = 5; F = 2.709; $p = 0.0539$; **Figure 9C**), *insb* transcript abundance was significantly affected by treatment (df = 5; F = 25.52; $p < 0.0001$; **Figure 9D**). The effect size (η2p) and observed power of the treatment were 0.43 and 0.68 for *insa* and 0.88 and 1.00 for *insb*. Post-hoc analysis revealed that BDE-47 significantly induced *insb* transcript abundance compared to all other treatment groups. Relative transcript abundance of *pck1* was similarly affected by treatment (df = 5; F = 6.293; $p = 0.0015$; **Figure 9E**), which post-hoc analysis resolved as significant increase in *pck1* transcript abundance in BDE-47 exposed zebrafish compared to control, high PS nanoplastics and co-exposure to high PS nanoplastics and BDE-47 ($p < 0.05$). The effect size (η2p) and observed power of the treatment were 0.64 and 0.98. Relative transcript abundance of *pomca* was significantly altered by treatment (df = 5; F = 21.24; $p < 0.0001$; **Figure 9F**), with significantly increased expression in BDE-47, low PS nanoplastic and low PS nanoplastic + BDE-47 exposed zebrafish compared to controls ($p < 0.05$). The effect size (η2p) and observed power of the treatment were 0.86 and 1.00. Relative transcript abundance of *pomcb* responded to treatment (df = 5; F = 4.932; $p = 0.0051$; **Figure 9G**), with significant increase in *pomcb* expression in BDE-47 exposed zebrafish compared to control and BDE-47 + high PS nanoplastic co-exposure. The effect size (η2p) and observed power of the treatment were 0.96 and 1.00.

4 DISCUSSION

4.1 PS Nanoplastics Accumulate in Exposed Zebrafish

A qualitative increase in fluorescence-labelled PS nanoplastics was observed especially in the anterior part of eleutheroembryos at both 2.5 and 25 ppm exposure concentrations, confirming uptake. In contrast to several studies, our study used a dialysis protocol before PS exposure, following reports of fluorescent dye leaching which may result in artifacts during imaging (Schür et al., 2019; Xu et al., 2019). Discernable increases in signal

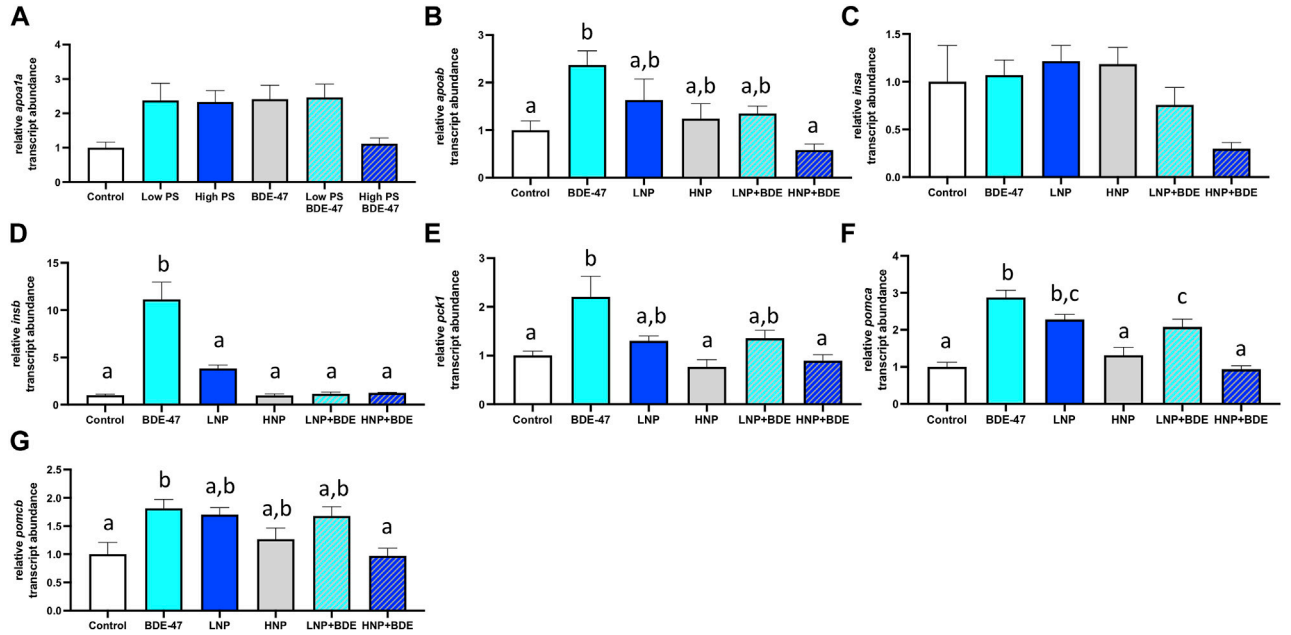

FIGURE 9 | Relative abundance of mRNA transcripts with characterized roles in energy metabolism in whole 7 dpf larvae. Treatment groups consist of exposures to vehicle control, 2.5 ppm PS, 25 ppm PS, 10 ppt BDE-47 or their combinations. Apolipoprotein transcripts *apoa1a* **(A)** and *apoab* **(B)**, insulin paralogue transcripts *insa* **(C)** and *insb* **(D)**, the gluconeogenic marker *pck1* **(E)** and *pomc* paralogues *pomca* **(F)** and *pomcb* **(G)**. Average mRNA transcript abundance +S.E.M. of $n = 4$ pooled replicates per treatment group containing $n = 10$ larvae per replicate are shown. Relative transcript abundance was normalized to control group to reflect fold-change. All data was analyzed using one-way ANOVAs with a significance cut-off of $p < 0.05$. Where omnibus tests revealed a significant treatment effect, Tukey's post-hoc test ($p < 0.05$) was used to discern significant differences between treatment groups, which are indicated by different letters.

intensity were observed in ventral regions containing the digestive tract at both 2.5 ppm and 25 ppm PS nanoplastic exposure concentrations. At the 25 ppm concentration, fluorescence-labelled PS nanoplastics, albeit to a lesser extent, were also detected in the tail region. To assess fluorescence labelled NP uptake at the tissue level, we exposed adult zebrafish to 25 ppm PS for 4 days. Subsequent histological analysis revealed increased fluorescence in the intestinal tract and liver, both of which also exhibited potential signs of inflammation such as enlarged goblet cells and hyperemia, respectively (**Supplementary Figure S1**).

These findings are in line with previous reports confirming uptake of PS nanoplastics principally in the intestine (Lu et al., 2016; Skjolding et al., 2017; Pitt et al., 2018; Brun et al., 2019; Trevisan et al., 2019; Trevisan et al., 2020). Oral ingestion following hatching has been characterized as the principal route of exposure in developing zebrafish, with limited biodistribution following ingestion for PS nanoparticles larger than 50 nm in size (van Pomeren et al., 2017). Together, these findings confirm PS nanoplastic uptake of 100 nm particles occurs especially in the dorsovisceral region of 7 dpf zebrafish in our study. While BDE-47 uptake or sorption to PS nanoplastics was not quantified in the current study, BDE-47 has, due to its high K_{OW} of >6.5, been shown to bioaccumulate in zebrafish embryos in previous studies with reported BCF exceeding 2000 (Zheng et al., 2012; Usenko et al., 2013; Liu et al., 2015). BDE-47 has also been shown to sorb to nanoplastics, especially PS (Xu et al., 2019; Horton et al., 2020; Wu et al., 2020). While our experimental design should ensure that both compounds are taken up in early developing zebrafish, the lack of analytical assessment of internal BDE-47 concentration measurement across treatment groups does not allow us to determine whether the 100 nm PS nanoplastic serve as a vector to increase internal BDE-47 concentration via ingestion, as reported for 20 nm PS nanoplastics and POPs (Zhang and Goss, 2020) or reduce BDE-47 uptake by sequestering free BDE-47 in the medium, as reported for 5 µm PS microplastics (Yang et al., 2020).

4.2 Individual PS Nanoplastic and BDE-47 Exposure Induces Organismal-Level Metabolic Changes in Early Zebrafish Development

Developing zebrafish exposed to PS nanoplastics as well as BDE-47 exhibit similar metabolic effects at the organismal level. Individual exposure to both compounds increased oxygen consumption rate at 2 dpf, a developmental window already characterized by high oxygen demand (**Figure 10**). An increase in oxygen consumption rate indicates an increased demand for oxidative metabolism to cover energetic needs. Higher energetic needs, in turn, may be linked to developmental timing (**Figure 10**), and increased cost of detoxification responses (Handy et al., 1999; Scott and Sloman, 2004), but may also reflect direct contaminant disruption of mitochondrial efficiency and ROS buffering (Souders et al., 2018; Yang et al., 2021). At the internal respiration level, 10 ppm PS

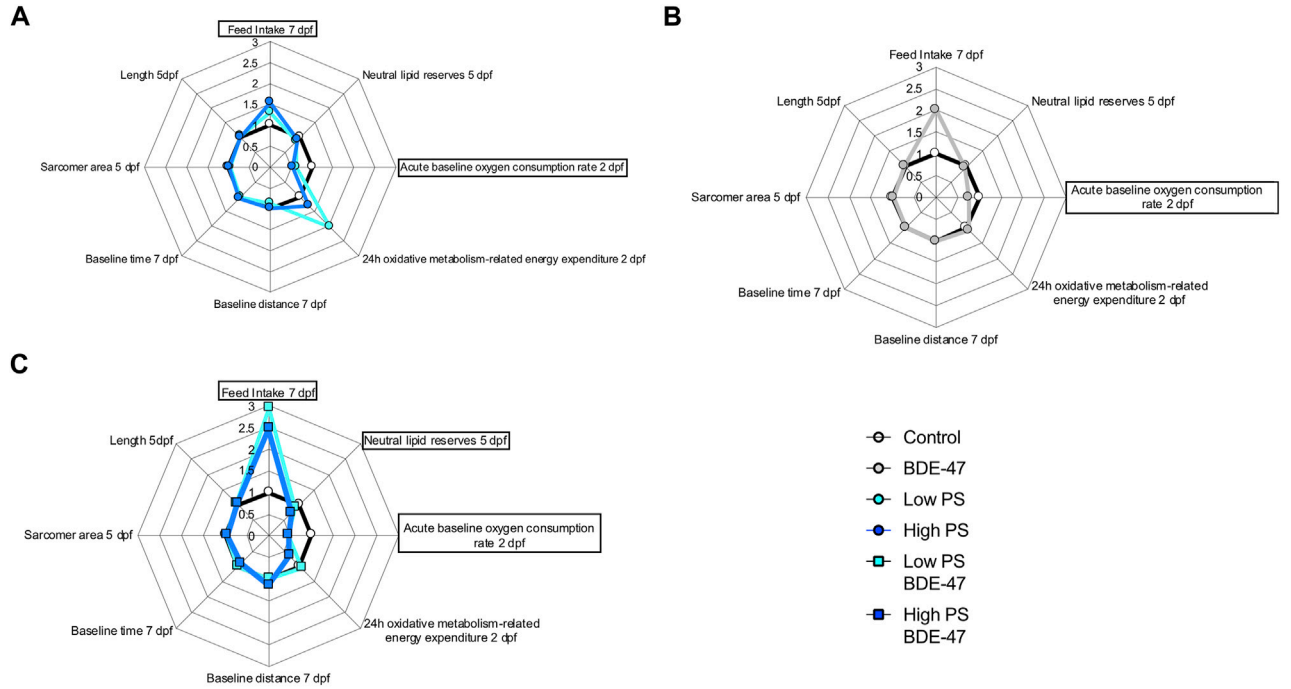

FIGURE 10 | Radar chart diagrams summarizing organismal level effects of different exposure treatments on the metabolic phenotype in developing zebrafish: Control, 2.5 ppm PS and 25 ppm PS exposures **(A)** Control and 10 ppt BDE-47 exposure, **(B)** Control and combined exposures of 2.5 ppm + 10 ppt BDE-47 and 25 ppm + 10 ppt BDE-47, **(C)** in comparison to vehicle control. Note that all average treatment group values have been normalized to control values (=1) and in some cases inverted so that datapoints >1 indicate quantified parameters with a positive contribution to energy balance, while datapoints <1 indicate parameters negatively contributing to organismal energy balance. Endpoints with significant effects of treatment are highlighted by surrounding rectangular shapes.

nanoplastic exposure has recently been shown to reduce coupling efficiency in developing zebrafish mitochondria at 2 and 4 dpf, without, however affecting baseline oxygen consumption rate (Trevisan et al., 2019). In the same study, a concurrent increase in NADH equivalents was reported, suggested to constitute either a consequential build-up of reducing equivalents in response to decreased coupling efficiency and/or a compensatory response driven by increased production of NADH equivalents. Metabolite level analysis provides further support PS induced mitochondrial uncoupling, as adult zebrafish exposure to 1.5 ppm PS nanoplastics resulted in increased ROS and decreased ATP concentrations in muscle tissues. Conversely, the increase in oxygen consumption rate was not accompanied by significant alterations of reduction equivalents in our study, although a strong tendency for a decrease was observed especially in the low PS exposed group. It is important to note that the Alamar Blue assay used to assess reducing equivalents fluorometrically quantifies both NADH and NADPH and is therefore sensitive to detoxification and oxidative stress responses fuelled by NADPH (Tu et al., 2019; Wu et al., 2019; Martínez et al., 2020). Indeed, robust induction of oxidative stress and detoxification responses have been reported for PS in developing zebrafish (Hu and Palić, 2020). Future studies should thus extend the Seahorse assay to probe a contribution of PS induced disruption of mitochondrial coupling efficiency and probe markers of oxidative stress such as glutathione lipid peroxidation or antioxidant gene expression and activity to differentiate between these two distinct possibilities. Irrespective of the key mechanism driving increased oxygen demand, however, we observe a concurrent increase in feeding rate, an organismal level response likely to meet increased demand for oxidizable fuel to provide ATP via mitochondrial respiration. Since PS nanoplastics are, following hatching, ingested and quantified in the intestinal tract and key tissues involved in the regulation of energy metabolism such as the liver and pancreas (van Pomeren et al., 2017; Pitt et al., 2018), it is possible that reduced nutrient absorption and metabolism, as well as disrupted endogenous nutrient sensing, may contribute to the increase in feeding rate (Jovanović, 2017). Nevertheless, these organismal level metabolic changes did not translate into altered growth as quantified by body length lateral surface area and sarcomere development, suggesting that at least in early life stages, zebrafish (eleuthero) embryos and larvae can mount sufficient homeostatic responses in response to 2.5 and 25 ppm PS exposure to maintain somatic growth. At the behavioural level, overall locomotion was generally not affected by PS exposure, indicating that metabolic challenges did also not necessitate compensatory hypolocomotory behaviour to conserve energy. However some exceptions to these general findings exist, such a significant increase in locomotor speed under dark conditions. These findings are in contrast to previous findings demonstrating a hypo- (Chen et al., 2017; Qiang and Cheng, 2019) or hyperlocomotory (Brun et al., 2019) phenotype in zebrafish larvae following PS nanoplastic exposure, albeit at higher, mg/L exposure concentrations and a smaller diameter. Interestingly, separation of short and long movement bouts revealed that while total locomotory behaviour remained largely unaffected, indices of short movement

(distance, time, speed) decreased, while the same indices increased for long movements under both baseline and different lighting conditions. Thus, while overall locomotion remains largely unaffected, the nature of locomotion exhibits specific responses to PS exposure, prioritizing long over short movements. Such changes may reflect foraging behaviour in line with increased feeding rates but may also be the consequence of peripheral feedback modulation or central control of locomotory behaviour, especially given that PS nanoplastics have been shown to affect lateral neuromasts in zebrafish (Brun et al., 2018) and have been shown to accumulate in the brain and muscle tissue where they have been shown to affect acetylcholine metabolism, concentration and neurons (Ding et al., 2018; Sarasamma et al., 2020; Yang et al., 2021). An integrated overview of the organismal level phenotypic consequences of PS exposure is presented in **Figure 10A**.

Similar to the PS exposure groups, BDE-47 exposure significantly increased oxygen consumption rate compared to control zebrafish (eleuthero)embryos. As previously discussed for PS, this may reflect higher energetic cost linked to detoxification and ROS buffering responses, as robust BDE-47 induced oxidative stress has been reported in a variety of species including (developing) zebrafish (Fernie et al., 2005; Shao et al., 2008; Tagliaferri et al., 2010; Costa et al., 2015; Usenko et al., 2015; Meng et al., 2020; Messina et al., 2020). Again, similar to described PS mode of actions, BDE-47 and its hydroxylated metabolite 6-OH BDE-47, have recently been described to decrease mitochondrial OXPHOS gene expression and ATP production and increase oxygen consumption indicative of OXPHOS disruption uncoupling in zebrafish (Legradi et al., 2017; Zhuang et al., 2020), suggesting a mitochondrial contribution to the observed increase in oxygen consumption rate. Like PS, BDE-47 exposure also increased the feeding rate. Increases in feeding in response to BDE-47 have recently also been reported in a marine rotifer, *Brachionus plicatilis*, where it has been linked to digestive suppression following BDE-47 induced mitochondrial disruption affecting cilia development on the one hand, and acetylcholine dependent control of feeding behaviour on the other (Yang et al., 2021). BDE-47 may promote zebrafish feed-intake as compensatory consequences of decreased nutrient absorption or mitochondrial function, or directly via disruption of central feeding circuits. The concomitant increase in oxygen consumption rate in response to BDE-47 exposure suggests that increased feeding rates may represent a homeostatic response to provide oxidizable fuel for energetically costly detoxification or mitochondria-derived ROS buffering processes widely reported for BDE-47 (Fernie et al., 2005; Shao et al., 2008; Tagliaferri et al., 2010; Costa et al., 2015; Usenko et al., 2015; Meng et al., 2020; Messina et al., 2020). However, possible directly inhibitory effects of BDE-47 on nutrient absorption and/or central suppression on feed-intake may represent alternative modes of action. Interestingly, cilia disruption has also been reported in zebrafish in response to other halogenated POPs such as PFOS (Huang et al., 2021), and histological examination of intestinal cell integrity including cilia development are warranted to probe potential effects on nutrient absorption. With regard to potential direct central effects of BDE-47 on feeding circuits, it is interesting to note that BDE-47 exposure decreased 5-HT-ir neurons in the zebrafish brain, a known anorexigenic factor in fish (Mennigen et al., 2009). In male mice, a 4 weeks exposure to 1 or 10 mg/kg/d BDE-47 resulted in ER-dependent alterations of several peptides involved in the regulation of feed intake and energy expenditure in the arcuate nucleus (Krumm et al., 2018). Overt effects on morphometric indices of growth were not observed, in line with reported findings of developmental delays or morphological effects of BDE-47 in zebrafish occur only at concentrations an order of magnitude higher than concentrations used in our experiment (Lema et al., 2007). Locomotory behaviour was unaffected by BDE-47 exposure, with the exception of reducing small movement speed under baseline conditions compared to control. These findings confirm previous locomotory analysis in zebrafish which revealed that zebrafish embryo single pulse static BDE-47 exposure at higher exposure concentrations (5–100 ppm) does not affect zebrafish locomotion at 4 and 6 dpf (Zhao et al., 2014). Together, the organismal level metabolic consequences of BDE-47 exposure affect similar endpoints as observed for PS exposure. An integrated overview of the organismal level phenotypic consequences of BDE-47 exposure is presented in **Figure 10B**.

4.3 Co-Exposure Enhances Organismal Level Metabolic Effects Observed for Individual PS and BDE-47 Exposures

Co-exposure of PS and BDE-47 increased zebrafish oxygen consumption-rate not only over control but also over BDE-47 and high PS. Similarly, feeding rate, a second endpoint observed to increase in response to PS and BDE-47 exposure alone further increased in PS + BDE-47 co-exposed zebrafish compared to BDE-47 and in the case of low PS exposed zebrafish, over PS alone. Thus, our data reveal that organismal level indices of energy balance are generally enhanced in co-exposures of PS and BDE-47. While the lack of internal BDE-47 and or PS sorption measurements precludes any conclusion regarding the importance of potential vector function of PS to enhance internal BDE-47 bioconcentration to mediate these effects, the additive and/or synergistic effects on early developing zebrafish energy metabolism, is further supported by a significant decrease of neutral lipid reserves in zebrafish co-exposed to high PS and BDE-47 compared to controls. This suggests that under high PS and BDE-47 co-exposure conditions, internal lipid energy reserves are increasingly mobilized to meet energetic demands. However, as in individual exposures, co-exposure did not affect morphometric indices and only mildly affected behaviour, which revealed a decrease in movement initiation events in high PS + BDE-47 compared to control, without however affecting distance, time spent on locomotion or speed. An integrated overview of the organismal level phenotypic consequences of enhanced organismal metabolic effects in response to PS and BDE-47 co-exposure is presented in **Figure 10C**. Given reports of mitochondrial disruption of both PS + BDE-47, further research should investigate whole zebrafish larval mitochondrial disruption of PS, BDE-47 and their combination in detail using adapted Seahorse assays (Souders et al., 2018).

4.5 High PS Exposure Attenuates BDE-47 Effects on Metabolic Gene Expression

To investigate potential molecular underpinnings indicative of metabolic disruption in PS, BDE-47 and PS + BDE-47 exposed zebrafish, we quantified the relative abundance of transcripts in whole larvae involved in lipid and glucose metabolism as well as peptides involved in (neuro)endocrine regulation of energy balance. Gene expression of *apoab,* but not *apoa1a,* was significantly induced by BDE-47, a response attenuated in co-exposure with high PS. The apolipoprotein genes *apoa1a* and *apoba* are comparatively well-characterized in early zebrafish development (Otis and Farber, 2016; Otis et al., 2019; Thierer et al., 2019; Templehof et al., 2021) and have been shown to be responsive to feeding status (Cruz-Garcia and Schlegel, 2014) and contaminants including BPA and PFOS as well as their replacement compounds BPS and F-53B (Sant et al., 2017; Wang W et al., 2018; Shi et al., 2019; Martínez et al., 2020). Gene expression of *apoba* is, similarly to *apoa1a* (Babin et al., 1997), strongly induced in the yolk syncytial layer at 2 dpf (Thierer et al., 2019; Templehof et al., 2021). Following the transition to exogenous feeding, *aboba* becomes restricted to liver (Thierer et al., 2019; Templehof et al., 2021) while *apoa1a* is expressed in endosomes and lysosomes in the liver and intestine (Otis and Farber, 2016; Otis et al., 2019). Its functional relevance in early developmental lipid metabolism remains however unknown, as homozygous gene deletion did not elicit changes in lipid metabolism (Templehof et al., 2021). BDE-47 also induced *insb* but not *insa* expression in zebrafish larvae, an effect attenuated by PS co-exposure. *Insa* and *insb* transcript abundance in early zebrafish development from 0–6 dpf has been shown to strongly increase and decrease, respectively (Papasani et al., 2006). While *insa* expression is restricted to the developing pancreas where it strongly increases after hatching, *insb* expression has been localized to both head region and pancreas using *in situ* hybridization and is minimal after 2 dpf, suggesting non-metabolic functions (Papasani et al., 2006). This expression pattern has been confirmed in CrispR/Cas9 mutants which revealed that while morphologically unaffected, pancreatic insulin was completely absent in *insa* but not *insb* mutants (Mullapudi et al., 2019). Functionally, this translates to severe metabolic disturbances including hyperglycemia and reduced yolk lipid metabolization in *insa* −/− larvae, but not *insb* −/− larvae. However, the lack of metabolic roles appears to be linked to low expression of *insb* after 2 dpf, as its overexpression successfully lowers glucose levels, revealing its metabolic function (Mullapudi et al., 2019). Interestingly, co-exposure of BDE-47 and PS revealed a marginally significant trend for decrease of pancreatic expressed *insa*, suggesting that co-exposure of high PS and BDE-47 may result in pancreatic toxicity reported in response to PS using *in situ* staining (Brun et al., 2019) and POPs using a zebrafish GFP-based insulin reporter line (Sant et al., 2017). Given the reported glucoregulatory function of *insb*, BDE-47-dependent induction of *insb* may be reflective of alterations of glucose metabolism. This is further corroborated by the simultaneous induction of *pck1,* a transcriptional indicator of glucose metabolism in early developing zebrafish (Elo et al., 2007; Gut et al., 2013; Brun et al., 2019). Both PS nanoplastics and BDE-47 have been linked to pancreatic toxicity and dysregulation of glucose metabolism (Zhang et al., 2016; Brun et al., 2019) and future studies should investigate the possibility of individual or cumulative effects of PS and BDE-47 on pancreatic oxidative stress and function using reporter lines in detail. Expression of *pomca* and *pomcb* was induced by BDE-47 and attenuated by co-exposure with high PS. The *pomca* was the only paralogue transcript investigated that was also responsive to PS, as low PS exposure also resulted in a significant increase. Expression of *pomc* is restricted to the pituitary corticotrophs at 1 dpf and responsive to modulation (Hansen et al., 2003; Liu et al., 2003). Compared to mammals, the zebrafish *pomc* gene has both conserved and differential roles on organismal energy metabolism (Shi et al., 2020). While *pomca* knockout in zebrafish induces increased body weight as in mammalian taxa, this increase in body weight represents, in contrast to mammalian *Pomc* knockout models, not a feed-intake mediated obesity phenotype. Instead, *pomca* knockout weight gain in zebrafish is dependent on *pomca* encoded ACTH, hypocortisolism associated hyperandrogenism, and is accompanied by a reduction in oxygen consumption (Shi et al., 2020). This is in direct contrast to mammalian *Pomc* knockout models, whose obesity phenotype is mediated by the loss of central inhibition of the feeding circuitry. Together, the targeted gene expression analysis is indicative of widespread stimulation of BDE-47 on energy metabolism pathways in zebrafish larvae which include induction of transcripts relevant to lipid and glucose metabolism, as well as endocrine factors involved in the regulation of energy metabolism. Comparatively, PS nanoplastic exposure only elicits an increase in *pomca* in the low PS exposure group. However, in all co-exposure groups, PS nanoplastics dose-dependently attenuate gene expression induced by BDE-47 to control group levels suggesting interaction of both compounds at the gene expression level.

5 CONCLUSION

Our study reveals that nanoplastics and BDE-47 similarly affect organismal level metabolic phenotype in zebrafish larvae and that co-exposure exacerbates this effect. Under the experimental conditions tested, zebrafish larvae appear to compensate for contaminant-induced increases in energy expenditure by increasing food intake and depleting lipid reserves while reducing acute oxygen consumptions rates. These changes generally do not manifestation in global behavioural or morphometric effects. Given the sensitivity of early developmental periods to long-term metabolic effects (Martínez et al., 2020), future studies should investigate possible metabolic consequences along developmental trajectories. As mitochondrial modes of actions have been described for both PS and BDE-47, future studies investigating whether additive and/or synergistic effects of PS and BDE-47 occur at the level of mitochondrial respiration are warranted. While the interaction between PS and BDE-47 on energy metabolism is also

evident at the transcript level, the directionality of changes is generally opposite to additive effects observed at the organismal level. Thus, caution is warranted when deducing functional interaction between PS nanoplastics and POPs based on (targeted) gene expression profiles. Indeed, the directionality (additivity/synergism or attenuation) of POP effects in zebrafish is not necessarily correlated with internal dosing, as microplastic absorption limited uptake of F-53B (a hydrophobic POP) but elicited both additive and attenuating effects on oxidative stress and immune function in zebrafish larvae (Wu et al., 2019; Yang et al., 2020).

Overall, this study clearly demonstrates cumulative effects of emerging nanoplastics compounds and persistent legacy contaminants on organismal energy balance in early development in zebrafish, a model relevant to both eco- and human toxicology. These findings thus provide novel mechanistic insight of cumulative metabolism-disrupting effects and raise concerns regarding possible impacts on aquatic wildlife and developmental origins of human metabolic disease.

DATA AVAILABILITY STATEMENT

The raw data supporting the conclusion of this article will be made available by the authors, without undue reservation.

ETHICS STATEMENT

The animal study was reviewed and approved by the ACVS University of Ottawa.

AUTHOR CONTRIBUTIONS

SA-G and FP-L initiated the project. SA-G, FP-L, and JM conceived and designed the study. RC, TE, EX, SM, FP-L, SA-G ER, NT, EH, and JAM contributed to the acquisition, analysis, and interpretation of the data. RC, TE and JAM wrote the first draft of the manuscript and all authors contributed to manuscript revision and edits and approved the submitted version. SA-G, FP-L, NT, EH, and JAM secured funding and/or supported the project through in-kind contributions.

FUNDING

This study was improved by input and advice from Jason O'Brien, Robert Letcher and Hans Larsson. This study was supported by funds from EcoCanada, the Environment and Climate Change Canada Science and Technology Branch, the Killam Research Fellowship, the Canada Research Chairs program, the Natural Sciences and Engineering Research Council of Canada through CREATE PURE and NSERC-DG grants, the FRQNT funded Regroupement des Écotoxicologues du Québec. The Canada Foundation for Innovation (John R. Evans Leaders' fund).

SUPPLEMENTARY MATERIAL

The Supplementary Material for this article can be found online at: https://www.frontiersin.org/articles/10.3389/fphar.2022.822111/full#supplementary-material

Supplementary Figure 1 | Fluorescence microscopy-based investigation of tissue distribution of fluorescently labelled PS nanoplastic particles in intestine, gill and liver of control. **(A-C)** and 25 ppm PS-exposed **(D-F)** adult zebrafish.

REFERENCES

Babin, P. J., Thisse, C., Durliat, M., Andre, M., Akimenko, M. A., and Thisse, B. (1997). Both apolipoprotein E and A-I Genes Are Present in a Nonmammalian Vertebrate and Are Highly Expressed during Embryonic Development. *Proc. Natl. Acad. Sci. U S A.* 94, 8622–8627. doi:10.1073/pnas.94.16.8622

Bambino, K., and Chu, J. (2017). Zebrafish in Toxicology and Environmental Health. *Curr. Top. Dev. Biol.* 124, 331–367. doi:10.1016/bs.ctdb.2016.10.007

Barnes, D. K., Galgani, F., Thompson, R. C., and Barlaz, M. (2009). Accumulation and Fragmentation of Plastic Debris in Global Environments. *Philos. Trans. R. Soc. Lond. B Biol. Sci.* 364, 1985–1998. doi:10.1098/rstb.2008.0205

Benchoula, K., Khatib, A., Jaffar, A., Ahmed, Q. U., Sulaiman, W. M. A. W., Wahab, R. A., et al. (2019). The Promise of Zebrafish as a Model of Metabolic Syndrome. *Exp. Anim.* 68, 407–416. doi:10.1538/expanim.18-0168

Berger, J., Sztal, T., and Currie, P. D. (2012). Quantification of Birefringence Readily Measures the Level of Muscle Damage in Zebrafish. *Biochem. Biophys. Res. Commun.* 423, 785–788. doi:10.1016/j.bbrc.2012.06.040

Brun, N. R., Koch, B. E. V., Varela, M., Peijnenburg, W. J. G. M., Spaink, H. P., and Vijver, M. G. (2018). Nanoparticles Induce Dermal and Intestinal Innate Immune System Responses in Zebrafish Embryos. *Environ. Sci. Nano* 5, 904–916. doi:10.1039/C8EN00002F

Brun, N. R., van Hage, P., Hunting, E. R., Haramis, A. G., Vink, S. C., Vijver, M. G., et al. (2019). Polystyrene Nanoplastics Disrupt Glucose Metabolism and Cortisol Levels with a Possible Link to Behavioural Changes in Larval Zebrafish. *Commun. Biol.* 2, 382. doi:10.1038/s42003-019-0629-6

Cedervall, T., Hansson, L. A., Lard, M., Frohm, B., and Linse, S. (2012). Food Chain Transport of Nanoparticles Affects Behaviour and Fat Metabolism in Fish. *PLoS One* 7, e32254. doi:10.1371/journal.pone.0032254

Chae, Y., Kim, D., Kim, S. W., and An, Y. J. (2018). Trophic Transfer and Individual Impact of Nano-Sized Polystyrene in a Four-Species Freshwater Food Chain. *Sci. Rep.* 8, 284. doi:10.1038/s41598-017-18849-y

Chen, X., Huang, C., Wang, X., Chen, J., Bai, C., Chen, Y., et al. (2012). BDE-47 Disrupts Axonal Growth and Motor Behavior in Developing Zebrafish. *Aquat. Toxicol.* 120-121, 35–44. doi:10.1016/j.aquatox.2012.04.014

Chen, Q., Gundlach, M., Yang, S., Jiang, J., Velki, M., Yin, D., et al. (2017). Quantitative Investigation of the Mechanisms of Microplastics and Nanoplastics toward Zebrafish Larvae Locomotor Activity. *Sci. Total Environ.* 584-585 (585), 1022–1031. doi:10.1016/j.scitotenv.2017.01.156

Clunies-Ross, P., Smith, G., Gordon, K., and Gaw, S. (2016). Synthetic Shorelines in New Zealand? Quantification and Characterisation of Microplastic Pollution on Canterbury's Coastlines. *New Zealand J. Mar. Freshw. Res.* 50, 317–325. doi:10.1080/00288330.2015.1132747

Costa, L. G., Pellacani, C., Dao, K., Kavanagh, T. J., and Roque, P. J. (2015). The Brominated Flame Retardant BDE-47 Causes Oxidative Stress and Apoptotic Cell Death *In Vitro* and *In Vivo* in Mice. *Neurotoxicology* 48, 68–76. doi:10.1016/j.neuro.2015.03.008

Cruz-Garcia, L., and Schlegel, A. (2014). Lxr-driven Enterocyte Lipid Droplet Formation Delays Transport of Ingested Lipids. *J. Lipid Res.* 55, 1944–1958. doi:10.1194/jlr.M052845

Dai, Y. J., Jia, Y. F., Chen, N., Bian, W. P., Li, Q. K., Ma, Y. B., et al. (2014). Zebrafish as a Model System to Study Toxicology. *Environ. Toxicol. Chem.* 33, 11–17. doi:10.1002/etc.2406

Ding, J., Zhang, S., Razanajatovo, R. M., Zou, H., and Zhu, W. (2018). Accumulation, Tissue Distribution, and Biochemical Effects of Polystyrene Microplastics in the Freshwater Fish Red tilapia (*Oreochromis niloticus*). *Environ. Pollut.* 238, 1–9. doi:10.1016/j.envpol.2018.03.001

Elo, B., Villano, C. M., Govorko, D., and White, L. A. (2007). Larval Zebrafish as a Model for Glucose Metabolism: Expression of Phosphoenolpyruvate Carboxykinase as a Marker for Exposure to Anti-diabetic Compounds. *J. Mol. Endocrinol.* 38, 433–440. doi:10.1677/JME-06-0037

Farrell, P., and Nelson, K. (2013). Trophic Level Transfer of Microplastic: *Mytilus edulis* (L.) to *Carcinus maenas* (L.). *Environ. Pollut.* 177, 1–3. doi:10.1016/j.envpol.2013.01.046

Fernie, K. J., Shutt, J. L., Mayne, G., Hoffman, D., Letcher, R. J., Drouillard, K. G., et al. (2005). Exposure to Polybrominated Diphenyl Ethers (PBDEs): Changes in Thyroid, Vitamin A, Glutathione Homeostasis, and Oxidative Stress in American Kestrels (*Falco sparverius*). *Toxicol. Sci.* 88, 375–383. doi:10.1093/toxsci/kfi295

Frederiksen, M., Vorkamp, K., Mathiesen, L., Mose, T., and Knudsen, L. E. (2010). Placental Transfer of the Polybrominated Diphenyl Ethers BDE-47, BDE-99 and BDE-209 in a Human Placenta Perfusion System: an Experimental Study. *Environ. Health* 9, 32. doi:10.1186/1476-069X-9-32

Garcia, G. R., Noyes, P. D., and Tanguay, R. L. (2016). Advancements in Zebrafish Applications for 21st century Toxicology. *Pharmacol. Ther.* 161, 11–21. doi:10.1016/j.pharmthera.2016.03.009

Gigault, J., El Hadri, H., Nguyen, B., Grassl, B., Rowenczyk, L., Tufenkji, N., et al. (2021). Nanoplastics Are Neither Microplastics Nor Engineered Nanoparticles. *Nat. Nanotechnol.* 16, 501–507. doi:10.1038/s41565-021-00886-4

Girden, E. R. (1992). *ANOVA: Repeated Measures*. Newbury Park, CA: Sage.

Gut, P., Baeza-Raja, B., Andersson, O., Hasenkamp, L., Hsiao, J., Hesselson, D., et al. (2013). Whole-organism Screening for Gluconeogenesis Identifies Activators of Fasting Metabolism. *Nat. Chem. Biol.* 9, 97–104. doi:10.1038/nchembio.1136

Handy, R. D., Sims, D. W., Giles, A., Campbell, H. A., and Musonda, M. M. (1999). Metabolic Trade-Off between Locomotion and Detoxification for Maintenance of Blood Chemistry and Growth Parameters by Rainbow trout (*Oncorhynchus mykiss*) during Chronic Dietary Exposure to Copper. *Aquat. Toxicol.* 47, 23–41. doi:10.1016/S0166-445X(99)00004-1

Hansen, I. A., To, T. T., Wortmann, S., Burmester, T., Winkler, C., Meyer, S. R., et al. (2003). The Pro-opiomelanocortin Gene of the Zebrafish (*Danio rerio*). *Biochem. Biophys. Res. Commun.* 303, 1121–1128. doi:10.1016/s0006-291x(03)00475-3

Heckmann, L. H., Sørensen, P. B., Krogh, P. H., and Sørensen, J. G. (2011). NORMA-Gene: a Simple and Robust Method for qPCR Normalization Based on Target Gene Data. *BMC Bioinformatics* 12, 250. doi:10.1186/1471-2105-12-250

Hendrickson, E., Minor, E. C., and Schreiner, K. (2018). Microplastic Abundance and Composition in Western Lake Superior as Determined via Microscopy, Pyr-GC/MS, and FTIR. *Environ. Sci. Technol.* 52, 1787–1796. doi:10.1021/acs.est.7b05829

Hites, R. A. (2004). Polybrominated Diphenyl Ethers in the Environment and in People: a Meta-Analysis of Concentrations. *Environ. Sci. Technol.* 38, 945–956. doi:10.1021/es035082g

Horton, A. A., Newbold, L. K., Palacio-Cortés, A. M., Spurgeon, D. J., Pereira, M. G., Carter, H., et al. (2020). Accumulation of Polybrominated Diphenyl Ethers and Microbiome Response in the Great Pond Snail *Lymnaea stagnalis* with Exposure to Nylon (Polyamide) Microplastics. *Ecotoxicol Environ. Saf.* 188, 109882. doi:10.1016/j.ecoenv.2019.109882

Hu, M., and Palić, D. (2020). Micro- and Nano-Plastics Activation of Oxidative and Inflammatory Adverse Outcome Pathways. *Redox Biol.* 37, 101620. doi:10.1016/j.redox.2020.101620

Huang, J., Sun, L., Mennigen, J. A., Liu, Y., Liu, S., Zhang, M., et al. (2021). Developmental Toxicity of the Novel PFOS Alternative OBS in Developing Zebrafish: An Emphasis on Cilia Disruption. *J. Hazard. Mater.* 409, 124491. doi:10.1016/j.jhazmat.2020.124491

Ibrahim, Y. S., Tuan Anuar, S., Azmi, A. A., Wan Mohd Khalik, W. M. A., Lehata, S., Hamzah, S. R., et al. (2021). Detection of Microplastics in Human Colectomy Specimens. *JGH Open* 5, 116–121. doi:10.1002/jgh3.12457

Jones, K. S., Alimov, A. P., Rilo, H. L., Jandacek, R. J., Woollett, L. A., and Penberthy, W. T. (2008). A High Throughput Live Transparent Animal Bioassay to Identify Non-toxic Small Molecules or Genes that Regulate Vertebrate Fat Metabolism for Obesity Drug Development. *Nutr. Metab. (Lond)* 5, 23. doi:10.1186/1743-7075-5-23

Jovanović, B. (2017). Ingestion of Microplastics by Fish and its Potential Consequences from a Physical Perspective. *Integr. Environ. Assess. Manag.* 13, 510–515. doi:10.1002/ieam.1913

Mansouri, K., Consonni, V., Durjava, M. K., Kolar, B., Öberg, T., and Todeschini, R. (2012). Assessing Bioaccumulation of Polybrominated Diphenyl Ethers for Aquatic Species by QSAR Modeling. *Chemosphere* 89, 433–444. doi:10.1016/j.chemosphere.2012.05.081

Kimmel, C. B., Ballard, W. W., Kimmel, S. R., Ullmann, B., and Schilling, T. F. (1995). Stages of Embryonic Development of the Zebrafish. *Dev. Dyn.* 203, 253–310. doi:10.1002/aja.1002030302

Koelmans, A. A., Besseling, E., and Shim, W. J. (2015a). "Nanoplastics in the Aquatic Environment. Critical Review," in *Marine Anthropogenic Litter*. Editors M. Bergmann, L. Gutow, and M. Klages (Cham: Springer International Publishing), 325–340. doi:10.1007/978-3-319-16510-3_12

Koelmans, A. A., Quik, J. T., and Velzeboer, I. (2015b). Lake Retention of Manufactured Nanoparticles. *Environ. Pollut.* 196, 171–175. doi:10.1016/j.envpol.2014.09.025

Koenig, C. M., Lango, J., Pessah, I. N., and Berman, R. F. (2012). Maternal Transfer of BDE-47 to Offspring and Neurobehavioral Development in C57BL/6J Mice. *Neurotoxicol. Teratol.* 34, 571–580. doi:10.1016/j.ntt.2012.09.005

Krumm, E. A., Patel, V. J., Tillery, T. S., Yasrebi, A., Shen, J., Guo, G. L., et al. (2018). Organophosphate Flame-Retardants Alter Adult Mouse Homeostasis and Gene Expression in a Sex-dependent Manner Potentially through Interactions with ERα. *Toxicol. Sci.* 162, 212–224. doi:10.1093/toxsci/kfx238

Lebreton, L. C. M., van der Zwet, J., Damsteeg, J. W., Slat, B., Andrady, A., and Reisser, J. (2017). River Plastic Emissions to the World's Oceans. *Nat. Commun.* 8, 15611. doi:10.1038/ncomms15611

Lee, H., Shim, W. J., and Kwon, J. H. (2014). Sorption Capacity of Plastic Debris for Hydrophobic Organic Chemicals. *Sci. Total Environ.* 470-471, 1545–1552. doi:10.1016/j.scitotenv.2013.08.023

Legradi, J., Pomeren, M. V., Dahlberg, A. K., and Legler, J. (2017). Effects of Hydroxylated Polybrominated Diphenyl Ethers in Developing Zebrafish Are Indicative of Disruption of Oxidative Phosphorylation. *Int. J. Mol. Sci.* 18, 970. doi:10.3390/ijms18050970

Lema, S. C., Schultz, I. R., Scholz, N. L., Incardona, J. P., and Swanson, P. (2007). Neural Defects and Cardiac Arrhythmia in Fish Larvae Following Embryonic Exposure to 2,2',4,4'-tetrabromodiphenyl Ether (PBDE 47). *Aquat. Toxicol.* 82, 296–307. doi:10.1016/j.aquatox.2007.03.002

Liu, N. A., Huang, H., Yang, Z., Herzog, W., Hammerschmidt, M., Lin, S., et al. (2003). Pituitary Corticotroph Ontogeny and Regulation in Transgenic Zebrafish. *Mol. Endocrinol.* 17, 959–966. doi:10.1210/me.2002-0392

Liu, H., Tang, S., Zheng, X., Zhu, Y., Ma, Z., Liu, C., et al. (2015). Bioaccumulation, Biotransformation, and Toxicity of BDE-47, 6-OH-BDE-47, and 6-MeO-BDE-47 in Early Life-Stages of Zebrafish (*Danio rerio*). *Environ. Sci. Technol.* 49, 1823–1833. doi:10.1021/es503833q

Lu, Y., Zhang, Y., Deng, Y., Jiang, W., Zhao, Y., Geng, J., et al. (2016). Response to Comment on "Uptake and Accumulation of Polystyrene Microplastics in Zebrafish (*Danio rerio*) and Toxic Effects in Liver". *Environ. Sci. Technol.* 50, 12523–12524. doi:10.1021/acs.est.6b04379

Lu, H.-C., Ziajahromi, S., Neale, P. A., and Leusch, F. D. L. (2021). A Systematic Review of Freshwater Microplastics in Water and Sediments: Recommendations for Harmonisation to Enhance Future Study Comparisons. *Sci. Total Environ.* 781, 146693. doi:10.1016/j.scitotenv.2021.146693

Martínez, R., Tu, W., Eng, T., Allaire-Leung, M., Piña, B., Navarro-Martín, L., et al. (2020). Acute and Long-Term Metabolic Consequences of Early Developmental Bisphenol A Exposure in Zebrafish (*Danio rerio*). *Chemosphere* 256, 127080. doi:10.1016/j.chemosphere.2020.127080

Mattsson, K., Johnson, E. V., Malmendal, A., Linse, S., Hansson, L. A., and Cedervall, T. (2017). Brain Damage and Behavioural Disorders in Fish Induced by Plastic Nanoparticles Delivered through the Food Chain. *Sci. Rep.* 7, 11452. doi:10.1038/s41598-017-10813-0

Mazdai, A., Dodder, N. G., Abernathy, M. P., Hites, R. A., and Bigsby, R. M. (2003). Polybrominated Diphenyl Ethers in Maternal and Fetal Blood Samples. *Environ. Health Perspect.* 111, 1249–1252. doi:10.1289/ehp.6146

McIntyre, R. L., Kenerson, H. L., Subramanian, S., Wang, S. A., Kazami, M., Stapleton, H. M., et al. (2015). Polybrominated Diphenyl Ether Congener, BDE-47, Impairs Insulin Sensitivity in Mice with Liver-specific Pten Deficiency. *BMC Obes.* 2, 3. doi:10.1186/s40608-014-0031-3

Meng, S., Chen, X., Gyimah, E., Xu, H., and Chen, J. (2020). Hepatic Oxidative Stress, DNA Damage and Apoptosis in Adult Zebrafish Following Sub-chronic Exposure to BDE-47 and BDE-153. *Environ. Toxicol.* 35, 1202–1211. doi:10.1002/tox.22985

Mennigen, J. A., Harris, E. A., Chang, J. P., Moon, T. W., and Trudeau, V. L. (2009). Fluoxetine Affects Weight Gain and Expression of Feeding Peptides in the Female Goldfish Brain. *Regul. Pept.* 155, 99–104. doi:10.1016/j.regpep.2009.01.001

Messina, C. M., Espinosa Ruiz, C., Regoli, F., Manuguerra, S., D'Agostino, F., Avellone, G., et al. (2020). BDE-47 Exposure Modulates Cellular Responses, Oxidative Stress and Biotransformation Related-Genes in *Mytilus galloprovincialis*. *Fish. Shellfish Immunol.* 107, 537–546. doi:10.1016/j.fsi.2020.11.015

Minchin, J. E., and Rawls, J. F. (2017). *In Vivo* imaging and Quantification of Regional Adiposity in Zebrafish. *Methods Cel Biol.* 138, 3–27. doi:10.1016/bs.mcb.2016.11.010

Mitrano, D. M., Wick, P., and Nowack, B. (2021). Placing Nanoplastics in the Context of Global Plastic Pollution. *Nat. Nanotechnol.* 16, 491–500. doi:10.1038/s41565-021-00888-2

Mohammed, A. (2013). "Why Are Early Life Stages of Aquatic Organisms More Sensitive to Toxicants Than Adults," in *New Insights into Toxicity and Drug Testing* (Rijeka, Croatia: IntechOpen). Available at: https://www.intechopen.com/chapters/42016 (Accessed August 13, 2021).

Mullapudi, S. T., Boezio, G. L. M., Rossi, A., Marass, M., Matsuoka, R. L., Matsuda, H., et al. (2019). Disruption of the Pancreatic Vasculature in Zebrafish Affects Islet Architecture and Function. *Development* 146, dev173674. doi:10.1242/dev.173674

Otis, J. P., and Farber, S. A. (2016). High-fat Feeding Paradigm for Larval Zebrafish: Feeding, Live Imaging, and Quantification of Food Intake. *JoVE* (116), 54735. doi:10.3791/54735

Otis, J. P., Shen, M. C., Caldwell, B. A., Reyes Gaido, O. E., and Farber, S. A. (2019). Dietary Cholesterol and Apolipoprotein A-I Are Trafficked in Endosomes and Lysosomes in the Live Zebrafish Intestine. *Am. J. Physiol. Gastrointest. Liver Physiol.* 316, G350–G365. doi:10.1152/ajpgi.00080.2018

Papasani, M. R., Robison, B. D., Hardy, R. W., and Hill, R. A. (2006). Early Developmental Expression of Two Insulins in Zebrafish (*Danio rerio*). *Physiol. Genomics* 27, 79–85. doi:10.1152/physiolgenomics.00012.2006

Pikuda, O., Xu, E., Berk, D., and Tufenkji, N. (2019). Toxicity Assessments of Micro- and Nanoplastics Can Be Confounded by Preservatives in Commercial Formulations. *Environ. Sci. Technol. Lett.* 6 (1), 21–25. doi:10.1021/acs.estlett.8b00614

Pitt, J. A., Kozal, J. S., Jayasundara, N., Massarsky, A., Trevisan, R., Geitner, N., et al. (2018). Uptake, Tissue Distribution, and Toxicity of Polystyrene Nanoparticles in Developing Zebrafish (*Danio rerio*). *Aquat. Toxicol.* 194, 185–194. doi:10.1016/j.aquatox.2017.11.017

Qiang, L., and Cheng, J. (2019). Exposure to Microplastics Decreases Swimming Competence in Larval Zebrafish (*Danio rerio*). *Ecotoxicol Environ. Saf.* 176, 226–233. doi:10.1016/j.ecoenv.2019.03.088

Reid, R. M., D'Aquila, A. L., and Biga, P. R. (2018). The Validation of a Sensitive, Non-toxic *In Vivo* Metabolic Assay Applicable across Zebrafish Life Stages. *Comp. Biochem. Physiol. C Toxicol. Pharmacol.* 208, 29–37. doi:10.1016/j.cbpc.2017.11.004

Renquist, B. J., Zhang, C., Williams, S. Y., and Cone, R. D. (2013). Development of an Assay for High-Throughput Energy Expenditure Monitoring in the Zebrafish. *Zebrafish* 10, 343–352. doi:10.1089/zeb.2012.0841

Revel, M., Châtel, A., and Mouneyrac, C. (2018). Micro(nano)plastics: A Threat to Human Health? *Curr. Opin. Environ. Sci. Health* 1, 17–23. doi:10.1016/j.coesh.2017.10.003

Sant, K. E., Jacobs, H. M., Borofski, K. A., Moss, J. B., and Timme-Laragy, A. R. (2017). Embryonic Exposures to Perfluorooctanesulfonic Acid (PFOS) Disrupt Pancreatic Organogenesis in the Zebrafish, *Danio rerio*. *Environ. Pollut.* 220, 807–817. doi:10.1016/j.envpol.2016.10.057

Sarasamma, S., Audira, G., Siregar, P., Malhotra, N., Lai, Y. H., Liang, S. T., et al. (2020). Nanoplastics Cause Neurobehavioral Impairments, Reproductive and Oxidative Damages, and Biomarker Responses in Zebrafish: Throwing up Alarms of Wide Spread Health Risk of Exposure. *Int. J. Mol. Sci.* 21, E1410. doi:10.3390/ijms21041410

Schür, C., Rist, S., Baun, A., Mayer, P., Hartmann, N. B., and Wagner, M. (2019). When Fluorescence Is Not a Particle: The Tissue Translocation of Microplastics in Daphnia Magna Seems an Artifact. *Environ. Toxicol. Chem.* 38, 1495. doi:10.1002/etc.4436

Schwabl, P., Köppel, S., Königshofer, P., Bucsics, T., Trauner, M., Reiberger, T., et al. (2019). Detection of Various Microplastics in Human Stool: A Prospective Case Series. *Ann. Intern. Med.* 171, 453–457. doi:10.7326/M19-0618

Scott, G. R., and Sloman, K. A. (2004). The Effects of Environmental Pollutants on Complex Fish Behaviour: Integrating Behavioural and Physiological Indicators of Toxicity. *Aquat. Toxicol.* 68, 369–392. doi:10.1016/j.aquatox.2004.03.016

Senathirajah, K., Attwood, S., Bhagwat, G., Carbery, M., Wilson, S., and Palanisami, T. (2021). Estimation of the Mass of Microplastics Ingested - A Pivotal First Step towards Human Health Risk Assessment. *J. Hazard. Mater.* 404, 124004. doi:10.1016/j.jhazmat.2020.124004

Seth, A., Stemple, D. L., and Barroso, I. (2013). The Emerging Use of Zebrafish to Model Metabolic Disease. *Dis. Model. Mech.* 6, 1080–1088. doi:10.1242/dmm.011346

Shao, J., White, C. C., Dabrowski, M. J., Kavanagh, T. J., Eckert, M. L., and Gallagher, E. P. (2008). The Role of Mitochondrial and Oxidative Injury in BDE 47 Toxicity to Human Fetal Liver Hematopoietic Stem Cells. *Toxicol. Sci.* 101, 81–90. doi:10.1093/toxsci/kfm256

Shi, G., Cui, Q., Wang, J., Guo, H., Pan, Y., Sheng, N., et al. (2019). Chronic Exposure to 6:2 Chlorinated Polyfluorinated Ether Sulfonate Acid (F-53B) Induced Hepatotoxic Effects in Adult Zebrafish and Disrupted the PPAR Signaling Pathway in Their Offspring. *Environ. Pollut.* 249, 550–559. doi:10.1016/j.envpol.2019.03.032

Shi, C., Lu, Y., Zhai, G., Huang, J., Shang, G., Lou, Q., et al. (2020). Hyperandrogenism in POMCa-Deficient Zebrafish Enhances Somatic Growth without Increasing Adiposity. *J. Mol. Cel Biol.* 12, 291–304. doi:10.1093/jmcb/mjz053

Skjolding, L. M., Ašmonaitė, G., Jølck, R. I., Andresen, T. L., Selck, H., Baun, A., et al. (2017). An Assessment of the Importance of Exposure Routes to the Uptake and Internal Localisation of Fluorescent Nanoparticles in Zebrafish (*Danio rerio*), Using Light Sheet Microscopy. *Nanotoxicology* 11, 351–359. doi:10.1080/17435390.2017.1306128

Smith, L. L., Beggs, A. H., and Gupta, V. A. (2013). Analysis of Skeletal Muscle Defects in Larval Zebrafish by Birefringence and Touch-Evoke Escape Response Assays. *JoVE* (82), e50925. doi:10.3791/50925

Souders, C. L., Liang, X., Wang, X., Ector, N., Zhao, Y. H., and Martyniuk, C. J. (2018). High-throughput Assessment of Oxidative Respiration in Fish Embryos: Advancing Adverse Outcome Pathways for Mitochondrial Dysfunction. *Aquat. Toxicol.* 199, 162–173. doi:10.1016/j.aquatox.2018.03.031

Streets, S. S., Henderson, S. A., Stoner, A. D., Carlson, D. L., Simcik, M. F., and Swackhamer, D. L. (2006). Partitioning and Bioaccumulation of PBDEs and PCBs in Lake Michigan. *Environ. Sci. Technol.* 40, 7263–7269. doi:10.1021/es061337p

Sun, B., Liu, J., Zhang, Y. Q., Leungb, K. M. Y., and Zeng, E. Y. (2021). Leaching of Polybrominated Diphenyl Ethers from Microplastics in Fish Oil: Kinetics and Bioaccumulation. *J. Hazard. Mater.* 406, 124726. doi:10.1016/j.jhazmat.2020.124726

Tagliaferri, S., Caglieri, A., Goldoni, M., Pinelli, S., Alinovi, R., Poli, D., et al. (2010). Low Concentrations of the Brominated Flame Retardants BDE-47 and BDE-99 Induce Synergistic Oxidative Stress-Mediated Neurotoxicity in Human Neuroblastoma Cells. *Toxicol. Vitro* 24, 116–122. doi:10.1016/j.tiv.2009.08.020

Templehof, H., Moshe, N., Avraham-Davidi, I., and Yaniv, K. (2021). Zebrafish Mutants Provide Insights into Apolipoprotein B Functions during Embryonic Development and Pathological Conditions. *JCI Insight* 6, 130399. doi:10.1172/jci.insight.130399

Ter Halle, A., Ladirat, L., Martignac, M., Mingotaud, A. F., Boyron, O., and Perez, E. (2017). To what Extent Are Microplastics from the Open Ocean Weathered? *Environ. Pollut.* 227, 167–174. doi:10.1016/j.envpol.2017.04.051

Thierer, J. H., Ekker, S. C., and Farber, S. A. (2019). The LipoGlo Reporter System for Sensitive and Specific Monitoring of Atherogenic Lipoproteins. *Nat. Commun.* 10, 3426. doi:10.1038/s41467-019-11259-w

Torres, L., Orazio, C. E., Peterman, P. H., and Patiño, R. (2013). Effects of Dietary Exposure to Brominated Flame Retardant BDE-47 on Thyroid Condition, Gonadal Development and Growth of Zebrafish. *Fish. Physiol. Biochem.* 39, 1115–1128. doi:10.1007/s10695-012-9768-0

Trevisan, R., Voy, C., Chen, S., and Di Giulio, R. T. (2019). Nanoplastics Decrease the Toxicity of a Complex PAH Mixture but Impair Mitochondrial Energy Production in Developing Zebrafish. *Environ. Sci. Technol.* 53, 8405–8415. doi:10.1021/acs.est.9b02003

Trevisan, R., Uzochukwu, D., and Di Giulio, R. T. (2020). PAH Sorption to Nanoplastics and the Trojan Horse Effect as Drivers of Mitochondrial Toxicity and Pah Localization in Zebrafish. *Front. Environ. Sci.* 8, 78. doi:10.3389/fenvs.2020.00078

Tu, W., Martínez, R., Navarro-Martin, L., Kostyniuk, D. J., Hum, C., Huang, J., et al. (2019). Bioconcentration and Metabolic Effects of Emerging PFOS Alternatives in Developing Zebrafish. *Environ. Sci. Technol.* 53, 13427–13439. doi:10.1021/acs.est.9b03820

Usenko, C. Y., Robinson, E. M., Bruce, E. D., and Usenko, S. (2013). Uptake and Metabolism of Individual Polybrominated Diphenyl Ether Congeners by Embryonic Zebrafish. *Environ. Toxicol. Chem.* 32, 1153–1160. doi:10.1002/etc.2163

Usenko, C. Y., Abel, E. L., Kudela, M., Janise, A., and Bruce, E. D. (2015). Comparison of PBDE Congeners as Inducers of Oxidative Stress in Zebrafish. *Environ. Toxicol. Chem.* 34, 1154–1160. doi:10.1002/etc.2922

van Pomeren, M., Brun, N. R., Peijnenburg, W. J. G. M., and Vijver, M. G. (2017). Exploring Uptake and Biodistribution of Polystyrene (Nano)particles in Zebrafish Embryos at Different Developmental Stages. *Aquat. Toxicol.* 190, 40–45. doi:10.1016/j.aquatox.2017.06.017

Wang D, D., Yan, J., Teng, M., Yan, S., Zhou, Z., and Zhu, W. (2018). In Utero and Lactational Exposure to BDE-47 Promotes Obesity Development in Mouse Offspring Fed a High-Fat Diet: Impaired Lipid Metabolism and Intestinal Dysbiosis. *Arch. Toxicol.* 92, 1847–1860. doi:10.1007/s00204-018-2177-0

Wang W, W., Zhang, X., Wang, Z., Qin, J., Wang, W., Tian, H., et al. (2018). Bisphenol S Induces Obesogenic Effects through Deregulating Lipid Metabolism in Zebrafish (*Danio rerio*) Larvae. *Chemosphere* 199, 286–296. doi:10.1016/j.chemosphere.2018.01.163

Watts, A. J., Lewis, C., Goodhead, R. M., Beckett, S. J., Moger, J., Tyler, C. R., et al. (2014). Uptake and Retention of Microplastics by the Shore Crab *Carcinus maenas*. *Environ. Sci. Technol.* 48, 8823–8830. doi:10.1021/es501090e

Webster, T., Vieira, V., and Schecter, A. (2005). Estimating Human Exposure to PBDE-47 via Air, Food and Dust Using Monte Carlo Methods. *Brominated Flame Retardants* 67, 505–508.

Wen, Q., Liu, H. L., Zhu, Y. T., Zheng, X. M., Su, G. Y., Zhang, X. W., et al. (2015). Maternal Transfer, Distribution, and Metabolism of BDE-47 and its Related Hydroxylated, Methoxylated Analogs in Zebrafish (*Danio rerio*). *Chemosphere* 120, 31–36. doi:10.1016/j.chemosphere.2014.05.050

Williams, S. Y., and Renquist, B. J. (2016). High Throughput Danio Rerio Energy Expenditure Assay. *JoVE* (107), e53297. doi:10.3791/53297

Wu, Y., Huang, J., Deng, M., Jin, Y., Yang, H., Liu, Y., et al. (2019). Acute Exposure to Environmentally Relevant Concentrations of Chinese PFOS Alternative F-53B Induces Oxidative Stress in Early Developing Zebrafish. *Chemosphere* 235, 945–951. doi:10.1016/j.chemosphere.2019.07.016

Wu, J., Xu, P., Chen, Q., Ma, D., Ge, W., Jiang, T., et al. (2020). Effects of Polymer Aging on Sorption of 2,2',4,4'-tetrabromodiphenyl Ether by Polystyrene Microplastics. *Chemosphere* 253, 126706. doi:10.1016/j.chemosphere.2020.126706

Xu, P., Ge, W., Chai, C., Zhang, Y., Jiang, T., and Xia, B. (2019). Sorption of Polybrominated Diphenyl Ethers by Microplastics. *Mar. Pollut. Bull.* 145, 260–269. doi:10.1016/j.marpolbul.2019.05.050

Yang, C., Harrad, S., Abdallah, M. A., Desborough, J., Rose, N. L., Turner, S. D., et al. (2014). Polybrominated Diphenyl Ethers (PBDEs) in English Freshwater Lakes, 2008-2012. *Chemosphere* 110, 41–47. doi:10.1016/j.chemosphere.2014.03.028

Yang, H., Lai, H., Huang, J., Sun, L., Mennigen, J. A., Wang, Q., et al. (2020). Polystyrene Microplastics Decrease F-53B Bioaccumulation but Induce Inflammatory Stress in Larval Zebrafish. *Chemosphere* 255, 127040. doi:10.1016/j.chemosphere.2020.127040

Yang, Y., Jian, X., Tang, X., Ma, W., Sun, Z., Zhang, X., et al. (2021). Feeding Behavior Toxicity in the marine Rotifer *Brachionus plicatilis* Caused by 2,2',4,4'-tetrabromodiphenyl Ether (BDE-47): Characteristics and Mechanisms. *Chemosphere* 271, 129512. doi:10.1016/j.chemosphere.2020.129512

Yee, M. S.-L., Hii, L.-W., Looi, C. K., Lim, W.-M., Wong, S.-F., Kok, Y.-Y., et al. (2021). Impact of Microplastics and Nanoplastics on Human Health. *Nanomaterials* 11, 496. doi:10.3390/nano11020496

Zhang, Y., and Goss, G. G. (2020). Potentiation of Polycyclic Aromatic Hydrocarbon Uptake in Zebrafish Embryos by Nanoplastics. *Environ. Sci. Nano* 7, 1730–1741. doi:10.1039/D0EN00163E

Zhang, Z., Li, S., Liu, L., Wang, L., Xiao, X., Sun, Z., et al. (2016). Environmental Exposure to BDE47 Is Associated with Increased Diabetes Prevalence: Evidence from Community-Based Case-Control Studies and an Animal experiment. *Sci. Rep.* 6, 27854. doi:10.1038/srep27854

Zhang, W., Zhang, S., Wang, J., Wang, Y., Mu, J., Wang, P., et al. (2017). Microplastic Pollution in the Surface Waters of the Bohai Sea, China. *Environ. Pollut.* 231, 541–548. doi:10.1016/j.envpol.2017.08.058

Zhao, J., Xu, T., and Yin, D. Q. (2014). Locomotor Activity Changes on Zebrafish Larvae with Different 2,2',4,4'-tetrabromodiphenyl Ether (PBDE-47) Embryonic Exposure Modes. *Chemosphere* 94, 53–61. doi:10.1016/j.chemosphere.2013.09.010

Zheng, X., Zhu, Y., Liu, C., Liu, H., Giesy, J. P., Hecker, M., et al. (2012). Accumulation and Biotransformation of BDE-47 by Zebrafish Larvae and Teratogenicity and Expression of Genes along the Hypothalamus-Pituitary-Thyroid axis. *Environ. Sci. Technol.* 46, 12943–12951. doi:10.1021/es303289n

Zhou, C., Pagano, J., McGoldrick, D. J., Chen, D., Crimmins, B. S., Hopke, P. K., et al. (2019). Legacy Polybrominated Diphenyl Ethers (PBDEs) Trends in Top Predator Fish of the Laurentian Great Lakes (GL) from 1979 to 2016: Will Concentrations Continue to Decrease? *Environ. Sci. Technol.* 53, 6650–6659. doi:10.1021/acs.est.9b00933

Zhuang, J., Pan, Z. J., Mengqiu-LiHong, F. S., Zhu, C. K., Wu, N., et al. (2020). BDE-47 Induced Apoptosis in Zebrafish Embryos through Mitochondrial ROS-Mediated JNK Signaling. *Chemosphere* 258, 127385. doi:10.1016/j.chemosphere.2020.127385

Conflict of Interest: The authors declare that the research was conducted in the absence of any commercial or financial relationships that could be construed as a potential conflict of interest.

frontiers in Pharmacology

REVIEW
published: 28 February 2022
doi: 10.3389/fphar.2022.837687

The Role of Estrogen and Thyroid Hormones in Zebrafish Visual System Function

Annastelle Cohen[1], *Jeremy Popowitz*[1], *Mikayla Delbridge-Perry*[2], *Cassie J. Rowe*[1,3] *and Victoria P. Connaughton*[1,3]*

[1]Department of Biology, American University, Washington, DC, WA, United States, [2]Department of Chemistry, American University, Washington, DC, WA, United States, [3]Center for Neuroscience and Behavior, American University, Washington, DC, WA, United States

Visual system development is a highly complex process involving coordination of environmental cues, cell pathways, and integration of functional circuits. Consequently, a change to any step, due to a mutation or chemical exposure, can lead to deleterious consequences. One class of chemicals known to have both overt and subtle effects on the visual system is endocrine disrupting compounds (EDCs). EDCs are environmental contaminants which alter hormonal signaling by either preventing compound synthesis or binding to postsynaptic receptors. Interestingly, recent work has identified neuronal and sensory systems, particularly vision, as targets for EDCs. In particular, estrogenic and thyroidogenic signaling have been identified as critical modulators of proper visual system development and function. Here, we summarize and review this work, from our lab and others, focusing on behavioral, physiological, and molecular data collected in zebrafish. We also discuss different exposure regimes used, including long-lasting effects of developmental exposure. Overall, zebrafish are a model of choice to examine the impact of EDCs and other compounds targeting estrogen and thyroid signaling and the consequences of exposure in visual system development and function.

Keywords: ***Danio rerio*** **(zebrafish), retina, estradiol, T3, T4, development**

OPEN ACCESS

Edited by:
Anna Siebel,
Universidade Comunitária da Região de Chapecó, Brazil

Reviewed by:
Jason Bondoc Alipio,
University of Maryland, Baltimore, United States
Lisa Baumann,
Heidelberg University, Germany

***Correspondence:**
Victoria P. Connaughton
vconn@american.edu

Specialty section:
This article was submitted to Experimental Pharmacology and Drug Discovery, a section of the journal Frontiers in Pharmacology

Received: *16 December 2021*
Accepted: *28 January 2022*
Published: *28 February 2022*

Citation:
Cohen A, Popowitz J, Delbridge-Perry M, Rowe CJ and Connaughton VP (2022) The Role of Estrogen and Thyroid Hormones in Zebrafish Visual System Function. Front. Pharmacol. 13:837687. doi: 10.3389/fphar.2022.837687

INTRODUCTION

The impacts of endocrine manipulation often result in a cascade of effects at the biomolecular level, reaching outside a single pathway, and many non-endocrine organs, such as kidney and gut, secrete hormones. Further, neuronal development, and sensory system development, are dependent on hormones. Recent work has revealed the importance of thyroid hormones (THs), estrogen, and their receptors in visual system development. Both hormones are able to cross cell membranes, bind intracellular receptors, and affect subsequent pathways and/or gene expression. Disruption of either estrogenic or thyroidogenic pathways, by clinical treatments or environmental endocrine disrupting compounds (EDCs), impact the visual system directly or indirectly, and early developmental exposure to endocrine disruptors can have long-term deleterious effects. In addition to the epidemiological significance of endocrine disruption in humans, these effects also impose consequences on ecological systems at a population level as visual perception is essential for the success, survival, and reproduction of many organisms. The purpose of this review is to compare/contrast the role(s) of thyroid hormone and estrogen in the proper function and development of the visual system in the zebrafish animal model.

Zebrafish

Zebrafish, *Danio rerio*, a small freshwater tropical fish native to Southeast Asia, are an existing vertebrate model for a variety of disciplines, including endocrinology, toxicology, developmental biology, and vision. Adult zebrafish measure 2.5–4 cm in length and, due to their small size, can be housed in large numbers at a low-cost relative to other available model organisms. The zebrafish genome has been sequenced in its entirety (https://www.sanger.ac.uk/data/zebrafish-genome-project/), making this species valuable for investigation of various disorders and disease. Zebrafish have more than 26,000 protein-coding genes and 70% of human genes have at least one obvious zebrafish orthologue (Howe et al., 2013). Mutant strains and transgenic lines can be easily and quickly produced and assessed using large-scale genetic screens. Further, large clutch sizes of externally developing, transparent embryos are amenable to exposure studies as compounds are administered directly into tank water resulting in behavioral and/or physiological responses that can be recorded.

In addition to the technical and practical advantages of zebrafish, they serve as a powerful model organism for studying visual system development, function, and underlying mechanisms of disease. Zebrafish eyes are similar in anatomy, circuitry, physiology, and gene expression to humans (Bibliowicz et al., 2012). The zebrafish retina contains similar cell types and circuitry to the human retina, and retina-specific diseases observed in humans, such as red color blindness (Brockerhoff et al., 1997) and congenital stationary night blindness (Peachey et al., 2012) occur in and are modeled with zebrafish.

Zebrafish have also been used to study early life and adult effects of hormones, at both organizational and activational levels. Zebrafish nervous and endocrine systems (Tata, 2005) are also similar to humans from development throughout adulthood (Kimmel et al., 1995; Kishida and Callard, 2001; Gerlai, 2016). Studies with EDCs reveal effects on development, reproduction, sensory systems, cell proliferation, and heart formation. EDC exposure has been linked to obesity (Hatch et al., 2010; Heindel et al., 2015), metabolic and reproductive issues (Wada et al., 2007; Casals-Casas and Desvergne, 2011), and neurological disorders (Kajta and Wojtowicz, 2013). Specific to this review, EDCs can affect the brain/neurogenesis (Kishida et al., 2001; Hamad et al., 2007; Pelligrini et al., 2007; Diotel et al., 2013), including negatively impacting the visual system (Dong et al., 2006; Hamad et al., 2007; Wang et al., 2012).

Here, we focus on the specific effects of estrogen and thyroid hormone signaling in retinal development and function. We begin with a general description of eye development and structure in zebrafish and signaling by estrogen and thyroid hormones. We then discuss the role of estrogenic and thyroidogenic signaling in vision. We conclude with a summary of these effects, revealing significant crosstalk among these two systems that is important for proper visual function.

Visual System Development

Morphogenesis of the zebrafish eye occurs very rapidly between 12 and 24 h post fertilization (hpf) and the structure of the eyes is thought to be fully realized by 36 hpf (Schmitt and Dowling, 1994; Schmitt and Dowling, 1999). Within the retina, differentiation first occurs in a ventronasal patch near the optic nerve, and like most other vertebrates, moves from inner to outer retina (Schmitt and Dowling, 1999). At 32 hpf, ganglion cells begin to form and the optic nerve exits the retina. By 50 hpf, amacrine and horizontal cells in the inner nuclear layer begin to differentiate. Bipolar cells in the inner nuclear layer begin to differentiate at 60 hpf, as do rod and cone synaptic terminals. At 74 hpf, the zebrafish eye is fully developed (Schmitt and Dowling, 1999). Optokinetic responses can be recorded from zebrafish larvae as young as 4 days postfertilization (dpf) (Neuhauss, 2003; Brockerhoff, 2006), and vision-based optomotor responses are reliably recorded at 7 dpf (Clark, 1981; Bilotta et al., 2002; Bahadori et al., 2003; Orger et al., 2004; Muto et al., 2005) (**Figure 1**).

The adult zebrafish retina includes four cone types (R—red, G—green, B—blue, UV—ultraviolet) arranged in an orderly mosaic. These cone types are present in larval retinas, though the mosaic is less organized (Allison et al., 2010). During embryogenesis, photoreceptors develop at 43–48 hpf and opsins in rods, R and B cones are first detected at ~50–52 hpf (Raymond et al., 1995; Tsujikawa and Malicki, 2004). The presence of four cone types confers rich color processing abilities (Meier et al., 2018), in both larvae and adults, with a diversity of color-evoked responses seen in second-order horizontal cells (Connaughton and Nelson, 2010) as well as third-order amacrine (Torvund et al., 2016) and ganglion cells (Connaughton and Nelson, 2010). Color responses in zebrafish retinal bipolar cells have not been recorded; though anatomical analysis of dendritic connections with cone pedicles suggests multiple spectral types (Li et al., 2012). Signal transduction in the retina is highly conserved across vertebrates, with the connections of retinal neurons, overall layered organization, parallel ON- and OFF-pathways, and excitatory glutamatergic inputs within the vertical transduction pathway (photoreceptors to bipolar cells to ganglion cells) observed in both zebrafish and humans. GABAergic, glycinergic, and dopaminergic cells are also present. A difference between zebrafish and mammals is seen in brain circuitry: the optic tectum, a midbrain structure, is responsible for all higher order visual processing in zebrafish. In humans, the midbrain LGN (lateral geniculate nucleus) receives and processes retinal inputs before projecting to visual cortex (V1) (Haynes et al., 2005). Though lacking V1, the zebrafish optic tectum is well developed and capable of cortical-level processing of visual stimuli, such as stimulus detection and orientation (Hunter et al., 2013), escape behaviors (Dunn et al., 2016), and prey capture (Muto and Kawakami, 2013). Thus, the overall similarities in anatomy and circuitry between zebrafish and humans, coupled with genetic techniques that can be easily applied, allows zebrafish to serve as a convenient and relevant model for testing the effects of endocrine disrupting compounds (EDCs) and for assessing deficits in visual physiology and behavior (Link and Collery, 2015).

Estrogen Localization, Signaling, Receptor Types

Classically, estrogen production occurs in the gonads and, to a lesser extent, the adrenal cortex, with release stimulated by the

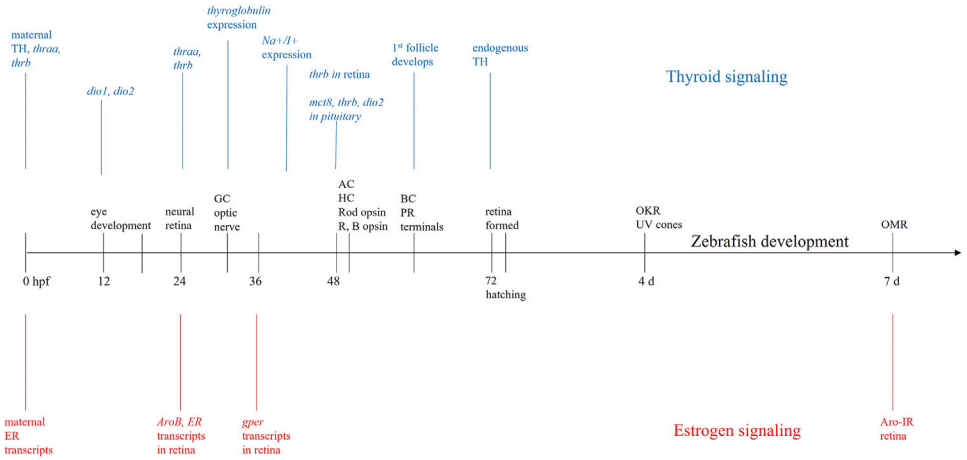

FIGURE 1 | Developmental timeline. Sequence of events in zebrafish eye and retinal development (black) beginning at fertilization (0 h postfertilization—hpf) and continuing until 7 days (days) postfertilization. During this time, maternally derived transcripts for estrogen receptors (ER—red) and maternally derived thyroid hormones (TH—blue) are present in yolk. At 24 hpf, when neural retina is developing, expression of ER and aromatase (*AroB*) are present in retina, and expression of the genes for both thyroid receptors (*thraa, thrb*) begins. Expression of G-protein coupled ER (*gper*) begins ~36 hpf; at 48 hpf *thrb* is expressed in retina. At hatching (72 hpf), there is endogenous production of both TH and estrogen. The overlap and concurrent development of thyroid, estrogen, and retinal development, suggests these hormones are important for proper retinal/visual system development. GC = ganglion cell, AC = amacrine cell, HC = horizontal cell, R = red cone, B = blue cone, BC = bipolar cell, PR = photoreceptor, OKR = optokinetic response, OMR = optomotor response.

hypothalamic-pituitary axis. Estradiol (17β-estradiol or E2), the biologically relevant estrogen, is synthesized directly from the aromatization of testosterone by the enzyme aromatase (estrogen synthase), a product of the *cyp19* gene. E2 is released from these glands directly into the bloodstream and, as it is best known for its roles in reproductive functions, is often referred to as a gonadal sex steroid (Menuet et al., 2005; Mccarthy, 2008). However, we have since learned that E2 synthesis and action are not restricted to reproductive tissues: E2 is locally produced via aromatase in a variety of non-reproductive tissues and throughout the nervous system (Lephart, 1996), inducing potent pleiotropic effects on central nervous system development, maturation, and function (Menuet et al., 2005).

For example, E2's effects extend to the visual system. The retina expresses aromatase, and estrogen receptors (ERs) are found in all retinal layers across vertebrate species (Gellinas and Callard, 1993; Callard et al., 2001; Cascio et al., 2007; Cascio et al., 2015), pointing to a conserved functional significance of local E2 synthesis and action. Indeed, E2 is neuroprotective in retina, preventing excitotoxic cell death and protecting against retinal degeneration in humans (Cascio et al., 2007). E2 also influences eye structure and function and the incidence of many ocular diseases (Cascio et al., 2007) and changes in E2 levels from aging or hormone therapies are associated with neurodegenerative retinal diseases and visual complications (Cascio et al., 2015).

Developmentally, ER transcripts in newly fertilized zebrafish embryos are maternally derived (Bardet et al., 2002; Lassiter et al., 2002; Tingaud-Sequeira et al., 2004) with endogenous transcription beginning around 24–48 hpf (**Figure 1**) (Bardet et al., 2002; Lassiter et al., 2002; Tingaud-Sequeira et al., 2004) and corresponding with the onset of aromatase mRNA expression (Mouriec et al., 2009). By 7 dpf, aromatase can be detected in retina using immunocytochemistry (Le Page et al., 2011), suggesting local E2 expression.

Aromatase in the Fish Brain

Teleost fish have remarkably high levels of neural aromatase, a finding pioneered in longhorn sculpin (Callard et al., 1978) and goldfish (Pasmanik and Callard, 1988; Gellinas and Callard, 1993; Callard et al., 1995) and confirmed in other teleosts (Trimmers et al., 1987; Borg et al., 1989; Mayer et al., 1991; Gonzalez and Piferrer, 2002), including zebrafish (Kishida and Callard, 2001; Sawyer et al., 2006). It is estimated that teleost neural aromatase is about 100 to 1000-fold greater when compared to mammals and birds (Pellegrini et al., 2005), and this high aromatase is thought to be involved in the regenerative abilities and plasticity of the teleost brain, optic nerve, and eye (Hamad et al., 2007). Furthermore, estrogens and estrogenic compounds upregulate the expression of developmental aromatase (Menuet et al., 2005; Sawyer et al., 2006), allowing neural aromatase in teleosts to serve as an indicator of estrogen signaling and modulation (Kishida et al., 2001).

Another unique feature of teleosts is that neural aromatase is exclusively expressed in a single and distinct cell type: radial glial cells (Menuet et al., 2005). These radial glial cells serve as progenitor cells that are essential in neurogenesis, where in mammals they act as embryonic neural stem cells that disappear shortly after birth (Schmidt and Scholpp, 2013). While these cell types are similarly important during zebrafish neurogenesis, they also persist into adulthood, continuing to express high levels of aromatase, proliferate, self-renew, and generate new neurons (Schmidt and Scholpp, 2013). Therefore, adult zebrafish seem to possess embryonic

mammalian features in terms of neurogenesis, allowing them to serve as sensitive models for estrogen signaling and the effects of disruption (Le Page et al., 2011).

Zebrafish have two separate and distinct aromatase expressing genes that have subdivided expression domains. The *cyp19a* gene encodes aromatase A (*AroA*) which is primarily expressed in the gonads, whereas the *cyp19b* gene encodes aromatase B (*AroB*) which is expressed in neural tissues, including the brain and retina (Callard et al., 2001; Menuet et al., 2005). In the retina of goldfish, *AroB* has been detected in horizontal, bipolar, and amacrine cells, and within ganglion cell projections to the brain from the optic nerve and tract (Callard et al., 1995). In support of a functional role of aromatase in the visual system, developmental exposure to known aromatase inhibitors causes thinning of retinal layers, delayed eye growth, and deficits in visually-guided behaviors (Hamad et al., 2007; Gould et al., 2017). Taken together, the localization of *AroB* in the retina and the anatomical and visual impacts from aromatase inhibition suggest a key role for E2 in the development and function of the visual system.

Estrogen Receptors and Signaling

Sequencing and phylogenetic analyses of human and zebrafish ERs reveal conserved functional motifs, high sequence homology, particularly in the DNA binding domain (C domain) (Bardet et al., 2002; Menuet et al., 2002) and near identical exon numbers and lengths (Lassiter et al., 2002). Further, human and teleost ERs exhibit similar binding characteristics (Thomas et al., 2010) and share the same intracellular signaling cascades (Thomas et al., 2010) and mechanisms of transcriptional activation (Klinge, 2001; Bardet et al., 2002). Thus, while we acknowledge that there may be species-specific differences in timing of events, the general signaling pathways and mechanisms of estrogen signaling are highly conserved across vertebrates (Klinge, 2001).

The actions of E2 are primarily mediated through two intracellular ERs, ERα and ERβ, that act as ligand-activated transcription factors to modulate estrogen target gene activity (Menuet et al., 2002). In the classical signaling pathway, intracellular ERs will form homo- or heterodimers upon E2 binding and translocate to the nucleus (Cascio et al., 2015). Once there, dimerized receptors bind to estrogen response elements (EREs) in promoter regions of DNA and recruit specific cofactors to alter gene expression (Belcher and Zsarnovszky, 2001; Mccarthy, 2008). E2 targets genes expressed in the retinal photoreceptor layer including *grk7a* and *pde6ga* (Hao et al., 2013). *grk7a*, or G-protein-coupled receptor kinase 7a, is involved in visual perception and phototransduction; *pde6ga* is predicted to be involved the activation of MAPK activity (Vogalis et al., 2011; Thisse and Thisse, 2014). E2 increases the expression of these genes, thus, lower E2 levels would decrease expression, causing lowered photosensitivity or lower level of function overall in retina (Vogalis et al., 2011; Thisse and Thisse, 2014).

In addition to direct interaction with EREs, E2-activated nuclear ERs can also regulate transcription via an indirect genomic mechanism by associating with and influencing activity of transcription factors, including stimulating protein 1 (SP-1), activator protein 1 (AP-1), nuclear factor-κB (NF-κB), and c-jun (Cui et al., 2013). Estrogen receptors can also participate in indirect "extranuclear signaling" through membrane-localized ERs in association with cytosolic kinases and growth factor signaling components to mediate rapid estrogenic effects (Levin, 2002). This extranuclear pathway can initiate multiple cytoplasmic signaling cascades that involve the downstream activation of MAPK/ERK, PI3K/AKT, and cAMP/PKA, which can ultimately also lead to transcriptional changes (Cortez et al., 2013).

The ERα and ERβ isoforms have distinct functions (Mccarthy, 2009), developmental expression patterns, tissue distributions, genes, and affinities for E2 (Menuet et al., 2002). However, the presence of ERα and ERβ in retina has been observed in many vertebrate animals, including rats, bovines, humans, and teleosts (Kobayashi et al., 1998; Cascio et al., 2015). In zebrafish, there are two forms of ERβ (zfERβ1 and zfERβ2), which likely resulted from a duplication event in the teleost lineage (Menuet et al., 2002). In development, it is thought that ERβ1 is most highly expressed (Paige et al., 1999; Froehlicher et al., 2009). All three ERs (zfERα, zfERβ1, and zfERβ2) are detected in zebrafish eyes where they begin to be highly expressed 24-48hpf (Menuet et al., 2002; Tingaud-Sequeira et al., 2004; Mouriec et al., 2009) (**Figure 1**).

E2 can also bind to a membrane-bound G protein-coupled estrogen receptor (GPER) to elicit indirect rapid non-genomic signaling (Belcher and Zsarnovszky, 2001). GPER binding E2 activates cAMP through adenylyl cyclase, which causes downstream activation of MAPK and CREB pathways, promoting neuronal growth and survival (Shi et al., 2013; Roque and Baltazar, 2019). GPER activation also promotes the activity of kinases involved in neuronal protection, such as PI3K/AKT (Roque and Baltazar, 2019).

Although the nervous system effects of E2 are largely attributed to classical ER genomic signaling, increasing evidence suggests that E2 mediated GPER activation is also involved (Luo and Liu, 2020). During zebrafish embryogenesis, GPER mRNA and protein shows a wide distribution throughout the central nervous system and can be detected from fertilization to 72 hpf, with high levels of expression occurring after 24 hpf (Jayasinghe and Volz, 2011; Shi et al., 2013). *gper* has also been detected in the zebrafish eye at 36 hpf and more recently in the retina, optic tract, and in nuclei of primary and secondary visual pathways of adult goldfish (Mangiamele et al., 2017). Further, genes involved in the MAPK/ERK pathway are present in zebrafish retina at various stages of development (Krens et al., 2006). GPER also plays a functional role as knockdowns induce apoptosis, decrease proliferation of brain cells, and cause abnormal development of sensory neurons (Shi et al., 2013). The presence of *gper* and downstream genes in the retina of embryonic zebrafish and the functional deficits of GPER knockdown suggest that E2 might rapidly modulate sensory processes via this non-genomic signaling pathway. Therefore, it appears that E2 exerts its effects in neurogenesis and neuroprotection using both long-term, transcriptional, and rapid, non-genomic mechanisms.

Thyroid Hormone Localization, Signaling, Receptor Types

The adult thyroid gland releases two thyroid hormones (THs): tri-iodothyronine (T3) and tetra-iodothyronine, or thyroxine (T4). Both T3 and T4 require iodine, which is taken up from the blood stream and, after binding tyrosine, is bound to thyroglobulin for storage within thyroid follicles (Sellitti and Suzuki, 2014). Though a greater amount of T4 is released, it is converted to T3 after release and T3, with greater affinity for thyroid receptors, is the more active form. Conversion of T4 and/or T3 occurs through the activity of three deiodinase enzymes: deiodinase type 2 (Dio2 or D2) converts T4 to T3, deiodinase type 3 (Dio3 or D3) inactivates T3 by converting it to reverse T3 (rT3) (Darras et al., 1999), and Dio1 (D1) performs both reactions, though it is considered the least efficient of the three (Bianco and Kim, 2006; Darras et al., 2011). All three deiodinases are present in zebrafish, and Dio2 is the major isoform producing useable T3 (Porazzi et al., 2009). Thyroid hormones impact all cells in the body, as they are important for growth and metabolic rate, and are involved in a variety of pathways during development (Silva et al., 2017).

In particular, THs are required for proper brain/CNS development (Boas et al., 2006; Darras et al., 1999; Howdeshell, 2002). In humans, initial TH levels are of maternal origin, with endogenous production occurring after 10–12 weeks gestation (Darras et al., 1999; Kohrle and Fradrich, 2021; Howdeshell, 2002). D3 activity in the placenta and fetus maintains constant fetal T3 levels (Patrick, 2009). Zebrafish embryos also have measurable levels of TH of maternal origin (**Figure 1**) (Silva et al., 2017; Gothie et al., 2019), resulting in stable whole body T3 and T4 levels until 60–72 hpf (Chang et al., 2012). At ~72 hpf, endogenous TH synthesis begins (Porazzi et al., 2009; Darras et al., 2011; Gothie et al., 2019; Vancamp et al., 2019) causing internal TH levels to increase significantly, peaking at 10 dpf (T3) and 21 dpf (T4) (Chang et al., 2012). A more recent study measuring T3 and T4 levels using fluorescent antibodies found hormone levels peak earlier, at 6 dpf, and then decrease (Rehberger et al., 2018). Prior to hatching, thyroglobulin expression begins at 32 hpf and Na^+/I^+ symporter expression starts at 40 hpf (Alt et al., 2006). The first thyroid follicle is evident ~55–60 hpf (Alt et al., 2006) and follicles can be clearly seen at 72 hpf, which coincides with the onset of endogenous T4 production (Porazzi et al., 2009). Interestingly, this development and early functioning of the thyroid gland does not require thyroid-stimulating hormone (TSH) (Alt et al., 2006) and is, therefore, independent of the hypothalamic-pituitary axis (Vancamp et al., 2019).

Altering T3 levels by knockdown of deiodinases disrupts eye development by decreasing eye size, reducing cone numbers, and altering visually guided responses in zebrafish (Houbrechts et al., 2016). Sensitivity of the retina to TH levels remains throughout life. Indeed, external application of T3 from 2 to 4 dpf alters cone opsin expression in exposed larvae, an effect also observed in juveniles exposed from 26 to 31 dpf (Mackin et al., 2019).

Thyroid Hormone Receptors and Signaling

T3 converted from T4 is transported into target cells via a high affinity membrane transporter (such as monocarboxylate transporter 8 or mct8) (Arjona et al., 2011), where it binds to a thyroid hormone receptor (TR). Similar to ERs and other members of the nuclear receptor superfamily, TRs act as ligand-activated transcription factors that influence transcription of target genes (Flamant et al., 2017). TRs bound to T3 form a dimer, commonly a heterodimer (Flamant et al., 2017), with the retinoid X receptor (TR/RXR) (Li et al., 2002; Li et al., 2004) or the retinoic acid receptor (TR/RAR) (Lee and Privalsky, 2005) before binding to a thyroid response element (TRE) on DNA to alter target gene transcription (Lazar et al., 1991). An interesting aspect of thyroid hormone signaling is that both RXR and RAR can also bind their natural ligand, retinoic acid, when bound to TR (Li et al., 2002; Li et al., 2004; Bohnsack and Kahana, 2013) and interactions between thyroid and retinoic acid signaling have been reported (Essner et al., 1997). In addition to this canonical genomic pathway, T3 can interact with plasma membrane integrin αvβ3 to initiate rapid intracellular signaling cascades involved in neuroprotection, growth, and apoptotic regulation, including MAPK (ERK1/2) and PI3K/AKT (Flamant et al., 2017).

In mammals there are 2 TR genes: TRα and TRβ (Bernal et al., 2003; Bernal, 2005). Zebrafish also have TRα and TRβ that respond to TH (Porazzi et al., 2009). In mammals, the TH receptor genes code for various protein products with TRα1, TRβ1, TRβ2, and TRβ3 able to bind to both T3 and to DNA (Bernal et al., 2003; Bernal, 2005). In zebrafish, one gene encodes TRβ (*thrb*), but two genes encode TRα (*thraa* and *thrab*) (Liu et al., 2000; Porazzi et al., 2009; Darras et al., 2011; Marelli et al., 2016), with all receptor isoforms expressed in retina. The *thraa* gene forms two proteins: TRαA-1 and TRαA1-2 (Porazzi et al., 2009; Darras et al., 2011), with TRαA-1 corresponding to mammalian TRα1 (Darras et al., 2011). *Thrb* encodes three isoforms: zTRβ1s (short), zTRβ1L (long) and zTRβ2 (Vancamp et al., 2019). All receptors bind T3 and are intracellular (Marelli et al., 2016).

During early embryogenesis, both *thraa* and *thrb* are expressed in zebrafish embryos (Liu et al., 2000; Porazzi et al., 2009; Vancamp et al., 2019), peaking at 18 hpf, then decreasing to undetectable levels until 24 hpf when expression again increases (Marelli et al., 2016). At 48 hpf, *thrb* is detectable in retina and it is still expressed in the eye and muscles of adult zebrafish (Marelli et al., 2016). Expression of *mct8* (Vancamp et al., 2019) and *Dio2* are also found in developing retina (Bohnsack and Kahana, 2013). Thus, though endogenous TH production does not begin until hatching, gene expression and/or development of thyroid signaling components are present much earlier, indicating high embryonic TH levels may drive expression of pathway components (Liu et al., 2000).

Role of Estrogen in Visual Function

As noted above, development of the retina/visual system and estrogenic signaling occur simultaneously (**Figure 1**), suggesting an interaction between these two processes. Indeed, many animal

studies have suggested that proper estrogenic signaling is critical for neurogenesis of the visual system: developmental manipulation of estradiol signaling or synthesis causes abnormal eye growth (Hamad et al., 2007; Hano et al., 2007), deficits in visually guided behaviors (Lovato et al., 2017; Crowley-Perry et al., 2021), and thinning and apoptosis in the retina (Dong et al., 2006; Hamad et al., 2007). Much of this research uses EDCs to determine the role of E2 in the visual system. Here, we discuss the visual system effects of EDCs acting as E2 agonists—BPA and EE2—and E2 antagonists—TBT and 4-OH-A.

Bisphenol-A (BPA) is a familiar, ubiquitous chemical (Arase et al., 2011) used primarily in the manufacture of polycarbonate and epoxy resins (Chapin et al., 2008) and it is present in plastic water bottles, food containers, and dental sealants. BPA levels in humans are measurable and significant (Ben-Jonathan and Steinmetz, 1998) and occur in ~93% of the population (Group, 2013). BPA is effective at extremely low (nM) doses (Ben-Jonathan and Steinmetz, 1998) which correspond to the median value reported in US streams (Kolpin et al., 2002). BPA levels can be measured in human tissues and fluids (Chapin et al., 2008; Vandenberg et al., 2010; Lakind and Naiman, 2011) and, significantly, BPA is able to cross the placenta (Takahashi and Oishi, 2000; Chapin et al., 2008; Vandenberg et al., 2009) resulting in measurable fetal levels (Schonfelder et al., 2002; Chapin et al., 2008). There are no reports documenting developmental effects of BPA on humans (Chapin et al., 2008); however, *in utero* exposure (Chapin et al., 2008) causes a variety of behavioral deficits (Farabollini et al., 1999; Jasarevic et al., 2011; Kim et al., 2011; Wolstenholme et al., 2012) and is linked to childhood asthma (Nakajima et al., 2012) in rodents.

Our lab, and others, have reported the deleterious effects of exposure to BPA on the visual system. BPA targets neuroendocrine systems as a weak E2 agonist that binds and activates both ERs (Chung et al., 2011; Cano-Nicolau et al., 2016) and GPER (Thomas and Dong, 2006). BPA is extremely effective at low concentrations (Ben-Jonathan and Steinmetz, 1998), with exposure causing hyperactivity (Saili et al., 2012; Kinch et al., 2015; Weber et al., 2015), reduced midbrain size (Tse et al., 2013), and reduced outgrowth of motor neurons (Wang et al., 2013) in zebrafish. Because ER and aromatase regulation are estrogen-dependent, BPA causes dramatic overexpression of aromatase (Chung et al., 2011; Cano-Nicolau et al., 2016) and ER mRNA (Kishida et al., 2001), resulting in abnormally high estrogen signaling with likely adverse effects on nervous system development and function (Cano-Nicolau et al., 2016). For example, acute (24–48 h) BPA exposure in embryonic zebrafish causes defects in otolith formation (Gibert et al., 2011) and decreases in hair cell survival and regeneration (Hayashi et al., 2015), demonstrating that short-term exposure to BPA can have deleterious effects on sensory systems. Specific to the visual system, a chronic 120-day exposure in embryonic zebrafish (2 hpf) to BPS, a BPA analogue with similar estrogenic actions (Qiu et al., 2016), decreased tracking ability and the thickness of the ganglion cell layer and retina, and induced irregular arrangement of photoreceptor cells (Liu et al., 2017). Lastly, acute (24 h) exposure to BPA in larval zebrafish aged 72 hpf and 7 dpf resulted in changes in eye diameter and visually guided behaviors that were evident 1–2 weeks after removal from treatment (Crowley-Perry et al., 2021). These findings suggest that short- and long-term exposure to BPA can evoke both immediate and sustained effects on sensory systems, including the visual system.

Ethinyl-estradiol (EE2) is another estrogen receptor agonist that has been tested in zebrafish. EE2 is a synthetic derivative of endogenous E2 and, due to its wide use as a constituent in oral contraceptives, reaches aquatic environments through wastewater effluents (Vilela et al., 2021); agricultural and aquaculture runoff are other sources (Tang et al., 2021). EE2 concentration in surface waters varies, ranging up to 62 ng/L (Versonnen and Janssen, 2004), and it is consistently identified worldwide make it a serious environmental contaminant (Tang et al., 2021). EE2 exhibits higher potency and ER binding affinity than E2 (Aten and Eisenfeld, 1982; Denny et al., 2009), thus eliciting estrogenic effects at and below levels detected in the environment. There are no available epidemiological reports of EE2 and its effects on human sensory systems. However, EE2 binds to teleost and mammalian ERs (Aten and Eisenfeld, 1982), and environmentally relevant levels adversely affect fish (Nikoleris et al., 2016; Tang et al., 2021; Ramirez-Montero et al., 2022).

Embryonic zebrafish at 8–10 dpf exposed to picomolar concentrations of EE2 (10–1,000 p.m.) between 1 and 7 dpf of development have significantly inhibited axonal nerve and hair cell regeneration, suggesting direct impairments to nervous and sensory system development (Nasri et al., 2021). Similar 7-day EE2 exposures using pM to low nM concentrations caused significant overexpression of brain AroB and ERα/β transcripts in juvenile Atlantic salmon (Lyssimachou et al., 2006) and 7 dpf zebrafish (Cano-Nicolau et al., 2016; Nasri et al., 2021). Specific EE2 effects have also been observed in retina, where a 32-day exposure to low nanomolar concentrations (4–100 ng/L) decreased the outer and inner plexiform layers and total retinal thickness of minnows assessed at 28 days post-hatch (Alcaraz et al., 2021), an effect likely attributed to disrupted and/or heightened estrogen signaling.

Tributyltin (TBT) is an EDC that targets estrogenic pathways, but with opposite effects to BPA and EE2. TBT is an organotin compound used commonly as a biocide in antifouling paints applied to boats and marine structures and was historically found at high concentrations in aquatic environments (Mcallister and Kime, 2003). Though the International Maritime Organization banned the use of TBT in anti-fouling paints in 2008 (Showalter and Savarese, 2004; Gipperth, 2009; IMO, 2019), which lead to reduced environmental levels (Liang et al., 2017) and wildlife recovery (Jones and Ross, 2018), recent reports identify spikes in TBT levels (μg/g) in coastal areas off of Latin America, Norway, and Panama (Batista-Andrade et al., 2018; Schoyen et al., 2019; Castro et al., 2021) and TBT-based paint is still sold (Uc-Peraza et al., 2022), suggesting continued exposure. TBT is not readily biodegradable (Mcallister and Kime, 2003) and, once ingested, bioaccumulates and crosses the blood brain barrier, concentrating in areas of the brain that receive sensory inputs (Roulea et al., 2003).

TBT exposure in humans is not well studied, though exposure is thought to occur through consumption of contaminated fish or shellfish (Chien et al., 2002; Antizar-Ladislao, 2008). Such dietary intake of TBT has been measured worldwide and TBT is reported to inhibit placental aromatase (reviewed in Antizar-Ladislao, 2008), suggesting an impact on development.

TBT exposure causes a range of adverse effects, including increasing oxidative stress, triggering an immune response, reducing neurotransmitter synthesis/levels, increasing lipid accumulation, and altering liver function (Zhang CN. et al., 2017; Zhang J. et al., 2017; Ortiz-Villanueva et al., 2018; Barbosa et al., 2019; Li and Li, 2021; Shi et al., 2021). Relevant to this review is that TBT is also a known aromatase inhibitor that prevents the synthesis of E2 and decreases AroB expression in zebrafish brain (Lyssimachou et al., 2006). Plasma levels of testosterone are correspondingly increased, leading to deleterious effects on the reproductive system and population sex ratios. High levels of imposex in gastropod mollusks (Schoyen et al., 2019) and masculinization in fish (Mcallister and Kime, 2003; Santos et al., 2006; Mcginnis and Crivello, 2011) occur after TBT exposure. Within the visual system, embryonic fish (<8 hpf) transiently exposed to TBT exhibit abnormal eye growth (Hano et al., 2007) and apoptosis of retinal neurons (Dong et al., 2006). Degeneration and abnormal ordering of retinal layers has also been observed in larvae exposed to TBT for 10 days (Fent and Meier, 1992). Additionally, transient 24-h exposure to TBT during development alters visually guided optomotor responses (OMRs) measured 1-week after removal from treatment (Bernardo and Connaughton, 2022). Effects were age-dependent, with reduced OMRs occurring if TBT exposure occurred at 72 hpf or 7 dpf; reduced eye diameters were also observed when exposure occurred at 7 dpf.

Exposure studies using the pharmaceutical EDC 4-hydroxy-androstendione (4-OH-A or Formestane), another potent aromatase inhibitor, provide further support for the role of E2 in visual system development. A 3-day application of 4-OH-A to 48 hpf zebrafish prevented expression of normal sensory motor behaviors, including swimming movement, tactile response, fin movement, and eye movement (Nelson et al., 2008). Co-application with E2 at a concentration determined to be optimal for the transcriptional activation of ERs (Menuet et al., 2002) and upregulation of AroB mRNA (Kishida et al., 2001) rescued all sensory responses (Nelson et al., 2008), pointing to a key functional role of E2 signaling via ERs in sensory system development. Additionally, acute, 24-h exposure to 4-OH-A significantly decreased eye diameter in 7 dpf zebrafish (Gould et al., 2019). We also observed that the visual system effects of 4-OH-A persist into adulthood, as a 24-h exposure at 24 hpf, 72 hpf, and 7 dpf larval zebrafish resulted in significantly decreased visually guided optomotor responses in adults (3–4 months removed from treatment) (Gould et al., 2017), suggesting that even a brief disruption to estrogen signaling during development can have effects on maturation and long-term function. Taken together, these studies indicate that modulating E2 signaling via EDCs imposes both immediate and long-term effects on visual system development and function at a wide range of concentrations, developmental timepoints, and exposure durations.

Role of Thyroid Hormones in Visual Function

Similar to estrogenic signaling, thyroid hormone signaling also coincides with retinal development (**Figure 1**). However, compared to E2, THs have a more direct involvement in retinal neurogenesis as they are required for neuronal maturation and cell fate of cone photoreceptors (Harpavat and Cepko, 2003; Roberts et al., 2006). In particular, TH binding to TRβ2 determines correct expression of cone opsins in both zebrafish (Harpavat and Cepko, 2003; Suzuki et al., 2013; Volkov et al., 2020) and rodents (Roberts et al., 2006). During development, zebrafish cones can express one of seven different opsins: lws1 (R1) or lws2 (R2) (red cones); rh2-1/rh2-2 (G1) or rh2-3 (G3) (green cones); sws2 (B1) or B2 (blue cones); sws1 (UV cones) (Takechi and Kawamura, 2005; Endeman et al., 2013; Nelson et al., 2019). *trβ2* expression is specifically required for expression of the red cone opsin (Suzuki et al., 2013) lws1 (Suzuki et al., 2013; Mackin et al., 2019; Volkov et al., 2020). Consequently, knockdown of *trβ2* reduces the number of red cones (Suzuki et al., 2013); zebrafish *thrb* mutants, as larvae or adults, have an anatomical loss of red cones (Volkov et al., 2020), which is associated with reduced response to red light and a loss of red cone inputs to the ERG (Deveau et al., 2020). Exposing zebrafish larvae to T3 from 2 to 4 dpf increased expression and distribution of lws1 (Mackin et al., 2019), consistent with effects in TRβ2 mutants. Interestingly, juveniles exposed to T4 from 26–31 dpf did not display a difference in lws1 expression (Mackin et al., 2019), though lws2 was altered. However, TH application upregulated *cyp27c1* in zebrafish juveniles (Mackin et al., 2019; Volkov et al., 2020). *cyp27c1* codes for the enzyme that converts vitamin A1 (the chromophore bound to opsin in zebrafish) to vitamin A2 in the retinal pigment epithelium (Allison et al., 2004; Enright et al., 2015; Volkov et al., 2020), consistent with a TH-induced shift toward longer wavelength sensitivity (Mackin et al., 2019; Volkov et al., 2020).

Though a major effect of *trβ2* expression is found in red cones, other cone types are also affected by changes in expression of this TR. For example, reductions in *trβ2* leads to an increase in the number of cones expressing UV opsin in zebrafish (Suzuki et al., 2013; Volkov et al., 2020), similar to the increase in S-cone number observed in TRβ2-null mice (Roberts et al., 2006), suggesting *trβ2*, and TH signaling, determines L-cone vs. UV-cone fate (Suzuki et al., 2013). Exposing *trβ2* mutant zebrafish larvae (2–4 dpf) to T3 caused a dose dependent increase in *rh2-2* and *rh2-3* expression (Mackin et al., 2019) in green cones, which was observed physiologically as reduced green sensitivity and a shift to a longer peak wavelength in photopic ERG recordings (Deveau et al., 2020), another example of a TH-induced shift to longer wavelength sensitivity. These results in zebrafish agree with those from human retinal organoid cultures, which show that TH binding to TRβ2 is required for L/M cone development (Eldred et al., 2018).

The thyroid axis is very sensitive to environmental chemicals. Many identified contaminants are able to affect this system and all levels are sensitive to disruption (Howdeshell, 2002; Boas et al., 2006; Patrick, 2009; Kohrle and Fradrich, 2021). Clinically, and experimentally, two EDCs are used to block TH synthesis: methimazole (MMI) or propylthiouracil (PTU). Both compounds are used as a treatment for hyperthyroidism (Yu et al., 2020) as they reduce the activity of thyroid peroxidase, the enzyme that catalyzes binding of iodine to tyrosine (Ohtaki et al., 1996); PTU also prevents formation of T4 from thyroglobulin (Bohnsack and Kahana, 2013). Song et al. (2017) performed a meta-analysis to assess the risk of congenital abnormalities in children born to mothers prescribed MMI vs. PTU during pregnancy. They conclude that MMI exposure resulted in a greater risk of congenital malformations, compared to mothers taking PTU (Song et al., 2017). Furter, disruption of or reduced TH signaling during pregnancy causes abnormal brain development and/or cognitive impairments (Patrick, 2009; Noyes et al., 2019). These deleterious effects can extend to "brain derivatives" that include retina, cochlea, and pacemaker cells (Howdeshell, 2002).

Exposing zebrafish embryos to 0.3 mM MMI between 60 and 72 hpf causes smaller eye diameters at 65 hpf which corresponded to a thinner GCL and IPL in treated retinas (Reider and Connaughton, 2014). Other neuronal, pharyngeal, and esophageal anomalies were also reported in zebrafish embryonically exposed to MMI (Komoike et al., 2013). These latter effects are similar to anomalies resulting from *in utero* exposure in humans (Komoike et al., 2013). MMI also reduces TH levels in adult rodents and reduces expression of Dio3 and Dio2 (Glaschke et al., 2011), suggesting not only reduced overall synthesis of TH, but a reduced ability to convert/activate circulating TH.

Exposure to PTU from 0 to 5 dpf reduced eye size in zebrafish larvae and alters optokinetic responses (Baumann et al., 2016; Gothie et al., 2019); effects correlated with PTU-induced downregulation of TR expression (Baumann et al., 2016). Subsequent microarray analysis revealed PTU exposure caused downregulation of phototransduction-related genes coding for opsins, phosphodiesterase, and arrestin (Baumann et al., 2019). In fact, of the genes involved in sensory perception, expression of >90% were found to be downregulated by PTU. The number of downregulated genes remained high when measured after a 3-day removal from treatment, though the levels of downregulation were less (Baumann et al., 2019), suggesting differential sensitivity to specific genes and long-term impacts of exposure.

TBBPA (tetrabromobisphenol-A) has also been used to examine TH signaling. TBBPA can bind to TR as either an agonist or antagonist, depending on the concentration used. TBBPA exposure reduced eye size and altered OKR in zebrafish larvae exposed from 0 to 5 dpf (Baumann et al., 2016; Gothie et al., 2019). The effect of TBBPA exposure on expression of specific genes was variable (Baumann et al., 2016), consistent with agonistic and/or antagonistic effects of this compound. Indeed, though opsin expression was upregulated after a 5-day exposure to TBBPA (from 0 to 5 dpf), overall TBBPA exposure caused more general effects than PTU (Baumann et al., 2019). However, compared to PTU-induced downregulation of genes involved in sensory perception, >80% were upregulated by TBBPA. Following 3 days of recovery/removal from treatment, opsin gene expression was still upregulated and detectable in TBBPA treated fish (Baumann et al., 2019).

Summarizing E2 and TH Effects Identifies Crosstalk Between Estrogenic and Thyroidogenic Pathways

E2 and TH-based signaling pathways have many similarities (**Figure 2**). These similarities, though highlighted in zebrafish, are highly conserved across vertebrates. Both hormones are released from glands that receive stimulation through the hypothalamic-pituitary axis and both cross the plasma membrane of cells, bind intracellular receptors, initiate overlapping cytoplasmic signaling cascades, and interact with hormone response elements (HREs) to influence gene expression. Significantly, the half-sites of thyroid response elements (TREs) and estrogen response elements (EREs) exhibit striking sequence similarities in various promoters (Glass et al., 1988; Scott et al., 1997; Vasudevan et al., 2002). TRs have been shown to bind the consensus ERE with high affinity, preventing ERα-ERE interaction and consequently ERα-mediated transcription (Glass et al., 1988; Vasudevan et al., 2001; Vasudevan et al., 2002). There is evidence that ERs can also take part in this competition by binding TREs to suppress the effect of T3 on target promoters (Yarwood et al., 1993) and mediate strong estrogen-dependent activation of transcription (Graupner et al., 1991). Therefore, it appears that competition between ERs and TRs can lead to antagonizing effects.

One of the significant published reports related to cross talk between E2 and TH signaling relates to the shared sensitivity to BPA. As noted above, BPA is a weak estrogen agonist; however, it is also an antagonist of TR that prevents binding of T3 (Moriyama et al., 2002; Zoeller et al., 2005; Jung et al., 2007; Heimeier et al., 2009), thereby inhibiting negative feedback by TH and increasing serum T4 levels (Zoeller et al., 2005). BPA is a better antagonist for TRβ than TRα (Zoeller et al., 2005). Importantly, binding of BPA to TH receptors occurs at relatively high (>10 μM) BPA doses (Moriyama et al., 2002; Zoeller et al., 2005; Vandenberg et al., 2009). Low doses of BPA are reported to increase androgen receptor mRNA expression (Richter et al., 2007) but not to have anti-androgenic activity *in vivo* (Chapin et al., 2008). These interactions between TH and E2 signaling pathways, coupled to maternally derived *TH* and *ER* transcripts, their localization in the same tissues and the ability of those tissues to locally regulate hormonal actions, suggests TH and E2 signaling could mediate specific developmental events, such as retinal development.

Both hormones are present in the developing retina and synthesized locally within retinal tissue. In teleosts, the localization of neural aromatase, ERs, and GPER within embryonic and adult retina, and the functional deficits observed upon experimental estrogenic modulation, points to a key role of E2 in the visual system. Further, the importance of TRβ2 in cone photoreceptors and the strong early presence of

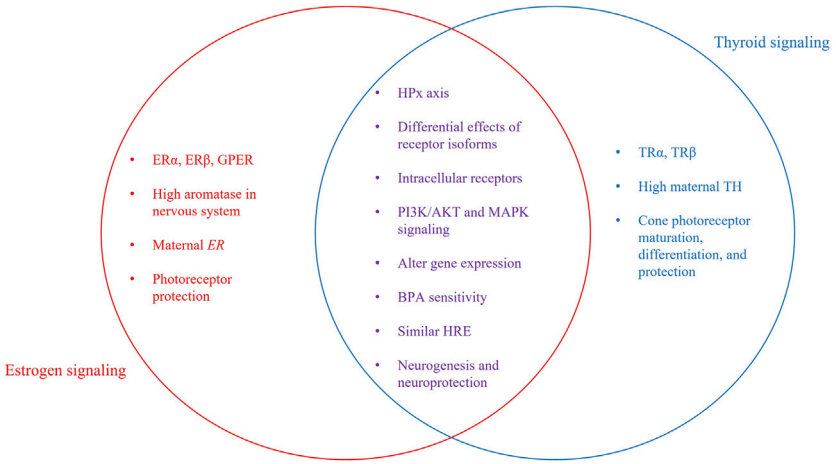

FIGURE 2 | Independent and interactive pathway components. Venn Diagram showing individual and interactive aspects of estrogen and thyroid signaling. Shared characteristics between both signaling pathways include the involvement of the hypothalamus-pituitary axis, intracellular receptors, some intracellular signaling molecules, and effects on gene transcription. Both E2 and TH are required for neurogenesis, including development of the visual system. Photoreceptors are the retinal cell type most sensitive, as TH is required for correct development and organization of cones. E2 is neuroprotective, preventing cell loss due to light-damage or disease.

maternal TH suggest a role for TH in the visual system. At 24 hpf, when the retina begins to develop, both *thraa* and *thrb* are expressed and TH levels are high due to maternally derived hormones in yolk. *AroB* and *ER* transcripts are detectable in retina at 24 hpf (Mouriec et al., 2009). Over the next ~12 h, thyroglobulin (Alt et al., 2006) and gper (Mangiamele et al., 2017) expression is detected and the optic nerve leaves the eye (Steurmer et al., 1988). By 48–50 hpf, amacrine and horizontal cells in the INL appear, opsin expression begins, and *thrb* expression is seen in retina. When hatching occurs, retina and thyroid are fully functional and E2 signaling is functional.

Though thyroid and estrogen signaling have been examined for decades, there are still effects/mechanisms of these hormones that are poorly understood. Further their interaction(s) and influence(s) on each other is clearly complex and even less understood. However, considering the consequences of TH and E2 dysregulation, crosstalk in signaling, and developmental co-localization of receptors presented in this review, it is likely that these hormones work synergistically in the development, maturation, and function of the visual system. It is also likely that other sensory systems are impacted in a similar manner and future work should address these questions.

AUTHOR CONTRIBUTIONS

All authors listed have made a substantial, direct, and intellectual contribution to the work and approved it for publication.

FUNDING

This project was funded by NIH Grant R15EY029866-01 (to VC).

REFERENCES

Alcaraz, A. J. G., Potěšil, D., Mikulášek, K., Green, D., Park, B., Burbridge, C., et al. (2021). Development of a Comprehensive Toxicity Pathway Model for 17α-Ethinylestradiol in Early Life Stage Fathead Minnows (*Pimephales promelas*). *Environ. Sci. Technol.* 55, 5024–5036. doi:10.1021/acs.est.0c05942

Allison, W. T., Barthel, L. K., Skebo, K. M., Takechi, M., Kawamura, S., and Raymond, P. A. (2010). Ontogeny of Cone Photoreceptor Mosaics in Zebrafish. *J. Comp. Neurol.* 518, 4182–4195. doi:10.1002/cne.22447

Allison, W. T., Haimberger, T. J., Hawryshyn, C. W., and Temple, S. E. (2004). Visual Pigment Composition in Zebrafish: Evidence for a Rhodopsin-Porphyropsin Interchange System. *Vis. Neurosci.* 21, 945–952. doi:10.1017/S0952523804216145

Alt, B., Reibe, S., Feitosa, N. M., Elsalini, O. A., Wendl, T., and Rohr, K. B. (2006). Analysis of Origin and Growth of the Thyroid Gland in Zebrafish. *Dev. Dyn.* 235, 1872–1883. doi:10.1002/dvdy.20831

Antizar-Ladislao, B. (2008). Environmental Levels, Toxicity and Human Exposure to Tributyltin (TBT)-contaminated marine Environment. A Review. b_antizar@hotmail.Com. *Environ. Int.* 34, 292–308. doi:10.1016/j.envint.2007.09.005

Arase, S., Ishii, K., Igarashi, K., Aisaki, K., Yoshio, Y., Matsushima, A., et al. (2011). Endocrine Disrupter Bisphenol A Increases *In Situ* Estrogen Production in the Mouse Urogenital Sinus. *Biol. Reprod.* 84, 734–742. doi:10.1095/biolreprod.110.087502

Arjona, F. J., De Vrieze, E., Visser, T. J., Flik, G., and Klaren, P. H. (2011). Identification and Functional Characterization of Zebrafish Solute Carrier Slc16a2 (Mct8) as a Thyroid Hormone Membrane Transporter. *Endocrinology* 152, 5065–5073. doi:10.1210/en.2011-1166

Aten, R. F., and Eisenfeld, A. J. (1982). Estradiol Is Less Potent Than Ethinyl Estradiol for *In Vivo* Translocation of the Mammalian Liver Estrogen Receptor to the Nucleus. *Endocrinology* 111, 1292–1298. doi:10.1210/endo-111-4-1292

Bahadori, R., Huber, M., Rinner, O., Seeliger, M. W., Geiger-Rudolph, S., Geisler, R., et al. (2003). Retinal Function and Morphology in Two Zebrafish Models of

Oculo-Renal Syndromes. *Eur. J. Neurosci.* 18, 1377–1386. doi:10.1046/j.1460-9568.2003.02863.x

Barbosa, M. A. G., Capela, R., Rodolfo, J., Fonseca, E., Montes, R., André, A., et al. (2019). Linking Chemical Exposure to Lipid Homeostasis: A Municipal Waste Water Treatment Plant Influent Is Obesogenic for Zebrafish Larvae. *Ecotoxicol Environ. Saf.* 182, 109406. doi:10.1016/j.ecoenv.2019.109406

Bardet, P. L., Horard, B., Robinson-Rechavi, M., Laudet, V., and Vanacker, J. M. (2002). Characterization of Oestrogen Receptors in Zebrafish (*Danio rerio*). *J. Mol. Endocrinol.* 28, 153–163. doi:10.1677/jme.0.0280153

Batista-Andrade, J. A., Caldas, S. S., Batista, R. M., Castro, I. B., Fillmann, G., and Primel, E. G. (2018). From TBT to Booster Biocides: Levels and Impacts of Antifouling along Coastal Areas of Panama. *Environ. Pollut.* 234, 243–252. doi:10.1016/j.envpol.2017.11.063

Baumann, L., Ros, A., Rehberger, K., Neuhauss, S. C., and Segner, H. (2016). Thyroid Disruption in Zebrafish (*Danio rerio*) Larvae: Different Molecular Response Patterns lead to Impaired Eye Development and Visual Functions. *Aquat. Toxicol.* 172, 44–55. doi:10.1016/j.aquatox.2015.12.015

Baumann, L., Segner, H., Ros, A., Knapen, D., and Vergauwen, L. (2019). Thyroid Hormone Disruptors Interfere with Molecular Pathways of Eye Development and Function in Zebrafish. *Int. J. Mol. Sci.* 20. doi:10.3390/ijms20071543

Belcher, S. M., and Zsarnovszky, A. (2001). Estrogenic Actions in the Brain: Estrogen, Phytoestrogens, and Rapid Intracellular Signaling Mechanisms. *J. Pharmacol. Exp. Ther.* 299, 408–414.

Ben-Jonathan, N., and Steinmetz, R. (1998). Xenoestrogens: The Emerging Story of Bisphenol A. *Trends Endocrinol. Metab.* 9, 124–128. doi:10.1016/s1043-2760(98)00029-0

Bernal, J., Guadaño-Ferraz, A., and Morte, B. (2003). Perspectives in the Study of Thyroid Hormone Action on Brain Development and Function. *Thyroid* 13, 1005–1012. doi:10.1089/105072503770867174

Bernal, J. (2005). Thyroid Hormones and Brain Development. *Vitam Horm.* 71, 95–122. doi:10.1016/S0083-6729(05)71004-9

Bernardo, R. C., and Connaughton, V. P. (2022). Transient Developmental Exposure to Tributyltin Reduces Optomotor Responses in Larval Zebrafish (*Danio rerio*). *Neurotoxicol Teratol* 89, 107055. doi:10.1016/j.ntt.2021.107055

Bianco, A. C., and Kim, B. W. (2006). Deiodinases: Implications of the Local Control of Thyroid Hormone Action. *J. Clin. Invest.* 116, 2571–2579. doi:10.1172/JCI29812

Bibliowicz, J., Tittle, R. K., and Gross, J. M. (2012). Toward a Better Understanding of Human Eye Disease Insights from the Zebrafish, *Danio rerio*. *Prog. Mol. Biol. Transl Sci.* 100, 287–330. doi:10.1016/B978-0-12-384878-9.00007-8

Bilotta, J., Saszik, S., Givin, C. M., Hardesty, H. R., and Sutherland, S. E. (2002). Effects of Embryonic Exposure to Ethanol on Zebrafish Visual Function. *Neurotoxicol Teratol* 24, 759–766. doi:10.1016/s0892-0362(02)00319-7

Boas, M., Feldt-Rasmussen, U., Skakkebaek, N. E., and Main, K. M. (2006). Environmental Chemicals and Thyroid Function. *Eur. J. Endocrinol.* 154, 599–611. doi:10.1530/eje.1.02128

Bohnsack, B. L., and Kahana, A. (2013). Thyroid Hormone and Retinoic Acid Interact to Regulate Zebrafish Craniofacial Neural Crest Development. *Dev. Biol.* 373, 300–309. doi:10.1016/j.ydbio.2012.11.005

Borg, B., Andersson, E., Mayer, I., and Lambert, J. G. (1989). Aromatase Activity in the Brain of the Three-Spined Stickleback, *Gasterosteus aculeatus*. III. Effects of Castration under Different Conditions and of Replacement with Different Androgens. *Exp. Biol.* 48, 149–152.

Brockerhoff, S. E., Hurley, J. B., Niemi, G. A., and Dowling, J. E. (1997). A New Form of Inherited Red-Blindness Identified in Zebrafish. *J. Neurosci.* 17, 4236–4242. doi:10.1523/jneurosci.17-11-04236.1997

Brockerhoff, S. E. (2006). Measuring the Optokinetic Response of Zebrafish Larvae. *Nat. Protoc.* 1, 2448–2451. doi:10.1038/nprot.2006.255

Callard, G. V., Kruger, A., and Betka, M. (1995). The Goldfish as a Model for Studying Neuroestrogen Synthesis, Localization, and Action in the Brain and Visual System. *Environ. Health Perspect.* 103 (Suppl. 7), 51–57. doi:10.1289/ehp.95103s751

Callard, G. V., Petro, Z., and Ryan, K. J. (1978). Phylogenetic Distribution of Aromatase and Other Androgen-Converting Enzymes in the Central Nervous System. *Endocrinology* 103, 2283–2290. doi:10.1210/endo-103-6-2283

Callard, G. V., Tchoudakova, A. V., Kishida, M., and Wood, E. (2001). Differential Tissue Distribution, Developmental Programming, Estrogen Regulation and Promoter Characteristics of Cyp19 Genes in Teleost Fish. *J. Steroid Biochem. Mol. Biol.* 79, 305–314. doi:10.1016/s0960-0760(01)00147-9

Cano-Nicolau, J., Vaillant, C., Pellegrini, E., Charlier, T. D., Kah, O., and Coumailleau, P. (2016). Estrogenic Effects of Several BPA Analogs in the Developing Zebrafish Brain. *Front. Neurosci.* 10, 112. doi:10.3389/fnins.2016.00112

Casals-Casas, C., and Desvergne, B. (2011). Endocrine Disruptors: from Endocrine to Metabolic Disruption. *Annu. Rev. Physiol.* 73, 135–162. doi:10.1146/annurev-physiol-012110-142200

Cascio, C., Deidda, I., Russo, D., and Guarneri, P. (2015). The Estrogenic Retina: The Potential Contribution to Healthy Aging and Age-Related Neurodegenerative Diseases of the Retina. *Steroids* 103, 31–41. doi:10.1016/j.steroids.2015.08.002

Cascio, C., Russo, D., Drago, G., Galizzi, G., Passantino, R., Guarneri, R., et al. (2007). 17beta-estradiol Synthesis in the Adult Male Rat Retina. *Exp. Eye Res.* 85, 166–172. doi:10.1016/j.exer.2007.02.008

Castro, Í. B., Machado, F. B., De Sousa, G. T., Paz-Villarraga, C., and Fillmann, G. (2021). How Protected Are marine Protected Areas: a Case Study of Tributyltin in Latin America. *J. Environ. Manage.* 278, 111543. doi:10.1016/j.jenvman.2020.111543

Chang, J., Wang, M., Gui, W., Zhao, Y., Yu, L., and Zhu, G. (2012). Changes in Thyroid Hormone Levels during Zebrafish Development. *Zoolog. Sci.* 29, 181–184. doi:10.2108/zsj.29.181

Chapin, R., Adams, J., Boekelheide, K., Gray, J., Le, Hayward, S., Lees, P., et al. (2008). NTP-CERHR Expret Panel Report on the Reproductive and Developmental Toxicity of Bisphenol A. *Birth Defects Res. B. Dev. Reprod. Toxicol.* 83 (3), 157–395. doi:10.1002/bdrb.20147

Chien, L. C., Hung, T. C., Choang, K. Y., Yeh, C. Y., Meng, P. J., Shieh, M. J., et al. (2002). Daily Intake of TBT, Cu, Zn, Cd and as for Fishermen in Taiwan. *Sci. Total Environ.* 285, 177–185. doi:10.1016/s0048-9697(01)00916-0

Chung, E., Genco, M. C., Megrelis, L., and Ruderman, J. V. (2011). Effects of Bisphenol A and Triclocarban on Brain-specific Expression of Aromatase in Early Zebrafish Embryos. *Proc. Natl. Acad. Sci. U S A.* 108, 17732–17737. doi:10.1073/pnas.1115187108

Clark, D. (1981). *Visual Responses in Developing Zebrafish (Brachydanio Rerio). PhD Thesis*. Eugene, OR: University of Oregon.

Connaughton, V. P., and Nelson, R. (2010). Spectral Responses in Zebrafish Horizontal Cells Include a Tetraphasic Response and a Novel UV-Dominated Triphasic Response. *J. Neurophysiol.* 104, 2407–2422. doi:10.1152/jn.00644.2009

Cortez, V., Mann, M., Brann, D. W., and Vadlamudi, R. K. (2013). Extranuclear Signaling by Estrogen: Role in Breast Cancer Progression and Metastasis. *Minerva Ginecol* 62, 573–583.

Crowley-Perry, M., Barberio, A. J., Zeino, J., Winston, E. R., and Connaughton, V. P. (2021). Zebrafish Optomotor Response and Morphology Are Altered by Transient, Developmental Exposure to Bisphenol-A. *J. Dev. Biol.* 9, 14. doi:10.3390/jdb9020014

Cui, J., Shen, Y., and Li, R. (2013). Estrogen Synthesis and Signaling Pathways during Aging: from Periphery to Brain. *Trends Mol. Med.* 19, 197–209. doi:10.1016/j.molmed.2012.12.007

Darras, V. M., Hume, R., and Visser, T. J. (1999). Regulation of Thyroid Hormone Metabolism during Fetal Development. *Mol. Cel Endocrinol* 151, 37–47. doi:10.1016/s0303-7207(99)00088-x

Darras, V. M., Van Herck, S. L., Heijlen, M., and De Groef, B. (2011). Thyroid Hormone Receptors in Two Model Species for Vertebrate Embryonic Development: Chicken and Zebrafish. *J. Thyroid Res.* 2011, 402320. doi:10.4061/2011/402320

Denny, J. S., Tapper, M. A., Schmieder, P. K., Hornung, M. W., Jensen, K. M., Ankley, G. T., et al. (2009). Comparison of Relative Binding Affinities of Endocrine Active Compounds to Fathead Minnow and Rainbow trout Estrogen Receptors. *Environ. Toxicol. Chem.* 24, 2948–2953. doi:10.1897/04-595r.1

Deveau, C., Jiao, X., Suzuki, S. C., Krishnakumar, A., Yoshimatsu, T., Hejtmancik, J. F., et al. (2020). Thyroid Hormone Receptor Beta Mutations Alter Photoreceptor Development and Function in *Danio rerio* (Zebrafish). *Plos Genet.* 16, e1008869. doi:10.1371/journal.pgen.1008869

Diotel, N., Vaillant, C., Gabbero, C., Mironov, S., Fostier, A., Gueguen, M. M., et al. (2013). Effects of Estradiol in Adult Neurogenesis and Brain Repair in Zebrafish. *Horm. Behav.* 63, 193–207. doi:10.1016/j.yhbeh.2012.04.003

Dong, W., Muramoto, W., Nagai, Y., Takehana, K., Stegeman, J. J., Teraoka, H., et al. (2006). Retinal Neuronal Cell Is a Toxicological Target of Tributyltin in Developing Zebrafish. *J. Vet. Med. Sci.* 68, 573–579. doi:10.1292/jvms.68.573

Dunn, T. W., Gebhardt, C., Naumann, E. A., Riegler, C., Ahrens, M. B., Engert, F., et al. (2016). Neural Circuits Underlying Visually Evoked Escapes in Larval Zebrafish. *Neuron* 89, 613–628. doi:10.1016/j.neuron.2015.12.021

Eldred, K. C., Hadyniak, S. E., Hussey, K. A., Brenerman, B., Zhang, P. W., Chamling, X., et al. (2018). Thyroid Hormone Signaling Specifies Cone Subtypes in Human Retinal Organoids. *Science* 362. doi:10.1126/science.aau6348

Endeman, D., Klaassen, L. J., and Kamermans, M. (2013). Action Spectra of Zebrafish Cone Photoreceptors. *PLOS ONE* 8, e68540. doi:10.1371/journal.pone.0068540

Enright, J. M., Toomey, M. B., Sato, S. Y., Temple, S. E., Allen, J. R., Fujiwara, R., et al. (2015). Cyp27c1 Red-Shifts the Spectral Sensitivity of Photoreceptors by Converting Vitamin A1 into A2. *Curr. Biol.* 25, 3048–3057. doi:10.1016/j.cub.2015.10.018

Essner, J. J., Breuer, J. J., Essner, R. D., Fahrenkrug, S. C., and Hackett, P. B. (1997). The Zebrafish Thyroid Hormone Receptor Alpha 1 Is Expressed during Early Embryogenesis and Can Function in Transcriptional Repression. *Differentiation* 62, 107–117. doi:10.1046/j.1432-0436.1997.6230107.x

Farabollini, F., Porrini, S., and Dessì-Fulgherit, F. (1999). Perinatal Exposure to the Estrogenic Pollutant Bisphenol A Affects Behavior in Male and Female Rats. *Pharmacol. Biochem. Behav.* 64, 687–694. doi:10.1016/s0091-3057(99)00136-7

Fent, K., and Meier, W. (1992). Tributyltin-induced Effects on Early Life Stages of Minnows *Phoxinus phoxinus*. *Arch. Environ. Contam. Toxicol.* 22, 428–438. doi:10.1007/BF00212563

Flamant, F., Cheng, S. Y., Hollenberg, A. N., Moeller, L. C., Samarut, J., Wondisford, F. E., et al. (2017). Thyroid Hormone Signaling Pathways: Time for a More Precise Nomenclature. *Endocrinology* 158, 2052–2057. doi:10.1210/en.2017-00250

Froehlicher, M., Liedtke, A., Groh, K., López-Schier, H., Neuhauss, S. C., Segner, H., et al. (2009). Estrogen Receptor Subtype Beta2 Is Involved in Neuromast Development in Zebrafish (*Danio rerio*) Larvae. *Dev. Biol.* 330, 32–43. doi:10.1016/j.ydbio.2009.03.005

Gellinas, D., and Callard, G. V. (1993). Immunocytochemical and Biochemical Evidence for Aromatase in Neurons of the Retina, Optic Tectum and Retinotectal Pathways in Goldfish. *J. Neuroendocrinology* 5, 635–641.

Gerlai, R. (2016). Learning and Memory in Zebrafish (*Danio rerio*). *Methods Cel Biol* 134, 551–586. doi:10.1016/bs.mcb.2016.02.005

Gibert, Y., Sassi-Messai, S., Fini, J. B., Bernard, L., Zalko, D., Cravedi, J. P., et al. (2011). Bisphenol A Induces Otolith Malformations during Vertebrate Embryogenesis. *BMC Dev. Biol.* 11, 4. doi:10.1186/1471-213X-11-4

Gipperth, L. (2009). The Legal Design of the International and European Union Ban on Tributyltin Antifouling Paint: Direct and Indirect Effects. *J. Environ. Manage.* 90 (Suppl. 1), S86–S95. doi:10.1016/j.jenvman.2008.08.013

Glaschke, A., Weiland, J., Del Turco, D., Steiner, M., Peichl, L., and Glösmann, M. (2011). Thyroid Hormone Controls Cone Opsin Expression in the Retina of Adult Rodents. *J. Neurosci.* 31, 4844–4851. doi:10.1523/JNEUROSCI.6181-10.2011

Glass, C. K., Holloway, J. M., Devary, O. V., and Rosenfeld, M. G. (1988). The Thyroid Hormone Receptor Binds with Opposite Transcriptional Effects to a Common Sequence Motif in Thyroid Hormone and Estrogen Response Elements. *Cell* 54, 313–323. doi:10.1016/0092-8674(88)90194-8

González, A., and Piferrer, F. (2002). Characterization of Aromatase Activity in the Sea Bass: Effects of Temperature and Different Catalytic Properties of Brain and Ovarian Homogenates and Microsomes. *J. Exp. Zool* 293, 500–510. doi:10.1002/jez.90005

Gothié, J. D., Vancamp, P., Demeneix, B., and Remaud, S. (2019). Thyroid Hormone Regulation of Neural Stem Cell Fate: from Development to Ageing. *Acta Physiol. (Oxf)* 228, e13316. doi:10.1111/apha.13316

Gould, C. J., Saldanha, C. J., and Connaughton, V. P. (2019). Acute Exposure to 4-OH-A, Not PCB1254, Alters Brain Aromatase Activity but Does Not Adversely Affect Growth in Zebrafish. *Environ. Toxicol. Pharmacol.* 68, 133–140. doi:10.1016/j.etap.2019.02.010

Gould, C. J., Wiegand, J. L., and Connaughton, V. P. (2017). Acute Developmental Exposure to 4-hydroxyandrostenedione Has a Long-Term Effect on Visually-Guided Behaviors. *Neurotoxicol Teratol* 64, 45–49. doi:10.1016/j.ntt.2017.10.003

Graupner, G., Zhang, X. K., Tzukerman, M., Wills, K., Hermann, T., and Pfahl, M. (1991). Thyroid Hormone Receptors Repress Estrogen Receptor Activation of a TRE. *Mol. Endocrinol.* 5, 365–372. doi:10.1210/mend-5-3-365

Group, E. W. (2013). *Dirty Dozen List of Endocrine Disruptors [Online]*. Available at: http://www.ewg.org/research/dirty-dozen-list-endocrine-disruptors (Accessed, 2016).

Hamad, A., Kluk, M., Fox, J., Park, M., and Turner, J. E. (2007). The Effects of Aromatase Inhibitors and Selective Estrogen Receptor Modulators on Eye Development in the Zebrafish (*Danio rerio*). *Curr. Eye Res.* 32, 819–827. doi:10.1080/02713680701573712

Hano, T., Oshima, Y., Kim, S. G., Satone, H., Oba, Y., Kitano, T., et al. (2007). Tributyltin Causes Abnormal Development in Embryos of Medaka, *Oryzias latipes*. *Chemosphere* 69, 927–933. doi:10.1016/j.chemosphere.2007.05.093

Hao, R., Bondesson, M., Singh, A. V., Riu, A., Mccollum, C. W., Knudsen, T. B., et al. (2013). Identification of Estrogen Target Genes during Zebrafish Embryonic Development through Transcriptomic Analysis. *PLoS One* 8, e79020. doi:10.1371/journal.pone.0079020

Harpavat, S., and Cepko, C. L. (2003). Thyroid Hormone and Retinal Development: an Emerging Field. *Thyroid* 13, 1013–1019. doi:10.1089/105072503770867183

Hatch, E. E., Nelson, J. W., Stahlhut, R. W., and Webster, T. F. (2010). Association of Endocrine Disruptors and Obesity: Perspectives from Epidemiological Studies. *Int. J. Androl.* 33, 324–332. doi:10.1111/j.1365-2605.2009.01035.x

Hayashi, L., Sheth, M., Young, A., Kruger, M., Wayman, G. A., and Coffin, A. B. (2015). The Effect of the Aquatic Contaminants Bisphenol-A and PCB-95 on the Zebrafish Lateral Line. *Neurotoxicology* 46, 125–136. doi:10.1016/j.neuro.2014.12.010

Haynes, J.-D., Deichmann, R., and Rees, G. (2005). Eye-specific Effects of Binocular Rivalry in the Human Lateral Geniculate Nucleus. *Nature* 438, 496–499. doi:10.1038/nature04169

Heimeier, R. A., Das, B., Buchholz, D. R., and Shi, Y. B. (2009). The Xenoestrogen Bisphenol A Inhibits Postembryonic Vertebrate Development by Antagonizing Gene Regulation by Thyroid Hormone. *Endocrinology* 150, 2964–2973. doi:10.1210/en.2008-1503

Heindel, J. J., Newbold, R., and Schug, T. T. (2015). Endocrine Disruptors and Obesity. *Nat. Rev. Endocrinol.* 11, 653–661. doi:10.1038/nrendo.2015.163

Houbrechts, A. M., Vergauwen, L., Bagci, E., Van Houcke, J., Heijlen, M., Kulemeka, B., et al. (2016). Deiodinase Knockdown Affects Zebrafish Eye Development at the Level of Gene Expression, Morphology and Function. *Mol. Cel Endocrinol* 424, 81–93. doi:10.1016/j.mce.2016.01.018

Howdeshell, K. L. (2002). A Model of the Development of the Brain as a Construct of the Thyroid System. *Environ. Health Perspect.* 110 (Suppl. 3), 337–348. doi:10.1289/ehp.02110s3337

Howe, K., Clark, M. D., Torroja, C. F., Torrance, J., Berthelot, C., Muffato, M., et al. (2013). The Zebrafish Reference Genome Sequence and its Relationship to the Human Genome. *Nature* 496, 498–503. doi:10.1038/nature12111

Hunter, P. R., Lowe, A. S., Thompson, I. D., and Meyer, M. P. (2013). Emergent Properties of the Optic Tectum Revealed by Population Analysis of Direction and Orientation Selectivity. *J. Neurosci.* 33, 13940–13945. doi:10.1523/JNEUROSCI.1493-13.2013

IMO (2019). *International Convention on the Control of Harmful Anti-fouling Systems on Ships [Online]*. London: International Maritime Organization. Available at: https://www.imo.org (Accessed, 2021).

Jašarević, E., Sieli, P. T., Twellman, E. E., Welsh, T. H., Jr, Schachtman, T. R., Roberts, R. M., et al. (2011). Disruption of Adult Expression of Sexually Selected Traits by Developmental Exposure to Bisphenol A. *Proc. Natl. Acad. Sci. U S A.* 108, 11715–11720. doi:10.1073/pnas.1107958108

Jayasinghe, B. S., and Volz, D. C. (2011). Aberrant Ligand-Induced Activation of G Protein-Coupled Estrogen Receptor 1 (GPER) Results in Developmental Malformations during Vertebrate Embryogenesis. *Toxicol. Sci.* 125, 262–273. doi:10.1093/toxsci/kfr269

Jones, M. R. L., and Ross, P. M. (2018). Recovery of the New Zealand Muricid Dogwhelk Haustrum Scobina from TBT-Induced Imposex. *Mar. Pollut. Bull.* 126, 396–401. doi:10.1016/j.marpolbul.2017.11.034

Jung, K. K., Kim, S. Y., Kim, T. G., Kang, J. H., Kang, S. Y., Cho, J. Y., et al. (2007). Differential Regulation of Thyroid Hormone Receptor-Mediated Function by Endocrine Disruptors. *Arch. Pharm. Res.* 30, 616–623. doi:10.1007/BF02977657

Kajta, M., and Wójtowicz, A. K. (2013). Impact of Endocrine-Disrupting Chemicals on Neural Development and the Onset of Neurological Disorders. *Pharmacol. Rep.* 65, 1632–1639. doi:10.1016/s1734-1140(13)71524-x

Kim, M. E., Park, H. R., Gong, E. J., Choi, S. Y., Kim, H. S., and Lee, J. (2011). Exposure to Bisphenol A Appears to Impair Hippocampal Neurogenesis and Spatial Learning and Memory. *Food Chem. Toxicol.* 49, 3383–3389. doi:10.1016/j.fct.2011.09.017

Kimmel, C. B., Ballard, W. W., Kimmel, S. R., Ullmann, B., and Schilling, T. F. (1995). Stages of Embryonic Development of the Zebrafish. *Dev. Dyn.* 203, 253–310. doi:10.1002/aja.1002030302

Kinch, C. D., Ibhazehiebo, K., Jeong, J. H., Habibi, H. R., and Kurrasch, D. M. (2015). Low-dose Exposure to Bisphenol A and Replacement Bisphenol S Induces Precocious Hypothalamic Neurogenesis in Embryonic Zebrafish. *Proc. Natl. Acad. Sci. U S A.* 112, 1475–1480. doi:10.1073/pnas.1417731112

Kishida, M., and Callard, G. V. (2001). Distinct Cytochrome P450 Aromatase Isoforms in Zebrafish (*Danio rerio*) Brain and Ovary Are Differentially Programmed and Estrogen Regulated during Early Development. *Endocrinology* 142, 740–750. doi:10.1210/endo.142.2.7928

Kishida, M., Mclellan, M., Miranda, J. A., and Callard, G. V. (2001). Estrogen and Xenoestrogens Upregulate the Brain Aromatase Isoform (P450aromB) and Perturb Markers of Early Development in Zebrafish (*Danio rerio*). *Comp. Biochem. Physiol. B Biochem. Mol. Biol.* 129, 261–268. doi:10.1016/s1096-4959(01)00319-0

Klinge, C. M. (2001). Estrogen Receptor Interaction with Estrogen Response Elements. *Nucleic Acids Res.* 29, 2905–2919. doi:10.1093/nar/29.14.2905

Kobayashi, K., Kobayashi, H., Ueda, M., and Honda, Y. (1998). Estrogen Receptor Expression in Bovine and Rat Retinas. *Invest. Ophthalmol. Vis. Sci.* 39, 2105–2110.

Köhrle, J., and Frädrich, C. (2021). Thyroid Hormone System Disrupting Chemicals. *Best Pract. Res. Clin. Endocrinol. Metab.* 35, 101562. doi:10.1016/j.beem.2021.101562

Kolpin, D. W., Furlong, E. T., Meyer, M. T., Thurman, E. M., and Zaugg, S. D. (2002). Pharmaceuticals, Hormones, and Other Organic Wastewater Contaminants in US Streams, 1999-2000: A National Reconnaissance. *Environ. Sci. Technol.* 36 (6), 1202–1211.

Komoike, Y., Matsuoka, M., and Kosaki, K. (2013). Potential Teratogenicity of Methimazole: Exposure of Zebrafish Embryos to Methimazole Causes Similar Developmental Anomalies to Human Methimazole Embryopathy. *Birth Defects Res. B Dev. Reprod. Toxicol.* 98, 222–229. doi:10.1002/bdrb.21057

Krens, S. F., He, S., Spaink, H. P., and Snaar-Jagalska, B. E. (2006). Characterization and Expression Patterns of the MAPK Family in Zebrafish. *Gene Expr. Patterns* 6, 1019–1026. doi:10.1016/j.modgep.2006.04.008

Lakind, J. S., and Naiman, D. Q. (2011). Daily Intake of Bisphenol A and Potential Sources of Exposure: 2005-2006 National Health and Nutrition Examination Survey. *J. Expo. Sci. Environ. Epidemiol.* 21, 272–279. doi:10.1038/jes.2010.9

Lassiter, C. S., Kelley, B., and Linney, E. (2002). Genomic Structure and Embryonic Expression of Estrogen Receptor Beta a (ERbetaa) in Zebrafish (*Danio rerio*). *Gene* 299, 141–151. doi:10.1016/s0378-1119(02)01050-8

Lazar, M. A., Berrodin, T. J., and Harding, H. P. (1991). Differential DNA Binding by Monomeric, Homodimeric, and Potentially Heteromeric Forms of the Thyroid Hormone Receptor. *Mol. Cel Biol* 11, 5005–5015. doi:10.1128/mcb.11.10.5005

Le Page, Y., Vosges, M., Servili, A., Brion, F., and Kah, O. (2011). Neuroendocrine Effects of Endocrine Disruptors in Teleost Fish. *J. Toxicol. Environ. Health B Crit. Rev.* 14, 370–386. doi:10.1080/10937404.2011.578558

Lee, S., and Privalsky, M. L. (2005). Heterodimers of Retinoic Acid Receptors and Thyroid Hormone Receptors Display Unique Combinatorial Regulatory Properties. *Mol. Endocrinol.* 19, 863–878. doi:10.1210/me.2004-0210

Lephart, E. D. (1996). A Review of Brain Aromatase Cytochrome P450. *Brain Res. Brain Res. Rev.* 22, 1–26. doi:10.1016/0165-0173(96)00002-1

Levin, E. R. (2002). Cellular Functions of Plasma Membrane Estrogen Receptors. *Steroids* 67, 471–475. doi:10.1016/s0039-128x(01)00179-9

Li, D., Li, T., Wang, F., Tian, H., and Samuels, H. H. (2002). Functional Evidence for Retinoid X Receptor (RXR) as a Nonsilent Partner in the Thyroid Hormone Receptor/RXR Heterodimer. *Mol. Cel Biol* 22, 5782–5792. doi:10.1128/mcb.22.16.5782-5792.2002

Li, D., Yamada, T., Wang, F., Vulin, A. I., and Samuels, H. H. (2004). Novel Roles of Retinoid X Receptor (RXR) and RXR Ligand in Dynamically Modulating the Activity of the Thyroid Hormone Receptor/RXR Heterodimer. *J. Biol. Chem.* 279, 7427–7437. doi:10.1074/jbc.M311596200

Li, Y. N., Tsujimura, T., Kawamura, S., and Dowling, J. E. (2012). Bipolar Cell-Photoreceptor Connectivity in the Zebrafish (*Danio rerio*) Retina. *J. Comp. Neurol.* 520, 3786–3802. doi:10.1002/cne.23168

Li, Z. H., and Li, P. (2021). Effects of the Tributyltin on the Blood Parameters, Immune Responses and Thyroid Hormone System in Zebrafish. *Environ. Pollut.* 268, 115707. doi:10.1016/j.envpol.2020.115707

Liang, X., Souders, C. L., Iii, Zhang, J., and Martyniuk, C. J. (2017). Tributyltin Induces Premature Hatching and Reduces Locomotor Activity in Zebrafish (*Danio rerio*) Embryos/larvae at Environmentally Relevant Levels. *Chemosphere* 189, 498–506. doi:10.1016/j.chemosphere.2017.09.093

Link, B. A., and Collery, R. F. (2015). Zebrafish Models of Retinal Disease. *Annu. Rev. Vis. Sci.* 1, 125–153. doi:10.1146/annurev-vision-082114-035717

Liu, W., Zhang, X., Wei, P., Tian, H., Wang, W., and Ru, S. (2017). Long-term Exposure to Bisphenol S Damages the Visual System and Reduces the Tracking Capability of Male Zebrafish (*Danio rerio*). *J. Appl. Toxicol.* 38, 248–258. doi:10.1002/jat.3519

Liu, Y. W., Lo, L. J., and Chan, W. K. (2000). Temporal Expression and T3 Induction of Thyroid Hormone Receptors Alpha1 and Beta1 during Early Embryonic and Larval Development in Zebrafish, *Danio rerio*. *Mol. Cel Endocrinol* 159, 187–195. doi:10.1016/s0303-7207(99)00193-8

Lovato, A. K., Creton, R., and Colwill, R. M. (2017). Effects of Embryonic Exposure to Polychlorinated Biphenyls (PCBs) on Larval Zebrafish Behavior. *Neurotoxicol Teratol* 53, 1–10. doi:10.1016/j.ntt.2015.11.002

Luo, J., and Liu, D. (2020). Does GPER Really Function as a G Protein-Coupled Estrogen Receptor *In Vivo*? *Front. Endocrinol. (Lausanne)* 11, 148. doi:10.3389/fendo.2020.00148

Lyssimachou, A., Jenssen, B. M., and Arukwe, A. (2006). Brain Cytochrome P450 Aromatase Gene Isoforms and Activity Levels in Atlantic Salmon after Waterborne Exposure to Nominal Environmental Concentrations of the Pharmaceutical Ethynylestradiol and Antifoulant Tributyltin. *Toxicol. Sci.* 91, 82–92. doi:10.1093/toxsci/kfj136

Mackin, R. D., Frey, R. A., Gutierrez, C., Farre, A. A., Kawamura, S., Mitchell, D. M., et al. (2019). Endocrine Regulation of Multichromatic Color Vision. *Proc. Natl. Acad. Sci. U S A.* 116, 16882–16891. doi:10.1073/pnas.1904783116

Mangiamele, L. A., Gomez, J. R., Curtis, N. J., and Thompson, R. R. (2017). GPER/GPR30, a Membrane Estrogen Receptor, Is Expressed in the Brain and Retina of a Social Fish (*Carassius auratus*) and Colocalizes with Isotocin. *J. Comp. Neurol.* 525, 252–270. doi:10.1002/cne.24056

Marelli, F., Carra, S., Agostini, M., Cotelli, F., Peeters, R., Chatterjee, K., et al. (2016). Patterns of Thyroid Hormone Receptor Expression in Zebrafish and Generation of a Novel Model of Resistance to Thyroid Hormone Action. *Mol. Cel Endocrinol* 424, 102–117. doi:10.1016/j.mce.2016.01.020

Mayer, I., Borg, B., Berglund, I., and Lambert, J. G. (1991). Effects of Castration and Androgen Treatment on Aromatase Activity in the Brain of Mature Male Atlantic salmon (*Salmo salar* L.) Parr. *Gen. Comp. Endocrinol.* 82, 86–92. doi:10.1016/0016-6480(91)90299-l

Mcallister, B. G., and Kime, D. E. (2003). Early Life Exposure to Environmental Levels of the Aromatase Inhibitor Tributyltin Causes Masculinisation and Irreversible Sperm Damage in Zebrafish (*Danio rerio*). *Aquat. Toxicol.* 65, 309–316. doi:10.1016/s0166-445x(03)00154-1

Mccarthy, M. M. (2008). Estradiol and the Developing Brain. *Physiol. Rev.* 88, 91–124. doi:10.1152/physrev.00010.2007

Mccarthy, M. M. (2009). The Two Faces of Estradiol: Effects on the Developing Brain. *Neuroscientist* 15, 599–610. doi:10.1177/1073858409340924

Mcginnis, C. L., and Crivello, J. F. (2011). Elucidating the Mechanism of Action of Tributyltin (TBT) in Zebrafish. *Aquat. Toxicol.* 103, 25–31. doi:10.1016/j.aquatox.2011.01.005

Meier, A., Nelson, R., and Connaughton, V. P. (2018). Color Processing in Zebrafish Retina. *Front Cel Neurosci* 12, 327. doi:10.3389/fncel.2018.00327

Menuet, A., Pellegrini, E., Anglade, I., Blaise, O., Laudet, V., Kah, O., et al. (2002). Molecular Characterization of Three Estrogen Receptor Forms in Zebrafish: Binding Characteristics, Transactivation Properties, and Tissue Distributions. *Biol. Reprod.* 66, 1881–1892. doi:10.1095/biolreprod66.6.1881

Menuet, A., Pellegrini, E., Brion, F., Gueguen, M. M., Anglade, I., Pakdel, F., et al. (2005). Expression and Estrogen-dependent Regulation of the Zebrafish Brain Aromatase Gene. *J. Comp. Neurol.* 485, 304–320. doi:10.1002/cne.20497

Moriyama, K., Tagami, T., Akamizu, T., Usui, T., Saijo, M., Kanamoto, N., et al. (2002). Thyroid Hormone Action Is Disrupted by Bisphenol A as an Antagonist. *J. Clin. Endocrinol. Metab.* 87, 5185–5190. doi:10.1210/jc.2002-020209

Mouriec, K., Lareyre, J. J., Tong, S. K., Le Page, Y., Vaillant, C., Pellegrini, E., et al. (2009). Early Regulation of Brain Aromatase (Cyp19a1b) by Estrogen Receptors during Zebrafish Development. *Dev. Dyn.* 238, 2641–2651. doi:10.1002/dvdy.22069

Muto, A., and Kawakami, K. (2013). Prey Capture in Zebrafish Larvae Serves as a Model to Study Cognitive Functions. *Front. Neural Circuits* 7, 110. doi:10.3389/fncir.2013.00110

Muto, A., Orger, M. B., Wehman, A. M., Smear, M. C., Kay, J. N., Page-Mccaw, P. S., et al. (2005). Forward Genetic Analysis of Visual Behavior in Zebrafish. *Plos Genet.* 1, e66. doi:10.1371/journal.pgen.0010066

Nakajima, Y., Goldblum, R. M., and Midoro-Horiuti, T. (2012). Fetal Exposure to Bisphenol A as a Risk Factor for the Development of Childhood Asthma: an Animal Model Study. *Environ. Health* 11, 8. doi:10.1186/1476-069X-11-8

Nasri, A., Mezni, A., Lafon, P.-A., Wahbi, A., Cubedo, N., Clair, P., et al. (2021). Ethinylestradiol (EE2) Residues from Birth Control Pills Impair Nervous System Development and Swimming Behavior of Zebrafish Larvae. *Sci. Total Environ.* 770, 145272. doi:10.1016/j.scitotenv.2021.145272

Nelson, B. P., Henriet, R. P., Holt, A. W., Bopp, K. C., Houser, A. P., Allgood, O. E., Jr, et al. (2008). The Role of Estrogen in the Developmental Appearance of Sensory-Motor Behaviors in the Zebrafish (*Danio rerio*): the Characterization of the "listless" Model. *Brain Res.* 1222, 118–128. doi:10.1016/j.brainres.2008.05.049

Nelson, R. F., Balraj, A., Suresh, T., Torvund, M., and Patterson, S. S. (2019). Strain Variations in Cone Wavelength Peaks *In Situ* during Zebrafish Development. *Vis. Neurosci.* 36, E010. doi:10.1017/S0952523819000075

Neuhauss, S. C. (2003). Behavioral Genetic Approaches to Visual System Development and Function in Zebrafish. *J. Neurobiol.* 54, 148–160. doi:10.1002/neu.10165

Nikoleris, L., Hultin, C. L., Hallgren, P., and Hansson, M. C. (2016). 17α-Ethinylestradiol (EE2) Treatment of Wild Roach (*Rutilus rutilus*) during Early Life Development Disrupts Expression of Genes Directly Involved in the Feedback Cycle of Estrogen. *Comp. Biochem. Physiol. C Toxicol. Pharmacol.* 180, 56–64. doi:10.1016/j.cbpc.2015.12.002

Noyes, P. D., Friedman, K. P., Browne, P., Haselman, J. T., Gilbert, M. E., Hornung, M. W., et al. (2019). Evaluating Chemicals for Thyroid Disruption: Opportunities and Challenges with *In Vitro* Testing and Adverse Outcome Pathway Approaches. *Environ. Health Perspect.* 127, 95001. doi:10.1289/EHP5297

Orger, M. B., Gahtan, E., Muto, A., Page-Mccaw, P., Smear, M. C., and Baier, H. (2004). Behavioral Screening Assays in Zebrafish. *Methods Cel Biol* 77, 53–68. doi:10.1016/s0091-679x(04)77003-x

Ortiz-Villanueva, E., Jaumot, J., Martínez, R., Navarro-Martín, L., Piña, B., and Tauler, R. (2018). Assessment of Endocrine Disruptors Effects on Zebrafish (*Danio rerio*) Embryos by Untargeted LC-HRMS Metabolomic Analysis. *Sci. Total Environ.* 635, 156–166. doi:10.1016/j.scitotenv.2018.03.369

Paige, L. A., Christensen, D. J., Grøn, H., Norris, J. D., Gottlin, E. B., Padilla, K. M., et al. (1999). Estrogen Receptor (ER) Modulators Each Induce Distinct Conformational Changes in ER Alpha and ER Beta. *Proc. Natl. Acad. Sci. U S A.* 96, 3999–4004. doi:10.1073/pnas.96.7.3999

Pasmanik, M., and Callard, G. V. (1988). Changes in Brain Aromatase and 5 Alpha-Reductase Activities Correlate Significantly with Seasonal Reproductive Cycles in Goldfish (*Carassius auratus*). *Endocrinology* 122, 1349–1356. doi:10.1210/endo-122-4-1349

Patrick, L. (2009). Thyroid Disruption: Mechanism and Clinical Implications in Human Health. *Altern. Med. Rev.* 14, 326–346.

Peachey, N. S., Ray, T. A., Florijn, R., Rowe, L. B., Sjoerdsma, T., Contreras-Alcantara, S., et al. (2012). GPR179 Is Required for Depolarizing Bipolar Cell Function and Is Mutated in Autosomal-Recessive Complete Congenital Stationary Night Blindness. *Am. J. Hum. Genet.* 90, 331–339. doi:10.1016/j.ajhg.2011.12.006

Pellegrini, E., Menuet, A., Lethimonier, C., Adrio, F., Gueguen, M. M., Tascon, C., et al. (2005). Relationships between Aromatase and Estrogen Receptors in the Brain of Teleost Fish. *Gen. Comp. Endocrinol.* 142, 60–66. doi:10.1016/j.ygcen.2004.12.003

Pellegrini, E., Mouriec, K., Anglade, I., Menuet, A., Le Page, Y., Gueguen, M. M., et al. (2007). Identification of Aromatase-Positive Radial Glial Cells as Progenitor Cells in the Ventricular Layer of the Forebrain in Zebrafish. *J. Comp. Neurol.* 501, 150–167. doi:10.1002/cne.21222

Porazzi, P., Calebiro, D., Benato, F., Tiso, N., and Persani, L. (2009). Thyroid Gland Development and Function in the Zebrafish Model. *Mol. Cel Endocrinol* 312, 14–23. doi:10.1016/j.mce.2009.05.011

Qiu, W., Zhao, Y., Yang, M., Farajzadeh, M., Pan, C., and Wayne, N. L. (2016). Actions of Bisphenol A and Bisphenol S on the Reproductive Neuroendocrine System during Early Development in Zebrafish. *Endocrinology* 157, 636–647. doi:10.1210/en.2015-1785

Ramírez-Montero, M. d. C., Gómez-Oliván, L. M., Gutiérrez-Noya, V. M., Orozco-Hernández, J. M., Islas-Flores, H., Elizalde-Velázquez, G. A., et al. (2022). Acute Exposure to 17-α-Ethinylestradiol Disrupt the Embryonic Development and Oxidative Status of *Danio rerio*. *Comp. Biochem. Physiol. C: Toxicol. Pharmacol.* 251, 109199. doi:10.1016/j.cbpc.2021.109199

Raymond, P. A., Barthel, L. K., and Curran, G. A. (1995). Developmental Patterning of Rod and Cone Photoreceptors in Embryonic Zebrafish. *J. Comp. Neurol.* 359, 537–550. doi:10.1002/cne.903590403

Rehberger, K., Baumann, L., Hecker, M., and Braunbeck, T. (2018). Intrafollicular Thyroid Hormone Staining in Whole-Mount Zebrafish (*Danio rerio*) Embryos for the Detection of Thyroid Hormone Synthesis Disruption. *Fish. Physiol. Biochem.* 44, 997–1010. doi:10.1007/s10695-018-0488-y

Reider, M., and Connaughton, V. P. (2014). Developmental Exposure to Methimazole Increases Anxiety Behavior in Zebrafish. *Behav. Neurosci.* 129, 634–642. doi:10.1037/bne0000087

Richter, C. A., Taylor, J. A., Ruhlen, R. L., Welshons, W. V., and Vom Saal, F. S. (2007). Estradiol and Bisphenol A Stimulate Androgen Receptor and Estrogen Receptor Gene Expression in Fetal Mouse Prostate Mesenchyme Cells. *Environ. Health Perspect.* 115, 902–908. doi:10.1289/ehp.9804

Roberts, M. R., Srinivas, M., Forrest, D., Morreale de Escobar, G., and Reh, T. A. (2006). Making the Gradient: Thyroid Hormone Regulates Cone Opsin Expression in the Developing Mouse Retina. *Proc. Natl. Acad. Sci. U S A.* 103, 6218–6223. doi:10.1073/pnas.0509981103

Roque, C., and Baltazar, G. (2019). G Protein-Coupled Estrogen Receptor 1 (GPER) Activation Triggers Different Signaling Pathways on Neurons and Astrocytes. *Neural Regen. Res.* 14, 2069–2070. doi:10.4103/1673-5374.262577

Rouleau, C., Xiong, Z. H., Pacepavicius, G., and Huang, G. L. (2003). Uptake of Waterborne Tributyltin in the Brain of Fish: Axonal Transport as a Proposed Mechanism. *Environ. Sci. Technol.* 37, 3298–3302. doi:10.1021/es020984n

Saili, K. S., Corvi, M. M., Weber, D. N., Patel, A. U., Das, S. R., Przybyla, J., et al. (2012). Neurodevelopmental Low-Dose Bisphenol A Exposure Leads to Early Life-Stage Hyperactivity and Learning Deficits in Adult Zebrafish. *Toxicology* 291, 83–92. doi:10.1016/j.tox.2011.11.001

Santos, M. M., Micael, J., Carvalho, A. P., Morabito, R., Booy, P., Massanisso, P., et al. (2006). Estrogens Counteract the Masculinizing Effect of Tributyltin in Zebrafish. *Comp. Biochem. Physiol. C Toxicol. Pharmacol.* 142, 151–155. doi:10.1016/j.cbpc.2005.11.014

Sawyer, S. J., Gerstner, K. A., and Callard, G. V. (2006). Real-time PCR Analysis of Cytochrome P450 Aromatase Expression in Zebrafish: Gene Specific Tissue Distribution, Sex Differences, Developmental Programming, and Estrogen Regulation. *Gen. Comp. Endocrinol.* 147, 108–117. doi:10.1016/j.ygcen.2005.12.010

Schmidt, R., Strähle, U., and Scholpp, S. (2013). Neurogenesis in Zebrafish - from Embryo to Adult. *Neural Dev.* 8, 3. doi:10.1186/1749-8104-8-3

Schmitt, E. A., and Dowling, J. E. (1994). Early Eye Morphogenesis in the Zebrafish, Brachydanio Rerio. *J. Comp. Neurol.* 344, 532–542. doi:10.1002/cne.903440404

Schmitt, E. A., and Dowling, J. E. (1999). Early Retinal Development in the Zebrafish, *Danio rerio*: Light and Electron Microscopic Analyses. *J. Comp. Neurol.* 404, 515–536. doi:10.1002/(sici)1096-9861(19990222)404:4<515::aid-cne8>3.0.co;2-a

Schönfelder, G., Wittfoht, W., Hopp, H., Talsness, C. E., Paul, M., and Chahoud, I. (2002). Parent Bisphenol A Accumulation in the Human Maternal-Fetal-

Placental Unit. *Environ. Health Perspect.* 110, A703–A707. doi:10.1289/ehp.110-1241091

Schøyen, M., Green, N. W., Hjermann, D. Ø., Tveiten, L., Beylich, B., Øxnevad, S., et al. (2019). Levels and Trends of Tributyltin (TBT) and Imposex in Dogwhelk (*Nucella lapillus*) along the Norwegian Coastline from 1991 to 2017. *Mar. Environ. Res.* 144, 1–8. doi:10.1016/j.marenvres.2018.11.011

Scott, R. E., Wu-Peng, X. S., Yen, P. M., Chin, W. W., and Pfaff, D. W. (1997). Interactions of Estrogen- and Thyroid Hormone Receptors on a Progesterone Receptor Estrogen Response Element (ERE) Sequence: a Comparison with the Vitellogenin A2 Consensus ERE. *Mol. Endocrinol.* 11, 1581–1592. doi:10.1210/mend.11.11.0003

Sellitti, D. F., and Suzuki, K. (2014). Intrinsic Regulation of Thyroid Function by Thyroglobulin. *Thyroid* 24, 625–638. doi:10.1089/thy.2013.0344

Shi, Y., Chen, C., Li, M., Liu, L., Dong, K., Chen, K., et al. (2021). Oral Exposure to Tributyltin Induced Behavioral Abnormality and Oxidative Stress in the Eyes and Brains of Juvenile Japanese Medaka (*Oryzias latipes*). *Antioxidants (Basel)* 10, 1647. doi:10.3390/antiox10111647

Shi, Y., Liu, X., Zhu, P., Li, J., Sham, K. W., Cheng, S. H., et al. (2013). G-protein-coupled Estrogen Receptor 1 Is Involved in Brain Development during Zebrafish (*Danio rerio*) Embryogenesis. *Biochem. Biophys. Res. Commun.* 435, 21–27. doi:10.1016/j.bbrc.2013.03.130

Showalter, S., and Savarese, J. (2004). *Restrictions on the Use of marine Antifouling Paints Containing Tributyltin and Copper*.

Silva, N., Louro, B., Trindade, M., Power, D. M., and Campinho, M. A. (2017). Transcriptomics Reveal an Integrative Role for Maternal Thyroid Hormones during Zebrafish Embryogenesis. *Sci. Rep.* 7 (1), 1–11. doi:10.1038/s41598-017-16951-9

Song, R., Lin, H., Chen, Y., Zhang, X., and Feng, W. (2017). Effects of Methimazole and Propylthiouracil Exposure during Pregnancy on the Risk of Neonatal Congenital Malformations: A Meta-Analysis. *PLoS One* 12, e0180108. doi:10.1371/journal.pone.0180108

Suzuki, S. C., Bleckert, A., Williams, P. R., Takechi, M., Kawamura, S., and Wong, R. O. (2013). Cone Photoreceptor Types in Zebrafish Are Generated by Symmetric Terminal Divisions of Dedicated Precursors. *Proc. Natl. Acad. Sci. U S A.* 110, 15109–15114. doi:10.1073/pnas.1303551110

Takahashi, O., and Oishi, S. (2000). Disposition of Orally Administered 2,2-Bis(4-Hydroxyphenyl)propane (Bisphenol A) in Pregnant Rats and the Placental Transfer to Fetuses. *Environ. Health Perspect.* 108, 931–935. doi:10.1289/ehp.00108931

Takechi, M., and Kawamura, S. (2005). Temporal and Spatial Changes in the Expression Pattern of Multiple Red and green Subtype Opsin Genes during Zebrafish Development. *J. Exp. Biol.* 208, 1337–1345. doi:10.1242/jeb.01532

Tang, Z., Liu, Z.-H., Wang, H., Dang, Z., and Liu, Y. (2021). A Review of 17α-Ethynylestradiol (EE2) in Surface Water across 32 Countries: Sources, Concentrations, and Potential Estrogenic Effects. *J. Environ. Manage.* 292, 112804. doi:10.1016/j.jenvman.2021.112804

Tata, J. R. (2005). One Hundred Years of Hormones. *EMBO Rep.* 6, 490–496. doi:10.1038/sj.embor.7400444

Thisse, B., and Thisse, C. (20142004). *Fast Release Clones: A High Throughput Expression analysisZFIN Direct Data Submission*. http://zfin.org.

Thomas, P., Alyea, R., Pang, Y., Peyton, C., Dong, J., and Berg, A. H. (2010). Conserved Estrogen Binding and Signaling Functions of the G Protein-Coupled Estrogen Receptor 1 (GPER) in Mammals and Fish. *Steroids* 75, 595–602. doi:10.1016/j.steroids.2009.11.005

Thomas, P., and Dong, J. (2006). Binding and Activation of the Seven-Transmembrane Estrogen Receptor GPR30 by Environmental Estrogens: A Potential Novel Mechanism of Endocrine Disruption. *J. Steroid Biochem. Mol. Biol.* 102, 175–179. doi:10.1016/j.jsbmb.2006.09.017

Tingaud-Sequeira, A., André, M., Forgue, J., Barthe, C., and Babin, P. J. (2004). Expression Patterns of Three Estrogen Receptor Genes during Zebrafish (*Danio rerio*) Development: Evidence for High Expression in Neuromasts. *Gene Expr. Patterns* 4, 561–568. doi:10.1016/j.modgep.2004.02.002

Torvund, M., Ma, T., Connaughton, V., Ono, F., and Nelson, B. (2016). Cone Signals in the Monostratified Amacrine Cells of Adult Zebrafish Retina. *J. Comp. Neurol.* 525 (7), 1532–1557. doi:10.1002/cne.24107

Trimmers, R., Labert, J., Peute, J., Vullings, H., and Van Oordt, P. (1987). Localization of Aromatase in the Brain of the Male African Catfish, *Clarias gariepinus* (Burchell), by Microdissection and Biochemical Identification. *J. Comp. Neurol.* 258, 369–377.

Tse, W. K., Yeung, B. H., Wan, H. T., and Wong, C. K. (2013). Early Embryogenesis in Zebrafish Is Affected by Bisphenol A Exposure. *Biol. Open* 2, 466–471. doi:10.1242/bio.20134283

Tsujikawa, M., and Malicki, J. (2004). Genetics of Photoreceptor Development and Function in Zebrafish. *Int. J. Dev. Biol.* 48, 925–934. doi:10.1387/ijdb.041890mt

Uc-Peraza, R. G., Castro, Í. B., and Fillmann, G. (2022). An Absurd Scenario in 2021: Banned TBT-Based Antifouling Products Still Available on the Market. *Sci. Total Environ.* 805, 150377. doi:10.1016/j.scitotenv.2021.150377

Vancamp, P., Houbrechts, A. M., and Darras, V. M. (2019). Insights from Zebrafish Deficiency Models to Understand the Impact of Local Thyroid Hormone Regulator Action on Early Development. *Gen. Comp. Endocrinol.* 279, 45–52. doi:10.1016/j.ygcen.2018.09.011

Vandenberg, L. N., Chahoud, I., Heindel, J. J., Padmanabhan, V., Paumgartten, F. J., and Schoenfelder, G. (2010). Urinary, Circulating, and Tissue Biomonitoring Studies Indicate Widespread Exposure to Bisphenol A. *Environ. Health Perspect.* 118, 1055–1070. doi:10.1289/ehp.0901716

Vandenberg, L. N., Maffini, M. V., Sonnenschein, C., Rubin, B. S., and Soto, A. M. (2009). Bisphenol-A and the Great divide: a Review of Controversies in the Field of Endocrine Disruption. *Endocr. Rev.* 30, 75–95. doi:10.1210/er.2008-0021

Vasudevan, N., Koibuchi, N., Chin, W. W., and Pfaff, D. W. (2001). Differential Crosstalk between Estrogen Receptor (ER)alpha and ERbeta and the Thyroid Hormone Receptor Isoforms Results in Flexible Regulation of the Consensus ERE. *Brain Res. Mol. Brain Res.* 95, 9–17. doi:10.1016/s0169-328x(01)00165-6

Vasudevan, N., Ogawa, S., and Pfaff, D. (2002). Estrogen and Thyroid Hormone Receptor Interactions: Physiological Flexibility by Molecular Specificity. *Physiol. Rev.* 82, 923–944. doi:10.1152/physrev.00014.2002

Versonnen, B. J., and Janssen, C. R. (2004). Xenoestrogenic Effects of Ethinylestradiol in Zebrafish (*Danio rerio*). *Environ. Toxicol.* 19, 198–206. doi:10.1002/tox.20012

Vilela, C. L. S., Villela, H. D. M., Duarte, G. A. S., Santoro, E. P., Rachid, C. T. C. C., and Peixoto, R. S. (2021). Estrogen Induces Shift in Abundances of Specific Groups of the Coral Microbiome. *Sci. Rep.* 11, 2767. doi:10.1038/s41598-021-82387-x

Vogalis, F., Shiraki, T., Kojima, D., Wada, Y., Nishiwaki, Y., Jarvinen, J. L., et al. (2011). Ectopic Expression of Cone-specific G-Protein-Coupled Receptor Kinase GRK7 in Zebrafish Rods Leads to Lower Photosensitivity and Altered Responses. *J. Physiol.* 589, 2321–2348. doi:10.1113/jphysiol.2010.204156

Volkov, L. I., Kim-Han, J. S., Saunders, L. M., Poria, D., Hughes, A. E. O., Kefalov, V. J., et al. (2020). Thyroid Hormone Receptors Mediate Two Distinct Mechanisms of Long-Wavelength Vision. *Proc. Natl. Acad. Sci. U S A.* 117, 15262–15269. doi:10.1073/pnas.1920086117

Wada, K., Sakamoto, H., Nishikawa, K., Sakuma, S., Nakajima, A., Fujimoto, Y., et al. (2007). Life Style-Related Diseases of the Digestive System: Endocrine Disruptors Stimulate Lipid Accumulation in Target Cells Related to Metabolic Syndrome. *J. Pharmacol. Sci.* 105, 133–137. doi:10.1254/jphs.fm0070034

Wang, X., Dong, Q., Chen, Y., Jiang, H., Xiao, Q., Wang, Y., et al. (2013). Bisphenol A Affects Axonal Growth, Musculature and Motor Behavior in Developing Zebrafish. *Aquat. Toxicol.* 142-143, 104–113. doi:10.1016/j.aquatox.2013.07.011

Wang, Y. P., Hong, Q., Qin, D. N., Kou, C. Z., Zhang, C. M., Guo, M., et al. (2012). Effects of Embryonic Exposure to Polychlorinated Biphenyls on Zebrafish (*Danio rerio*) Retinal Development. *J. Appl. Toxicol.* 32, 186–193. doi:10.1002/jat.1650

Weber, D. N., Hoffmann, R. G., Hoke, E. S., and Tanguay, R. L. (2015). Bisphenol A Exposure during Early Development Induces Sex-specific Changes in Adult Zebrafish Social Interactions. *J. Toxicol. Environ. Health A.* 78, 50–66. doi:10.1080/15287394.2015.958419

Wolstenholme, J. T., Edwards, M., Shetty, S. R., Gatewood, J. D., Taylor, J. A., Rissman, E. F., et al. (2012). Gestational Exposure to Bisphenol A Produces Transgenerational Changes in Behaviors and Gene Expression. *Endocrinology* 153, 3828–3838. doi:10.1210/en.2012-1195

Yarwood, N. J., Gurr, J. A., Sheppard, M. C., and Franklyn, J. A. (1993). Estradiol Modulates Thyroid Hormone Regulation of the Human Glycoprotein Hormone Alpha Subunit Gene. *J. Biol. Chem.* 268, 21984–21989. doi:10.1016/s0021-9258(20)80637-1

Yu, W., Wu, N., Li, L., Wang, J., Ouyang, H., and Shen, H. (2020). Side Effects of PTU and MMI in the Treatment of Hyperthyroidism: a Systematic Review and Meta-Analysis. *Endocr. Pract.* 26, 207–217. doi:10.4158/EP-2019-0221

Zhang, C. N., Zhang, J. L., Ren, H. T., Zhou, B. H., Wu, Q. J., and Sun, P. (2017a). Effect of Tributyltin on Antioxidant Ability and Immune Responses of Zebrafish (*Danio rerio*). *Ecotoxicol Environ. Saf.* 138, 1–8. doi:10.1016/j.ecoenv.2016.12.016

Zhang, J., Zhang, C., Sun, P., Huang, M., Fan, M., and Liu, M. (2017b). RNA-sequencing and Pathway Analysis Reveal Alteration of Hepatic Steroid Biosynthesis and Retinol Metabolism by Tributyltin Exposure in Male Rare Minnow (Gobiocypris Rarus). *Aquat. Toxicol.* 188, 109–118. doi:10.1016/j.aquatox.2017.03.015

Zoeller, R. T., Bansal, R., and Parris, C. (2005). Bisphenol-A, an Environmental Contaminant that Acts as a Thyroid Hormone Receptor Antagonist *In Vitro*, Increases Serum Thyroxine, and Alters RC3/neurogranin Expression in the Developing Rat Brain. *Endocrinology* 146, 607–612. doi:10.1210/en.2004-1018

Conflict of Interest: The authors declare that the research was conducted in the absence of any commercial or financial relationships that could be construed as a potential conflict of interest.

frontiers in Pharmacology

ORIGINAL RESEARCH
published: 07 March 2022
doi: 10.3389/fphar.2022.822359

Intravitreal Administration of rhNGF Enhances Regenerative Processes in a Zebrafish Model of Retinal Degeneration

Pasquale Cocchiaro[1†], Vincenzo Di Donato[2†], Davide Rubbini[2], Rodolfo Mastropasqua[3], Marcello Allegretti[1], Flavio Mantelli[1], Andrea Aramini[1] and Laura Brandolini[1*]*

[1]Dompé Farmaceutici SpA, Napoli, Italy, [2]ZeClinics SL, IGTP (Germans Trias I Pujol Research Institute), Barcelona, Spain, [3]Institute of Ophthalmology, University of Modena and Reggio Emilia, Modena, Italy

OPEN ACCESS

Edited by:
Anna Siebel,
Universidade Comunitária da Região de Chapecó, Brazil

Reviewed by:
Xu Zhang,
Nanchang University, China
Salvatore Lucia Stella,
The Pennsylvania State University, United States
Olivia García Suárez,
Universidad de Oviedo Mieres, Spain

***Correspondence:**
Vincenzo Di Donato
vincenzo.didonato@zeclinics.com
Laura Brandolini
laura.brandolini@dompe.com

[†]These authors contributed equally to this work and share first authorship

Specialty section:
This article was submitted to Experimental Pharmacology and Drug Discovery, a section of the journal Frontiers in Pharmacology

Received: 25 November 2021
Accepted: 28 January 2022
Published: 07 March 2022

Citation:
Cocchiaro P, Di Donato V, Rubbini D, Mastropasqua R, Allegretti M, Mantelli F, Aramini A and Brandolini L (2022) Intravitreal Administration of rhNGF Enhances Regenerative Processes in a Zebrafish Model of Retinal Degeneration. Front. Pharmacol. 13:822359. doi: 10.3389/fphar.2022.822359

Nerve growth factor (NGF) is the best characterized neurotrophin, and it is known to play an important role in ocular homeostasis. Here, we demonstrated the expression of NGF receptors in adult zebrafish retina and optimized a light-induced retina degeneration (LID) zebrafish model that mimics human cone-rod disorders, demonstrating that intravitreal (IV) administration of rhNGF can boost zebrafish retinal regeneration in this model. Adult zebrafish retinae exposed to 60 h of light irradiation (60 h LID) displayed evident reduction of outer nuclear layer (ONL) thickness and cell number with presence of apoptotic cells. Retinal histologic evaluation at different time points showed that IV therapeutic injection of rhNGF resulted in an increase of ONL thickness and cell number at late time points after damage (14 and 21 days post injury), ultimately accelerating retinal tissue recovery by driving retinal cell proliferation. At a molecular level, rhNGF activated the ERK1/2 pathway and enhanced the regenerative potential of Müller glia *gfap*- and *vim*-expressing cells by stimulating at early time points the expression of the photoreceptor regeneration factor Drgal1-L2. Our results demonstrate the highly conserved nature of NGF canonical pathway in zebrafish and thus support the use of zebrafish models for testing new compounds with potential retinal regenerative properties. Moreover, the pro-regenerative effects of IV-injected NGF that we observed pave the way to further studies aimed at evaluating its effects also in mammals, in order to expedite the development of novel rhNGF-based therapeutic approaches for ophthalmological disorders.

Keywords: nerve growth factor (NGF), age-related macular degeneration (AMD), retinitis pigmentosa (RP), zebrafish, retinal regeneration, Müller glia cells, neuroprotection, translational research

INTRODUCTION

Inherited, acquired, or iatrogenic, the retinal conditions are complex and multi-factorial diseases characterized by progressive bilateral degeneration of the rod and cone photoreceptors (Narayan et al., 2016; Al-Zamil and Yassin 2017). Photoreceptor degeneration ultimately leads to either partial or total visual impairment, thus severely compromising the quality of life of affected individuals (Teutsch et al., 2016; Welp et al., 2016). Over the years, several potential therapeutic approaches have been developed with the aim of delaying the progression of these diseases (Connors et al., 2021), but

currently, a therapy that is able to promote the reversion of the phenotype remains an unmet medical need.

Photoreceptor apoptotic death is the final step of several retinal disorders, and the deregulation of the nerve growth factor (NGF) pathway observed in retinal degeneration models supports the hypothesis that a profound alteration of NGF pathway balance may account for the progressive neuronal cell death and photoreceptor loss (Santos et al., 2012; Garcia et al., 2017). NGF is the best characterized member of the neurotrophin family and has been widely described as a critical neuronal survival factor (Colafrancesco et al., 2011; L.; Mesentier-Louro et al., 2017; L. A.; Mesentier-Louro et al., 2018). It plays a crucial role also in regulating the homeostasis of ocular tissues (Aloe et al., 2012), where it is expressed with its receptors TrkA and p75 (Garcia et al., 2017): TrkA has high affinity and selectivity for NGF binding and can trigger different signaling pathways related to cell survival, proliferation, and differentiation, which involve the activation of ERK, PI3K, and PLC-γ (Wang et al., 2014); on the contrary, p75 has low affinity for NGF and high affinity for proNGF and is implicated in cell death mediation (Coassin et al., 2008). The role of NGF in visual function has been largely attributed to its ability to regulate phenotypic features of the neuro-retina, innervation density and plasticity (Sacchetti et al., 2017), cell body size, axonal terminal sprouting, and dendritic growth (Rocco et al., 2018). Notably, increasing lines of evidence have shown that NGF can be crucial for the treatment of blinding diseases, such as retinal degenerations, and several studies have already described the protective effect of NGF administration in experimental models of retinitis pigmentosa (RP) (Rocco et al., 2015) and age-related macular degeneration (AMD) (Lambiase et al., 2009).

In eye research, the availability of appropriate animal models has been extremely valuable to investigate pathological molecular mechanisms and to test new therapeutic interventions (Shah et al., 2019). Among the various species, zebrafish has progressively become a powerful model system especially for studying complex diseases, as the conservation between organization and function in human and zebrafish retinas has been a great advantage. Unlike mammals that cannot regenerate their retina after damage or degeneration, the zebrafish retina displays a robust regenerative response upon injury, and this feature can be exploited to gain insights into molecular mechanisms underlying healing of damaged tissues in eye human pathology (Wan and Goldman 2016; Richardson et al., 2017). Regeneration of the zebrafish retina (Nagashima et al., 2013; Wan and Goldman 2016) occurs *via* the ciliary marginal zone (CMZ), which is a stem cell niche that constantly adds new retinal neurons as the retina grows throughout life and *via* Müller glia (MG) cells, accounting for differentiated quiescent cells that normally help in maintaining retinal architecture and homeostasis but that can also be primed by a photic, chemical, or mechanical damage of the retina. In case of retinal injury, MG cells undergo a reprogramming event that leads to the generation of multipotent neuronal progenitors, which can then migrate and differentiate into any of the lost retinal cell type (Powell et al., 2016). The molecular circuitry driving MG reprogramming is poorly understood, but studies indicate that a remarkable variety of secreted factors contribute to retina regeneration in zebrafish and modulate MG reprogramming and proliferation in the injured retina (Faillace et al., 2002; Kassen et al., 2009; Ramachandran et al., 2011; Wan et al., 2012; Nelson et al., 2013).

Both NGF and its canonical receptors, known in the zebrafish as *ntrk1* and *ngfrb*, are conserved and widely expressed in zebrafish neurons, suggesting a conserved pathway activation *via* binding of neuronal cell surface receptors (Götz and Schartl 1994; Martin et al., 1995; Nittoli et al., 2018; Cacialli et al., 2019; Hahn et al., 2020).

Here, we sought to assess the potential regenerative effect of intravitreal (IV) administration of rhNGF using a retinal degeneration paradigm in adult zebrafish based on constant light irradiation.

Our results show that NGF receptors are expressed in adult zebrafish retina and that administration of rhNGF can boost zebrafish retinal regeneration upon injury.

RESULTS

Expression Pattern of *ngfrb* and *ntrk1* in Zebrafish Adult Retinae

Although a recent study confirmed the expression of *ngfrb* (ortologue of mammalian p75) and *ntrk1* (ortologue of mammalian TrkA) genes in sensory neurons during zebrafish early development (Hahn et al., 2020), the expression of the two NGF receptors in adult zebrafish retina has not been reported yet. Thus, in order to evaluate the potential regenerative effect of rhNGF administration in adult zebrafish retinal degeneration model, we first assessed the expression of NGF receptors in adult zebrafish retina. With this aim, we performed *in situ* hybridization (ISH) on retinal sections for detection of *ngfrb* and *ntrk1* in adult zebrafish eyes. Transcript localization of *ngfrb* and *ntrk1* revealed a mild widespread expression in the adult zebrafish retina and showed that both NGF receptors are expressed predominantly in the photoreceptor cells of the outer nuclear cell layer (ONL) (**Figure 1**). These data demonstrate that NGF receptors are present in the adult zebrafish retina, thus suggesting that the tissue is potentially responsive to endogenous or exogenous NGF.

Optimization of a Zebrafish-Based Retinal Degeneration Paradigm for Ophthalmological Studies

Since loss of photoreceptors is a hallmark of human retinal conditions such as AMD and RP (Marc et al., 2003; Kalloniatis and Fletcher 2004), we sought to assess whether IV administration of rhNGF might have a regenerative effect on photoreceptor cell population upon damage. With this aim, we first optimized a zebrafish model of retinal degeneration induced by constant light irradiation. Injury

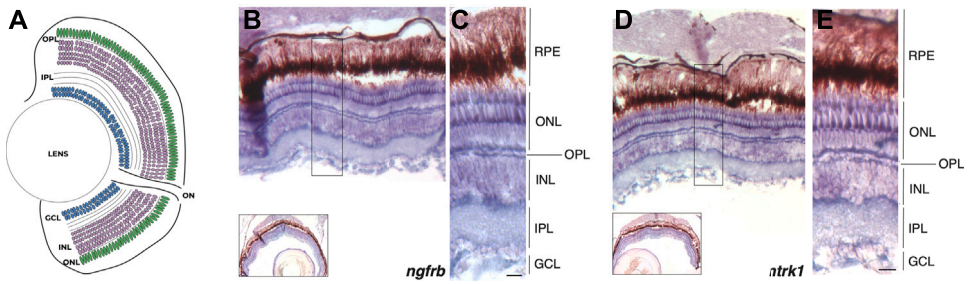

FIGURE 1 | *ngfrb* and *ntrk1* mRNA expression pattern in adult zebrafish eye. **(A)** Schematic representation of the zebrafish retina with nuclear and plexiform layers highlighted. **(B)** *In situ* hybridization (ISH) for *ngfrb* expression in cross sections of adult zebrafish retina (signal in blue/violet). **(C)** High magnification showing the expression of *ngfrb* gene in the different retinal layers and cell types. **(D)** ISH for *ntrk1* expression in adult zebrafish retina (signal in blue/violet). **(E)** High magnification showing *ntrk1* transcript localization in the different retinal layers and cell types. RPE: retinal pigmented epithelium. ONL: outer nuclear layer. OPL: outer plexiform layer. INL: inner nuclear layer. IPL: inner plexiform layer. GCL: ganglion cell layer. Scale bar: 50 μm.

models based on photo-induced retinal degeneration have been developed in several species (Donovan et al., 2001; Saito et al., 2016; Sudharsan et al., 2017) and showed that constant light exposure induces loss of rod and cone photoreceptors and, macroscopically, thinning of the retinal outer nuclear layer (ONL), where these photoreceptors are located. Since fish have long-life ability to heal the retinal tissue, we first had to establish the appropriate time of light exposure needed to induce degeneration of the retinal tissue. Thus, after a period of dark acclimatization of 14 days, adult zebrafish were exposed to constant light (18,000–20,000 lumens) and eyes were enucleated at time 0 (not exposed to light) and then at different time points after light irradiation onset. Immunohistochemistry with Zpr1 antibody on enucleated eyes was performed to label red/green double cone photoreceptors (Matsuoka et al., 2013), used as reference cell population of the ONL, and thickness and cell number of ONL were established as phenotypic readouts to assess the severity of the injury. Initially, we exposed adult zebrafish to constant bright light for 48 h, as it was previously described as a stimulus able to induce a mild to drastic reduction of photoreceptors (Thomas et al., 2012; Saito et al., 2016). However, in our hands, 48 h of light-induced degeneration (48 h LID) only slightly reduced ONL thickness and cell number compared to non-injured retinae (NO LID) (**Supplementary Figure S1**). In order to induce a more consistent damage to photoreceptors, we increased the light treatment to 60 h, and indeed, at this time point, the integrity of double cone photoreceptors, in terms of density, was severely compromised compared to non-injured retinae (NO LID) (**Figure 2A,B**). Moreover, photoreceptor layer damage was confirmed by evident reduction of ONL thickness and cell number in LID retinae (**Figure 2C,D**). Injured retinal tissue displayed on average a significantly thinner ONL (7.671 ± 0.5606 SE μm) characterized by a significantly lower number of cells (25.42 ± 2.953 SEM) compared to control retinae thickness (20.05 ± 0.7203 SE μm) and cell number (103.6 ± 2.904 SEM). To further assess the injury effect on cell viability, we performed terminal deoxynucleotidyl transferase-mediated dUTP nick-end labeling (TUNEL) assay for the detection of apoptotic photoreceptors. While no cell death could be observed in the ONL of control retinae (NO LID), several apoptotic cells were detected upon 60 h of light treatment (**Figure 2E,G**) in retinal tissues analyzed.

Based on these results, we determined that 60 h was the most appropriate light exposure time needed to induce degeneration of adult zebrafish retinal tissue in our model.

rhNGF Enhances Retinal Regeneration After Light-Induced Damage

Having defined the appropriate retina degeneration conditions (60 h LID), we used this experimental model to test the potential effect of rhNGF on zebrafish retinal recovery upon injury. To this end, we administered 5 μg/eye of rhNGF through eye incision and posterior IV injection in adult zebrafish immediately after 60 h of light exposure. Thereafter, groups of fish were sacrificed at five different time points [0 days post injury (dpi), 7 dpi, 14 dpi, 21 dpi, and 28 dpi] and eyes were removed. Incised and non-rhNGF-injected contralateral eyes were enucleated at the same time points and used as control, as no differences—in terms of ONL thickness and ONL cell number—were observed in a preliminary study in which we compared 60 LID non-injected (sham) and 60 LID saline-injected animals (data not shown).

As previously described, the readouts of the experiment were the ONL thickness and cell number per retinal length (**Figure 3**). As expected, at 0 dpi, analyzed retinal tissue displayed a reduced ONL (5.295 ± 0.3808 SEM μm) that was characterized by a low number of cells (22.30 ± 2.129 SEM) (**Figure 3B**). At 7 dpi, a comparable recovery in both readouts was observed in both rhNGF-injected and untreated retinae (**Figure 3C,D**). Notably, at 14 dpi, the recovery in rhNGF-injected retinae was significantly higher compared to untreated retinae and was demonstrated by an amelioration of ONL thickness and cell number (**Figure 3E,F,K,L**). A similar result was observed at 21 dpi, when rhNGF-treated retinal tissue displayed an improved

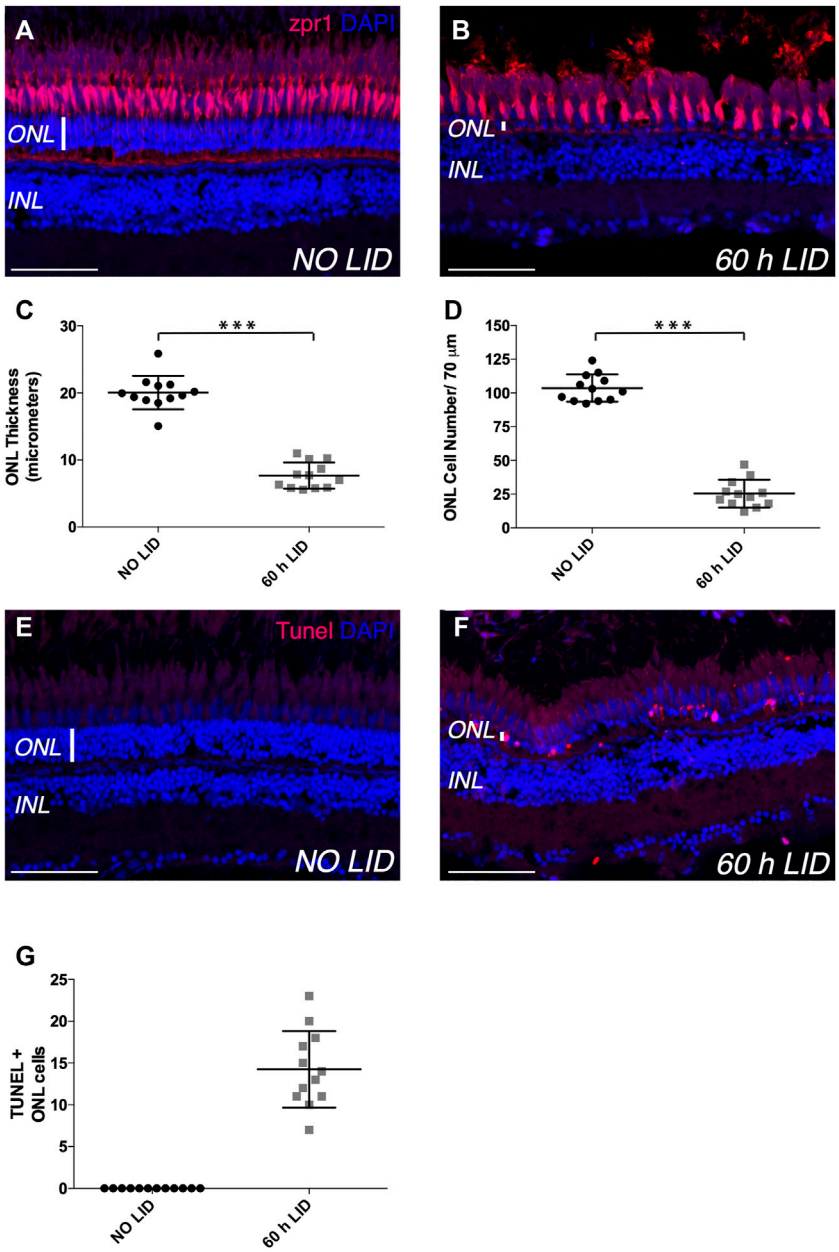

FIGURE 2 | Light-induced retinal degeneration zebrafish model. **(A,B)** Representative images of retinal cryosections of adult zebrafish eyes immunostained with Zpr1 antibody (red), which labels photoreceptor cells, and stained with DAPI (blue), which labels nuclei. **(A)** Retinal cryosection of adult zebrafish eye not exposed to constant light (NO LID). **(B)** Retinal cryosection of adult zebrafish eye exposed to 60 h of constant light (light-induced degeneration—LID). **(C)** Quantification of ONL thickness (number of retinae analyzed = 12). **(D)** Quantification of ONL cell number (number of retinae analyzed = 12, total number of cells: 305 for injured and 1,243 for control retinae). **(E,F)** Representative images of retinal cryosections of adult zebrafish eyes stained with TUNEL (red), which labels apoptotic cells, and with DAPI (blue), which labels nuclei. **(E)** Retinal cryosection of adult zebrafish eye not damaged by light exposure (NO LID). **(F)** Retinal cryosection of adult zebrafish eye after 60 h of LID. **(G)** Quantification of TUNEL-positive cells shown as mean number per retina (number of retinae analyzed = 12). Data are shown as means ± SEM. ***$p < 0.001$ (Mann–Whitney test). Scale bar: 50 µm.

recovery rate in both parameters compared to the untreated retinae (**Figure 3G,H,K,L**). At 28 dpi, treated and untreated retinae showed similar values of ONL thickness and cell number (**Figure 3I,J**).

To further investigate whether the improved condition of the photoceptor cell layer observed in rhNGF-treated retinae compared to untreated tissue was determined by an increase in cell proliferation or a reduction in apoptotic processes, we analyzed cell proliferation and apoptosis on retinae of the same groups of animals sacrificed for the ONL evaluation at all five time points. Cell proliferation was evaluated by immunohistochemical analysis of proliferation cell

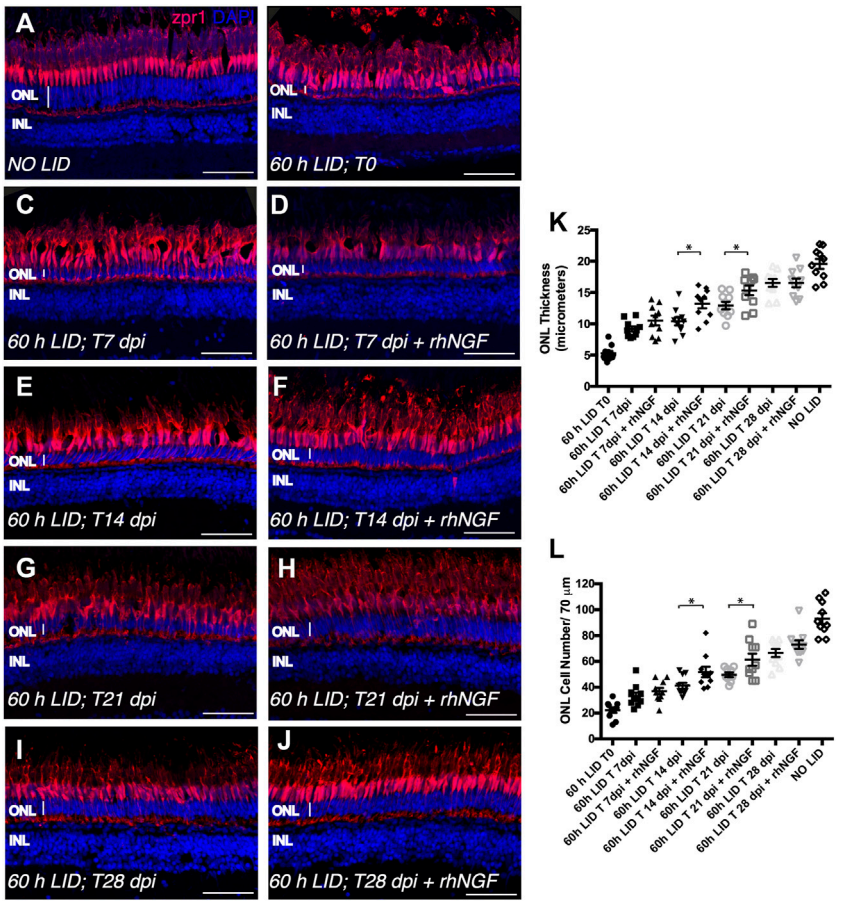

FIGURE 3 | Analysis of rhNGF-induced retinal tissue recovery upon light-induced degeneration (LID). (A–J) Representative images of retinal cryosection of adult zebrafish eyes immunostained for Zpr1 antibody (red) and stained with DAPI (blue). **(A)** Retinal cryosection of an adult zebrafish eye not exposed to light. **(B)** Retinal cryosection of an adult zebrafish eye exposed to 60 h of LID at T = 0 (*N* animals:10; *N* total cells: 223). **(C)** Cryosection of an untreated adult zebrafish retina at 7 dpi (*N* animals:10; *N* total cells: 332). **(D)** Retinal cryosection of rhNGF-injected adult zebrafish eye at 7 dpi (*N* animals:10; *N* total cells: 369). **(E)** Cryosection of an untreated adult zebrafish retina at 14 dpi (*N* animals:10; *N* total cells: 412). **(F)** Retinal cryosection of rhNGF-injected adult zebrafish eye at 14 dpi (*N* animals:10; *N* total cells: 518). **(G)** Cryosection of an untreated adult zebrafish retina at 21 dpi (*N* animals:10; *N* total cells: 498). **(H)** Retinal cryosection of rhNGF-injected adult zebrafish eye at 21 dpi (*N* animals:10; *N* total cells: 614). **(I)** Cryosection of an untreated adult zebrafish retina at 28 dpi (*N* animals:10; *N* total cells: 665).**(J)** Retinal cryosection of rhNGF-injected adult zebrafish eye at 28 dpi (*N* animals:10; *N* total cells: 731). **(K)** Quantification of ONL thickness in the different conditions. Data are shown as means ± SEM: **p* < 0.05 (one-way ANOVA test followed by a Sidak's multiple comparison test); 60 h LID T 14 dpi vs. 60 h LID T 14 dpi + rhNGF: Adjusted *p*-value: 0.0108; 60 h LID T 21 dpi vs. 60 h LID T 21 dpi + rhNGF: Adjusted *p*-value: 0.0394. **(L)** Quantification of ONL cell number in the different conditions. Data are shown as means ± SEM: **p* < 0.05 (one-way ANOVA test followed by a Sidak's multiple comparison test); 60 h LID T 14 dpi vs. 60 h LID T 14 dpi + rhNGF: Adjusted *p*-value: 0.0424; 60 h LID T 21 dpi vs. 60 h LID T 21 dpi + rhNGF: Adjusted *p*-value: 0.0240. DPI: days post injury. Scale bar: 50 µm.

nuclear antigen (PCNA)-positive cells. Although, after 60 h of light irradiation, some degree of cell proliferation was visible also in untreated retinae compared to retinae of fish not exposed to light, a significantly higher number of dividing cells per tissue area was detected in retinae from rhNGF-injected eyes compared to untreated ones at all the analyzed time points, with the exception of 28 days, the time point corresponding to a *plateau* of tissue recovery, as also described in previous reports (**Figure 4**) (Thummel et al., 2008a; Thummel et al., 2008b; Thomas et al., 2016). In contrast, photoreceptor apoptosis detected by TUNEL staining did not vary between treated and non-treated groups over the 28 days of analysis (**Supplementary Figure S2**).

Overall, these results suggest that IV injection of rhNGF induces retinal tissue recovery by driving cell proliferation upon injury in our zebrafish retinal degeneration model, whereas it has no effect on photoreceptor cell death.

rhNGF-Mediated Pathway Activation and Gene Expression After Light-Induced Retinal Degeneration

In order to determine whether IV injection of rhNGF led to the activation of NGF canonical pathway, we analyzed the changes in ERK protein expression levels, a known NGF downstream effector, after light-induced retinal degeneration. The phosphorylation of these proteins indicates activation of the

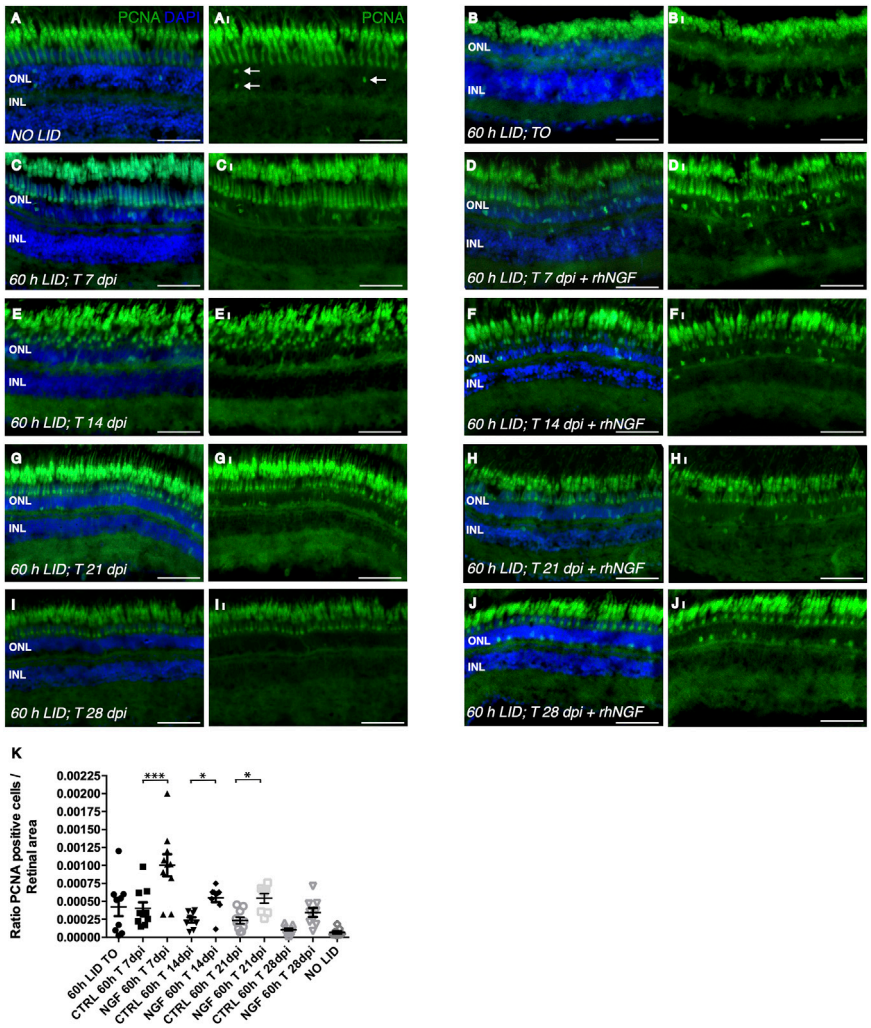

FIGURE 4 | Analysis of rhNGF-induced cell proliferation upon light-induced degeneration (LID). (A–J) Representative images of retinal cryosection of adult zebrafish eyes immunostained with anti-PCNA antibody, which labels proliferating cells (green), and stained with DAPI (blue). (A_I–J_I) Images extrapolated from A–J displaying exclusively the PCNA signal. **(A,A)$_I$** Retinal cryosection of an adult zebrafish eye not exposed to light (*N* retinae: 9). **(B,B$_I$)** Retinal cryosection of adult zebrafish eye exposed to 60 h of LID (*N* retinae: 9). **(C,C$_I$)** Cryosection of untreated adult zebrafish retina at 7 dpi (*N* retinae: 10). **(D,D$_I$)** Retinal cryosection of rhNGF-injected adult zebrafish eye at 7 dpi (*N* retinae: 10). **(E,E$_I$)**. Cryosection of untreated adult zebrafish retina at 14 dpi (*N* retinae: 9). **(F,F$_I$)** Retinal cryosection of rhNGF-injected adult zebrafish eye at 14 dpi (*N* retinae: 9). **(G,G$_I$)** Cryosection of untreated adult zebrafish retina at 21 dpi (*N* retinae: 10).**(H,H$_I$)** Retinal cryosection of rhNGF-injected adult zebrafish eye at 21 dpi (*N* retinae: 8). **(I,I$_I$)** Cryosection of untreated adult zebrafish retina at 28 dpi (*N* retinae: 9). **(J,J$_I$)** Retinal cryosection of untreated rhNGF-injected adult zebrafish eye at 28 dpi (*N* retinae: 9).(K) Quantification of proliferating cells. Ratio of PCNA-positive cells over the analyzed area is shown. Data are shown as means ± SEM ($n = 10$). ***$p < 0.001$; **$p < 0.01$; *$p < 0.05$ (one-way ANOVA test followed by a Sidak's multiple comparison test); 0 h LID T 7 dpi vs. 60 h LID T 7 dpi + rhNGF: Adjusted *p*-value:< 0.001; 60 h LID T 14 dpi vs. 60 h LID T 14 dpi + rhNGF: Adjusted *p*-value: 0.0379; 60 h LID T 21 dpi vs. 60 h LID T 21 dpi + rhNGF: Adjusted *p*-value: 0.0412. DPI: days post injury. Scale bar: 50 µm.

pathway; therefore, the ratio between phosphorylated ERK and total protein was evaluated. A significant increase in phosphorylated ERK levels was observed 36 h after the IV injection in eyes treated with rhNGF compared to non-injected contralateral eyes and to eyes extracted immediately after 60 h of light injury (**Figures 5A–C**), suggesting that rhNGF administration is able to induce activation of the canonical pathway.

We next sought to evaluate the effect of rhNGF injection on regenerative mechanisms investigating the potential role of rhNGF on MG by analyzing the expression of genes specific of this cell population, *gfap* (glial fibrillary acidic protein) and *vim* (vimentin) (**Figure 5D,E**) (Ranski et al., 2018). In order to detect potential changes in expression from early activation to later regeneration phases, for the expression analysis, we selected a range of time spanning from 36 h post injury (hpi) to 21 dpi. Since the peak of photoreceptor apoptosis has been shown to occur at 24 hpi and is followed by MG cell-cycle re-entry at approximately 30 hpi (Vihtelic and Hyde 2000), changes in gene expression were evaluated at two additional time points (36 and 72 hpi) not included in the ONL regeneration analysis, while 28 dpi was identified as a *plateau* stage for regeneration analysis and therefore was considered not

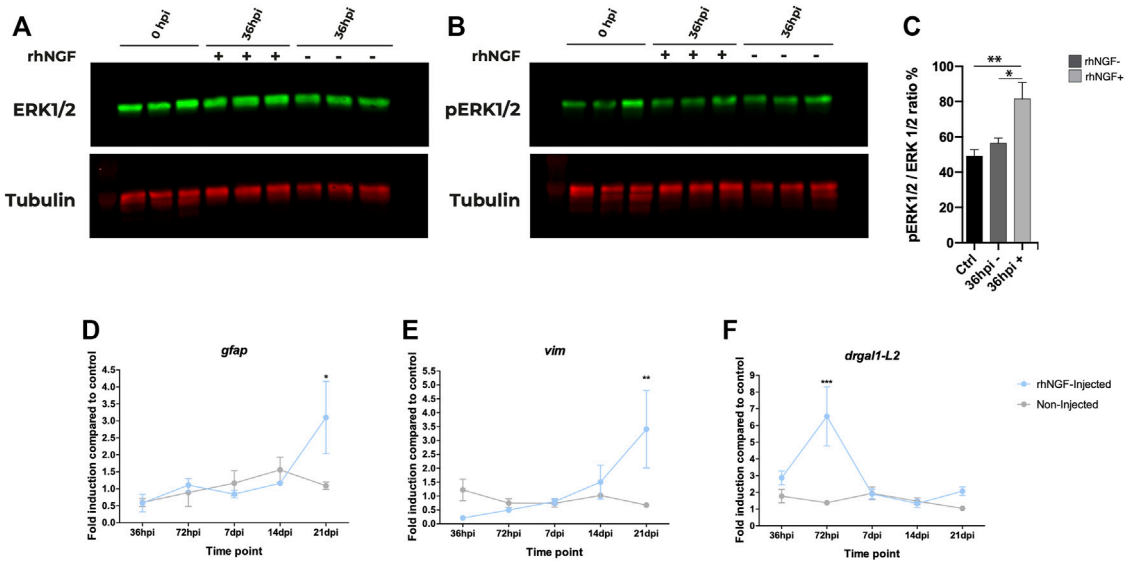

FIGURE 5 | rhNGF-mediated pathway activation and gene expression in adult zebrafish during retinal regeneration. (A, B) Western blot analysis of ERK during retinal regeneration. **(A)** Total ERK protein levels in non-injected and rhNGF-injected adult zebrafish eyes at 0 h post injury (hpi) and at 36 hpi. Ctr-0 hpi (*N*: 15 eyes); 36 hpi rhNGF – (*N*: nine eyes); 36 hpi rhNGF + (*N*: 9 eyes) (3 eyes × time point × condition). **(B)** Phosphorylated ERK protein levels in the same samples analyzed in A. **(C)** Bar plot of pERK/ERK ratio as normalized fluorescence intensity relative to protein levels. Data are shown as means and standard error of the mean (SEM). The statistical analysis test used was one-way ANOVA followed by a Dunnett's multiple comparisons test; 0 hpi vs. 36 hpi rhNGF +: Adjusted *p*-value: 0.0078; 36 hpi un-injected *N*: nine eyes; 36 hpi rhNGF – vs. 36 hpi rhNGF +: Adjusted *p*-value: 0.0347. **(D–F)**. Expression levels of Müller glia-specific genes *gfap*, *vim*, and *drgal1-L2* during retinal regeneration (*N* three eyes time point condition). Data are shown as mean ± SEM. ***$p < 0.001$; **$p < 0.01$; *$p < 0.05$ (two-way ANOVA test followed by a Sidak's multiple comparisons test). *gfap*: 21 dpi un-injected vs. 21 dpi rhNGF-injected. Adjusted *p*-value: 0.0134; *vim*: 21 dpi un-injected vs. 21 dpi rhNGF-injected: Adjusted *p*-value: 0.0052. *drgal*: 72 hpi un-injected vs. 72 hpi rhNGF-injected: Adjusted *p*-value: <0.001. rhNGF: recombinant human nerve growth factor.

informative. No differences in expression levels were detected at the analyzed time points, with the exception of the last one. At 21 dpi, in fact, transcriptional levels of both *gfap* and *vim* increased threefold in rhNGF-injected eyes compared to the control eyes.

To investigate the mechanisms underlying the late effect of NGF on MG, we also analyzed also the expression of *drgal1-L2* (galectin 1–like 2), a secreted factor that is expressed by microglia and regenerative MG and their lineage starting approximately 24 hpi, which is required for rod photoreceptor regeneration (Marc et al., 2003) and thus represents a molecular signature of regenerating zebrafish retina. At 36 hpi, an upregulation of *drgal1-L2* transcription was observed in both injected and untreated eyes compared to the basal expression level (2 folds change); however, at 72 hpi, a drastic threefold increase was detected in rhNGF-injected retinal tissues compared to the untreated ones.

Overall, these results suggest that activation of NGF pathway by injection of exogenous growth factor might enhance the regenerative potential of the tissue, and this effect is possibly mediated by a rhNGF-induced proliferation of MG cell populations in the early post-injury time points, which would result in an increased size in the pool of MG in later time points.

DISCUSSION

Retinal degeneration and damage progressively lead to low vision and blindness, and no radical treatment is currently available (Jin and Takahashi 2012). Here, we evaluated the potential retinal regenerative effects of intravitreal injection of rhNGF in a model of light-induced retinal degeneration in adult zebrafish.

NGF and its receptors, TrkA and p75, are widely expressed in mammal central visual pathway (lateral geniculate nucleus and visual cortex), as well as in the optic nerve and retina (Chakrabarti et al., 1990). In the neural retina of adult rodents, NGF is mainly expressed by retinal ganglion cells (RGCs) and glial cells, like Müller cells and microglia, as well as by photoreceptors and in photoreceptor outer segments (Sun et al., 2008). The presence of TrkA and p75 in photoreceptors, RGCs, and Müller cells suggests that these cells can respond to NGF signaling, which might modulate their survival or death (Garcia et al., 2017). In line with this hypothesis, it has been shown that exogenous NGF protects retinal cells from degeneration and apoptosis in experimental retinal detachment (Sun et al., 2007) and in models of RP (Rocco et al., 2015; Sacchetti et al., 2017). In zebrafish, the expression of NGF receptors (ntrk1 and ngfrb) had been investigated and reported only during the early development of the nervous system (Nittoli et al., 2018; Hahn et al., 2020), while no data are available regarding the expression of these receptors in the adult fish. In this context, our result demonstrated the presence of *ntrk1* and *ngfrb*, orthologues of TrkA and p75 in different layers in the retina of adult zebrafish and represent the first piece of evidence of the conservation of NGF retinal expression pattern between adult mammals and fish,

suggesting that the potential therapeutic effects of rhNGF can be assessed in a zebrafish model of retinal degeneration.

During the last years, zebrafish have been extensively studied to understand molecular mechanisms underlying retinal regeneration, which, in this organism, lasts throughout the entire lifespan (Wan and Goldman 2016). Models of retinal disease have been described in zebrafish and mouse based on bright or UV light irradiation that leads to photoreceptor cell apoptosis and degeneration of the sensory retina (Belmonte et al., 2006; Saito et al., 2016). However, the reported experimental procedures vary among research groups and present different degrees of phenotype severity, as a standardized protocol has not been established yet. Some models involve the exposure of the animals to a constant bright light of a density of ~8,000 lux (Vihtelic and Hyde 2000; Thomas et al., 2012) or even less, i.e., 2,800 lux (Thummel et al., 2008a), for a prolonged time (up to 4 days) to obtain significant reduction of outer nuclear layer (ONL) thickness and increase of apoptotic cells. Other studies, however, have reported the establishment of a light-induced retinal degeneration model in adult pigmented zebrafish using a greater light density (~16–20,000 lux). Under these conditions, Rajaram et al. (2014) described severe damage of ONL at 51 hpi, while in another study (Saito et al., 2016), the effect on fish retinae could be achieved even by a lower exposure time (up to 48 h). Starting from these previous reports, we irradiated fish with a constant light intensity of 18,000–20,000 lumens and carefully set up our model checking for retinal damage at 48 and 60 h, finally choosing this latter time point based on ONL thickness and cell number. In the present study, we thus defined a robust experimental procedure for light-induced retinal degeneration based on 60 h of constant bright light irradiation. We have shown that such exposure causes photoreceptor apoptosis, which leads to a striking reduction of ONL thickness and cell number, the readouts used to assess retinal tissue damage. In this model, IV administration of rhNGF speeded up the amelioration of damaged retinal tissue in treated animals compared to untreated siblings, which was especially evident and significant in the late stages of regeneration. In fact, injected and control retinae showed a similar phenotype during the first phases of regeneration (7 dpi), while a significant improvement in ONL thickness and cell number was observed at later (14 and 21 dpi) time points. These results suggest that rhNGF might activate underlying molecular mechanisms in the early regeneration processes, such as MG dedifferentiation and proliferation, and this would result in faster recovery from damage at late stages of regeneration, until reaching the plateau in the final phases.

In zebrafish, the primary source of regeneration is the MG, which can generate and replace all types of retinal neurons after injury (Ramachandran et al., 2010). Thus, the improvement that we observed in ONL thickness and cell number after the treatment with NGF could be the result of two processes: on one side, NGF could have stimulated MG division, thus leading to the repopulation of retinal tissue through the differentiation of different classes of retinal neurons; on the other hand, NGF-induced proliferation could have led to an expansion of the MG pool at later time points, when the regeneration process was completed. The high expression of proliferating cell nuclear antigen (PCNA) that we observed in NGF-treated retinae and data from a seminal work demonstrating the mitogenic effect of NGF in culture MG and the expression of NGF receptors in this cell population (Ikeda and Puro 1994) might validate the second scenario supporting a direct proliferating effect of NGF on the MG.

Analysis of the downstream effectors of NGF in treated zebrafish revealed a significant upregulation of the ERK1/2 pathway at 36 hpi in rhNGF-injected eyes compared to controls, indicating that injection of rhNGF activates the pathway at early time points inducing cell proliferation, which accounts for the enhanced retinal regeneration documented by later ONL thickness improvement and increment of MG-specific gene expression, *gfap* and *vim*. In line with this, the injection of rhNGF also drastically increased the levels of Drgal1-L2, a secreted factor that plays a key role in retinal development and photoreceptor regeneration. This upregulation of regeneration-specific gene programs at 72 hpi, in association with the faster recovery of the photoreceptor cell layer observed by cytological analysis, indicates that rhNGF treatment boosts the regenerative potential of zebrafish retinal tissue upon injury.

Although the use of zebrafish as a model to test the effects of therapeutic or neuroprotective compounds has been scarce until now (Cunvong et al., 2013; Saito et al., 2016), our results on NGF receptors' expression and pathway activation in adult zebrafish strongly sustain the potential successful exploitation of zebrafish as a powerful alternative model for testing the efficacy of novel IV injection-based treatments for retinal diseases. Moreover, the regenerative effects that we observed in zebrafish retinae upon NGF treatment have an important translational impact. An increasing body of evidence in fact indicates that MG retains multipotency and can be reprogrammed in neurons to restore cellular function in damaged retina stem cells also in adult mammals (Yao et al., 2018), and thus similar regenerative effects can be expected after the treatment with rhNGF also in mammal MG, potentially leading to retinal regeneration after injury or degeneration.

In light of our data and considerations, our study opens the way to the use of zebrafish as a useful model to test new compounds potentially able to stimulate the regeneration properties of the retina and paves the ground to further studies aimed at evaluating in particular the effects of IV-injected NGF also in mammals, in order to expedite the development of novel and promising alternative therapeutic approaches for ophthalmological indications based on rhNGF administration.

MATERIALS AND METHODS

In vivo Experiments

Zebrafish (*Danio rerio*) were maintained at 24°C on a 12-h light/12-h dark cycle. Collected embryos were cultured in fish water containing 0.01% methylene blue to prevent fungal growth. Fish were grown in the fish facility of ZeClinics SL. Light-induced retinal damage protocol was adapted and optimized from

TABLE 1 | List of the primers used for ISH.

Gene	Protein encoded	Transcript ID	Primer name	Sequence
ngfra	*nerve growth factor receptor a*	ENSDART00000125281.3	*ngfra*Fw	GGAGTGATCAAGGAGTGTGGAG
ngfra	*nerve growth factor receptor a*	ENSDART00000125281.3	*ngfra*Rev	AGATGGGGATCAGGTTCTCATTTAG
ntrk1	*neurotrophic tyrosine kinase, receptor, type 1*	ENSDART00000027013.5	*ntrk1*Fw1	TAGACCTCGCCAACTACAGAGA
ntrk1	*neurotrophic tyrosine kinase, receptor, type 1*	ENSDART00000027013.5	*ntrk1*Rev1	TCCGTTGATTGGTTAGTGGGAG
ntrk1	*neurotrophic tyrosine kinase, receptor, type 1*	ENSDART00000027013.5	*ntrk1*Fw2	AATGGCTGTACAACAACATGCC
ntrk1	*neurotrophic tyrosine kinase, receptor, type 1*	ENSDART00000027013.5	*ntrk1*Rev2	TTCACCCAGTTCCCACTTCAAA
ntrk1	*neurotrophic tyrosine kinase, receptor, type 1*	ENSDART00000027013.5	*ntrk1*Fw3	TTTGAAGTGGGAACTGGGTGAA
ntrk1	*neurotrophic tyrosine kinase, receptor, type 1*	ENSDART00000027013.5	*ntrk1*Rev3	CCTTGATGACCAACCTTTGCTG

previous reports (Belmonte et al., 2006; Saito et al., 2016). Adult fish anesthetized with 100 mg/L of MS-222 (Millipore Sigma, St. Louis, MO) were positioned on one side and the outer cornea was removed. Next, a small hole was opened close to the lens and 5 μg of rhNGF (Dompé farmaceutici s.p.a) was injected intravitreally, after 60 h of light irradiation (60 h LID). All procedures performed were in accordance with Spanish and European Union animal welfare guidelines and approved by the Animal Testing Ethics Committee (CEEA; n:20–005-ISA).

Immunohistochemistry and Imaging

Following euthanasia with 300 mg/L of MS-222 at 0, 7, 14, 21, and 28 dpi, zebrafish eyes were removed, fixed in 4% paraformaldehyde/1 × phosphate buffered saline (PBS; pH 7.4) overnight at 4°C and cryoprotected overnight (O/N) in 30% sucrose/0.02% sodium azide/PBS before embedding in O.C.T. compound (Sakura Finetech, Torrance, CA). Embedded samples were then frozen on dry ice, and 14-μm sections were mounted on Fisherbrand Superfrost Plus slides (Fisher Scientific, Waltham, MA). Cryosections were washed three times in 1 × PBS/0.1% Tween-20 (PBS-T) solution and incubated for 1 h at room temperature (RT) in 10% Normal Goat Serum (ThermoFisher, Carlsbad, CA) in PBS-T blocking solution. Sections were stained O/N at 4°C with mouse Zpr1 antibody (1:250) (AbCam, Cambridge, United Kingdom), a monoclonal antibody that recognizes zebrafish cone arrestin 3a, which is expressed specifically by both red and green cones from the synaptic pedicle of the apex of the inner segment. Goat anti-mouse IgG AF594 antibody (1:200) (ThermoFisher, Carlsbad, CA) and DAPI (4′,6-diamidino-2-phenylindole) DNA fluorescent stain (1:500) (Sigma) in blocking solution were added for 2 h at RT. Sections washed in PBS-T were mounted with Vectashield mounting media (Vector Laboratories, Burlingame, CA). Slides were left at RT for 1 h before imaging with a Leica SP5 confocal microscope. Images were analyzed with ImageJ software 3, 25. Statistical significance was assessed with GraphPad Prism One-way ANOVA followed by Dunnett's or Sidak's test.

TABLE 2 | List of the primers used for real-time PCR.

Gene	Primer sequence
ntrk1_fw	CTATGCCTACACTGAACTCATC
ntrk1_rv	TGCCCAGTTTGTTCTTCAC
ngfrb_fw	TCTGTCAAGATTTCGATGCTCCT
ngfrb_rv	GCTCTCCGTAGGATTGTCCG
drgal1-L2_fw	TGTGCAATTCATTCCAGAGC
drgal1-L2_rv	AACCCCTTGGATCCTGACTT
vim_fw	TAA GCC TGC GAG AGT CCA TGA
vim_rv	TCG TTT TGG GTG GAC TCG TT
gfap_fw	GCA GAC AGG TGG ATG GAC TCA
gfap_rv	GGC CAA GTT GTC TCT CTC GAT C

Gene Expression Analysis by Real-Time PCR

At 36 hpi, 72 hpi, 7 dpi, 14 dpi, and 21 dpi, three eyes per condition were homogenized in TRIreagent (MilliporeSigma), and total RNA was extracted following the manufacturer's protocol. RNA concentration was estimated using a NanoDrop Spectrophotometer ND-1000 (NanoDrop Technologies; Wilmington, DE). One hundred nanograms of RNA was retrotranscribed to cDNA by reverse transcriptase (Superscript III RT-Enzyme, ThermoFisher) and stored at −20°C. Gene expression was assessed with a Lightcycler® 480 system (Roche) using the SYBR GREEN method from 1:10 cDNA and β-actin as a housekeeping gene (stability determined by Bestkeeper© software). Relative expression levels were quantified using the ΔΔCt method.

Riboprobe Synthesis for *In Situ* Hybridization (ISH)

In vitro transcription of probes was performed using RNA Labeling Kit (Roche) following the manufacturer's instructions. cDNAs were amplified by PCR from a custom zebrafish cDNA library obtained by RT-PCR performed on mRNA from 4 months adult zebrafish. SP6 sequence linker was included in reverse primers to directly use synthesized PCR products as templates to amplify the reverse riboprobe for ISH. After ISH, embryos were analyzed on a Leica M165 FC microscope. Images were processed using Adobe Illustrator software.

In Situ Hybridization on Cryosections

Slides were digested with 20 μg/ml proteinase K in pre-warmed 50 mM Tris for 10–20 min at 37°C and thus rinsed 5 × in distilled water. Afterwards, sections were immersed in ice-cold

20% (v/v) acetic acid for 20 s and dehydrated by washing for approximately 1 min per wash in 70% ethanol, 95% ethanol, and 100% ethanol. Hybridization solution (100 µl) was then added to each slide. The slides were incubated for 1 h in a humidified hybridization chamber at 62°C while the probes were diluted in hybridization solution and heated at 95°C for 2 min. We added 100 µl of diluted probe per section and incubated the slides in a humidified chamber at 65°C overnight. Cover the sample with a cover slip to prevent evaporation. Thus, we performed stringency washes to remove non-specific bindings. Thereafter, slides were washed twice in MABT (maleic acid buffer containing Tween 20) for 30 min at room temperature. We proceeded with blocking and revealing according to standard protocol by Abcam (https://www.abcam.com/protocols/ish-in-situ-hybridization-protocol).

PCNA Detection and TUNEL Detection

The 14-µm sections were mounted on Fisherbrand Superfrost Plus slides. Prior to anti-PCNA immunostaining, an antigen retrieval step has been performed. Slides were incubated with 10 mM NaCitrate 0.05% Tween 20 Buffer pH 6.0 in a steamer for 20 min and then cooled down at room temperature for 30 min. Immunohistochemistry has been performed incubating the slides overnight at 4°C with anti-PCNA primary antibody diluted 1/500 in blocking solution. After three washes with PBST, slides were incubated for 2 h at room temperature with anti-Mouse Alexa Fluor 488 secondary antibody diluted 1/500 in blocking solution and finally washed with PBST. For TUNEL assay, retinal cross sections were fixed with 4% PFA for 15 min at RT and apoptotic cells were labeled with *In Situ* Cell Death Detection Kit and TMR red kit following the manufacturer's instructions (Roche).

Image Analysis

Adult fish retinae were cryo-sectioned with 14 µm thickness. For analysis, we used sections of the central part of the dorsal half of the retina. Section orientation was established and maintained throughout the different experiments in order to obtain retinal regions that could be compared in the study. The entire volume of a representative cryosection was imaged with a Leica SP5 confocal microscope (for imaging of samples in **Figures 2–4**), employing a ×20 objective (1 µm per stack). For quantification of the thickness and cell number parameters, the imaged acquired were processed through ImageJ software. As the thinning of the ONL upon damage makes it difficult to use parameters other than length for the analysis of retinal tissue, we identified a "retinal length unit" in the central part of the dorsal half of the retina, which has been then used as reference for all the experiments. In particular, we established a retinal length of 70 µm as our reference region of interest (ROI) for ONL nuclei counting, which was then used also for comparison with other conditions. A maximum projection of the total number of the stacks was performed for each imaged retina. ONL thickness measurement was performed in Maximum projection images through ImageJ software in the central part of the ROI by using the straight-line tool. ONL cell count measurement was performed in Maximum projection images through ImageJ by using the point selection tool after background subtraction. For PCNA and TUNEL staining, cryosections were analyzed on a Leica DMI6000B microscope system. For quantification, positive cells were counted using the point selection tool after background subtraction. The number of stained cells were then divided by area of retina analyzed. Area was calculated using ImageJ Fiji function "measurement" across the ROI used for the counting. Results were plotted using GraphPad Prism software and statistical significance was assessed using the most appropriate statistical test.

Western Blot

Three eyes per condition were lysed in 150 ml of RIPA buffer (MilliporeSigma) plus proteinase inhibitors (Roche), homogenized, incubated on ice for 15 min, and finally sonicated for 15 s. Samples were kept on ice for an additional 15 min and centrifuged for 20 min at 4°C. Supernatant was stored at −80°C. Proteins were quantified using Bradford assay (MilliporeSigma). Twenty milligrams of protein per sample was combined with 3 ml of 5 × Laemmli loading buffer and water to a final 15-ml volume, boiled at 98°C for 5 min, and loaded onto a 10% SDS-PAGE gel (Bio-Rad, Hercules, CA). Proteins were transferred to a PVDF membrane, blocked for 1 h at RT, and incubated with antibodies for MAPK (1:500) and pMAPK (1:1,000) (Cell Signaling Technology Danvers, MA) in blocking buffer (Licor, Lincoln, NE) diluted 1:2 with TBS-T (0.2%) O/N at 4°C. Blots were then incubated in secondary antibodies (1: 5,000) (Licor) in TBS-T for 1 h at RT. Antibody against tubulin (Sigma) and its corresponding secondary were incubated for 1 h at RT. Blots were developed with Odyssey instrument and analyzed using Image Studio Lite software.

Primers for ISH

A list of the primers used for ISH is reported in **Table 1**.

Primers for Real-Time PCR

A list of the primers used for real-time PCR is reported in **Table 2**.

DATA AVAILABILITY STATEMENT

The original contributions presented in the study are included in the article/**Supplementary Materials**, further inquiries can be directed to the corresponding authors.

ETHICS STATEMENT

All procedures performed were in accordance with Spanish and European Union animal welfare guidelines and approved by the Animal Testing Ethics Committee (CEEA; n: 20–005-ISA).

AUTHOR CONTRIBUTIONS

MA, AA, FM, LB, PC, and VD conceptualized this study, and reviewed and edited the manuscript; the methodology was designed by PC, LB, VD, and DR; the investigation was carried out by VD and DR. PC, VD, and DR prepared the original draft; VD, DR, PC, and LB analyzed data. All authors have read and agreed to the published version of the manuscript.

FUNDING

This research was funded by the Italian Ministry of Economic Development (project F/090033/01/X36 - Piattaforma tecnologica integrata per l'identificazione e lo sviluppo di nuovi farmaci per il trattamento di patologie rare o ad elevato bisogno di cura insoddisfatto. Grant DM 1 GIUGNO 2016 "Grandi Progetti R&S - PON 2014/2020" - Agenda digitale o Industria sostenibile). VDD was funded by a Marie Skłodowska-Curie Individual Fellowship (UE; IF-845713).

ACKNOWLEDGMENTS

We acknowledge Michele Pagliarella, Kateřina Apolínová, Sylvia Dyballa, Lucia Lozano, Valeria Di Giacomo, Sergio Jarque and Jone Ibarra for crucial technical work and help in the interpretation of the results. We thank Javier Terriente and Carles Cornet for fruitful discussion on the data. We thank Novelli Rubina for writing support.

SUPPLEMENTARY MATERIAL

The Supplementary Material for this article can be found online at: https://www.frontiersin.org/articles/10.3389/fphar.2022.822359/full#supplementary-material

REFERENCES

Aloe, L., Rocco, M. L., Bianchi, P., and Manni, L. (2012). Nerve Growth Factor: From the Early Discoveries to the Potential Clinical Use. *J. Transl Med.* 10 (1), 239. doi:10.1186/1479-5876-10-239

Al-Zamil, W. M., and Yassin, S. A. (2017). Recent Developments in Age-Related Macular Degeneration: A Review. *Clin. Interv. Aging* 12, 1313–1330. doi:10.2147/CIA.S143508

Belmonte, M. A., Santos, M. F., Kihara, A. H., Yan, C. Y., and Hamassaki, D. E. (2006). Light-Induced Photoreceptor Degeneration in the Mouse Involves Activation of the Small GTPase Rac1. *Invest. Ophthalmol. Vis. Sci.* 47 (3), 1193–1200. doi:10.1167/iovs.05-0446

Cacialli, P., Gatta, C., D'Angelo, L., Leggieri, A., Palladino, A., de Girolamo, P., et al. (2019). Nerve Growth Factor Is Expressed and Stored in Central Neurons of Adult Zebrafish. *J. Anat.* 235 (1), 167–179. doi:10.1111/joa.12986

Chakrabarti, S., Sima, A. A., Lee, J., Brachet, P., and Dicou, E. (1990). Nerve Growth Factor (NGF), ProNGF and NGF Receptor-like Immunoreactivity in BB Rat Retina. *Brain Res.* 523 (1), 11–15. doi:10.1016/0006-8993(90)91630-Y

Coassin, M., Lambiase, A., Sposato, V., Micera, A., Bonini, S., and Aloe, L. (2008). Retinal P75 and Bax Overexpression Is Associated with Retinal Ganglion Cells Apoptosis in a Rat Model of Glaucoma. *Graefes Arch. Clin. Exp. Ophthalmol.* 246 (12), 1743–1749. doi:10.1007/s00417-008-0913-5

Colafrancesco, V., Parisi, V., Sposato, V., Rossi, S., Russo, M. A., Coassin, M., et al. (2011). Ocular Application of Nerve Growth Factor Protects Degenerating Retinal Ganglion Cells in a Rat Model of Glaucoma. *J. Glaucoma* 20 (2), 100–108. doi:10.1097/IJG.0b013e3181d787e5

Connors, E., Curtis, A., Kim, D., and Freeland, A. (2021). The Effect of Age and Vision on Functional Measures of Medication Management, across Different Prescription Drug Container Shapes in Persons with Visual Impairment. *Br. J. Vis. Impairment* 39 (2), 161–174. doi:10.1177/0264619620918893

Cunvong, K., Huffmire, D., Ethell, D. W., and Cameron, D. J. (2013). Amyloid-β Increases Capillary Bed Density in the Adult Zebrafish Retina. *Invest. Ophthalmol. Vis. Sci.* 54 (2), 1516–1521. doi:10.1167/iovs.12-10821

Donovan, M., Carmody, R. J., and Cotter, T. G. (2001). Light-Induced Photoreceptor Apoptosis *In Vivo* Requires Neuronal Nitric-Oxide Synthase and Guanylate Cyclase Activity and Is Caspase-3-independent. *J. Biol. Chem.* 276 (25), 23000–23008. doi:10.1074/jbc.M005359200

Faillace, M. P., Julian, D., and Korenbrot, J. I. (2002). Mitotic Activation of Proliferative Cells in the Inner Nuclear Layer of the Mature Fish Retina: Regulatory Signals and Molecular Markers. *J. Comp. Neurol.* 451 (2), 127–141. doi:10.1002/cne.10333

Garcia, T. B., Hollborn, M., and Bringmann, A. (2017). Expression and Signaling of NGF in the Healthy and Injured Retina. *Cytokine Growth Factor. Rev.* 34, 43–57. doi:10.1016/j.cytogfr.2016.11.005

Götz, R., and Schartl, M. (1994). The Conservation of Neurotrophic Factors during Vertebrate Evolution. *Comp. Biochem. Physiol. C: Pharmacol. Toxicol. Endocrinol.* 108 (1), 1–10. doi:10.1016/1367-8280(94)90082-5

Hahn, K., Manuel, P., and Bouldin, C. (2020). Expression of the Neurotrophic Tyrosine Kinase Receptors,ntrk1andntrk2a, Precedes Expression of Otherntrkgenes in Embryonic Zebrafish. *PeerJ* 8, e10479. doi:10.7717/peerj.10479

Jin, Z. B., and Takahashi, M. (2012). Generation of Retinal Cells from Pluripotent Stem Cells. *Prog. Brain Res.* 201, 171–181. doi:10.1016/B978-0-444-59544-7.00008-1

Kalloniatis, M., and Fletcher, E. L. (2004). Retinitis Pigmentosa: Understanding the Clinical Presentation, Mechanisms and Treatment Options. *Clin. Exp. Optom.* 87 (2), 65–80. doi:10.1111/j.1444-0938.2004.tb03152.x

Kassen, S. C., Thummel, R., Campochiaro, L. A., Harding, M. J., Bennett, N. A., and Hyde, D. R. (2009). CNTF Induces Photoreceptor Neuroprotection and Müller Glial Cell Proliferation through Two Different Signaling Pathways in the Adult Zebrafish Retina. *Exp. Eye Res.* 88 (6), 1051–1064. doi:10.1016/j.exer.2009.01.007

Lambiase, A., Coassin, M., Tirassa, P., Mantelli, F., and Aloe, L. (2009). Nerve Growth Factor Eye Drops Improve Visual Acuity and Electrofunctional Activity in Age-Related Macular Degeneration: A Case Report. *Ann. Ist Super Sanita* 45 (4), 439–442. doi:10.1590/S0021-25712009000400014

Marc, R. E., Jones, B. W., Watt, C. B., and Strettoi, E. (2003). Neural Remodeling in Retinal Degeneration. *Prog. Retin. Eye Res.* 22 (5), 607–655. doi:10.1016/S1350-9462(03)00039-9

Martin, S. C., Marazzi, G., Sandell, J. H., and Heinrich, G. (1995). Five Trk Receptors in the Zebrafish. *Develop. Biol.* 169 (2), 745–758. doi:10.1006/dbio.1995.1184

Matsuoka, R. L., Sun, L. O., Katayama, K., Yoshida, Y., and Kolodkin, A. L. (2013). Sema6B, Sema6C, and Sema6D Expression and Function during Mammalian Retinal Development. *PLoS ONE* 8 (4), e63207. doi:10.1371/journal.pone.0063207

Mesentier-Louro, L. A., De Nicolò, S., Rosso, P., De Vitis, L. A., Castoldi, V., Leocani, L., et al. (2017). Time-Dependent Nerve Growth Factor Signaling Changes in the Rat Retina during Optic Nerve Crush-Induced Degeneration of Retinal Ganglion Cells. *Int. J. Mol. Sci.* 18 (1), 98. doi:10.3390/ijms18010098

Mesentier-Louro, L. A., Rosso, P., Carito, V., Mendez-Otero, R., Santiago, M. F., Rama, P., et al. (2018). Nerve Growth Factor Role on Retinal Ganglion Cell Survival and Axon Regrowth: Effects of Ocular Administration in Experimental

Model of Optic Nerve Injury. *Mol. Neurobiol.* 56, 1056–1069. doi:10.1007/s12035-018-1154-1

Nagashima, M., Barthel, L. K., and Raymond, P. A. (2013). A Self-Renewing Division of Zebrafish MÃ¼ller Glial Cells Generates Neuronal Progenitors that Require N-Cadherin to Regenerate Retinal Neurons. *Development* 140 (22), 4510–4521. doi:10.1242/dev.090738

Narayan, D. S., Wood, J. P., Chidlow, G., and Casson, R. J. (2016). A Review of the Mechanisms of Cone Degeneration in Retinitis Pigmentosa. *Acta Ophthalmol.* 94 (8), 748–754. doi:10.1111/aos.13141

Nelson, C. M., Ackerman, K. M., O'Hayer, P., Bailey, T. J., Gorsuch, R. A., and Hyde, D. R. (2013). Tumor Necrosis Factor-Alpha Is Produced by Dying Retinal Neurons and Is Required for Muller Glia Proliferation during Zebrafish Retinal Regeneration. *J. Neurosci.* 33 (15), 6524–6539. doi:10.1523/JNEUROSCI.3838-12.2013

Nittoli, V., Sepe, R. M., Coppola, U., D'Agostino, Y., De Felice, E., Palladino, A., et al. (2018). A Comprehensive Analysis of Neurotrophins and Neurotrophin Tyrosine Kinase Receptors Expression during Development of Zebrafish. *J. Comp. Neurol.* 526 (6), 1057–1072. doi:10.1002/cne.24391

Powell, C., Cornblath, E., Elsaeidi, F., Wan, J., and Goldman, D. (2016). Zebrafish Müller Glia-Derived Progenitors Are Multipotent, Exhibit Proliferative Biases and Regenerate Excess Neurons. *Sci. Rep.* 6 (1), 24851. doi:10.1038/srep24851

Rajaram, K., Harding, R. L., Bailey, T., Patton, J. G., and Hyde, D. R. (2014). Dynamic miRNA Expression Patterns during Retinal Regeneration in Zebrafish: Reduced Dicer or miRNA Expression Suppresses Proliferation of Müller Glia-Derived Neuronal Progenitor Cells. *Dev. Dyn.* 243 (12), 1591–1605. doi:10.1002/dvdy.24188

Ramachandran, R., Fausett, B. V., and Goldman., D. (2010). Ascl1a Regulates Müller Glia Dedifferentiation and Retinal Regeneration through a Lin-28-dependent, Let-7 microRNA Signalling Pathway. *Nat. Cel Biol* 12 (11), 1101–1107. doi:10.1038/ncb2115

Ramachandran, R., Zhao, X. F., and Goldman, D. (2011). Ascl1a/Dkk/beta-catenin Signaling Pathway Is Necessary and Glycogen Synthase Kinase-3beta Inhibition Is Sufficient for Zebrafish Retina Regeneration. *Proc. Natl. Acad. Sci. U S A.* 108 (38), 15858–15863. doi:10.1073/pnas.1107220108

Ranski, A. H., Kramer, A. C., Morgan, G. W., Perez, J. L., and Thummel, R. (2018). Characterization of Retinal Regeneration in Adult Zebrafish Following Multiple Rounds of Phototoxic Lesion. *PeerJ* 6, e5646. doi:10.7717/peerj.5646

Richardson, R., Tracey-White, D., Webster, A., and Moosajee, M. (2017). The Zebrafish Eye-A Paradigm for Investigating Human Ocular Genetics. *Eye (Lond)* 31 (1), 68–86. doi:10.1038/eye.2016.198

Rocco, M. L., Balzamino, B. O., Petrocchi Passeri, P., Micera, A., and Aloe, L. (2015). Effect of Purified Murine NGF on Isolated Photoreceptors of a Rodent Developing Retinitis Pigmentosa. *PLOS ONE* 10 (4), e0124810. doi:10.1371/journal.pone.0124810

Rocco, M. L., Soligo, M., Manni, L., and Aloe, L. (2018). Nerve Growth Factor: Early Studies and Recent Clinical Trials. *Curr. Neuropharmacol* 16 (10), 1455–1465. doi:10.2174/1570159X16666180412092859

Sacchetti, M., Mantelli, F., Rocco, M. L., Micera, A., Brandolini, L., Focareta, L., et al. (2017). Recombinant Human Nerve Growth Factor Treatment Promotes Photoreceptor Survival in the Retinas of Rats with Retinitis Pigmentosa. *Curr. Eye Res.* 42 (7), 1064–1068. doi:10.1080/02713683.2017.1279634

Saito, Y., Tsuruma, K., Shimazawa, M., Nishimura, Y., Tanaka, T., and Hara, H. (2016). Establishment of a Drug Evaluation Model against Light-Induced Retinal Degeneration Using Adult Pigmented Zebrafish. *J. Pharmacol. Sci.* 131 (3), 215–218. doi:10.1016/j.jphs.2016.05.009

Santos, A. M., López-Sánchez, N., Martín-Oliva, D., de la Villa, P., Cuadros, M. A., and Frade, J. M. (2012). Sortilin Participates in Light-dependent Photoreceptor Degeneration *In Vivo*. *PLoS ONE* 7 (4), e36243. doi:10.1371/journal.pone.0036243

Shah, M., Cabrera-Ghayouri, S., Christie, L. A., Held, K. S., and Viswanath, V. (2019). Translational Preclinical Pharmacologic Disease Models for Ophthalmic Drug Development. *Pharm. Res.* 36 (4), 58. doi:10.1007/s11095-019-2588-5

Sudharsan, R., Simone, K. M., Anderson, N. P., Aguirre, G. D., and Beltran, W. A. (2017). Acute and Protracted Cell Death in Light-Induced Retinal Degeneration in the Canine Model of Rhodopsin Autosomal Dominant Retinitis Pigmentosa. *Invest. Ophthalmol. Vis. Sci.* 58 (1), 270–281. doi:10.1167/iovs.16-20749

Sun, X., Xu, X., Wang, F., Zhang, X., Yu, Z., Lu, H., et al. (2007). Effects of Nerve Growth Factor for Retinal Cell Survival in Experimental Retinal Detachment. *Curr. Eye Res.* 32 (9), 765–772. doi:10.1080/02713680701531082

Sun, X., Xu, X., Wang, F., Zhang, X., Ho, P. C., Liu, H., et al. (2008). Nerve Growth Factor Helps Protect Retina in Experimental Retinal Detachment. *Ophthalmologica* 222 (1), 58–61. doi:10.1159/000109281

Steven M. Teutsch, Margaret A. McCoy, R. Brian Woodbury, and Annalyn Welp, Editors (2016). *Making Eye Health a Population Health Imperative*. (Washington, D.C.: National Academies Press). doi:10.17226/23471

Thomas, J. L., Nelson, C. M., Luo, X., Hyde, D. R., and Thummel, R. (2012). Characterization of Multiple Light Damage Paradigms Reveals Regional Differences in Photoreceptor Loss. *Exp. Eye Res.* 97 (1), 105–116. doi:10.1016/j.exer.2012.02.004

Thomas, J. L., Ranski, A. H., Morgan, G. W., and Thummel, R. (2016). Reactive Gliosis in the Adult Zebrafish Retina. *Exp. Eye Res.* 143, 98–109. doi:10.1016/j.exer.2015.09.017

Thummel, R., Kassen, S. C., Enright, J. M., Nelson, C. M., Montgomery, J. E., and Hyde, D. R. (2008a). Characterization of Müller Glia and Neuronal Progenitors during Adult Zebrafish Retinal Regeneration. *Exp. Eye Res.* 87 (5), 433–444. doi:10.1016/j.exer.2008.07.009

Thummel, R., Kassen, S. C., Montgomery, J. E., Enright, J. M., and Hyde, D. R. (2008b). Inhibition of Müller Glial Cell Division Blocks Regeneration of the Light-Damaged Zebrafish Retina. *Dev. Neurobiol.* 68 (3), 392–408. doi:10.1002/dneu.20596

Vihtelic, T. S., and Hyde, D. R. (2000). Light-Induced Rod and Cone Cell Death and Regeneration in the Adult Albino Zebrafish (Danio Rerio) Retina. *J. Neurobiol.* 44 (3), 289–307. doi:10.1002/1097-4695(20000905)44:3<289:aid-neu1>3.0.co;2-h

Wan, J., and Goldman, D. (2016). Retina Regeneration in Zebrafish. *Curr. Opin. Genet. Develop.* 40, 41–47. doi:10.1016/j.gde.2016.05.009

Wan, J., Ramachandran, R., and Goldman, D. (2012). HB-EGF Is Necessary and Sufficient for Müller Glia Dedifferentiation and Retina Regeneration. *Dev. Cel* 22 (2), 334–347. doi:10.1016/j.devcel.2011.11.020

Wang, H., Wang, R., Thrimawithana, T., Little, P. J., Xu, J., Feng, Z. P., et al. (2014). The Nerve Growth Factor Signaling and its Potential as Therapeutic Target for Glaucoma. *Biomed. Res. Int.* 2014, 759473. doi:10.1155/2014/759473

Welp, A., Meier, L. L., and Manser, T. (2016). The Interplay between Teamwork, Clinicians' Emotional Exhaustion, and Clinician-Rated Patient Safety: a Longitudinal Study. *Crit. Care* 20 (1), 110. doi:10.1186/s13054-016-1282-9

Yao, K., Qiu, S., Wang, Y. V., Park, S. J. H., Mohns, E. J., Mehta, B., et al. (2018). Restoration of Vision after De Novo Genesis of Rod Photoreceptors in Mammalian Retinas. *Nature* 560 (7719), 484–488. doi:10.1038/s41586-018-0425-3

Conflict of Interest: The authors PC, MA, FM, AA, and LB are employees of Dompé farmaceutici s.p.a. The authors VD and DR are employees of ZeClinics SL, IGTP.

The remaining author declares that the research was conducted in the absence of any commercial or financial relationships that could be construed as a potential conflict of interest.

Publisher's Note: All claims expressed in this article are solely those of the authors and do not necessarily represent those of their affiliated organizations, or those of the publisher, the editors, and the reviewers. Any product that may be evaluated in this article, or claim that may be made by its manufacturer, is not guaranteed or endorsed by the publisher.

frontiers in Pharmacology

REVIEW
published: 15 March 2022
doi: 10.3389/fphar.2022.835827

A Critical Review of Zebrafish Models of Parkinson's Disease

Jillian M. Doyle and Roger P. Croll*

Department of Physiology and Biophysics, Faculty of Medicine, Dalhousie University, Halifax, NS, Canada

A wide variety of human diseases have been modelled in zebrafish, including various types of cancer, cardiovascular diseases and neurodegenerative diseases like Alzheimer's and Parkinson's. Recent reviews have summarized the currently available zebrafish models of Parkinson's Disease, which include gene-based, chemically induced and chemogenetic ablation models. The present review updates the literature, critically evaluates each of the available models of Parkinson's Disease in zebrafish and compares them with similar models in invertebrates and mammals to determine their advantages and disadvantages. We examine gene-based models, including ones linked to Early-Onset Parkinson's Disease: *PARKIN, PINK1, DJ-1*, and *SNCA*; but we also examine *LRRK2,* which is linked to Late-Onset Parkinson's Disease. We evaluate chemically induced models like MPTP, 6-OHDA, rotenone and paraquat, as well as chemogenetic ablation models like metronidazole-nitroreductase. The article also reviews the unique advantages of zebrafish, including the abundance of behavioural assays available to researchers and the efficiency of high-throughput screens. This offers a rare opportunity for assessing the potential therapeutic efficacy of pharmacological interventions. Zebrafish also are very amenable to genetic manipulation using a wide variety of techniques, which can be combined with an array of advanced microscopic imaging methods to enable *in vivo* visualization of cells and tissue. Taken together, these factors place zebrafish on the forefront of research as a versatile model for investigating disease states. The end goal of this review is to determine the benefits of using zebrafish in comparison to utilising other animals and to consider the limitations of zebrafish for investigating human disease.

Keywords: zebrafish (brachydanio rerio), parkinson's disease (PD), animal models, neurodegeneration, dopamine

OPEN ACCESS

Edited by:
Carla Denise Bonan, Pontifical Catholic University of Rio Grande do Sul, Brazil

Reviewed by:
Marc Ekker, University of Ottawa, Canada
Arianna Bellucci, University of Brescia, Italy

****Correspondence:***
Jillian M. Doyle
jillian.doyle@dal.ca

Specialty section:
This article was submitted to Neuropharmacology, a section of the journal Frontiers in Pharmacology

Received: *15 December 2021*
Accepted: *08 February 2022*
Published: *15 March 2022*

Citation:
Doyle JM and Croll RP (2022) A Critical Review of Zebrafish Models of Parkinson's Disease. Front. Pharmacol. 13:835827. doi: 10.3389/fphar.2022.835827

1 INTRODUCTION

1.1 Parkinson's Disease

Parkinson's Disease (PD) is the second most common neurodegenerative disorder after Alzheimer's Disease. It typically affects individuals over the age of 65, although Early Onset Parkinson's Disease (EOPD) is well-noted. With the current aging world population, the number of people living with PD is expected to reach 12 million by the year 2040 (Dorsey and Bloem, 2018; Dorsey et al., 2018). Symptoms primarily affect movement, including tremors, bradykinesia (slow movements), rigidity and postural instability; in addition, patients may also manifest cognitive symptoms like impaired memory and executive dysfunction (Rana et al., 2015). Despite extensive research, no definitive cause has been identified. Numerous genes have been implicated, including, but not limited to: *LRRK2, SNCA* (*PARK1/4*), *DJ-1, PINK1,* and *PARKIN* (Best and Alderton, 2008). The majority of PD cases, however, are sporadic and not

associated with any particular gene (Lang and Lozano, 1998; Coulom and Birman, 2004). Environmental factors, like chemical exposure to MPTP, pesticides and solvents, may also play a role in the onset of PD (Best and Alderton, 2008; Vázquez-Vélez and Zoghbi, 2021).

The two main physiological characteristics of PD are the loss of nigrostriatal dopaminergic neurons and diffuse brain deposition of Lewy bodies, proteinaceous inclusions mainly containing α-synuclein fibrils. (Braak and Braak, 2000; Davie, 2008). Many interconnected factors contribute to the pathophysiology of PD, some of which are not fully elucidated (Vázquez-Vélez and Zoghbi, 2021).

Alpha-synuclein, produced by the *SNCA* gene, has been associated with several linked cellular pathways that are altered in PD pathophysiology. Impairments in lysosomal pathways, whether genetically induced or not, cause a reduction in α-synuclein degradation (Cuervo et al., 2004; Vogiatzi et al., 2008; Vázquez-Vélez and Zoghbi, 2021). Dysregulation and/or improper processing of α-synuclein also leads to mitochondrial dysfunction and the generation of reactive oxygen species (ROS). Although the mechanisms are not precisely clear, mitochondrial dysfunction can also affect α-synuclein in a feedback loop (Nakamura et al., 2011; Di Maio et al., 2016).

Mitochondrial dysfunction itself is a fundamental part of PD pathophysiology and is an important factor in dopaminergic cell death (Malpartida et al., 2021). The genes *PINK1* and *PARKIN* have been linked to mitophagy and recent studies suggest that mutations in the genes *LRRK2* and *SNCA* also contribute to mitochondrial dysfunction (Malpartida et al., 2021). Several of the chemical substances identified as environmental risk factors for developing PD specifically target Complex I of the mitochondrial electron transport chain (ETC) and subsequently cause neuron death (Moore et al., 2005).

ROS also play a large role in PD pathophysiology and are tightly connected with dysregulation of α-synuclein and mitochondrial dysfunction (Weng et al., 2018). Alpha-synuclein promotes pro-inflammatory factors in microglia, the immune cells of the central nervous system, which results in ROS production (Block et al., 2007; Thameem Dheen et al., 2007). Mitochondrial dysfunction leads to production of ROS which then interferes with the ETC and leads to a reduction in cellular energy stores, and subsequently causes cell death (Bhat et al., 2015; Hang et al., 2015). Even dopamine, the neurotransmitter at the heart of PD, is notably unstable and can auto-oxidize and form ROS, in addition to ROS being generated as by-products of dopamine degradation by monoamine oxidase B (MAO-B) (Youdim et al., 2006; Hastings, 2009). Many other elements have been implicated in PD; however a full review of the disease pathophysiology is beyond the scope of this article. For a more in-depth treatment, the reader is referred to excellent reviews on the topic (Moore et al., 2005; Weng et al., 2018; Malpartida et al., 2021; Vázquez-Vélez and Zoghbi, 2021).

Due to the myriad of mechanisms and potential causes involved in PD, the development of a model recapitulating the main features of the disease, including the selective degeneration of nigrostriatal neurons, Lewy bodies-like pathology and motor deficits has proven to be problematic.

1.2 Using Animal Models to Investigate Causes

Studying *in vitro* human cell models can impart substantial information, but such models cannot yet replicate the multi-system interactions observed in the human disease or *in vivo* animal models. When choosing a model organism, a critical analysis must be performed to determine the value of findings with respect to human disease. Most importantly, studies of a model must possess a high level of replicability (Caramillo and Echevarria, 2017). A meta-analysis of transcriptional profiles of transgenic mouse models of Alzheimer's Disease found that those models were not always similar within their own group, between groups or to human Alzheimer's Disease models, indicating poor replicability and it is expected that this finding would also be relevant to models of PD (Hargis and Blalock, 2017). Accordingly, many of the therapies developed with animal models do not translate well to human clinical trials for a host of reasons (van der Worp et al., 2010). These challenges must be addressed when developing animal models of human disease.

Mice and rats are traditional animal models for studying human diseases (Jucker, 2010). As mammals, they possess relatively similar anatomy and physiology to humans; and in the case of mice, numerous transgenic strains have been developed. However, despite their small size, mice are still expensive to keep in large numbers, and transgenic strains are labour-intensive to produce (Jucker, 2010). Conversely, invertebrates like the fruit fly, *Drosophila melanogaster*, and the nematode, *Caenorhabditis elegans,* have been used for many years as medical models. Such invertebrates possess many of the same basic cellular processes and basic gene functions as mammals but are inexpensive and suitable for large scale experiments (Ségalat, 2007). The obvious drawback of these invertebrates is that they lack similar brain structures and organ systems to humans, so they may not model human disease accurately. The zebrafish has become widely established as a medical model in recent years, conveniently combining the versatility of invertebrates with the anatomical similarity of mammals (Spence et al., 2008).

1.3 Benefits of Using Zebrafish

Zebrafish have been used to study numerous human diseases, including neuropsychiatric and neurodegenerative diseases, owing to similarities with human brain physiology and anatomy (Xi et al., 2011; Fontana et al., 2018). To date, models have been developed for some of these diseases including amyotrophic lateral sclerosis (ALS) and Huntington's Disease, with the bulk of extant research focused on Alzheimer's and Parkinson's Diseases (Xi et al., 2011; Babin et al., 2014; Martín-Jiménez et al., 2015). The zebrafish brain is comparable to the mammalian brain, with fore-, mid- and hindbrain sections also containing a diencephalon and telencephalon and primary neurotransmitter function is generally similar to that in humans (Panula et al., 2006;

Lieschke and Currie, 2007; Toledo-Ibarra et al., 2013; Stoyek et al., 2015; Caramillo and Echevarria, 2017). Like mammals, zebrafish possess a blood brain barrier, and permeability tests indicate that its physiological properties are conserved between zebrafish and humans (Cuoghi and Mola, 2007; Wager and Russell, 2013). In addition to their physiological benefits, zebrafish also exhibit sophisticated cognitive behaviours, such as learning and retaining associations, and they manifest well-documented anxiety behaviours (Lieschke and Currie, 2007).

One of the key advantages of zebrafish is their suitability for genetic manipulation, which has led to the development of thousands of mutant, transgenic and otherwise genetically-altered strains (See **Section 2.1**) (Ruzicka et al., 2019). For example, adult zebrafish of some mutant strains are optically transparent, enabling *in vivo* imaging of internal tissues and cells (White et al., 2008). These transparent mutations extend the optical transparency that is already a useful feature of all larval zebrafish into adulthood (Parichy et al., 2009). Genetically altered zebrafish featuring a genotype or phenotype of interest can be produced with less effort than their rodent counterparts, as DNA or RNA can more easily be injected at the single cell stage, due to external fertilisation and development of the fish (Clark et al., 2011). Fluorescent reporters linked to specific promotors provide an array of imaging opportunities (Halpern et al., 2008). Besides traditional reporters, like green fluorescent protein (GFP), genetically encoded calcium indicators like GCaMP and the optogenetic reporter channel rhodopsin can easily be incorporated into transgenic zebrafish lines (Halpern et al., 2008; Howe et al., 2017). Combining the ability to create custom transgenic lines with current imaging techniques presents a unique opportunity to study the functions of genes in a living animal, something not easily achieved with other models. With advanced microscopy techniques imaging live transgenic lines is becoming more accessible. Light sheet microscopy enables the user to illuminate and image an entire plane of tissue, which has advantages over traditional point-scanning methods like confocal and two-photon (Hillman et al., 2019). Fluorescence lifetime imaging microscopy (FLIM) offers the ability to perform *in vivo* observations of zebrafish over the temporal lifespan of the fluorophore, and can provide additional data on overlapping emission spectra and the intensity of the fluorophore (Zhang et al., 2021). In addition to the advantages described above, zebrafish are becoming increasingly popular for use in high-throughput screens due to their prolific reproduction and cost-efficient size. Based on these factors, potential therapeutics and genes can be quickly identified in a fraction of the time required for rodents (See **Section 5**: Discussion).

1.4 Dopaminergic Neurons in Zebrafish

The dopaminergic system, the primary site of PD, has been extensively studied in zebrafish. Retrograde tracing studies in the adult zebrafish brain found that dopaminergic neurons projecting to the ventral telencephalon are located in the posterior tuberculum of the ventral diencephalon (Xi et al., 2011). Although it has been suggested that these dopaminergic neurons in the ventral diencephalon may be analogous to the midbrain dopaminergic neurons of the nigrostriatal pathway, this has been questioned by others (Wullimann and Rink, 2001; Tay et al., 2011). The dopaminergic system in embryonic zebrafish is also well characterized. Dopaminergic neurons are first detected at 18 h post fertilization (hpf) in a cluster in the ventral diencephalon, and by 72 hpf, the organization of the central nervous system is complete and subsequent development only adds increased numbers of neurons (Kimmel et al., 1995; Wullimann and Rink, 2001). In addition to the ventral diencephalon, dopaminergic neurons are also found in the olfactory bulb, preoptic region, retina and pretectum (Rink and Wullimann, 2002). Zebrafish had been found to have similar dopaminergic signalling pathways to mammals, and transcription factors have been shown to play evolutionarily conserved roles in the development of zebrafish dopaminergic neurons (Xi et al., 2011). Dopaminergic neurons in zebrafish are sensitive to oxidative stress, which is one of the main causes of their death in PD (McCormack et al., 2006; Rappold et al., 2011; also see above). The well-characterized dopaminergic system, along with the other benefits mentioned above, make the zebrafish a suitable model for studying PD.

1.5 Goals of This Review

Reviews published in the last few years have catalogued the numerous gene and chemically based models of PD in zebrafish (Razali et al., 2021; Wang et al., 2021). However, it is still unclear how these models compare to PD models in more established animals, like rodents, *Drosophila* and *C. elegans*. This paper presents a critical review of several gene-based and chemical-based models of PD in zebrafish. Each of the currently available models will be evaluated on its strengths, weaknesses and contributions, or potential future contributions, to knowledge of the disease; however, emphasis will be placed on the most characterized and relevant models.

2 GENE-BASED MODELS

2.1 Creating Gene-Based Models in Zebrafish

The models described in this section use various methods of genomic manipulation, each with its own advantages and disadvantages.

One of the earliest methods of creating models was to expose zebrafish to mutagenic substances and then perform extensive phenotyping to identify fish with mutations of interest (Driever et al., 1996; van Eeden et al., 1998). This labour intensive process was facilitated by the advent of TILLING (targeting induced local lesions in genomes) which can easily identify genes of interest (Amsterdam and Hopkins, 2006; Rafferty and Quinn, 2018). Another method for disabling genes is using zinc-finger nucleases (ZFNs), restriction enzymes which cleave a target section of DNA. ZFNs are very accurate at targeting specific nucleotide sequences, but sometimes mutations occur at the repair site. Furthermore, this process is expensive and can be difficult to design (Carroll, 2011; Hruscha et al., 2013).

In the past, one of the most popular tools for genetic manipulation had been the transient gene knock down using

TABLE 1 | Gene-based zebrafish models of Parkinson's Disease.

Human gene	Zebrafish gene	Study	Adults/ Larvae	Method	Dopamine	Results
DJ-1	dj-1	Baulac et al. (2009)	Larvae	MO knock down of *dj-1*	Increased sensitivity of DNs to oxidative stress	Dysregulation in proteins related to mitophagy, redox, stress and inflammation
		Edson et al. (2019)	Adults	CRISPR/Cas 9 removal of *dj-1*	Loss of TH-positive cells	
PINK1	pink1	Anichtchik et al. (2008)	Larvae	MO knock down of *pink1*	Loss of dopaminergic neurons	Severe phenotype
		Sallinen et al. (2009)	Larvae	MO knock down of *pink1*	Increased sensitivity of DNs to MPTP	
		Xi et al. (2010)	Larvae	MO knock down of *pink1*	Disruption of DN organization	Decreased swimming, reduced startle response, reduced mitochondria
		Flinn et al. (2013)	Larvae/ Adults	*pink1*$^{-/-}$ mutant (identified with TILLING)	Loss of DNs, ↓ mitochondrial activity	Upregulation of TigarB (MO knockdown rescued *pink1*$^{-/-}$ effects)
PARKIN	parkin	Flinn et al. (2009)	Larvae	MO knock down of *parkin*	Loss of DN, increased sensitivity	Decreased mitochondrial activity
		Fett et al. (2010)	Larvae	MO knock down of *parkin*	Increased sensitivity	
LRRK2	lrrk2	Sheng et al. (2010)	Larvae	MO knock down *lrrrk2*	Loss of TH-positive cells	Severe lethality
		Sheng et al. (2010)	Larvae	MO knock down of *lrrk2* (WD40)	Loss of DN neurons	Reduced swimming activity
		Ren et al. (2011)	Larvae	MO knock down of *lrrk2* (WD40)	No loss of DNs	No swimming deficits
		Prabhudesai et al. (2016)	Larvae	MO knock down of *lrrk2* (50%)	Loss of DNs	Moderate defects, β-synuclein aggregates
SNCA	β- and γ_1-synuclein	Milanese et al. (2012)	Larvae	MO knock down of *β* and/ or *γ-synuclein*	Alters DN development	Impaired motor functions, rescued by human α-synuclein
	α-synuclein (human)	Prabhudesai et al. (2012)	Larvae	Human *α-synuclein* overexpression		α-synuclein aggregates, apoptosis, rescued by CLR01
	γ_1-synuclein	Lulla et al. (2016)	Larvae	*γ$_1$-synuclein* overexpression		γ_1-synuclein aggregates, rescued by CLR01

**MO, Morpholino oligonucleotides DNs, Dopaminergic neurons TH, Tyrosine hydroxylase.*

morpholino oligonucleotides (MOs). MOs work by either blocking translation of target mRNA or preventing splicing of pre-mRNA. This method revolutionized gene manipulation, as it was cost effective and relatively easy to use, with many of the studies reviewed here employing this method. It is well documented that MOs may inhibit off-target genes in addition to, or instead of, the target gene (Bill et al., 2009; Blum et al., 2015). Furthermore, it is difficult to inject precise and reproducible volumes of MOs into zebrafish eggs (Eisen and Smith, 2008).

Many of the gene-based models in this review utilised genetically altered strains of zebrafish, which were created using several methods. In one method, a plasmid containing a gene or nucleotide sequence of interest is injected into zebrafish eggs, and this DNA is eventually integrated into the genome. However, this method has a low rate of success, as only about 5% of the resultant fish possess the desired genotype (Kawakami, 2007). A notable improvement uses the *tol2* system which depends on identified *tol2* sequences, which are found throughout zebrafish DNA. Injected transposase mRNA cleaves the DNA at these sequences, and a plasmid containing a *tol2* construct with desired new DNA inserts into the resulting gap. This method is much more accurate and 50–70% of the offspring inherit the inserted DNA.

The advent of new genomic editing techniques presents the opportunity to create knock downs with fewer off-target effects. One of the most accurate is TALEN (transcription activator-like effector nucleases), which utilises TALEs (transcription activator-like effectors) designed to bind to specific DNA sequences (Joung and Sander, 2013). TALEs are combined with nucleases, which enable them to cleave DNA at precise locations. This method can be used to excise a gene or generate a site for a gene to be inserted. TALEs are relatively easy to design but have labour-intensive cloning steps and may not be accessible to all labs (Hruscha et al., 2013). The newest method is the CRISPR (clustered, regularly interspaced, short palindromic repeats)/Cas9 system, which was developed from a bacterial immune defence mechanism. Emmanuelle Charpentier and Jennifer Doudna won the Nobel Prize in Chemistry in 2020 for their work on CRISPR and it has rapidly become one of the most widely used genetic editing techniques, generally and specifically in zebrafish (Westermann et al., 2021). The first step is the construction of a short piece of synthetic RNA that targets a complementary segment of desired DNA. The Cas9 protein, an enzyme that cleaves DNA, uses the synthetic RNA to identify the site of DNA cleavage (Ran et al., 2013). Like TALEN, it can be used to excise genes or introduce a new gene. CRISPR/Cas9 is cheaper and much less time consuming than either ZFN or TALEN. In

zebrafish, CRISPR/Cas9 is highly effective: the mutation can be induced in 86% percent of fish on average and be completely heritable (Hruscha et al., 2013). This technique shows immense promise for the creation of new zebrafish lines.

For a summary of the following specific models refer to **Table 1**.

2.2 Parkin

Mutations in the *Parkin* gene are the most common autosomal-recessive mutations in EOPD (Kitada et al., 1998). The *Parkin* gene encodes an E3 ubiquitin ligase which is involved in the proteasome degradation system and also may be involved in mitochondrial function along with the other PD-related genes *PINK1* and *DJ-1* (Flinn et al., 2009). The ParkinQ311X mouse, which expresses a human parkin variant, exhibited dysfunction and degeneration in dopaminergic neurons (Regoni et al., 2020, 2021). However, *Parkin*-null mice showed no evidence of dopaminergic neuron loss, decreased mitochondrial function or abnormal behaviour (Dawson et al., 2010). Conversely, loss of *Parkin* function in *Drosophila* results in decreased numbers of dopaminergic neurons and a reduction of mitochondria in the indirect flight muscles (Greene et al., 2003; Whitworth et al., 2005).

Zebrafish parkin has 62% similarity with the human counterpart and is expressed ubiquitously in larval and adult fish (Flinn et al., 2009). An MO knock down of *parkin* caused a 20% decrease in the numbers of diencephalic dopaminergic neurons, and an increased sensitivity of these neurons to the neurotoxin MPP+ (See **Section 3.1**) at 3 days post fertilization (dpf) (Flinn et al., 2009). The knock down did not have abnormal mitochondria morphology but did have reduced mitochondrial Complex I activity, something also noted in human patients with *Parkin* mutations (Durcan and Fon, 2015). There was no effect on the normal onset of swimming behaviour at 5 dpf, but it is unclear whether the observed 20% neuron loss would have been sufficient to cause such motor symptoms.

In contrast, another MO knock down of *parkin* in zebrafish showed no loss of dopaminergic neurons but did show increased susceptibility to stress-induced cell death (Fett et al., 2010). There was no effect on mitochondrial morphology, but *parkin* was transcriptionally upregulated in response to mitochondrial stress, as in humans. *Parkin* may also have a protective effect because overexpression inhibits proteotoxic stress, which causes cell death.

Flinn et al. (2009) stated that their MO knock down of *parkin* has biochemical and pathological changes analogous to those in humans with *Parkin* mutations. However, as with other MO knock downs, there is a definite discrepancy between the results in these studies, which may indicate different off-target effects or different knock down efficiencies. Both Flinn et al. (2009) and Fett et al. (2010) indicate that *parkin* has similar protective functions, and they are comparable to the effects seen in humans. A *parkin*-deficient fish created using a more consistent method is required to clarify these results.

2.3 PINK1

Mutations in the gene encoding PINK1 (PTEN (phosphatase/tensin homolog)-induced putative kinase I) are the second most common cause of autosomal-recessive EOPD (Xi et al., 2011). Loss of *PINK1* function in humans causes increased lipid peroxidation and decreased function of mitochondrial Complex I (Exner et al., 2007). In *PINK1*-deficient mouse models, no dopaminergic neuron loss was characterized, but dopamine release was impaired (Kitada et al., 2007; Zhou et al., 2007). In *Drosophila*, deactivation of *PINK1* caused various effects, notably death of dopaminergic neurons and muscle degeneration (Yang et al., 2006).

Zebrafish pink1, which is 54% similar to human PINK1, is expressed ubiquitously in larvae but found only in the periventricular zones and in some diencephalic dopaminergic neurons of the adult fish brain (Anichtchik et al., 2008). An MO knock down of *pink1* reduced the number of dopaminergic neurons by 40% in the ventral diencephalon and was accompanied by severe defects in body morphology. This severe phenotype was partially rescued by wild-type human PINK1 but not mutant PINK1. There were also differences in mitochondrial function, including increased caspase-3 activity and ROS levels (Anichtchik et al., 2008).

A different MO knock down of *pink1* (Sallinen et al., 2010) was not able to replicate the results from Anichtchik et al. (2008). The severe morphological effects seen in Anichtchik et al. were only noted in the Sallinen et al. study in MOs with strong off-target effects that could not be rescued by *pink1* mRNA. It is likely that the MO developed by Anichtchik et al. may have had strong off-target effects and this knock down should be replicated using a different genetic editing technique. Sallinen et al. (2010) noted no loss of dopaminergic neurons in their knock down, but they did show an increased sensitivity to the neurotoxin MPTP (See **Section 3.1**). The *pink1* knock down fish, when exposed to MPTP, swam significantly less and experienced a greater loss of tyrosine hydroxylase (TH)-immunoreactive neurons than controls exposed to MPTP alone. TH is the rate limiting enzyme in the synthetic pathway for dopamine and often used to identify dopaminergic cells.

A third MO knock down of *pink1* also found little loss of dopaminergic neurons but did note some abnormal morphology of said neurons (Xi et al., 2010). The *pink1* deficient fish exhibited altered locomotor activity, including decreased swimming behaviour and response to touch. There was also decreased mitochondrial function due to reduced numbers of mitochondria and a loss of cristae (Xi et al., 2010, 2011).

A *pink1*$^{-/-}$ mutant zebrafish, identified using TILLING, showed loss of dopaminergic neurons, increased mitochondrial size and decreased mitochondrial Complex I and III activity in both larvae and adults (Flinn et al., 2013). These fish also upregulated the apoptosis regulator *TigarB* (orthologue to human *TIGAR*), and an MO knock down of *TigarB* completely rescued dopaminergic neuron loss in the *pink1* mutants. Flinn et al. (2013) verified the results by creating first a MO knock down of *pink1,* which mirrored the mutant results, and then a double knock down of *pink1* and *TigarB*, which rescued the dopaminergic neurons and mitochondrial function.

The many contradictory results from knock downs of *pink1* in zebrafish are suggestive of off-target effects, stemming from

the different MOs used (See **Section 5**: Discussion). The mutant model presented by Flinn et al. (2013) may present a more stable platform to study the function of *pink1*. The congruence between the findings of their MO knock down and mutant models is strong evidence of a successful MO knock down. This study also indicated that *pink1* plays an important role in dopaminergic neuron development and mitochondrial function and suggests a target (*TigarB*) for future therapeutic intervention.

2.4 DJ-1

DJ-1 is a redox-sensitive chaperone that protects against oxidative stress. Mutations in the gene encoding DJ-1 (also known as PARK7) have been linked to autosomal-recessive EOPD, causing altered mitochondrial morphology and increased production of ROS (Cookson, 2005). *DJ-1* null mice showed no apparent direct effects in dopaminergic neurons, but those neurons were more sensitive to oxidative stress (Kim et al., 2005). *Drosophila* studies of an interference RNA knock down of *DJ-1* showed degrees of dopaminergic neuron loss and an increased sensitivity to oxidative stress (Meulener et al., 2005; Yang et al., 2005).

Zebrafish dj-1 is 83% identical to the human version and is expressed throughout the brain, including in dopaminergic neurons in the CNS (specifically cell groups in the olfactory bulbs, diencephalon and telencephalon) (Bai et al., 2006).

An immunohistochemical study of a *dj-1* MO knock down showed no decrease in the numbers of dopaminergic (TH-positive) neurons. As in the mouse model, the zebrafish dopaminergic neurons were more susceptible to apoptosis and showed increased sensitivity to hydrogen peroxide or to a proteasome inhibitor. In zebrafish subjected to oxidative stress, *dj-1* is upregulated. This indicates that mutations in *dj-1* may impair the response of dopaminergic neurons to environmental stress, leaving them susceptible to cell death (Baulac et al., 2009).

Recently, the CRISPR-Cas9 method was used to produce a dj-1 deficient zebrafish, which developed normally until the adult stage, at which point the fish began to exhibit low body mass and lower levels of TH. A proteomic analysis on the brains revealed a dysregulation in proteins involved with mitochondrial mitophagy, redox regulation, stress response and inflammation (Edson et al., 2019).

As only one knock down study of *dj-1* was characterized in zebrafish, it is difficult to assess its effectiveness (Baulac et al., 2009). The CRISPR study is very promising as the fish can be studied in adulthood, compared to the MO knock downs that could only be achieved in larvae. In general, the results mirror those from the mice study, and therefore the gene appears to have a similar function to its mammalian counterpart and may provide a good basis for future study.

2.5 LRRK2

Mutations in the gene encoding LRRK2 (Leucine-rich repeat kinase 2) are the most prevalent cause of autosomal dominant PD in humans (Blandini and Armentero, 2012). Not much is known about the function of LRRK2, but it seems to be involved in neurodegeneration and kidney function (MacLeod et al., 2006). There are contradictory results with *Drosophila* models of *LRRK2* deficiency. One study reports reduction of dopaminergic neuron numbers (Lee et al., 2007), but the other saw no change in the neurons (Wang et al., 2008). In mice, disruption of *LRRK2* had no obvious effect on dopaminergic neurons and no increased sensitivity to the neurotoxin, MPTP (Andres-Mateos et al., 2009).

The zebrafish orthologue lrrk2 has a 38% similarity to its human counterpart (Sager et al., 2010). An MO knock down of *lrrk2* caused severe morphological defects, a loss of diencephalic TH-positive cells and death by 3 dpf (Sheng et al., 2010). Due to the severe phenotype, another MO knock down was created targeting a domain of *LRRK2* called WD40, which is associated with PD-inducing mutations in humans. These fish showed increasing loss of diencephalic dopaminergic neurons with increasing MO concentration. The WD40 knock downs also had reduced swimming activity that could be rescued by wild-type zebrafish or human LRRK2 or L-DOPA, a common treatment for the symptoms of PD (Cools, 2006; Sheng et al., 2010).

A replication of the study by Sheng et al. (2010), however, showed no dopaminergic neuron loss in a knock down of the WD40 domain of *LRRK2* (Ren et al., 2011). An analysis of swimming behaviour showed no differences between the knock downs and controls.

A recent study developed a knock down which reduced the levels of lrrk2 by 50%, and showed a reduction in the numbers of dopaminergic neurons and moderate defects in body morphology (Prabhudesai et al., 2016). The knock down also upregulated other PD-associated genes and caused β-synuclein (see below) aggregates in the diencephalon, midbrain and hindbrain.

There is some evidence to suggest that loss of *lrrk2* function is associated with dopaminergic neuron loss, but results present too much variation to be definitive. Again, such findings highlight the variety of results from MO knock downs. A direct replication of Sheng et al. (2010) failed to achieve the same outcomes. Ren et al. (2011) suggested the recreation of the knock down using ZFNs; this or CRISPR would help to clarify the function of *lrrk2* in zebrafish.

2.6 Alpha-Synuclein

Lewy bodies made of insoluble α-synuclein aggregates are a feature of PD and are thought to be caused by the dysregulation of α-synuclein, which is produced by the gene *SNCA* (Spillantini et al., 1998). In addition to α-synuclein, mammals also have β- and γ-synucleins, each encoded by its own gene (Clayton and George, 1998). In zebrafish, there is no evidence of a gene encoding α-synuclein. This gene may have been lost over time because of the overlapping function between the other synucleins (Chen et al., 2009); zebrafish do possess β-synuclein and co-orthologues for γ-synuclein (γ_1 and γ_2), but only β and γ_1 are expressed in the CNS (Sun and Gitler, 2008).

An MO knock down of β- or γ_1-synuclein caused decreased motor activity; and knock down of both β and γ_1 caused delayed differentiation of dopaminergic neurons, reduced

TABLE 2 | Chemical-based zebrafish models of Parkinson's Disease.

Chemical	Adults/ Larvae	Studies	Results
MPTP	Adults/ Larvae	Bretaud et al. (2004), Lam et al. (2005), McKinley et al. (2005), Sallinen et al. (2009)	Loss of DNs in diencephalon, decreases in swimming responses
	Adults	Anichtchik et al. (2004)	Intracerebral/intramuscular injections cause locomotor defects and decreased dopamine levels
	Larvae	Wen et al. (2008)	GFP line to visualize TH-positive neurons. Loss of neurons in posterior and the hypothalamus
	Larvae	Dukes et al. (2016)	GFP line to visualize mitochondria in DNs. Reduction of mitochondrial transport
	Adults	Babu et al. (2016)	Injection. Increased synuclein, identified 73 proteins upregulated with MPTP exposure
6-OHDA	Adults	Anichtchik et al. (2004)	Intracerebral/intramuscular injections cause locomotor defects and decreased dopamine levels
	Larvae	Parng et al. (2007)	Reduction TH-positive neurons in hypothalamus, posterior tuberculum, ventral thalamus and pretectum
	Larvae	Feng et al. (2014)	Minocycline, Vitamin E and Sinemet can rescue locomotor defects
	Adults	Vijayanathan et al. (2017)	Decreased TH-positive neurons, decreased swim speed, spontaneous recovery by 30 dpf
Rotenone	Adults	Bretaud et al. (2004)	High doses: lethality, low doses: no morphological or locomotor defects
	Adults	Wang et al. (2017)	Decrease in DA and TH expression, behavioural abnormality, olfactory deficits
Paraquat	Adults	Bortolotto et al. (2014)	Injection. Learning and motor deficits, increase in DA
	Larvae	Nellore and Nandita, (2015)	Morphological defects, increased apoptosis
	Adults	Wang et al. (2016)	Upregulation of antioxidant genes
	Adults	Nunes et al. (2017)	Abnormal behaviour, increase in aggression
	Adults	Müller et al. (2018)	Injection. Learning and motor deficits, Sodium selenite diet prevents motor symptoms
	Larvae	Wang et al. (2018)	Locomotor defects, reduced mitochondrial activity
Titanium dioxide nanoparticles	Larvae	Hu et al. (2017)	Loss of DNs, increase PD-associated gene expression, increase in ROS

**DNs, Dopaminergic neurons DA - Dopamine TH, Tyrosine hydroxylase GFP, Green fluorescent protein ROS, reactive oxygen species.*

dopamine levels and impaired motor functions. Interestingly, expression of human α-synuclein can rescue this phenotype in zebrafish (Milanese et al., 2012).

Using a DNA plasmid, researchers created a zebrafish model that expresses large amounts of human α-synuclein, which resulted in high mortality rates but also α-synuclein aggregates and α-synuclein-induced apoptosis. This severe phenotype was greatly improved by the addition of CLR01, a "molecular tweezer" known to inhibit the assembly and toxicity of many amyloidogenic proteins (Prabhudesai et al., 2012).

Additionally when γ_1-synuclein was overexpressed, fish developed aggregates within neurons similar to those found within fish expressing human α-synuclein (O'Donnell et al., 2014; Lulla et al., 2016). Zebrafish larvae were exposed to ziram, a fungicide that increases α-synuclein expression in rat cells. The larvae showed neuronal aggregates and dopaminergic neuron toxicity, which could be prevented when treated with CLR01.

In summary, studies suggest that although zebrafish do not possess an α-synuclein orthologue, γ_1-synuclein may perform a comparable function to human α-synuclein, however more research is required to confirm this hypothesis. The human α-synuclein gene can be successfully expressed in zebrafish and causes aggregates within neurons. Studies also confirmed the successful use of CLR01, a potential PD therapy, in zebrafish.

3 CHEMICAL-BASED MODELS OF PARKINSON'S DISEASE

For a summary of these models refer to **Table 2**

3.1 MPTP

Administration of 1-methyl-4-phenyl-1,2,3,6-tetrahydropyridine (MPTP) has been a well-documented method of inducing dopaminergic neurodegeneration in a variety of animals (Dauer and Przedborski, 2003). The highly lipophilic MPTP crosses the blood brain barrier and is converted to the metabolite 1-methyl-4phenylpyridinium ion (MPP+) by monoamine oxidase B (Blandini and Armentero 2012). MPP+ has a high affinity for the dopamine transporter and is carried into the dopaminergic neurons of the substantia nigra where it

blocks mitochondrial Complex I activity (Blandini and Armentero, 2012). It produces Parkinsonian-like symptoms in humans; however, it does not create the Lewy body-like inclusions that are present in PD (Blandini and Armentero, 2012). Exposure of *C. elegans* to MPTP causes reduced movement and degeneration of dopaminergic neurons (Braungart et al., 2004). Similarly, MPTP exposure in *Drosophila* causes oxidative stress and inflammation as well as behavioural deficits (Abolaji et al., 2018; Aryal and Lee, 2019). Rats injected with MPTP do not develop Parkinsonian-like symptoms, for unknown reasons (Beal, 2001). To achieve dopaminergic depletion in mice, large doses of MPTP must be administered regularly. Injecting MPTP in conjunction with probenecid prevents the clearance of MPTP from the brain and kidneys, such that a chronic depletion of dopamine may be realised (Petroske et al., 2001; Meredith et al., 2008).

When exposed to MPTP, larval zebrafish exhibited a 39% loss of dopaminergic neurons in the ventral diencephalon (Lam et al., 2005; Kalyn et al., 2020). Both larval and adult zebrafish showed decreases in swimming responses after treatment with MPTP (Bretaud et al., 2004; Sallinen et al., 2009). Inhibition of monoamine oxidase B or the dopamine transporter mitigates the neuronal loss following administration of MPTP, which confirms the same mechanism of action as in mammals (Lam et al., 2005; McKinley et al., 2005).

A transgenic zebrafish, expressing green fluorescing protein (GFP) in neurons expressing vesicular monoamine transporter 2, was created to characterize the loss of TH-positive neurons within the context of all monoaminergic neurons present in the nervous system (Wen et al., 2008). They noted loss of TH-positive neurons in the posterior tuberculum of the ventral diencephalon and the hypothalamus following MPTP exposure. Another transgenic GFP line was developed to visualize the mitochondria of dopaminergic neurons (Dukes et al., 2016). After exposure to MPP+, there was a reduction of all mitochondrial transport, which likely plays a role in the dopaminergic neuron loss.

A study on adult zebrafish injected intraperitoneally with MPTP showed a decrease in swimming behaviour and increased "freezing," as a response to stress, but also increased γ_1-and γ_2-synuclein expression, which was visualized with an antibody against human α-synuclein (Babu et al., 2016). This study was mainly proteomic in nature and identified 73 proteins that demonstrated altered expression in the MPTP-induced state.

In summary, one of the most popular chemical models of PD, MPTP and its metabolite (MPP+) cause reliable dopaminergic neuron loss in both larval and adult zebrafish and the dosages for both are well established. Like most chemical models, this one does not cause Lewy body-like inclusions in the brain. The use of transgenic GFP lines make the characterization of neuron loss and intracellular activities easy to visualize *in vivo*. In addition, Babu et al. (2016) identified new, potential targets for study when they identified proteins that have altered expression after MPTP exposure.

3.2 6–Hydroxydopamine

The hydroxylated analogue of dopamine, 6-hydroxydopamine (6-OHDA), was used to create one of the first animal models of PD (Schober, 2004). It has a high affinity for the dopamine transporter, which carries 6-OHDA inside dopaminergic neurons where it accumulates and causes cell death (Blandini and Armentero, 2012). In mice and rats, administration of 6-OHDA caused reduction in dopaminergic neuron numbers and marked locomotor defects but no evidence of Lewy body-like inclusions (Schober, 2004; Stott and Barker, 2014). *C. elegans* exposed to 6-OHDA showed selective degeneration of dopaminergic neurons (Nass et al., 2002).

Intramuscular injections of 6-OHDA in zebrafish caused locomotor defects and decreased dopamine levels which indicate that 6-OHDA crosses the blood-brain barrier (BBB) more readily in zebrafish than in mammals (Murray et al., 1975; Anichtchik et al., 2004). When 6-OHDA was administered to larval zebrafish there was increased oxidation throughout the brain and a significant reduction in the number of TH-positive neurons in the diencephalon (hypothalamus, posterior tuberculum, ventral thalamus, and pretectum) (Parng et al., 2007). Another study of larval fish found that the antioxidant Vitamin E was able to rescue the locomotor defects and the decrease in TH expression caused by 6-OHDA exposure (Feng et al., 2014). They also found that the microglia inhibitor, minocycline, can reverse both locomotor defects and the expression of inflammatory genes in 6-OHDA-treated fish. Feng et al. (2014) also assessed a clinical PD treatment, Sinemet (a combination of L-dopa and carbidopa), and found that it can also rescue locomotor activity and reduced the expression of *pink1* and *parkin* in treated animals.

A more recent study injected 6-OHDA directly into the diencephalon and demonstrated both decreases in TH immunoreactive neurons and decreases in swim speed and distance travelled of the fish (Vijayanathan et al., 2017). Interestingly, animals showed recovery of the lost TH immunoreactive neurons 30 days after injection.

The effects of 6-OHDA have been well characterized in both adult and larval zebrafish, and although the toxin does not induce Lewy bodies found in PD, it seems to be a good model for screening therapeutic options for PD. There is a suggestion that 6-OHDA has greater effects on the brain of zebrafish than in rodents because of the ease with which it crosses the blood-brain barrier (Murray et al., 1975). Vijayanathan et al. (2017) found that the fish recover from 6-OHDA spontaneously. This may indicate that neurogenesis is occurring, which is common in zebrafish (Kizil et al., 2012).

3.3 Rotenone

Rotenone is widely used as both an insecticide and piscicide (fish toxin). It readily crosses the blood brain barrier and is a high-affinity inhibitor of Complex I of the mitochondrial ETC (Sherer et al., 2003; Bové et al., 2005). Humans exposed to high levels of rotenone are 2.5 times more likely to develop Parkinsonian-like symptoms than the general population (Innos and Hickey, 2021). In rats, rotenone exposure causes degradation of the nigrostriatal dopaminergic neurons and behavioural symptoms characteristic of PD (Sherer et al., 2003). The affected neurons possess intracellular inclusions that appear to be Lewy bodies, showing immunoreactivity for α-

synuclein and ubiquitin as with human Lewy bodies (Blesa and Przedborski, 2014). In *Drosophila* and *C. elegans*, rotenone causes locomotor deficits and loss of dopaminergic neurons (Coulom and Birman, 2004; Zhou et al., 2013). Chronic oral administration of rotenone to mice resulted in behavioural impairments and a significant loss of TH-positive neurons. In addition α-synuclein expression was increased in remaining neurons as the treatment progressed (Inden et al., 2011).

Exposure of larval zebrafish to rotenone at LD_{50} concentration (50 nM) resulted in moderate locomotor defects and 36% reduction in the amount dopaminergic neurons in the ventral diencephalon (Kalyn et al., 2020). A study of environmental neurotoxins found that high dosages of rotenone were lethal to adult zebrafish after a few days, and embryos exposed to high dosages expressed increased pigmentation and eventually death (Bretaud et al., 2004). However, lower doses caused no morphological or locomotor defects.

In another study, adult zebrafish administered rotenone (chronic exposure over 4 weeks) exhibited both motor and non-motor (cognitive) effects of PD which mirrors the effects of the Kalyn et al. (2020) study in larvae (Wang et al., 2017). This contradicts the findings of Bretaud et al. (2004), which showed no locomotor defects after 4 weeks of exposure to the same dosage of rotenone (2 μg/L). In the Wang et al. (2017) study, rotenone-treated fish showed a reduction in dopamine concentrations in the brain as well as a decrease in TH expression. They also exhibited a 70% reduction in swimming duration and distance travelled, which may be comparable to the bradykinesia observed in PD patients. In a light/dark box test, treated fish spent more time in the light and showed a longer latency to enter the dark component, which Wang et al. (2017) suggests indicates depression-like behaviour. Treated fish also showed a decreased affinity for amino acids, which may indicate a loss of olfactory function, a common symptom in PD (Ruan et al., 2012). This study also examined the expression of PD-related genes and found that in treated fish, *dj-1* was down-regulated by 60% and *lrrk2* was up-regulated. Other genes, *synuclein* (unspecified), *parkin* and *pink1* remained unchanged.

The chronic exposure of zebrafish to rotenone and the development of clinical and biochemical symptoms common to PD make this an interesting model to study the disease. There is some contention about dosage and reported symptoms. The role of rotenone as an aquatic pesticide means only small dosages can be used in any fish model. Rotenone also causes Lewy body-like inclusions in rodents, although it is unclear if that is the case in zebrafish.

3.4 Paraquat

Paraquat or N,N′-dimethyl-4-4′-bipiridinium is a widely used agricultural herbicide that subsequently becomes an aquatic contaminant due to run-off (Dinis-Oliveira et al., 2006). It is thought that paraquat impairs mitochondrial Complex I, leading to problems with the ETC and consequently the overproduction of ROS (Wang et al., 2018). It is very similar in structure to the MPTP metabolite MPP+ and also has specificity for the same dopamine transporter, and therefore it acts mainly on dopaminergic neurons (Manning-Bog et al., 2003; Bové et al., 2005). Like rotenone, humans exposed to high levels of paraquat, usually during the manufacture or use of the herbicide, develop Parkinsonian-like symptoms (Boyd et al., 2020). Chronic paraquat exposure in rats caused an increase in anxiety-like behaviour, a loss of olfactory function and a marked decrease in mitochondrial function (Czerniczyniec et al., 2011). In *Drosophila and C. elegans,* paraquat exposure caused severe locomotor deficits (Jahromi et al., 2015; Bora et al., 2021).

An early study of paraquat found that chronic water exposure did not cause any motor defects or changes in TH levels of adult or larval zebrafish (Bretaud et al., 2004). However, subsequent studies report that paraquat-exposed larval fish showed increased oxidative stress, upregulation of antioxidant genes and general apoptosis (Nellore and Nandita, 2015; Wang et al., 2016). Mitochondrial respiration was reduced by 70% in treated fish (Wang et al., 2018). At LD50 concentrations, paraquat did not cause locomotor defects but did cause a 16% reduction in the number of dopaminergic neurons in the ventral diencephalon of larval zebrafish (Kalyn et al., 2020).

However, adult zebrafish injected intraperitoneally with paraquat showed locomotor defects, increased "freezing" behaviour indicative of anxiety and increased aggression when presented with their own reflection (Nunes et al., 2017; Müller et al., 2018). The fish experienced some cognitive deficiencies, as they could not learn associations in a Y-maze as well as controls. There was no decrease in dopamine levels, but depending on the paraquat dosage, dopamine transporter (DAT) expression decreased (Bortolotto et al., 2014). Sodium selenite (Na_2SeO_3), an antioxidant, rescues some of the behavioural symptoms (Müller et al., 2018).

As with the other chemical models, there seems to be a disagreement with effective dosages to induce PD-like symptoms. Like rotenone, paraquat does not seem to cause Lewy body-like inclusions in zebrafish, but some of the later studies seem to have developed stable models to investigate the underlying mechanisms and potential therapeutic substances.

3.5 Titanium Dioxide Nanoparticles

Titanium dioxide nanoparticles are widely produced for various commercial applications. Unfortunately, they can also cause health issues due to environmental or workplace exposure (Shi et al., 2013). Large scale exposure of mice to titanium dioxide nanoparticles caused motor deficits and reduction of dopaminergic neurons in the midbrain substantia nigra (Heidari et al., 2019). When embryonic zebrafish were exposed to titanium dioxide nanoparticles from 0–96 hpf, the titanium accumulated in the brain, causing the generation of ROS and ultimately cell death in the hypothalamus. The nanoparticles also caused loss of dopaminergic neurons and increased the expression of *pink1* and *parkin* (Hu et al., 2017). This shows promise as a method of inducing a Parkinsonian-like state, and future work could confirm its validity.

4 CHEMOGENETIC ABLATIONS

These models are unique in that they employ a combination of genetic and chemical methods to achieve the ablation of specific

cells. The models discussed in this review use nitroreductase (NTR), a bacterial enzyme derived from *Escherichia coli*, which converts the antibiotic metronidazole into a cytotoxic metabolite (Curado et al., 2008). By creating a transgenic zebrafish line that expresses NTR under a specific promoter, metronidazole will only be converted into a toxin in those cells where NTR is present and when metronidazole is administered. This leads to spatially and temporally specific ablation of targeted cells (Pisharath and Parsons, 2009).

4.1 Cytotoxic Metabolite of Metronidazole

A study created a transgenic zebrafish expressing NTR fused to cyan fluorescent protein (CFP) under the control of the dopamine transporter (DAT), in the telencephalon, diencephalon, olfactory bulb and caudal hypothalamus (Godoy et al., 2015). Administration of the anti-bacterial pro-drug metronidazole at 1 dpf resulted in loss of DAT-expressing neurons at 5 dpf in addition to motor impairments. Some motor function was re-established by 7 dpf when there was evidence of new DAT-expressing cells; however, there was still a deficit at 14 dpf. A follow-up study in adult transgenic zebrafish found that a 24 h exposure to metronidazole resulted in significant loss of dopaminergic neurons in the olfactory bulb and a decrease in the ability to smell (Godoy et al., 2020). Another study has suggested that using a similar drug, ronidazole, can achieve comparable results at lower concentrations (Lai et al., 2021). The cytotoxic metabolites of these drugs appear to induce Parkinsonian-like symptoms, like other chemical models, and may provide a basis for understanding mechanisms underlying neuronal loss.

5 DISCUSSION

As discussed throughout this review zebrafish present numerous promising avenues for research. They generally possess the same genes as humans with comparable functions and most of the toxins mentioned produce similar outcomes. This provides an outstanding opportunity to study basic underlying mechanisms in a more tractable model than offer by traditional mammalian species. Advanced imaging techniques in conjunction with genetic manipulation make zebrafish a highly versatile model for researching PD. The specific aspects of each model were reviewed in detail in **Sections 2**, **3**, **4**. In this section, the strengths and weaknesses of models are discussed. For instance, many orthologues of PD-related genes have been identified in zebrafish and evidence suggests that fish can provide useful insights into both their normal functions and their roles in disease progression. However, the major issue with many of the gene-based models of PD is their current reliance on MO antisense oligonucleotides to create gene knock downs. It became evident during the evaluation of these models that there was great variation in findings between different studies, even when targeting the same gene. For example, three different knock downs of *pink1* had vastly different results (Anichtchik et al., 2008; Sallinen et al., 2010; Xi et al., 2010). In another case, a direct replication of an *lrrk2* knock down was unable to reproduce the same results, even when using the same methods (Ren et al., 2011). This lack of reproducibility obscures the function of these genes in zebrafish because it is unclear whether the knock downs have off target effects. It has been well-documented that MOs can often have severe off-target effects, and it is difficult to differentiate between specific and non-specific effects (Schulte-Merker and Stainier, 2014; Blum et al., 2015). Some researchers, therefore, suggest that MOs should not be used as a primary method of studying gene function (Kok et al., 2015), but others insist that they are still valuable if the proper controls are in place. Eisen and Smith (2008) outlined guidelines for using MOs appropriately and avoiding off-target effects. While some of the reviewed studies employed one or more of these techniques, few followed all of the recommended guidelines. Consequently, the relative accuracy of these studies cannot be directly compared, except in cases where they were employed alongside a strain made by another technique as accomplished by Flinn et al. (2013) (See **Section 2.3**). Otherwise, the accuracy of models that utilise MOs may be compromised. The CRISPR/Cas9 system however, shows immense promise for the creation of genetically altered zebrafish lines and this genomic editing technique presents an opportunity to create more accurate gene knock downs/ins, which may elucidate some of the gene functions that are unclear in other models. It also enables researchers to examine gene knock downs in adult animals, as MOs generally only work until the larvae is a few days old. The study by Edson et al. (2019), created a *dj-1* knock down with CRISPR that successfully grew to adulthood.

In addition to evaluating the methods of creating genetic models, a critical review of the literature must also consider the unique characteristics of zebrafish. A possibly problematic feature of zebrafish is their duplicated genome, when compared to mammals. As mentioned in the reviews of gene-based models, zebrafish may have one or two homologous genes corresponding to a single human gene (Lieschke and Currie, 2007). Unfortunately, there is no evidence of consistency in the duplicated gene functions. The doubled genes may have unrelated functions, or alternatively, they may have semi-overlapping functions, which may be exploited to provide insight into different aspects of the genes' functions by selectively knocking out one or the other (Newman et al., 2014).

Another feature of the zebrafish that sets it apart from mammals and that is relevant to both gene-based and chemically-induced models is the high level of post-embryonic neurogenesis that persists into adulthood in the fish. This is potentially problematic in studies of neuronal loss, as recovery from these states is very possible in zebrafish, unlike in mammals where recovery of neurons it is greatly limited (Kizil et al., 2012).

A further issue with current genetic models of PD in zebrafish is that PD is usually a disease of adults or older individuals. However, most of the models discussed in this review were performed on larvae, juvenile or young adult zebrafish. In fact, MOs are only effective when injected in the single cell stage and only function for a few days, therefore serious questions arise as to how well any such model can represent the disease as a whole (Eisen and Smith, 2008). With the advent of new genetic manipulation techniques mentioned above, it is possible to generate animals that express these PD phenotypes into

adulthood. Generally, housing animals into senescence can become expensive and add years to potential studies, however the cost can be mitigated with economical animals like zebrafish.

Another general problem with attempts to replicate PD in any animals is that they do not naturally develop the full array of symptoms associated with the disease in humans. The genetic models can elicit some of the features of PD, but they never precisely replicate it. The chemical models generally do not induce PD, but instead use different mechanisms to achieve similar phenotypes. These mechanisms do not necessarily represent all aspects of the disease accurately. For instance, most of the chemical models of PD successfully induce a Parkinsonian-like state in zebrafish with losses of dopaminergic neurons and some behavioural symptoms, but none of them recreate the Lewy body-like inclusions seen in humans with the disease.

A final common issue with the reviewed models is that there is very little replication of experiments. Compared to other medical models, zebrafish are relatively new on the scene. Therefore, many of these models have only been the subject of one or two studies to date, with the notable exception of a handful of well-established models induced by chemicals such as MPTP. In contrast, there are many transgenic mouse models of PD (Duty and Jenner, 2011; Sharma et al., 2017). In time, further replication of previous studies may serve to solidify the status of these models and provide a basis to develop more complex models.

Despite some of the issues that one must consider when developing a zebrafish model of PD, there are several distinct advantages. As mentioned above, zebrafish are relatively easy to manipulate genetically, and a wide variety of custom strains can be created to allow sophisticated imaging techniques to be performed. With the CRISPR/Cas9 system, gene knock downs can be achieved in adult animals to examine this typically adult disease in older fish. This genetic adaptability can also be applied in conjunction with other areas of research, such as behavioural screens and high-throughput screens.

5.1 Future Directions

5.1.1 Behavioural Screens

A practical method of assessing disease model effects on a normal phenotype is to examine changes in behaviour (Khan et al., 2017). For rodent models, there is a wide range of paradigms available to examine the effects of experimental treatment on behaviour, ranging from simple evaluation of locomotion to complex cognitive abilities like learning and memory (Sousa et al., 2006). Accordingly, rodent behavioural paradigms have been used extensively to study PD (Ameen-Ali et al., 2017; Vingill et al., 2018).

Zebrafish also possess a wide repertoire with many normal and abnormal behaviours catalogued (Kalueff et al., 2013). Zebrafish are inherently communal animals, living in shoals, so they display a wide variety of social behaviours. They also have well-documented expressions of fear and anxiety, and they can learn complex associations (Lieschke and Currie, 2007). Consequently, there have been many behavioural tests developed for zebrafish that are suitable for models of PD.

Several zebrafish paradigms are analogous to well established ones developed for rodents (Champagne et al., 2010). For instance, the novel tank test is an assessment of anxiety-like behaviour in zebrafish to a new stark environment and can be compared to the open-field test in rodents (Blaser and Rosemberg, 2012; Harro, 2018). There are also numerous paradigms that test cognitive behaviours, as the fish can rapidly learn associations using various unconditioned stimuli (Karnik and Gerlai, 2012). Zebrafish are highly visual animals and can differentiate between basic colours or patterns, but they can also form associations using olfactory or auditory stimuli (Colwill et al., 2005; Braubach et al., 2009; Avdesh et al., 2012; Doyle et al., 2017). Many common apparatuses used for studying cognitive behaviours in rodents have been adapted for zebrafish, including shuttle boxes, Y-mazes, T-mazes, and plus-mazes (Pather and Gerlai, 2009; Gerlai, 2010; Sison and Gerlai, 2010). Zebrafish training is highly reproducible and can therefore be automated and performed using groups of animals (Wyeth et al., 2011; Miller and Gerlai, 2012; Doyle et al., 2017). Commercially-available software offers three-dimensional, automated tracking of multiple fish simultaneously (Stewart et al., 2015).

Most of these learning paradigms are suitable for use with adult zebrafish; however, only the simplest behavioural assays are suitable for larvae (Colwill and Creton, 2011; Kalueff et al., 2013). Larvae can be examined for general behavioural abnormalities, but larvae under 5 dpf do not swim well (Lindsey et al., 2010). By 30 dpf, however, juvenile fish can perform in adult-appropriate paradigms (Kalueff et al., 2013; Merovitch, 2016).

In summary, many of the models reviewed in this study use some form of behavioural analysis to examine different aspects of PD. Several experiments use larvae, which limits the available behavioural analysis paradigms; however, the use of genetically altered zebrafish that can survive to adulthood in a disease-like state, presents the opportunity to examine disease models in older animals. Chemical-based models utilising adults are also viable and have been studied with behavioural paradigms, as reviewed in **Section 3**. Adult animals display more complex cognitive abilities than larvae, which may be studied to provide greater insight into the cognitive deficits seen in PD. However, while some paradigms can be used with groups of animals, none of the reviewed models utilised large-scale behavioural tests. Adaptation of some of these paradigms to use larger numbers of fish would allow rapid and efficient assessment of cognitive or behavioural defects induced in the disease models.

5.1.2 High-Throughput Screening

One of the most touted benefits of the zebrafish is their suitability for high-throughput screening (Gerlai, 2010). Rodents are expensive and relatively large, which makes them less practical to use in drug screens. High throughput screens with *C. elegans* and *Drosophila* also exist, but as invertebrates, they are less similar to humans. These species also possess tough cuticles, which may present barriers to the diffusion of drugs (Wells, 1998; Manev et al., 2003). By contrast, chemicals can enter the larval zebrafish by diffusion from the surrounding water (Langheinrich, 2003). Dissolving chemicals into water is simpler and quicker

than injecting each animal (Parng et al., 2002). Moreover, larval zebrafish are quite small and can subsist in only 200 µl of water, so they fit efficiently in a 96-well plate, and only small amounts of test chemicals are needed (Best and Alderton, 2008). Often, larval zebrafish can be dosed with microliters of solution, compared to milliliters that may be required for rodents. This allows a greater number of animals to be tested with the same quantity of drugs (Parng et al., 2002). However, the aquatic environment does present some challenges. The precise delivery of some chemicals in water can be problematic. There may be some difficulty determining dosage, and chemicals may not be soluble in water, although this can often be remedied via solvents (i.e. dimethyl sulfoxide) (Rubinstein, 2003; Maes et al., 2012).

A further advantage is that the characterization of drug effects can be much simpler in larval zebrafish than in rodents (Parng et al., 2002). As previously mentioned, their transparent bodies, combined with the availability of numerous fluorescent reporters, make target areas or cell types relatively easy to visualize (Vaz et al., 2018). Each zebrafish larva can be tracked, and commercial systems are available to facilitate automated tracking (Stewart et al., 2015). The zebrafish has therefore shown promise as a subject for high throughput screening of potential disease treatments or discovery of novel compounds (Langheinrich, 2003; Bowman and Zon, 2010; Stewart et al., 2014; Vaz et al., 2018). Many of the gene knock downs mentioned in this review created altered phenotypes; high-throughput screening of drugs may be used to readily identify treatments that rescue these phenotypes.

There are, however, limitations to these high-throughput screens. Although this review found several cases of human drugs having the same function in zebrafish, physiological differences mean that some drugs that are effective on zebrafish may not work on humans (Bowman and Zon, 2010). Even in cases where drugs have the same function on the molecular level, they may interact differently within the context of human physiology (Van Dam and De Deyn, 2011). Most screens utilise chemical libraries of previously approved drugs, with the goal of finding new therapeutic applications for old drugs (North et al., 2007; Hao et al., 2010). These drugs have already been deemed safe for human use, so approval depends exclusively on effectiveness, thus streamlining the process. Larval zebrafish are well suited for these large-scale drug screens, but with the development of new genetically altered strains, there are increasing numbers of gene knock outs in adult fish that can be investigated (Kalueff et al., 2014). There have recently been increased efforts to develop large scale testing of adult fish. While adult fish do not have the same advantages as larvae in terms of water requirements, they do present opportunities for different types of behavioural screening.

As discussed in **Section 5.1.1**, several of the common behavioural paradigms are easily adaptable to accommodate large numbers of fish. One study presents a high volume study to identify fluorophores in adult zebrafish (Blackburn et al., 2011). This was performed in normally pigmented fish, but there are also strains of mutant zebrafish (e.g. CASPER) that remain transparent into adulthood, which would facilitate the visualization of fluorescence (White et al., 2008). The intersecting developments in genomic editing, high-throughput screening and behavioural screening collectively represent fertile ground for future research into zebrafish disease models of PD.

6 CONCLUSION

No animal model can perfectly mimic human disease, especially highly complex neurodegenerative diseases such as PD. However, the use of multiple animal models can mitigate their limitations. For such a nascent model organism, there is a surprising array of zebrafish models that investigate various aspects of PD.

Gene-based studies have established that zebrafish possess genes to that are homologous to human PD genes, and they generally serve similar functions. However, gene-based models that rely on MOs tend to show conflicting results, which detract from their value. Their use should follow strict guidelines to ensure repeatability, but off-target effects remain problematic regardless. Alternatively, new methods of genomic editing such as CRISPR show immense promise for more consistent generation of gene knock outs/ins. Whatever the method, researchers must account for the duplication within the zebrafish genome, which in some cases may even present promising avenues for future research.

Chemical methods can readily induce disease-like states but do not accurately model all aspects of the disease. There are several well-established chemically induced models of PD, which provide stable bases for study; and newer methods show great potential but are not currently as well studied. Zebrafish models typically show the same effects as the mammalian models when exposed to the same chemicals, indicating the validity of zebrafish for this application.

As a relatively new model organism, the zebrafish initially lacked the well-established body of research that surrounds some other animals, but with the advent of new genomic editing technology and the development of advanced imaging techniques zebrafish are swiftly becoming a highly favoured model. With the array of behavioural paradigms and high-throughput screens available, the zebrafish as a disease model is on the threshold of new discoveries.

AUTHOR CONTRIBUTIONS

JD wrote majority of manuscript. RC co-authored and edited.

FUNDING

Funding was provided by a Discovery Grant (38863) from the Natural Sciences and Engineering Research Council of Canada (NSERC) to RC. JD was supported by scholarships from NSERC and Dalhousie University.

ACKNOWLEDGMENTS

The authors would like to thank for Drs. Alan Fine, George Robertson, Alex Quinn and Richard Brown for their feedback on earlier drafts. Special thanks to Anthony Edmonds for additional proofreading of multiple versions of this article. We would also like to thank the two reviewers for their detailed and constructive comments on an earlier version of this article.

REFERENCES

Abolaji, A. O., Adedara, A. O., Adie, M. A., Vicente-Crespo, M., and Farombi, E. O. (2018). Resveratrol Prolongs Lifespan and Improves 1-Methyl-4-Phenyl-1,2,3,6-Tetrahydropyridine-Induced Oxidative Damage and Behavioural Deficits in *Drosophila melanogaster*. *Biochem. Biophys. Res. Commun.* 503, 1042–1048. doi:10.1016/j.bbrc.2018.06.114

Ameen-Ali, K. E., Wharton, S. B., Simpson, J. E., Heath, P. R., Sharp, P., and Berwick, J. (2017). Review: Neuropathology and Behavioural Features of Transgenic Murine Models of Alzheimer's Disease. *Neuropathol. Appl. Neurobiol.* 43, 553–570. doi:10.1111/nan.12440

Amsterdam, A., and Hopkins, N. (2006). Mutagenesis Strategies in Zebrafish for Identifying Genes Involved in Development and Disease. *Trends Genet.* 22, 473–478. doi:10.1016/j.tig.2006.06.011

Andres-Mateos, E., Mejias, R., Sasaki, M., Li, X., Lin, B. M., and Biskup, S. (2009). Unexpected Lack of Hypersensitivity in LRRK2 Knock-Out Mice to MPTP (1-Methyl-4-Phenyl-1,2,3,6-Tetrahydropyridine). *J. Neurosci.* 29, 15846–15850. doi:10.1523/JNEUROSCI.4357-09.2009

Anichtchik, O., Diekmann, H., Fleming, A., Roach, A., Goldsmith, P., and Rubinsztein, D. C. (2008). Loss of PINK1 Function Affects Development and Results in Neurodegeneration in Zebrafish. *J. Neurosci.* 28, 8199–8207. doi:10.1523/JNEUROSCI.0979-08.2008

Anichtchik, O. V., Kaslin, J., Peitsaro, N., Scheinin, M., and Panula, P. (2004). Neurochemical and Behavioural Changes in Zebrafish *Danio rerio* after Systemic Administration of 6-hydroxydopamine and 1-Methyl-4-Phenyl-1,2,3,6-Tetrahydropyridine. *J. Neurochem.* 88, 443–453. doi:10.1111/j.1471-4159.2004.02190.x

Aryal, B., and Lee, Y. (2019). Disease Model Organism for Parkinson Disease: *Drosophila melanogaster*. *BMB Rep.* 52, 250–258. doi:10.5483/BMBRep.2019.52.4.204

Avdesh, A., Martin-Iverson, M. T., Mondal, A., Chen, M., Askraba, S., Morgan, N., et al. (2012). Evaluation of Color Preference in Zebrafish for Learning and Memory. *J. Alzheimer's Dis.* 28, 459–469. doi:10.3233/JAD-2011-110704

Babin, P. J., Goizet, C., and Raldúa, D. (2014). Zebrafish Models of Human Motor Neuron Diseases: Advantages and Limitations. *Prog. Neurobiol.* 118, 36–58. doi:10.1016/j.pneurobio.2014.03.001

Babu, N. S., Murthy, C. L. N., Kakara, S., Sharma, R., Brahmendra Swamy, C. V., and Idris, M. M. (2016). 1-Methyl-4-phenyl-1,2,3,6-tetrahydropyridine Induced Parkinson's Disease in Zebrafish. *Proteomics* 16, 1407–1420. doi:10.1002/pmic.201500291

Bai, Q., Mullett, S. J., Garver, J. A., Hinkle, D. A., and Burton, E. A. (2006). Zebrafish DJ-1 Is Evolutionarily Conserved and Expressed in Dopaminergic Neurons. *Brain Res.* 1113, 33–44. doi:10.1016/j.brainres.2006.07.057

Baulac, S., Lu, H., Strahle, J., Yang, T., Goldberg, M. S., Shen, J., et al. (2009). Increased DJ-1 Expression under Oxidative Stress and in Alzheimer's Disease Brains. *Mol. Neurodegener.* 4, 12. doi:10.1186/1750-1326-4-12

Beal, M. F. (2001). Experimental Models of Parkinson's Disease. *Nat. Rev. Neurosci.* 2, 325–332. doi:10.1038/35072550

Best, J. D., and Alderton, W. K. (2008). Zebrafish: An *In Vivo* Model for the Study of Neurological Diseases. *Neuropsychiatr. Dis. Treat.* 4, 567–576. doi:10.1006/dbio.2001.020110.2147/ndt.s2056

Bhat, A. H., Dar, K. B., Anees, S., Zargar, M. A., Masood, A., Sofi, M. A., et al. (2015). Oxidative Stress, Mitochondrial Dysfunction and Neurodegenerative Diseases; a Mechanistic Insight. *Biomed. Pharmacother.* 74, 101–110. doi:10.1016/j.biopha.2015.07.025

Bill, B. R., Petzold, A. M., Clark, K. J., Schimmenti, L. A., and Ekker, S. C. (2009). A Primer for Morpholino Use in Zebrafish. *Zebrafish* 6, 69–77. doi:10.1089/zeb.2008.0555

Blackburn, J. S., Liu, S., Raimondi, A. R., Ignatius, M. S., Salthouse, C. D., and Langenau, D. M. (2011). High-throughput Imaging of Adult Fluorescent Zebrafish with an LED Fluorescence Macroscope. *Nat. Protoc.* 6, 229–241. doi:10.1038/nprot.2010.170

Blandini, F., and Armentero, M.-T. (2012). Animal Models of Parkinson's Disease. *FEBS J.* 279, 1156–1166. doi:10.1111/j.1742-4658.2012.08491.x

Blaser, R. E., and Rosemberg, D. B. (2012). Measures of Anxiety in Zebrafish (*Danio rerio*): Dissociation of Black/White Preference and Novel Tank Test. *PLoS One* 7, e36931. doi:10.1371/journal.pone.0036931

Blesa, J., and Przedborski, S. (2014). Parkinson's Disease: Animal Models and Dopaminergic Cell Vulnerability. *Front. Neuroanat.* 8, 155. doi:10.3389/fnana.2014.00155

Block, M. L., Zecca, L., and Hong, J. S. (2007). Microglia-mediated Neurotoxicity: Uncovering the Molecular Mechanisms. *Nat. Rev. Neurosci.* 8, 57–69. doi:10.1038/nrn2038

Blum, M., De Robertis, E. M., Wallingford, J. B., and Niehrs, C. (2015). Morpholinos: Antisense and Sensibility. *Dev. Cel.* 35, 145–149. doi:10.1016/j.devcel.2015.09.017

Bora, S., Vardhan, G. S. H., Deka, N., Khataniar, L., Gogoi, D., and Baruah, A. (2021). Paraquat Exposure over Generation Affects Lifespan and Reproduction through Mitochondrial Disruption in *C. elegans*. *Toxicology* 447, 152632. doi:10.1016/j.tox.2020.152632

Bortolotto, J. W., Cognato, G. P., Christoff, R. R., Roesler, L. N., Leite, C. E., Kist, L. W., et al. (2014). Long-Term Exposure to Paraquat Alters Behavioral Parameters and Dopamine Levels in Adult Zebrafish (Danio Rerio). *Zebrafish* 11, 142–153. doi:10.1089/zeb.2013.0923

Bové, J., Prou, D., Perier, C., and Przedborski, S. (2005). Toxin-Induced Models of Parkinson ' S Disease. *Am. Soc. Exp. Neurother.* 2, 484–494. doi:10.4061/2011/52064010.1602/neurorx.2.3.484

Bowman, T. V., and Zon, L. I. (2010). Swimming into the Future of Drug Discovery: *In Vivo* Chemical Screens in Zebrafish. *ACS Chem. Biol.* 5, 159–161. doi:10.1021/cb100029t

Boyd, W. A., Blain, R. B., Skuce, C. R., Thayer, K. A., and Rooney, A. A. (2020). NTP Research Report on the Scoping Review of Paraquat Dichloride Exposure and Parkinson's Disease. Research Triangle Park, NC: National Toxicology Program. Research Report 16. doi:10.22427/NTP-RR-16

Braak, H., and Braak, E. (2000). Pathoanatomy of Parkinson's Disease. *J. Neurol.* 247 Suppl 2, 3–10. doi:10.1007/pl00007758

Braubach, O., Wood, H., Gadbois, S., Fine, A., and Croll, R. P. (2009). Olfactory Conditioning in the Zebrafish. *Behav. Brain* 18, 9977–9988. Available at: http://www.sciencedirect.com/science/article/pii/S0166432808006049 (Accessed September 24, 2015). doi:10.1016/j.bbr.2008.10.044

Braungart, E., Gerlach, M., Riederer, P., Baumeister, R., and Hoener, M. C. (2004). *Caenorhabditis elegans* MPP+ Model of Parkinson's Disease for High-Throughput Drug Screenings. *Neurodegener. Dis.* 1, 175–183. doi:10.1159/000080983

Bretaud, S., Lee, S., and Guo, S. (2004). Sensitivity of Zebrafish to Environmental Toxins Implicated in Parkinson's Disease. *Neurotoxicol Teratol.* 26, 857–864. doi:10.1016/j.ntt.2004.06.014

Caramillo, E. M., and Echevarria, D. J. (2017). Alzheimer's Disease in the Zebrafish: Where Can We Take it? *Behav. Pharmacol.* 28, 179–186. doi:10.1097/FBP.0000000000000284

Carroll, D. (2011). Genome Engineering with Zinc-finger Nucleases. *Genetics* 188, 773–782. doi:10.1534/genetics.111.131433

Champagne, D. L., Hoefnagels, C. C. M., de Kloet, R. E., and Richardson, M. K. (2010). Translating Rodent Behavioral Repertoire to Zebrafish (*Danio rerio*): Relevance for Stress Research. *Behav. Brain Res.* 214, 332–342. doi:10.1016/J.BBR.2010.06.001

Chen, Y.-C., Cheng, C.-H., Chen, G.-D., Hung, C.-C., Yang, C.-H., Hwang, S.-P. L., et al. (2009). Recapitulation of Zebrafish *Sncga* Expression Pattern and Labeling the Habenular Complex in Transgenic Zebrafish Using green Fluorescent Protein Reporter Gene. *Dev. Dyn.* 238, 746–754. doi:10.1002/dvdy.21877

Clark, K. J., Urban, M. D., Skuster, K. J., and Ekker, S. C. (2011). "Transgenic Zebrafish Using Transposable Elements," in *Methods in Cell Biology* (Academic Press), 137–149. doi:10.1016/B978-0-12-374814-0.00008-2

Clayton, D. F., and George, J. M. (1998). The Synucleins: A Family of Proteins Involved in Synaptic Function, Plasticity, Neurodegeneration and Disease. *Trends Neurosci.* 21, 249–254. doi:10.1016/S0166-2236(97)01213-7

Colwill, R. M., and Creton, R. (2011). Imaging Escape and Avoidance Behavior in Zebrafish Larvae. *Rev. Neurosci.* 22, 63–73. doi:10.1515/RNS.2011.008

Colwill, R. M., Raymond, M. P., Ferreira, L., and Escudero, H. (2005). Visual Discrimination Learning in Zebrafish (*Danio rerio*). *Behav. Process.* 70, 19–31. doi:10.1016/j.beproc.2005.03.001

Cookson, M. R. (2005). The Biochemistry of Parkinson's Diease. *Annu. Rev. Biochem.* 74, 29–52. doi:10.1146/annurev.biochem.74.082803.133400

Cools, R. (2006). Dopaminergic Modulation of Cognitive Function-Implications for L-DOPA Treatment in Parkinson's Disease. *Neurosci. Biobehav. Rev.* 30, 1–23. doi:10.1016/j.neubiorev.2005.03.024

Coulom, H., and Birman, S. (2004). Chronic Exposure to Rotenone Models Sporadic Parkinson's Disease in *Drosophila melanogaster*. *J. Neurosci.* 24, 10993–10998. doi:10.1523/JNEUROSCI.2993-04.2004

Cuervo, A. M., Stafanis, L., Fredenburg, R., Lansbury, P. T., and Sulzer, D. (2004). Impaired Degradation of Mutant α-synuclein by Chaperone-Mediated Autophagy. *Science* 305, 1292–1295. doi:10.1126/science.1101738

Cuoghi, B., and Mola, L. (2007). Microglia of Teleosts: Facing a challenge in Neurobiology. *Eur. J. Histochem.* 51, 231–239. Available at: https://search-proquest-com.ezproxy.library.dal.ca/docview/876292801?accountid=10406 (Accessed November 21, 2018).

Curado, S., Stainier, D. Y. R., and Anderson, R. M. (2008). Nitroreductase-mediated Cell/tissue Ablation in Zebrafish: A Spatially and Temporally Controlled Ablation Method with Applications in Developmental and Regeneration Studies. *Nat. Protoc.* 3, 948–954. doi:10.1038/nprot.2008.58

Czerniczyniec, A., Karadayian, A. G., Bustamante, J., Cutrera, R. A., and Lores-Arnaiz, S. (2011). Paraquat Induces Behavioral Changes and Cortical and Striatal Mitochondrial Dysfunction. *Free Radic. Biol. Med.* 51, 1428–1436. doi:10.1016/j.freeradbiomed.2011.06.034

Dauer, W., and Przedborski, S. (2003). Parkinson's Disease: Mechanisms and Models. *Neuron* 39, 889–909. doi:10.1016/S0896-6273(03)00568-3

Davie, C. A. (2008). A Review of Parkinson's Disease. *Br. Med. Bull.* 86, 109–127. doi:10.1093/bmb/ldn013

Dawson, T. M., Ko, H. S., and Dawson, V. L. (2010). Genetic Animal Models of Parkinson's Disease. *Neuron* 66, 646–661. doi:10.1016/j.neuron.2010.04.034

Di Maio, R., Barrett, P. J., Hoffman, E. K., Barrett, C. W., Zharikov, A., Borah, A., et al. (2016). α-Synuclein Binds to TOM20 and Inhibits Mitochondrial Protein Import in Parkinson's Disease. *Sci. Transl. Med.* 8, 1–14. doi:10.1126/scitranslmed.aaf3634

Dinis-Oliveira, R. J., Remião, F., Carmo, H., Duarte, J. A., Navarro, A. S., Bastos, M. L., et al. (2006). Paraquat Exposure as an Etiological Factor of Parkinson's Disease. *Neurotoxicology* 27, 1110–1122. doi:10.1016/j.neuro.2006.05.012

Dorsey, E. R., and Bloem, B. R. (2018). The Parkinson Pandemic - A Call to Action. *JAMA Neurol.* 75, 9–10. doi:10.1001/jamaneurol.2017.3299

Dorsey, E. R., Elbaz, A., Nichols, E., Abbasi, N., Abd-Allah, F., Abdelalim, A., et al. (2018). Global, Regional, and National burden of Parkinson's Disease, 1990-2016: a Systematic Analysis for the Global Burden of Disease Study 2016. *Lancet Neurol.* 17, 939–953. Available at: https://reader.elsevier.com/reader/sd/pii/S1474442218302953?token=C9BAB5F81C9DD1A6ACDB128C3A758458FB57E5785E4650740DFBC5240CBE09BEE25A6C91D1206FDCD461E8153CC0DAA1&originRegion=us-east-1&originCreation=20220119215452 (Accessed January 19, 2022). doi:10.1016/S1474-4422(18)30295-3

Doyle, J. M., Merovitch, N., Wyeth, R. C., Stoyek, M. R., Schmidt, M., Wilfart, F., et al. (2017). A Simple Automated System for Appetitive Conditioning of Zebrafish in Their home Tanks. *Behav. Brain Res.* 317, 444–452. doi:10.1016/j.bbr.2016.09.044

Driever, W., Solnica-Krezel, L., Schier, A. F., Neuhauss, S. C. F., Malicki, J., Stemple, D. L., et al. (1996). A Genetic Screen for Mutations Affecting Embryogenesis in Zebrafish. *Development* 123, 37–46. doi:10.1242/DEV.123.1.37

Dukes, A. A., Bai, Q., Van Laar, V. S., Zhou, Y., Ilin, V., David, C. N., et al. (2016). Live Imaging of Mitochondrial Dynamics in CNS Dopaminergic Neurons *In Vivo* Demonstrates Early Reversal of Mitochondrial Transport Following MPP+exposure. *Neurobiol. Dis.* 95, 238–249. doi:10.1016/j.nbd.2016.07.020

Durcan, T. M., and Fon, E. A. (2015). The Three 'P's of Mitophagy: PARKIN, PINK1, and post-translational Modifications. *GENES Dev.* 29, 989–999. Available at: http://genesdev.cshlp.org/content/29/10/989.short (Accessed October 18, 2018). doi:10.1101/gad.262758.115

Duty, S., and Jenner, P. (2011). Animal Models of Parkinson's Disease: A Source of Novel Treatments and Clues to the Cause of the Disease. *Br. J. Pharmacol.* 164, 1357–1391. doi:10.1111/j.1476-5381.2011.01426.x

Edson, A. J., Hushagen, H. A., Frøyset, A. K., Elda, I., Khan, E. A., Di Stefano, A., et al. (2019). Dysregulation in the Brain Protein Profile of Zebrafish Lacking the Parkinson's Disease-Related Protein DJ-1. *Mol. Neurobiol.* 56, 8306–8322. doi:10.1007/S12035-019-01667-W/FIGURES/6

Eisen, J. S., and Smith, J. C. (2008). Controlling Morpholino Experiments: Don't Stop Making Antisense. *Development* 135, 1735–1743. doi:10.1242/dev.001115

Exner, N., Treske, B., Paquet, D., Holmström, K., Schiesling, C., Gispert, S., et al. (2007). Loss-of-function of Human PINK1 Results in Mitochondrial Pathology and Can Be Rescued by Parkin. *J. Neurosci.* 27, 12413–12418. doi:10.1523/JNEUROSCI.0719-07.2007

Feng, C.-W., Wen, Z.-H., Huang, S.-Y., Hung, H.-C., Chen, C.-H., Yang, S.-N., et al. (2014). Effects of 6-Hydroxydopamine Exposure on Motor Activity and Biochemical Expression in Zebrafish (Danio Rerio) Larvae. *Zebrafish* 11, 227–239. doi:10.1089/zeb.2013.0950

Fett, M. E., Pilsl, A., Paquet, D., van Bebber, F., Haass, C., Tatzelt, J., et al. (2010). Parkin Is Protective against Proteotoxic Stress in a Transgenic Zebrafish Model. *PLoS One* 5. doi:10.1371/journal.pone.0011783

Flinn, L. J., Keatinge, M., Bretaud, S., Mortiboys, H., Matsui, H., De Felice, E., et al. (2013). TigarB Causes Mitochondrial Dysfunction and Neuronal Loss in PINK1 Deficiency. *Ann. Neurol.* 74, 837–847. doi:10.1002/ana.23999

Flinn, L., Mortiboys, H., Volkmann, K., Kster, R. W., Ingham, P. W., and Bandmann, O. (2009). Complex I Deficiency and Dopaminergic Neuronal Cell Loss in Parkin-Deficient Zebrafish (*Danio rerio*). *Brain* 132, 1613–1623. doi:10.1093/brain/awp108

Fontana, B. D., Mezzomo, N. J., Kalueff, A. V., and Rosemberg, D. B. (2018). The Developing Utility of Zebrafish Models of Neurological and Neuropsychiatric Disorders: A Critical Review. *Exp. Neurol.* 299, 157–171. doi:10.1016/J.EXPNEUROL.2017.10.004

Gerlai, R. (2010). High-throughput Behavioral Screens: The First Step towards Finding Genes Involved in Vertebrate Brain Function Using Zebrafish. *Molecules* 15, 2609–2622. doi:10.3390/molecules15042609

Godoy, R., Hua, K., Kalyn, M., Cusson, V. M., Anisman, H., and Ekker, M. (2020). Dopaminergic Neurons Regenerate Following Chemogenetic Ablation in the Olfactory Bulb of Adult Zebrafish (*Danio rerio*). *Sci. Rep.* 10, 12825. doi:10.1038/s41598-020-69734-0

Godoy, R., Noble, S., Yoon, K., Anisman, H., and Ekker, M. (2015). Chemogenetic Ablation of Dopaminergic Neurons Leads to Transient Locomotor Impairments in Zebrafish Larvae. *J. Neurochem.* 135, 249–260. doi:10.1111/jnc.13214

Greene, J. C., Whitworth, A. J., Kuo, I., Andrews, L. A., Feany, M. B., and Pallanck, L. J. (2003). Mitochondrial Pathology and Apoptotic Muscle Degeneration in Drosophila Parkin Mutants. *Proc. Natl. Acad. Sci.* 100, 4078–4083. doi:10.1073/pnas.0737556100

Halpern, M. E., Rhee, J., Goll, M. G., Akitake, C. M., Parsons, M., and Leach, S. D. (2008). Gal4/UAS Transgenic Tools and Their Application to Zebrafish. *Zebrafish* 5, 97–110. doi:10.1089/zeb.2008.0530

Hang, L., Thundyil, J., and Lim, K. L. (2015). Mitochondrial Dysfunction and Parkinson Disease: a Parkin–AMPK alliance in Neuroprotection. *Ann. N. Y. Acad. Sci.* 1350, 37–47. doi:10.1111/nyas.12820

Hao, J., Ho, J. N., Lewis, J. A., Karim, K. A., Daniels, R. N., Gentry, P. R., et al. (2010). *In Vivo* structure - Activity Relationship Study of Dorsomorphin Analogues Identifies Selective VEGF and BMP Inhibitors. *ACS Chem. Biol.* 5, 245–253. doi:10.1021/cb9002865

Hargis, K. E., and Blalock, E. M. (2017). Transcriptional Signatures of Brain Aging and Alzheimer's Disease: What Are Our Rodent Models Telling Us? *Behav. Brain Res.* 322, 311–328. doi:10.1016/J.BBR.2016.05.007

Harro, J. (2018). Animals, Anxiety, and Anxiety Disorders: How to Measure Anxiety in Rodents and Why. *Behav. Brain Res.* 352, 81–93. doi:10.1016/J.BBR.2017.10.016

Hastings, T. G. (2009). The Role of Dopamine Oxidation in Mitochondrial Dysfunction: Implications for Parkinson's Disease. *J. Bioenerg. Biomembr.* 41, 469–472. doi:10.1007/S10863-009-9257-Z

Heidari, Z., Mohammadipour, A., Haeri, P., and Ebrahimzadeh-Bideskan, A. (2019). The Effect of Titanium Dioxide Nanoparticles on Mice Midbrain Substantia Nigra. *Iranj. Basic Med. Sci.* 22, 745–751. doi:10.22038/ijbms.2019.33611.8018

Hillman, E. M. C., Voleti, V., Li, W., and Yu, H. (2019). Light-Sheet Microscopy in Neuroscience. *Annu. Rev. Neurosci.* 42, 295–313. doi:10.1146/annurev-neuro-070918-050357

Howe, D. G., Bradford, Y. M., Eagle, A., Fashena, D., Frazer, K., Kalita, P., et al. (2017). The Zebrafish Model Organism Database: New Support for Human Disease Models, Mutation Details, Gene Expression Phenotypes and Searching. *Nucleic Acids Res.* 45, D758–D768. doi:10.1093/nar/gkw1116

Hruscha, A., Krawitz, P., Rechenberg, A., Heinrich, V., Hecht, J., Haass, C., et al. (2013). Efficient CRISPR/Cas9 Genome Editing with Low Off-Target Effects in Zebrafish. *Development* 140, 4982–4987. doi:10.1242/dev.099085

Hu, Q., Guo, F., Zhao, F., and Fu, Z. (2017). Effects of Titanium Dioxide Nanoparticles Exposure on Parkinsonism in Zebrafish Larvae and PC12. *Chemosphere* 173, 373–379. doi:10.1016/j.chemosphere.2017.01.063

Inden, M., Kitamura, Y., Abe, M., Tamaki, A., Takata, K., and Taniguchi, T. (2011). Parkinsonian Rotenone Mouse Model: Reevaluation of Long-Term Administration of Rotenone in C57BL/6 Mice. *Biol. Pharm. Bull.* 34, 92–96. doi:10.1248/bpb.34.92

Innos, J., and Hickey, M. A. (2021). Using Rotenone to Model Parkinson's Disease in Mice: A Review of the Role of Pharmacokinetics. *Chem. Res. Toxicol.* 34, 1223–1239. doi:10.1021/ACS.CHEMRESTOX.0C00522

Jahromi, S. R., Haddadi, M., Shivanandappa, T., and Ramesh, S. R. (2015). Attenuation of Neuromotor Deficits by Natural Antioxidants of Decalepis Hamiltonii in Transgenic Drosophila Model of Parkinson's Disease. *Neuroscience* 293, 136–150. doi:10.1016/j.neuroscience.2015.02.048

Joung, J. K., and Sander, J. D. (2013). TALENs: A Widely Applicable Technology for Targeted Genome Editing. *Nat. Rev. Mol. Cel. Biol.* 14, 49–55. doi:10.1038/nrm3486

Jucker, M. (2010). The Benefits and Limitations of Animal Models for Translational Research in Neurodegenerative Diseases. *Nat. Med.* 16, 1210–1214. doi:10.1038/nm.2224

Kalueff, A. V., Gebhardt, M., Stewart, A. M., Cachat, J. M., Brimmer, M., Chawla, J. S., et al. (2013). Towards a Comprehensive Catalog of Zebrafish Behavior 1.0 and beyond. *Zebrafish* 10, 70–86. doi:10.1089/zeb.2012.0861

Kalueff, A. V., Echevarria, D. J., and Stewart, A. M. (2014). Gaining Translational Momentum: More Zebrafish Models for Neuroscience Research. *Prog. Neuropsychopharmacology Biol. Psychiatry* 55, 1–6. doi:10.1016/J.PNPBP.2014.01.022

Kalyn, M., Hua, K., Noor, S. M., Wong, C. E. D., and Ekker, M. (2020). Comprehensive Analysis of Neurotoxin-Induced Ablation of Dopaminergic Neurons in Zebrafish Larvae. *Biomedicines* 8, 1. doi:10.3390/biomedicines8010001

Karnik, I., and Gerlai, R. (2012). Can Zebrafish Learn Spatial Tasks? an Empirical Analysis of Place and Single CS-US Associative Learning. *Behav. Brain Res.* 233, 415–421. doi:10.1016/j.bbr.2012.05.024

Kawakami, K. (2007). Tol2: a Versatile Gene Transfer Vector in Vertebrates. *Genome Biol.* 8 (Suppl. 1), S7. doi:10.1186/gb-2007-8-s1-s7

Khan, K. M., Collier, A. D., Meshalkina, D. A., Kysil, E. V., Khatsko, S. L., Kolesnikova, T., et al. (2017). Zebrafish Models in Neuropsychopharmacology and CNS Drug Discovery. *Br. J. Pharmacol.* 174, 1925–1944. doi:10.1111/bph.13754

Kim, R. H., Smith, P. D., Aleyasin, H., Hayley, S., Mount, M. P., Pownall, S., et al. (2005). Hypersensitivity of DJ-1-Deficient Mice to 1-Methyl-4-Phenyl-1,2,3,6-Tetrahydropyrindine (MPTP) and Oxidative Stress. *Proc. Natl. Acad. Sci.* 102, 5215–5220. doi:10.1073/pnas.0501282102

Kimmel, C. B., Ballard, W. W., Kimmel, S. R., Ullmann, B., and Schilling, T. F. (1995). Stages of Embryonic Development of the Zebrafish. *Dev. Dyn.* 203, 253–310. doi:10.1002/aja.1002030302

Kitada, T., Asakawa, S., Hattori, N., Matsumine, H., Yamamura, Y., Minoshima, S., et al. (1998). Mutations in the Parkin Gene Cause Autosomal Recessive Juvenile Parkinsonism. *Nature* 392, 605–608. doi:10.1038/33416

Kitada, T., Pisani, A., Porter, D. R., Yamaguchi, H., Tscherter, A., Martella, G., et al. (2007). Impaired Dopamine Release and Synaptic Plasticity in the Striatum of PINK1-Deficient Mice. *Proc. Natl. Acad. Sci. U. S. A.* 104, 11441–11446. doi:10.1073/pnas.0702717104

Kizil, C., Kaslin, J., Kroehne, V., and Brand, M. (2012). Adult Neurogenesis and Brain Regeneration in Zebrafish. *Dev. Neurobiol.* 72, 429–461. doi:10.1002/dneu.20918

Kok, F. O., Shin, M., Ni, C.-W., Gupta, A., Grosse, A. S., van Impel, A., et al. (2015). Reverse Genetic Screening Reveals Poor Correlation between Morpholino-Induced and Mutant Phenotypes in Zebrafish. *Dev. Cel.* 32, 97–108. doi:10.1016/J.DEVCEL.2014.11.018

Lai, S., Kumari, A., Liu, J., Zhang, Y., Zhang, W., Yen, K., et al. (2021). Chemical Screening Reveals Ronidazole Is a superior Prodrug to Metronidazole for Nitroreductase-Induced Cell Ablation System in Zebrafish Larvae. *J. Genet. Genomics* 48, 1081–1090. doi:10.1016/j.jgg.2021.07.015

Lam, C. S., Korzh, V., and Strahle, U. (2005). Zebrafish Embryos Are Susceptible to the Dopaminergic Neurotoxin MPTP. *Eur. J. Neurosci.* 21, 1758–1762. doi:10.1111/j.1460-9568.2005.03988.x

Lang, A. E., and Lozano, A. M. (1998). Parkinson's Disease. *New Engl. J. Med.* 339, 1130–1143. doi:10.1056/NEJM199810153391607

Langheinrich, U. (2003). Zebrafish: A New Model on the Pharmaceutical Catwalk. *BioEssays* 25, 904–912. doi:10.1002/bies.10326

Lee, S. B., Kim, W., Lee, S., and Chung, J. (2007). Loss of LRRK2/PARK8 Induces Degeneration of Dopaminergic Neurons in Drosophila. *Biochem. Biophys. Res. Commun.* 358, 534–539. doi:10.1016/j.bbrc.2007.04.156

Lieschke, G. J., and Currie, P. D. (2007). Animal Models of Human Disease: Zebrafish Swim into View. *Nat. Rev. Genet.* 8, 353–367. doi:10.1038/nrg2091

Lindsey, B. W., Smith, F. M., and Croll, R. P. (2010). From Inflation to Flotation: Contribution of the Swimbladder to Whole-Body Density and Swimming Depth during Development of the Zebrafish (*Danio rerio*). *Zebrafish* 7, 85–96. doi:10.1089/ZEB.2009.0616/ASSET/IMAGES/LARGE/FIG-7.JPEG

Lulla, A., Barnhill, L., Bitan, G., Ivanova, M. I., Nguyen, B., O'Donnell, K., et al. (2016). Neurotoxicity of the Parkinson Disease-Associated Pesticide Ziram Is Synuclein-dependent in Zebrafish Embryos. *Environ. Health Perspect.* 124, 1766–1775. doi:10.1289/EHP141

MacLeod, D., Dowman, J., Hammond, R., Leete, T., Inoue, K., and Abeliovich, A. (2006). The Familial Parkinsonism Gene LRRK2 Regulates Neurite Process Morphology. *Neuron* 52, 587–593. doi:10.1016/j.neuron.2006.10.008

Maes, J., Verlooy, L., Buenafe, O. E., de Witte, P. A. M., Esguerra, C. V., and Crawford, A. D. (2012). Evaluation of 14 Organic Solvents and Carriers for Screening Applications in Zebrafish Embryos and Larvae. *PLoS One* 7, e43850. doi:10.1371/journal.pone.0043850

Malpartida, A. B., Williamson, M., Narendra, D. P., Wade-Martins, R., and Ryan, B. J. (2021). Mitochondrial Dysfunction and Mitophagy in Parkinson's Disease: From Mechanism to Therapy. *Trends Biochem. Sci.* 46, 329–343. doi:10.1016/j.tibs.2020.11.007

Manev, H., Dimitrijevic, N., and Dzitoyeva, S. (2003). Techniques: Fruit Flies as Models for Neuropharmacological Research. *Trends Pharmacol. Sci.* 24, 41–43. doi:10.1016/S0165-6147(02)00004-4

Manning-Bog, A. B., McCormack, A. L., Purisai, M. G., Bolin, L. M., and Di Monte, D. A. (2003). Alpha-synuclein Overexpression Protects against Paraquat-Induced Neurodegeneration. *J. Neurosci.* 23, 3095–3099. doi:10.1523/JNEUROSCI.23-08-03095.2003

Martín-Jiménez, R., Campanella, M., and Russell, C. (2015). New Zebrafish Models of Neurodegeneration. *Curr. Neurol. Neurosci. Rep.* 15, 1–7. doi:10.1007/s11910-015-0555-z

McCormack, A. L., Atienza, J. G., Langston, J. W., and Di Monte, D. A. (2006). Decreased Susceptibility to Oxidative Stress Underlies the Resistance of Specific Dopaminergic Cell Populations to Paraquat-Induced Degeneration. *Neuroscience* 141, 929–937. doi:10.1016/j.neuroscience.2006.03.069

McKinley, E. T., Baranowski, T. C., Blavo, D. O., Cato, C., Doan, T. N., and Rubinstein, A. L. (2005). Neuroprotection of MPTP-Induced Toxicity in Zebrafish Dopaminergic Neurons. *Mol. Brain Res.* 141, 128–137. doi:10.1097/SAP.0b013e3180d099fa10.1016/j.molbrainres.2005.08.014

Meredith, G. E., Totterdell, S., Potashkin, J. A., and Surmeier, D. J. (2008). Modeling PD Pathogenesis in Mice: Advantages of a Chronic MPTP Protocol. *Parkinsonism Relat. Disord.* 14, S112–S115. doi:10.1016/j.parkreldis.2008.04.012

Merovitch, N. H. (2016). *A Simple Automated System for Appetitive Conditioning of Zebrafish in Their home Tank and Underlying Neural Activation*. Halifax, Canada: Dalhousie University.

Meulener, M., Whitworth, A. J., Armstrong-Gold, C. E., Rizzu, P., Heutink, P., Wes, P. D., et al. (2005). Drosophila DJ-1 Mutants Are Selectively Sensitive to Environmental Toxins Associated with Parkinson's Disease. *Curr. Biol.* 15, 1572–1577. doi:10.1016/j.cub.2005.07.064

Milanese, C., Sager, J. J., Bai, Q., Farrell, T. C., Cannon, J. R., Greenamyre, J. T., et al. (2012). Hypokinesia and Reduced Dopamine Levels in Zebrafish Lacking β- and γ1-synucleins. *J. Biol. Chem.* 287, 2971–2983. doi:10.1074/jbc.M111.308312

Miller, N., and Gerlai, R. (2012). "Automated Tracking of Zebrafish shoals and the Analysis of Shoaling Behavior," in *Zebrafish Protocols for Neurobehavioral Research* (Totowa, NJ: Humana Press), 217–230. doi:10.1007/978-1-61779-597-8_16

Moore, D. J., West, A. B., Dawson, V. L., and Dawson, T. M. (2005). Molecular Pathophysiology of Parkinson's Disease. *Annu. Rev. Neurosci.* 28, 57–87. doi:10.1146/annurev.neuro.28.061604.135718

Müller, T. E., Nunes, M. E., Menezes, C. C., Marins, A. T., Leitemperger, J., Gressler, A. C. L., et al. (2018). Sodium Selenite Prevents Paraquat-Induced Neurotoxicity in Zebrafish. *Mol. Neurobiol.* 55, 1928–1941. Available at: https://link.springer.com/article/10.1007/s12035-017-0441-6 (Accessed October 18, 2018). doi:10.1007/s12035-017-0441-6

Murray, M., Jones, H., Cserr, H. F., and Rall, D. P. (1975). The Blood-Brain Barrier and Ventricular System of *Myxine glutinosa*. *Brain Res.* 99, 17–33. Available at: http://www.ncbi.nlm.nih.gov/pubmed/1188978 (Accessed November 16, 2018). doi:10.1016/0006-8993(75)90605-8

Nakamura, K., Nemani, V. M., Azarbal, F., Skibinski, G., Levy, J. M., Egami, K., et al. (2011). Direct Membrane Association Drives Mitochondrial Fission by the Parkinson Disease-Associated Protein α-synuclein. *J. Biol. Chem.* 286, 20710–20726. doi:10.1074/jbc.M110.213538

Nass, R., Hall, D. H., Miller, D. M., and Blakely, R. D. (2002). Neurotoxin-induced Degeneration of Dopamine Neurons in *Caenorhabditis elegans*. *Proc. Natl. Acad. Sci. U. S. A.* 99, 3264–3269. doi:10.1073/pnas.042497999

Nellore, J., and Nandita, P. (2015). Paraquat Exposure Induces Behavioral Deficits in Larval Zebrafish during the Window of Dopamine Neurogenesis. *Toxicol. Rep.* 2, 950–956. doi:10.1016/J.TOXREP.2015.06.007

Newman, M., Ebrahimie, E., and Lardelli, M. (2014). Using the Zebrafish Model for Alzheimer's Disease Research. *Front. Genet.* 5, 189. doi:10.3389/fgene.2014.00189

North, T. E., Goessling, W., Walkley, C. R., Lengerke, C., Kopani, K. R., Lord, A. M., et al. (2007). Prostaglandin E2 Regulates Vertebrate Haematopoietic Stem Cell Homeostasis. *Nature* 447, 1007–1011. doi:10.1038/nature05883

Nunes, M. E., Müller, T. E., Braga, M. M., Fontana, B. D., Quadros, V. A., Marins, A., et al. (2017). Chronic Treatment with Paraquat Induces Brain Injury, Changes in Antioxidant Defenses System, and Modulates Behavioral Functions in Zebrafish. *Mol. Neurobiol.* 54, 3925–3934. doi:10.1007/s12035-016-9919-x

O'Donnell, K. C., Lulla, A., Stahl, M. C., Wheat, N. D., Bronstein, J. M., and Sagasti, A. (2014). Axon Degeneration and PGC-1α-Mediated protection in a Zebrafish Model of α-synuclein Toxicity. *Dis. Model. Mech.* 7, 571–582. doi:10.1242/dmm.013185

Panula, P., Sallinen, V., Sundvik, M., Kolehmainen, J., Torkko, V., Tiittula, A., et al. (2006). Modulatory Neurotransmitter Systems and Behavior: towards Zebrafish Models of Neurodegenerative Diseases. *Zebrafish* 3, 235–247. Available at: https://www.liebertpub.com/doi/abs/10.1089/zeb.2006.3.235 (Accessed October 11, 2018). doi:10.1089/zeb.2006.3.235

Parichy, D. M., Elizondo, M. R., Mills, M. G., Gordon, T. N., and Engeszer, E. (2009). Normal Table of Post-Embryonic Zebrafish Development: Staging by Externally Visible Anatomy of the Living Fish. *Dev. Dyn.* 238, 2975–3015. doi:10.1002/dvdy.22113.Normal

Parng, C., Roy, N. M., Ton, C., Lin, Y., and McGrath, P. (2007). Neurotoxicity Assessment Using Zebrafish. *J. Pharmacol. Toxicol. Methods* 55, 103–112. doi:10.1016/j.vascn.2006.04.004

Parng, C., Seng, W. L., Semino, C., and McGrath, P. (2002). Zebrafish: A Preclinical Model for Drug Screening. *Assay Drug Dev. Technol.* 1, 41–48. doi:10.1089/154065802761001293

Pather, S., and Gerlai, R. (2009). Shuttle Box Learning in Zebrafish (*Danio rerio*). *Behav. Brain Res.* 196, 323–327. doi:10.1016/j.bbr.2008.09.013

Petroske, E., Meredith, G. E., Callen, S., Totterdell, S., and Lau, Y. S. (2001). Mouse Model of Parkinsonism: A Comparison between Subacute MPTP and Chronic MPTP/probenecid Treatment. *Neuroscience* 106, 589–601. doi:10.1016/S0306-4522(01)00295-0

Pisharath, H., and Parsons, M. J. (2009). Nitroreductase-mediated Cell Ablation in Transgenic Zebrafish Embryos. *Methods Mol. Biol.* 546, 133–143. doi:10.1007/978-1-60327-977-2_9

Prabhudesai, S., Bensabeur, F. Z., Abdullah, R., Basak, I., Baez, S., Alves, G., et al. (2016). LRRK2 Knockdown in Zebrafish Causes Developmental Defects, Neuronal Loss, and Synuclein Aggregation. *J. Neurosci. Res.* 94, 717–735. doi:10.1002/jnr.23754

Prabhudesai, S., Sinha, S., Attar, A., Kotagiri, A., Fitzmaurice, A. G., Lakshmanan, R., et al. (2012). A Novel "Molecular Tweezer" Inhibitor of α-Synuclein Neurotoxicity *In Vitro* and *In Vivo*. *Neurotherapeutics* 9, 464–476. doi:10.1007/s13311-012-0105-1

Rafferty, S. A., and Quinn, T. A. (2018). A Beginner's Guide to Understanding and Implementing the Genetic Modification of Zebrafish. *Prog. Biophys. Mol. Biol.* 138, 3–19. doi:10.1016/j.pbiomolbio.2018.07.005

Ran, F. A., Hsu, P. D., Wright, J., Agarwala, V., Scott, D. A., and Zhang, F. (2013). Genome Engineering Using the CRISPR-Cas9 System. *Nat. Protoc.* 8, 2281–2308. doi:10.1038/nprot.2013.143

Rana, A. Q., Ahmed, U. S., Chaudry, Z. M., and Vasan, S. (2015). Parkinson's Disease: A Review of Non-motor Symptoms. *Expert Rev. Neurother.* 15, 549–562. doi:10.1586/14737175.2015.1038244

Rappold, P. M., Cui, M., Chesser, A. S., Tibbett, J., Grima, J. C., Duan, L., et al. (2011). Paraquat Neurotoxicity Is Mediated by the Dopamine Transporter and Organic Cation Transporter-3. *Proc. Natl. Acad. Sci.* 108, 20766–20771. doi:10.1073/pnas.1115141108

Razali, K., Othman, N., Mohd Nasir, M. H., Doolaanea, A. A., Kumar, J., Ibrahim, W. N., et al. (2021). The Promise of the Zebrafish Model for Parkinson's Disease: Today's Science and Tomorrow's Treatment. *Front. Genet.* 12, 553. doi:10.3389/FGENE.2021.655550/BIBTEX

Regoni, M., Cattaneo, S., Mercatelli, D., Novello, S., Passoni, A., Bagnati, R., et al. (2020). Pharmacological Antagonism of Kainate Receptor Rescues Dysfunction and Loss of Dopamine Neurons in a Mouse Model of Human Parkin-Induced Toxicity. *Cell Death Dis.* 11, 1–11. doi:10.1038/s41419-020-03172-8

Regoni, M., Zanetti, L., Comai, S., Mercatelli, D., Novello, S., Albanese, F., et al. (2021). Early Dysfunction of Substantia Nigra Dopamine Neurons in the Parkinq311x Mouse. *Biomedicines* 9, 1–15. doi:10.3390/biomedicines9050514

Ren, G., Xin, S., Li, S., Zhong, H., and Lin, S. (2011). Disruption of Lrrk2 Does Not Cause Specific Loss of Dopaminergic Neurons in Zebrafish. *PLoS One* 6, e20630. doi:10.1371/journal.pone.0020630

Rink, E., and Wullimann, M. F. (2002). Connections of the Ventral Telencephalon and Tyrosine Hydroxylase Distribution in the Zebrafish Brain (*Danio rerio*) lead to Identification of an Ascending Dopaminergic System in a Teleost. *Brain Res. Bull.* 57, 385–387. doi:10.1016/S0361-9230(01)00696-7

Ruan, Y., Zheng, X. Y., Zhang, H. L., Zhu, W., and Zhu, J. (2012). Olfactory Dysfunctions in Neurodegenerative Disorders. *J. Neurosci. Res.* 90, 1693–1700. doi:10.1002/jnr.23054

Rubinstein, A. L. (2003). Zebrafish : From Disease Modeling to Drug Discovery. *Curr. Opin. Drug Discov. Devel.* 6, 218–223.

Ruzicka, L., Howe, D. G., Ramachandran, S., Toro, S., Van Slyke, C. E., Bradford, Y. M., et al. (2019). The Zebrafish Information Network: New Support for Non-coding Genes, Richer Gene Ontology Annotations and the Alliance of Genome Resources. *Nucleic Acids Res.* 47, D867–D873. doi:10.1093/nar/gky1090

Sager, J. J., Bai, Q., and Burton, E. A. (2010). Transgenic Zebrafish Models of Neurodegenerative Diseases. *Brain Struct. Funct.* 214, 285–302. doi:10.1007/s00429-009-0237-1

Sallinen, V., Kolehmainen, J., Priyadarshini, M., Toleikyte, G., Chen, Y. C., and Panula, P. (2010). Dopaminergic Cell Damage and Vulnerability to MPTP in Pink1 Knockdown Zebrafish. *Neurobiol. Dis.* 40, 93–101. doi:10.1016/j.nbd.2010.06.001

Sallinen, V., Torkko, V., Sundvik, M., Reenilä, I., Khrustalyov, D., Kaslin, J., et al. (2009). MPTP and MPP+ Target Specific Aminergic Cell Populations in Larval Zebrafish. *J. Neurochem.* 108, 719–731. doi:10.1111/j.1471-4159.2008.05793.x

Schober, A. (2004). Classic Toxin-Induced Animal Models of Parkinson's Disease: 6-OHDA and MPTP. *Cell Tissue Res.* 318, 215–224. doi:10.1007/s00441-004-0938-y

Schulte-Merker, S., and Stainier, D. Y. R. (2014). Out with the Old, in with the New: Reassessing Morpholino Knockdowns in Light of Genome Editing Technology. *Development* 141, 3103–3104. doi:10.1242/dev.112003

Ségalat, L. (2007). Invertebrate Animal Models of Diseases as Screening Tools in Drug Discovery. *ACS Chem. Biol.* 2, 231–236. doi:10.1021/cb700009m

Sharma, N., Khurana, N., and Muthuraman, A. (2017). Lower Vertebrate and Invertebrate Models of Alzheimer's Disease – A Review. *Eur. J. Pharmacol.* 815, 312–323. doi:10.1016/j.ejphar.2017.09.017

Sheng, D., Qu, D., Kwok, K. H. H., Ng, S. S., Lim, A. Y. M., Aw, S. S., et al. (2010). Deletion of the WD40 Domain of LRRK2 in Zebrafish Causes Parkinsonism-like Loss of Neurons and Locomotive Defect. *Plos Genet.* 6, e1000914. doi:10.1371/journal.pgen.1000914

Sherer, T. B., Betarbet, R., Testa, C. M., Seo, B. B., Richardson, J. R., Kim, J. H., et al. (2003). Mechanism of Toxicity in Rotenone Models of Parkinson's Disease. *J. Neurosci.* 23, 10756–10764. doi:10.1523/jneurosci.23-34-10756.2003

Shi, H., Magaye, R., Castranova, V., and Zhao, J. (2013). Titanium Dioxide Nanoparticles: A Review of Current Toxicological Data. *Part. Fibre Toxicol.* 10, 1–33. doi:10.1186/1743-8977-10-15

Sison, M., and Gerlai, R. (2010). Associative Learning in Zebrafish (*Danio rerio*) in the Plus Maze. *Behav. Brain Res.* 207, 99–104. doi:10.1016/j.bbr.2009.09.043

Sousa, N., Almeida, O. F. X., and Wotjak, C. T. (2006). A Hitchhiker's Guide to Behavioral Analysis in Laboratory Rodents. *Genes, Brain Behav.* 5, 5–24. doi:10.1111/j.1601-183X.2006.00228.x

Spence, R., Gerlach, G., Lawrence, C., and Smith, C. (2008). The Behaviour and Ecology of the Zebrafish, *Danio rerio*. *Biol. Rev.* 83, 13–34. doi:10.1111/j.1469-185X.2007.00030.x

Spillantini, M. G., Crowther, R. A., Jakes, R., Hasegawa, M., and Goedert, M. (1998). α-Synuclein in Filamentous Inclusions of Lewy Bodies from Parkinson's Disease and Dementia with Lewy Bodies. *Proc. Natl. Acad. Sci.* 95, 6469–6473. doi:10.1073/pnas.95.11.6469

Stewart, A. M., Braubach, O., Spitsbergen, J., Gerlai, R., and Kalueff, A. V. (2014). Zebrafish Models for Translational Neuroscience Research: From Tank to Bedside. *Trends Neurosci.* 37, 264–278. doi:10.1016/j.tins.2014.02.011

Stewart, A. M., Grieco, F., Tegelenbosch, R. A. J., Kyzar, E. J., Nguyen, M., Kaluyeva, A., et al. (2015). A Novel 3D Method of Locomotor Analysis in Adult Zebrafish: Implications for Automated Detection of CNS Drug-Evoked Phenotypes. *J. Neurosci. Methods* 255, 66–74. doi:10.1016/j.jneumeth.2015.07.023

Stott, S. R. W., and Barker, R. A. (2014). Time Course of Dopamine Neuron Loss and Glial Response in the 6-OHDA Striatal Mouse Model of Parkinson's Disease. *Eur. J. Neurosci.* 39, 1042–1056. doi:10.1111/EJN.12459

Stoyek, M. R., Croll, R. P., and Smith, F. M. (2015). Intrinsic and Extrinsic Innervation of the Heart in Zebrafish (*Danio rerio*). *J. Comp. Neurol.* 523, 1683–1700. doi:10.1002/cne.23764

Sun, Z., and Gitler, A. D. (2008). Discovery and Characterization of Three Novel Synuclein Genes in Zebrafish. *Dev. Dyn.* 237, 2490–2495. doi:10.1002/dvdy.21569

Tay, L. T., Ronneberger, O., Ryu, S., Nitschke, R., and Driever, W. (2011). Comprehensive Catecholaminergic Projectome Analysis Reveals Single-Neuron Integration of Zebrafish Ascending and Descending Dopaminergic Systems. *Nat. Commun.* 2, 1–12. doi:10.1038/ncomms1171

Thameem Dheen, S., Kaur, C., and Ling, E.-A. (2007). Microglial Activation and its Implications in the Brain Diseases. *Curr. Med. Chem.* 14, 1189–1197. doi:10.2174/092986707780597961

Toledo-Ibarra, G. A., Rojas-Mayorquín, A. E., and Girón-Pérez, M. I. (2013). Influence of the Cholinergic System on the Immune Response of Teleost Fishes: Potential Model in Biomedical Research. *Clin. Dev. Immunol.* 2013, 536534. doi:10.1155/2013/536534

Van Dam, D., and De Deyn, P. P. (2011). Animal Models in the Drug Discovery Pipeline for Alzheimer's Disease. *Br. J. Pharmacol.* 164, 1285–1300. doi:10.1111/j.1476-5381.2011.01299.x

van der Worp, H. B., Howells, D. W., Sena, E. S., Porritt, M. J., Rewell, S., O'Collins, V., et al. (2010). Can Animal Models of Disease Reliably Inform Human Studies? *Plos Med.* 7, 1–8. doi:10.1371/journal.pmed.1000245

van Eeden, F. J. M., Granato, M., Odenthal, J., and Haffter, P. (1998). Chapter 2 Developmental Mutant Screens in the Zebrafish. *Methods Cel. Biol.* 60, 21–41. doi:10.1016/S0091-679X(08)61892-0

Vaz, R. L., Outeiro, T. F., and Ferreira, J. J. (2018). Zebrafish as an Animal Model for Drug Discovery in Parkinson's Disease and Other Movement Disorders: A Systematic Review. *Front. Neurol.* 9. doi:10.3389/fneur.2018.00347

Vázquez-Vélez, G. E., and Zoghbi, H. Y. (2021). Parkinson's Disease Genetics and Pathophysiology. *Annu. Rev. Neurosci.* 44, 87–108. doi:10.1146/annurev-neuro-100720-034518

Vijayanathan, Y., Lim, F. T., Lim, S. M., Long, C. M., Tan, M. P., Majeed, A. B. A., et al. (2017). 6-OHDA-Lesioned Adult Zebrafish as a Useful Parkinson's Disease Model for Dopaminergic Neuroregeneration. *Neurotox. Res.* 32, 496–508. doi:10.1007/s12640-017-9778-x

Vingill, S., Connor-Robson, N., and Wade-Martins, R. (2018). Are Rodent Models of Parkinson's Disease Behaving as They Should? *Behav. Brain Res.* 352, 133–141. doi:10.1016/j.bbr.2017.10.021

Vogiatzi, T., Xilouri, M., Vekrellis, K., and Stefanis, L. (2008). Wild Type α-synuclein Is Degraded by Chaperone-Mediated Autophagy and Macroautophagy in Neuronal Cells. *J. Biol. Chem.* 283, 23542–23556. doi:10.1074/jbc.M801992200

Wager, K., and Russell, C. (2013). Mitophagy and Neurodegeneration: The Zebrafish Model System. *Autophagy* 9, 1693–1709. doi:10.4161/auto.25082

Wang, D., Tang, B., Zhao, G., Pan, Q., Xia, K., Bodmer, R., et al. (2008). Dispensable Role of Drosophila Ortholog of LRRK2 Kinase Activity in Survival of Dopaminergic Neurons. *Mol. Neurodegener.* 3, 3. doi:10.1186/1750-1326-3-3

Wang, Q., Liu, S., Hu, D., Wang, Z., Wang, L., Wu, T., et al. (2016). Identification of Apoptosis and Macrophage Migration Events in Paraquat-Induced Oxidative Stress Using a Zebrafish Model. *Life Sci.* 157, 116–124. doi:10.1016/j.lfs.2016.06.009

Wang, X. H., Souders, C. L., Zhao, Y. H., and Martyniuk, C. J. (2018). Paraquat Affects Mitochondrial Bioenergetics, Dopamine System Expression, and Locomotor Activity in Zebrafish (*Danio rerio*). *Chemosphere* 191, 106–117. doi:10.1016/j.chemosphere.2017.10.032

Wang, X., Zhang, J. B., He, K. J., Wang, F., and Liu, C. F. (2021). Advances of Zebrafish in Neurodegenerative Disease: From Models to Drug Discovery. *Front. Pharmacol.* 12, 1802. doi:10.3389/FPHAR.2021.713963/BIBTEX

Wang, Y., Liu, W., Yang, J., Wang, F., Sima, Y., Zhong, Z. M., et al. (2017). Parkinson's Disease-like Motor and Non-motor Symptoms in Rotenone-Treated Zebrafish. *Neurotoxicology* 58, 103–109. doi:10.1016/j.neuro.2016.11.006

Wells, W. A. (1998). High-throughput Worms. *Chem. Biol.* 5, R147–R148. Available at: http://www.ncbi.nlm.nih.gov/pubmed/9653546 (Accessed November 21, 2018). doi:10.1016/s1074-5521(98)90174-0

Wen, L., Wei, W., Gu, W., Huang, P., Ren, X., Zhang, Z., et al. (2008). Visualization of Monoaminergic Neurons and Neurotoxicity of MPTP in Live Transgenic Zebrafish. *Dev. Biol.* 314, 84–92. doi:10.1016/j.ydbio.2007.11.012

Weng, M., Xie, X., Liu, C., Lim, K. L., Zhang, C. W., and Li, L. (2018). The Sources of Reactive Oxygen Species and its Possible Role in the Pathogenesis of Parkinson's Disease. *Parkinsons. Dis.* 2018, 9163040. doi:10.1155/2018/9163040

Westermann, L., Neubauer, B., and Köttgen, M. (2021). Nobel Prize 2020 in Chemistry Honors CRISPR: a Tool for Rewriting the Code of Life. *Pflugers Arch. Eur. J. Physiol.* 473, 1. doi:10.1007/s00424-020-02497-9

White, R. M., Sessa, A., Burke, C., Bowman, T., LeBlanc, J., Ceol, C., et al. (2008). Transparent Adult Zebrafish as a Tool for *In Vivo* Transplantation Analysis. *Cell Stem Cell* 2, 183–189. doi:10.1016/j.stem.2007.11.002

Whitworth, A. J., Theodore, D. A., Greene, J. C., Benes, H., Wes, P. D., and Pallanck, L. J. (2005). Increased Glutathione S-Transferase Activity Rescues Dopaminergic Neuron Loss in a Drosophila Model of Parkinson's Disease. *Proc. Natl. Acad. Sci. U. S. A.* 102, 8024–8029. doi:10.1073/pnas.0501078102

Wullimann, M., and Rink, E. (2001). Detailed Immunohistology of Pax6 Protein and Tyrosine Hydroxylase in the Early Zebrafish Brain Suggests Role of Pax6 Gene in Development of Dopaminergic. *Dev. Brain Res.* 131, 173–191. Available at: http://www.sciencedirect.com/science/article/pii/S016538060100270X (Accessed September 6, 2017). doi:10.1016/s0165-3806(01)00270-x

Wyeth, R. C., Braubach, O. R., Fine, A., and Croll, R. P. (2011). Videograms: A Method for Repeatable Unbiased Quantitative Behavioral Analysis without Scoring or Tracking. *Neuromethods* 51, 15–33. doi:10.1007/978-1-60761-953-6_2

Xi, Y., Noble, S., and Ekker, M. (2011). Modeling Neurodegeneration in Zebrafish. *Curr. Neurol. Neurosci. Rep.* 11, 274–282. doi:10.1007/s11910-011-0182-2

Xi, Y., Ryan, J., Noble, S., Yu, M., Yilbas, A. E., and Ekker, M. (2010). Impaired Dopaminergic Neuron Development and Locomotor Function in Zebrafish with Loss of Pink1 Function. *Eur. J. Neurosci.* 31, 623–633. doi:10.1111/j.1460-9568.2010.07091.x

Yang, Y., Gehrke, S., Haque, M. E., Imai, Y., Kosek, J., Yang, L., et al. (2005). Inactivation of Drosophila DJ-1 Leads to Impairments of Oxidative Stress Response and Phosphatidylinositol 3-kinase/Akt Signaling. *Proc. Natl. Acad. Sci. U. S. A.* 102, 13670–13675. doi:10.1073/pnas.0504610102

Yang, Y., Gehrke, S., Imai, Y., Huang, Z., Ouyang, Y., Wang, J.-W., et al. (2006). Mitochondrial Pathology and Muscle and Dopaminergic Neuron Degeneration Caused by Inactivation of Drosophila Pink1 Is Rescued by Parkin. *Proc. Natl. Acad. Sci.* 103, 10793–10798. doi:10.1073/pnas.0602493103

Youdim, M. B. H., Edmondson, D., and Tipton, K. F. (2006). The Therapeutic Potential of Monoamine Oxidase Inhibitors. *Nat. Rev. Neurosci.* 7, 295–309. doi:10.1038/nrn1883

Zhang, Y., Guldner, I. H., Nichols, E. L., Benirschke, D., Smith, C. J., Zhang, S., et al. (2021). Instant FLIM Enables 4D *In Vivo* Lifetime Imaging of Intact and Injured Zebrafish and Mouse Brains. *Optica* 8, 885. doi:10.1364/optica.426870

Zhou, H., Falkenburger, B. H., Schulz, J. B., Tieu, K., Xu, Z., and Xu, G. X. (2007). Silencing of the Pink1 Gene Expression by Conditional RNAi Does Not Induce Dopaminergic Neuron Death in Mice. *Int. J. Biol. Sci.* 3, 242–250. doi:10.7150/ijbs.3.242

Zhou, S., Wang, Z., and Klaunig, J. E. (2013). *Caenorhabditis elegans* Neuron Degeneration and Mitochondrial Suppression Caused by Selected Environmental Chemicals. *Int. J. Biochem. Mol. Biol.* 4, 191. Available at:/pmc/articles/PMC3867705/ (Accessed November 25, 2021). doi:10.1007/s11010-013-1641-7

Conflict of Interest: The authors declare that the research was conducted in the absence of any commercial or financial relationships that could be construed as a potential conflict of interest.

Publisher's Note: All claims expressed in this article are solely those of the authors and do not necessarily represent those of their affiliated organizations, or those of the publisher, the editors and the reviewers. Any product that may be evaluated in this article, or claim that may be made by its manufacturer, is not guaranteed or endorsed by the publisher.

frontiers in Pharmacology

ORIGINAL RESEARCH
published: 18 March 2022
doi: 10.3389/fphar.2022.837756

In Vivo Dopamine Neuron Imaging-Based Small Molecule Screen Identifies Novel Neuroprotective Compounds and Targets

Gha-hyun J. Kim[1,2], Han Mo[1,3], Harrison Liu[4,5], Meri Okorie[1,2], Steven Chen[4,6], Jiashun Zheng[7], Hao Li[7], Michelle Arkin[4,6], Bo Huang[4,5,8] and Su Guo[1,2]**

[1]Department of Bioengineering and Therapeutic Sciences and Programs in Biological Sciences and Human Genetics, University of California San Francisco, San Francisco, CA, United States, [2]Graduate Program of Pharmaceutical Sciences and Pharmacogenomics, University of California San Francisco, San Francisco, CA, United States, [3]Tsinghua-Peking Center for Life Sciences, McGovern Institute for Brain Research, Tsinghua University, Beijing, China, [4]Department of Pharmaceutical Chemistry, San Francisco, CA, United States, [5]Graduate Program of Bioengineering, San Francisco, CA, United States, [6]Small Molecule Discovery Center, University of California San Francisco, San Francisco, CA, United States, [7]Department of Biochemistry and Biophysics, University of California San Francisco, San Francisco, CA, United States, [8]Chan Zuckerberg Biohub, San Francisco, CA, United States

OPEN ACCESS

Edited by:
Anna Siebel, Universidade Comunitária da Região de Chapecó, Brazil

Reviewed by:
Daniëlle Copmans, KU Leuven, Belgium
Marta d''Amora, Italian Institute of Technology (IIT), Italy

***Correspondence:**
Gha-hyun J. Kim
happyiowa@gmail.com
Su Guo
su.guo@ucsf.edu

Specialty section:
This article was submitted to Experimental Pharmacology and Drug Discovery, a section of the journal Frontiers in Pharmacology

Received: *17 December 2021*
Accepted: *21 February 2022*
Published: *18 March 2022*

Citation:
Kim Gj, Mo H, Liu H, Okorie M, Chen S, Zheng J, Li H, Arkin M, Huang B and Guo S (2022) In Vivo Dopamine Neuron Imaging-Based Small Molecule Screen Identifies Novel Neuroprotective Compounds and Targets. Front. Pharmacol. 13:837756. doi: 10.3389/fphar.2022.837756

Parkinson's disease (PD) is the second most common neurodegenerative disorder with prominent dopamine (DA) neuron degeneration. PD affects millions of people worldwide, but currently available therapies are limited to temporary relief of symptoms. As an effort to discover disease-modifying therapeutics, we have conducted a screen of 1,403 bioactive small molecule compounds using an *in vivo* whole organism screening assay in transgenic larval zebrafish. The transgenic model expresses the bacterial enzyme nitroreductase (NTR) driven by the tyrosine hydroxylase (th) promotor. NTR converts the commonly used antibiotic pro-drug metronidazole (MTZ) to the toxic nitroso radical form to induce DA neuronal loss. 57 compounds were identified with a brain health score (BHS) that was significantly improved compared to the MTZ treatment alone after FDR adjustment (padj<0.05). Independently, we curated the high throughput screening (HTS) data by annotating each compound with pharmaceutical classification, known mechanism of action, indication, IC50, and target. Using the Reactome database, we performed pathway analysis, which uncovered previously unknown pathways in addition to validating previously known pathways associated with PD. Non-topology-based pathway analysis of the screening data further identified apoptosis, estrogen hormone, dipeptidyl-peptidase 4, and opioid receptor Mu1 to be potentially significant pathways and targets involved in neuroprotection. A total of 12 compounds were examined with a secondary assay that imaged DA neurons before and after compound treatment. The z'-factor of this secondary assay was determined to be 0.58, suggesting it is an excellent assay for screening. Etodolac, nepafenac, aloperine, protionamide, and olmesartan showed significant neuroprotection and was also validated by blinded manual DA neuronal counting. To determine whether these compounds are broadly relevant for

neuroprotection, we tested them on a conduritol-b-epoxide (CBE)-induced Gaucher disease (GD) model, in which the activity of *glucocerebrosidase* (GBA), a commonly known genetic risk factor for PD, was inhibited. Aloperine, olmesartan, and nepafenac showed significant protection of DA neurons in this assay. Together, this work, which combines high content whole organism *in vivo* imaging-based screen and bioinformatic pathway analysis of the screening dataset, delineates a previously uncharted approach for identifying hit-to-lead candidates and for implicating previously unknown pathways and targets involved in DA neuron protection.

Keywords: neurodegeneration, NTR-MTZ, aloperine, Parkinson's disease, GBA, gaucher disease, larval screening, zebrafish

INTRODUCTION

Neurodegenerative diseases, characterized by progressive loss of neuronal types in the central or peripheral nervous systems (CNS or PNS) followed by multi-organ dysfunction or dementia, are a major source of disability worldwide. Parkinson's disease (PD) is of particular concern as its prevalence is increasing rapidly but the development of disease-modifying therapeutics has been stagnant (Jankovic and Tan, 2020; Paolini Paoletti et al., 2020). PD is the second most common neurodegenerative disorder that affects more than 10 million people worldwide as of 2020, with an economic burden of $51.9 billion in the United States alone (Yang et al., 2020). Loss of dopamine (DA) neurons in the PD patients results in the cardinal motor symptoms that include bradykinesia, resting tremor, postural instability, and rigidity. Additionally, many PD patients also experience comorbidities including cardiac disorders and increased infection rates that can significantly impede the quality of life and pose severe burdens on their families and caregivers (DeMaagd and Philip, 2015; Armstrong and Okun, 2020). While there are several treatment options for PD that work by enhancing dopamine action, decreasing metabolism of dopamine, or replacing the natural form of dopamine with exogenous drugs tailored for each patient, these therapies provide symptomatic relief only (Armstrong and Okun, 2020). Levodopa is considered the gold standard therapy but is associated with significant complications such as the "wearing off" effect and levodopa-induced dyskinesia. The surgical method with deep brain stimulation has been established for alleviating some of these motor complications and possibly offering neuroprotection in animal models, but the mechanism remains inconclusive (Koprich et al., 2017; Jakobs et al., 2020). Thus, there is an urgent need for identifying disease-modifying therapeutics for PD.

While current therapeutic drug discovery is largely target-based, the implementation of phenotypic drug discovery has significant advantages particularly for neurodegenerative diseases (Ibhazehiebo et al., 2018; Lam and Peterson, 2019; Kim et al., 2021; Zhang et al., 2021). Phenotypic assays for a direct impact on neuronal integrity can bypass the need to fully understand complex biological processes underlying neurodegeneration, and in many cases provide leads to novel targets (Liu et al., 2016; Moffat et al., 2017). By directly imaging brain DA neuronal loss which is the hallmark of PD, our phenotypic screen aims to overcome the current challenge in target-based drug discovery, that is, difficulty in identifying suitable targets for idiopathic conditions. Larval zebrafish is an attractive model for phenotypic drug discovery as it possesses a high degree of genetic, physiological and morphological similarity with humans. Zebrafish genes share 70% homology with human counterparts and 82% disease-related genes have at least one zebrafish orthologue (Howe et al., 2013). The diencephalic region of the zebrafish brain is homologous to the substantia nigra pars compacta in humans which is the region of DA loss in PD patients. DA neurons are readily detectable in larvae as young as 3 days post-fertilization (dpf). zebrafish can produce many embryos on a weekly basis, which can grow up to seven dpf without the need for feeding or handling. The transgenic model used in the screening assay expresses the E. coli nitroreductase (NTR) controlled by the promoter of tyrosine hydroxylase (th), a rate-limiting enzyme in DA synthesis. This model, upon addition of the commonly used antibiotic metronidazole (MTZ), shows robust DA neuronal loss at the larval stage that is suitable for high throughput screening (HTS) screening. Neither genetic models nor neurotoxin (e.g., MPTP) models of PD offer such strength, due to late onset, weak or variable DA neuronal loss. The NTR converts MTZ to the toxic nitroso radical form (Curado et al., 2008; Pisharath and Parsons, 2009; Williams et al., 2015) *in vivo* causing DA neuronal loss that is quantifiable in the ventral forebrain region and involves mitochondrial dysfunction (Kim et al., 2021).

HTS generates large amounts of data and there are many different approaches towards deciding which compounds to pursue further for secondary validation. A widely accepted method for estimating the variability and effect size of the data is through the strictly standardized mean difference (SSMD) (Zhang et al., 2007). While SSMD scores can capture data variability, simply selecting the highest scoring compounds may not be sufficient to uncover candidate hits because SSMD is based on the ratio of mean to standard deviation which could lead to high SSMD scores even with a small mean, resulting in less desirable compounds. Likewise, simply looking at the mean scores (e.g., the brain health scores-BHS) may also result in false positives due to one skewed sample data.

Previously, we developed a high throughput DA neuron imaging method (Liu et al., 2016) and reported the identification of renin-angiotensin-aldosterone system (RAAS)

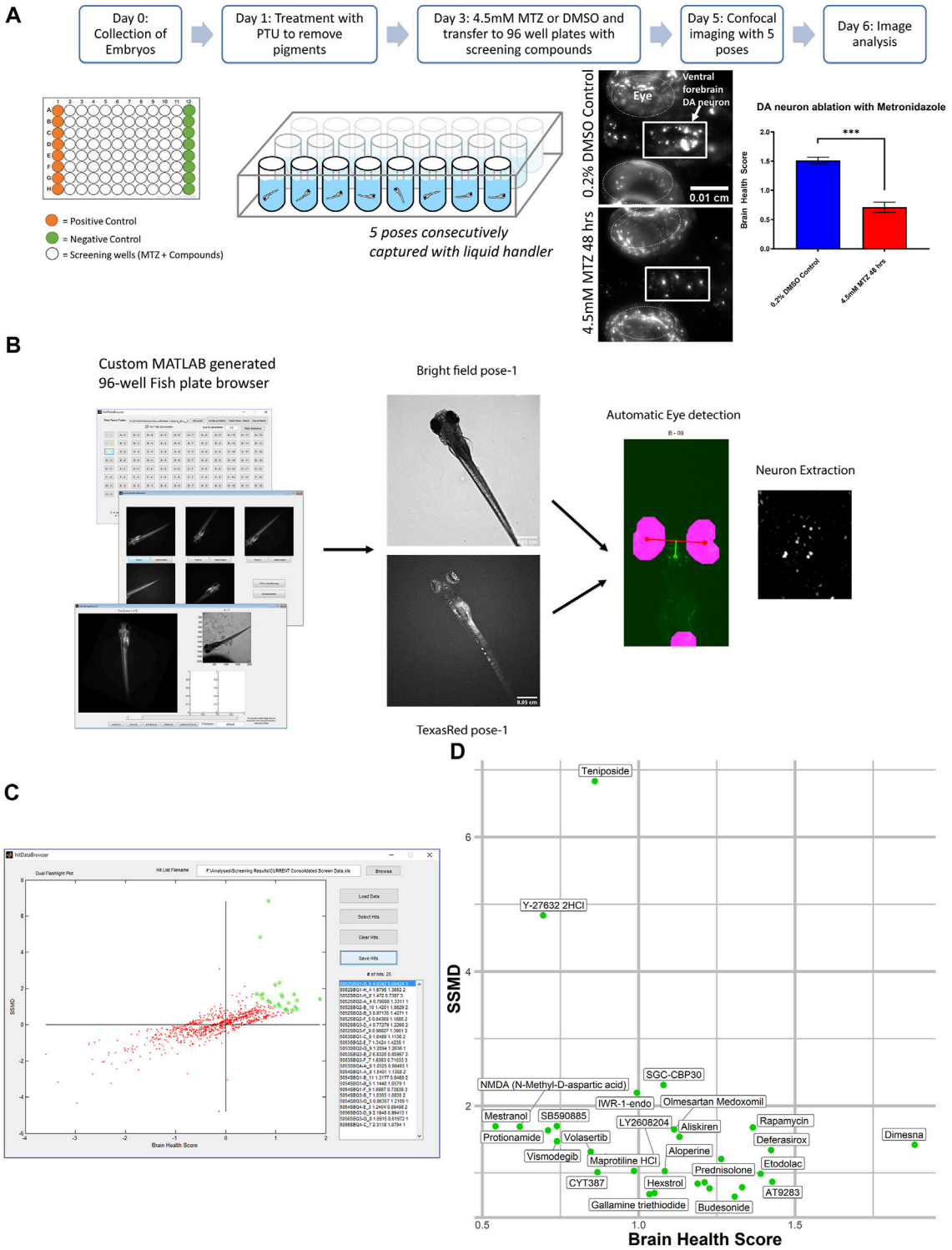

FIGURE 1 | *In vivo* dopamine neuron imaging-based high throughput screening in larval zebrafish identifies potential neuroprotective compounds. **(A)** Overview of the high throughput screening assay. 3 dpf larvae are transferred to 96 well plates with 10 μM screening compounds. DMSO (positive control) or 4.5 mM MTZ (negative control) was added 3 hours later and the treatment lasted for 24 hr, followed by imaging with brightfield and TexRed channels on InCell 6,000. Images were analyzed with the Cellprofiler pipeline. **(B)** Schematic of the image processing pipeline using the custom generated MATLAB "fishplatebrowser" and Cellprofiler. The brightfield and TexRed images were used to automatically detect the eye and diencephalic region of the brain and to quantify DA neurons. **(C)** Dual flashlight plot generated from custom made GUI "HitDataBrowser" with MATLAB. Compounds can be selected and exported with SSMD, BHS, and corresponding sample number. **(D)** Compounds in the top right quadrant with high BHS and SSMD scores based on manual selection. Details of the compounds are shown in **Table 1**. PTU: 1-phenyl 2-thiourea MTZ: Metronidazole DMSO: dimethyl sulfoxide.

inhibition as neuroprotective via mitochondrial targeting in DA neurons (Kim et al., 2021). In this study, we present for the first time the results of the entire 1403 HTS bioactive compound screen and uncover additional neuroprotective candidates after secondary validation. We apply a multi-pronged approach that incorporates the threshold-based method, topology-based analysis using the Reactome pathway database, and a non-topology-based method. By analyzing the entire screening datasets obtained from the HTS, significant and previously unknown pathways were identified to be involved in neuroprotection.

MATERIALS AND METHODS

Ethics Statement

The study was reviewed and approved by University of California, San Francisco Institutional Animal Care and Use Committee (approval number AN179000). The zebrafish system was regularly inspected by the University of California, San Francisco Laboratory Animal Resource Center.

Zebrafish Husbandry and Transgenic Lines

For all experiments in the study, homozygous Transgenic *Tg [fuguth:gal4-uas:GFP; uas-NTRmCherry]* and AB wild type were used. Zebrafish were raised on a 14:10 h light/dark cycle and maintained in the zebrafish facility according to the University of California San Francisco Institutional Animal Care and Use Committee standards. Embryos were raised in Blue Egg Water (0.12 g CaSO4, 0.2 g IO Salt, 30 μL of 1% Methylene per L).

High Throughput Screening of 1,403 Bioactive Compounds

For the *in vivo* high throughput screening assay we utilized a bioactive compound library from SelleckChem obtained from the UCSF Small Molecule Discovery Center (SMDC). As many of these compounds are FDA approved or validated in preclinical research, the target profiles and pharmacodynamics have been established. The assay was performed on a weekly protocol (**Figure 1A**) spanning from the initial collection of *Tg[fuguth:gal4-uas:GFP; uas:NTRmCherry]* embryos at day 0 and treatment with 200 μM 1-phenyl 2-thiourea (PTU) on 1dpf to remove the pigment. On 3dpf, larvae were transferred to round bottom 96-well plates containing 10 μM of screening compounds and treated with 4.5 mM MTZ for 48 h. The concentration and treatment period of MTZ was determined based on our previous work (Liu et al., 2016), which resulted in robust DA neuron loss (~60%) without affecting larval zebrafish development and morphology. On 5dpf the larvae were treated with tricaine at a low concentration of 160 ug/mL 30 min prior to imaging the ventral forebrain dopamine (DA) neurons using the InCell 2000 (GE healthcare 28–9,534–63) automated microscope with the TexasRed channel and bright field using a 4 × 0.2NA objective (Nikon) using the built-in 2.5 D deconvolution setting. A total of five different poses were acquired by reorienting the larvae with a liquid handler (Biomek FXp) that mixed 40 μL of the solution in each well to change the orientation.

The images were analyzed on a custom generated MATLAB script (**Figure 1B**) that allows the manual selection of the best pose and the neurons are automatically extracted using the brightfield images with eyes as landmarks to automatically identify and extract the DA neurons. The analysis was based on a custom CellProfiler (McQuin et al., 2018) pipeline that processes and quantifies the fluorescent intensity and calculates the brain health score (BHS) based on the logarithm of the covariance between the brain image and a reference image generated from multiple healthy brains that was previously described (Liu et al., 2016). The BHS equation is as follows: BHS = log2 Σi,j IijMij, where I is the pixel intensity of the image and M is the pixel intensity of a template image based on the average of 35 brain images at pixel i, j. The SSMD was defined as the ratio of mean to the standard deviation of the difference between the MTZ treated negative control and the sample. The custom pipeline can be found in the Zenodo repository https://doi.org/10.5281/zenodo.5787480. All the experiments were performed in a blinded manner from compound treatment to analysis.

Topology and Non-Topology-Based Pathway Analysis

The bioactive compound library data was annotated with the Hugo Gene Nomenclature Committee (HGNC) database (Tweedie et al., 2021) and the Therapeutics target database (Wang et al., 2020). For each compound, the pharmaceutical class, known mechanism of action, indication, the half maximal inhibitory concentration (IC50), target, and the activity information was recorded (**Figure 2A**). For the SSMD and BHS scores of the compounds with opposing mechanisms of action such as inducer versus inhibitor, and agonist versus antagonist, the scores for the compounds with negative SSMD and BHS scores were inverted during the pathway analysis. The Reactome pathway analysis was conducted using the HGNC gene symbols as the identifier and the BHS as the numeric value. The non-topology-based pathway analysis was conducted with the entire HTS dataset. The annotated targets or pathways were analyzed with a Wilcoxon rank sum test to determine whether any had a brain health score that was significantly higher than the average of the entire dataset (FDR adj $p < 0.05$).

Secondary Assay Optimization and Hit Validation

To validate candidate hit compounds from the primary screen, we developed a medium throughput secondary assay that incorporates larger sample size, higher resolution, and statistical effect size. 5 dpf larvae were embedded in 1.2% agarose and imaged both before chemical treatment and 24 h after treatment, using the same x,y,z coordinates (**Figure 3A**). Image analysis was conducted by determining the ratio of "after treatment BHS" to "before treatment BHS". Since embedding did not need the multi-pose method from the initial screen (Liu et al.,

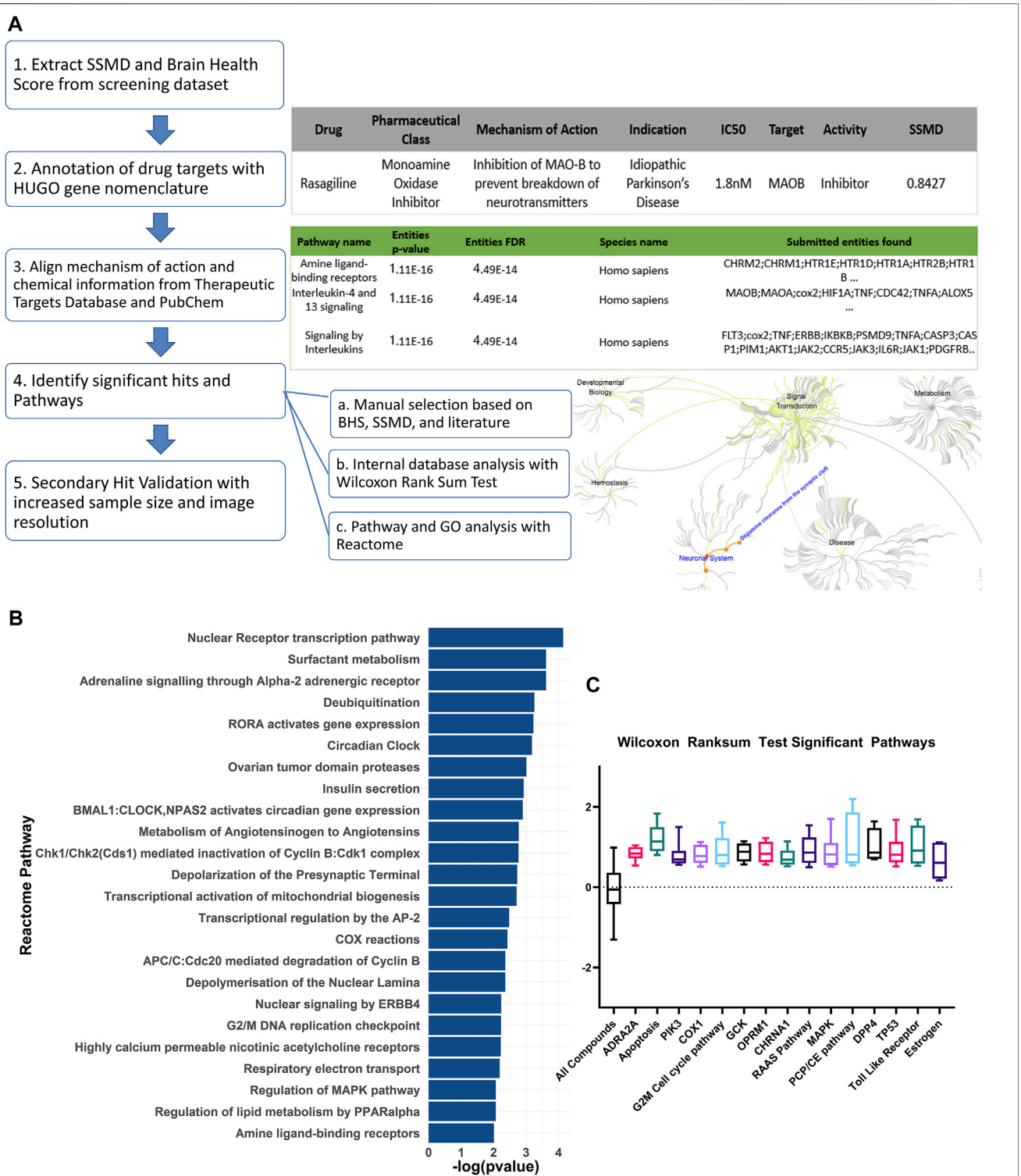

FIGURE 2 | Curation and pathway analysis of the screening dataset identify novel mechanisms of neuroprotection. **(A)** Schematic showing the data processing and analysis pipeline. The example output of the annotations are shown on the right side with the corresponding numbers of each step. Hit calling was based on three criteria, including manual selection with good BHS and SSMD score, Wilcoxon rank sum test, and Reactome pathway analysis. **(B)** A list of significant pathways from the Reactome pathway analysis sorted from highest to lowest significance (Padj <0.01). **(C)** Significant pathways from the non-topology-based pathway analysis of the screening dataset. BHS of the chemicals in the same pathway were compared against BHS of all compounds in the dataset. (n = 5 to 13; Padj <0.05, Wilcoxon rank sum test). ADRA2A: Alpha-2A adrenergic receptor, PIK3: Phosphoinositide 3-kinase, COX1: Cytochrome c oxidase subunit I, OPRM1: Mu type opioid receptor, CHRNA1: Cholinergic Receptor Nicotinic Alpha 1 Subunit, RAAS: Renin angiotensin system, MAPK: Mitogen-activated protein kinase, PCP/CE: Planar cell polarity and convergent extension, DPP4: Dipeptidyl peptidase-4, TP53: Tumor protein P53.

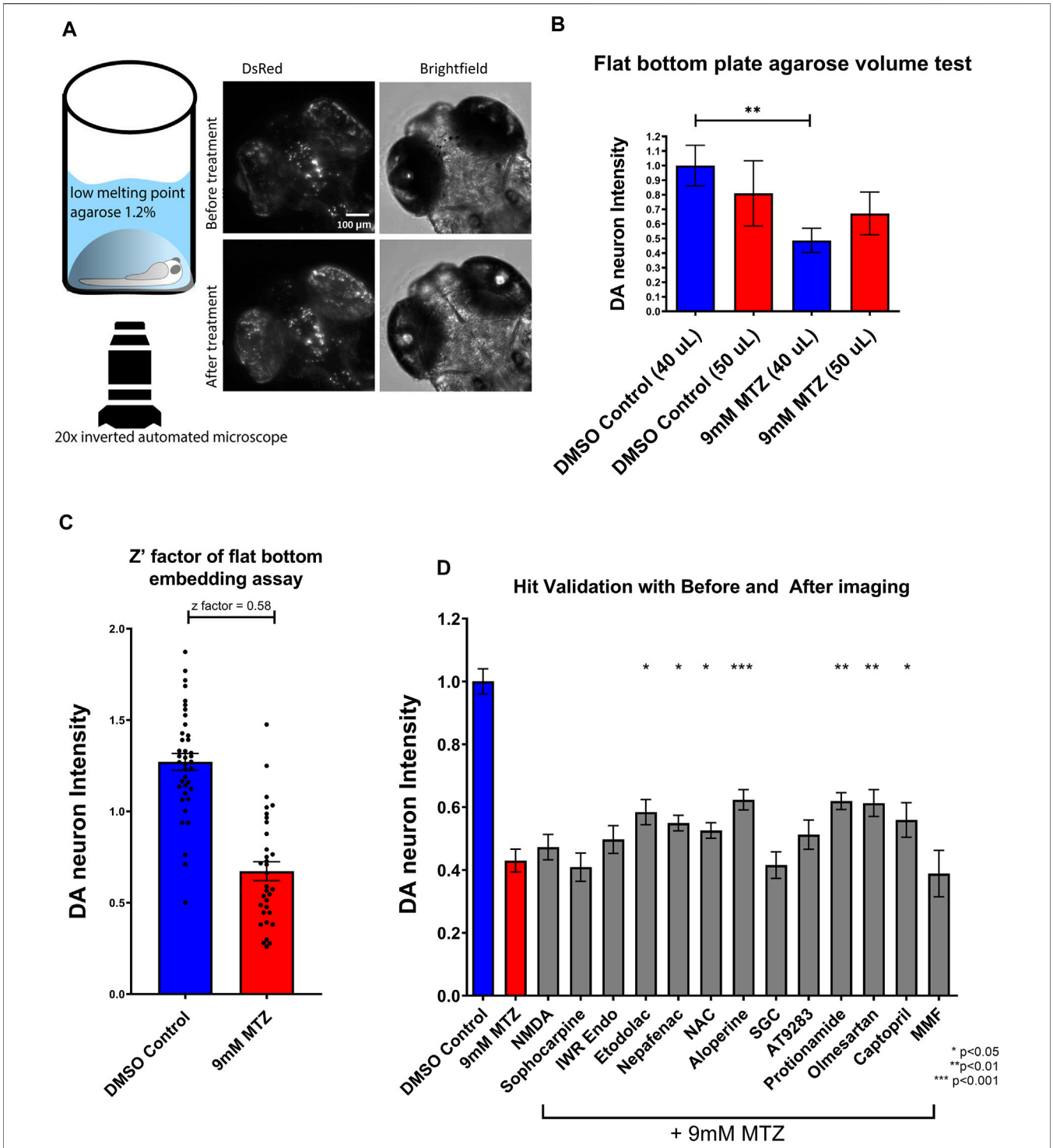

FIGURE 3 | Establishment of a secondary hit validation assay and validation of candidate hit compounds. **(A)** Schematic of the secondary hit validation assay using agarose embedding and automated imaging. At 5 dpf, larvae were embedded in 1.2% agarose and imaged under brightfield and DsRed channels. The larvae were treated with 0.2% DMSO or 9 mM MTZ with or without hit compounds. At 6 dpf, larvae were again imaged with the same x,y,z coordinates on the microscope. Image shown is an example of a 0.2% DMSO control. **(B)** Comparison of 40 and 50 µL 1.2% low melting point agarose for embedding. Samples embedded with 40 µL agarose showed significant difference between DMSO control and 9 mM MTZ ($n = 8$; $p < 0.05$, unpaired t test), whereas those with 50 µL agarose did not, due to increased distance between the objective and the samples. **(C)** Evaluation of Z′-factor for the secondary hit validation assay. The 0.2% DMSO control and 24 h of 9 mM MTZ treatment showed a significant difference in DA neuron intensity with a z'factor of 0.58. **(D)** Secondary hit validation of compounds with the embedding assay. Samples were treated with 10 µM of each candidate compound and 9 mM MTZ for 24 h. Etodolac, nepafenac, NAC, aloperine, Protionamide, olmesartan, and captopril showed significantly greater "BHS After treatment" to "BHS before treatment" ratio compared to the negative control (9 mM MTZ) ($n = 22$ to 30; one-way ANOVA $F = 12.33$, $p = 0.003$, post-hoc Fishers LSD $^{*}p < 0.05$, $^{**}p < 0.01$, $^{***}p < 0.001$). MTZ: metronidazole, DMSO: dimethyl sulfoxide, NAC: N-Acetyl Cysteine, NMDA: N-methyl-D-aspartate, MMF: Mycophenolate mofetil, SGC: SGC-CBP30.

TABLE 1 | Top 30 hit compounds from the bioactive high throughput screen with high SSMD and BHS (ranked by BHS).

Compound name	SSMD	Brain health score	*p*-value	Selleckchem ID	Mechanism of action
Dimesna	1.4201	1.8829	0.0120	S1201	Inactivation of acrolein
AT9283	0.8713	1.4271	0.0134	S1134	JAK2/3 kinase inhibitor
Deferasirox	1.3424	1.4235	0.0152	S1712	Iron chelator
Etodolac	0.9883	1.3901	0.0155	S1328	COX inhibitor
Rapamycin	1.6795	1.3652	0.0165	S1039	mTOR inhibitor
AG-490 (Tyrphostin B42)	0.7901	1.3311	0.0167	S1143	EGFR inhibitor
Budesonide	0.6488	1.3074	0.0170	S1286	Glucocorticoid steroid
Prednisolone	1.2094	1.2636	0.0171	S1737	Glucocorticoid steroid
Nepafenac	0.7728	1.2268	0.0176	S1255	COX inhibitor
Sophocarpine	0.8636	1.2109	0.0176	S2405	Tetracyclic quinolizidine alkaloid
Ganetespib (STA-9090)	0.8437	1.1885	0.0203	S1159	HSP90 inhibitor
Aliskiren Hemifumarate	1.5401	1.1308	0.0205	S2199	Direct renin inhibitor
Olmesartan Medoxomil	1.6489	1.1136	0.0208	S1604	Angiotensin II receptor blocker
Aloperine	1.0303	1.0835	0.0210	S2420	PI3K/Akt inhibitor
SGC-CBP30	2.3118	1.0794	0.0222	S7256	CREBBP inhibitor
LY2608204	1.1448	1.0579	0.0238	S2155	Glucokinase activator
Hexstrol	0.7018	1.0509	0.0241	S2473	Nonsteroidal estrogen
Gallamine triethiodide	0.6848	1.0341	0.0336	S2471	Cholinergic receptor blocker
IWR-1-endo	2.1948	0.9941	0.0342	S7086	Wnt inhibitor
Cyproterone Acetate	1.0325	0.9849	0.0365	S2042	Androgen receptor antagonist
Maprotiline HCl	1.2404	0.8950	0.0375	S2517	Noradrenalin reuptake inhibitor
CYT387	1.0129	0.8683	0.0430	S2219	JAK1/2 kinase inhibitor
Teniposide	6.8325	0.8597	0.0403	S1787	DNA topoisomerase II inhibitor
Volasertib (BI 6727)	1.3177	0.8468	0.0411	S2235	Plk1 inhibitor
Vismodegib	1.4720	0.7387	0.0417	S1082	Hedgehog inhibitor
SB590885	1.6987	0.7384	0.0423	S2220	B-raf inhibitor
Protionamide	1.6363	0.7103	0.0432	S1881	Class 1A anti-arrhythmic, Sodium Channel Blocker
Y-27632	4.8342	0.6942	0.0433	S1049	ROCK1 inhibitor
NMDA (N-Methyl-D-aspartic acid)	1.6915	0.6197	0.0436	S7072	NMDA agonist
Mestranol	1.6959	0.5421	0.0447	S2125	Estrogen receptor activation

2016), a flat bottom 96 well plate was used for greater efficiency in embedding and better tracking of well coordinates and resolution.

The hit candidates selected from the pathway analysis underwent a secondary assay validation with greater sample size. Unlike the primary HTS assay, the secondary assay was designed as a low throughput assay that involves manual embedding of each larval zebrafish in a thin layer of agarose to obtain the most optimal position for visualizing the DA neurons, followed by imaging using a ×20 objective under a confocal microscope with both before and after images taken. The assay was optimized by determining the shape of the well, agarose concentration, and volume of agarose used for embedding. A flat bottom 96 well plate (Griener cat no 655096) was used. The candidate hits were added in 10 μM concentration for 3 h prior to the administration of 9 mM MTZ. The 5 dpf before treatment images were taken on the InCell 6,000 (GE healthcare) and subsequently taken again post 24 h incubation. The images were taken with an inverted ×20 objective under dsRed and brightfield channels (0.45NA, 7.5 mm working distance). 3 μm Z-slices for a total of 40 slices were obtained and the max intensity projection was processed with ImageJ. The BHS was calculated based on the Cellprofiler pipeline as described above. The ratio of BHS before treatment and BHS after treatment was used to quantify the neuroprotective effect and to account for any changes due to brain development during the incubation period. For the dose response studies, concentrations of the compounds were prepared from a series of 5-fold dilutions that were determined by a range based on the known EC50 properties. The candidate compounds were purchased from SelleckChem (NMDA: S7072, Sophocarpine: S2405, IWR Endo: S7086, Etodolac: S1328, Nepafenac: S1255, Aloperine: S2420, SGC-CBP30: S7256, NAC: S1623, AT9283: S1134, Protionamide: S1881, olmesartan: S1604, captopril: S2051, Mycophenolate Mofetil: S1501). The manual screening was performed in a blinded manner by having a single investigator code the compounds and another investigator counting the medium- and large-sized DA neurons under the 20x epifluorescent compound microscope (Zeiss).

RESULTS

In Vivo DA Neuron Imaging-Based High Throughput Screening Identifies Neuroprotective Compounds

A total of 1,403 bioactive compounds (SelleckChem) were screened at 10 μM concentration that were obtained from the UCSF Small Molecule Discovery Center (SMDC). The dual flashlight plot was created to visualize the strictly standardized mean difference (SSMD) and the BHS (**Figures 1C,D**). A total of 57 compounds had a BHS score

TABLE 2 | Significant compounds and pathways identified from the Reactome and Wilcoxon Rank sum test. Detailed information of the 83 compounds from the initial compound library that were shown to be significant in both the Reactome pathway analysis and wilcoxon rank sum test. The strictly standardized mean difference (SSMD) score measures the effect size and the variance amongst the triplicate larval samples for each compound. The brain health score (BHS) was defined as the logarithm of the covariance between the brain image and a template image. During the analysis pipeline, the SSMD and BHS scores were converted for directionality based on the pharmacological activity profile obtained from the Therapeutic Target database. The pathway names were outputted directly based on the target and activity profile from Reactome.

Compound	Pathway name	SSMD	BHS	Target	Activity	FDA status
Dexmedetomidine	Adrenaline signalling through Alpha-2 adrenergic receptor	1.040	−2.928	ADRA2A	AGONIST	Approved
Guanabenz Acetate	Adrenaline signalling through Alpha-2 adrenergic receptor	0.984	−0.868	ADRA2A	AGONIST	Approved
Noradrenaline	Adrenaline signalling through Alpha-2 adrenergic receptor	0.855	−1.021	ADRA2A	STIMULATOR	Approved
Phentolamine Mesylate	Adrenaline signalling through Alpha-2 adrenergic receptor	−0.818	0.624	ADRA2A	INHIBITOR	Approved
Medetomidine	Adrenaline signalling through Alpha-2 adrenergic receptor	0.777	−0.729	ADRA2A	AGONIST	Approved
Ivabradine HCl	Adrenaline signalling through Alpha-2 adrenergic receptor	0.539	0.156	ADRA2A	INHIBITOR	Approved
Y-27632 2HCl	Apoptosis	4.834	0.694	ROCK1	INHIBITOR	
Oprozomib	Apoptosis	1.558	0.221	PSMB8	INHIBITOR	
Apoptosis Activator 2	Apoptosis	1.291	−3.112	CASP3	ACTIVATOR	
Evodiamine	Apoptosis	−1.150	−0.525	BCL2	INDUCER	
RKI-1447	Apoptosis	1.124	−0.097	ROCK1	INHIBITOR	
Dynasore	Apoptosis	0.913	−0.232	DNM1	INHIBITOR	
PF-573228	Apoptosis	0.891	0.305	PTK2	INHIBITOR	
Carfilzomib (PR-171)	Apoptosis	−0.801	−0.066	PSMD9	AGONIST	Approved
ZSTK474	Cell surface interactions at the vascular wall	1.500	0.322	PIK3CA	INHIBITOR	
Dactolisib (BEZ235, NVP-BEZ235)	Cell surface interactions at the vascular wall	0.904	0.571	PIK3CA	INHIBITOR	
RepSox	Cell surface interactions at the vascular wall	0.746	−0.112	TGFB1	INHIBITOR	
Dasatinib	Cell surface interactions at the vascular wall	0.690	0.261	SRC	INHIBITOR	Approved
ML347	Cell surface interactions at the vascular wall	0.625	−0.090	TGFB1	INHIBITOR	
CAL-101 (Idelalisib, GS-1101)	Cell surface interactions at the vascular wall	0.590	0.360	PIK3CA	INHIBITOR	
Bosutinib (SKI-606)	Cell surface interactions at the vascular wall	0.558	0.134	SRC	INHIBITOR	Approved
Ibuprofen (Dolgesic)	COX reactions	1.124	0.217	COX	INHIBITOR	Approved
Mefenamic acid	COX reactions	1.074	0.446	COX	INHIBITOR	Approved
Etodolac (Lodine)	COX reactions	0.988	1.390	COX	INHIBITOR	Approved
Bromfenac	COX reactions	0.778	1.053	COX	INHIBITOR	Approved
Nepafenac	COX reactions	0.773	1.227	COX	INHIBITOR	Approved
Diclofenac Sodium	COX reactions	0.694	0.428	PTSG2	INHIBITOR	Approved
Ketorolac (ketorolac tromethamine)	COX reactions	0.577	0.504	COX	INHIBITOR	Approved
Suprofen (Profenal)	COX reactions	0.510	0.423	COX	INHIBITOR	Approved
Enzastaurin (LY317615)	Depolymerisation of the Nuclear Lamina	0.522	0.610	PRKCB	INHIBITOR	
JTC-801	G-protein activation	−1.223	−3.519	OPRM1	ANTAGONIST	
Matrine ((+)-Matrine)	G-protein activation	0.800	0.787	OPRM1	AGONIST	
Naloxone HCl	G-protein activation	0.564	0.964	OPRM1	AGONIST	Approved
Tenovin-1	G2/M DNA damage checkpoint	−1.612	−0.715	TP53	ACTIVATOR	
VE-821	G2/M DNA damage checkpoint	0.923	0.332	ATM	INHIBITOR	
VE-822	G2/M DNA damage checkpoint	0.781	0.041	ATR	ANTAGONIST	
LY2608204	Glycolysis	1.145	1.058	GCK	INHIBITOR	
Clorsulon	Glycolysis	0.907	0.518	GPM1	INHIBITOR	
Vismodegib (GDC-0449)	Hh mutants that don't undergo autocatalytic processing are degraded by ERAD	1.472	0.739	SHH	INHIBITOR	Approved
PNU-120596	Highly calcium permeable nicotinic acetylcholine receptors	−1.142	−3.868	CHRNA1	AGONIST	
Tropicamide	Highly calcium permeable nicotinic acetylcholine receptors	0.952	0.697	CHRNA1	INHIBITOR	Approved
Darifenacin	Highly calcium permeable nicotinic acetylcholine receptors	0.869	0.064	CHRNA1	INHIBITOR	Approved
Pancuronium dibromide	Highly calcium permeable nicotinic acetylcholine receptors	0.860	0.930	CHRNA1	INHIBITOR	Approved
Gallamine triethiodide (Flaxedil)	Highly calcium permeable nicotinic acetylcholine receptors	0.685	1.034	CHRNA1	INHIBITOR	Approved
Adiphenine	Highly calcium permeable nicotinic acetylcholine receptors	0.671	0.306	CHRNA1	INHIBITOR	
Bethanechol chloride	Highly calcium permeable nicotinic acetylcholine receptors	0.570	−0.201	CHRNA1	AGONIST	Approved
Atropine sulfate monohydrate	Highly calcium permeable nicotinic acetylcholine receptors	0.551	0.416	CHRNA1	INHIBITOR	Approved
Cytisine	Highly calcium permeable nicotinic acetylcholine receptors	−0.520	−0.750	CHRNA4	AGONIST	
Aliskiren hemifumarate	Metabolism of Angiotensinogen to Angiotensins	1.540	1.1308	REN	INHIBITOR	Approved
Imidapril HCl	Metabolism of Angiotensinogen to Angiotensins	0.938	0.5801	ACE	INHIBITOR	
Enalapril Maleate	Metabolism of Angiotensinogen to Angiotensins	0.860	2.947	ACE	INHIBITOR	
Quinapril hydrochloride (accupril)	Metabolism of Angiotensinogen to Angiotensins	0.707	0.385	ACE	INHIBITOR	Approved
Ramipril	Metabolism of Angiotensinogen to Angiotensins	0.498	0.253	ACE	INHIBITOR	Approved
SB590885	Negative feedback regulation of MAPK pathway	1.699	0.738	RAF1	INHIBITOR	
Selumetinib (AZD6244)	Negative feedback regulation of MAPK pathway	1.098	0.172	MEK1	INHIBITOR	

(Continued on following page)

TABLE 2 | (*Continued*) Significant compounds and pathways identified from the Reactome and Wilcoxon Rank sum test. Detailed information of the 83 compounds from the initial compound library that were shown to be significant in both the Reactome pathway analysis and wilcoxon rank sum test. The strictly standardized mean difference (SSMD) score measures the effect size and the variance amongst the triplicate larval samples for each compound. The brain health score (BHS) was defined as the logarithm of the covariance between the brain image and a template image. During the analysis pipeline, the SSMD and BHS scores were converted for directionality based on the pharmacological activity profile obtained from the Therapeutic Target database. The pathway names were outputted directly based on the target and activity profile from Reactome.

Compound	Pathway name	SSMD	BHS	Target	Activity	FDA status
RAF265 (CHIR-265)	Negative feedback regulation of MAPK pathway	0.886	0.537	RAF1	INHIBITOR	
SL327	Negative feedback regulation of MAPK pathway	0.812	0.668	MEK1	INHIBITOR	
Vemurafenib (PLX4032, RG7204)	Negative feedback regulation of MAPK pathway	0.625	0.962	BRAF	INHIBITOR	Approved
Tanshinone IIA (Tanshinone B)	Negative feedback regulation of MAPK pathway	0.547	1.823	MAP2K1	INHIBITOR	
PD0325901 (PD325901)	Negative feedback regulation of MAPK pathway	0.511	0.597	MEK1	INHIBITOR	
IWR-1 (endo-IWR 1)	PCP/CE pathway	2.195	0.994	WNT1	INHIBITOR	
EHop-016	PCP/CE pathway	0.879	−0.273	RAC1	INHIBITOR	
XAV-939	PCP/CE pathway	0.544	0.853	WNT1	INHIBITOR	
Protionamide	Peptide hormone metabolism	1.636	0.710	INHA	INHIBITOR	
Alogliptin	Peptide hormone metabolism	0.988	0.720	DPP4	INHIBITOR	Approved
TAK-875	Peptide hormone metabolism	0.733	1.320	gpr40	ANTAGONIST	
SGC-CBP30	Regulation of Hypoxia-inducible Factor (HIF) by oxygen	2.312	1.079	DOT1L	INHIBITOR	
Rapamycin	Regulation of TP53 Activity	1.679	1.365	MTOR	INHIBITOR	Approved
P22077	Regulation of TP53 Activity	1.145	0.694	USP7	INHIBITOR	
ETP-46464	Regulation of TP53 Activity	1.085	0.023	MTOR	INHIBITOR	
Ridaforolimus	Regulation of TP53 Activity	1.078	0.298	MTOR	INHIBITOR	
PP242	Regulation of TP53 Activity	0.896	0.892	MTOR	INHIBITOR	
KU-0063794	Regulation of TP53 Activity	0.618	1.254	MTOR	INHIBITOR	
PHT-427	Regulation of TP53 Activity	0.616	0.553	AKT1	INHIBITOR	
Entinostat (MS-275)	Regulation of TP53 Activity	0.574	0.524	HDAC1	INHIBITOR	
AZD1152-HQPA (Barasertib)	Regulation of TP53 Activity	0.517	1.01	AURKB	INHIBITOR	
Carprofen	Respiratory electron transport	0.697	0.858	cox2	INHIBITOR	Approved
Cilengitide	Smooth Muscle Contraction	0.718	−0.104	ITGA1	INHIBITOR	
(-)-Huperzine A	Synthesis of PC	1.320	0.550	ACHE	INHIBITOR	
Odanacatib (MK 0822)	Toll-Like Receptors Cascades	−1.054	−0.098	CTSK	AGONIST	
EUK 134	Toll-Like Receptors Cascades	0.529	0.279	APP	INHIBITOR	
NMDA	TP53 Regulates Metabolic Genes	1.691	0.619	NMDA	AGONIST	
BAM 7	TP53 Regulates Transcription of Genes Involved in G2 Cell Cycle Arrest	0.763	0.027	BAX	INDUCER	

that was significantly greater when compared to MTZ treatment alone (FDR adjusted $p < 0.05$) (**Table 1**). 67% of the hit compounds identified were inhibitors while 14% were agonists or activators. The remaining compounds were synthetic hormones or glucocorticoids including prednisolone, budesonide, hexestrol, and mestranol. Four compounds were natural products from plants including aloperine, matrine, and sesamin. The primary therapeutic class for the compounds consisted of 32% anti-cancer, 31% neurological, 15% infectious diseases, 12% cardiovascular, and 10% endocrinology drugs.

Pathway Analyses Identify Previously Unknown and Validate Previously Known Pathways Associated With PD

The Reactome pathway analysis identified 24 significant pathways after correcting for false discoveries (**Figure 2B**) ($p < 0.05$, FDR = 0.01). With PD being highly related to mitochondrial dysfunction, pathways including deubiquitylation, cyclooxygenase (COX), respiratory electron transport, mitochondrial biogenesis were found to be significant. Other pathways relevant to PD such as acetylcholine receptors, adrenergic signaling, mitogen activated protein kinase (MAPK) were also found to be significant. Additionally, cell cycle and development pathways were found significant including transcriptional regulation by AP-2 and G2/M DNA replication checkpoint. Several pathways were novel or have limited implications in PD, including RAR Related Orphan Receptor A (RORA) gene activation, circadian clock, ovarian tumor proteases, Peroxisome proliferator-activated receptor alpha (PPARα), renin angiotensin system, and insulin regulation.

The non-topology-based pathway analysis using the Wilcoxon rank sum test of the entire dataset showed 15 targets and pathways to be significant ($p < 0.05$, FDR = 0.05) (**Figure 1C**). Apoptosis, estrogen hormone, dipeptidyl-peptidase 4 (DPP4), and opioid receptor Mu 1 were significant in the Wilcoxon rank sum test but not in the Reactome analysis. A total of 83 compounds were shown to be significant in both the Reactome and Wilcoxon rank sum test (**Table 2**). 32 compounds were already FDA approved and 20 compounds were in early phase clinical trials.

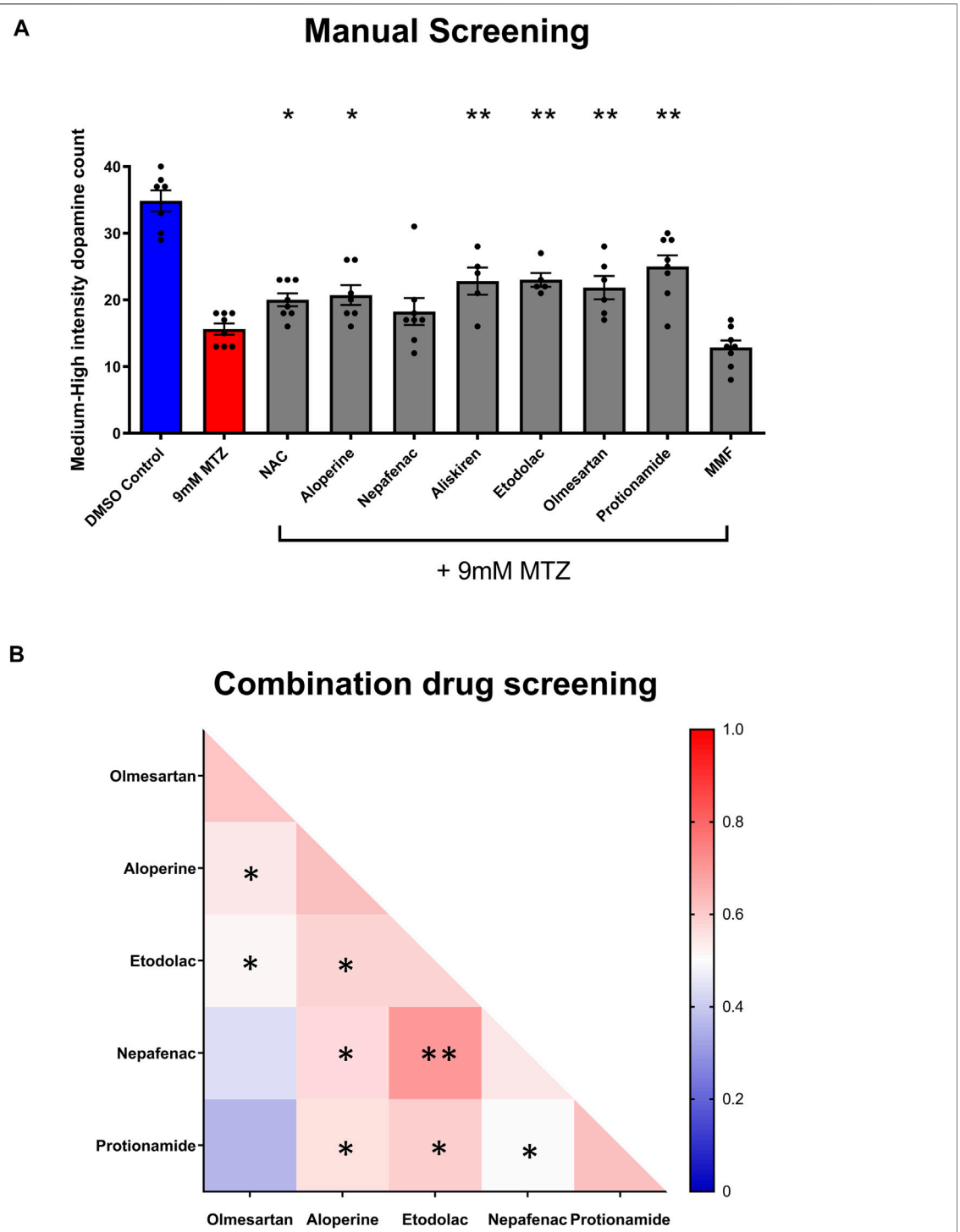

FIGURE 4 | Manual screening and combination screening of hit candidates based on secondary assay. **(A)** Manual screening of the significant compounds identified from the secondary hit validation assay. All samples were manually quantified in a blinded manner after 24 h treatment with candidate compounds and MTZ as described above. (n = 7 to 8; one-way ANOVA F = 16.72, $p < 0.001$, post-hoc Fishers LSD $^{*}p < 0.05$, $^{**}p < 0.01$). **(B)** Heatmap matrix showing the BHS for testing hit compounds in combination. All candidate compounds were 10 μM in concentration. The combination of etodolac-nepafenac, etodolac-protionamide, and etodolac-aloperine showed greater BHS compared to the administration of either alone. 0.2% DMSO for positive control and 9 mM MTZ for negative control. (n = 12 to 16; $^{*}p < 0.05$, $^{**}p < 0.01$, unpaired t test).

Secondary Hit Validation Identifies Non-Steroidal Anti-inflammatory Drugs, Renin Angiotensin System, Aloperine, and Protionamide to Be Neuroprotective

For secondary hit validation, we developed an agarose embedding method to achieve better resolution for imaging DA neurons. We first experimented with the volume of agarose used for embedding. 40 µL was chosen as it did not harm or stress larvae during the 24 h incubation period (**Figure 3B**). The higher 50 uL volume of agarose resulted in worsening image quality due to the distance between the DA neurons and inverted objective lens. Furthermore, having too much agarose possibly resulted in less air exchange, thus impairing the health of the larvae when embedded for a prolonged period of time. The calculated z' factor of the secondary assay was 0.58, which is considered an excellent assay with less within-group variation compared to the z' factor 0.35 of the primary assay (**Figure 3C**, **Supplementary Figure S1**).

Utilizing the secondary hit validation assay, a total of 12 candidate compounds were tested for neuroprotection. We selected these compounds based on a combination of statistical thresholding using SSMD and BHS and pathway analyses. Additionally, N-Acetyl Cysteine (NAC) was used as a reference compound based on previous studies showing significant neuroprotection in other DA models (Monti et al., 2019). After treatment with 9 mM MTZ for 48 h and comparing the BHS of the before and after images, 10 µM etodolac, nepafenac, aloperine, NAC, protionamide, olmesartan, and captopril showed significant neuroprotection (**Figure 3D**). These compounds were then manually validated in a single blinded design by counting the medium to high intensity dopamine neurons after 24 h of MTZ treatment. All compounds except for nepafenac were shown to be significant compared to control ($p < 0.05$) (**Figure 4A**). A dose response study of nepafenac showed lower doses (0.04 and 2.0 µM) to be neuroprotective (**Supplementary Figure S2**). For the dose response study, there were no linear dose response relationships observed in the BHS scores and toxicity was observed for all compounds at the highest concentrations.

Significantly neuroprotective drugs were also tested in combination to determine the possible drug pairs that could provide additive or synergistic effects on neuroprotection. The combination of etodolac-nepafenac, etodolac-protionamide, and etodolac-aloperine showed a greater BHS compared to the administration of either compound alone (**Figure 4B**).

Validation of Candidate Compounds in a Chemically Induced Gaucher Disease Model Uncovers DA Neuron Protection

As the NTR-MTZ induced DA neuron degeneration does not directly relate to the etiology of PD in humans, we next tested the candidate compounds using a chemically induced Gaucher's disease model. Gaucher's disease involves mutations in the glucocerebrosidase (gba1) gene, which is known to be the most common genetic risk factor for PD (Riboldi and Di Fonzo, 2019). Chemical inhibition of GBA was achieved using conduritol B-epoxide, which has been previously established in both mice and zebrafish (Vardi et al., 2016; Artola et al., 2019). 5 dpf larvae were treated with 10 µM of the candidate compounds etodolac, nepafenac, olmesartan, protionamide, and aloperine along with 500 µM CBE for 48 h. At 7 dpf, the larvae were imaged with the InCell 6,000 high throughput confocal imaging platform and the ventral DA neurons were analyzed with the custom CellProfiler pipeline (**Figure 5A**). The compounds nepafenac, olmesartan, and aloperine showed significant neuroprotection compared to the CBE treatment alone ($p < 0.01$, $p < 0.01$, and $p < 0.001$ respectively, one-way ANOVA with post-hoc Fischer's LSD) (**Figure 5B**).

Statistical Analysis

The SSMD and BHS data from high throughput screening studies were analyzed by one-way ANOVA and post-hoc Fishers LSD (lease squares difference) test with the R program and is expressed as means ± SEM unless otherwise stated. When only two groups were present (i.e., DMSO versus MTZ control or 40uL agarose versus 50uL agarose), an unpaired *t*-test was performed. The pathway analysis with Reactome was conducted with an over-representation (hypergeometric) test. The non-topology-based pathway analysis was carried out using the Wilcoxon rank sum test to identify significant targets from the entire screen. All the secondary hit validations were conducted with a one-way ANOVA and post-hoc LSD between the sample and negative control (MTZ treatment).

DISCUSSION

By developing a whole organism screening assay that directly images DA neurons of larval zebrafish in a high throughput manner, we have introduced a phenotype-based method for identifying compounds that protect against DA neuron degeneration. The secondary hit validation assay that utilizes the embedding technique to image before and after treatment showed an excellent z' factor score. Since a threshold-based hit calling method using SSMD and BHS scores focuses primarily on the selection of top scored hits, this is limited due to the small sample size of $n = 3$ in the primary screen, some true hit may be missed due to low affinity of the compounds that may be improvable by future medicinal chemistry. We therefore employed additional bioinformatic analysis to select candidates based on significant results from the pathway analysis. These efforts led to the identification of new pathways previously not linked to PD, as well as the validation of pathways previously implicated in PD.

Pathway analysis revealed mitochondrial dysfunction and respiratory transport chain pathways that are known to be closely tied to the etiology of PD (Park et al., 2018). This finding further strengthens the relevance of our screening assay to PD. The relevance of our screening assay has also been established in our recent report of an in-depth analysis of the RAAS inhibitors in PD (Kim et al., 2021). Etodolac and nepafenac identified in our screen are known COX-2 selective

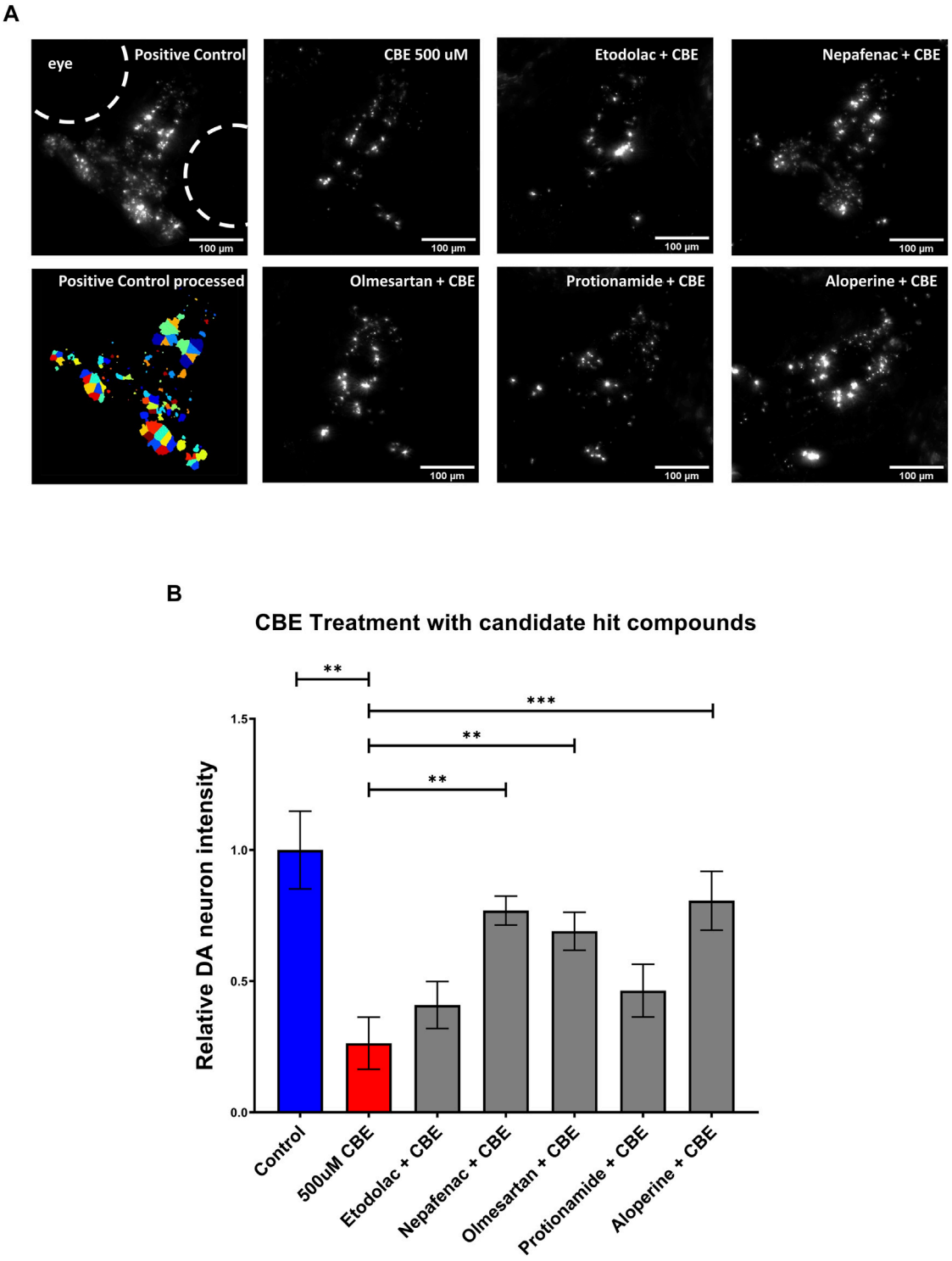

FIGURE 5 | Validation of candidate compounds in a chemically induced Gaucher disease model. **(A)** High throughput imaging of DA neurons with the InCell 6,000 platform for the positive control, CBE, and the candidate compounds. The bottom left image shows the DA neuron isolation process in the custom Cellprofiler pipeline used for image analysis. **(B)** Hit validation of candidate compounds with 48 h treatment of 500 µM CBE. At 5 dpf, larvae were treated with 0.2% DMSO (positive control), 500 µM CBE (negative control), and the CBE+ 10 µM candidate compounds for 48 h. At 7 dpf, the larvae were imaged with a confocal microscope. The 500 µM CBE showed significant reduction in DA neurons compared to the 0.2% DMSO control (N = 12; $p = 0.0012$, unpaired *t*-test). Nepafenac, olmesartan, and aloperine showed significant neuroprotection when co-treated with CBE ($N = 10$ to 12; one-way ANOVA F = 6.205, $p < 0.001$, post-hoc Fishers LSD $^{**}p < 0.01$, $^{***}p < 0.001$, unpaired *t*-test). CBE: Conduritol B epoxide.

inhibitors, which have been previously studied as potential PD therapeutics with its anti-inflammatory properties. Particularly COX-2 is involved in microglia activation, production of radicals, and protects against DA neuron loss in 6-OHDA rat models (Sánchez-Pernaute et al., 2004; Bartels and Leenders, 2010).

Pathways that are not previously associated with PD could lead to new targets and therapeutics. The pathway related to circadian rhythm regulation was found significant from the Reactome pathway analysis. These include the BMAL1: CLOCK:NPAS2 circadian gene expression pathway. Sleep disturbance is a common nonmotor complaint in PD but the etiology is not well understood (Breen et al., 2014). The circadian clock gene BMAL1 is important in sleep control and leukocytes of PD patients have shown to have altered expression that also correlates with PD severity (Cai et al., 2010). Studies in mice have shown that cholinergic neurons of the basal forebrain are more active in Bmal1 muscle-overexpressed mice (Ehlen et al., 2017). In zebrafish, circadian genes modulate dopamine levels (Huang et al., 2015). Insulin regulation and glucose control was also found to be significantly linked to neuroprotection in the pathway analysis. This is supported by a previous report that hyperglycemia increases the production of reactive oxygen species from the mitochondrial electron transport chain and type 2 diabetes is associated with an increased risk of PD (Hu et al., 2007).

The natural product aloperine showed strong and validated neuroprotective effects in this study. Aloperine is a quinolizidine-type alkaloid that is known to have antioxidant properties through suppression of NF-κB signaling (Xu et al., 2014), activation of nuclear factor erythroid-related factor 2 (Song et al., 2018). Aloperine can also inhibit apoptosis in amyloid induced mouse cells in a mitochondria-dependent pathway (Zhao et al., 2018). The neuroprotective benefits of natural compounds are a promising topic of interest but further efforts on elucidating their pharmacokinetic and pharmacodynamic properties are needed (Sharifi-Rad et al., 2020).

The initial screen had a relatively low sample size of $n = 3$ which could have led to variability and potential false errors. However, this was mitigated by calculating the SSMD score and evaluating not single compounds, but a group of compounds based on pharmacological targets and pathway analysis. Furthermore, secondary validation was conducted with greater sample size along with a blinded manual screen. With the NTR/MTZ assay, it is possible that the compounds that act as inhibitors of NTR could come across as being neuroprotective. These compounds should not show neuroprotection in the second model, the CBE-induced GD model. Therefore, by using both assays in our study, we shall be able to identify broad neuroprotective compounds and distinguish them from NTR inhibitors. The hit compounds identified in this paper will require follow up studies in other animal models and at the mechanistic levels to understand their potential neuroprotective effects in PD.

DATA AVAILABILITY STATEMENT

The original contributions presented in the study are included in the article/**Supplementary Material**, further inquiries can be directed to the corresponding authors.

ETHICS STATEMENT

The animal study was reviewed and approved by University of California, San Francisco Institutional Animal Care and Use Committee (approval number AN179000).

AUTHOR CONTRIBUTIONS

SG and GJK conceived the project. GJK, HM, HL, SC, MO performed the experiments. GJK, HM, SC, HL, JZ, analyzed data. HL, MA, BH, and SG provided resources, supervision, and funding acquisition. GJK and SG wrote the paper with the contributions from all authors.

FUNDING

This project was supported by NIH R21 NS082938, R01 NS120219, and DoD CDMRP PD170068 (to SG), NIH R01AG058742 (to HL), the UCSF Mary Anne Koda-Kimble Seed Award for Innovation and the Luis Zeh Fellowship (to GJK).

ACKNOWLEDGMENTS

We thank Michael Munchua and Vivian Yuan for excellent animal care and maintenance of the zebrafish facility and the Guo lab members for helpful discussions throughout the study design and analysis.

SUPPLEMENTARY MATERIAL

The Supplementary Material for this article can be found online at: https://www.frontiersin.org/articles/10.3389/fphar.2022.837756/full#supplementary-material

REFERENCES

Armstrong, M. J., and Okun, M. S. (2020). Diagnosis and Treatment of Parkinson Disease: A Review. *JAMA* 323, 548–560. doi:10.1001/jama.2019.22360

Artola, M., Kuo, C. L., Lelieveld, L. T., Rowland, R. J., van der Marel, G. A., Codée, J. D. C., et al. (2019). Functionalized Cyclophellitols Are Selective Glucocerebrosidase Inhibitors and Induce a Bona Fide Neuropathic Gaucher Model in Zebrafish. *J. Am. Chem. Soc.* 141, 4214–4218. doi:10.1021/jacs.9b00056

Bartels, A. L., and Leenders, K. L. (2010). Cyclooxygenase and Neuroinflammation in Parkinson's Disease Neurodegeneration. *Curr. Neuropharmacol.* 8, 62–68. doi:10.2174/157015910790909485

Breen, D. P., Vuono, R., Nawarathna, U., Fisher, K., Shneerson, J. M., Reddy, A. B., et al. (2014). Sleep and Circadian Rhythm Regulation in Early Parkinson Disease. *JAMA Neurol.* 71, 589–595. doi:10.1001/jamaneurol.2014.65

Cai, Y., Liu, S., Sothern, R. B., Xu, S., and Chan, P. (2010). Expression of Clock Genes Per1 and Bmal1 in Total Leukocytes in Health and Parkinson's Disease. *Eur. J. Neurol.* 17, 550–554. doi:10.1111/j.1468-1331.2009.02848.x

Curado, S., Stainier, D. Y., and Anderson, R. M. (2008). Nitroreductase-mediated Cell/tissue Ablation in Zebrafish: a Spatially and Temporally Controlled Ablation Method with Applications in Developmental and Regeneration Studies. *Nat. Protoc.* 3, 948–954. doi:10.1038/nprot.2008.58

DeMaagd, G., and Philip, A. (2015). Parkinson's Disease and its Management: Part 1: Disease Entity, Risk Factors, Pathophysiology, Clinical Presentation, and Diagnosis. *P. T.* 40, 504–532. Available at: https://pubmed.ncbi.nlm.nih.gov/26236139.

Ehlen, J. C., Brager, A. J., Baggs, J., Pinckney, L., Gray, C. L., DeBruyne, J. P., et al. (2017). Bmal1 Function in Skeletal Muscle Regulates Sleep. *Elife* 6, e26557. doi:10.7554/eLife.26557

Howe, K., Clark, M. D., Torroja, C. F., Torrance, J., Berthelot, C., Muffato, M., et al. (2013). The Zebrafish Reference Genome Sequence and its Relationship to the Human Genome. *Nature* 496, 498–503. doi:10.1038/nature12111

Hu, G., Jousilahti, P., Bidel, S., Antikainen, R., and Tuomilehto, J. (2007). Type 2 Diabetes and the Risk of Parkinson's Disease. *Diabetes Care* 30, 842–847. doi:10.2337/dc06-2011

Huang, J., Zhong, Z., Wang, M., Chen, X., Tan, Y., Zhang, S., et al. (2015). Circadian Modulation of Dopamine Levels and Dopaminergic Neuron Development Contributes to Attention Deficiency and Hyperactive Behavior. *J. Neurosci.* 35, 2572–2587. doi:10.1523/JNEUROSCI.2551-14.2015

Ibhazehiebo, K., Gavrilovici, C., de la Hoz, C. L., Ma, S. C., Rehak, R., Kaushik, G., et al. (2018). A Novel Metabolism-Based Phenotypic Drug Discovery Platform in Zebrafish Uncovers HDACs 1 and 3 as a Potential Combined Anti-seizure Drug Target. *Brain* 141, 744–761. doi:10.1093/brain/awx364

Jakobs, M., Lee, D. J., and Lozano, A. M. (2020). Modifying the Progression of Alzheimer's and Parkinson's Disease with Deep Brain Stimulation. *Neuropharmacology* 171, 107860. doi:10.1016/j.neuropharm.2019.107860

Jankovic, J., and Tan, E. K. (2020). Parkinson's Disease: Etiopathogenesis and Treatment. *J. Neurol. Neurosurg. Psychiatry* 91, 795–808. doi:10.1136/jnnp-2019-322338

Kim, G.-H. J., Mo, H., Liu, H., Wu, Z., Chen, S., Zheng, J., et al. (2021). A Zebrafish Screen Reveals Renin-Angiotensin System Inhibitors as Neuroprotective via Mitochondrial Restoration in Dopamine Neurons. *Elife* 10, e69795. doi:10.7554/eLife.69795

Koprich, J. B., Kalia, L. V., and Brotchie, J. M. (2017). Animal Models of α-synucleinopathy for Parkinson Disease Drug Development. *Nat. Rev. Neurosci.* 18, 515–529. doi:10.1038/nrn.2017.75

Lam, P. Y., and Peterson, R. T. (2019). Developing Zebrafish Disease Models for *In Vivo* Small Molecule Screens. *Curr. Opin. Chem. Biol.* 50, 37–44. doi:10.1016/j.cbpa.2019.02.005

Liu, H., Chen, S., Huang, K., Kim, J., Mo, H., Iovine, R., et al. (2016). A High-Content Larval Zebrafish Brain Imaging Method for Small Molecule Drug Discovery. *PLoS One* 11, e0164645. doi:10.1371/journal.pone.0164645

McQuin, C., Goodman, A., Chernyshev, V., Kamentsky, L., Cimini, B. A., Karhohs, K. W., et al. (2018). CellProfiler 3.0: Next-Generation Image Processing for Biology. *PLOS Biol.* 16, e2005970. doi:10.1371/journal.pbio.2005970

Moffat, J. G., Vincent, F., Lee, J. A., Eder, J., and Prunotto, M. (2017). Opportunities and Challenges in Phenotypic Drug Discovery: An Industry Perspective. *Nat. Rev. Drug Discov.* 16, 531–543. doi:10.1038/nrd.2017.111

Monti, D. A., Zabrecky, G., Kremens, D., Liang, T. W., Wintering, N. A., Bazzan, A. J., et al. (2019). N-Acetyl Cysteine Is Associated with Dopaminergic Improvement in Parkinson's Disease. *Clin. Pharmacol. Ther.* 106, 884–890. doi:10.1002/cpt.1548

Paolini Paoletti, F., Gaetani, L., and Parnetti, L. (2020). The Challenge of Disease-Modifying Therapies in Parkinson's Disease: Role of CSF Biomarkers. *Biomolecules* 10, 335. doi:10.3390/biom10020335

Park, J. S., Davis, R. L., and Sue, C. M. (2018). Mitochondrial Dysfunction in Parkinson's Disease: New Mechanistic Insights and Therapeutic Perspectives. *Curr. Neurol. Neurosci. Rep.* 18, 21. doi:10.1007/s11910-018-0829-3

Pisharath, H., and Parsons, M. J. (2009). Nitroreductase-mediated Cell Ablation in Transgenic Zebrafish Embryos. *Methods Mol. Biol.* 546, 133–143. doi:10.1007/978-1-60327-977-2_9

Riboldi, G. M., and Di Fonzo, A. B. (2019). GBA, Gaucher Disease, and Parkinson's Disease: From Genetic to Clinic to New Therapeutic Approaches. *Cells* 8, 364. doi:10.3390/cells8040364

Sánchez-Pernaute, R., Ferree, A., Cooper, O., Yu, M., Brownell, A. L., and Isacson, O. (2004). Selective COX-2 Inhibition Prevents Progressive Dopamine Neuron Degeneration in a Rat Model of Parkinson's Disease. *J. Neuroinflammation* 1, 6. doi:10.1186/1742-2094-1-6

Sharifi-Rad, M., Lankatillake, C., Dias, D. A., Docea, A. O., Mahomoodally, M. F., Lobine, D., et al. (2020). Impact of Natural Compounds on Neurodegenerative Disorders: From Preclinical to Pharmacotherapeutics. *J. Clin. Med.* 9, 1061. doi:10.3390/jcm9041061

Song, S., Chen, Y., Han, F., Dong, M., Xiang, X., Sui, J., et al. (2018). Aloperine Activates the Nrf2-ARE Pathway when Ameliorating Early Brain Injury in a Subarachnoid Hemorrhage Model. *Exp. Ther. Med.* 15, 3847–3855. doi:10.3892/etm.2018.5896

Tweedie, S., Braschi, B., Gray, K., Jones, T. E. M., Seal, R. L., Yates, B., et al. (2021). Genenames.org: the HGNC and VGNC Resources in 2021. *Nucleic Acids Res.* 49, D939–D946. doi:10.1093/nar/gkaa980

Vardi, A., Zigdon, H., Meshcheriakova, A., Klein, A. D., Yaacobi, C., Eilam, R., et al. (2016). Delineating Pathological Pathways in a Chemically Induced Mouse Model of Gaucher Disease. *J. Pathol.* 239, 496–509. doi:10.1002/path.4751

Wang, Y., Zhang, S., Li, F., Zhou, Y., Zhang, Y., Wang, Z., et al. (2020). Therapeutic Target Database 2020: Enriched Resource for Facilitating Research and Early Development of Targeted Therapeutics. *Nucleic Acids Res.* 48, D1031–D1041. doi:10.1093/nar/gkz981

Williams, E. M., Little, R. F., Mowday, A. M., Rich, M. H., Chan-Hyams, J. V., Copp, J. N., et al. (2015). Nitroreductase Gene-Directed Enzyme Prodrug Therapy: Insights and Advances toward Clinical Utility. *Biochem. J.* 471, 131–153. doi:10.1042/BJ20150650

Xu, Y. Q., Jin, S. J., Liu, N., Li, Y. X., Zheng, J., Ma, L., et al. (2014). Aloperine Attenuated Neuropathic Pain Induced by Chronic Constriction Injury via Anti-oxidation Activity and Suppression of the Nuclear Factor Kappa B Pathway. *Biochem. Biophys. Res. Commun.* 451, 568–573. doi:10.1016/j.bbrc.2014.08.025

Yang, W., Hamilton, J. L., Kopil, C., Beck, J. C., Tanner, C. M., Albin, R. L., et al. (2020). Current and Projected Future Economic burden of Parkinson's Disease in the U.S. *NPJ Parkinsons Dis.* 6, 15. doi:10.1038/s41531-020-0117-1

Zhang, L., Chen, C., Fu, J., Lilley, B., Berlinicke, C., Hansen, B., et al. (2021). Large-scale Phenotypic Drug Screen Identifies Neuroprotectants in Zebrafish and Mouse Models of Retinitis Pigmentosa. *Elife* 10, e57245. doi:10.7554/eLife.57245

Zhang, X. D., Ferrer, M., Espeseth, A. S., Marine, S. D., Stec, E. M., Crackower, M. A., et al. (2007). The Use of Strictly Standardized Mean Difference for Hit Selection in Primary RNA Interference High Throughput Screening Experiments. *J. Biomol. Screen.* 12, 497–509. doi:10.1177/1087057107300646

Zhao, J., Zhang, G., Li, M., Luo, Q., Leng, Y., and Liu, X. (2018). Neuro-protective Effects of Aloperine in an Alzheimer's Disease Cellular Model. *Biomed. Pharmacother.* 108, 137–143. doi:10.1016/j.biopha.2018.09.008

Conflict of Interest: The authors declare that the research was conducted in the absence of any commercial or financial relationships that could be construed as a potential conflict of interest.

Publisher's Note: All claims expressed in this article are solely those of the authors and do not necessarily represent those of their affiliated organizations, or those of the publisher, the editors and the reviewers. Any product that may be evaluated in this article, or claim that may be made by its manufacturer, is not guaranteed or endorsed by the publisher.

frontiers in Pharmacology

ORIGINAL RESEARCH
published: 22 March 2022
doi: 10.3389/fphar.2022.668065

Differentiating the Neuropharmacological Properties of Nicotinic Acetylcholine Receptor-Activating Alkaloids

Omar Alijevic[1], Oihane Jaka[2†], Ainhoa Alzualde[2†], Diana Maradze[3†], Wenhao Xia[4], Stefan Frentzel[1], Andrew N. Gifford[3], Manuel C. Peitsch[1], Julia Hoeng[1] and Kyoko Koshibu[1]**

[1]PMI R&D, Philip Morris Products S.A., Neuchâtel, Switzerland, [2]Biobide, Donostia-San Sebastian, Spain, [3]Gifford Bioscience Ltd., The BioHub Birmingham, Birmingham, United Kingdom, [4]PMI R&D, Philip Morris International Research Laboratories Pte. Ltd., Singapore, Singapore

OPEN ACCESS

Edited by:
Helene Tricoire-Leignel, Université d'Angers, France

Reviewed by:
Styliani (Stella) Vlachou, Dublin City University, Ireland
Robert Warren Gould, Wake Forest School of Medicine, United States

***Correspondence:**
Julia Hoeng
Julia.Hoeng@pmi.com
Kyoko Koshibu
kyoko_koshibu@yahoo.com

†These authors have contributed equally to this work

Specialty section:
This article was submitted to Neuropharmacology, a section of the journal Frontiers in Pharmacology

Received: *15 February 2021*
Accepted: *21 February 2022*
Published: *22 March 2022*

Citation:
Alijevic O, Jaka O, Alzualde A, Maradze D, Xia W, Frentzel S, Gifford AN, Peitsch MC, Hoeng J and Koshibu K (2022) Differentiating the Neuropharmacological Properties of Nicotinic Acetylcholine Receptor-Activating Alkaloids. Front. Pharmacol. 13:668065. doi: 10.3389/fphar.2022.668065

Alkaloids that target nicotinic acetylcholine receptors (nAChR) are of great interest because of the critical role they play in mood and anxiety. However, understanding of the neuropharmacological effects of nicotinic alkaloids, such as cotinine and anatabine, is very limited. In this study, we investigated the neuropharmacological effects of three naturally occurring alkaloids—nicotine, cotinine, and anatabine—*in vitro* and *in vivo*. A single injection of nicotine induced anxiolytic-like behavioral features in mice by using the SmartCube® behavioral profiling system, while cotinine and anatabine had no detectable effect. The results were corroborated by using the zebrafish novel tank test (NTT), which showed a profound anxiolytic-like effect induced by multiple doses of nicotine after a single 20-min treatment. When the regulation of dopamine and norepinephrine release—the neurotransmitter systems relevant for anxiety—were examined *in vitro*, we found that nicotine stimulated the release of both norepinephrine and dopamine, while cotinine and anatabine mainly stimulated the dopamine release. The molecular targets of nicotine were confirmed to be nAChRs with its most potent activities against α4β2 and α6/3β2β3 subtypes *in vitro*. Anatabine was a weaker agonist for these receptors than nicotine. Cotinine was the least potent nAChR compound, only being able to activate α4β2 and α6/3β2β3 subtypes at high doses and no detectable activities against α3β4 and α7 subtypes at the concentrations tested. The observed effects were unlikely due to the off-target effect, because these alkaloids did not bind or regulate >160 other molecular targets *in vitro*. Thus, the present results suggest that natural nicotinic alkaloids can induce an anxiolytic-like behavior in nonclinical animal models, potency of which may depend on the activation of various nAChRs and regulation of various neurotransmitter systems. Further investigations would help understand their effects on humans, because non-clinical studies should not be taken as a direct indication for human behavior and nicotine is not risk free.

Keywords: nicotine, cotinine, anatabine, alkaloids, nicotinic acetylcholine receptor (nAChR), anxiety

1 INTRODUCTION

Alkaloids are naturally occurring compounds present in a wide spectrum of plants, and their effects on animal behavior are being investigated for their therapeutic potential in various mood disorders and neurodegenerative diseases (Maione et al., 2013; Perviz et al., 2016; Hussain et al., 2018). There are more than 3,000 alkaloids identified, and their botanical and biochemical origins as well as chemical structures and pharmacological actions vary (Vina et al., 2012). In particular, pyridine alkaloids that target nicotinic acetylcholine receptors (nAChRs) are of great interest due to the critical role they play in neuropharmacology of mood and anxiety (Koob and Le Moal, 1997; Picciotto et al., 2002; Picciotto et al., 2015; Perviz et al., 2016). Nicotinic acetylcholine receptors are composed of *a* (α1–α10), *ß* (β1–β4), and other (δ, γ, ε) subunits, forming ligand-gated pentameric cation channels. Among the nAChRs, the homomeric α7 and heteromeric α4β2 nAChRs are the best characterized and most abundant subtypes in the central nervous system (Gotti et al., 2006). Other nAChRs in the brain can contain α3, α4, α5, α6, β2, β3, and β4 subunits in various combinations (Gotti and Clementi, 2004; Gotti et al., 2006). It is believed that the various receptor subtypes, inducing different time courses of activation and sensitization in various cell types involved in the diverse neurotransmitter systems, are responsible for the behavioral complexity induced by nicotinic compounds (Picciotto et al., 2002). For example, clinical studies suggest that abnormalities in cholinergic signaling are associated with major depressive disorder, whereas nonclinical studies have implicated both β2 subunit-containing (β2) and α7 nAChRs in anxiety- and depression-like behaviors (Perera et al., 2007; Mineur et al., 2013; Yu et al., 2014; Mineur et al., 2016). Thus, both nonclinical animal studies and clinical trials suggest that compounds that alter nAChR activity can affect behaviors related to mood and anxiety (Breslau, 1995; Diwan et al., 1998).

Among numerous alkaloids that activates nAChRs, nicotine is the most well-known natural alkaloid that can be found in many plants of the Solanaceae family with well-established activities on nAChRs (Alijevic et al., 2020; Xing et al., 2020). However, nicotine is not risk-free with reported negative effects on respiratory, gastrointestinal, cardiovascular functions and on addiction (Mishra, et al., 2015). A number of studies have also reported efficacy of nicotine in regulating memory, anxiety, and depression in rodents and humans (Levin, 2002; Terry et al., 2015; Bertrand and Terry, 2018; Terry and Callahan, 2019). In contrast, the effects of other alkaloids from the same chemical class in Solanaceae plans, such as cotinine and anatabine, are less well known (Dwoskin et al., 1995; Lippiello et al., 1996; Andersson et al., 2003; Vazquez-Palacios et al., 2004; Suemaru et al., 2006; Andreasen and Redrobe, 2009; Levin et al., 2014; Anderson and Brunzell, 2015; Terry et al., 2015; Xia et al., 2019). For example, anatabine is mainly known for its anti-inflammatory effect in neurodegenerative models in rodents (Paris et al., 2013a; Paris et al., 2013b; Verma et al., 2015), with a single study suggesting anxiolytic-like effect and improved social interaction and social memory in PS1/APPswe transgenic mice (Verma et al., 2015). In addition, little is known about the behavioral effects of anatabine when administered acutely.

In this study, the behavioral effects of three nicotinic alkaloids—nicotine, cotinine, and anatabine—were first assessed by using a proprietary machine learning system, SmartCube®, in order to discover their potential acute neurological effects in a relatively high-throughput manner. The SmartCube® system allows phenotypic classification of test compounds by comparing the behavioral features induced by the compounds against a reference behavioral database built from known marketed drugs, including for example, buspirone, ipsapirone, and flesinoxan (Alexandrov et al., 2015; Alexandrov et al., 2016). The advantages of this system are automation of scoring and analysis and relatively high throughput, considering more than 2,000 of behavioral features obtained in one session. Using this innovative technology, the behavioral features induced by the three nicotinic alkaloids after a single intraperitoneal (i.p.) injection in mice were analyzed to understand their possible drug classifications. We chose to treat the animals acutely to understand the direct effect of the compounds on behavior without potential tolerability-related changes that are known to occur for nicotine (Perkins, 2002). In addition, the clinical references used to establish the behavior profile database for SmartCube® used an acute single injection paradigm.

The three alkaloids were then examined by using the zebrafish novel tank test (NTT) of anxiety. The zebrafish NTT takes advantage of the innate behavior of zebrafish to dive and dwell at the bottom of a body of water when anxious. This behavioral paradigm is increasingly being accepted as a relative high-throughput method with some translational value to humans (Levin et al., 2007; Papke et al., 2012; Stewart et al., 2012). Nicotinic compounds as well as anxiolytic drugs, such as diazepam and buspirone, have been shown to induce anxiolytic-like effect in this zebrafish paradigm (Levin and Rezvani, 2007; Bencan and Levin, 2008; Bencan et al., 2009; Stewart et al., 2012). Lastly, the effects of these alkaloids on the neurotransmitter release and their molecular targets were assessed *in vitro* to understand the possible mechanisms underlying the behavioral findings.

2 MATERIALS AND METHODS

2.1 Chemicals

(-)-Nicotine free base (CAS no. 54-11-5) and (-)-cotinine free base (CAS no. 486-56-6) were purchased from Sigma-Aldrich® (St. Louis, MO, United States). (±)-Anatabine citrate (purity 98.92% by HPLC) was purchased from Concept Life Sciences (Manchester, UK). (±)-Anatabine free base (purity >95% by HPLC) used for the SmartCube® study was a generous gift from Indena® S. p.A. (Milan, Italy) (Rossia et al., 2018). (±)-Anatabine free base used for the zebrafish NTT was custom synthesized by WuXi AppTec (purity ≥95%; Shanghai, China). PNU282987 (CAS no. 711085-63-1) and buspirone hydrochloride (CAS No. 33386-08-2) were purchased from

Tocris Bioscience (Bio-Techne®, Minneapolis, MN, United States). AZD1446 (CAS no. 1025007-04-8) was purchased from Key Organics Limited (Cornwall, UK).

2.2 Animals

2.2.1 Mice for the SmartCube® Experiment

Male C57Bl/6 mice (8-9 weeks old; Jackson Laboratories, Bar Harbor, ME, United States) were group-housed in OPTImice® ventilated cages (4 mice/cage). Mice were acclimated to the colony room for at least 1 week prior to testing and subsequently tested at approximately 9-10 weeks of age. All animals were examined, handled, and weighed prior to the initiation of the study to assure adequate health and suitability and to minimize handling stress. During the course of the study, 12/12-h light/dark cycles were maintained. The room temperature was maintained between 20 and 23°C with a relative humidity between 30 and 70%. Chow and water were provided *ad libitum* in the home cages. Mice were randomly assigned to the treatment groups. For tolerability tests, mice were single-housed in OPTImice® ventilated cages for the duration of the study. All behavioral studies were conducted by PsychoGenics Inc. (Paramus, NJ, United States), a facility accredited by the Association for Assessment and Accreditation of Laboratory Animal Care International. The procedures were approved by the Institutional Animal Care and Use Committee in accordance with the National Institute of Health Guide for the Care and Use of Laboratory Animals (protocols 195-0513, 233-0214 and 277-1113).

2.2.2 Zebrafish for NTT

Wild-type zebrafish (*Danio rerio*; strain AB) were bred and housed at Biobide (San Sebastián, Gipuzkoa, Spain) in accordance with standard procedures (Zebrafish Information Network) as described previously (Alzualde et al., 2018; Quevedo et al., 2019). In brief, the fish were maintained in a 300-L aquarium with a maximum of 1,000 fish per tank. System water was maintained at 28.5°C, pH 7–7.8, conductivity at 500–800 μS, and 80–100% oxygen and continuously filtered. The system water condition was monitored daily and regulated, if required. The fish were kept under a 14-/10-h light/dark cycle (light on at 7:30 a.m.). Adults were fed ground dry pellets (Gemma Micro 300; Sketting Zebrafish, Westbrook, ME, United States) and live food (Artemia; Catvis B.V, 's-Hertogenbosch, Netherlands) once a day. All behavioral experiments were performed on male and female adult zebrafish (approximately 36–52 weeks post fertilization) in accordance with European standards of animal welfare on animal use for scientific purposes (2010/63/EU), compiled with national regulations for the care of experimental animals, and were approved as described in national regulations (RD 53/2013) by local and regional committees: PRO-AE-SS-121 and PRO-AE-SS-134.

2.2.3 Rats for Neurotransmitter Assay

Adult male Sprague Dawley rats (200—225 g body weight) were purchased from Charles River UK, Ltd. (Kent, United Kingdom) and were housed at the University of Birmingham animal facility, which has a procedure establishment license issued by the Secretary of State and conforms to all relevant United Kingdom legislation. The animals were terminated in accordance with schedule one procedures issued by the UK home office.

2.3 Tolerability

Tolerability tests were conducted by both manually scored observations and open-field activity tests to ensure that the doses used for the SmartCube® test did not have any adverse effects on basic physiology and behavior. In brief, mice were single-housed prior to the test and evaluated for baseline body weight, body temperature, and other parameters. Animals exhibiting abnormal parameters were removed from the tolerability test, and the remaining mice were randomly assigned to the treatment groups, balanced by their body weight and body temperature. On day 1, the mice were i. p. injected with saline (vehicle) or a test compound at 10 ml/kg body weight. Then, body temperature was measured at 15 min, 4 h, and 24 h and body weight on days 1 and 2. Neurological and motor parameters were evaluated at 15 min, 2 h, and 4 h after administration. The list of parameters is provided in **Supplementary Figure S1** in **Supplementary Material S1**. Behaviors that were significantly different from the vehicle-treated mice were considered abnormal.

In addition, within 5 min after the 15-min observation period, mice were placed in open-field chambers for 30 min to determine their general motor activity (distance traveled), ambulatory time, and number of rears. The open-field chambers were made of Plexiglas (27.3 × 27.3 × 20.3 cm; Med Associates Inc, St Albans, VT, United States) surrounded by infrared photobeam sources (16 × 16 × 16 beams). Horizontal activity (distance and time traveled) and vertical activity (number and frequency of rears) were measured by consecutive beam breaks. At the end of each open-field test session, the chambers were thoroughly cleaned with NOLVASAN® solution (Zoetis Services LLC, Parsippany, NJ, United States). Four mice were used per treatment condition. Mice were terminated after completion of the last tolerability observation.

All compounds were diluted in saline, and the pH was adjusted to approximately 7.0 with HCl or NaOH on the day of the experiment. The doses of the chemicals tested were as follows: nicotine (0.25, 0.5, and 1 mg/kg body weight), cotinine (2.5, 5, 10 mg/kg body weight), anatabine (1, 2, and 4 mg/kg body weight), AZD1446 (0.1, 0.3, 1, 3, and 10 mg/kg body weight), PNU282987 (0.1, 1, and 10 mg/kg body weight). The doses were calculated based on the free base molecular weight of the compounds.

2.4 SmartCube® Behavioral Profiling

The SmartCube® system is a unique mouse behavior profiling system developed by PsychoGenics Inc. It extracts over 2000 spontaneous and challenge-induced behavioral features during a session (Alexandrov et al., 2015; Alexandrov et al., 2016). The recorded behavioral parameters are then compared against the behavioral profiles of marketed reference compounds in the database, and the test compounds are classified into known

drug classes using PsychoGenics' proprietary bioinformatics algorithms. In brief, mice were i. p. injected with vehicle or test compound at 10 ml/kg body weight and placed in the SmartCube® arena (24 cm × 25 cm) 15 min later. Spontaneous and stimulus-induced behaviors of mice were recorded using force sensors distributed throughout the arena during a 45-min test session. In addition, three high-resolution video cameras provided a constant 3-dimensional (3D) view of the mouse behavior in the SmartCube® arena throughout the testing period. The bedding was vacuumed, and the arena was cleaned with NOLVASAN® solution between each run. Data from the SmartCube® test were processed using PsychoGenics' proprietary Computer Vision feature extraction, Bayesian probabilistic density models, and data mining algorithms, trained on a large library of reference compounds with known therapeutic indications to predict the underlying class of each test compound (Alexandrov et al., 2015; Alexandrov et al., 2016). Twelve mice were tested per condition. Mice were terminated after the completion of the SmartCube® test.

The doses of the tested chemicals were chosen based on the tolerability test findings as follows: nicotine (0.125, 0.25, and 0.5 mg/kg body weight), cotinine (0.25, 0.5, 1, 2.5, 5, and 10 mg/kg body weight), anatabine (0.5, 1, and 2 mg/kg body weight), AZD1446 (0.01, 0.03, 0.1, 0.3, 1, 3, and 10 mg/kg body weight), PNU282987 (0.1, 0.3, 1, 3, and 10 mg/kg body weight). The doses were calculated based on the free base molecular weight. The doses were selected based on the tolerability test results.

2.5 Zebrafish NTT

Adult male and female wild-type zebrafish were treated with the compounds for 20 min in a final volume of 50 ml in a 250-ml treatment beaker one fish at a time. The fish were briefly rinsed in fresh system water, and then immediately transferred to a trapezoidal tank (14.6 cm height x 5.5 cm width x 27.9 cm top length and x 23.6 cm bottom length) filled with 1.5 L system water. The behavior of the fish was monitored for the next 5 min by using the Noldus EthoVision XT system (Wageningen, Netherlands), with the camera placed approximately 1 m from the test tank. The part of the tank filled with water (11.5 cm height) was virtually divided into top, center, and bottom of equal heights (approximately 3.8 cm per segment) for the analysis. The average time spent at the top and bottom portions of the tank was analyzed to determine the anxiety-like behavior of fish. The average total distance travelled and freezing time were calculated to determine the effects of the compounds on the general behavior of fish. Freezing was defined by a complete cessation of movement except for gills and eyes (Kalueff et al., 2013). A minimum of 12 fish (6 females and 6 males) per condition were used for the study. The experimenter was blind to the test conditions. Any fish that stayed immobile for longer than 200 s out of a total of 5-min test period were considered as an outlier as it was generally >2 standard deviations away from the mean and excluded from the analysis. Three fish from vehicle control, one fish from 10 mg/L anatabine, and three fish from 100 mg/L buspirone were removed from the final analysis, but these changes did not alter the significance of statistical results.

The test concentrations were determined by first testing the compounds at 30 mg/L. If the fish tolerated the dose (as determined by the lack of abnormal behavior such as tail or body tremors or floating at the surface of the water), then higher doses were tested. If not, the dose was reduced until no obvious signs of tolerability problems were observed. The test concentrations for the NTT were as follows: nicotine (0.3, 1, 3, and 10 mg/L; equivalent to 2, 6, 19, and 62 μM), cotinine (30, 100, and 300 mg/L; equivalent to 171, 568, and 1705 μM), anatabine (0.3, 1, 3, and 10 mg/L, equivalent to 2, 6, 19, and 63 μM), and buspirone (10, 30, and 100 mg/L; equivalent to 26, 78, and 259 μM). The concentrations were calculated based on the free base molecular weight. Buspirone—a clinical anxiolytic drug used acutely and chronically to investigate the change in the anxiety-like behavior (Maximino, et al., 2011; Maximino, et al., 2013)—was included as a positive control.

2.6 *In vitro* Neurotransmitter Release Assay

In vitro neurotransmitter assays using crude synaptosome preparations were conducted by Gifford Biosciences Limited (Birmingham, UK) based on the previously described protocols (Clarke and Reuben, 1996; Gifford et al., 2000). In brief, male Sprague Dawley rats (200–225 g) were terminated by cervical dislocation followed by decapitation. The striatums or hippocampi were dissected and homogenized in ice-cold 0.32 M sucrose using a Dounce homogenizer. The homogenates were centrifuged at 100 x g for 5 min to pellet cell debris. The supernatants were collected and centrifuged at 17,000 x g for 10 min at 4°C to pellet crude synaptosomes. The pellets were resuspended in 5 ml Krebs buffer, pH 7.4 (in mM (pH 7.4): 120 NaCl, 3.3 KCl, 1.2 $MgSO_4$, 1.3 $CaCl_2$, 1.2 K_2HPO_4, 25 HEPES, 11 glucose, 0.01 ascorbic acid, 0.025 pargyline, and 0.1% BSA containing 2 μCi/ml [^{3}H]norepinephrine for hippocampal synaptosomes or 1 μCi/ml [^{3}H]dopamine for striatal synaptosomes and incubated for 15 min at 35°C with gentle shaking.

The [^{3}H]norepinephrine- or [^{3}H]dopamine-treated crude synaptosomes were loaded onto closed filter chambers containing Whatman® Grade GF/C Glass Microfiber filters (Sigma-Aldrich, Merck KGaA, Darmstadt, Germany) and placed in a superfusion system. Preoxygenated Krebs buffer was perfused through the chambers at a rate of 1 ml/min at 37 °C using an 8-channel peristaltic pump. To ensure an even flow over the synaptosomal bed, trapped air bubbles were removed from the filters prior to collection of the fractions. After a superfusion period of 40 min, three basal fractions (1.5 ml/fraction) were collected first, followed by three fractions (1.5 ml/fraction) containing the test compound. Two additional fractions were collected in the presence of 30 mM KCl to depolarize the synaptosomes. A 0.4-ml aliquot of each fraction was then transferred to a counting plate, and a scintillation cocktail was added to measure the radioactivity using a Wallac® TriLux 1450 MicroBeta counter (PerkinElmer Life Sciences, Zaventem, Belgium). Once all fractions were collected, the filters holding the crude synaptosome samples were removed and dried overnight at room temperature. On the following day, the

scintillation cocktail was added and the filters were counted to determine residual radioactivity.

Compound-evoked release of neurotransmitters was calculated by subtracting the counts per minute (CPM) in the two basal fractions collected immediately prior to compound addition from those in the two fractions collected immediately following compound addition. The compound-evoked release was then expressed as a percentage of the basal release from that chamber. Potassium-evoked release was calculated by subtracting the CPM in the fraction immediately prior to KCl addition from the CPM in the three fractions immediately following potassium addition. Stimulated release was calculated as the percentage of basal release for that chamber. The increase in stimulated release above the baseline (no compound) release for that experimental run was determined, and the latter values were plotted on the graphs. Dose–response curves were determined using non-linear curve fitting in Prism (GraphPad Software, Inc, San Diego, CA, United States). All experiments were repeated at least three times.

2.7 *In vitro* nAChR Functional Assay

Electrophysiological responses were recorded using an automated patch-clamp Patchliner Octo® system (Nanion Technologies, Munich, Germany) equipped with two EPC-10 Quadro patch-clamp amplifiers (HEKA Elektronik, Lambrecht, Germany) as described by (Alijevic et al., 2020). In brief, Chinese hamster ovary (CHO) or human embryonic kidney-293 (HEK-293) cells stably expressing human nAChRs (Charles River Laboratories, Wilmington, MA, United States) were maintained in DMEM/F12 medium (Gibco, Thermo Fisher Scientific, Waltham, MA, United States) supplemented with 10% heat-inactivated fetal bovine serum (FBS; Gibco) and penicillin–streptomycin (100 U/mL and 0.1 mg/ml, respectively; Sigma-Aldrich, St. Louis, MO, United States) at 37°C in 5% CO_2 and 70% humidity. The following selection antibiotics were used for the cell lines: G418 (0.25 mg/ml; Sigma-Aldrich) and Zeocin™ (0.4 mg/ml; InvivoGen, San Diego, CA, United States) for α7/Ric3 nAChR and α3β4 nAChR cells; puromycin (8 μg/ml; InvivoGen) and hygromycin B (0.4 mg/ml; Gibco) for α4β2 nAChR cells; and G418 (0.5 mg/ml), puromycin (0.25 μg/ml), and hygromycin B (0.02 mg/ml) for α6/3β2/β3 nAChR cells. The cells were used for characterizing nAChR pharmacology, because no endogenous ionotropic nicotinic receptors are found (Roncarati et al., 2008; Papke and Smith-Maxwell, 2009; Kirsch et al., 2016; Scheffel et al., 2018). The subunit distributions in the cells have been previously described (Alijevic et al., 2020). The human nAChRs were selected due to the lack of commercially available nAChR expression systems for mouse or zebrafish. The translatability of findings between zebrafish and human nAChR activities have been previously reported (Papke and Smith-Maxwell, 2009; Papke et al., 2012; Alijevic et al., 2020).

On the day of the experiment, nAChR-expressing cells were suspended in extracellular solution (in mM: 140 NaCl, 4KCl, one $MgCl_2$, two $CaCl_2$, five glucose, and 10 HEPES, adjusted to pH 7.4 with NaOH (298 mOsmol)), then placed in the Patchliner Octo® system. The internal solution contained in mM: 50 KCl, 60 kF, 10 NaCl, 20 EGTA, and 10 HEPES, adjusted to pH 7.2 with KOH (285 mOsmol). A seal-enhancer solution (in mM: 80 NaCl, 3 KCl, 10 $MgCl_2$, 35 $CaCl_2$, and 10 HEPES (pH 7.4, adjusted with HCl; 298 mOsmol) was used and replaced with the external solution once the whole-cell configuration was established. For activating the nAChRs, cells were stimulated with 5–10 μL of the test compounds in 0.3% DMSO, applied at 114 μL/s, followed by a washout using 120 μL external solution. Their response was recorded at a holding potential of−70 mV and a sampling rate of 20 kHz and filtered at 3 kHz using the PatchControlHT software (Nanion Technologies, v2.01.31) in combination with the Patchmaster software (HEKA Elektronik, v2×90.4 beta). Data were analyzed using the Patchmaster software and corrected for leak current. The data acceptance criteria were as follows: seal resistance >100 MΩ; seal resistance loss variation <50%; access resistance <20 MΩ; and minimum current amplitude elicited by maximal effect concentration acetylcholine >50 pA. Offline data analysis was performed in OpenOffice™ (v4.1.2; The Apache Software Foundation, Wakefield, MA, United States). Data are presented as mean ± S.D. All experiments were performed at room temperature (24°C) and repeated at least three times. Igor Pro (v6.2.2.2; WaveMetrics, Lake Oswego, OR, United States) or Prism (v8.2.1) were used for assessing the concentration–response curves.

2.8 *In vitro* Molecular Target Profiling

One hundred sixty five molecular targets were selected based on various references and databases. Majority of targets were selected by using SuperPred database as a guide for known and predicted targets of the three compounds (Nickel et al., 2014). SuperPred is a publicly accessible database that provides both experimentally reported drug–target interactions (DTIs) and predicted DTIs derived by a molecular similarity approach, covering a total of 665,000 DTIs connecting 31,000 compounds and 1800 targets (Nickel et al., 2014). This database was chosen because of its comprehensive coverage for nicotine, anatabine, and cotinine compared to other databases (Fang et al., 2017). Additional targets were included based on previous in-house proteomics and SmartCube® investigations, the abuse potential guidelines published by the United States Food and Drug Administration in 2017 (U.S. Department of Health and Human Services Food and Drug Administration (FDA) Center for Drug Evaluation and Research (CDER), 2017), and preclinical drug safety screening guidelines (Whitebread et al., 2005; Bowes et al., 2012). Combining the results of these resources, nicotine, cotinine, and anatabine were tested in technical duplicates against 175 assays including, for example, 86 GPCRs, 23 ion channels, 7 transporters, 15 kinases, and 35 other enzymes.

All binding and functional assays for molecular target characterization were conducted by Eurofins Cerep SA (Celle-Lévescault, France) and Eurofins Panlabs Discovery Services Taiwan, Ltd. (New Taipei City, Taiwan) using their standard *in vitro* binding and functional assays (**Supplementary Material S2**). A single concentration of each compound (10 μM in 0.1% DMSO) was used for the initial screen, followed by a full dose–response analysis for those targets for which the compounds showed an effect greater than 50%. Negative values were considered to be an artifact arising from, for

example, compounds interfering with the assay readout. The initial dose was selected based on our findings that 0.5 mg/kg nicotine showed an effect in the SmartCube®, which corresponded to a plasma concentration of approximately 5–6 μM according to the pharmacokinetics data reported by Petersen et al. (1984).

The radioligand displacement binding assays employed the gold standard filtration method using membrane preparations from stable cell lines (HEK-293 or CHO cells) expressing human or rodent target proteins to determine the interaction of the compounds with specific receptors, channels, and transporters. For this purpose, the competitive binding of test compounds against a [^{125}I]- [^{3}H]-, or [^{35}S]-labelled agonist and/or antagonist was determined. The specific list of radiolabeled ligands and experimental conditions are summarized in **Supplementary Material S2**.

2.9 Statistical Analysis

For the tolerability tests, passive signs and manipulation responses were analyzed for effects of the treatment by the Kruskal–Wallis test. Body temperature and body weight data were analyzed by two-way repeated measures analysis of variance (ANOVA). The total distance and time traveled and number and frequency of rears in the open-field activity test were analyzed by one-way ANOVA, followed by the Tukey *post-hoc* test. For the analyses of the zebrafish NTT data, one-way ANOVA was used, followed by Dunnett's multiple comparison test, if it passed the Shapiro-Wilk normality test. If the data set did not pass the normality test, then Kruskal–Wallis test followed by Dunn's multiple comparison test was used. An effect was considered significant if $p < 0.05$. The half maximal effective concentration (EC_{50}) and half-maximal inhibitory concentration (IC_{50}) for the receptor pharmacology and neurotransmitter release assay were determined by using nonlinear regression analysis. Statistical analyses were conducted using GraphPad Prism.

3 RESULTS

3.1 SmartCube® Behavioral Profiling and Classification

To investigate a wide range of neurobehavioral effects, nicotine, cotinine, and anatabine were tested in the SmartCube® system after a single i.p. injection in mice. Two reference compounds, AZD1446 and PNU282987, were included as α4β2 and α7 nAChR-specific agonists, respectively. The treatment protocol was chosen to be consistent with the treatment protocol used to establish the SmartCube® reference database. To determine the test doses, three doses of each compound were tested for tolerability. The results indicated that the highest dose (10 mg/kg) of cotinine, AZD1446, and PNU282987 were well tolerated and thus, 10 mg/kg was selected as the highest dose to be tested on the SmartCube® system (**Supplementary Material S3**; **Supplementary Figure S2** in **Supplementary Material S1**). For anatabine and nicotine, the highest dose tested (4 mg/kg and 1 mg/kg, respectively) decreased the body temperature of the mice 15 min after the injection (**Supplementary Figure S3** in **Supplementary Material S1**; main treatment effect: F (6, 21) = 12.619; $p < 0.001$; treatment × time interaction effect: F (6, 21) = 11.755; $p < 0.001$; LSD post hoc: $p < 0.05$ for both). Thus, a lower dose (2 mg/kg and 0.5 mg/kg, respectively) was chosen to be tested as the highest dose for the SmartCube® experiment.

Among the compounds tested on the SmartCube® system, only nicotine at the highest dose (0.5 mg/kg body weight) showed anxiolytic-like behavior features in mice. Other compounds did not induce any behavioral changes that significantly differed from those induced by the vehicle control (**Figure 1**).

3.2 Effects of Alkaloids on Zebrafish NTT Response

The zebrafish NTT was used to assess the anxiolytic-like effects of three alkaloids. In this experiment, zebrafish were placed in a beaker containing nicotine, cotinine, or anatabine for 20 min, then placed in a novel tank. The top three concentrations of nicotine (1, 3, and 10 mg/L) increased the time spent at the top and reduced the time spent at the bottom (**Figures 2B, E, H**; H (4) = 36.38; $p < 0.001$; Dunn's post hoc: $p = 0.001$, 0.013, <0.0001 for 1, 3, and 10 mg/L, respectively for the time spent at the top; H (4) = 59.66; Dunn's post hoc: $p < 0.0001$ for 1 and 10 mg/L, $p < 0.004$ for 3 mg/L for the time spent at the bottom). Zebrafish exposed to 100 mg/kg cotinine spent less time at the bottom of the tank, but other concentrations had no effect (**Figures 2C,F,I;** H (3) = 23.86; $p < 0.0001$; Dunn's post hoc: $p < 0.0001$). The time spent at the top was not affected by any doses of cotinine. Anatabine increased the time spent at the top and reduced the time spent at the bottom only at the highest dose tested (**Figures 2D,G,J**; H (4) = 24.40; $p < 0.0001$; Dunn's post hoc: $p = 0.001$ for the time spent at the top; H (4) = 30.73; $p < 0.0001$; Dunn's post hoc: $p < 0.0001$ for the time spent at the bottom). The anxiolytic reference compound buspirone increased the time spent at the top for all three doses tested and reduced the time spent at the bottom for the middle two doses (**Supplementary Figures S4A, B** in **Supplementary Material S1**; F (3, 58) = 22.60; $p < 0.0001$; Dunnett's post hoc: $p = 0.0002$, <0.0001, 0.0078 for 10, 30, and 100 mg/L, respectively for the time spent at the top; H (3) = 33.21; $p < 0.0001$; Dunn's post hoc: $p = 0.014$ and <0.0001 for 10 and 30 mg/L, respectively for the time spent at the bottom), supporting the validity of the zebrafish NTT to detect anxiolytic-like compounds.

When the general behavior was examined, the fish treated with 1 and 10 mg/L nicotine showed decreased total distance traveled, but showed no freezing response (**Figures 3A,D** in **Supplementary Material S1**; F (4, 100) = 8.520; $p < 0.0001$; Dunnetts' post hoc: $p < 0.0001$ for 1 mg/L, $p = 0.010$ for 10 mg/L for total distance traveled). Total distance traveled in fish exposed to 100 mg/L cotinine was reduced without affecting their freezing time (**Figures 3B,E** in **Supplementary Material S1**; F (3, 77) = 4.832; $p = 0.0039$; Dunnett's post hoc: $p = 0.049$). Total distance travelled was reduced in zebrafish exposed to 0.3 and 10 mg/L anatabine (**Figure 3C** in **Supplementary Material S1**; H (4) = 19.19; $p < 0.001$; Dunn's post hoc: $p = 0.002$ and 0.001 for 0.3 and 10 mg/L, respectively). The freezing time was increased only at 0.3 mg/L (**Figure 3F**; H (4) = 14.53; $p < 0.006$; Dunn's post hoc:

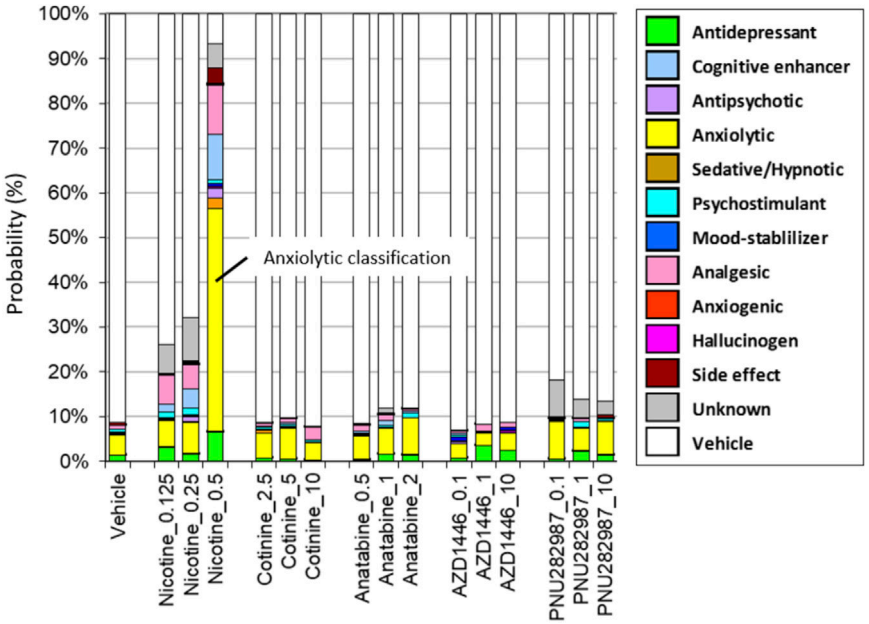

FIGURE 1 | Drug classifications of the plant alkaloids. The drug classifications of nicotine, cotinine, anatabine, and nAChR reference compounds (AZD1446 and PNU282987) determined by using the SmartCube® system in mice are presented. Only nicotine induced anxiolytic-like behavioral signature (yellow bar). Neither the free base nor citrate form of anatabine showed any changes in behavior. Thus, only the free base data are shown for anatabine. The doses are indicated on the *x*-axis as mg/kg. The color code is described in the figure legend on the left. N = 12 mice.

p = 0.002). The total distance traveled was decreased and the freezing time was increased at 100 mg/L buspirone (**Supplementary Figures S4C, D** in **Supplementary Material S1**; F (3, 58) = 4.785; p = 0.005; Dunnett's post hoc: p = 0.009 for total distance; H (3) = 29.22; p < 0.0001; Dunnett's post hoc: p < 0.0001 for freezing time), suggesting potential tolerability challenge at this very high dose of buspirone. The changes in total distance travelled for all compounds were rather small albeit significant, and the reduced activity did not always result in anxiolytic-like behavior and vice versa (e.g., 3 mg/L nicotine and 0.3 mg/L anatabine). There were also no significant differences between male and female zebrafish responses for all the parameters examined.

3.3 Neurotransmitter Release

To understand the possible regulatory role of nicotine, cotinine, and anatabine on neurotransmitter systems relevant for emotionality such as anxiety, we investigated the effects of these alkaloids on dopamine and norepinephrine release *in vitro*. The AZD1446 and PNU282987 were included as α4β2 and α7 nAChR specific reference compounds, respectively (Bodnar et al., 2005; Mazurov et al., 2012), and acetylcholine as an endogenous nAChR ligand. Our results showed that dopamine release from striatal synaptosomes was partially induced by nicotine, anatabine, AZD1446, and acetylcholine (EC_{50}: 0.19, 1.76, 8.4, and 0.27 μM, respectively) (**Figure 4**). Cotinine and PNU282987 at higher concentrations induced 20–30% dopamine release, but the results were either too variable or not sufficiently potent to reliably assess EC_{50} values. Norepinephrine release from hippocampal synaptosomes was induced only by nicotine and acetylcholine (EC_{50}: 4.22 and 13.5 μM, respectively) (**Figure 5**). Anatabine induced a slight increase (~20%) in norepinephrine release at the higher doses, but its EC_{50} could not be reliably assessed due to the high variability of the data at the highest concentration tested. The α4β2 nAChR agonist AZD1446 and the α7 nAChR agonist PNU282987 induced negligible change in norepinephrine release.

3.4 *In vitro* Molecular Target Profiling of Nicotine, cotinine, and Anatabine

To understand the molecular mechanisms, dose–response binding and/or functional studies were conducted for α3β4, α4β2, α6/3β2β3, and α7 nAChR subtypes *in vitro* (**Figure 6**; **Table 1**, and **Supplementary Figure S5** in **Supplementary Material S1**). Nicotine was a potent full agonist for α4β2 and α6/3β2β3 nAChRs (EC_{50} = 1.0 ± 0.2 and 0.7 ± 0.1 μM, respectively) and showed weak activity against α3β4 and α7 nAChRs (EC_{50} = 42.4 ± 2.2 and 54.5 ± 10.6 μM, respectively). Anatabine showed a slightly weaker potency for all receptor subtypes compared to nicotine (EC_{50} for α3β4 nAChR = 70.6 ± 8.2 μM; for α4β2 nAChR = 6.1 ± 1.4 μM; for α6/3β2β3 nAChR = 3.6 ± 0.3 μM; for α7 nAChR = 158.5 ± 11.4 μM). Cotinine was the least potent of the three alkaloids with EC_{50} for α4β2 and α6/3β2β3 nAChRs greater than 100 μM and no detectable activities for α3β4 and α7 nAChRs for the range of concentrations tested in this study. In support of this weak activity, the cotinine binding for α3β4 and α7 nAChRs were also undetectable and for α4β2 was barely detectable (**Supplementary Figures S5B, E, and H** in **Supplementary**

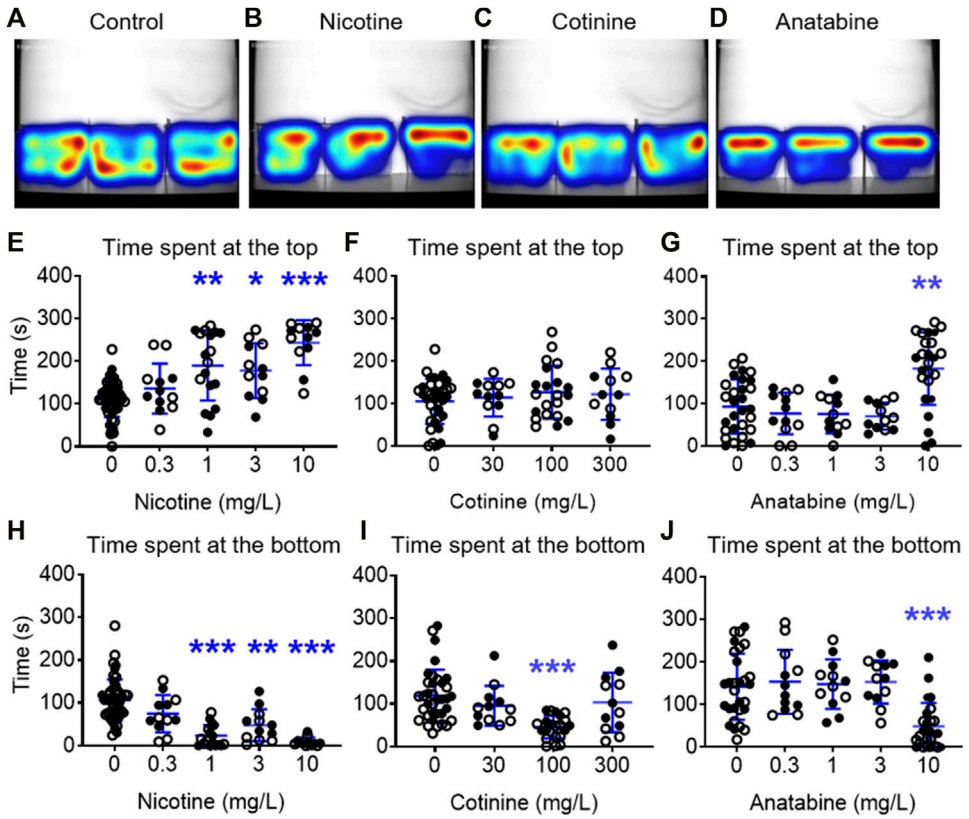

FIGURE 2 | Effects of alkaloids on anxiety-like behavior in zebrafish. Heatmaps of the general activity of zebrafish after **(A)** vehicle, **(B)** nicotine (1 mg/L), **(C)** cotinine (100 mg/L), or **(D)** anatabine (10 mg/L) treatment are shown. Nicotine increased the time spent at the top and decreased the time spent at the bottom for the three highest doses, 1, 3, and 10 mg/L **(E, H)**. Cotinine decreased the time spent at the bottom only at 100 mg/L and did not affect the time spent at the top **(F, I)**. Anatabine increased the time spent at the top and decreased the time spent at the bottom at only the highest dose tested (10 mg/L; **(G, J)**. Each individual circle represent one zebrafish. Solid circles = males; open circles = females; n = 12–36; $^{*}p < 0.05$ and $^{***}p < 0.001$. Data are presented as mean ± S.D.

Material S1). In contrast, nicotine and anatabine showed a strong binding affinity towards α3β4 and α4β2 nAChRs (α3β4 nAChR IC_{50} for nicotine and anatabine = 1.00 ± 0.08 and 0.96 ± 0.20 μM, respectively; α4β2 nAChR IC_{50} for nicotine and anatabine = 0.04 ± 0.002 and 0.71 ± 0.09 μM, respectively) (**Supplementary Figure S5A, D** in **Supplementary Material S1,** for nicotine; 6C and F for anatabine). The EC_{50} values for α7 nAChR were barely detectable at 10 μM for both nicotine and anatabine (**Supplementary Figures S5G, I** in **Supplementary Material S1**). Binding assays could not be conducted for α6/3β2β3 nAChRs due to the lack of commercially available compounds that are specific to α6-contatining subtypes. It is worth noting that independent functional assays were conducted for each compound, and, thus, the possible roles of the compounds as non-competitive or silent agonists or allosteric modulators were not assessed.

To understand potential off-target effects of these alkaloids, we selected 175 *in vitro* binding and enzymatic assays to determine the molecular target specificity of nicotine, cotinine, and anatabine based on the database and previous studies. The result indicated that all three alkaloids showed specific binding to α4β2 and muscle-type nAChR, but did not bind or regulate the activities of other molecular targets *in vitro* (**Figure 7**).

4 DISCUSSION

In this study, we investigated the neurobehavioral effects of three alkaloids—nicotine, cotinine, and anatabine—by using two relatively high-throughput behavioral paradigms, the SmartCube® system and zebrafish NTT. We were able to demonstrate the anxiolytic-like effect of nicotine by using both systems, supporting the robustness of the finding across species. Cotinine induced a weak anxiolytic-like effect at a concentration 100-fold higher than nicotine in zebrafish, with the effect only observable when the time spent at the bottom was considered. Similarly, anatabine also induced an anxiolytic-like effect, but only at the highest tolerated concentration, which was 10-fold higher than nicotine. The relative low potency of cotinine and anatabine may have been reflected by the lack of anxiolytic-like effect detected in the SmartCube® system. The fact that cotinine did not induce a strong neurobehavioral effect suggests that the observed effect of nicotine was likely due to the direct effect of

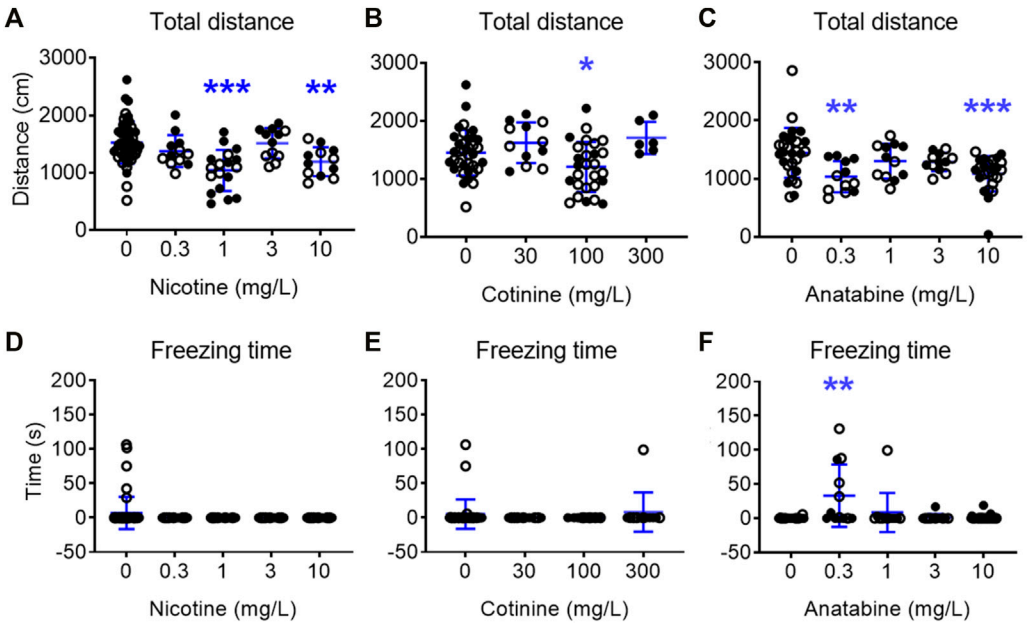

FIGURE 3 | Effects of alkaloids on general movement in zebrafish. Total distance traveled over 5 min test period for **(A)** nicotine, **(B)** cotinine, and **(C)** anatabine and freezing time for **(D)** nicotine, **(E)** cotinine, and **(F)** anatabine are presented. A slight reduction in the movement was detected for fish exposed to nicotine at 1 and 10 mg/L, cotinine at 100 mg/L, and anatabine at 0.3 and 10 mg/L. Freezing time was only increased by 0.3 mg/L anatabine treatment. Each individual circle represent one zebrafish. Solid circles = males; open circles = females; n = 12–36; $^{*}p < 0.05$ and $^{***}p <$ Data are presented as mean ± S.D.

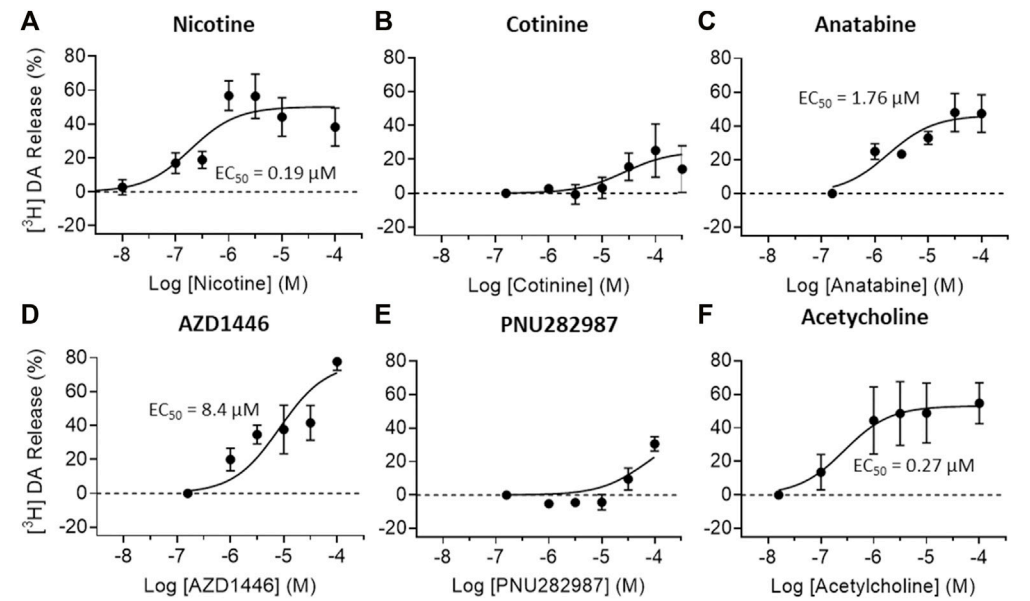

FIGURE 4 | Effects of nAChR ligands on dopamine release *in vitro*. Dopamine (DA) release from crude striatal synaptosome preparations were measured after **(A)** nicotine, **(B)** cotinine, **(C)** anatabine, **(D)** AZD1446 **(E)** PNU282987, and **(F)** acetylcholine treatment. All tested compounds elicited robust DA release except for cotinine and PNU282987 at the concentrations tested. Data are presented as mean ± S.D.

nicotine and not due to its metabolic product. Furthermore, nicotine was able to induce dopamine and norepinephrine release *in vitro*, while cotinine and anatabine mainly induced dopamine release only. Previous studies have demonstrated the translational value of dopamine and norepinephrine signaling systems among zebrafish, rodents, and humans (Singh et al.,

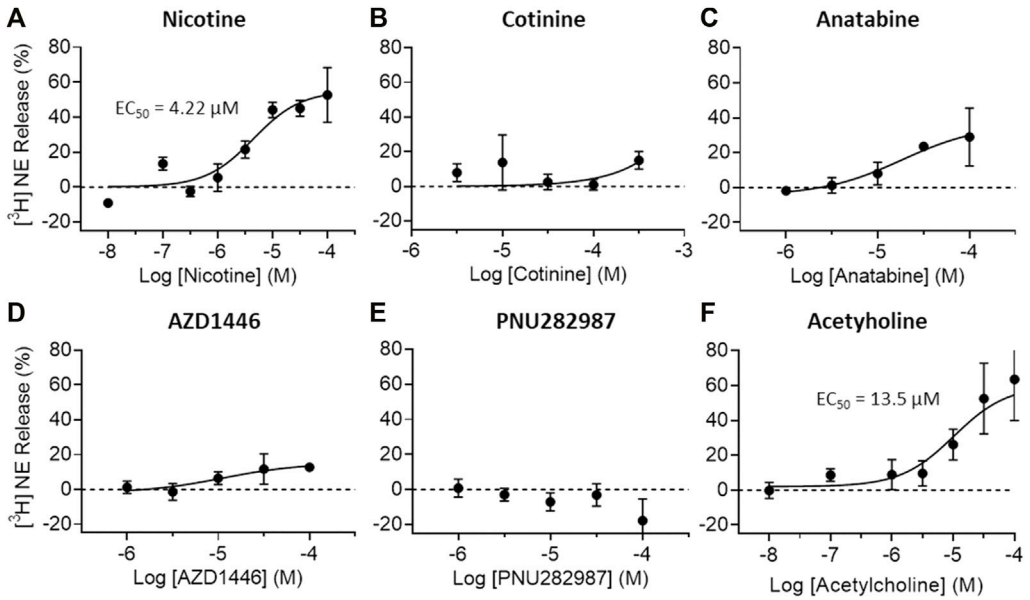

FIGURE 5 | Effects of nAChR ligands on *in vitro* norepinephrine release. Norepinephrine (NE) release from crude hippocampal synaptosome preparations were measured after **(A)** nicotine **(B)** cotinine, **(C)** anatabine, **(D)** AZD1446, **(E)** PNU282987, and **(F)** acetylcholine treatment. Only nicotine and acetylcholine seem to elicit clear NE release at the concentrations tested. Data are presented as mean ± S.D.

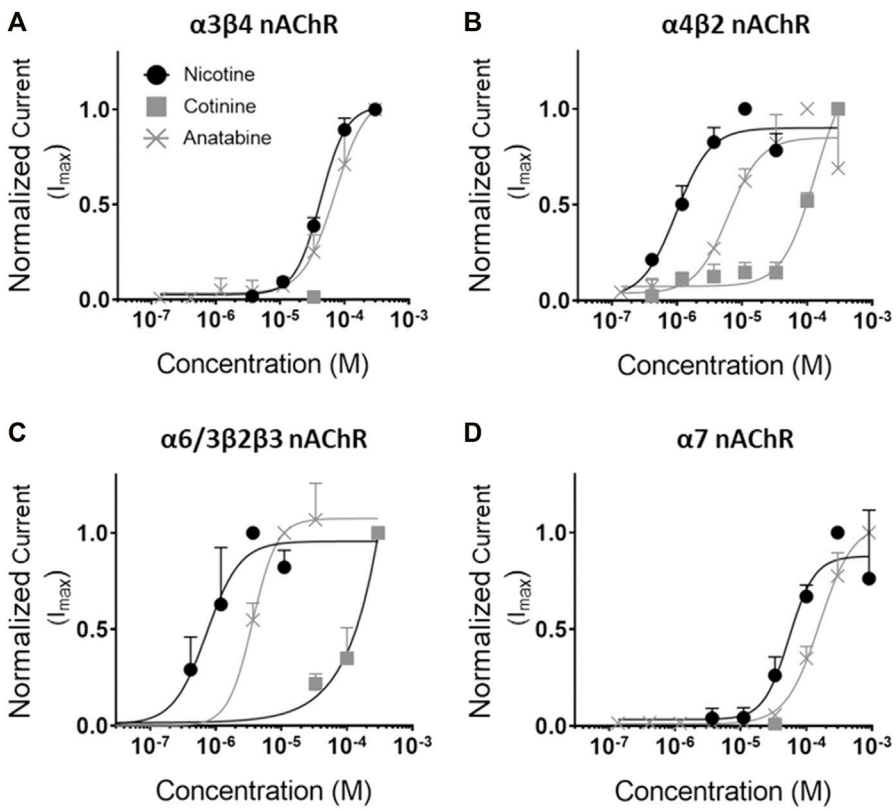

FIGURE 6 | Concentration response curves of the alkaloids for various nAChRs. Functional activity of nicotine, cotinine, and anatabine were tested against **(A)** α3β4, **(B)** α4β2, **(C)** α6/3β2β3, and **(D)** α7 *in vitro*. Mean EC_{50} values (in μM) are indicated in **Table 1**. Nicotine = black lines with solid circles; Cotinine = grey lines with solid squares; anatabine = grey lines with crosses. Data are presented as mean ± S.D.

TABLE 1 | The EC_{50} values of alkaloids for various nAChR subtypes.

	α3β4 nAChR EC50 in μM	α4β2 nAChR EC50 in μM	α6/3β2β3 EC50 in μM	α7 nAChR EC50 in μM
Nicotine	42.4 ± 2.2	1.0 ± 0.2	0.7 ± 0.1	54.5 ± 10.6
Cotinine	No effect *	Undetermined	Undetermined	No effect*
Anatabine	70.6 ± 8.2	6.1 ± 1.4	3.6 ± 0.3	158.5 ± 11.4

*The EC_{50} values of all compounds are presented as mean ± S.D. * Up to 33 μM.*

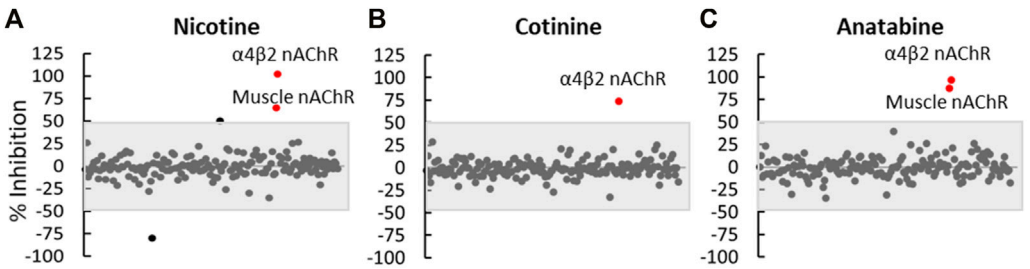

FIGURE 7 | Off-target effect assessment. **(A)** Nicotine, **(B)** cotinine, and **(C)** anatabine were tested in 175 *in vitro* binding or functional assays as summarized in **Supplementary Material S2**. Each dot represents the outcome of one assay. The grey shaded area covers any assay that showed an effect smaller than 50%. Red dots represent assays that showed greater than 50% change by the respective compounds compared to the vehicle control. N = three repeats.

2015; Ek et al., 2016; Feng et al., 2019). Thus, although the *in vitro* dopamine and norepinephrine release assays were conducted using rat synaptosomes, the findings should be applicable across species. The differences of these alkaloids in regulating neurobehavioral effects and neurotransmitter release may be reflected by the different levels of nAChR activation, where nicotine showed the strongest potency against almost all receptor subtypes examined. In addition, our preliminary results suggested that anatabine may not fully activate α3β4, α4β2, and α6/3β2β4 nAChRs, inducing perhaps, 40, 60, and 70% of the full receptor activity, respectively (data not shown).

Dopamine and norepinephrine are tightly regulated to control anxiety in animals (Garcia-Garcia et al., 2014; Montoya et al., 2016). It has been well-documented that activation of nAChRs induces the release of norepinephrine in the hippocampus from terminals originating in the locus coeruleus and of dopamine in the striatum from terminals originating in the substantia nigra or the ventral tegmentum (Rapier et al., 1988; Rapier et al., 1990; Sacaan et al., 1995; Clarke and Reuben, 1996). Various reports suggest that presynaptic nAChRs associated with striatal dopaminergic and hippocampal noradrenergic terminals differ pharmacologically to finely regulate their neurotransmitter release mechanisms. For example, nigrostriatal dopaminergic terminals have been suggested to have at least two types of nAChRs: *a*-conotoxin MII (α-CtxMII)-sensitive and -insensitive nAChRs (Kulak et al., 1997). The β2 subunit of nAChRs is absolutely required for both *a*-CtxMII-sensitive and -insensitive nAChR-mediated dopamine release, while the β4 and α7 subunits are not (Salminen et al., 2004). The distinguishing composition of these nAChRs is that the *a*-CtxMII-sensitive response requires the β3 and α6 subunits and is partially dependent on the α4 subunit (e.g., α6β3β2 and α4α6β3β2), whereas the *a*-CtxMII-resistant release requires the α4 subunit and is partially dependent on the α5 subunit (e.g., α4β2 and α4α5β2) (Champtiaux et al., 2002; Champtiaux et al., 2003; Luetje, 2004; Salminen et al., 2004). The contribution of α7 receptors to the control of dopamine release and, in fact, of norepinephrine release also, is mediated indirectly via an increase in glutamate release (Salminen et al., 2004; Barik and Wonnacott, 2006). Consistent with these results, Zoli et al. (2002) concluded that nicotinic binding sites expressed in rats include α4β2, α4α5β2, α6β2 (β3), and α4α6β2 (β3) nAChRs (Zoli et al., 2002). Thus, α4β2 nAChR-activating compounds, such as nicotine, anatabine, and AZD1446 used in the current study, can strongly induce dopamine release *in vitro*, while α7 nAChR agonists, such as PNU282987, induce a marginal effect.

Similarly, locus coeruleus noradrenergic neurons projecting to the hippocampus also show specific nAChR subunit compositions that can be differentially modulated by various nAChR ligands. Two populations of neurons can be distinguished on the basis of nAChR mRNA expression patterns and electrophysiological properties (Wada et al., 1989; Wada et al., 1990; Dineley-Miller and Patrick, 1992; Lena et al., 1999). One population of small cells systematically express α3 and β4 mRNAs (and often α6, β3, α5, and α4 mRNAs). Another population of cells with large soma systematically express α6 and β3 (and often α4), but not α3 and β4 mRNAs. Nicotine preferentially elicits large currents in the large cells, while cytisine preferentially elicits large currents in the small cells. This nAChR-specific and, thus, cell-type specific activation allows nicotine to more potently induce norepinephrine release than cytisine in the hippocampus, indicating that the noradrenergic terminals in the hippocampus most likely originate from the large α6-and β3-expressing cells (e.g., α6β3β2 and α4α6β3β2) in the locus

coeruleus (Lena et al., 1999). This fine-tuning of norepinephrine release by receptor subtype-specific activation may explain why nicotine was uniquely classified as an anxiolytic-like compound using mice in this study, while others, such as cotinine and anatabine with no potency or low potency and partial activation (approximately 67% of nicotine; preliminary data) of α6-containing nAChRs, respectively, were not.

It is worthy to note that previous studies have reported both anxiolytic and anxiogenic effects of nicotine in other nonclinical models (Lippiello et al., 1996; Lippiello et al., 2007; Mineur et al., 2007; Terry et al., 2012; Grizzell et al., 2014; Levin et al., 2014; Grizzell and Echeverria, 2015; Terry et al., 2015; Elhassan et al., 2017; Xia et al., 2019). Similarly, nAChR antagonists, such as mecamylamine, have also been reported to possess both anxiolytic and anxiogenic properties in nonclinical studies (Zarrindast et al., 2000; Newman et al., 2001; Picciotto et al., 2002). The ability of nAChR agonists and antagonists to act as an anxiolytic or anxiogenic substance is quite complex and dependent on the regimen of administration (acute vs chronic regimens, or withdrawal), route of administration (i.p., subcutaneous, intravenous, or inhaled), and behavioral state of the experimental subjects (relaxed vs stressed) (Picciotto et al., 2002; Picciotto et al., 2015). In particular, the baseline level of endogenous acetylcholine, which can vary depending on, for example, the stress level of the animal, could be rather important to understand the drug effects (Imperato et al., 1989; Imperato et al., 1991). The changing endogenous acetylcholine levels can modify nAChR sensitization or desensitization state, which ultimately determine the drug effect on behavioral outcome (Lu et al., 1999; Giniatullin et al., 2005; Yu et al., 2014). These various factors in nonclinical models, influencing the effect of nicotine and anxiety, in general, also make it challenging to interpret their implications in human neuropharmacology and ultimately, human behavior. Thus, future research is certainly worthwhile to assess if chronic treatment of nicotinic alkaloids or other considerations can produce similar anxiolytic-like effects.

Taken together, our results indicate that nicotinic ligands can induce an anxiolytic-like effect. The differential neurobehavioral effects induced by the three alkaloids suggest a fine regulation of neurotransmitter systems orchestrated by a complex combination of various nAChR subtypes. Previous studies showing nAChR-mediated mechanisms using specific antagonists (Levin, 2002; Terry et al., 2015; Bertrand and Terry, 2018; Terry and Callahan, 2019) support these concepts outlined in this study. Although cotinine and anatabine did not induce a strong anxiolytic-like effect, cotinine, in particular was well tolerated in both fish and mice. Thus, these findings support the importance of investigating the therapeutic potential of natural compounds that are well tolerated.

DATA AVAILABILITY STATEMENT

The raw data supporting the conclusion of this article will be made available by the authors, without undue reservation.

ETHICS STATEMENT

The animal study was reviewed and approved by the National Institute of Health Guide for the Care and Use of Laboratory Animals (protocols 195-0513, 233-0214 and 277-1113.

AUTHOR CONTRIBUTIONS

OA designed, conducted, and analyzed the *in vitro* functional assays. OJ and AA designed, conducted, and analyzed the zebrafish experiment. DM and AG designed, conducted, and analyzed the neurotransmitter release assays. WX contributed to the design and interpretation of the SmartCube® experiment. SF contributed to the design and interpretation of the *in vitro* binding and functional assays. JH and MP provided critical feedbacks to the projects and reviewed the manuscript. KK initiated, designed, and interpreted all experiments, managed and coordinated the studies, and wrote the manuscript. All authors critically reviewed and approved the manuscript.

FUNDING

This work was funded solely by Philip Morris International.

ACKNOWLEDGMENTS

We thank Dr. Taleen Hanania (PsychoGenics Inc.) for our tireless discussions and her invaluable help in understanding the SmartCube® test system and results, Eurofins for their valuable contribution in the hundreds of binding and functional assays conducted, and Indena® S. p.A. for their generous contribution of (±)-anatabine free base. We thank Dr. Karsta Luettich and Dr. Damian McHugh for valuable scientific discussions.

SUPPLEMENTARY MATERIAL

The Supplementary Material for this article can be found online at: https://www.frontiersin.org/articles/10.3389/fphar.2022.668065/full#supplementary-material

REFERENCES

Alexandrov, V., Brunner, D., Hanania, T., and Leahy, E. (2015). High-throughput Analysis of Behavior for Drug Discovery. *Eur. J. Pharmacol.* 750, 82–89. doi:10.1016/j.ejphar.2014.11.047

Alexandrov, V., Brunner, D., Menalled, L. B., Kudwa, A., Watson-Johnson, J., Mazzella, M., et al. (2016). Large-scale Phenome Analysis Defines a Behavioral Signature for Huntington's Disease Genotype in Mice. *Nat. Biotechnol.* 34, 838–844. doi:10.1038/nbt.3587

Alijevic, O., Mchugh, D., Rufener, L., Mazurov, A., Hoeng, J., and Peitsch, M. (2020). An Electrophysiological Characterization of Naturally Occurring

Tobacco Alkaloids and Their Action on Human α4β2 and α7 Nicotinic Acetylcholine Receptors. *Phytochemistry* 170, 112187. doi:10.1016/j.phytochem.2019.112187

Alzualde, A., Behl, M., Sipes, N. S., Hsieh, J. H., Alday, A., Tice, R. R., Paules, R. S., Muriana, A., and Quevedo, C. (2018). Toxicity Profiling of Flame Retardants in Zebrafish Embryos Using a Battery of Assays for Developmental Toxicity, Neurotoxicity, Cardiotoxicity and Hepatotoxicity Toward Human Relevance. *Neurotoxicol. Teratol.* 70, 40–50. doi:10.1016/j.ntt.2018.10.002

Anderson, S. M., and Brunzell, D. H. (2015). Anxiolytic-like and Anxiogenic-like Effects of Nicotine Are Regulated via Diverse Action at β2*nicotinic Acetylcholine Receptors. *Br. J. Pharmacol.* 172, 2864–2877. doi:10.1111/bph.13090

Andersson, C., Wennström, P., and Gry, J. (2003). *Nicotine Alkaloids in Solanaceous Food Plants*. Copenhagen, Sweden: Ekspressen Tryk & Kopicenter.

Andreasen, J. T., and Redrobe, J. P. (2009). Antidepressant-like Effects of Nicotine and Mecamylamine in the Mouse Forced Swim and Tail Suspension Tests: Role of Strain, Test and Sex. *Behav. Pharmacol.* 20, 286–295. doi:10.1097/FBP.0b013e32832c713e

Barik, J., and Wonnacott, S. (2006). Indirect Modulation by Alpha7 Nicotinic Acetylcholine Receptors of Noradrenaline Release in Rat Hippocampal Slices: Interaction with Glutamate and GABA Systems and Effect of Nicotine Withdrawal. *Mol. Pharmacol.* 69, 618–628. doi:10.1124/mol.105.018184

Bencan, Z., and Levin, E. D. (2008). The role of Alpha7 and Alpha4 beta2 Nicotinic Receptors in the Nicotine-Induced Anxiolytic Effect in Zebrafish. *Physiol. behav.*, 95 (3), 408–412. doi:10.1016/j.physbeh.2008.07.009

Bencan, Z., Sledge, D., and Levin, E. D. (2009). Buspirone, Chlordiazepoxide and Diazepam Effects in a Zebrafish Model of Anxiety. *Pharmacol. Biochem. Behav.* 94 (1), 75–80. doi:10.1016/j.pbb.2009.07.009

Bertrand, D., and Terry, A. V., Jr. (2018). The Wonderland of Neuronal Nicotinic Acetylcholine Receptors. *Biochem. Pharmacol.* 151, 214–225. doi:10.1016/j.bcp.2017.12.008

Bodnar, A. L., Cortes-Burgos, L. A., Cook, K. K., Dinh, D. M., Groppi, V. E., Hajos, M., et al. (2005). Discovery and Structure-Activity Relationship of Quinuclidine Benzamides as Agonists of Alpha7 Nicotinic Acetylcholine Receptors. *J. Med. Chem.* 48, 905–908. doi:10.1021/jm049363q

Bowes, J., Brown, A. J., Hamon, J., Jarolimek, W., Sridhar, A., Waldron, G., et al. (2012). Reducing Safety-Related Drug Attrition: the Use of *In Vitro* Pharmacological Profiling. *Nat. Rev. Drug Discov.* 11, 909–922. doi:10.1038/nrd3845

Breslau, N. (1995). Psychiatric Comorbidity of Smoking and Nicotine Dependence. *Behav. Genet.* 25, 95–101. doi:10.1007/BF02196920

Champtiaux, N., Han, Z. Y., Bessis, A., Rossi, F. M., Zoli, M., Marubio, L., et al. (2002). Distribution and Pharmacology of Alpha 6-containing Nicotinic Acetylcholine Receptors Analyzed with Mutant Mice. *J. Neurosci.* 22, 1208–1217. doi:10.1523/jneurosci.22-04-01208.2002

Champtiaux, N., Gotti, C., Cordero-Erausquin, M., David, D. J., Przybylski, C., Léna, C., et al. (2003). Subunit Composition of Functional Nicotinic Receptors in Dopaminergic Neurons Investigated with Knock-Out Mice. *J. Neurosci.* 23, 7820–7829. doi:10.1523/jneurosci.23-21-07820.2003

Clarke, P. B., and Reuben, M. (1996). Release of [3H]-Noradrenaline from Rat Hippocampal Synaptosomes by Nicotine: Mediation by Different Nicotinic Receptor Subtypes from Striatal [3H]-Dopamine Release. *Br. J. Pharmacol.* 117, 595–606. doi:10.1111/j.1476-5381.1996.tb15232.x

Dineley-Miller, K., and Patrick, J. (1992). Gene Transcripts for the Nicotinic Acetylcholine Receptor Subunit, Beta4, Are Distributed in Multiple Areas of the Rat central Nervous System. *Brain Res. Mol. Brain Res.* 16, 339–344. doi:10.1016/0169-328x(92)90244-6

Diwan, A., Castine, M., Pomerleau, C. S., Meador-Woodruff, J. H., and Dalack, G. W. (1998). Differential Prevalence of Cigarette Smoking in Patients with Schizophrenic vs Mood Disorders. *Schizophr Res.* 33, 113–118. doi:10.1016/s0920-9964(98)00045-0

Dwoskin, L. P., Teng, L., Buxton, S. T., Ravard, A., Deo, N., and Crooks, P. A. (1995). Minor Alkaloids of Tobacco Release [3H]dopamine from Superfused Rat Striatal Slices. *Eur. J. Pharmacol.* 276, 195–199. doi:10.1016/0014-2999(95)00077-x

Ek, F., Malo, M., Åberg Andersson, M., Wedding, C., Kronborg, J., Svensson, P., et al. (2016). Behavioral Analysis of Dopaminergic Activation in Zebrafish and Rats Reveals Similar Phenotypes. *ACS Chem. Neurosci.* 7, 633–646. doi:10.1021/acschemneuro.6b00014

Elhassan, S., Bagdas, D., and Damaj, M. I. (2017). Effects of Nicotine Metabolites on Nicotine Withdrawal Behaviors in Mice. *Nicotine Tob. Res.* 19, 763–766. doi:10.1093/ntr/ntx045

Fang, J., Liu, C., Wang, Q., Lin, P., and Cheng, F. (2017). In Silico polypharmacology of Natural Products. *Brief Bioinform* 19, 1153. doi:10.1093/bib/bbx045

Feng, J., Zhang, C., Lischinsky, J. E., Jing, M., Zhou, J., Wang, H., et al. (2019). A Genetically Encoded Fluorescent Sensor for Rapid and Specific *In Vivo* Detection of Norepinephrine. *Neuron* 102, 745–e8. doi:10.1016/j.neuron.2019.02.037

Garcia-Garcia, A. L., Newman-Tancredi, A., and Leonardo, E. D. (2014). 5-HT(1A) [corrected] Receptors in Mood and Anxiety: Recent Insights into Autoreceptor versus Heteroreceptor Function. *Psychopharmacology (Berl)* 231, 623–636. doi:10.1007/s00213-013-3389-x

Gifford, A. N., Bruneus, M., Gatley, S. J., and Volkow, N. D. (2000). Cannabinoid Receptor-Mediated Inhibition of Acetylcholine Release from Hippocampal and Cortical Synaptosomes. *Br. J. Pharmacol.* 131, 645–650. doi:10.1038/sj.bjp.0703599

Giniatullin, R., Nistri, A., and Yakel, J. L. (2005). Desensitization of Nicotinic ACh Receptors: Shaping Cholinergic Signaling. *Trends Neurosci.* 28, 371–378. doi:10.1016/j.tins.2005.04.009

Gotti, C., and Clementi, F. (2004). Neuronal Nicotinic Receptors: from Structure to Pathology. *Prog. Neurobiol.* 74, 363–396. doi:10.1016/j.pneurobio.2004.09.006

Gotti, C., Zoli, M., and Clementi, F. (2006). Brain Nicotinic Acetylcholine Receptors: Native Subtypes and Their Relevance. *Trends Pharmacol. Sci.* 27, 482–491. doi:10.1016/j.tips.2006.07.004

Grizzell, J. A., and Echeverria, V. (2015). New Insights into the Mechanisms of Action of Cotinine and its Distinctive Effects from Nicotine. *Neurochem. Res.* 40, 2032–2046. doi:10.1007/s11064-014-1359-2

Grizzell, J. A., Iarkov, A., Holmes, R., Mori, T., and Echeverria, V. (2014). Cotinine Reduces Depressive-like Behavior, Working Memory Deficits, and Synaptic Loss Associated with Chronic Stress in Mice. *Behav. Brain Res.* 268, 55–65. doi:10.1016/j.bbr.2014.03.047

Hussain, G., Rasul, A., Anwar, H., Aziz, N., Razzaq, A., Wei, W., et al. (2018). Role of Plant Derived Alkaloids and Their Mechanism in Neurodegenerative Disorders. *Int. J. Biol. Sci.* 14, 341–357. doi:10.7150/ijbs.23247

Imperato, A., Puglisi-Allegra, S., Casolini, P., Zocchi, A., and Angelucci, L. (1989). Stress-induced Enhancement of Dopamine and Acetylcholine Release in Limbic Structures: Role of Corticosterone. *Eur. J. Pharmacol.* 165, 337–338. doi:10.1016/0014-2999(89)90735-8

Imperato, A., Puglisi-Allegra, S., Casolini, P., and Angelucci, L. (1991). Changes in Brain Dopamine and Acetylcholine Release during and Following Stress Are Independent of the Pituitary-Adrenocortical axis. *Brain Res.* 538, 111–117. doi:10.1016/0006-8993(91)90384-8

Kalueff, A. V., Gebhardt, M., Stewart, A. M., Cachat, J. M., Brimmer, M., Chawla, J. S., et al. (2013). Towards a Comprehensive Catalog of Zebrafish Behavior 1.0 and beyond. *Zebrafish* 10, 70–86. doi:10.1089/zeb.2012.0861

Kirsch, G. E., Fedorov, N. B., Kuryshev, Y. A., Liu, Z., Armstrong, L. C., and Orr, M. S. (2016). Electrophysiology-Based Assays to Detect Subtype-Selective Modulation of Human Nicotinic Acetylcholine Receptors. *Assay Drug Dev. Technol.* 14, 333–344. doi:10.1089/adt.2015.688

Koob, G. F., and Le Moal, M. (1997). Drug Abuse: Hedonic Homeostatic Dysregulation. *Science* 278, 52–58. doi:10.1126/science.278.5335.52

Kulak, J. M., Nguyen, T. A., Olivera, B. M., and Mcintosh, J. M. (1997). Alpha-conotoxin MII Blocks Nicotine-Stimulated Dopamine Release in Rat Striatal Synaptosomes. *J. Neurosci.* 17, 5263–5270. doi:10.1523/jneurosci.17-14-05263.1997

Léna, C., De Kerchove D'exaerde, A., Cordero-Erausquin, M., Le Novère, N., Del Mar Arroyo-Jimenez, M., and Changeux, J. P. (1999). Diversity and Distribution of Nicotinic Acetylcholine Receptors in the Locus Ceruleus Neurons. *Proc. Natl. Acad. Sci. U S A.* 96, 12126–12131. doi:10.1073/pnas.96.21.12126

Levin, E. D., Hao, I., Burke, D. A., Cauley, M., Hall, B. J., and Rezvani, A. H. (2014). Effects of Tobacco Smoke Constituents, Anabasine and Anatabine, on Memory and Attention in Female Rats. *J. Psychopharmacol.* 28, 915–922. doi:10.1177/0269881114543721

Levin, E. D. (2002). Nicotinic Receptor Subtypes and Cognitive Function. *J. Neurobiol.* 53, 633–640. doi:10.1002/neu.10151

Levin, E. D., and Rezvani, A. H. (2007). Nicotinic Interactions With Antipsychotic Drugs, Models of Schizophrenia and Impacts on Cognitive Function. *Biochem. pharmacol.* 74 (8), 1182–1191. doi:10.1016/j.bcp.2007.07.019

Lippiello, P. M., Bencherif, M., Caldwell, W. S., Arrington, S. R., Fowler, K. W., Lovette, M. E., et al. (1996). Metanicotine: A Nicotinic Agonist with central Nervous System Selectivity?*In Vitro* and *In Vivo* Characterization. *Drug Dev. Res.* 38, 169–176. doi:10.1002/(sici)1098-2299(199607/08)38:3/4<169::aid-ddr5>3.0.co;2-k

Lippiello, P., Bencherif, M., Hauser, T., Jordan, K., Letchworth, S., and Mazurov, A. (2007). Nicotinic Receptors as Targets for Therapeutic Discovery. *Expert Opin. Drug Discov.* 2, 1185–1203. doi:10.1517/17460441.2.9.1185

Lu, Y., Marks, M. J., and Collins, A. C. (1999). Desensitization of Nicotinic Agonist-Induced [3H]gamma-Aminobutyric Acid Release from Mouse Brain Synaptosomes Is Produced by Subactivating Concentrations of Agonists. *J. Pharmacol. Exp. Ther.* 291, 1127–1134.

Luetje, C. W. (2004). Getting Past the Asterisk: the Subunit Composition of Presynaptic Nicotinic Receptors that Modulate Striatal Dopamine Release. *Mol. Pharmacol.* 65, 1333–1335. doi:10.1124/mol.65.6.1333

Maione, F., Cicala, C., Musciacco, G., De Feo, V., Amat, A. G., Ialenti, A., et al. (2013). Phenols, Alkaloids and Terpenes from Medicinal Plants with Antihypertensive and Vasorelaxant Activities. A Review of Natural Products as Leads to Potential Therapeutic Agents. *Nat. Prod. Commun.* 8, 539–544. doi:10.1177/1934578x1300800434

Maximino, C., Silva, A. W. B., Gouveia, A., Jr, and Herculano, A. M. (2011). Pharmacological Analysis of Zebrafish (*Danio rerio*) Scototaxis. *Prog. Neuropsychopharmacol. Biol. Psychiatry* 30 (352), 624–631. doi:10.1016/j.pnpbp.2011.01.006

Maximino, C., Puty, B., Benzecry, R., Araújo, J., Lima, M. G., de Jesus Oliveira Batista, E., et al. (2013). Role of Serotonin in Zebrafish (*Danio rerio*) Anxiety: Relationship with Serotonin Levels and Effect of Buspirone, WAY 100635, SB 224289, Fluoxetine and Para-Chlorophenylalanine (pCPA) in Two Behavioral Models. *Neuropharmacology* 71, 83–97. doi:10.1016/j.neuropharm.2013.03.006

Mazurov, A. A., Miao, L., Bhatti, B. S., Strachan, J. P., Akireddy, S., Murthy, S., et al. (2012). Discovery of 3-(5-chloro-2-furoyl)-3,7-diazabicyclo[3.3.0]octane (TC-6683, AZD1446), a Novel Highly Selective α4β2 Nicotinic Acetylcholine Receptor Agonist for the Treatment of Cognitive Disorders. *J. Med. Chem.* 55, 9181–9194. doi:10.1021/jm3006542

Mineur, Y. S., Somenzi, O., and Picciotto, M. R. (2007). Cytisine, a Partial Agonist of High-Affinity Nicotinic Acetylcholine Receptors, Has Antidepressant-like Properties in Male C57BL/6J Mice. *Neuropharmacology* 52, 1256–1262. doi:10.1016/j.neuropharm.2007.01.006

Mineur, Y. S., Obayemi, A., Wigestrand, M. B., Fote, G. M., Calarco, C. A., Li, A. M., et al. (2013). Cholinergic Signaling in the hippocampus Regulates Social Stress Resilience and Anxiety- and Depression-like Behavior. *Proc. Natl. Acad. Sci. U S A.* 110, 3573–3578. doi:10.1073/pnas.1219731110

Mineur, Y. S., Fote, G. M., Blakeman, S., Cahuzac, E. L., Newbold, S. A., and Picciotto, M. R. (2016). Multiple Nicotinic Acetylcholine Receptor Subtypes in the Mouse Amygdala Regulate Affective Behaviors and Response to Social Stress. *Neuropsychopharmacology* 41, 1579–1587. doi:10.1038/npp.2015.316

Mishra, A., Chaturvedi, P., Datta, S., Sinukumar, S., Joshi, P., and Garg, A. (2015). Harmful Effects of Nicotine. *Indian J. Med. Paediatr. Oncol.* 36, 24–31. doi:10.4103/0971-5851.151771

Montoya, A., Bruins, R., Katzman, M. A., and Blier, P. (2016). The Noradrenergic Paradox: Implications in the Management of Depression and Anxiety. *Neuropsychiatr. Dis. Treat.* 12, 541–557. doi:10.2147/NDT.S91311

Newman, M. B., Nazian, S. J., Sanberg, P. R., Diamond, D. M., and Shytle, R. D. (2001). Corticosterone-attenuating and Anxiolytic Properties of Mecamylamine in the Rat. *Prog. Neuropsychopharmacol. Biol. Psychiatry* 25, 609–620. doi:10.1016/s0278-5846(00)00178-0

Nickel, J., Gohlke, B. O., Erehman, J., Banerjee, P., Rong, W. W., Goede, A., et al. (2014). SuperPred: Update on Drug Classification and Target Prediction. *Nucleic Acids Res.* 42, W26–W31. doi:10.1093/nar/gku477

Papke, R. L., and Smith-Maxwell, C. (2009). High Throughput Electrophysiology with Xenopus Oocytes. *Comb. Chem. High Throughput Screen.* 12, 38–50. doi:10.2174/138620709787047975

Papke, R. L., Ono, F., Stokes, C., Urban, J. M., and Boyd, R. T. (2012). The Nicotinic Acetylcholine Receptors of Zebrafish and an Evaluation of Pharmacological Tools Used for Their Study. *Biochem. Pharmacol.* 84, 352–365. doi:10.1016/j.bcp.2012.04.022

Paris, D., Beaulieu-Abdelahad, D., Abdullah, L., Bachmeier, C., Ait-Ghezala, G., Reed, J., et al. (2013a). Anti-inflammatory Activity of Anatabine via Inhibition of STAT3 Phosphorylation. *Eur. J. Pharmacol.* 698, 145–153. doi:10.1016/j.ejphar.2012.11.017

Paris, D., Beaulieu-Abdelahad, D., Mullan, M., Ait-Ghezala, G., Mathura, V., Bachmeier, C., et al. (2013b). Amelioration of Experimental Autoimmune Encephalomyelitis by Anatabine. *PLoS One* 8, e55392. doi:10.1371/journal.pone.0055392

Perera, T. D., Coplan, J. D., Lisanby, S. H., Lipira, C. M., Arif, M., Carpio, C., et al. (2007). Antidepressant-induced Neurogenesis in the hippocampus of Adult Nonhuman Primates. *J. Neurosci.* 27, 4894–4901. doi:10.1523/JNEUROSCI.0237-07.2007

Perkins, K. A. (2002). Chronic Tolerance to Nicotine in Humans and its Relationship to Tobacco Dependence. *Nicotine Tob. Res.* 4, 405–422. doi:10.1080/1462220021000018425

Perviz, S., Khan, H., and Pervaiz, A. (2016). Plant Alkaloids as an Emerging Therapeutic Alternative for the Treatment of Depression. *Front. Pharmacol.* 7, 28. doi:10.3389/fphar.2016.00028

Petersen, D. R., Norris, K. J., and Thompson, J. A. (1984). A Comparative Study of the Disposition of Nicotine and its Metabolites in Three Inbred Strains of Mice. *Drug Metab. Dispos* 12, 725–731.

Picciotto, M. R., Brunzell, D. H., and Caldarone, B. J. (2002). Effect of Nicotine and Nicotinic Receptors on Anxiety and Depression. *NeuroReport* 13, 1097–1106. doi:10.1097/00001756-200207020-00006

Picciotto, M. R., Lewis, A. S., Van Schalkwyk, G. I., and Mineur, Y. S. (2015). Mood and Anxiety Regulation by Nicotinic Acetylcholine Receptors: A Potential Pathway to Modulate Aggression and Related Behavioral States. *Neuropharmacology* 96, 235–243. doi:10.1016/j.neuropharm.2014.12.028

Quevedo, C., Behl, M., Ryan, K., Paules, R. S., Alday, A., Muriana, A., and Alzualde, A. (2019). Detection and Prioritization of Developmentally Neurotoxic and/or Neurotoxic Compounds Using Zebrafish. *Toxicol. Sci.* 168 (1), 225–240. doi:10.1093/toxsci/kfy291

Rapier, C., Lunt, G. G., and Wonnacott, S. (1988). Stereoselective Nicotine-Induced Release of Dopamine from Striatal Synaptosomes: Concentration Dependence and Repetitive Stimulation. *J. Neurochem.* 50, 1123–1130. doi:10.1111/j.1471-4159.1988.tb10582.x

Rapier, C., Lunt, G. G., and Wonnacott, S. (1990). Nicotinic Modulation of [3H] dopamine Release from Striatal Synaptosomes: Pharmacological Characterisation. *J. Neurochem.* 54, 937–945. doi:10.1111/j.1471-4159.1990.tb02341.x

Roncarati, R., Seredenina, T., Jow, B., Jow, F., Papini, S., Kramer, A., et al. (2008). Functional Properties of Alpha7 Nicotinic Acetylcholine Receptors Co-expressed with RIC-3 in a Stable Recombinant CHO-K1 Cell Line. *Assay Drug Dev. Technol.* 6, 181–193. doi:10.1089/adt.2007.120

Rossia, F. V., Ballinia, R., Barbonia, L., Allegrinib, P., and Palmieri, A. (2018). A Practical and Efficient Synthesis of (±)-Anatabine. *Synthesis* 50 (09), 1921–1925. doi:10.1055/s-0036-1591538

Sacaan, A. I., Dunlop, J. L., and Lloyd, G. K. (1995). Pharmacological Characterization of Neuronal Acetylcholine Gated Ion Channel Receptor-Mediated Hippocampal Norepinephrine and Striatal Dopamine Release from Rat Brain Slices. *J. Pharmacol. Exp. Ther.* 274, 224–230.

Salminen, O., Murphy, K. L., Mcintosh, J. M., Drago, J., Marks, M. J., Collins, A. C., et al. (2004). Subunit Composition and Pharmacology of Two Classes of Striatal Presynaptic Nicotinic Acetylcholine Receptors Mediating Dopamine Release in Mice. *Mol. Pharmacol.* 65, 1526–1535. doi:10.1124/mol.65.6.1526

Scheffel, C., Niessen, K. V., Rappenglück, S., Wanner, K. T., Thiermann, H., Worek, F., et al. (2018). Counteracting Desensitization of Human α7-nicotinic Acetylcholine Receptors with Bispyridinium Compounds as an Approach against Organophosphorus Poisoning. *Toxicol. Lett.* 293, 149–156. doi:10.1016/j.toxlet.2017.12.005

Singh, C., Oikonomou, G., and Prober, D. A. (2015). Norepinephrine Is Required to Promote Wakefulness and for Hypocretin-Induced Arousal in Zebrafish. *Elife* 4, e07000. doi:10.7554/eLife.07000

Stewart, A., Gaikwad, S., Kyzar, E., Green, J., Roth, A., and Kalueff, A. V. (2012). Modeling Anxiety Using Adult Zebrafish: A Conceptual Review. *Neuropharmacology* 62 (1), 135–143. doi:10.1016/j.neuropharm.2011.07.037

Suemaru, K., Yasuda, K., Cui, R., Li, B., Umeda, K., Amano, M., et al. (2006). Antidepressant-like Action of Nicotine in Forced Swimming Test and Brain Serotonin in Mice. *Physiol. Behav.* 88, 545–549. doi:10.1016/j.physbeh.2006.05.007

Terry, A. V., and Callahan, P. M. (2019). Nicotinic Acetylcholine Receptor Ligands, Cognitive Function, and Preclinical Approaches to Drug Discovery. *Nicotine Tob. Res.* 21, 383–394. doi:10.1093/ntr/nty166

Terry, A. V., Jr., Buccafusco, J. J., Schade, R. F., Vandenhuerk, L., Callahan, P. M., Beck, W. D., et al. (2012). The Nicotine Metabolite, Cotinine, Attenuates Glutamate (NMDA) Antagonist-Related Effects on the Performance of the Five Choice Serial Reaction Time Task (5C-SRTT) in Rats. *Biochem. Pharmacol.* 83, 941–951. doi:10.1016/j.bcp.2011.12.043

Terry, A. V., Jr., Callahan, P. M., and Hernandez, C. M. (2015). Nicotinic Ligands as Multifunctional Agents for the Treatment of Neuropsychiatric Disorders. *Biochem. Pharmacol.* 97, 388–398. doi:10.1016/j.bcp.2015.07.027

U.S. Department of Health and Human Services Food and Drug Administration (FDA) Center for Drug Evaluation and Research (CDER) (2017). Assessment of Abuse Potential of Drugs: Guidance for Industry. *Clin. Med.*. FDA-2010-D-0026.

Vázquez-Palacios, G., Bonilla-Jaime, H., and Velázquez-Moctezuma, J. (2004). Antidepressant-like Effects of the Acute and Chronic Administration of Nicotine in the Rat Forced Swimming Test and its Interaction with Fluoxetine [correction of Flouxetine]. *Pharmacol. Biochem. Behav.* 78, 165–169. doi:10.1016/j.pbb.2004.03.002

Verma, M., Beaulieu-Abdelahad, D., Ait-Ghezala, G., Li, R., Crawford, F., Mullan, M., et al. (2015). Chronic Anatabine Treatment Reduces Alzheimer's Disease (AD)-Like Pathology and Improves Socio-Behavioral Deficits in a Transgenic Mouse Model of AD. *PLoS One* 10, e0128224. doi:10.1371/journal.pone.0128224

Viña, D., Serra, S., Lamela, M., and Delogu, G. (2012). Herbal Natural Products as a Source of Monoamine Oxidase Inhibitors: a Review. *Curr. Top. Med. Chem.* 12, 2131–2144. doi:10.2174/156802612805219996

Wada, E., Wada, K., Boulter, J., Deneris, E., Heinemann, S., Patrick, J., et al. (1989). Distribution of Alpha 2, Alpha 3, Alpha 4, and Beta 2 Neuronal Nicotinic Receptor Subunit mRNAs in the central Nervous System: a Hybridization Histochemical Study in the Rat. *J. Comp. Neurol.* 284, 314–335. doi:10.1002/cne.902840212

Wada, E., Mckinnon, D., Heinemann, S., Patrick, J., and Swanson, L. W. (1990). The Distribution of mRNA Encoded by a New Member of the Neuronal Nicotinic Acetylcholine Receptor Gene Family (Alpha 5) in the Rat central Nervous System. *Brain Res.* 526, 45–53. doi:10.1016/0006-8993(90)90248-a

Whitebread, S., Hamon, J., Bojanic, D., and Urban, L. (2005). Keynote Review: *In Vitro* Safety Pharmacology Profiling: an Essential Tool for Successful Drug Development. *Drug Discov. Today* 10, 1421–1433. doi:10.1016/S1359-6446(05)03632-9

Xia, W., Veljkovic, E., Koshibu, K., Peitsch, M. C., and Hoeng, J. (2019). Neurobehavioral Effects of Selected Tobacco Constituents in Rodents Following Subchronic Administration. *Eur. J. Pharmacol.* 865, 172809. doi:10.1016/j.ejphar.2019.172809

Xing, H., Keshwah, S., Rouchaud, A., and Kem, W. R. (2020). A Pharmacological Comparison of Two Isomeric Nicotinic Receptor Agonists: The Marine Toxin Isoanatabine and the Tobacco Alkaloid Anatabine. *Mar. Drugs* 18, 106. doi:10.3390/md18020106

Yu, L. F., Zhang, H. K., Caldarone, B. J., Eaton, J. B., Lukas, R. J., and Kozikowski, A. P. (2014). Recent Developments in Novel Antidepressants Targeting α4β2-nicotinic Acetylcholine Receptors. *J. Med. Chem.* 57, 8204–8223. doi:10.1021/jm401937a

Zarrindast, M. R., Homayoun, H., Babaie, A., Etminani, A., and Gharib, B. (2000). Involvement of Adrenergic and Cholinergic Systems in Nicotine-Induced Anxiogenesis in Mice. *Eur. J. Pharmacol.* 407, 145–158. doi:10.1016/s0014-2999(00)00628-2

Zoli, M., Moretti, M., Zanardi, A., Mcintosh, J. M., Clementi, F., and Gotti, C. (2002). Identification of the Nicotinic Receptor Subtypes Expressed on Dopaminergic Terminals in the Rat Striatum. *J. Neurosci.* 22, 8785–8789. doi:10.1523/jneurosci.22-20-08785.2002

Conflict of Interest: OA, SF, MP, JH, and KK were employed by Philip Morris International. WX is employed by Philip Morris International Research Laboratories Pte. Ltd. DM, and AG were employed by Gifford Bioscience Ltd. OJ and AA were employed by Biobide. Philip Morris International employed Biobide service for zebrafish assay and Gifford Bioscience service for neurotransmitter assay.

The remaining authors declare that the research was conducted in the absence of any commercial or financial relationships that could be construed as a potential conflict of interest.

Publisher's Note: All claims expressed in this article are solely those of the authors and do not necessarily represent those of their affiliated organizations, or those of the publisher, the editors and the reviewers. Any product that may be evaluated in this article, or claim that may be made by its manufacturer, is not guaranteed or endorsed by the publisher.

frontiers | Frontiers in Pharmacology

ORIGINAL RESEARCH
published: 04 April 2022
doi: 10.3389/fphar.2022.841826

Atrazine and Diuron Effects on Survival, Embryo Development, and Behavior in Larvae and Adult Zebrafish

Amanda B. Zaluski[1†], Melissa T. Wiprich[2†], Luiza F. de Almeida[1†], Andressa P. de Azevedo[1†], Carla D. Bonan[2†] and Monica R. M. Vianna[1†]*

[1]*Laboratório de Biologia e Desenvolvimento do Sistema Nervoso, Escola de Ciências da Saúde e da Vida, Pontifícia Universidade Católica do Rio Grande do Sul, Porto Alegre, Brazil,* [2]*Laboratório de Neuroquímica e Psicofarmacologia, Escola de Ciências da Saúde e da Vida, Pontifícia Universidade Católica do Rio Grande do Sul, Porto Alegre, Brazil*

Atrazine and Diuron are widely used herbicides. The use of pesticides contaminates the aquatic environment, threatening biodiversity and non-target organisms such as fish. In this study, we investigated the effects of acute exposure for 96 h hours to atrazine and diuron commercial formulations in zebrafish (*Danio rerio*, wild-type AB) embryos and larvae and adult stages. We observed a significant concentration-dependent survival decrease and hatching delays in animals exposed to both herbicides and in the frequency of malformations compared to the control groups. Morphological defects included cardiac edema, tail reduction, and head malformation. At 7 days post-fertilization (dpf), atrazine exposure resulted in a reduction in the head length at 2, 2.5, and 5 mg/L and increased the ocular distance at 1, 2, 2.5, and 5 mg/L atrazine when compared to controls. At the same age, diuron increased the ocular distance in animals exposed to diuron (1.0 and 1.5 mg/L) and no effects were observed on the head length. We also evaluated a behavioral repertoire in larvae at 7 dpf, and there were no significant differences in distance traveled, mean speed, time in movement, and thigmotaxis for atrazine and diuron when animals were individually placed in a new environment. The cognitive ability of the larvae was tested at 7 dpf for avoidance and optomotor responses, and neither atrazine nor diuron had significant impacts when treated groups were compared to their corresponding controls. Adults' behavior was evaluated 7 and 8 days after the end of the acute herbicide exposure. Exploration of a new environment and associated anxiety-like parameters, social interaction, and aggressiveness were not altered. Our results highlight the need for further studies on the sublethal effects of both herbicides and the consideration of the effects of commercial formulas vs. isolated active ingredients. It also emphasizes the need to take sublethal effects into consideration when establishing the environmental limits of residues.

Keywords: survival, teratogenesis, exploratory behavior, cognition, social interaction, atrazine, diuron, zebrafish

OPEN ACCESS

Edited by:
Aramandla Ramesh, Meharry Medical College, United States

Reviewed by:
Frederick E. Williams, University of Toledo, United States
Jonathan H. Freedman, University of Louisville, United States

***Correspondence:**
Monica R. M. Vianna
monica.vianna@pucrs.br
orcid.org/0000-0002-1881-127X

***ORCID:**
Amanda B. Zaluski
orcid.org/0000-0003-1638-5331
Melissa T. Wiprich
orcid.org/0000-0002-1415-038X
Luiza F. de Almeida
orcid.org/0000-0002-3399-1969
Andressa P. de Azevedo
orcid.org/0000-0001-8272-1239
Carla D. Bonan
orcid.org/0000-0001-9715-6244

Specialty section:
This article was submitted to Predictive Toxicology, a section of the journal Frontiers in Pharmacology

Received: *22 December 2021*
Accepted: *15 February 2022*
Published: *04 April 2022*

Citation:
Zaluski AB, Wiprich MT, de Almeida LF, de Azevedo AP, Bonan CD and Vianna MRM (2022) Atrazine and Diuron Effects on Survival, Embryo Development, and Behavior in Larvae and Adult Zebrafish. Front. Pharmacol. 13:841826. doi: 10.3389/fphar.2022.841826

1 INTRODUCTION

The demand for greater agricultural productivity over the last few decades was accompanied by the increased use of agrochemicals, such as herbicides, in pest and weed control. The fate of these substances on the environment depends on several factors, such as the concentration and frequency of use, application methods, and environmental biotic and abiotic characteristics (Rodrigues et al., 2017; Tang et al., 2021). The extensive use of these substances leads to air and soil contamination not only at the planting sites but also in local water bodies and groundwater (Fernandes et al., 2020). The persistence of these substances in the environment and the combined use of more than one agrochemical in the same area result in added contamination hazards. Presently, some notoriously toxic substances are still used in several global areas, contributing to biodiversity threats and environmental pollution (Sharma et al., 2019; Maggi et al., 2020; Tang et al., 2021). Country specific regulatory limits and guideline levels for pesticide residues in drinking water and groundwater are mostly based on animal mortality studies that estimate the median lethal concentration (LC50) (Hamilton et al., 2003), but do not include sublethal teratogenic and behavioral effects that may compromise animals' endurance.

Atrazine and diuron are globally used herbicides associated with significant threat to the ecosystem and human health, despite their ban from some developed countries. In Brazil, diuron and atrazine are used in pre- and post-emergent control of annual grasses and broadleaf weeds in several crops, mainly in cotton, corn, soybean, sugarcane, and pineapple (Lyer, 2003; Solomon et al., 2008; Švorc et al., 2013). Both are water soluble and can leach from fields to surface and groundwater persisting in the environment and possibly affecting the non-target aquatic species (Pereira et al., 2009; Velki et al., 2017). Increased concern is associated with the current lack of information regarding the effect of recurrent and combined exposure to pesticides and their derivatives in more realistic setups, including their environmental and non-target organism impacts (Dellamatrice and Monteiro 2014).

Diuron [3-(3,4-dichlorophenyl)-1,1-dimethylurea] is a phenylurea herbicide extensively used to control weeds in agriculture, urban, and industrial settings (Liu et al., 2013). Stable to hydrolysis at neutral pH (pH 5–9), it is generally persistent in soil with a half-life of more than 200 days (Tang et al., 2021), reaching water bodies through leaching or surface runoff (Giacomazzi and Cochet 2004; Langeron et al., 2014; Liu et al., 2016) and even atmospheric deposition. Moreover, its main degradation product, 3,4-dichloroaniline, exhibits higher toxicity and increased persistence in soils (Giacomazzi and Cochet 2004; Tasca et al., 2018). Atrazine (2-chloro-4-ethylamino-6-isopropylamino-1,3,5-triazine) is the most widely used triazine herbicide in crops globally and acts as a selective systemic herbicide by inhibiting photosynthesis (Plhalova et al., 2012). Its half-life is around 4 weeks and may persist in the environment for up to 2 years (Liu et al., 2016; Tai et al., 2021; Tang et al., 2021). Atrazine is metabolized to desethyl atrazine (DEA), desisopropyl atrazine (DIA), and diaminochlorotriazine (DACT) through cytochrome P450 enzymes in mammals but its mechanism is not fully understood in other species (Liu et al., 2016; Tai et al., 2021) so that its metabolites cause greater toxicity in non-target species. Both substances are also suggested to act as endocrine disruptors (Amaral, 2014; Wirbisky et al., 2015; Akcha et al., 2016; Horzmann et al., 2021). Diuron and atrazine LC50 for fish are 4.50 and 6.70 mg/L, respectively (Tang et al., 2021).

Zebrafish (*Danio rerio*) is an oviparous species with rapid organogenesis, especially suited for toxicological testing through water exposure in all life stages (Sipes et al., 2011; MacRae and Peterson 2015). This social species has a diverse and complex behavioral repertoire (Gerlai et al., 2000; Kalueff et al., 2013) that can contribute for the identification of sublethal effects of agrochemicals and their underlying cellular and molecular mechanisms.

In Brazil, the National Council for the Environment (CONAMA) establishes, through normative resolution CONAMA 357 (2005), limits and allowed environmental concentrations for the agrochemical's active principles and their environmental hazard classification. However, commercial formulations, known to have increased toxicity due to synergistic effects between components (Liu et al., 2013; Mansano et al., 2016), are not tested to establish such limits, neither are other biological parameters that can hinder species survival due to long-term effects on development, behavior, and reproduction. Also, while isolated atrazine is listed, for diuron these parameters have not been established in the country. For this reason, we decided to test both in parallel.

This study was designed to evaluate the individual toxicity of commercial formulations of atrazine and diuron on survival, hatching, and malformations in zebrafish early life stages. We also evaluated the behavioral parameters of ecological significance, such as exploration of a new environment, cognitive responses, social interaction, and aggression at different life stages, including larvae and adults.

2 MATERIALS AND METHODS

2.1 Animals and Ethics

Zebrafish (wild-type, AB strain) embryos and larvae (0–7 days post-fertilization, dpf) and adults (12–18 months) were used. Animals were obtained from our breeding colony and maintained in recirculating systems (Zebtec, Tecniplast, Italy) with equilibrated filtered water to reach the species standard temperature (28 ± 2°C), pH (7.0–7.5), conductivity (300–700 μS), ammonia (<0.02 mg/L), nitrite (<1 mg/L), nitrate (<50 mg/L), and chloride (0 mg/L) levels. Between 5 and 14 dpf, larvae were fed three times a day with crushed commercial flakes (TetraMin Tropical Flake Fish®), once including live paramecium. From 14 dpf, animals were also fed thrice a day and received commercial flakes and brine shrimp (*Artemia salina*) (Westerfield, 2000).

For breeding, female and males (1:2) were placed in breeding tanks (Tecniplast, Italy) overnight, and separated by a transparent barrier that was removed after lights went on, the following morning. The embryos, no more than 4 hpf were collected, sanitized, and randomly assigned to each

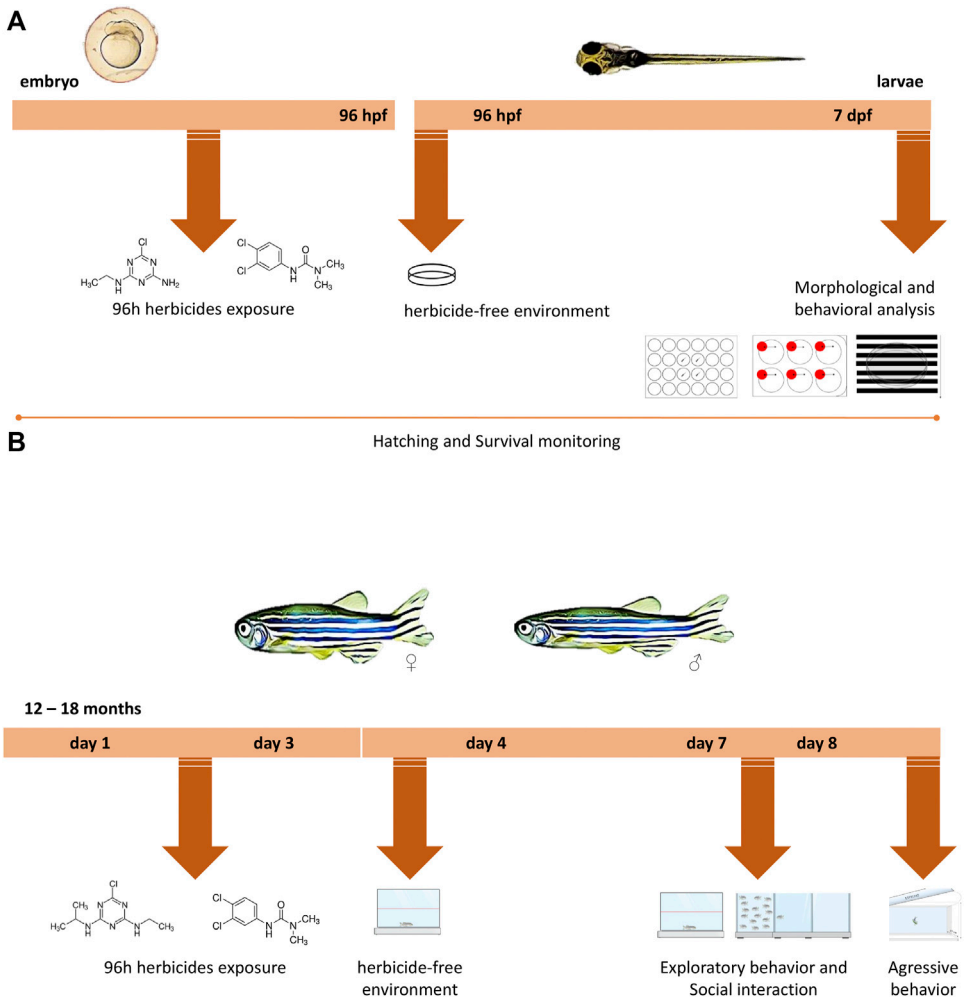

FIGURE 1 | Experimental design timeline for different life stages. **(A)** Zebrafish embryos up to 4 h post-fertilization (hpf) were exposed to water (control groups) or to different concentrations of the two herbicides (atrazine or diuron) for 96 h, after which they were transferred to an environment free of herbicides in which they remained until 7 days post-fertilization (dpf). During 7 dpf, morphological parameters, survival, and hatching rates were daily monitored. At 7 dpf, behavioral analyzes were performed and included the exploration of a new environment, aversive behavior, and optomotor response and individuals were photographed. **(B)** Adult animals aged 12–18 months were exposed to water (control groups) or to different concentrations of atrazine or diuron. Animals were exposed for 96 h, after which they were transferred to an environment free of herbicides where they remained for more than 3 days. On the third day, their performance on a new environment and the social interaction were evaluated. In the following day, an analysis of aggressive behavior was performed.

treatment group or control. All procedures followed the guidelines of the Brazilian Council of Animal Experimentation for Use of Fish in Research (CONCEA, 2016), and all protocols were approved by the Animal Care Committee of the Pontifical Catholic University of Rio Grande do Sul (10136/20—CEUA PUCRS). This study is registered at the Sistema Nacional de Gestão do Patrimônio Genético e Conhecimento Tradicional Associado—SISGEN (Protocol No. AD9D212). We followed the ARRIVE guidelines for reporting *in vivo* experiments (Percie du Sert et al., 2020).

2.2 Atrazine and Diuron Acute Exposure

Commercial herbicide formulations of atrazine (AclamadoBR®, 500 g/L, 50% purity—SC) and diuron (Diuron Nortox®, 500 g/L, 50% purity—SC) were diluted in water from recirculating tank systems (Tecniplast, Italy) and the solutions' pH was adjusted with sodium hydroxide (NaOH) solution to be within the aforementioned range and was verified daily. Embryos and adults were subjected to acute treatment for 96 h, as follows.

The herbicide concentration range was established based on the recommended working solutions and the environmental limits for atrazine. Experiments with embryos and larvae were performed chronologically first and additional concentrations were included for diuron, as it was not regulated in Brazil, and we aimed to explore a greater set of sampling points. Based on the initial findings, subsequent experiments with adults included the same concentrations for both herbicides. Each herbicide had a dedicated control group, to which treated animals were compared, hereafter called as the corresponding control group.

2.2.1 Larval Treatment

Embryos up to 4 h post-fertilization (hpf) were placed in Petri dishes (20 embryos per dish, in triplicate) and exposed to concentrations of the isolated herbicides atrazine (0.5, 1.0, 2.0, 2.5, and 5.0 mg/L) or diuron (0.1, 0.5, 1.0, 1.5, 2.0, 2.5, and 5.0 mg/L) for 96 h. After 96 hpf, the embryos were transferred to a pesticide-free environment until 168 hpf, that is, 7 dpf (**Figure 1A**). The control group went through the same manipulation; however, it was exposed just to the recirculating tank system water (Tecniplast, Italy). The dishes were kept in a biochemical oxygen demand (B.O.D) incubator with a constant temperature of 28°C and light/dark period of 14/10 h.

2.2.2 Adults Treatment

Adult animals, aged between 12 and 18 months of both sexes, were exposed to the concentrations of 0.5, 1.0, 2.0, 2.5, and 5.0 mg/L for both herbicides for 96 h. Animals were maintained in dedicated glass 3L tanks (30 cm long × 15 cm high × 10 cm wide), with aeration at a density of six zebrafish per liter, in triplicate. After the treatment, the animals were transferred to a pesticide-free environment for 3 days until behavioral analysis (**Figure 1B**). The control group also went through the same manipulation; however, it was exposed just to the recirculating tank system water (Tecniplast, Italy).

2.3 Survival and Hatching Rates

Embryos and hatched larvae were daily monitored for 7 dpf for survival defined by the presence of heartbeat and monitored under an inverted stereomicroscope (SMZ 1500 Nikon, Melville, EUA). Daily hatching was determined by the absence of chorion and was expected to occur between 48 and 72 hpf (Westerfield, 2000). The sample size was 60 embryos per group (n = 60).

2.4 Morphological and Teratogenic Evaluation

Treatment-induced morphological defects were estimated by morphological evaluation of 7 dpf larvae (n = 10 in triplicate) under a stereomicroscope (×3 magnification) and included the following parameters: body length (μm), head length (μm), ocular distance (μm), and forebrain and mesencephalon distance (μm), measured after photographic registration using NIS-Elements D software for Windows 3.2 (Nikon Instruments Inc., Melville, United States). Kimmel et al. (1995) staging series were used as a reference from normal development. The body length was defined as the distance from the mouth to the pigmented tip of the tail; the head length was measured from the mouth to the beginning of the pectoral fins; the ocular distance was the distance between the inner edge of the two eyes (Lutte et al., 2015; Wiprich et al., 2020), and the forebrain and mesencephalon width were measured in a coronal body orientation.

2.5 Larval Behavioral Analysis

All larvae behavioral experiments were conducted between 11 a.m. and 5 p.m. in a temperature-controlled room (27 ± 2°C) (Altenhofen et al., 2017a; Wiprich et al., 2020). Data quantification and analysis were performed automatedly using EthoVision XT tracking software (version 11.5, Noldus) and by experimenter's blind-to-individuals' group assignment.

2.5.1 Exploratory Behavior

At 7 dpf, larvae with no morphological defects were used for general exploratory and locomotion analysis (9 individuals per group, in triplicate) on a protocol adapted from Colwill and Creton (2011; Nabinger et al., 2018; Wiprich et al., 2020). Larvae were individually placed in a 24-well cell culture dish filled with 2 ml of recirculating tank system water (Tecniplast, Italy) and video recorded for automated analysis using EthoVision XT tracking software (version 11.5, Noldus) for 6 min, in a designed protocol that virtually divided each 15 mm diameter well in the inside (7.5 mm diameter) and outside areas (7.5 mm diameter) (Wiprich et al., 2020). Exploratory behavior was analyzed for 5 min after the 1-min acclimatization (Colwill and Creton 2011; Wiprich et al., 2020), and the video-tracking data was used to determine the following parameters: total distance traveled (m) and velocity (m/s, the ratio between distance traveled and movement), and were considered as parameters of exploration of the new environment. The parameter movement was defined as the period during which the zebrafish exceeded the start velocity (defined as 0.06 cm/s) and remained moving until reaching the stop velocity (defined as 0.01 cm/s; Mahmood et al., 2013). The anxiety-like behavior was also measured, and the time spent in each well position (outside area vs. inside area) was considered an index of anxiety. This task exploits the natural tendency of zebrafish to spend most of the time in the outside area when introduced to a novel environment, and then, the animals gradually extend the swimming range to include the inside portion of the test well. A longer time spent in the outside area and the less time spent in the inside of the well indicate increased anxiety (Colwill and Creton 2011).

2.5.2 Avoidance Behavior

The avoidance behavior evaluates animals' ability to escape an aversive stimulus. After the exploratory behavior, larvae were placed in a 6-well plate (5 larvae per well, in triplicate, per group) over an LCD monitor for the estimation of their avoidance behavior from an aversive visual stimulus (Pelkowski et al., 2011; Nery et al., 2014; Nabinger et al., 2018) for a 5-min session following 2 min of acclimation. A red bouncing ball (1.35 cm diameter) traveled from left to right over a straight 2 cm trajectory under one half of the well (stimulus area), which could be avoided by swimming to the other (non-stimulus) half. The number of larvae in the non-stimulus area was counted every 20 s during the 5-min session and was considered indicative of their cognitive ability of escaping an aversive stimulus (response of escape). Data are reported as the mean percentage of individuals from each group on each trial in the non-stimulus area.

2.5.3 Optomotor Behavior

The optomotor response is a visually driven behavior, in which larvae orientate and move their bodies according to the direction of white and black moving stripes (24.5 cm wide and 1.5 cm high)

adapted from Creton (2009) (Nery et al., 2017; Nabinger et al., 2020). Seven dpf larvae (15 larvae per dish, in triplicate, per group) were placed in a Petri dish over an LCD monitor, in which a sequence of animated images of moving stripes were presented for 10 min, following 2 min of acclimation. The stripes moved in alternating directions every 1 min, separated by a blank white screen that lasted 5 s. At the end of each min, when the blank background was presented, animals position inside the well was analyzed. Cognitively and visually apt individuals were expected to follow the stripes movement and therefor to be positioned at the end of the dish into which the stripes were moving. Data are expressed as the mean percentage of individuals from each group on each trial positioned on the far end into which sense the stripes were moving.

2.6 Adults Behavioral Analysis

All adult behavioral analyses were performed in a temperature-controlled room (27 ± 2°C) between 8:30 a.m. and 1:00 p.m. to avoid overlapping with their feeding schedule and unspecific effects on performance (Nabinger et al., 2018; Wiprich et al., 2020). Data quantification and analysis were performed automatedly using EthoVision XT tracking software (version 11.5, Noldus) or by experimenter's blind-to-individuals' group assignment.

2.6.1 Exploratory Behavior

Three days after the end of the 96 h treatment, each adult animal (six animals per group, in triplicate) was placed individually in experimental tanks (30 cm long × 15 cm high × 10 cm wide) with the recirculating tank system water (Tecniplast, Italy) and the locomotion and exploratory behavior was recorded for 6 min. After 1 min of habituation, the subsequent 5 min was analyzed by using EthoVision XT software (version 11.5, Noldus). The following behavioral parameters were analyzed: distance traveled (m), velocity (m/s, the ratio between distance traveled and movement), time in movement (s), and time spent in upper half of the water column (upper zone) (s). When zebrafish are introduced into a new environment, especially when isolated from their shoal, they tend to spend more time at the bottom of the tank until gradually moving to the upper zone (Levin et al., 2007). Increased time at the half bottom of the water column is indicative of an anxiety-like behavior (Cachat et al., 2010). Time mobile was defined as the period during which animals exceeded the start velocity (0.6 cm/s) and remained moving until reaching the stop velocity (0.59 cm/s), (Tran et al., 2016).

2.6.2 Social Interaction Test

Adults' social interaction was evaluated 3 days after the end of 96-h acute treatment (6 animals per group, in triplicate), with the same animals used to evaluate exploratory behavior, immediately after, in the same tank to minimize the manipulation interference. Zebrafish are schooling fish that may exhibit a preference for their conspecifics under certain circumstances (Breder and Halpern, 1946; Gerlai et al., 2000). For this, each fish remained individually placed in the experimental tanks (30 cm long × 15 cm high × 10 cm wide). On each smaller side wall of the experimental tank was a glass tank, identically sized (10 cm long × 15 cm high × 10 cm wide): one without fish and one with six adult zebrafish, the latter designated as the "stimulus tank." To quantify social interaction and innate preference for conspecifics, the experimental tank was virtually divided into three parts: a "stimulus zone" closer to the "stimulus tank" and a "non-stimulus zone" closer to the empty tank, separated by a third central one of equal size. Individual preferences between the stimulus tank zone and the non-stimulus tank zone were automatedly analyzed using EthoVision XT® tracking software (version 11.5, Noldus) (Gusso et al., 2021). Data are presented as mean time (s) spent by individuals from each group in the stimulus zone.

2.6.3 Aggression Test

Four days after the end of 96-h acute treatment, that is, on the day following the exploratory behavior and social interaction tests to ensure experiments were performed within the same time-window for all groups, aggressive behavior was estimated in adult animals (6 animals per group, in triplicate) using the mirror test according to the procedure described by Gerlai et al. (2000) and adapted by Wiprich et al. (2020). Each fish was individually placed in an experimental tank (30 cm long × 15 cm high × 10 cm wide). A mirror (45 cm long) was placed outside the tank at an angle of 22.5° from the 30 cm long wall so that the left vertical edge of the mirror touched the side of the tank, and the right edge was further away. Thus, when the experimental fish swam to the left side of the tank, their mirror image appeared closer to them. After 1-min acclimatization, a 5 min session was recorded for subsequent quantification of aggression behaviors using EthoVision XT tracking software (version 11.5, Noldus). Virtual vertical lines were used to divide the tank into six equally sized sections to allow the investigators to record the number of entries the fish made into each section. Entry to the left-most segment, the sixth part closer to the mirror, indicated a preference for proximity to the "opponent," whereas entry to the right-most segments implied avoidance. This segment was designated as the stimulus zone. The amount of time the experimental fish spent in each segment was measured as the number of bites against the mirror image, another parameter of aggression. Data are presented as mean time (s) spent by individuals in the stimulus zone, closer to the mirror and the mean number of bites from each group.

2.7 Statistical Analysis

Data analyses were performed using Graphpad Prism software version 8.0 (GraphPad Software, Inc.). The data were checked for normality prior to further analysis by the Shapiro–Wilk normality test. Larval survival and hatching rates during the initial 7 dpf were examined with the Kaplan–Meier test. Data from multiple groups of the same herbicide and their respective controls were compared by ANOVA followed by the Tukey's *post-hoc* test. The data are presented as the mean ± standard error of the mean (S.E.M), except for larval survival and hatching rates that are presented as percentage. For all comparisons, the significance level was set at $p < 0.05$. Statistical differences are graphically indicated as follows: * represents significant

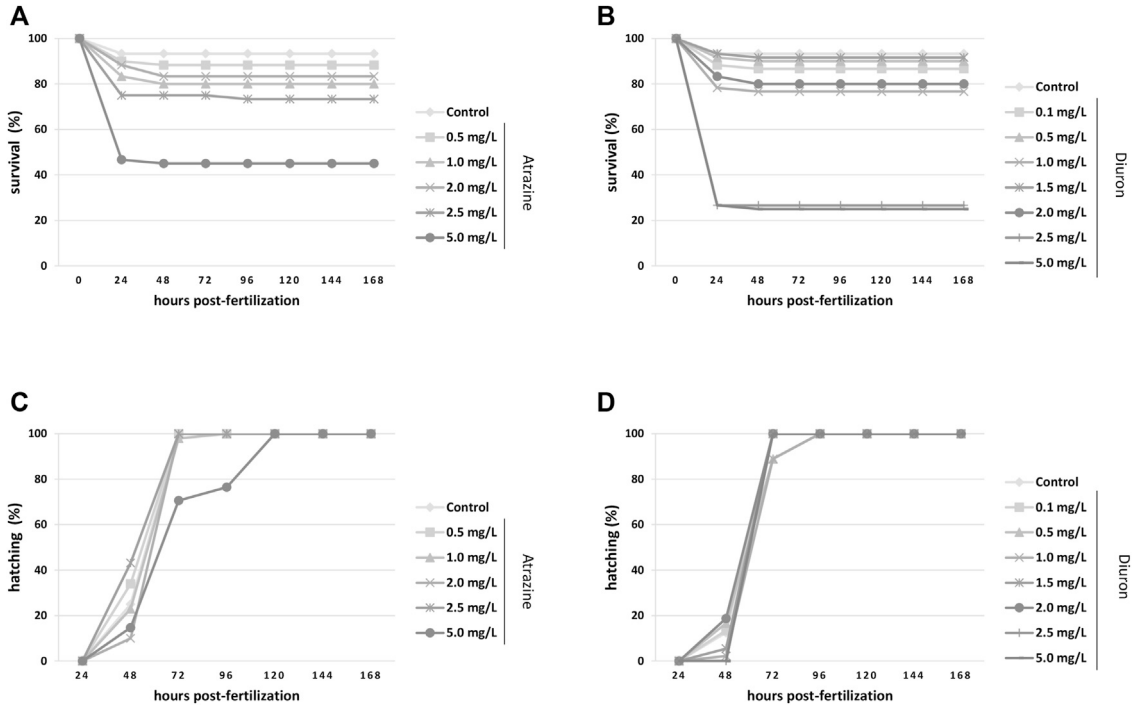

FIGURE 2 | Kaplan–Meier survival and hatching rates for zebrafish embryos and larvae exposed to the herbicides atrazine and diuron during their first 96 hpf and monitored for 7 days (168 hpf). **(A)** Atrazine effects on survival rates. Atrazine significantly reduced survival ($p < 0.0001$) at 5 mg/L when compared to controls; **(B)** Diuron effects on survival rates. Diuron significantly reduced survival ($p < 0.0001$) at 2.5 and 5 mg/L when compared to controls; **(C)** atrazine effects on the hatching rate. Atrazine did not impact hatching on surviving animals ($p = 0.1231$); **(D)** diuron effects on the hatching rate. Diuron significantly delayed hatching ($p = 0.0359$). Rates are expressed as percentage of the total number of animals from each group. Experiments were performed in triplicate, $n = 60$.

differences at $p \leq 0.05$, ** at $p \leq 0.01$, *** at $p \leq 0.001$, and **** at $p \leq 0.0001$ in relation to the corresponding control group.

3 RESULTS

3.1 Survival and Hatching Rates

The survival and hatching rates were evaluated from 4 hpf until 168 hpf, that is, 7 dpf, and analyzed by the Kaplan–Meier test. Exposure to atrazine commercial formula decreased the survival rate when all groups were compared ($p < 0.0001$, $n = 60$). The control group showed more than 90% survival, as expected for animals from our breeding colony, while only 46% of the animals exposed to 5 mg/L atrazine survived, mostly died at 24 hpf (**Figure 2A**). Diuron commercial formula also caused a significant decrease in the survival rate ($p < 0.0001$, $n = 60$) when all groups were compared. Dedicated controls also had a 93% of survival rate, whereas animals exposed to 2.5 and 5 mg/L diuron showed 26 and 25% of survival, respectively (**Figure 2C**).

There was no significant difference in the hatching rate of surviving embryos exposed to atrazine ($p = 0.1231$, $n = 60$). Most groups hatched between 48 and 96 hpf, as expected for this species (Kimmel et al., 1995; Westerfield, 2000), whereas in animals exposed to 5 mg/L atrazine hatching spanned for more than 96 hpf (**Figure 2B**). The hatching rate was significantly impacted when all groups were compared ($p = 0.0359$, $n = 60$), delayed in groups exposed to the herbicide at 2.5 and 5 mg/L in relation to controls. Whereas most animals started hatching at 48 hpf, and animals exposed to 2.5 and 5 mg/L hatched at 72 hpf (**Figure 2D**).

3.2 Morphology and Teratogenic Evaluation

The teratogenic effects of atrazine and diuron herbicides were daily evaluated over 7 dpf in embryos and larvae previously exposed to the herbicides for the initial 96 hpf and photographed at 7 dpf for quantification. For both herbicides, we observed a concentration-dependent increase in the incidence of deformations on body shape, including severe edema of the yolk sac, yolk sac deformation, reduced tail, and absence of head at all concentrations tested, while controls had 1.6% individuals with minor malformation, 0.5, 1.0, and 2.0 mg/L atrazine exposed groups had 5% of altered individuals, 2.5 mg/L had 8% and 5.0 mg/L had 10% (**Figure 3F**). Similarly, for diuron, controls only had one altered animal (1.6%) while the increasing concentrations of 0.1, 0.5, 1.0, 1.5, 2.0, 2.5, and 5 mg/L also had a progressively increased incidence of 3.3, 5, 6.6, 6.6, 11.6, and 15%, respectively (**Figure 3L**).

Quantification of discrete morphological parameters at 7 dpf showed that exposure to both herbicides significantly induced malformations on the head structure and brain vesicles, between treatment concentrations and in relation to their dedicated controls.

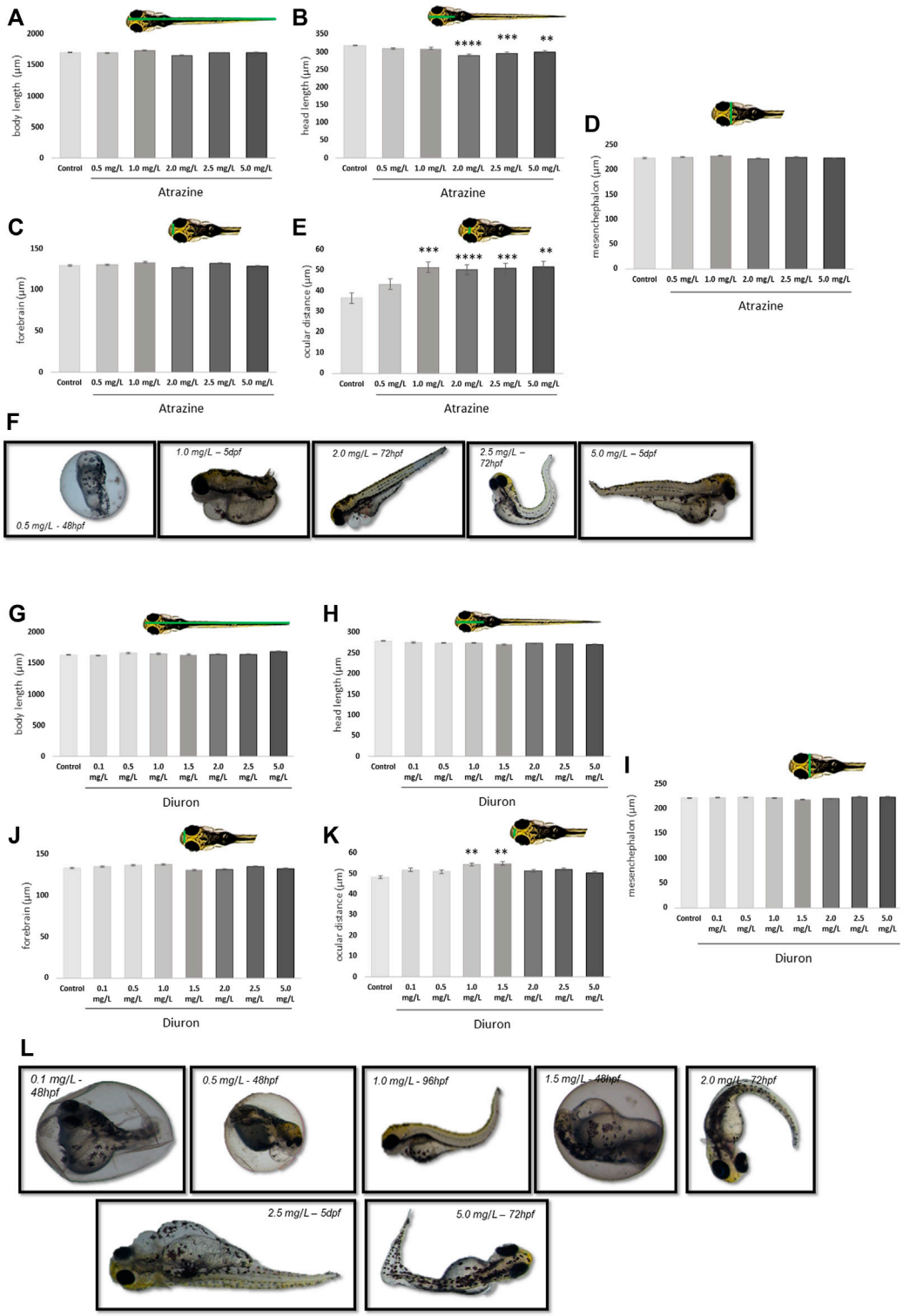

FIGURE 3 | Morphological effects of exposure to the herbicides atrazine and diuron during their first 96 hpf in zebrafish larvae at 7 dpf. **(A)** Atrazine exposure effects on the body length (µm); **(B)** atrazine exposure effects on the head length (µm); **(C)** atrazine exposure effects on the mesencephalon width (µm); **(D)** atrazine exposure effects on the forebrain width (µm); **(E)** atrazine exposure effects on the ocular distance (µm); **(F)** representative images of the most prominent morphology or teratogenic effects observed in individuals exposed to atrazine during the 7 dpf; **(G)** diuron exposure effects on the body length (µm); **(H)** diuron exposure effects on the head length (µm); **(I)** diuron exposure effects on the mesencephalon width (µm); **(J)** diuron exposure effects on the forebrain width (µm); **(K)** diuron exposure effects on the ocular distance (µm); **(L)** representative images of the most prominent morphology or teratogenic effects observed in individuals exposed to diuron during 7 dpf. Data were analyzed by one-way ANOVA followed by a *post-hoc* Tukey's test. ** represents significant differences at $p \leq 0.01$, ***$p \leq 0.001$, and ****$p \leq 0.0001$ in relation to control.

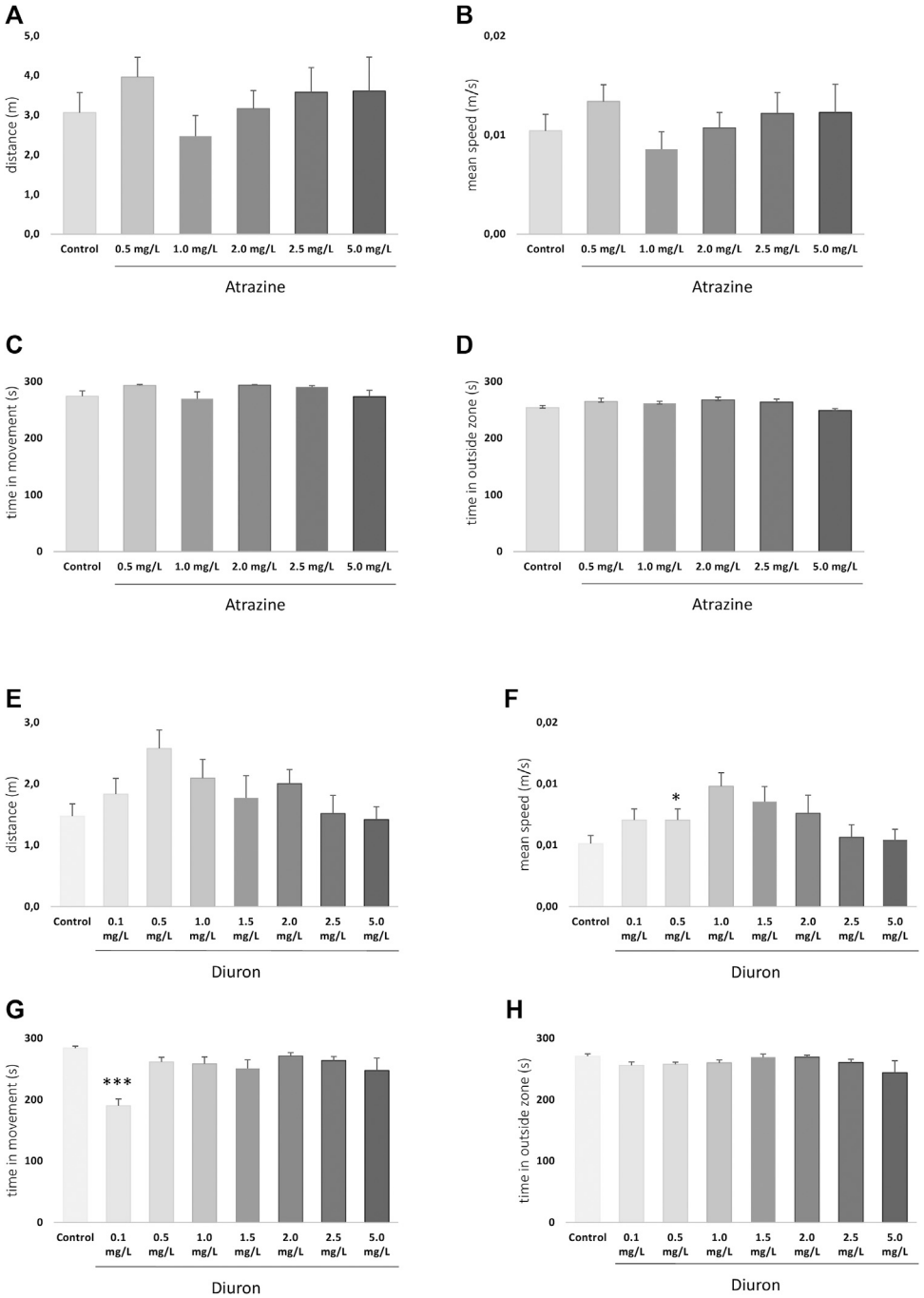

FIGURE 4 | Exploratory behavior of zebrafish larvae at 7 dpf after atrazine or diuron exposure during the initial 96 hpf. Columns depict means ± S.E.M. Sample sizes are $n = 27$ for each group. **(A)** Atrazine exposure effects on total distance traveled (m); **(B)** atrazine exposure effects on mean speed (m/s); **(C)** atrazine exposure effects on time in movement (s); **(D)** atrazine exposure effects on time in the outer area (s) of the well; **(E)** diuron exposure effects on total distance traveled (m); **(F)** diuron exposure effects on mean speed (m/s); **(G)** diuron exposure effects on time in movement (s); **(H)** diuron exposure effects on time in the outside area (s). Data were analyzed by one-way ANOVA followed by a *post-hoc* Tukey's test. Asterisks represent significant differences at $^{*}p \leq 0.01$ and $^{***}p \leq 0.001$ in relation to controls.

The body length was different between 1.0 and 2.0 mg/L groups exposed to atrazine ($p = 0.0005$). Atrazine resulted in a reduction in the head length at 2, 2.5, and 5 mg/L at $p < 0.0001$, $p = 0.0001$, and $p = 0.00027$ ($F_{(5,114)} = 9.307$), respectively, when compared to controls (**Figure 3A**). The head length also differed between 2.0 mg/L and 0.5 and 1.0 mg/L groups and $p = 0.0017$ and 0.0012, respectively (**Figure 3B**). A significant increase in the ocular distance in all atrazine groups, except the lower

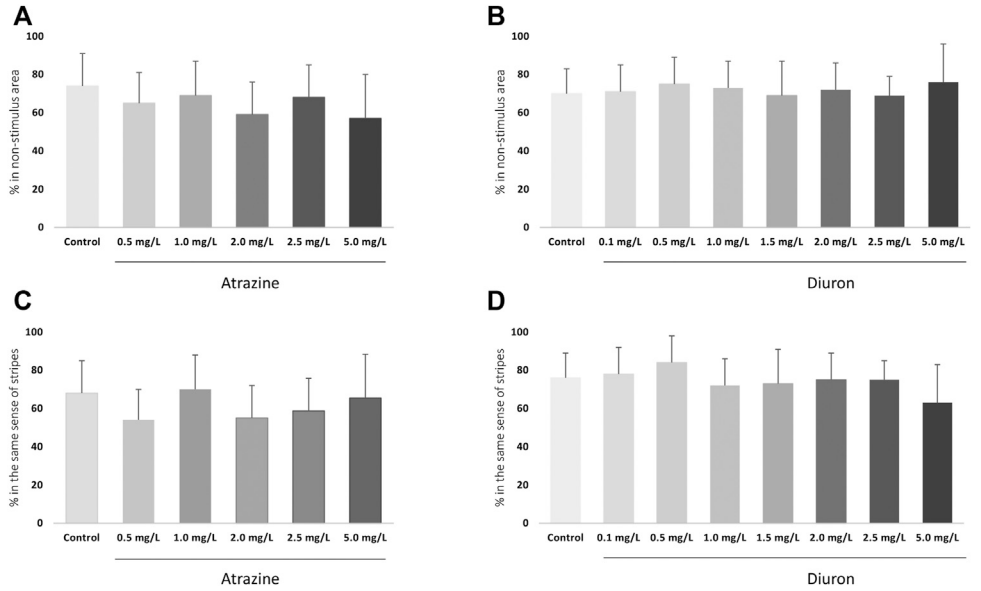

FIGURE 5 | Cognitive effects of atrazine or diuron exposure during the initial 96 hpf at 7 dpf larvae. Columns depict means ± S.E.M. Sample sizes are $n = 45$ for each group. **(A)** Atrazine exposure effects on the avoidance from an aversive visual stimulus; **(B)** Diuron exposure effects on the avoidance from an aversive visual stimulus; **(C)** Atrazine exposure effects on the optomotor response to moving stripes; **(D)** Diuron exposure effects on effects on the optomotor response to moving stripes. Data were analyzed by one-way ANOVA followed by a *post-hoc* Tukey's test.

concentration, was observed when compared to controls at $p < 0.0001$ ($F_{(5,97)} = 11.85$) was observed (**Figure 3E**). No differences between groups were observed in mesencephalon ($p = 0.1543$; $F_{(5,114)} = 1.643$) and forebrain ($p = 0.1027$; $F_{(5,114)} = 1.883$) dimensions (**Figures 3C,D**).

Animals exposed to diuron also had effects in morphological parameters. The body length differed between 1.0 and 5.0 mg/L groups at $p = 0.0177$ (**Figure 3G**). The ocular distance was increased in animals exposed to diuron 1.0 and 1.5 mg/L at $p = 0.0016$ and $p = 0.0006$ ($F_{(7,216)} = 4.164$), respectively (**Figure 3K**). This parameter was also increased in animals exposed to 1.5 mg/L in relation to 5.0 mg/L, suggesting an inverted U concentration-response curve. Forebrain dimensions were significantly reduced in animals exposed to 1.5 mg/L diuron when compared to 1.0 mg/L ($p = 0.0432$) (**Figure 3J**). The head length was not significantly impacted in animals exposed to diuron ($p = 0.7072$, $F_{(7,216)} = 0.6582$) or the mesencephalon dimensions ($p = 0.5762$; $F_{(7,216)} = 0.8143$) (**Figures 3H,I**).

3.3 Behavior Analysis in Larvae

3.3.1 Exploratory and Locomotor Behavior

The exploratory behavior of larvae in a new environment was analyzed at 7 dpf to determine whether atrazine or diuron exposure could alter larvae locomotion and anxiety. For atrazine, there were no significant differences in distance traveled (m) ($p = 0.5597$; $F_{(5,155)} = 0.7881$) (**Figure 4A**), mean speed (m/s) ($p = 0.5934$; $F_{(5,155)} = 0.7415$) (**Figure 4B**), time in movement (s) ($p = 0.8542$; $F_{(5,154)} = 1.982$) (**Figure 4C**), and the time spent outside the well area (s) ($p = 0.2765$; $F_{(5,154)} = 1.277$) when all groups were compared (**Figure 4D**). Despite the lack of statistical significance, when the mean distance traveled in controls (3.1 m) is contrasted with treated groups, an increase is observed in all tested concentrations (4, 3.2, 3.6, and 3.6 m in 0.5, 1.5, 2.0, 2.5, and 5.0 mgL, respectively), except 1.0 mg/L (2.5 m). The same pattern was observed regarding the mean speed.

For diuron, a similar inverted U pattern of mean total distance traveled, and speed is seen (**Figures 4E,F**) mostly due to the increased values on the lower concentrations in these parameters. Statistically significant differences were seen in the total distance traveled between 0.1 and 0.5 mg/L groups ($p = 0.0309$), and mean speed between 0.5 mg/L and controls ($p = 0.0309$). Time in movement was increased in diuron 0.1 mg/L in relation to controls ($p = 0.0021$) (**Figure 4G**). No differences were observed between groups regarding the time spent in the outside area ($p = 0.1388$; $F_{(7,208)} = 1.594$) (**Figure 4H**).

3.3.2 Avoidance Behavior

Avoidance from a red bouncing ball was evaluated at 7 dpf to test individuals' cognitive ability to escape an aversive stimulus and the effects of herbicide exposure. There were no changes in avoidance responses after acute exposure to atrazine ($p = 0.0798$; $F_{(5,48)} = 2.114$) or diuron ($p = 0.6342$; $F_{(7,61)} = 0.7459$) when exposed groups were compared to their corresponding controls (**Figures 5A,B**). Nonetheless, when mean responses of herbicide-exposed groups were examined in relation to their controls, that escaped the stimulus in average 74–75%, larvae exposed to all herbicide concentrations showed a lower mean ability to escape the stimulus and move to the non-stimulus zone.

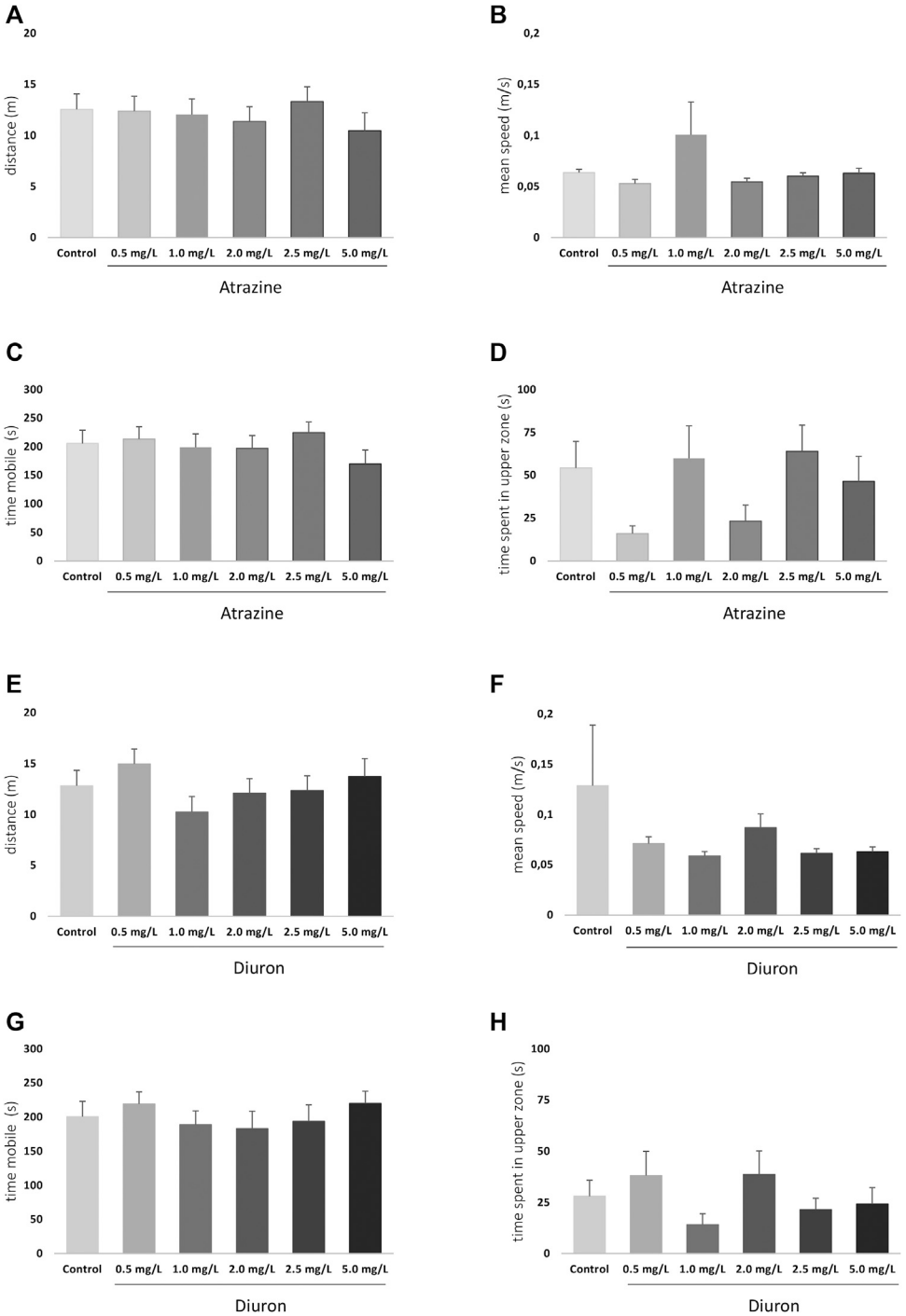

FIGURE 6 | Effects of acute exposure to atrazine or diuron on locomotion and exploratory behavior in adult zebrafish. Columns depict means ± S.E.M. Sample sizes are n = 18 for each group **(A)** Atrazine exposure effects on total distance traveled (m); **(B)** atrazine exposure effects on mean speed (m/s); **(C)** atrazine exposure effects on time mobile (s); **(D)** atrazine exposure effects on time spent in the upper tank zone (s); **(E)** diuron exposure effects on total distance traveled (m); **(F)** diuron exposure effects mean speed (m/s); **(G)** diuron exposure effects time mobile (s); **(H)** diuron exposure effects time spent in the upper zone (s). Data were analyzed by one-way ANOVA followed by a *post-hoc* Tukey's test.

3.3.3 Optomotor Response

The optomotor response to black and white moving stripes in alternating directions was analyzed at 7 dpf. There were no changes on optomotor response after acute exposure to atrazine (p = 0.1137; ($F_{(5,12)}$ = 2.269)) and diuron (p = 0.4399; ($F_{(7,15)}$ = 1.049)) when exposed groups were

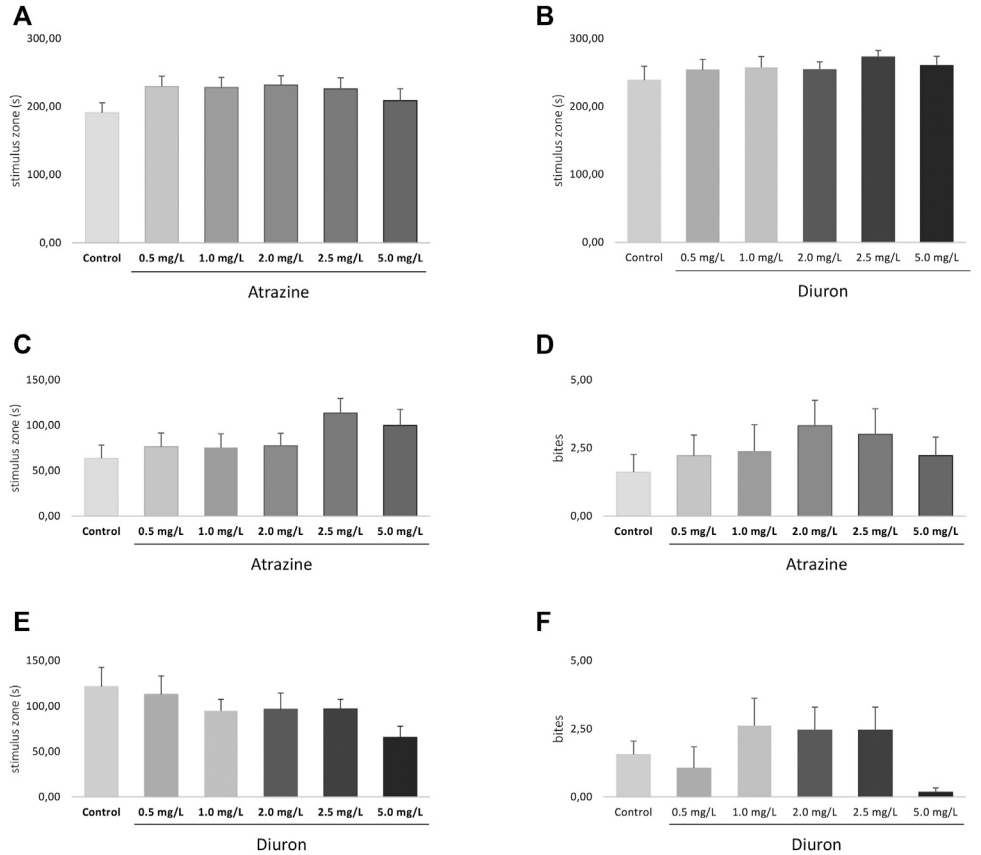

FIGURE 7 | Effects of acute exposure to atrazine or diuron on aggression and social interaction in adult zebrafish. Columns depict means ± S.E.M. Sample sizes are $n = 18$ for each group. **(A)** Atrazine exposure effects on aggressive behavior estimated by the time spent at the stimulus zone closer to the mirror (s); **(B)** atrazine exposure effects on the number of bites; **(C)** diuron exposure effects on aggressive behavior estimated by the time spent at the stimulus zone closer to the mirror (s); **(D)** diuron exposure effects on the number of bites; atrazine exposure effects on time mobile (s); **(E)** atrazine exposure effects on social behavior estimated by the time spent at the stimulus zone closer to the mirror (s); **(F)** atrazine exposure effects on social behavior estimated by the time spent at the stimulus zone closer to the mirror (s). Data were analyzed by one-way ANOVA followed by a *post-hoc* Tukey's test.

compared to their corresponding controls. Animals from all groups showed a positive optomotor response, following the same direction as the stripes, both up and down (**Figures 5C,D**).

3.4 Behavior Analysis in Adults

3.4.1 Exploratory

The exploratory and swimming pattern of adult animals in a new environment was analyzed 3 days after the end of the 96 h acute exposure to herbicides. There were no significant differences at any analyzed parameter when herbicide-exposed groups were compared to their dedicated controls. When atrazine groups and their controls were compared, the herbicide exposure did not impact the total traveled distance ($p = 0.8351$, $F_{(5,118)=}$ 0.4185) (**Figure 6A**), means speed ($p = 0.4441$; $F_{(5,118)} = 0.9620$) (**Figure 6B**), time mobile ($p = 0.6198$; $F_{(5,118)} = 0.7063$) (**Figure 6C**), and not the time spent in the upper zone of the tank ($p = 0.0929$; $F_{(5,118)} = 1.945$) (**Figure 6D**).

For diuron, a similar pattern was observed. Distance traveled ($p = 0.4484$; $F_{(5,121)} = 0.9572$), (**Figure 6E**) mean speed ($p = 0.4011$; $F_{(5,121)} = 1.034$) (**Figure 6F**), time mobile ($p = 0.7554$; $F_{(5,121)} = 0.5271$) (**Figure 6G**), and time in the upper area ($p = 0.3300$; $F_{(5,121)} = 1.166$) (**Figure 6H**) were not statistically different between groups. The mean time spent in the upper tank zone varied between groups, but probably due to dispersion, the comparisons were not statistically significant.

3.4.2 Social Interaction

Social interaction was evaluated after the exploratory behavioral test, also 3 days after the end of the 96-h exposure to atrazine and diuron herbicides, in the same apparatus. Atrazine and diuron acute exposure at all concentrations tested did not induce any social interaction deficits measured by the time spent in the stimulus zone when all groups were compared ($p = 0.5900$; $F_{(5,120)} = 0.7468$ and $p = 0.7297$; $F_{(5,118)} = 0.5610$) for atrazine and diuron, respectively. Despite the lack of significant effect, a subtle increase is observed in all herbicide-exposed groups in

relation to the mean responses of their dedicated controls (**Figures 7A,B**).

3.4.3 Aggression

Aggressive behavior was analyzed 4 days after the end of 96 h exposure to herbicides and two parameters were used, the time spent in most proximity of the mirror (stimulus zone) and the number of bites directed to their own reflection in the mirror. There were no significant differences in the time spent in the stimulus zone for atrazine ($p = 0.2250$, $F_{(5,94)=}1.418$) (**Figure 7C**) and diuron ($p = 0.2268$, $F_{(5,98)=}1.411$) (**Figure 7E**) when all groups are compared. The number of bites were also not statistically different between atrazine ($p = 0.7520$; $F_{(5,100)} = 0.5314$) (**Figure 7D**) and diuron ($p = 0.1742$; $F_{(5,102)} = 1.574$) (**Figure 7F**) exposed groups and their controls.

Despite the lack of statistical effect, animals exposed to all concentrations tested of atrazine spent in average more time in the segment nearest to the mirror when compared to the control group and showed an increased average number of biting episodes. In turn, for diuron-exposed groups, the average time spent in the stimulus zone was lower than that of controls, while the number of bites fluctuated.

4 DISCUSSION

Non-target species contamination by herbicides in aquatic environments occurs as a result of leaching, direct spraying, or during heavy rainfall of agricultural fields (Roy et al., 2016; Bridi et al., 2017). In the last years, Brazil was the country that had the highest consumption of pesticides and that most approved new commercial formulations in a few months (Ferrari et al., 2014; Frota et al., 2021). Most of these formulations have not been tested or regulated by CONAMA, so they do not have residue limit levels despite current use. For this reason, we analyzed, in a wide range of decreasing concentrations in relation to the known fish LC50 for the active principles of each, two herbicides: atrazine, a regulated pesticide, and diuron, currently unregulated in Brazil. In Brazil, it has been reported that diuron and atrazine herbicides are the second and the fourth most used herbicides, respectively, mostly found in surface waters, mainly near sugarcane crops (Bortoluzzi et al., 2006; Britto et al., 2011) at concentrations much higher than those allowed for the triazine group, and that should not exceed 2.0 μg/L (CONAMA 357, 2005).

Atrazine and diuron usage concentrations differ in the literature, but most studies with animal models and zebrafish use the isolated substance with >92% purity, which is not representative of the potential impacts due to the well reported synergistic toxicity between principle and vehicle substances (Corvi et al., 2012; Wang et al., 2015; Akcha et al., 2016; Liu et al., 2016; Velki et al., 2017, 2019; Horzmann et al., 2021; Tai et al., 2021). This is, to our knowledge, one of the very few studies that assess sublethal effects using commercial formulation as starter solution for treatment preparation, which is expected to be more realistic in estimating potential contamination effects on off-target organisms and environment.

Atrazine has a long history of toxicological tests and debatable toxicity, and data for model organisms vary according to species, developmental stage, exposure duration, concentrations, and formulation used. For diuron, however, there is a shortage of studies in non-target species such as fish (Velki et al., 2017), especially in adults, but also in embryos, and larvae zebrafish (Velki et al., 2017; Velki et al., 2019; 1314 Kao et al., 2018). Other species such as Nile tilapia *Oreochromis niloticus*) (Felício et al., 2017; Boscolo et al., 2018) and Javanese medaka also have a very limited number of studies (*Oryzias javanicus*) (Ibrahim et al., 2020).

Importantly, we observed a significant concentration-dependent survival decrease and hatching delays in animals exposed to both herbicides (**Figure 2**). Our survival curves are in accordance with the LC50 range for both substances, and differences may result from species and formulations used, in addition to manipulation. Our findings agree with Velki et al. (2017), that found 96 h-LC50 values of 6.31 ± 0.19 mg/L for zebrafish embryos exposed to diuron non-commercial formulation on the FET assay. Walker et al. (2018), also using isolated atrazine, found atrazine-induced mortality in an equivalent time window, but at lower concentrations.

The hatching delays observed are in accordance with previous reports using the isolated atrazine pure principle at lower concentrations (Liu et al., 2016; Walker et al., 2018). The interrelation between survival and hatching rates may hinder some deleterious effects that are not evident in the later parameter, as the lack of hatching delay in 5.0 mg/L atrazine-exposed animals only includes the surviving half population and may be considered when interpreting data.

Morphological defects and malformations were also more prevalent in herbicide-exposed groups than controls and included cardiac edema, tail reduction, and absence of head. The malformation types were found to agree with those expected for the species embryotoxicity tests (Beekhuijzen et al., 2015). The low incidence of malformations observed is typically seen in control animals from our AB wild-type breeding colony (Velki et al., 2017; Horzmann et al., 2021; Tai et al., 2021) and may vary depending on the vehicle solution controls exposed to, but are in accordance to other studies testing atrazine toxicity in similar and lower concentrations (Liu et al., 2016). Our findings are also in agreement with Blahova et al. (2020) that tested a wide range of environmentally relevant atrazine concentrations, using the isolated principle and found a significant increase in the occurrence of pericardial edema in the 10 mg/L group in relation to controls. They also paralleled those from Velki et al. (2017) which also observed body defects induced by pure diuron at 1.0, 2.0, and 3.8 mg/L.

In addition to a concentration-dependent effect on the frequency of malformations, specific morphological differences were observed between herbicide-exposed groups and their controls. The ocular distance was the most affected parameter, followed by the head length. Atrazine had more robust morphological effects than diuron, inducing reduced head length and increased ocular distance at several concentrations, while diuron increased the ocular distance in specific groups. Increased ocular distance may be associated with several factors,

including changes in overall head morphology and reduced ocular dimensions. Craniofacial abnormalities resulting from the developmental defects on chondrogenesis and osteogenesis may underly these effects, as atrazine exposure was previously shown to result in craniofacial defects in zebrafish embryos (Walker et al., 2018), but it has not been associated with diuron and deserve further investigation. The observed decrease in the head length and increase in the ocular distance may also be associated with the brain developmental effects of the herbicide exposure. Horzmann et al. (2021) demonstrated that early atrazine exposure results in neurotoxic changes in adult males, behavioral changes and anxiety, and cellular density on raphe brain cell population months after exposure.

Even discrete morphological effects may have lasting impacts on individuals' behavioral performance and physiology, endangering animals through their life cycle. To try to separate the morphological effects from exploratory and cognitive impacts of herbicide exposure, we only included individuals free from morphological defects on the behavioral analysis of 7 dpf larvae. This, of course, resulted in less pronounced behavioral effects than if abnormal animals were included, but may be strategic when looking for discrete effects (Velki et al., 2017). Despite the resulting lack of effect on exploratory parameters, traveled distances and mean speeds for each set of herbicide-exposed groups show a similar profile, as can be observed in **Figure 4**. Additionally, no effect was observed regarding thigmotaxis, suggesting anxiety was not impacted under these conditions and that has not been tested in other studies.

We also investigated exploratory parameters of 7 dpf larvae in a new environment. Swimming and responding to threats are critical abilities for larval fish, as is responding to visual cues. We did not observe any significant impact on exploratory and cognitive responses under tested conditions. The lack of effect is not in agreement with Liu et al (2016) that found reduced locomotion in zebrafish larvae after exposure to 100 and 300 ug/L atrazine. Velki et al (2017) also found an increase in the total distance moved by zebrafish larvae 118 h after exposure to diuron at concentrations of 1 and 2 mg/L, but not 3 mg/L, in a sudden light–dark transition test. Despite statistically significant, their effects were very subtle and may be related to the specific task, in which sudden transitions in lighting foster behavioral changes. These differences may be related to exposure conditions and may be attributed to research suggesting that the effects of exposure to atrazine are reversible once the exposure ends (Solomon et al., 2008).

Despite a reduced cognitive repertoire in comparison to adults, zebrafish larvae show specific visual-driven cognitive responses. We used previously established and validated protocols (Pelkowski et al., 2011; Nery et al., 2014, 2017; Nabinger et al., 2018; Nabinger et al., 2020) to measure aversive and optomotor responses in 7 dpf larvae exposed to atrazine and diuron. No significant differences were observed when treated animals were compared to their corresponding controls. Studies conducted with other pesticides showed a decrease in response to a visual stimulus, for glyphosate and Roundup® (Bridi et al., 2017) and the tebuconazole insecticide (Altenhofen et al., 2017b). Differences may be attributed to the different substances, underlying mechanisms and concentrations tested.

Adult zebrafish has a well-characterized behavioral repertoire (Kalueff et al., 2013) and consistent protocols to evaluate them under experimental conditions (Nery et al., 2014, 2017; Altenhofen et al., 2017a; Bridi et al., 2017; Nabinger et al., 2018; Nabinger et al., 2020; Wiprich et al., 2020; Gusso et al., 2021). This is, however, the first study assessing the acute toxic effects of diuron on the adult zebrafish behavior. We chose to evaluate ecologically relevant sets of behaviors: exploration of a new environment and associated anxiety-like parameters, social interaction, and aggressiveness. We did not find any significant effect on exploratory parameters and anxiety when they were individually placed in a new environment, while studies investigating the effects of diuron on behavior of zebrafish are scarce, diuron influences on the behavior of other fish have been assessed, that is, goldfish observed a higher burst swimming activity after exposure to diuron (Saglio and Trijasse 1998).

Adult zebrafish are social and interdependent of their school conspecifics. Social behavior, including aggression, social interaction, dominance, and inter-dependence tends to be impacted by separation from their conspecifics (Pagnussat et al., 2013). Under the conditions tested, we did not observe significant impacts of herbicide exposure on the parameters of social interaction. Our data diverges from the decreased social interaction found by Schmidel et al. (2014), showing increased inter-fish distance and an overall shoal area after 1.0 mg/L atrazine exposure. Differences between their and our findings regarding the social interaction may be attributed to the treatment regimen, which was subchronic and lasted 14 days, in contrast to ours that only lasted 4 days.

The lack of behavioral effects does not the exempt these substances from inducing other deleterious impacts. Sposito et al. (2018) demonstrated that atrazine and diuron on ng/L concentration range could alter zebrafish embryos gene expression after 3 days of exposure beginning at 48 hpf. Importantly, our findings agree to the expected increased susceptibility of early life stages, parallel to increased tolerance of adults. However, it is important to consider the possible long-term effects of the early life exposure in adults, which was not tested here, but were reported by Horzmann et al. (2021). In their study, they demonstrated that embryonic atrazine exposure during the initial 72 hpf decreases locomotor activity in males and alters gene expression.

5 CONCLUSION

This study investigated toxicological effects of atrazine and diuron exposure in sublethal concentrations—below the estimated LC50 for fish—and found impacts of survival, hatching, and morphology of zebrafish embryos, and larvae. These effects may be further explored to characterize its underlying mechanisms and potential impacts in other outcomes that can hinder animals' health span and lead to significant population decline.

Despite the lack of significant effects on behavioral outcomes in larvae and adult individuals, future studies may deepen the behavioral characterization of the herbicides' effects of fish, as behavioral changes may represent advantageous endpoints to estimate sublethal toxicity and fishes are vulnerable to the environmental contamination by agrochemicals.

DATA AVAILABILITY STATEMENT

The raw data supporting the conclusion of this article will be made available by the authors, without undue reservation.

ETHICS STATEMENT

The animal study was reviewed and approved by the Institutional Animal Care Committee of the Pontifical Catholic University of Rio Grande do Sul (approval under number 10136/20—CEUA PUCRS).

AUTHOR CONTRIBUTIONS

AZ, MW, CB, and MV contributed to conception and design of the study. LA and AA performed the herbicide exposure experiments and contributed to the animal care. AZ performed toxicological and morphological parameters. AZ and MW performed the behavioral experiments and the statistical analysis. AZ wrote the first draft of the manuscript that was completed by MV. MW and CB contributed to specific manuscript sections. All authors contributed to manuscript revision, read, and approved the submitted version.

FUNDING

This study was supported by the Brazilian Federal Agency CNPq (425818/2018-7), Coordenação de Aperfeiçoamento de Pessoal de Nível Superior—Brasil (CAPES)—Finance Code 001, and Instituto Nacional de Ciências e Tecnologia para Doenças Cerebrais, Excitotoxicidade e Neuroproteção. CB and MV are CNPq fellowship recipients. LA and AA received undergraduate fellowships from CNPq, Fundação de Amparo à Pesquisa do Estado do Rio Grande do Sul (FAPERGS) and PUCRS. AZ and MW received graduate fellowships from Coordenação de Aperfeiçoamento de Pessoal de Nível Superior—Brasil (CAPES)—FinanceCode 001 and CNPq, respectively.

REFERENCES

Akcha, F., Barranger, A., Bachère, E., Berthelin, C. H., Piquemal, D., Alonso, P., et al. (2016). Effects of an Environmentally Relevant Concentration of Diuron on Oyster Genitors during Gametogenesis: Responses of Early Molecular and Cellular Markers and Physiological Impacts. *Environ. Sci. Pollut. Res.* 23 (8), 8008–8020. doi:10.1007/s11356-015-5969-2

Altenhofen, S., Nabinger, D. D., Wiprich, M. T., Pereira, T. C. B., Bogo, M. R., and Bonan, C. D. (2017a). Tebuconazole Alters Morphological, Behavioral and Neurochemical Parameters in Larvae and Adult Zebrafish (*Danio rerio*). *Chemosphere* 180, 483–490. doi:10.1016/j.chemosphere.2017.04.029

Altenhofen, S., Wiprich, M. T., Nery, L. R., Leite, C. E., Vianna, M. R. M. R., and Bonan, C. D. (2017b). Manganese(II) Chloride Alters Behavioral and Neurochemical Parameters in Larvae and Adult Zebrafish. *Aquat. Toxicol.* 182, 172–183. doi:10.1016/j.aquatox.2016.11.013

Amaral, B. d., de Araujo, J. A., Peralta-Zamora, P. G., and Nagata, N. (2014). Simultaneous Determination of Atrazine and Metabolites (DIA and DEA) in Natural Water by Multivariate Electronic Spectroscopy. *Microchemical J.* 117, 262–267. doi:10.1016/j.microc.2014.07.008

Beekhuijzen, M., de Koning, C., Flores-Guillén, M. E., de Vries-Buitenweg, S., Tobor-Kaplon, M., van de Waart, B., et al. (2015). From Cutting Edge to Guideline: A First Step in Harmonization of the Zebrafish Embryotoxicity Test (ZET) by Describing the Most Optimal Test Conditions and Morphology Scoring System. *Reprod. Toxicol.* 56, 64–76. doi:10.1016/j.reprotox.2015.06.050

Blahova, J., Cocilovo, C., Plhalova, L., Svobodova, Z., and Faggio, C. (2020). Embryotoxicity of Atrazine and its Degradation Products to Early Life Stages of Zebrafish (*Danio rerio*). *Environ. Toxicol. Pharmacol.* 77 (March), 103370. doi:10.1016/j.etap.2020.103370

Boscolo, C. N. P., Pereira, T. S. B., Batalhão, I. G., Dourado, P. L. R., Schlenk, D., and de Almeida, E. A. (2018). Diuron Metabolites Act as Endocrine Disruptors and Alter Aggressive Behavior in Nile tilapia (*Oreochromis niloticus*). *Chemosphere* 191, 832–838. doi:10.1016/j.chemosphere.2017.10.009

Bortoluzzi, E. C., Rheinheimer, D. S., Gonçalves, C. S., Pellegrini, J. B. R., Zanella, R., and Copetti, A. C. C. (2006). Contamination of Surface Water by Pesticides as a Function of Soil Use in the Agudo Watershed. *RS. Ver. Bras. Eng. Agríc. Ambient.* 10 (4), 881–887. doi:10.1590/S1415-43662006000400015

Breder, C. M., and Halpern, F. (1946). Affecting, Acquired Behavior, and Aggregation of Fishes. *Physiol. Zoolog.* 19, 154–190.

Bridi, D., Altenhofen, S., Gonzalez, J. B., Reolon, G. K., and Bonan, C. D. (2017). Glyphosate and Roundup® Alter Morphology and Behavior in Zebrafish. *Toxicology* 392 (October), 32–39. doi:10.1016/j.tox.2017.10.007

Britto, F. B., do Vasco, A. N., Pereira, A. P. S., Méllo, A. V., and Nogueira, L. C. (2011). Herbicides in the Upper Poxim River, Sergipe, and the Risk of Contamination of Water Resources. *Rev. Ciênc. Agron.* 43 (2), 390–398. doi:10.1590/S1806-66902012000200024

Cachat, J., Stewart, A., Grossman, L., Gaikwad, S., Kadri, F., Chung, K. M., et al. (2010). Measuring Behavioral and Endocrine Responses to novelty Stress in Adult Zebrafish. *Nat. Protoc.* 5 (11), 1786–1799. doi:10.1038/nprot.2010.140

Colwill, R. M., and Creton, R. (2011). Locomotor Behaviors in Zebrafish (*Danio rerio*) Larvae. *Behav. Process.* 86 (2), 222–229. doi:10.1016/j.beproc.2010.12.003

Conama 357 (2005). Resolução CONAMA N° 357, De 17 De Março De 2005* (Retificada). *Conselho Nacional do Meio Ambiente* 204, 36.

Concea (2016). Normativas Do Concea Para Produção, Manutenção Ou Utilização de Animais Em Atividades de Ensino Ou Pesquisa Científica. *Conselho Nacional de COntrole de experimentação Anim.* 387, 1.

Corvi, M. M., Stanley, K. A., Peterson, T. S., Kent, M. L., Feist, S. W., La Du, J. K., et al. (2012). Investigating the Impact of Chronic Atrazine Exposure on Sexual Development in Zebrafish. *Birth Defects Res. B Dev. Reprod. Toxicol.* 95 (4), 276–288. doi:10.1002/bdrb.21016

Creton, R. (2009). Automated Analysis of Behavior in Zebrafish Larvae. *Behav. Brain Res.* 203 (1), 127–136. doi:10.1016/j.bbr.2009.04.030

Dellamatrice, P. M., and Monteiro, R. T. R. (2014). Principais aspectos da poluição de rios brasileiros por pesticidas. *Rev. Bras. Eng. Agríc. Ambient.* 18 (12), 1296–1301. doi:10.1590/1807-1929/agriambi.v18n12p1296-1301

Felício, A. A., Freitas, J. S., Scarin, J. B., de Souza Ondei, L., Teresa, F. B., Schlenk, D., et al. (2018). Isolated and Mixed Effects of Diuron and its Metabolites on Biotransformation Enzymes and Oxidative Stress Response of Nile Tilapia (Oreochromis Niloticus). *Ecotoxicology Environ. Saf.* 149, 248–256. doi:10.1016/j.ecoenv.2017.12.009

Fernandes, C. L. F., Volcão, L. M., Ramires, P. F., Moura, R. R. D., and Da Silva Júnior, F. M. R. (2020). Distribution of Pesticides in Agricultural and Urban Soils of Brazil: a Critical Review. *Environ. Sci. Process. Impacts* 22 (2), 256–270. doi:10.1039/c9em00433e

Ferrari, R. A. (2014). Uso de Agrotóxicos No Brasil e Problemas Para a Saúde Pública Pesticide Use in Brazil and Problems for Public Health Uso de Pesticidas En Brasil y Los Problemas Para La Salud Pública. *Ciência e Agrotecnologia* 10 (1), 101–102. Available at: https://revista.francomontoro.com.br/intercienciaesociedade/article/view/57/50.

Frota, A., Tereza Borges, M., and Siqueira, C. E. (2021). Pesticides: The Hidden Poisons on Our Table.". *Cadernos de Saude Publica* 37 (2), 1–5. doi:10.1590/0102-311x00004321

Gerlai, R., Lahav, M., Guo, S., and Rosenthal, A. (2000). Drinks like a Fish: Zebra Fish (*Danio rerio*) as a Behavior Genetic Model to Study Alcohol Effects. *Pharmacol. Biochem. Behav.* 67 (4), 773–782. doi:10.1016/s0091-3057(00)00422-6

Giacomazzi, S., and Cochet, N. (2004). Environmental Impact of Diuron Transformation: a Review. *Chemosphere* 56 (11), 1021–1032. doi:10.1016/j.chemosphere.2004.04.061

Gusso, D., Cruz, F. F., Fritsch, P. M., Gobbo, M. O., Morrone, F. B., Bonan, C. D., et al. (2021). "Oxytetracycline Induces Anxiety-like Behavior in Adult Zebrafish.". *Toxicol. Appl. Pharmacol.* 426 (June), 8–15. doi:10.1016/j.taap.2021.115616

Hamilton, D. J., Ambrus, Á., Dieterle, R. M., Felsot, A. S., Harris, C. A., Holland, P. T., et al. (2003). Regulatory Limits for Pesticide Residues in Water (IUPAC Technical Report). *Pure Appl. Chem.* 75 (8), 1123–1155. doi:10.1351/pac200375081123

Horzmann, K. A., Lin, L. F., Taslakjian, B., Yuan, C., and Freeman, J. L. (2021). Embryonic Atrazine Exposure and Later in Life Behavioral and Brain Transcriptomic, Epigenetic, and Pathological Alterations in Adult Male Zebrafish. *Cell Biol Toxicol* 37 (3), 421–439. doi:10.1007/s10565-020-09548-y

Ibrahim, M. A., Zulkifli, S. Z., Azmai, M. N. A., Mohamat-Yusuff, F., and Ismail, A. F. (2020). *Effect of Diuron on Embryo-Larval Development of Javanese Medaka (Oryzias Javanicus, Bleeker 1854)*. Available at: https://www.preprints.org/manuscript/202009.0290/v1.Preprints

Kalueff, A. V., Gebhardt, M., Stewart, A. M., Cachat, J. M., Brimmer, M., Chawla, J. S., et al. (2013). Towards a Comprehensive Catalog of Zebrafish Behavior 1.0 and beyond. *Zebrafish* 10 (1), 70–86. doi:10.1089/zeb.2012.0861

Kao, C. M., Ou, W. J., Lin, H. D., Eva, A. W., Wang, T. L., and Chen, S. C. (2018). Toxicity of Diuron in HepG2 Cells and Zebrafish Embryos. *Ecotoxicol Environ. Saf.* 172, 432–438. doi:10.1016/j.ecoenv.2019.01.036

Kimmel, C. B., Ballard, W. W., Kimmel, W. W. S. R., Ullmann, B., and Schilling, T. F. (1995). Stages of Embryonic Development of the Zebrafish. *Dev. Dyn.* 203 (3), 253–310. doi:10.1002/aja.1002030302

Langeron, J., Sayen, S., Couderchet, M., and Guillon, E. (2014). Leaching Potential of Phenylurea Herbicides in a Calcareous Soil: Comparison of Column Elution and Batch Studies. *Environ. Sci. Pollut. Res.* 21 (7), 4906–4913. doi:10.1007/s11356-012-1244-y

Levin, E. D., Bencan, Z., and Cerutti, D. T. (2007). Anxiolytic Effects of Nicotine in Zebrafish. *Physiol. Behav.* 90 (1), 54–58. doi:10.1016/j.physbeh.2006.08.026

Liu, S.-S., Wang, C.-L., Zhang, J., Zhu, X.-W., and Li, W.-Y. (2013). Combined Toxicity of Pesticide Mixtures on green Algae and Photobacteria. *Ecotoxicology Environ. Saf.* 95, 98–103. doi:10.1016/j.ecoenv.2013.05.018

Liu, Z., Wang, Y., Zhu, Z., Yang, E., Feng, X., Fu, Z., et al. (2016). Atrazine and its Main Metabolites Alter the Locomotor Activity of Larval Zebrafish (*Danio rerio*). *Chemosphere* 148, 163–170. doi:10.1016/j.chemosphere.2016.01.007

Lutte, A. H., Capiotti, K. M., da Silva, N. L., da Silva, C. S., Kist, L. W., Bogo, M. R., et al. (2015). Contributions from Extracellular Sources of Adenosine to the Ethanol Toxicity in Zebrafish Larvae. *Reprod. Toxicol.* 53, 82–91. doi:10.1016/j.reprotox.2015.04.001

MacRae, C. A., and Peterson, R. T. (2015). Zebrafish as Tools for Drug Discovery. *Nat. Rev. Drug Discov.* 14 (10), 721–731. doi:10.1038/nrd4627

Maggi, F., Cecilia, D. L., Tang, F. H. M., and McBratney, A. (2020). The Global Environmental hazard of Glyphosate Use. *Sci. Total Environ.* 717, 137167. doi:10.1016/j.scitotenv.2020.137167

Mahmood, F., Fu, S., Cooke, J., Wilson, S. W., Cooper, J. D., and Russell, C. (2013). A Zebrafish Model of CLN2 Disease Is Deficient in Tripeptidyl Peptidase 1 and Displays Progressive Neurodegeneration Accompanied by a Reduction in Proliferation. *Brain* 136 (5), 1488–1507. doi:10.1093/brain/awt043

Mansano, A. S., Moreira, R. A., Dornfeld, H. C., Freitas, E. C., Vieira, E. M., Sarmento, H., et al. (2016). Effects of Diuron and Carbofuran and Their Mixtures on the Microalgae Raphidocelis Subcapitata. *Ecotoxicol Environ. Saf.* 142, 312–321. doi:10.1016/j.ecoenv.2017.04.024

Nabinger, D. D., Altenhofen, S., Peixoto, J. V., da Silva, J. M. K., Gerlai, R., Bonan, C. D., et al. (2021). Feeding Status Alters Exploratory and Anxiety-like Behaviors in Zebrafish Larvae Exposed to Quinpirole. *Prog. Neuro-Psychopharmacology Biol. Psychiatry* 108, 110179. doi:10.1016/j.pnpbp.2020.110179

Nabinger, D. D., Altenhofen, S., Bitencourt, P. E. R., Nery, L. R., Leite, C. E., Vianna, M. R. M. R., et al. (2018). Nickel Exposure Alters Behavioral Parameters in Larval and Adult Zebrafish. *Sci. Total Environ.* 624, 1623–1633. doi:10.1016/j.scitotenv.2017.10.057

Nery, L. R., Eltz, N. S., Hackman, C., Fonseca, R., Altenhofen, S., Guerra, H. N., et al. (2014). Brain Intraventricular Injection of Amyloid-β in Zebrafish Embryo Impairs Cognition and Increases Tau Phosphorylation, Effects Reversed by Lithium. *PLoS One* 9 (9), e105862. doi:10.1371/journal.pone.0105862

Nery, L. R., Silva, N. E., Fonseca, R., Vianna, M. R. M., and Ryff, Monica. (2017). Presenilin-1 Targeted Morpholino Induces Cognitive Deficits, Increased Brain Aβ1–42 and Decreased Synaptic Marker PSD-95 in Zebrafish Larvae"Presenilin-1 Targeted Morpholino Induces Cognitive Deficits. *Neurochem. Res.* 42 (10), 2959–2967. doi:10.1007/s11064-017-2327-4

Lyer, P. (2003). Evidence on the Developmental and Reproductive Toxicity of Diuron," in *Reproductive and Cancer Hazard Assessment Section Office of Environmental Health Hazard Assessment California Environmental Protection Agency* Editor Oehha. (California), 1–43.

Pagnussat, N., Piato, A. L., Schaefer, I. C., Blank, M., Tamborski, A. R., Guerim, L. D., et al. (2013). One for All and All for One: the Importance of Shoaling on Behavioral and Stress Responses in Zebrafish. *Zebrafish* 10 (3), 338–342. doi:10.1089/zeb.2013.0867

Pelkowski, S. D., Kapoor, M., Richendrfer, H. A., Wang, X., Colwill, R. M., and Creton, R. (2011). A Novel High-Throughput Imaging System for Automated Analyses of Avoidance Behavior in Zebrafish Larvae. *Behav. Brain Res.* 223 (1), 135–144. doi:10.1016/j.bbr.2011.04.033

Percie du Sert, N., Hurst, V., Ahluwalia, A., Alam, S., Avey, M. T., Baker, M., et al. (2020). The Arrive Guidelines 2.0: Updated Guidelines for Reporting Animal Research. *PLoS Biol.* 18 (7), 1–12. doi:10.1371/journal.pbio.3000410

Pereira, J. L., Antunes, S. C., Castro, B. B., Marques, C. R., Gonçalves, A. M. M., Gonçalves, F., et al. (2009). Toxicity Evaluation of Three Pesticides on Non-target Aquatic and Soil Organisms: Commercial Formulation versus Active Ingredient. *Ecotoxicology* 18 (4), 455–463. doi:10.1007/s10646-009-0300-y

Plhalova, L., Blahova, J., Mikulikova, I., Stepanova, S., Dolezelova, P., Praskoval, E., et al. (2012). Effects of Subchronic Exposure to Atrazine on Zebrafish (*Danio rerio*). *Pol. J. Vet. Sci.* 15 (3), 417–423. doi:10.2478/v10181-012-0065-8

Rodrigues, E. T., Alpendurada, M. F., Ramos, F., Pardal, M. Â., and Pardal, M. Â. (2017). Environmental and Human Health Risk Indicators for Agricultural Pesticides in Estuaries. *Ecotoxicol Environ. Saf.* 150, 224–231. doi:10.1016/j.ecoenv.2017.12.047

Roy, N. M., Carneiro, B., and Ochs, J. (2016). Glyphosate Induces Neurotoxicity in Zebrafish. *Environ. Toxicol. Pharmacol.* 42, 45–54. doi:10.1016/j.etap.2016.01.003

Saglio, P., and Trijasse, S. (1998). Behavioral Responses to Atrazine and Diuron in Goldfish. *Arch. Environ. Contam. Toxicol.* 35 (3), 484–491. doi:10.1007/s002449900406

Schmidel, A. J., Assmann, K. L., Werlang, C. C., Bertoncello, K. T., Francescon, F., Rambo, C. L., et al. (2014). Subchronic Atrazine Exposure Changes Defensive Behaviour Profile and Disrupts Brain Acetylcholinesterase Activity of Zebrafish. *Neurotoxicol Teratol* 44, 62–69. doi:10.1016/j.ntt.2014.05.006

Sharma, A., Kumar, V., Shahzad, B., Tanveer, M., Sidhu, G., Handa, N., et al. (2019). Worldwide Pesticide Usage and its Impacts on Ecosystem.". *SN Appl. Sci.* 1 (11), 1–16. doi:10.1007/s42452-019-1485-1

Sipes, N. S., Padilla, S., and Knudsen, T. B. (2011). Zebrafish-As an Integrative Model for Twenty-First century Toxicity Testing. *Birth Defects Res. C: Embryo Today Rev.* 93 (3), 256–267. doi:10.1002/bdrc.20214

Solomon, K. R., Carr, J. A., Du Preez, L. H., Giesy, J. P., Kendall, R. J., Smith, E. E., et al. (2008). Effects of Atrazine on Fish, Amphibians, and Aquatic Reptiles: a Critical Review. *Crit. Rev. Toxicol.* 38 (9), 721–772. doi:10.1080/10408440802116496

Sposito, J. C. V., Montagner, C. C., Casado, M., Navarro-Martín, L., Jut Solórzano, J. C., Piña, B., et al. (2018). Emerging Contaminants in Brazilian Rivers:

Occurrence and Effects on Gene Expression in Zebrafish (*Danio rerio*) Embryos. *Chemosphere* 209, 696–704. doi:10.1016/j.chemosphere.2018.06.046

Švorc, Ľ., Rievaj, M., and Bustin, D. (2013). Green Electrochemical Sensor for Environmental Monitoring of Pesticides: Determination of Atrazine in River Waters Using a Boron-Doped Diamond Electrode. *Sensors Actuators, B: Chem.* 181, 294–300. doi:10.1016/j.snb.2013.02.036

Tai, A. C., Janiel, K., Horzmann, K. A., Franco, J., Jannasch, A. S., Cooper, B. R., et al. (2021). Developmental Atrazine Exposure in Zebrafish Produces the Same Major Metabolites as Mammals along with Altered Behavioral Outcomes. *Neurotoxicology and Teratology* 85, 106971. doi:10.1016/j.ntt.2021.106971

Tang, F. H. M., Lenzen, M., McBratney, A., and Maggi, F. (2021). Risk of Pesticide Pollution at the Global Scale. *Nat. Geosci.* 14 (4), 206–210. doi:10.1038/s41561-021-00712-5

Tasca, A. L., Fletcher, A., and Fletcher, A. (2018). State of the Art of the Environmental Behaviour and Removal Techniques of the Endocrine Disruptor 3,4-dichloroaniline. *J. Environ. Sci. Health A* 53 (3), 260–270. doi:10.1080/10934529.2017.1394701

Tran, S., Nowicki, M., Fulcher, N., Chatterjee, D., and Gerlai, R. (2016). Interaction between Handling Induced Stress and Anxiolytic Effects of Ethanol in Zebrafish: A Behavioral and Neurochemical Analysis. *Behav. Brain Res.* 298, 278–285. doi:10.1016/j.bbr.2015.10.061

Velki, M., Di Paolo, C., Nelles, J., Seiler, T. B., and Hollert, H. (2017). Diuron and Diazinon Alter the Behavior of Zebrafish Embryos and Larvae in the Absence of Acute Toxicity. *Chemosphere* 180, 65–76. doi:10.1016/j.chemosphere.2017.04.017

Velki, M., Lackmann, C., Barranco, A., and Artabe, A. E. (2019). Pesticides Diazinon and Diuron Increase Glutathione Levels and Affect Multixenobiotic Resistance Activity and Biomarker Responses in Zebrafish (Danio Rerio) Embryos and Larvae. *Environ. Sci. Europe* 31 (1), 1–18. doi:10.1186/s12302-019-0186-0

Walker, B. S., KramerKramer, A. G., and Lassiter, C. S. (2018). Atrazine Affects Craniofacial Chondrogenesis and Axial Skeleton Mineralization in Zebrafish (*Danio rerio*). *Toxicol. Ind. Health* 34 (5), 329–338. doi:10.1177/0748233718760419

Wang, H., Mu, S., Zhang, F., Wang, H., Liu, H., Zhang, H., et al. (2015). Effects of Atrazine on the Development of Neural System of Zebrafish, Danio Rerio. *Biomed. Res. Int.* 2015, 1. doi:10.1155/2015/976068

Westerfield, M. (2000). "The Zebrafish Book," in *A Guide for the Laboratory Use of Zebrafish (Danio rerio)* 4th edition. Eugene: University of Oregon Press.

Wiprich, M. T., Zanandrea, R., Altenhofen, S., and Bonan, C. D. (2020). Influence of 3-Nitropropionic Acid on Physiological and Behavioral Responses in Zebrafish Larvae and Adults. *Comp. Biochem. Physiol. Part - C: Toxicol. Pharmacol.* 234, 108772. doi:10.1016/j.cbpc.2020.108772

Wirbisky, S. E., Weber, G. J., Sepulveda, M. S., Lin, T.-L., Jannasch, A. S., and Freeman, J. L. (2016). An Embryonic Atrazine Exposure Results in Reproductive Dysfunction in Adult Zebrafish and Morphological Alterations in Their Offspring. *Scientific Rep.* 6, 1–13. doi:10.1038/srep21337

Conflict of Interest: The authors declare that the research was conducted in the absence of any commercial or financial relationships that could be construed as a potential conflict of interest.

Publisher's Note: All claims expressed in this article are solely those of the authors and do not necessarily represent those of their affiliated organizations, or those of the publisher, the editors, and the reviewers. Any product that may be evaluated in this article, or claim that may be made by its manufacturer, is not guaranteed or endorsed by the publisher.

frontiers | Frontiers in Pharmacology

ORIGINAL RESEARCH
published: 12 April 2022
doi: 10.3389/fphar.2022.836573

Neural Activity Correlates With Behavior Effects of Anti-Seizure Drugs Efficacy Using the Zebrafish Pentylenetetrazol Seizure Model

*Patrick C. Milder, Agnes S. Zybura, Theodore R. Cummins and James A. Marrs **

Department of Biology, Indiana University Purdue University Indianapolis, Indianapolis, IN, United States

OPEN ACCESS

Edited by:
Anna Siebel,
Universidade Comunitária da Região de Chapecó, Brazil

Reviewed by:
Angelo Piato,
Federal University of Rio Grande do Sul, Brazil
Justin James Botterill,
University of Toronto Scarborough, Canada
Bin Gu,
The Ohio State University, United States
Jyotirmoy Banerjee,
All India Institute of Medical Sciences, India

***Correspondence:**
James A. Marrs
jmarrs@iu.edu

Specialty section:
This article was submitted to Neuropharmacology, a section of the journal Frontiers in Pharmacology

Received: *15 December 2021*
Accepted: *03 March 2022*
Published: *12 April 2022*

Citation:
Milder PC, Zybura AS, Cummins TR and Marrs JA (2022) Neural Activity Correlates With Behavior Effects of Anti-Seizure Drugs Efficacy Using the Zebrafish Pentylenetetrazol Seizure Model. Front. Pharmacol. 13:836573. doi: 10.3389/fphar.2022.836573

Approximately 30% of patients with epilepsy do not achieve adequate seizure control through current anti-seizure drugs and treatment methods. Therefore, a critical need exists to efficiently screen anti-seizure drugs to enhance our ability to tailor treatment protocols and improve patient outcomes. The zebrafish pentylenetetrazol (PTZ) seizure model has become an increasingly popular screening paradigm for novel anti-seizure compounds. However, previous research using this model was variable due to differing experimental methods. Here, we present a method that was optimized to improve reliability and reproducibility in our laboratory using this PTZ model to develop a more robust screening of anti-seizure drugs comparing behavior and neural activity. Our behavior assay, spanning 90 min using 10 mM PTZ on 7 days post fertilization zebrafish, provides a broad window to observe anti-seizure drug efficacy. To compare our method with previously published data, we tested carbamazepine, lamotrigine, and topiramate, which have been tested in previous PTZ zebrafish assays. In addition, we assessed the candidate anti-seizure compound GS967, which has not been previously tested in the zebrafish seizure model. We examined the efficacy of anti-seizure drugs by acute administration concurrent with PTZ application and by pretreatment prior to exposure with PTZ. Pretreatment permitted us to examine potential neuroprotection and determine whether treatment time affects anti-seizure drugs' responses. As independent validation of anti-seizure drugs' effects, we evaluated whether the anti-seizure drug efficacy in the behavioral assay correlated with neural activity measurements, using electroencephalogram (EEG) and calcium signaling using GCaMP. There was no significant difference in the reduction of PTZ-induced seizure behavior activity between the pretreatment groups and acute treatment groups. Acute treatment with anti-seizure drugs in the EEG and GCaMP assays from 15 to 30 min post-anti-seizure drug exposure revealed consistent results between behavioral, EEG, and GCaMP assays for two of the three anti-seizure drugs. Lamotrigine only reduced neural activity (EEG and GCaMP assays). Carbamazepine, topiramate, and GS967 reduced activity in all three assays. The findings show that EEG and GCaMP assays largely correlate with the behavior findings, helping us connect physiological and behavior responses to anti-seizure drug and better assess anti-seizure drug efficacy.

Keywords: epilepsy, zebrafish, pentylenetetrazol (PTZ), behavior models, anti-seizure drugs

INTRODUCTION

Epilepsy is a disease classified by the recurrent state of seizures due to an imbalance between neuronal inhibition and excitation (Scharfman, 2007). Physicians manage individual patients with epilepsy, often by trying different medications to effectively control their seizures. However, using currently available treatments, at least 30% percent are unable to achieve adequate seizure control (Romanelli et al., 2012). There is a critical need to screen current and novel anti-seizure drugs to more effectively aid those individuals who are treatment refractory.

The zebrafish pentylenetetrazol (PTZ) seizure behavioral model has been employed to test anti-seizure drugs using a variety of methods, producing divergent results across the field because no standard protocol currently exists (Baraban et al., 2005; Gupta et al., 2014; Afrikanova et al., 2013; Kundap et al., 2017). For example, zebrafish adults were used to evaluate anti-seizure drugs on a PTZ treated behavior paradigm (Gupta et al., 2014; Kundap et al., 2017). Also, different concentrations of PTZ treatments using larvae are reported: 15–20 mM (Afrikanova et al., 2013) and 2.5–15 mM (Baraban et al., 2005). There are also various lengths of observation windows, and administration routes of anti-seizure drugs being used. Afrikanova et al. (2013) pretreated 7 days post fertilization (dpf) zebrafish with anti-seizure drugs for 18 h before PTZ was added, and the fish were given 5 min to habituate to a dark chamber before monitoring and quantifying movement for 30 min using a ZebraBox™. Baraban et al. (2005) took 2 min recordings of seven dpf zebrafish in control medium using a CCD camera and locomotion tracking software, comparing this to fish that were placed in 2.5–15 mM PTZ solution for 10 min. Again, 2 min recordings of movements were quantified. They also evaluated seizure type and percentage of fish affected.

The experimental approach was standardized and optimized in our laboratory to evaluate seizure activity in zebrafish, including behavioral, EEG, and GCaMP assays, producing reliable, and comparable results and to test a candidate anti-seizure compound. The zebrafish PTZ model has construct validity by inducing seizures, and it models seizure events in humans providing face validity. Previously tested anti-seizure drugs that work in humans also reduce seizures in the zebrafish PTZ model, indicating potential predictive validity. This study optimized the zebrafish PTZ model of seizure by examining the impact of varied PTZ concentrations and the duration of its effects. We tested carbamazepine, lamotrigine, topiramate, and the candidate anti-seizure compound, GS967 (a persistent sodium channel modulator; Anderson et al., 2014; Baker et al., 2018). Using longer assay time (90 min) and a concentration of 10 mM PTZ allowed for a broader view of anti-seizure drug efficacy. We tested carbamazepine, lamotrigine, topiramate which have been tested in previous PTZ zebrafish assays (Baraban et al., 2005; Gupta et al., 2014; Afrikanova et al., 2013). We also evaluated the candidate anti-seizure compound GS967 in our PTZ model, which has been used in mouse models and shown to be specifically effective for SCN8A (Baker et al., 2018) and SCN2A epilepsy (Anderson et al., 2014). We used our optimized assay to then test two hypotheses: 1) the efficacy of anti-seizure drugs may depend on whether anti-seizure drugs are administered acutely with PTZ or whether with pretreatment of the anti-seizure drugs before PTZ exposure; and 2) the efficacy of anti-seizure drug variability is consistent using different assays, like behavior, EEG, and GCaMP. Pretreatment versus acute application permitted us to examine whether anti-seizure drug/candidate pretreatment protects against PTZ induced seizures or whether only acute administration is needed. The outcomes of our experiments provide a consistent and effective model that will facilitate comparisons of various drugs.

Comparing different anti-seizure drugs using one reliable behavioral assay allowed us to resolve contradictory behavioral assay results in the literature. Observing behavior with the assistance of Viewpoint ZebraBox™ technology allowed for a consistent and high throughput assessment of anti-seizure drug efficacy. EEG readings and GCaMP imaging provided an independent evaluation of seizure activity for the behavioral assay. Using these zebrafish assays, rapid and robust comparison were made between known anti-seizure drugs and a candidate anti-seizure compound.

MATERIALS AND METHODS

Zebrafish Husbandry

The Indiana University Policy on Animal Care and Use guidelines were followed, and all experiments and procedures were approved by the IUPUI School of Science Institutional Animal Care and Use Committee. Zebrafish (*Danio rerio*) AB strain were raised and maintained under standard laboratory conditions (Westerfield, 2007). Fertilized eggs were collected from mating chambers and rinsed with embryo medium (EM). Zebrafish larva and embryos were maintained at 28.5°C, on a 14/10 h light/dark cycle under standard conditions.

Drug Administration

At six dpf, zebrafish were moved to individual wells of a 96-well plate and placed in 300 µL EM. Two different methods were used to administer anti-seizure drugs: pretreatment and acute. The pretreated groups were placed in 150 µl EM along with 150 µl at 2x of the final concentration of the respective anti-seizure drugs 24 h before the behavioral assay was performed. Thus seven dpf was the development stage used for EEG, GCaMP, and behavioral testing. Ten to 12 larvae were used per treatment parameter, and five to eight 96-well plates were used per experiment. All groups were tested together on each plate to control for potential differences in per plate variation. All larvae were raised in the same embryo medium and in the same Petri plate to control for variation in incubation conditions. On day

7, larvae were allowed to habituate for 30 min in the light at room temperature. After pre-incubation, 300 µl of embryo medium or 300 µl of a 2x solution for the acute group was added to obtain a final concentration of 1x for all treatment groups. This method was used for all larvae in all experiments.

Three anti-seizure drugs, carbamazepine (CBZ), lamotrigine (LTG), topiramate (TPR), and one candidate anti-seizure compound, GS967 were tested in our assay. Anti-seizure drugs were tested at several concentrations using previous studies as a guide. The candidate compound, GS967, has not been tested in zebrafish and required more testing at several concentrations (data not shown). Optimal concentrations were reported as follows. CBZ and LTG were both used at a final concentration of 100 µM. TPR was used at a final concentration of 200 µM in line with previous research (Bradford, 1995; Afrikanova et al., 2013; Gupta et al., 2014). As GS967 had not been used previously in zebrafish PTZ behavioral assays, a dose response test was performed, and 0.05 µM GS967 was found to be the most effective concentration at reducing seizure activity without anesthetizing the fish (i.e., high enough to reduce seizures, low enough that the control fish still move). These concentrations remained consistent throughout all assays. The anti-seizure drugs were evaluated based on duration and acute vs pretreatment. Only acute treatment of anti-seizure drugs was used in the EEG and GCaMP Assays.

Movement Tracking System

After adding PTZ, larvae were immediately moved to an automated tracking device, the ZebraBox™ apparatus. The large movement count was then quantified using ZebraLab™ software. Large count activity is defined as the number of movement events over a speed of 8 mm/s. Integration periods were grouped into 15 min intervals. Locomotion was tracked and measured over a total 90 min assay. This longer period of tracking differs from previous studies that used shorter periods. The ZebraBox™ collects data on fish movement, eliminating subjectivity in the observation of seizures to control for experimental bias.

GCaMP Assay

A seven dpf larva was embedded in 1% low-melting-point agarose. The plate containing the embedded larva had 2 ml of EM added to it. The larvae were allowed to habituate in embryo medium for 10 min. Once the initial 10 min of habituation had concluded, a Z-stack image was taken using a confocal microscope using a ×10 objective (Zeiss LSM 700). The maximum projection feature was used to create a single image of the zebrafish larva's baseline synaptic activity in EM. The GCaMP assay treatments were not blinded. An equal volume of 2x solution (DMSO, anti-seizure drug, PTZ or PTZ + anti-seizure drug) was then added to each plate and the larva was given 15 min to incubate in the testing solution. After 15 min a second Z-stack image was taken and once again the 21 slices were used to create a single image *via* maximum projection. All settings remained the same between both Z-stack sessions. The GCaMP assay used ImageJ for objective measurement of fluorescence.

EEG Assay

Each 7 dpf larva was then embedded in 1% low-melting-point agarose. The plate containing the embedded larva had 2 ml of EM added to it. A glass electrode filled with 2 M NaCl was placed into the optic tectum and recordings were performed in current clamp mode, low-pass filtered at 1 kHz, high-pass filtered at 0.1 Hz, digital gain 10, sampling interval 10 µs (EPC10, Heka Electronic). The larvae were allowed to habituate with electrode in place for 10 min. Once the initial 10 min of habituation was complete, a 10 min baseline reading occurred. The EEG treatments were not blinded. An equal volume of 2x solution (DMSO, anti-seizure drug, PTZ or PTZ + anti-seizure drug) was then added to each plate. The recordings started each time exactly 5 min after removal of the larva from proconvulsant solution and were continued for 10 min. Thus, EEG recordings were performed consistently from minutes 20 through 30 following exposure to PTZ. Recordings from eight larvae were taken per experimental condition. Seizure activity was analyzed according to the amount of spiking paroxysmal events or local field potentials (LFP). The EEG assay uses a set level of voltage (2 mV) to standardize the evaluation of potential seizure activity. This threshold is approximately 5 times the noise level and allowed detection of major events in the recordings.

Statistical Analysis

ARRIVE guidelines 2.0 were used in our animal experiments for reproducibility and rigor assurance. Sample sizes of larvae were determined using pilot experiments rather than power analysis to determine numbers needed. This approach was pursued because the ZebraBox™ apparatus has a variable number of wells in the plates that show excessive background. Thus, we have variable numbers of larvae per experiment. All larvae were included that did not show background in the measurements.

Behavior

Locomotor behavior data from replicate tracking run time points were subsequently averaged and analyzed by two-way ANOVA. Tukey's post-hoc comparisons were appropriate. The total large counts of each treatment group within 90 min were compared using one-way ANOVA followed by a Tukey's post hoc test where appropriate (GraphPad Prism software version 8.2). Embryo medium was used as the control group for untreated, dimethyl sulfoxide (DMSO) was used as the vehicle control, and 10 mM PTZ groups were used to represent the untreated epileptic condition.

GCaMP

In order to assess calcium signaling, a line of Tg (elavl3: GCaMP6s) zebrafish were obtained from the zebrafish resource center (zfin.org). The fish were heterozygous for the transgenic gene upon arrival and were backcrossed until a homozygous line was created and kept. We used these homozygous Tg (elavl3:GCaMP6s) zebrafish for our calcium signaling experiments. Fluorescence of the midbrain was

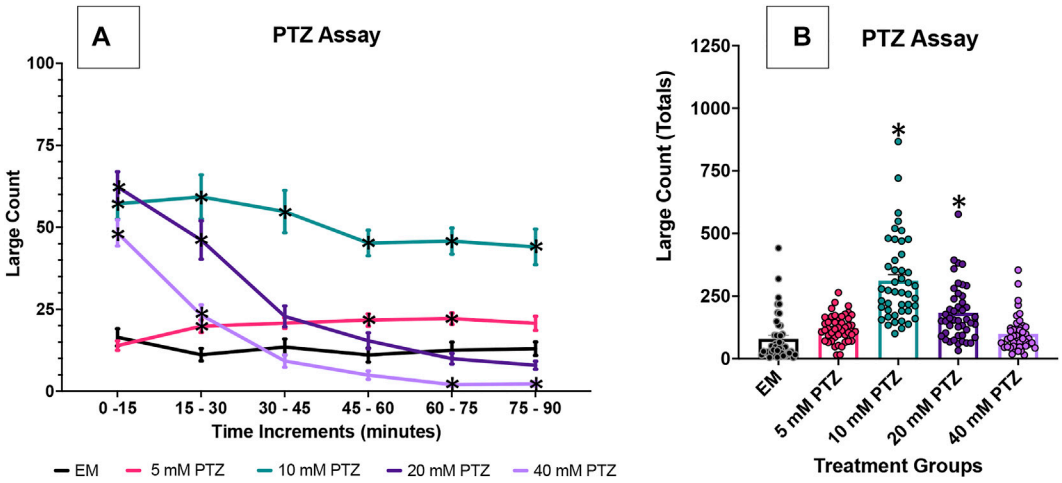

FIGURE 1 | Behavioral profile of zebrafish larvae exposed to PTZ. The following graphs displays the average large count (*y*-axis) of larvae. **(A)** The average larval large count is depicted per 15 min interval (*x*-axis) of the tracking session. Zebrafish larvae were tested PTZ concentrations at 5 mM, 10 mM, 20 mM, and 40 mM (n = 70 fish/solution/concentration). Embryo medium (EM) was used as the control. Significance indicated by *$p < 0.05$ PTZ vs. EM, two-way ANOVA, Tukey's post-hoc. **(B)** The total large count (*y*-axis) over 90 min is displayed. The respective treatment groups (*x*-axis). Analyses (one-way ANOVA, Tukey's post-hoc) are marked * ($p < 0.05$) to indicate significant differences to embryo medium (EM).

measured using ImageJ. The initial image was measured and normalized to 1. The treated image fluorescence was divided by the initial image fluorescence and was recorded as a normalized value compared to the initial embryo medium fluorescence. We followed this procedure for all treatments. Normalizing the fluorescence based on the same fish allowed us to rule out noise based on differences in fluorescence scores between different larvae. The normalized fluorescence scores were grouped by solution and were compared using one-way ANOVA followed by a Tukey's post hoc test (GraphPad Prism software version 8.2). Embryo medium was used as the control group for untreated, dimethyl sulfoxide (DMSO) was used as the vehicle control, embryo medium-15 (EM-15), which was used as the control group for the 15 min time difference in between Z-stacks, and 10 mM PTZ groups were used to represent the untreated epileptic condition.

EEG Assay

We took the total number of spiking paroxysmal events in the initial baseline recording. We then divided the total number of spiking paroxysmal events during baseline for individual larvae by the total number of spiking paroxysmal events during treatment for the same larvae to eliminate variability between different larvae. All spikes of 2 mV or higher were counted and totaled to compare the EEG spikes before and after administration of treatments. The initial baseline paroxysmal events count was normalized to one, which was divided by the paroxysmal events after treatment. Scores were grouped by solution and were compared using one-way ANOVA followed by a Tukey's post hoc test (GraphPad Prism software version 8.2). Embryo medium was used as the control group for untreated, dimethyl sulfoxide (DMSO) was used as the vehicle control, and embryo medium-15 (EM-15), which was used as the control group for the 15 min time difference in between recordings and 10 mM PTZ groups were used to represent the untreated epileptic condition.

RESULTS

Anti-Seizure Drugs Effects on PTZ-Induced Seizure Behavioral Activity of Zebrafish 7 dpf Larvae: Assay Description

We first investigated the effects of several PTZ concentrations on the zebrafish behavior profile over an extended 90 min time duration. Concentrations of 10 mM PTZ, 20 mM PTZ and 40 mM PTZ produced robust seizure activity. With 5 mM PTZ, an increased large count was observed but was inconsistent between replicates. 10 mM PTZ produced seizure activity that was more consistent than other concentrations over the course of the 90 min assay in repeated trials. In contrast, 20 and 40 mM PTZ significantly increased large (>8 mm/s) movement counts at the beginning of the assay (**Figure 1**). However, the seizure-like behavior subsided substantially over the course of the 90 min assay.

Given the consistent increases in seizure activity over 90 min seen in 7 dpf zebrafish larvae exposure, 10 mM PTZ was used as the optimal concentration for the experiments exploring the effectiveness of three distinct anti-seizure drugs and GS967, a candidate anti-seizure compound, on reducing PTZ-induced seizure activity (**Figure 1**; **Supplementary Tables S1-S7**).

Figures 2–5 show the results of the various anti-seizure drugs and anti-seizure compound assays performed over an extended 90 min duration in independent assays. There were

seven treatment groups in each assay. The groups were as follows: embryo medium; 0.1% DMSO: 10 mM PTZ; anti-seizure drug alone (pretreated); anti-seizure drug alone (acute); 10 mM PTZ + anti-seizure drug (pretreated); and 10 mM PTZ + anti-seizure drug (acute). Significance indicated vs. EM by * and vs. PTZ alone by &.

CBZ Effects on Seizure Behavioral Activity in 7 dpf Larvae

In this set of experiments, the effect of 100 μM CBZ was examined on the zebrafish activity. Compared to EM exposed zebrafish, acute exposure to CBZ alone (no PTZ exposure) induced a significant decrease in large movement counts throughout all six time periods (0–90 min). A decrease in activity was observed at four of the six assay time periods: 0–15 min, 30–45 min, 60–75 min, and–90 min. By contrast, the vehicle, DMSO, did not impact zebrafish behavior. Zebrafish exposed to PTZ (10 mM) exhibited a significant increase in large movement counts (compared to EM) across six time periods (0–90 min).

A significant decrease in large movement counts was observed during three time periods (30–45 min, 45–60 min and 60–75 min) when pretreatment with CBZ was followed by PTZ, and during two time periods (30–45 min and 45–60 min) for the acute CBZ group where CBZ and PTZ exposures were compared (**Figure 2A**).

To further compare these data, we summed the large count over the entire 90 min assay for the various treatment groups (**Figure 2B**). The DMSO and CBZ-pretreatment alone groups had similar large count totals compared to EM. Acute CBZ treatment alone decreased total large count movement (**Figure 2B**) compared to EM. PTZ significantly increased large count movement compared to EM. CBZ, both acute and pretreated reduced PTZ induced seizure activity over multiple time periods (**Figure 2A**) and in total large count (**Figure 2B**).

LTG Effects on Seizure Behavioral Activity in 7 dpf Larvae

The effect of 100 μM LTG was examined on the zebrafish activity. Compared to EM exposed zebrafish, DMSO, the vehicle, did not significantly impact zebrafish behavior and neither did the addition of LTG alone regardless of administration method (acute or pretreatment). In this set of experiments, zebrafish exposed to PTZ (10 mM) exhibited a significant increase in large movement counts (compared to EM) across all six time periods (0–90 min). PTZ with acute LTG administration did not significantly reduce seizure activity at any individual time point However, PTZ with larvae pretreated with LTG did experience significantly reduced large movement counts for the last 30 min of the assay compared to PTZ alone. To further compare these data, we summed the large count over the entire 90 min assay for the seven treatment groups shown in **Figure 3B**. The DMSO, LTG-acute alone, and LTG-pretreatment alone groups had similar large count totals compared to EM. PTZ, PTZ + LTG (both acute and pretreated) significantly increased large count movement compared to EM. LTG, both acute and pretreated, did not significantly reduce PTZ induced seizure activity in total large count (**Figure 3B**).

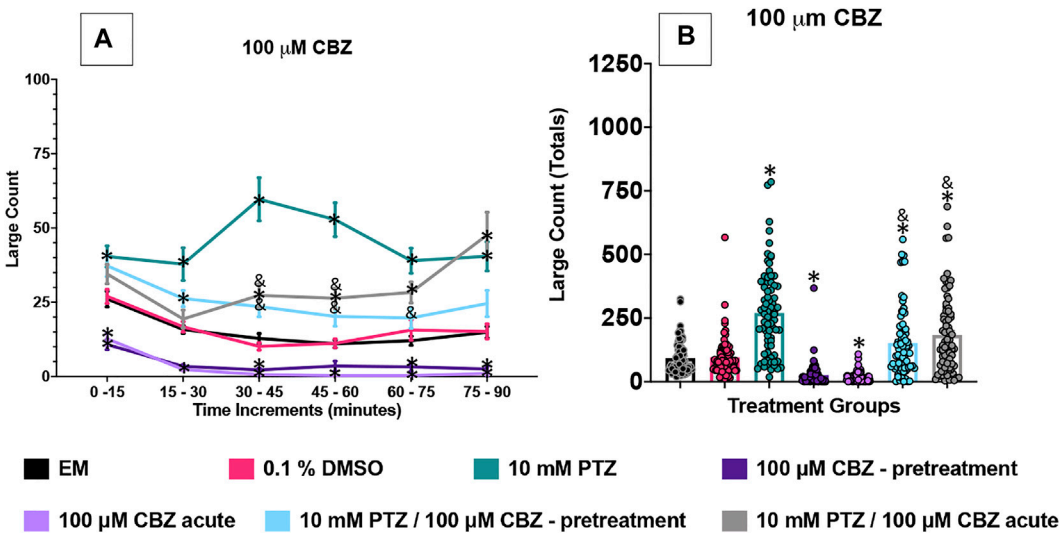

FIGURE 2 | Behavioral profile of zebrafish larvae exposed to carbamazepine **(A)** displays the average large count (*y*-axis) of larvae. The average larval large count is depicted per 15 min interval (*x*-axis) of the tracking session. The respective treatment groups are listed on the *x*-axis. Analyses (two-way ANOVA, Tukey's post-hoc) are marked * ($p < 0.05$) to indicate significant differences to embryo medium (EM). Standard error of the means is shown. Analyses (two-way ANOVA, Tukey's post-hoc) are marked and ($p < 0.05$) to indicate significant differences to 10 mM PTZ. **(B)** The total large count (*y*-axis) over 90 min is displayed. The respective treatment groups (*x*-axis). Analyses (one-way ANOVA, Tukey's post-hoc) are marked * ($p < 0.05$) to indicate significant differences to embryo medium (EM). Standard error of the means is shown. Analyses (one-way ANOVA, Tukey's post-hoc) are marked & ($p < 0.05$) to indicate significant differences to 10 mM PTZ. ($n = 76$ fish/treatment group).

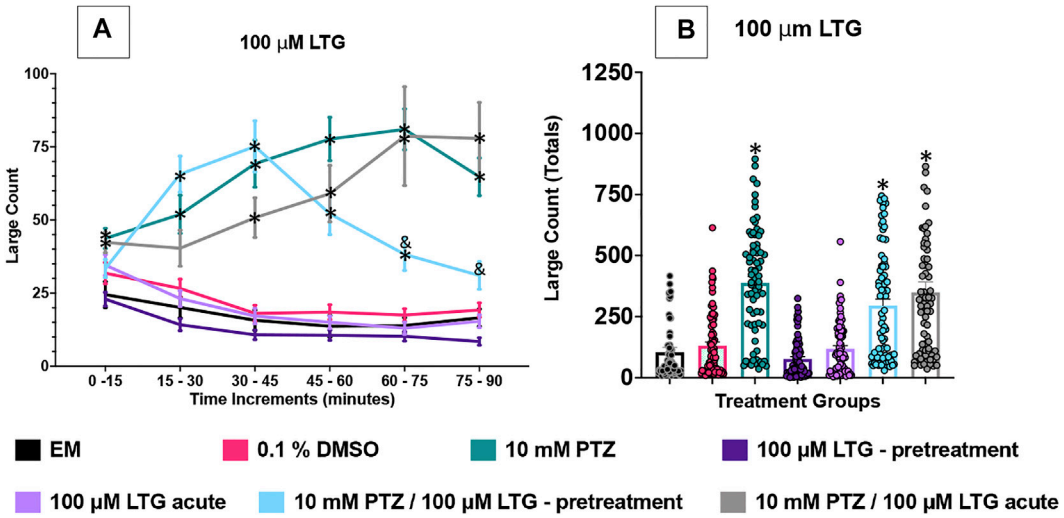

FIGURE 3 | Behavioral profile of zebrafish larvae exposed to lamotrigine. **(A)** The average large count (*y*-axis) of larvae is depicted per 15 min interval (*x*-axis) of the tracking session. The respective treatment groups are listed on the *x*-axis. Analyses (two-way ANOVA, Tukey's post-hoc) are marked * ($p < 0.05$) to indicate significant differences to embryo medium (EM). Standard error of the means is shown. Analyses (two-way ANOVA, Tukey's post-hoc) are marked & ($p < 0.05$) to indicate significant differences to 10 mM PTZ. **(B)** The total large count (*y*-axis) over 90 min is displayed. The respective treatment groups (*x*-axis). Analyses (one-way ANOVA, Tukey's post-hoc) are marked * ($p < 0.05$) to indicate significant differences to embryo medium (EM). Standard error of the means is shown. Analyses (one-way ANOVA, Tukey's post-hoc) are marked & ($p < 0.05$) to indicate significant differences to 10 mM PTZ. ($n = 76$ fish/treatment group).

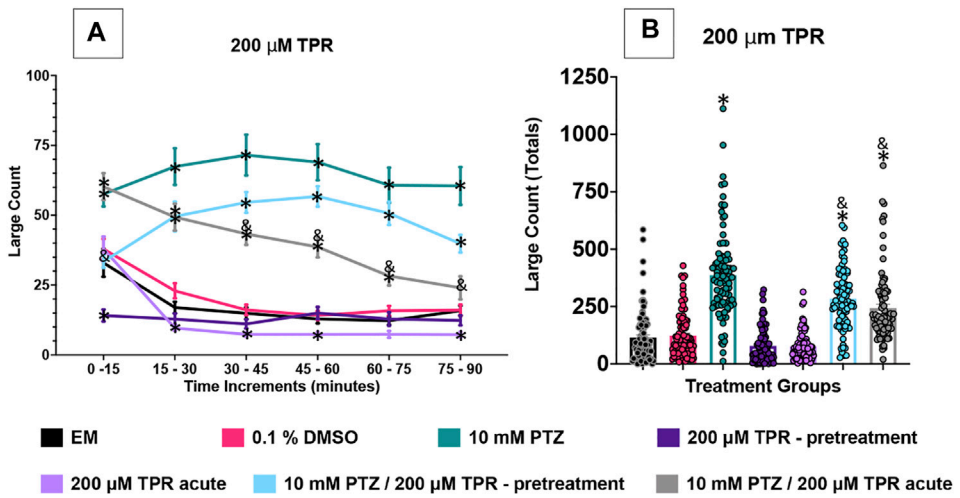

FIGURE 4 | Behavioral profile of zebrafish larvae exposed to topiramate. **(A)** The average large count (*y*-axis) of larvae is depicted per 15 min interval (*x*-axis) of the tracking session. The respective treatment groups (*x*-axis). Analyses (two-way ANOVA, Tukey's post-hoc) are marked * ($p < 0.05$) to indicate significant differences to embryo medium (EM). Standard error of the means is shown. Analyses (two-way ANOVA, Tukey's post-hoc) are marked & ($p < 0.05$) to indicate significant differences to 10 mM PTZ. **(B)** The total large count (*y*-axis) over 90 min is displayed. The respective treatment groups (*x*-axis). Analyses (one-way ANOVA, Tukey's post-hoc) are marked * ($p < 0.05$) to indicate significant differences to embryo medium (EM). Standard error of the means is shown. Analyses (one-way ANOVA, Tukey's post-hoc) are marked & ($p < 0.05$) to indicate significant differences to 10 mM PTZ. ($n = 91$ fish/treatment group).

TPR Effects on Seizure Behavioral Activity in 7 dpf Larvae

The effect of 200 µM TPR was examined on the zebrafish activity. Compared to EM exposed zebrafish, acute exposure to TPR alone induced a significant decrease in large movement counts in four time periods (15–30 min, 30–45 min, 45–60 min, and 75–90 min). With TPR pre-treatment alone, a decrease in large movement counts was observed at two time periods (0–15 min and 15–30 min). DMSO did not impact zebrafish behavior. The zebrafish exposed to PTZ (10 mM) exhibited a significant increase in large movement counts (compared to EM) across all six time periods (0–90 min).

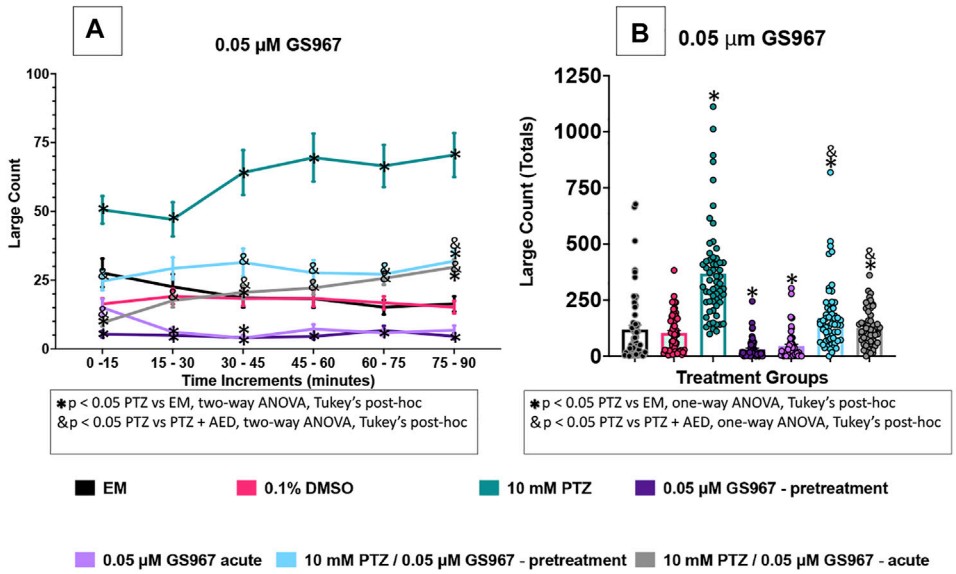

FIGURE 5 | Behavioral profile of zebrafish larvae exposed to GS967. **(A)** The average large count (*y*-axis) of larvae. The average larval large count is depicted per 15 min interval (*x*-axis) of the tracking session. The respective treatment groups (*x*-axis). Analyses (two-way ANOVA, Tukey's post-hoc) are marked * ($p < 0.05$) to indicate significant differences to embryo medium (EM). Standard error of the means is shown. Analyses (two-way ANOVA, Tukey's post-hoc) are marked & ($p < 0.05$) to indicate significant differences to 10 mM PTZ. **(B)** The total large count (*y*-axis) over 90 min is displayed. The respective treatment groups (*x*-axis). Analyses (one-way ANOVA, Tukey's post-hoc) are marked * ($p < 0.05$) to indicate significant differences to embryo medium (EM). Standard error of the means is shown. Analyses (one-way ANOVA, Tukey's post-hoc) are marked & ($p < 0.05$) to indicate significant differences to 10 mM PTZ. ($n = 60$ fish/treatment group).

The large movement counts were summed over the entire 90 min assay for the various TPR treatment groups (**Figure 4B**). The DMSO, and both TPR groups had similar large count totals compared to EM. The total large movement counts for both the TPR pretreatment + PTZ group and the acute TPR + PTZ group were significantly lower than the PTZ group total large counts.

GS967 Effects on Seizure Behavioral Activity in 7 dpf Larvae

In this set of experiments the effect of 0.05 µM GS967 was examined on the zebrafish activity. Compared to EM exposed zebrafish, acute exposure to GS967 alone induced a significant decrease in large movement counts throughout three time periods (15–30 min, 30–45 min, and 60–75 min). With GS967 pre-treatment, a decrease in activity was observed at five of the six time periods (0–60 min, 75–90 min). By contrast, the vehicle, DMSO did not impact zebrafish behavior. Zebrafish exposed to PTZ (10 mM) exhibited a significant increase in large movement counts (compared to EM) across six time periods (0–90 min).

A significant decrease in large movement counts was observed during five time periods (0–15 min, 30–45 min, 60–75 min and 75–90 min) when pretreatment with GS967 was followed by PTZ, and during six time periods (0–90 min) for the acute GS967 group when GS967 and PTZ exposures were compared to PTZ alone (**Figure 5A**).

To further compare these data, we summed the large count over the entire 90 min assay for the various treatment groups (**Figure 5B**). The DMSO group had similar large count totals compared to EM. GS967 treatments decreased total large count movement (**Figure 5B**) compared to EM. PTZ significantly increased large count movement compared to EM and GS967 with PTZ groups. Acute and pretreated GS967 both reduced PTZ induced seizure activity over multiple time periods (**Figure 5A**) and in total large count (**Figure 5B**). Interestingly, GS967 with PTZ groups had similar large count movements to EM.

PTZ and Anti-Seizure Drug Effects on Calcium Signaling Activity in 7 dpf Larvae

Transgenic Tg (elavl3:GCaMP6s) zebrafish have been used to monitor PTZ induced seizures (Turrini et al., 2017). We were able to observe and measure the difference in fluorescence between baseline activity in embryo medium, the increased fluorescence seen once zebrafish were allowed to habituate in a 10 mM PTZ solution, and the difference between PTZ fluorescence and PTZ + anti-seizure drug. The midbrain was chosen as the region of interest to measure so we would be able to pair it with the EEG data in which the probe is placed in the optic tectum, the largest midbrain structure (Baraban et al., 2007). We found that in the behavioral experiments there was not a significant difference between the pretreatment groups and acute treatment groups' ability to reduce PTZ induced seizure activity for each of the anti-seizure drugs tested. Based on this result, we tested only acute treatment of the anti-seizure drug in the EEG and GCaMP assays using the observation window of 15 min post exposure to 30 min post exposure to see if the results matched the results observed in the behavioral assays.

It was observed during this experiment that DMSO, EM-15, and PTZ + GS967 all had similar fluorescence scores

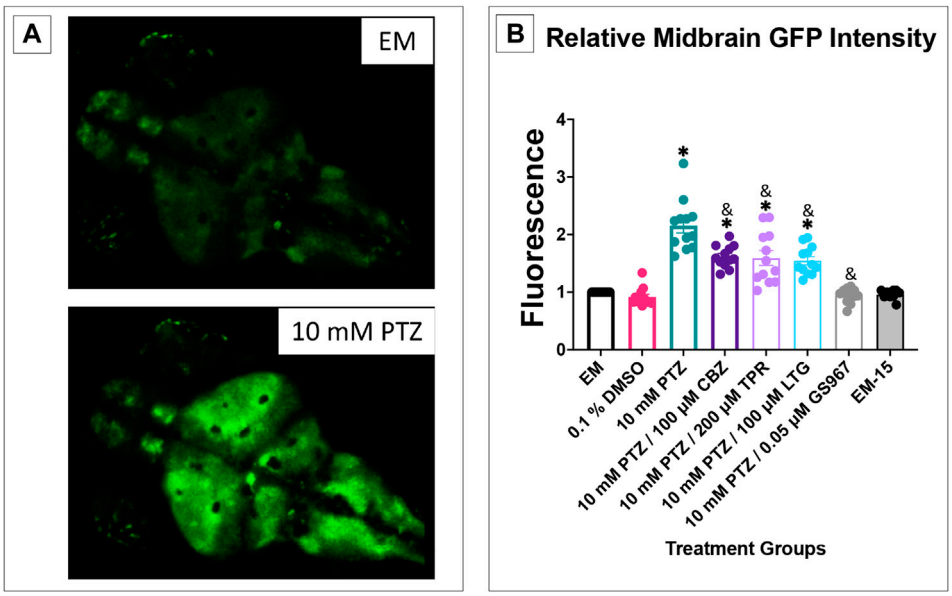

FIGURE 6 | Calcium signaling activity in 7 dpf larvae. The fluorescence score is displayed on the *y*-axis. The respective treatment groups are shown on the *x*-axis. Analyses (one-way ANOVA, Tukey's post-hoc) are marked * ($p < 0.05$) to indicate significant differences to embryo medium (EM). Standard error of the means is shown. Analyses (one-way ANOVA, Tukey's post-hoc) are marked & ($p < 0.05$) to indicate significant differences to 10 mM PTZ. ($n = 12$ fish/treatment group).

compared to EM (**Figure 6**). PTZ had significantly higher fluorescence than EM and all PTZ + anti-seizure drug groups. This result further correlates the ability of the four respective anti-seizure drugs/compound (CBZ, LTG, TPR, and GS967) ability to reduce seizure activity and corroborates the data shown in the behavioral assays.

PTZ and Anti-Seizure Drug Effects on EEG Activity in 7 dpf Larvae

We observed and measured the difference in the number of LFP for baseline activity in embryo medium, once zebrafish were allowed to habituate in a 10 mM PTZ solution, and additionally the difference between PTZ and PTZ + anti-seizure drugs. EEG data was taken from the optic tectum providing consistency with calcium signaling data. Choosing the optic tectum allowed us to target a portion of the brain that could be consistently seen and probed similarly between all groups and larvae, thus, reducing variability between individual zebrafish.

DMSO, EM-15, and all PTZ + anti-seizure drug groups had similar LFP counts compared to EM (**Figure 7**). PTZ had significantly higher LFP than EM and all PTZ + anti-seizure drug groups. This result, in combination with the GCaMP and behavioral assays results, corroborates the reliability of the behavioral model in measuring an anti-seizure drugs effectiveness on reducing seizure activity.

DISCUSSION

Inconsistencies in methods evaluating anti-seizure drugs could make it difficult to determine the relative effects. Our findings evaluated PTZ and anti-seizure effects over a longer time period using a moderate PTZ concentration. Higher PTZ concentrations can produce synaptic fatigue, exhaustion, or death, producing a reduction in swimming behavior in later time increments. This variability could confound comparisons of anti-seizure drugs.

The optimized PTZ assay conditions were used to determine whether three clinically useful anti-seizure drugs and a candidate anti-seizure compound exhibited efficacy against 10 mM PTZ induced seizure like behavior when given acutely with PTZ or pretreated for 24 h with the anti-seizure drug before PTZ exposure. Large movement counts were compared in our assay, but other measures, including small movement counts, large distance travelled, and small distance travelled, also showed effects of the PTZ and anti-seizure compounds. The large movement measure showed the most sensitivity. Anti-seizure drugs were also tested using two distinct assays, EEG and GCaMP, to see if there were discrepancies between the results found in the behavioral assays and those observed in the EEG and/or GCaMP assays. Three of the four anti-seizure drugs/compounds reduced PTZ-induced seizures in all the three assay types. Overall, there was no significant difference between pretreating and acute treatment of anti-seizure drugs in the behavioral models; thus only acute administration was used in the EEG and GCaMP assays. Future experiments could be used to determine whether pretreatment in EEG and GCaMP assays shows any difference with behavior. These assays corroborated the effectiveness of the behavioral assays' ability to determine anti-seizure drug efficacy.

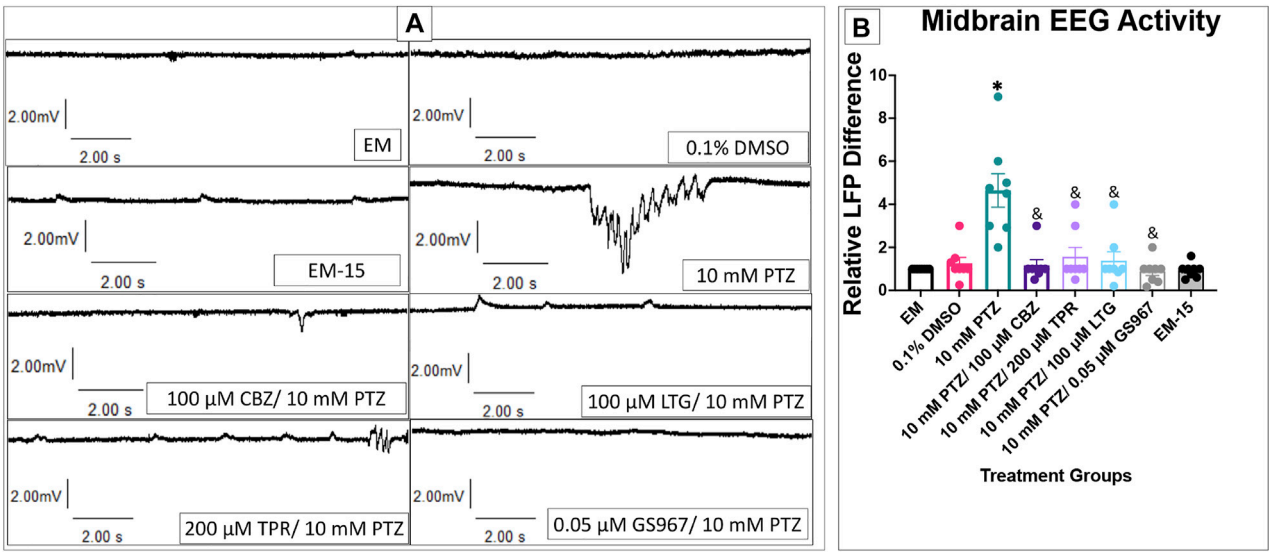

FIGURE 7 | Local field potentials in 7 dpf larvae. **(A)** Representative tracings recorded in the presence of EM (top) and 10 mM PTZ (bottom) are shown. **(B)** The relative LFP difference is displayed on the *y*-axis. The respective treatment groups are shown on the *x*-axis. Analyses (one-way ANOVA, Tukey's post-hoc) are marked * ($p < 0.05$) to indicate significant differences to embryo medium (EM). Standard error of the means is shown. Analyses (one-way ANOVA, Tukey's post-hoc) are marked & ($p < 0.05$) to indicate significant differences to 10 mM PTZ. ($n = 8$ fish/treatment group).

In this study our aim was to use the optimized assay to assess the efficacy of four different anti-seizure drugs/compounds and validate our behavioral assessments using two additional activity measures. CBZ was previously found to be ineffective in reducing seizure behavior and EEG activity in the zebrafish PTZ model (Bariban et al., 2005; Afrikanova et al., 2013), which contrasts with our findings. However, we used a lower concentration of PTZ over a longer time period. Interestingly, Gupta et al. (2014) found that CBZ reduced PTZ induced seizure behavior in adult zebrafish. LTG was previously shown to be ineffective in reducing seizure behavior and EEG activity in the zebrafish PTZ model (Afrikanova et al., 2013). Our behavior results were consistent with these findings, but our EEG and GCaMP studies showed LTG reduced neural activity in the zebrafish PTZ model. TPR was previously shown to be effective in reducing seizure behavior and ineffective in EEG activity in the zebrafish PTZ model (Afrikanova et al., 2013). Our results showed TPR reduced behavior and neural activity in the zebrafish PTZ model. It is worth noting that while LTG did not reduce seizure activity in our behavioral model. LTG and TPR were shown to have an anticonvulsant effect in an adult zebrafish behavioral (Pierog et al., 2021).

A candidate anti-seizure compounds, GS967, that has shown efficacy in preclinical models (Anderson et al., 2014; Baker et al., 2018) showed the greatest attenuation of PTZ induced seizure like behavior, and this compound reduced EEG and GCaMP activity, thus reducing PTZ-induced seizures in all the three assay types. We were able to clearly determine the effectiveness these anti-seizure drugs have on seizures by comparing the drugs over different assays, which helped resolve variation seen in the literature. The behavioral assay allows higher throughput evaluation of candidate compounds, and the EEG and GCAMP assays can validate potential anti-seizure compounds.

DATA AVAILABILITY STATEMENT

The raw data supporting the conclusion of this article will be made available by the authors, without undue reservation.

ETHICS STATEMENT

The animal study was reviewed and approved by The IUPUI School of Science Institutional Animal Care and Use Committee.

AUTHOR CONTRIBUTIONS

Conceived and designed the experiments: PM, JM, and TC Performed the experiments: AZ and PM Analyzed the data: PM Wrote the paper: PM, AZ, TC, and JM Supervised JM and TC.

FUNDING

This work was partially supported by funding from the Cute Syndrome Foundation to JM and TC.

ACKNOWLEDGMENTS

We acknowledge help with animal husbandry from the Marrs Lab and we thank the Marrs and Cummins Laboratory members for helpful discussion.

SUPPLEMENTARY MATERIAL

The Supplementary Material for this article can be found online at: https://www.frontiersin.org/articles/10.3389/fphar.2022.836573/full#supplementary-material

REFERENCES

Afrikanova, T., Serruys, A. S., Buenafe, O. E., Clinckers, R., Smolders, I., de Witte, P. A., et al. (2013). Validation of the Zebrafish Pentylenetetrazol Seizure Model: Locomotor versus Electrographic Responses to Antiepileptic Drugs. *PloS ONE* 8, e54166. doi:10.1371/journal.pone.0054166

Anderson, L. L., Thompson, C. H., Hawkins, N. A., Nath, R. D., Petersohn, A. A., Rajamani, S., et al. (2014). Antiepileptic Activity of Preferential Inhibitors of Persistent Sodium Current. *Epilepsia* 55, 1274–1283. doi:10.1111/epi.12657

Baker, E. M., Thompson, C. H., Hawkins, N. A., Wagnon, J. L., Wengert, E. R., Patel, M. K., et al. (2018). The Novel Sodium Channel Modulator GS-458967 (GS967) Is an Effective Treatment in a Mouse Model of SCN8A Encephalopathy. *Epilepsia* 59, 1166–1176. doi:10.1111/epi.14196

Baraban, S. C., Dinday, M. T., Castro, P. A., Chege, S., Guyenet, S., and Taylor, M. R. (2007). A Large-Scale Mutagenesis Screen to Identify Seizure-Resistant Zebrafish. *Epilepsia* 48, 1151–1157. doi:10.1111/j.1528-1167.2007.01075.x

Baraban, S. C., Taylor, M. R., Castro, P. A., and Baier, H. (2005). Pentylenetetrazole Induced Changes in Zebrafish Behavior, Neural Activity and C-Fos Expression. *Neuroscience* 131, 759–768. doi:10.1016/j.neuroscience.2004.11.031

Bradford, H. F. (1995). Glutamate, GABA and Epilepsy. *Prog. Neurobiol.* 47, 477–511. doi:10.1016/0301-0082(95)00030-5

Gupta, P., Khobragade, S. B., and Shingatgeri, V. M. (2014). Effect of Various Antiepileptic Drugs in Zebrafish PTZ-Seizure Model. *Indian J. Pharm. Sci.* 76, 157–163.

Kundap, U. P., Kumari, Y., Othman, I., and Shaikh, M. F. (2017). Zebrafish as a Model for Epilepsy-Induced Cognitive Dysfunction: A Pharmacological, Biochemical and Behavioral Approach. *Front. Pharmacol.* 8, 515. doi:10.3389/fphar.2017.00515

Pieróg, M., Socała, K., Doboszewska, U., Wyska, E., Guz, L., Szopa, A., et al. (2021). Effects of New Antiseizure Drugs on Seizure Activity and Anxiety-like Behavior in Adult Zebrafish. *Toxicol. Appl. Pharmacol.* 427, 115655. doi:10.1016/j.taap.2021.115655

Romanelli, P., Striano, P., Barbarisi, M., Coppola, G., and Anschel, D. J. (2012). Non-resective Surgery and Radiosurgery for Treatment of Drug-Resistant Epilepsy. *Epilepsy Res.* 99, 193–201. doi:10.1016/j.eplepsyres.2011.12.016

Scharfman, H. E. (2007). The Neurobiology of Epilepsy. *Curr. Neurol. Neurosci. Rep.* 7, 348–354. doi:10.1007/s11910-007-0053-z

Turrini, L., Fornetto, C., Marchetto, G., Müllenbroich, M. C., Tiso, N., Vettori, A., et al. (2017). Optical Mapping of Neuronal Activity during Seizures in Zebrafish. *Sci. Rep.* 7, 3025. doi:10.1038/s41598-017-03087-z

Westerfield, M. (2007). *Zebrafish Book: A Guide for the Laboratory Use of Zebrafish*. Eugene OR: University of Oregon Press.

Conflict of Interest: The authors declare that the research was conducted in the absence of any commercial or financial relationships that could be construed as a potential conflict of interest.

Publisher's Note: All claims expressed in this article are solely those of the authors and do not necessarily represent those of their affiliated organizations, or those of the publisher, the editors and the reviewers. Any product that may be evaluated in this article, or claim that may be made by its manufacturer, is not guaranteed or endorsed by the publisher.

frontiers | Frontiers in Pharmacology

ORIGINAL RESEARCH
published: 25 April 2022
doi: 10.3389/fphar.2022.827686

A Combined Human *in Silico* and CRISPR/Cas9-Mediated *in Vivo* Zebrafish Based Approach to Provide Phenotypic Data for Supporting Early Target Validation

Matthew J. Winter[1†], Yosuke Ono[2†], Jonathan S. Ball[1†], Anna Walentinsson[3], Erik Michaelsson[4], Anna Tochwin[1], Steffen Scholpp[2], Charles R. Tyler[1], Steve Rees[5], Malcolm J Hetheridge[1] and Mohammad Bohlooly-Y[6]**

[1]Biosciences, College of Life and Environmental Sciences, University of Exeter, Exeter, United Kingdom, [2]Living Systems Institute, College of Life and Environmental Sciences, University of Exeter, Exeter, United Kingdom, [3]Translational Science and Experimental Medicine, Research and Early Development, Cardiovascular, Renal and Metabolism, BioPharmaceuticals R&D, AstraZeneca, Gothenburg, Sweden, [4]Early Clinical Development, Research and Early Development, Cardiovascular, Renal and Metabolism, BioPharmaceuticals R&D, AstraZeneca, Gothenburg, Sweden, [5]Discovery Biology, Discovery Sciences, BioPharmaceuticals R&D, AstraZeneca, Cambridge, United Kingdom, [6]Translational Genomics, Discovery Sciences, BioPharmaceuticals R&D, AstraZeneca, Gothenburg, Sweden

The clinical heterogeneity of heart failure has challenged our understanding of the underlying genetic mechanisms of this disease. In this respect, large-scale patient DNA sequencing studies have become an invaluable strategy for identifying potential genetic contributing factors. The complex aetiology of heart failure, however, also means that *in vivo* models are vital to understand the links between genetic perturbations and functional impacts as part of the process for validating potential new drug targets. Traditional approaches (e.g., genetically-modified mice) are optimal for assessing small numbers of genes, but less practical when multiple genes are identified. The zebrafish, in contrast, offers great potential for higher throughput *in vivo* gene functional assessment to aid target prioritisation, by providing more confidence in target relevance and facilitating gene selection for definitive loss of function studies undertaken in mice. Here we used whole-exome sequencing and bioinformatics on human patient data to identify 3 genes (*API5*, *HSPB7*, and *LMO2*) suggestively associated with heart failure that were also predicted to play a broader role in disease aetiology. The role of these genes in cardiovascular system development and function was then further investigated using *in vivo* CRISPR/Cas9-mediated gene mutation analysis in zebrafish. We observed multiple impacts in F0 knockout zebrafish embryos (crispants) following effective somatic mutation, including changes in ventricle size, pericardial oedema, and chamber malformation. In the case of *lmo2*, there was also a significant impact on cardiovascular function as well as an expected reduction in erythropoiesis. The data generated from both the human *in silico* and zebrafish *in vivo* assessments undertaken supports further investigation of the potential roles of *API5*, *HSPB7*, and *LMO2* in human cardiovascular disease. The data presented also supports the use of human *in silico* genetic variant analysis, in combination

OPEN ACCESS

Edited by:
Anna Siebel, Universidade Comunitária da Região de Chapecó, Brazil

Reviewed by:
Sergey Prykhozhij, University of Ottawa, Canada
Vincenzo Di Donato, ZeClinics SL, Spain
Dimitris Beis, Biomedical Research Foundation of the Academy of Athens (BRFAA), Greece

***Correspondence:**
Matthew J. Winter
m.winter@exeter.ac.uk
https://orcid.org/0000-0002-3668-6564
Mohammad Bohlooly-Y
Mohammad.Bohlooly@astrazeneca.com

[†]These authors have contributed equally to this work

Specialty section:
This article was submitted to Experimental Pharmacology and Drug Discovery, a section of the journal Frontiers in Pharmacology

Received: *02 December 2021*
Accepted: *16 February 2022*
Published: *25 April 2022*

Citation:
Winter MJ, Ono Y, Ball JS, Walentinsson A, Michaelsson E, Tochwin A, Scholpp S, Tyler CR, Rees S, Hetheridge MJ and Bohlooly-Y M (2022) A Combined Human in Silico and CRISPR/Cas9-Mediated in Vivo Zebrafish Based Approach to Provide Phenotypic Data for Supporting Early Target Validation. Front. Pharmacol. 13:827686. doi: 10.3389/fphar.2022.827686

with zebrafish crispant phenotyping, as a powerful approach for assessing gene function as part of an integrated multi-level drug target validation strategy.

Keywords: CRISPR/Cas9, zebrafish, heart failure, drug target identification and validation, human whole exome sequencing

INTRODUCTION

Chronic heart failure is characterised by a mismatch between cardiac output and the oxygen demands of organs. Behind the clinical syndrome there is a well-established sequence of pathophysiological events eventually resulting in maladaptive cardiac remodelling, ventricular dilatation and poor cardiac performance manifested as reduced ejection fraction (Konstam et al., 2011). Despite this, at least half of the heart failure population falls outside of the definition of heart failure associated with reduced ejection fraction (HFrEF), and although the aetiology of heart failure in HFrEF patients is largely unknown, a paradigm has been proposed arguing that the root cause is extracardiac (Senni et al., 2014). This multifactorial aetiology makes identifying new drug targets for the treatment of chronic heart failure challenging. Target identification has been greatly aided by the emergence of large-scale patient DNA sequencing approaches (Suwinski et al., 2019; Povysil et al., 2020), although this strategy has its own limitations. Candidate gene progression, for example, is often complicated by identification of multiple potential genes that require subsequent functional characterisation and prioritisation. This is compounded by the fact that higher throughput screening approaches are currently limited to *in silico* or *in vitro* methods that lack the ability to score organ system-dependent gene function. On the other hand, higher-tier genetic target validation assessments in traditional animal models are not practical for screening multiple candidate genes. As an alternative *in vivo* model, the embryo-larval zebrafish could fill this gap. The zebrafish combines genetic tractability, higher throughput amenability, and optical transparency allowing the relatively simple assessment of organ system morphology, and functionality, across multiple candidate genes (Gut et al., 2017). Such studies can, therefore, provide more confidence in target relevance and facilitate gene selection for definitive loss of function studies undertaken in mice. Importantly, the zebrafish is also widely considered to be an appropriate animal model for studying human cardiovascular biology (MacRae and Peterson, 2015). Furthermore, recent studies have demonstrated the great utility of zebrafish in CRISPR/Cas9 mediated screens using F0 knockouts (crispants) as rapid, highly reproducible and scalable knockout models (Burger et al., 2016; Kroll et al., 2021), including for investigating the role of genes in cardiovascular development and functionality (Wu et al., 2018; Quick et al., 2021). Here, we used this approach to investigate the function of 3 genes implicated in human cardiovascular disease from a large-scale patient DNA sequencing study.

Whole exome sequencing (WES) and subsequent bioinformatics were used to identify genes from clinical cohorts that were suggestively associated with heart failure (Povysil et al., 2020). We identified a subset of three genes (*API5*, *HSPB7*, and *LMO2*) predicted to play a broader role in heart failure aetiology, and undertook *in vivo* phenotypic assessment in zebrafish. These specific genes were selected as they were representative of genes that: had broad pleiotropic functions without evidence of preferential cardiac expression (*API5*); showed preferential expression in the heart, but with ambiguous function (*HSPB7*); or were expressed in the haematopoietic compartment and thus had potential impacts on erythrocyte physiology, oxygen delivery and leukocyte biology (*LMO2*). The positive control gene selected was *GATA5*, which has a critical role in heart development and has been implicated in multiple human cardiovascular disease aetiologies (Gu et al., 2012; Wei et al., 2013; Zhang et al., 2015).

Functional knockout of *gata5* resulted in zebrafish larvae exhibiting the expected cardiovascular phenotype, and mutation of each of *api5*, *hspb7*, and *lmo2* resulted in some degree of negative impact on the physiology and/or development of the zebrafish cardiovascular system. The evidence presented supports the use of human *in silico* gene variant analysis in combination with zebrafish crispant assessment as a powerful screening approach for initially assessing gene function as part of early target identification activities. Furthermore, the data generated provides strong *in vivo* evidence to support the further investigation of these genes and their role in human cardiovascular disease.

MATERIALS AND METHODS

Case-Control Collapsing Analysis and Bioinformatics

Candidate genes were initially identified by WES in heart failure patients from two clinical trials: candesartan in Heart Failure-Assessment of Reduction in Mortality and Morbidity (CHARM) (Pfeffer et al., 2003); and Controlled rosuvastatin Multinational Trial in Heart Failure (CORONA) (Kjekshus et al., 2007). 5,942 heart failure cases from these trials were compared to controls without reported heart disease using gene-based rare-variant collapsing analysis, the results of which were published by Povysil et al. (2020). One gene, TTN (encoding Titin), reached study-wide significance, with the strongest association in the dominant protein-truncating variant (PTV) model ($p = 3.35 \times 10^{-13}$), a finding that was replicated in the United Kingdom Biobank WES data (Povysil et al., 2020) and was supported by our subsequent *in silico* analysis. From this, a list of 255 genes that had *p*-values above the study-wide significance threshold, but below 1×10^{-4}, were further explored for data supporting a role in cardiovascular disease using a bioinformatics prioritisation assessment as described below.

The subsequent *in silico* analysis of candidate genes largely relied upon public on-line resources. Each candidate gene was first assessed for genetic association to human disease phenotypes based on large-scale genome-wide association (GWAS) and WES studies encompassing common to low frequency variants (Common Metabolic Diseases Knowledge Portal or CMDKP (https://hugeamp.org/), GWAS Catalog (https://www.ebi.ac.uk/gwas/), Phenoscanner (http://www.phenoscanner.medschl.cam.ac.uk/). Rare variant associations reported in Online Mendelian Inheritance in Man (OMIM, https://www.omim.org/) and ClinVar (www.ncbi.nlm.nih.gov/clinvar/) were also captured.

Next, baseline tissue and cellular expression of candidate genes were investigated based on bulk and single cell RNA sequencing data from human tissues (Human Protein Atlas (HPA), https://www.proteinatlas.org/ and GTex portal, https://gtexportal.org/home/). Studies of expression dysregulation in cardiovascular disease were also conducted using patient transcriptomics data deposited in NCBI Gene Expression Omnibus (GEO, https://www.ncbi.nlm.nih.gov/geo/), using QIAGEN's OmicSoft DiseaseLand (release humandisease_B37_20191215_v14a), which applies generalised linear models on log2 transformed intensities (microarray data), and DESeq2 for raw counts data (RNAseq data). Genes were considered significantly differentially expressed at an adjusted $p < 0.05$. For mechanistic inference assessment, network-based functional enrichment analysis was performed using three separate tools (STRING (https://string-db.org/), Harmonizome (https://maayanlab.cloud/Harmonizome/) and GeneMANIA (https://genemania.org/)), all relying on multiple data types including protein-protein interactions, co-expression, database and text mining. The differential expression analysis of candidate genes was considered particularly important when assessing links to heart failure, as this is a clinical syndrome involving many comorbidities, any of which may be the culprit disease driver. From these *in silico* analyses, we prioritised 3 genes for subsequent *in vivo* assessment in zebrafish. *API5* was selected as a gene possessing broad pleiotropic functions without evidence of preferential cardiac expression; *HSPB7* showed preferential expression in the heart but without clearly defined cardiac functionality; and *LMO2* as it had potential for an indirect role in heart failure through its known role in haematopoiesis.

Guide RNA Design and Preparation

For the zebrafish orthologues of each gene assessed (*gata5*~ENSDARG00000017821; *api5*~ENSDARG00000033597; *hspb7*~ENSDARG00000104441; *lmo2*~ENSDARG00000095019), three individual guide RNAs (gRNAs) were designed using CHOPCHOP (https://chopchop.cbu.uib.no) to target discrete sections of coding exon 1 or 2 (**Supplementary Figure S1**). When selecting gRNAs, we excluded candidate target sites that had potential off-target sites with less than 2 mismatch sequences in the genome, and also confirmed that off-target target sites with 3 mismatch sequences were not located in any exon or UTR region of the protein-coding gene. Selected gRNAs were also BLAST-checked to confirm a lack of off-target gene interaction. Three gRNAs were designed within a 200 bp region, except *api5*, to promote PCR amplification of the region using a single primer set during subsequent molecular analyses. For *api5*, two gRNAs were designed at exon 1 and one gRNA at exon 2, as we were not able to design three gRNAs within a single coding exon. Each gRNA was applied alone (termed g#1, g#2 or g#3) to assess the consistency of phenotypes across different target sites, and as a combined injection containing all three gRNAs (termed g#1,2,3) to ensure functionally-effective mutation, alongside Cas9-only injection controls. Cas9 protein was considered likely to be the most biologically active component of the experimental injection mixture and, therefore, the most appropriate injection control for use when assessing multiple candidate genes as part of a higher throughput screening protocol. Although alternative gRNAs could have been used as additional controls, this was not considered necessary as we had already demonstrated phenotype variability across the genes and gRNA designs used (see results section). A comparison of the data from the different controls tested during method development is presented in **Supplementary Figure S2**.

Prior to injection, gene-specific crRNA and tracrRNA (Integrated DNA Technologies Inc. Coralville, United States) were diluted to a final concentration of 12 μM in nuclease-free duplex buffer and the resultant gRNA mixture incubated at 95°C for 5 min. Immediately prior to use, 5 μl of the gRNA mixture was mixed with Cas9-NLS protein (final concentration of 5 μM. New England Biolabs, Ipswich, United States), 2M KCl (final concentration of 300 mM), and 0.5% v/v Phenol red solution (Sigma Aldrich Ltd. Poole, United Kingdom) in a total volume of 10 μl. The resultant mixture was incubated at 37°C for 10 min to assemble the gRNA/Cas9 ribonucleoprotein complex, and then held at room temperature until use.

Zebrafish Culture

Adult WIK (Wild-type India Kolkata) strain zebrafish (*Danio rerio*), originally obtained from the Zebrafish International Resource Center (ZIRC, University of Oregon, Eugene, United States), were held under optimal spawning conditions (12 h light: 12 h dark cycle, with 20 min dusk-dawn transition periods, 28 ± 1°C), in mixed sex groups in flow through aquaria. Each injection day embryos were collected from individual male-female pairs and injected at the one-cell stage. In addition, the *cmlc2::DsRed2-nuc* transgenic zebrafish (Mably et al., 2003) used for confocal cardiomyocyte microscopic analysis were cultured under identical conditions.

Microinjection

Microinjection needles were prepared from thin wall borosilicate glass capillaries with filament (Outer diameter 1.0 mm, inner diameter 0.75 mm. World Precision Instruments, Sarasota, United States) on a micropipette puller (P-1000, Sutter Instruments, Novato, United States) using the following settings: Heat 501, Pull 60, Velocity 60, Time 20, Pressure 300, Ramp 499.

From pairs of spawning zebrafish, eggs were assessed for the desired development stage (1-cell) and for condition before being transferred in batches of 50–60 into the furrows of an injection mould-imprinted agar plate. Next, the injection needle was loaded with the injection mixture calibrated using a microscale

graticule to deliver 1–1.7 nl per injection and each egg was injected (FemtoJet 4x, Eppendorf, Hamburg, Germany), once, close to the cell/yolk boundary layer. Successful injection was indicated by the presence of phenol red. Injected eggs were then transferred to a Petri dish containing culture water and methylene blue (2 drops per litre of water) and cultured on a black background under the same conditions as the adult fish. At the end of day 0, all unfertilised and dead embryos were removed and 48 viable embryos, selected at random for each treatment, were individually transferred to wells of 48-well microplates (each in 1 ml) for later assessment.

Morphological Assessment at 2 and 4 dpf

At 2 days post fertilization (dpf), the general morphological phenotype of all embryos across all three individual and a combined gRNA injected group (named g#1, g#2, g#3 and g#1,2,3 respectively) was assessed. This was undertaken to identify the most effective guides (i.e., those resulting in the most prominent phenotype vs. the Cas9-only injected controls) for complete morphological and functional phenotyping at 4 dpf. Scoring was undertaken (without anaesthesia) using a dissecting microscope against a list of criteria shown in **Supplementary Table S1**. In addition, 8 embryos were removed from each treatment for the analysis of gene mutation efficiency (**see below**).

At 3 dpf, if necessary, embryos were manually dechorionated using fine forceps allowing the spine to straighten to facilitate complete phenotyping at 4 dpf. At 4 dpf, 10 animals were selected at random from the 2 most effective treatments groups, alongside 10 embryos from the Cas9-only injected control group for full morphological scoring using a method based upon Gustafson et al. (2012), and Ball et al. (2014). To facilitate scoring, animals were lightly anaesthetised by immersion in 0.165 g/L tricaine methanesulfonate (pH 7.5) and scored according to the criteria shown in **Supplementary Table S2**. Images were taken from representative animals within each treatment group. In addition to scoring the frequency of abnormalities, an estimate of the size of the pericardial oedema was made from each image saved. For this, the shortest distance was measured between the ventricle outer wall and the pericardial sac edge using Leica Application Suite (LAS) X core and LAS X measurements® (Leica Microsystems Ltd, Milton Keynes, United Kingdom). Note that in some cases it was not possible to obtain a clear anterior-posterior image of the larva and thus accurate measurement was not possible.

After assessment, each animal was directly transferred to benzocaine solution (1 g/L in 1% ethanol) for euthanasia. The guide-injected group providing the most robust phenotype was also selected for a second run to confirm the observed effect in a separate batch of embryos.

Analysis of Mutation Efficiency

Genomic DNA was extracted from individual 2 dpf larvae using the HotSHOT method (Meeker et al., 2007). Briefly, all water was removed from each PCR tube containing an embryo, 50 µl of 50 mM NaOH added, and the sample heated for 10 min at 95°C. The samples were then vigorously vortexed and subsequently cooled on ice. Next 5 µl of 1M Tris-HCl (pH 8.0) was added and the samples were well mixed. The samples were then centrifuged and the supernatant containing the genomic DNA was removed and stored at −20°C until further processing. The PCR primers were designed and obtained from Eurofins Genomics (Ebersberg, Germany). The primers used were: *gata5* (forward: GGAAAC CATCGCATTTGGAG and reverse: AGGGCACTTCCATAT TGATC); *api5* (exon 1 forward: ATACAGCGGAAGTATCCG AC, exon 1 reverse: TCAATTCTCGCTCAGGCTTG. exon 2 forward: TCTGGATGGTGTCAAAGGAG, and exon 2 reverse: CGGACAACATGTAAATACCAG); *hspb7* (forward: GAATAA GAACTTGATCACCGG and reverse: GCATATAGCTTTCCA CTCAC); and *lmo2* (Forward: TGGATGAGGTGCTCCAGATG and reverse: ATCTCTCCTGCACAGCTTTC). The PCR mixture was prepared as follows: 10 µl of 2x PCRBIO Taq Mix Red (PCR Biosystems Ltd, London, United Kingdom); 0.8 µl each of 10 µM forward and reverse primers; 1 µl of genomic DNA; and 7.4 µl of water. The PCR machine settings were as follows: 1 min at 95°C; 30 cycles of 15 s at 95°C, 15 s at 58°C, 15 s at 72°C; and finally 1 min at 72°C. DNA amplification was checked on a 3% agar gel. T7 endonuclease I (T7E1) assays were undertaken to detect heteroduplexes in the PCR product. For this, PCR products were denatured at 95°C for 5 min and then cooled down. Next, the T7E1 reaction mixture was made as follows: 10 µl of each PCR product; 1.5 µl NEBuffer 2 (New England Biolabs, Ipswich, United States); 0.3 µl T7E1 enzyme at 10 Units/µl (New England Biolabs, Ipswich, United States); and 3.2 µl water. Next digestion was undertaken for 15 min at 37°C and the resultant products were assessed on a 3% agar gel. A sub-sample of amplified DNA from each PCR product was also sent for Sanger sequencing by Eurofins Genomics (Ebersberg, Germany) using the forward or reverse primers described previously. The rates and types of insertions and deletions (indels) in the PCR products were analysed by Inference of CRISPR Edits (ICE; https://ice.synthego.com).

Histology

For histological analysis, 4 dpf animals were terminated by anaesthetic overdose in fixation tubes (2 g/L tricaine methanesulfonate, pH 7.5). Next the anaesthetic was replaced with 10% neutral buffered formalin for 4 h, followed by 70% alcohol in which they were stored at 4°C until further processing. For sectioning, animals were transferred into agar moulds for orientation (Sabaliauskas et al., 2006; Copper et al., 2018), and subsequently into tissue cassettes and embedded in paraffin using an automatic tissue processor (Thermo Scientific Excelsior AS, Thermo Fisher Scientific Ltd, Waltham, United States). The sequence of fixation and embedding steps applied are summarised in **Supplementary Table S3**. Following fixation, 5 µm sections were cut from each paraffin block using a microtome (Shandon AS325, ThermoFisher Scientific Ltd., Waltham, United States). The resultant sections were haemoxylin and eosin (H&E) stained on an automatic stainer (Shandon Varistain 24–4, ThermoFisher Scientific Ltd., Waltham, United States) using the sequence summarised in **Supplementary Table S4**. After staining, images of each section were captured on a binocular microscope (Axioskop

40, Zeiss, Oberkochen, Germany) equipped with a colour digital camera (DP70, Olympus, Tokyo, Japan) to allow histopathological analysis.

Cardiovascular Functional Assessment at 4 dpf

Cardiovascular function was assessed in ten 4 dpf embryos selected at random from each treatment, using the method outlined in Parker et al. (2014). Briefly, each animal was lightly anaesthetised by immersion in tricaine methanesulfonate (0.1 g/L pH 7.5) and then transferred into low melting point agarose (1 g/100 ml of the same tricaine methanesulfonate solution to maintain anaesthesia during imaging) and then deposited on its side on a clear microscope slide. Imaging was undertaken on an inverted light microscope (Leica DM IRB, Leica Microsystems United Kingdom Ltd, Milton Keynes, United Kingdom, ×10 magnification) equipped with two video cameras: one recording the heart at 25 frames per second (fps. Grasshopper® GRAS-50S5C-C, Point Grey, Richmond, Canada); and the second recording the dorsal aorta at 120 fps (Grasshopper® GRAS-03K2M-C, Point Grey, Richmond, Canada). Recording was undertaken for 10 min following which animals were directly transferred to benzocaine solution (1 g/L in 1% ethanol) for euthanasia without recovery.

Heart videos were analysed using MicroZebraLab™ (v3.5, ViewPoint, Lyon, France) from which beat frequencies were provided for each of the atrium (atrial beat rate or ABR) and the ventricle (ventricular beat rate or VBR). This allowed global heart rate measurement and the detection of certain arrhythmias such as the decoupling of atrial and ventricular beat frequencies, which has been previously described in association with exposure to some QT-prolonging drugs. Blood flow videos were analysed using ZebraBlood™ (v1.3.2, ViewPoint, Lyon, France), which provided measures of blood flow (nL/sec), blood linear velocity (μm/sec) and vessel diameter (μm). In addition to the directly determined parameters, estimates of stroke volume and cardiac output were calculated using measurements of heart rate and blood flow (termed surrogate stroke volume (SSV) and surrogate cardiac output (SCO)). Normally stroke volume is precisely calculated using the difference between end-systolic and end-diastolic volumes (see below). However, using our system a surrogate measure of SSV was calculated by dividing the dorsal aorta flow rate (in nL/sec), by the VBR per second. Similarly, cardiac output is normally calculated by dividing the stroke volume by the heart rate to provide a volume of blood pumped per minute. Here, however, SCO was calculated by multiplying the SSV by the VBR in bpm.

Ventricular Dimension-Related Parameter Measurements

Using the videos of the heart captured for functional analyses, 10 animals were randomly selected per treatment (5 per run) from which a manual measurement of ventricle diameters was undertaken. Using VirtualDub (http://www.virtualdub.org/), heart videos were converted to JPEGs from which 10 images showing the minimum (end-systolic) and 10 showing the maximum (end-diastolic) ventricle chamber extension were selected at random from each animal. On each image, the long and short axis ventricle chamber lengths were measured using ImageJ (https://imagej.net/). Next, using the Equation 1/6*π*long axis*short axis^2 and assuming a prolate spheroidal shape (Yalcin et al., 2017), end-systolic and end-diastolic ventricle volumes were calculated (in nL). From these measurements, stroke volume (end-diastolic minus end-systolic volumes, in nL), cardiac output (stroke volume*ventricular beat rate, in nL/min), and ejection fraction (stroke volume/end-diastolic volume*100, as a %) were calculated to supplement the surrogate measures of cardiac performance described previously. Although of much slower throughput, manual measurement of ventricular diameters is particularly useful where the absence of measurable blood flow means that SSV and SCO values are effectively zero. It should be noted, however, that as 2D images were derived from videos that were used for the functional analysis, in some cases precise determination of chamber edges was difficult and as such the actual dimensions should be considered approximations. In addition, it was not possible to normalise these measurements to the length of the specific animals used for functional assessment. However, ventricle measurements have been considered within the context of the average total body length of embryos within the same batch of animals used for the morphological evaluation.

Confocal Analysis of Cardiomyocyte Development and Morphology

To assess the impact of gene mutation on cardiomyocyte hyperplasia or hypertrophy, additional injections were undertaken in 4 dpf *cmlc2::DsRed2-nuc* transgenic zebrafish. For each gene and for Cas9-only injected animals, 10 randomly selected animals were assessed on a Nikon A1R laser scanning confocal microscope (Nikon, Tokyo, Japan) using 568 nm laser excitation (power 90, PMT 85) and transmitted light (PMT 25). At 20x magnification, Z-slices were taken every 5 μm through the heart from which maximum intensity z-projections were then generated. For imaging, the embryo's hearts were stopped by immersion in 1 g/L tricaine methanesulfonate (pH 7.5) after which they were transferred to 1 g/100 ml low melting point agarose made using the same tricaine methanesulfonate solution for immobilization during imaging. As before, after imaging larvae were directly transferred to a solution of benzocaine (1 g/L in 1% ethanol) for euthanasia without recovery. Each maximum intensity projection was imported into ImageJ, and the brightness was adjusted to aid visualization of cardiomyocyte nuclei. From these images, cardiomyocyte number was estimated in the ventricle of each animal using a manual cell counter.

Data Analysis

All measured parameters were averaged per animal to provide a series of individual values from which the treatment mean and standard error of the mean (SEM) were calculated. For statistical

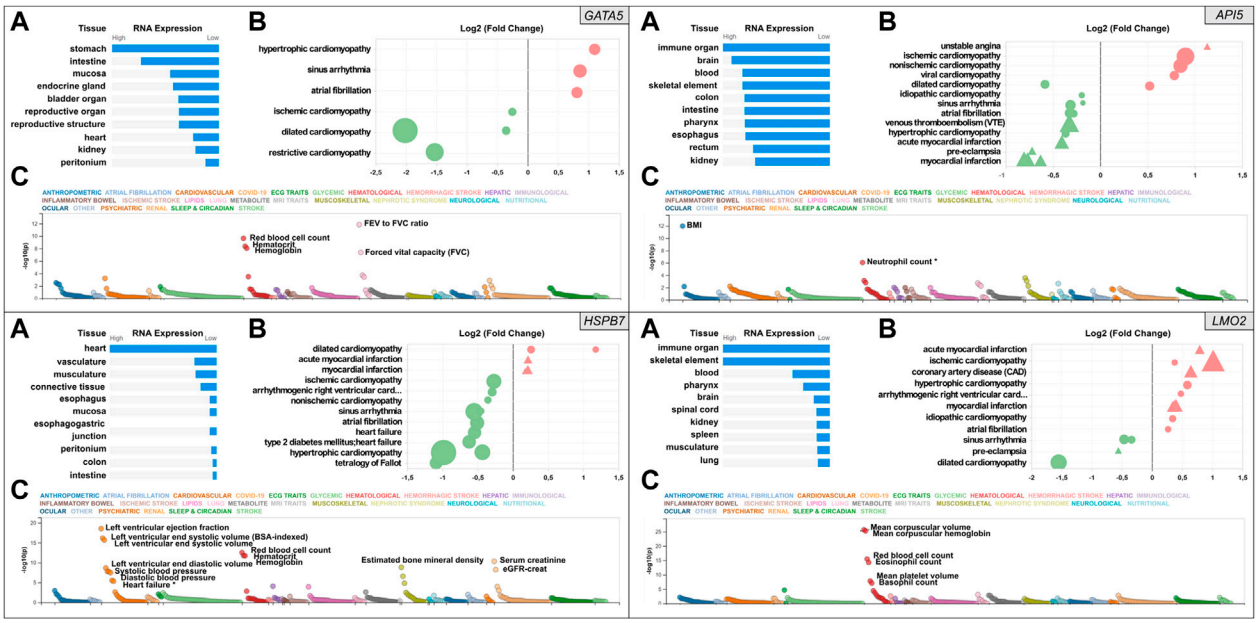

FIGURE 1 | Snapshot of the results from the *in silico* assessment of the heart failure candidate genes *API5* (top right), *HSPB7* (bottom left), *LMO2* (bottom right), and positive control gene *GATA5* (top left panel). **(A)**. The top 10 tissues showing expression based on RNA sequencing data from the Human Protein Atlas (HPA) and EMBL-EBI Expression Atlas as summarized by Open Targets Platform (https://www.targetvalidation.org). **(B)**. Gene expression changes in cardiovascular disease conditions based on publicly available transcriptome studies from NCBI Gene Expression Omnibus (GEO). Disease conditions are shown on the *Y*-axis and log2 fold changes (vs. normal controls) on the *X*-axis. Icons are coloured by direction of change; red and green represent up- and downregulation in that disease, respectively. Icon shapes represent tissue type subjected to transcriptomics; circles and triangles represent heart and blood, respectively. Finally, icon size reflects statistical significance; the larger the icon the lower the *p*-value. All findings shown are significant (Adjusted *p*-value<0.05). **(C)**. Common variant gene locus association data from 190 datasets and 251 traits in Common Metabolic Diseases Knowledge Portal (CMDKP). Traits considered genome-wide significant (p-value $\leq 5 \times 10^{-8}$) are highlighted (border-line significant traits are marked with *).

analysis, each group was first tested for normality (Anderson-Darling Test) and homogeneity of variance (Levene's, Bartlett's, or F-test). Each treatment was then compared with the Cas9-injected control group using either the Student's T-tests or 1-way ANOVA and Tukey's HSD tests (parametric), or the Mann Whitney U-tests or Kruskal Wallis and Dunn's Tests (non-parametric). All analyses were undertaken using Minitab™. Throughout data are shown as the mean, ± SEM (n), with a minimum α level of 0.05 applied (with a Bonferroni correction in the case of multiple comparisons).

RESULTS

From WES and subsequent bioinformatics, three genes were identified as suggestively associated with heart failure and were considered representative of groups of genes predicted to play a broader role in heart failure aetiology (Povysil et al., 2020). These genes were then subjected to *in vivo* phenotypic assessment in zebrafish alongside the positive control gene *gata5*, in order to further investigate their role in vertebrate cardiovascular development and function.

In Silico Analysis of Clinical Data

Key results of the *in silico* analysis are summarised in **Figure 1**. Additional data are contained within **Supplementary Figures S3, S4** and **Supplementary Data S1–S4**, and literature-derived information summarised in **Supplementary Table S5**.

Relative human tissue mRNA expression levels of the positive control gene *GATA5*, and the three candidate genes *API5*, *HSPB7* and *LMO2* are shown in **Figure 1** under normal (**Panel A** in each case) and cardiovascular disease conditions (**Panel B** in each case), alongside analysis of common variant gene-level associations (**Panel C** in each case). As expected, heart *GATA5* mRNA expression was significantly altered in association with various cardiovascular disease states the most significant being downregulated expression in association with dilated cardiomyopathy. The most pronounced changes in cardiac and blood *API5* expression included downregulated expression in association with myocardial infarction, and upregulated heart *API5* expression in association with ischemic and non-ischemic cardiomyopathies. Heart *HSPB7* expression was largely downregulated in association with various cardiac disease conditions, except for dilated cardiomyopathy in which *HSPB7* was found to be upregulated in two independent studies. *LMO2* blood mRNA expression predominantly showed upregulation, including in association with ischemic cardiomyopathy, coronary artery disease and myocardial infarction. In contrast, cardiac *LMO2* mRNA expression showed multiple increases and decreases across the same range of disease states, for example expression was increased in association with

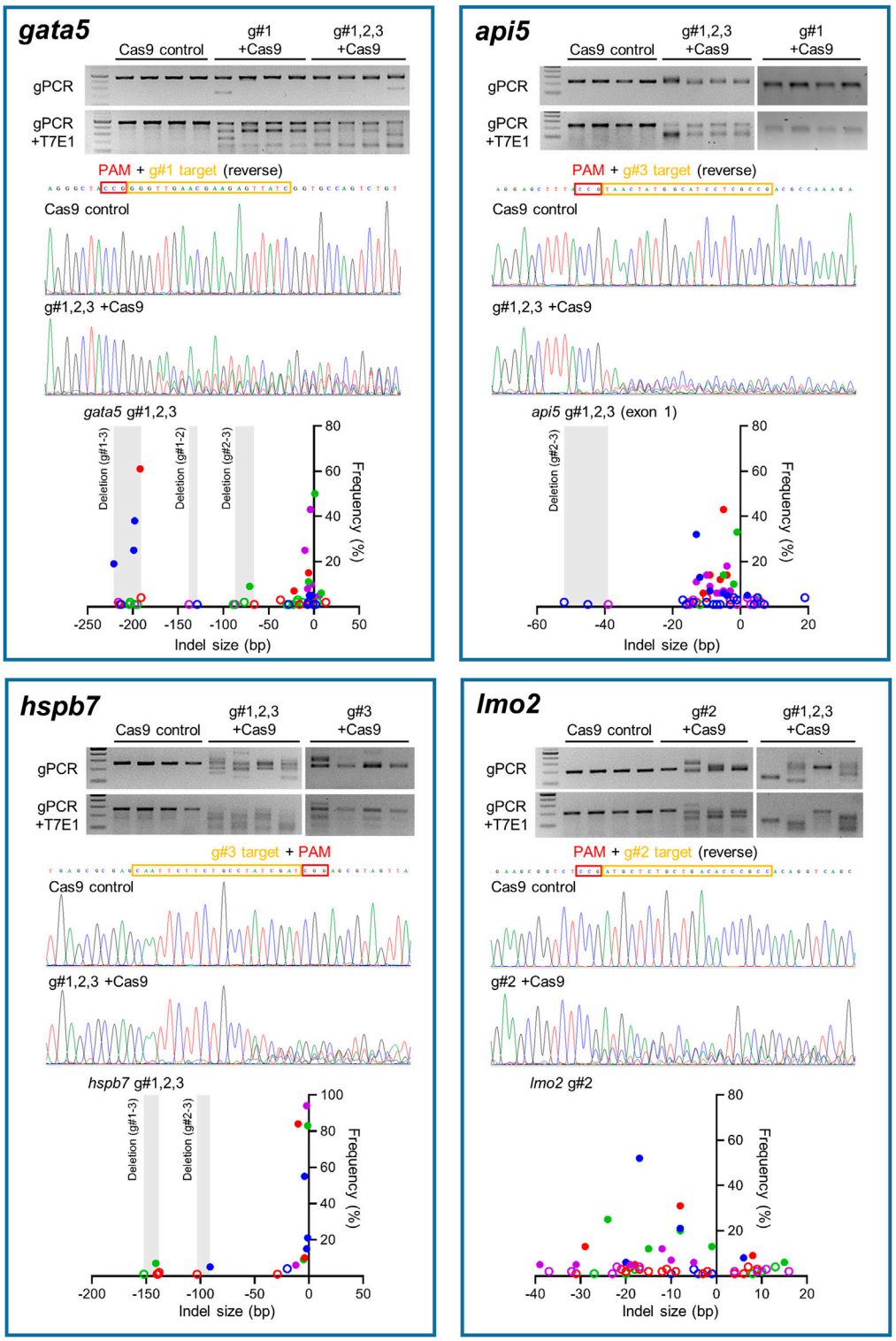

FIGURE 2 | Mutation efficiency of the gRNAs for each candidate gene. Data for *gata5* are shown in top left panel, *api5* in top right panel, *hspb7* in bottom left panel, and *lmo2* in bottom right panel. In each panel, the upper gel images show the bands obtained following targeted PCR of genomic DNA extracted from four individual animals injected with the two most effective CRISPR gRNAs + Cas9 (based on 2 dpf morphological analysis), compared with the Cas9 injected control animals. The lower gel images show the same samples following T7E1 assay undertaken to reveal the cleavage of heteroduplex DNA. The chromatogram images in the middle of each panel show the result of Sanger sequencing undertaken on representative genomic DNA samples from the most effective gRNA + Cas9, per gene, compared with that from a representative Cas9-injected control animal. The lower scatter plot graphs in each panel show the indel size and frequency in the PCR products from most

(*Continued*)

FIGURE 2 | effective gRNA + Cas9 group (n = 4) per gene. Data points with same colour indicate the indels identified in the same individual embryo within the group. The size ranges of deletions between gRNA target sites are shaded. Indels with less than 5% frequency are presented by open circles. Note in all cases the most effective gRNA was the combined guide group (g#1,2,3) except for *lmo2* which, due to high mortality in the g#1,2,3 group, the g#2-injected animals were selected for full analysis.

hypertrophic cardiomyopathy but decreased in association with dilated cardiomyopathy. Analysis of common variant gene-level associations (**Figure 1**, **Panel C** for each gene) revealed that *GATA5* was significantly associated with various lung functions and haematological traits. Despite this, no significant common variant associations with heart disease were found, although rare loss-of-function mutations in *GATA5* have been reported to cause congenital heart defects (Jiang et al., 2013). Assessment of *API5* revealed a significant association with body mass index (BMI) and a borderline significant association with neutrophil count (p-value = 9×10^{-7}). Among the cardiovascular traits assessed, low frequency 3′UTR or intron *API5* genetic variants showed a significant association with "Cause of death: atrial fibrillation and flutter" ($p = 6.4^{-22}$), and "Cause of death: acute and subacute infective endocarditis" ($p = 6.7^{-13}$). *HSPB7* common variant data showed a significant association with cardiovascular, renal, haematological and musculoskeletal traits with the most significant association to cardiac function including left ventricular ejection fraction, and left ventricular end-systolic volume. Other GWAS data revealed significant associations between common variants in *HSPB7* intron 3′ and 5′UTR and idiopathic dilated and sporadic cardiomyopathy ($p = 5.3^{-13}$ and $p = 1.4^{-9}$ respectively), as well as with systolic blood pressure ($p = 7^{-12}$). Finally, analysis of the *LMO2* data revealed significant associations with various haematological traits including mean corpuscular volume, haemoglobin and red blood cell count. The most significant cardiovascular trait association was only suggestive (P-wave duration at $p = 2.1^{-5)}$. Further analysis did, however, reveal that *LMO2* intron variants were significantly associated with "Cause of death: cardiomegaly" ($p = 3.0^{-9}$) and "Cause of death: dilated cardiomyopathy" ($p = 1.3^{-8}$).

In Vivo Gene Mutation Efficiency

Site-specific mutagenesis in zebrafish embryos was evaluated using the T7E1 assay for rapid assessment, reinforced with sequencing of genomic PCR products amplifying the region that gRNAs target for confirmation (**Figure 2**). Initially the T7E1 assay was assessed for consistency across all gRNAs designed to target *gata5* (**Supplementary Figure S5**). The data from this initial assessment suggested the method was suitable for rapidly detecting effective mutation across all gRNAs plus Cas9, but not in the Cas9 injected controls. This supported its application to indicate effective mutagenesis using analysis of the g#1,2,3 + Cas9 group only for the other genes assessed.

There was clear cleavage of PCR products by T7E1 in the presence of Cas9 and gRNAs, and sequencing confirmed that effective site-specific gene mutation was achieved for all genes, but not in the case of the Cas9-only injected controls. The efficiency of site-specific mutagenesis was estimated further by ICE analysis. For *gata5*, the average overall indel rates in the injected embryos using individual gRNAs ranged between 68 and 77% (**Supplementary Figure S5**, n = 4 per group), and the efficiency was 100% in g#1,2,3 + Cas9 injected animals. In the combined gRNA group, a large deletion between gRNA target sites (g#1 and g#3) in the genome was identified as well as small indels (**Figure 2**). Average overall indel rates in the *api5*, *hspb7* and *lmo2* crispants were 92.8, 100, and 86.3%, respectively, demonstrating highly efficient mutagenesis across the four genes assessed.

Morphology and Function of Crispants

At 2 dpf, the most robust *gata5* crispant phenotypes occurred after injection of g#1,2,3, followed by injection of g#1 alone (**Supplementary Figure S6**). By 4 dpf (**Figure 3**), all *gata5* crispants showed elevated pericardial oedema (in terms of frequency and size), and there were high incidences of misshapen and small heart chambers (e.g., 85% of the combined gRNA group) together with a frequent lack of chamber definition (e.g., 40% of the combined gRNA group). In addition, both groups of *gata5* crispants exhibited a range of non-cardiac developmental abnormalities (**Figure 3**) that included an increased incidence of poorly defined somites, malformed fins, small and malformed eyes, reduced neural tube size, a lack of definition of the fore-midbrain boundary and reduced size of the olfactory region. In addition, the g#1,2,3 group exhibited a comparatively high incidence of malformed brachial arches and deficient or absent jaw structures. Histological analysis of the heart (**Figure 4A** and **Supplementary Figure S7**) revealed that *gata5* crispants generally exhibited cardiac hypoplasia, chamber malformation, an absence of visible heart valves and pericardial distension. This abnormal cardiac phenotype was further supported after the analysis of ventricle dimensional parameters (**Figure 4B**), which revealed significantly smaller end-diastolic and end-systolic ventricle diameters and volumes, as well as reduced stroke volume, cardiac output and ejection fraction in the *gata5* crispants vs. the Cas9 control animals. Furthermore, *gata5* crispants (**Figure 4C** and **Supplementary Figure S8**) exhibited weaker and patchy DsRed2 fluorescence, reduced numbers of cardiomyocytes (estimated at 18 ± 4.2 vs 70 ± 3.06 in the Cas9 controls. Mean, ± SEM, n = 10) and predominantly misshapen and small cardiomyocyte nuclei. The abnormal cardiac phenotype was reflected in reduced cardiovascular function in the *gata5* crispants. For all endpoints measured except vessel diameter (only measurable where blood flow occurred), *gata5* crispants showed reduced cardiovascular function compared with the Cas9 controls (**Figure 5**, with accompanying videos in **Supplementary Videos**). Collectively these data supported a negative impact of *gata5* mutation on 4 dpf zebrafish cardiovascular physiology,

A

	% Malformations at 4 days post fertilisation (4dpf)																	
	n-number (scored)	Larvae abnormal	Body shape	Somites	Notochord	Tail	Fins	Heart	Face	Neural tube	Arches/Jaws	Group mean length (mm)	Swim bladder not inflated	Swim bladder not evident	Yolk ball -Remnant excessive	Liver - not evident	Liver -enlarged	Abdomen distended/yolk oedema
Cas9	20	20%	0%	0%	0%	0%	0%	20%	0%	0%	0%	3.58	50%	0%	0%	0%	0%	0%
gata5 g#1 + Cas9	10	100%	10%	50%	0%	0%	40%	100%	60%	60%	0%	3.31	100%	60%	0%	60%	0%	50%
gata5 g#1,2,3 + Cas9	20	100%	0%	80%	20%	0%	90%	100%	85%	90%	95%	3.15	100%	85%	0%	25%	0%	75%
Cas9	20	5%	0%	0%	0%	0%	0%	5%	0%	0%	0%	3.62	0%	0%	0%	0%	0%	0%
api5 g#1 + Cas9	10	40%	0%	0%	0%	0%	0%	40%	0%	0%	0%	3.69	0%	0%	0%	0%	0%	0%
api5 g#1,2,3 + Cas9	20	0%	0%	0%	0%	0%	0%	0%	0%	0%	0%	3.67	0%	0%	0%	0%	0%	0%
Cas9	20	5%	0%	0%	0%	0%	0%	5%	0%	0%	0%	3.65	100%	0%	0%	0%	0%	0%
hspb7 g#3 + Cas9	10	90%	0%	0%	0%	0%	40%	80%	10%	30%	70%	3.55	100%	0%	0%	0%	0%	0%
hspb7 g#1,2,3 + Cas9	20	75%	20%	20%	20%	15%	60%	60%	30%	45%	55%	3.28	100%	15%	20%	15%	5%	5%
Cas9	20	15%	0%	0%	0%	0%	0%	10%	0%	5%	10%	3.58	100%	0%	0%	0%	0%	0%
lmo2 g#1,2,3 + Cas9	10	100%	40%	90%	50%	60%	100%	100%	100%	100%	100%	2.30	100%	100%	100%	100%	100%	0%
lmo2 g#2 + Cas9	20	100%	15%	100%	20%	20%	90%	100%	100%	100%	100%	3.08	100%	100%	100%	60%	20%	50%

Ai

	% Heart-specific malformations at 4dpf							
	Slow heartbeat	No heartbeat	Pericardial sac swollen	Pericardial oedema size (µm)	Chambers not well defined	Misshapen	Small	Enlarged
Cas9	0	0%	20%	13 ±2 (16)	0%	0%	0%	0%
gata5 g#1 + Cas9	0	0%	100%	207 ± 42 (10)***	60%	60%	60%	0%
gata5 g#1,2,3 + Cas9	0	5%	100%	269 ±34 (14)***	40%	85%	85%	0%
Cas9	0	0%	10%	8 ±2 (14)	0%	0%	0%	0%
api5 g#1 + Cas9	0	0%	40%	10 ±2 (7)	0%	0%	0%	0%
api5 g#1,2,3 + Cas9	0	0%	0%	7 ±2 (17)	0%	0%	0%	0%
Cas9	0	0%	45%	5 ±1 (18)	0%	0%	0%	0%
hspb7 g#3 + Cas9	0	0%	90%	40 ±15 (8)**	0%	0%	0%	0%
hspb7 g#1,2,3 + Cas9	0	5%	70%	68 ±27 (17)***	15%	20%	20%	0%
Cas9	0	0%	5%	11 ±1 (19)	0%	0%	0%	0%
lmo2 g#1,2,3 + Cas9	0	0%	100%	212 ±29 (8)***	100%	100%	100%	0%
lmo2 g#2 + Cas9	0	0%	100%	206 ±13 (19)***	100%	100%	100%	0%

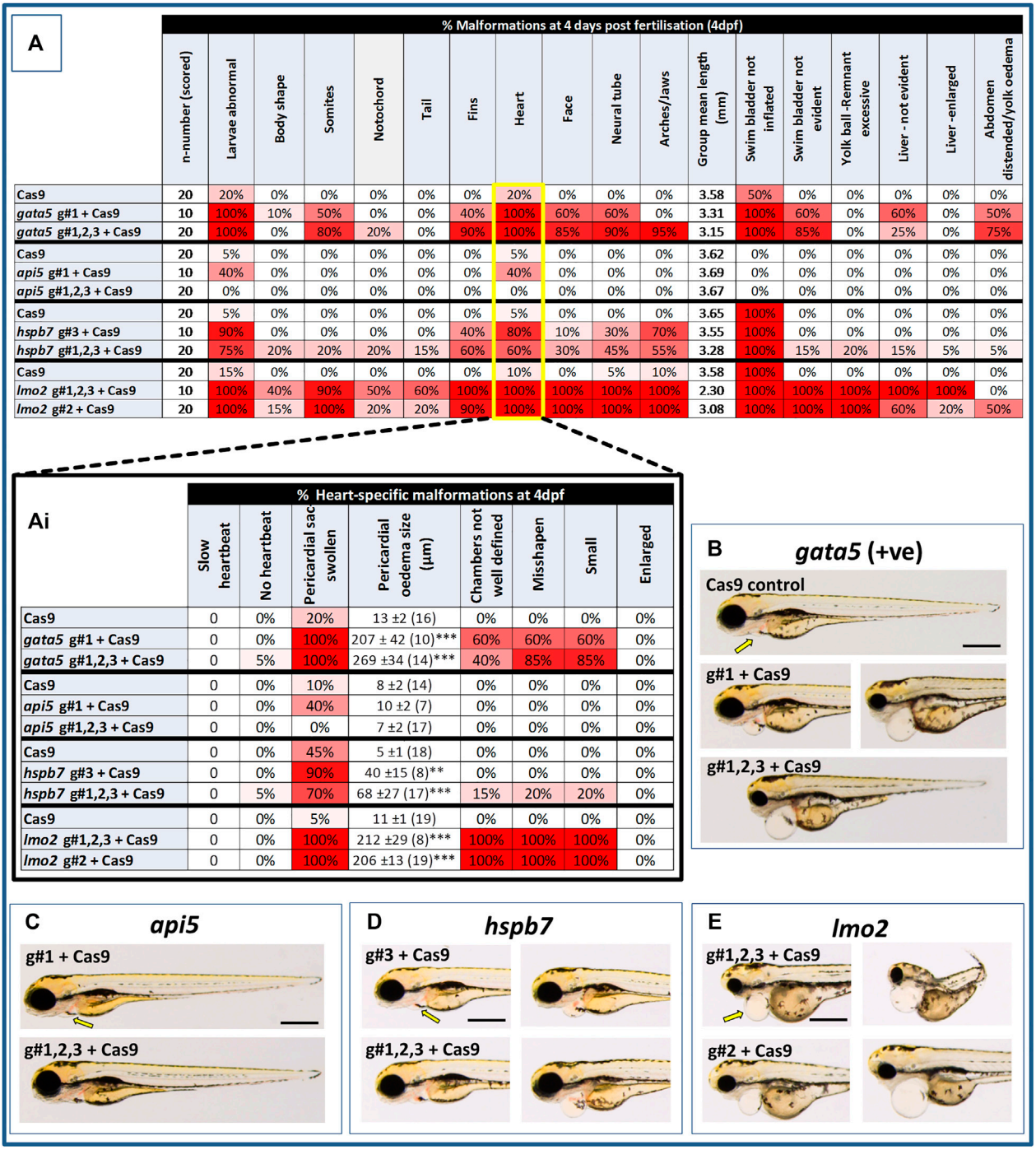

FIGURE 3 | Results of the morphological analysis of 4 dpf *gata5* (positive control), *api5*, *hspb7* and *lmo2* zebrafish crispants vs. the Cas9-injected control animals. Panel **(A)**: General whole body morphological endpoints measured following injection of Cas9 alone, or after mutation of each of the genes assessed. Data are shown as the % incidence of abnormalities under each category, with shades from white (0%) through to red (100%) providing an indication of the proportion of animals exhibiting a malformation within that category. Note different n-numbers present as two runs were undertaken for the Cas9 control and the gRNA + Cas9-injected group showing the most robust phenotype from run 1 (for *lmo2* g#2 was run twice due to concerns about excessive mortality in the g#1,2,3 group). The guide combination used for two runs in each case is shown in the lower panel of the example images for each gene. **Ai**: Expansion of heart-specific endpoints showing the full range scored including estimates of the size of pericardial oedema. Data are shown as the mean, ±SEM and (n = number of measures possible) for each treatment, For these data, **signifies a statistically significant difference vs. the Cas9 control at $p < 0.01$, and *** at $p < 0.001$ (*t*-test or Mann Whitney U-tests for the combined guide injected groups, or 1-way ANOVA and Tukey's HSD tests or Kruskal–Wallis and Dunn's tests for the single guide injected groups, in which run 1 and 2 data were combined). **(B)**: example larvae following *gata5* mutation vs. the Cas9-injected control. The yellow arrows indicate the position of the pericardial membrane and the extent of pericardial oedema, which was minimal in the controls but extensive in most crispant animals (two examples are shown for g#1-injected animals as there was some variability in the severities seen). **(C–E)**: examples of larvae following knockout of each of the other genes assessed (note the apparent lack of effect of *api5* mutation on general morphology). The scale bar shown in the first image of panels B–E represents 500 µm.

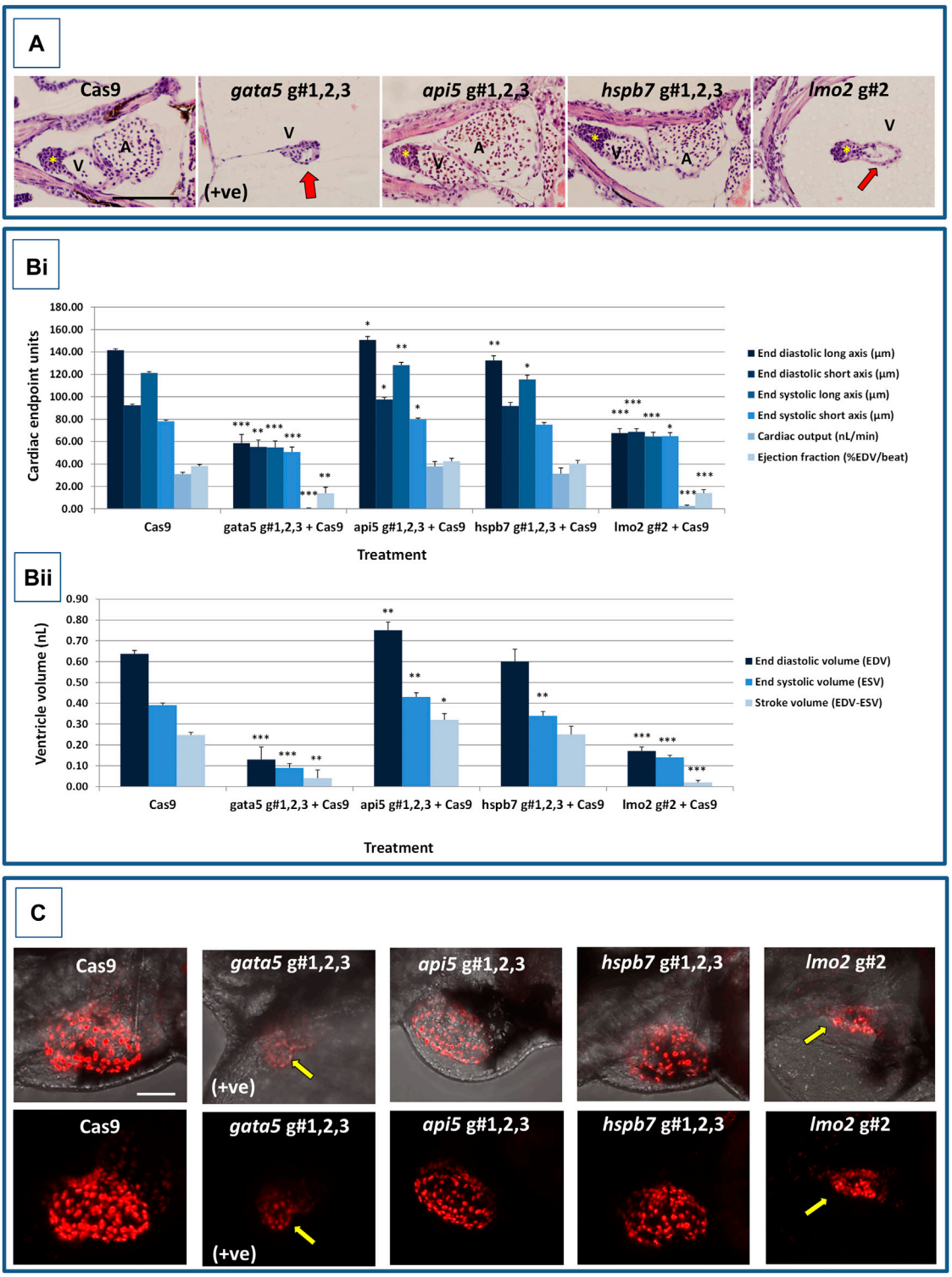

FIGURE 4 | Results of the cardiac pathological analysis of 4 dpf *gata5* (positive control), *api5*, *hspb7* and *lmo2* zebrafish crispants vs. the Cas9-injected control animals. Panel **(A)** Example haematoxylin and eosin stained coronal sections through the heart (top, A = atrium, V = ventricle, *bulbous arteriosus) from each of the treatment groups vs. the Cas9-injected controls (left-hand panels). Note in particular the extreme cardiac hypoplasia after *gata5* and *lmo2* mutation (indicated by a red arrow in the images) in which the atrium is not visible probably due to the severe pericardial oedema and resultant distension of the heart muscle. In each panel, animals are orientated with the head to the left, and viewed in the dorsal plane at a magnification of ×40 (the scale bar shown in left-hand image represents 200 μm). Panel B) Results of the analysis of ventricular dimensional analysis of the crispant vs. Cas9 control animals. Shown are the ventricle dimensions and cardiac functional

(*Continued*)

FIGURE 4 | parameters, calculated from the measurement of ventricle dimensions in 5 randomly selected embryos from each of the two runs undertaken on each gene. Panel **(Bi)** shows a graph of the ventricle diameter, cardiac output and ejection fraction data, and Panel **(Bii)** a graph of the ventricle volume-related measurements. In all cases data are shown as the mean and ±SEM of the animals in each group (n = 10 per group except n = 9 for the *gata5* cardiac output data due to the absence of a heart beat in one animal). For brevity the Cas9 data are shown as the mean across all 4 Cas9 datasets (n = 40 animals), however, statistical analysis was undertaken on the crispants versus the corresponding Cas9 control data in each case. *signifies a statistically significant difference vs. the Cas9 control for that parameter at $p < 0.05$, ** at $p < 0.01$, and *** at $p < 0.001$ (Student's *t*-test or Mann Whitney U-tests). Note: the overall body lengths of the *gata5* and the *lmo2* crispants were also significantly reduced ($p < 0.001$). Panel **(C)** Example images of hearts from *cmlc2:DsRed2-nuc* larvae in which the cardiomyocytes are labelled red, especially prominently in the ventricle. The top row of panels shows the image with transmitted light and *cmlc2::DsRed2-nuc* fluorescence signals, and the lower row shows the same example but with the *cmlc2::DsRed2-nuc* signal alone. Note the severe oedema, weaker *cmlc2::DsRed2-nuc* fluorescence signal, reduced number of cells and smaller chamber size typical of the *gata5* crispant (indicated by the yellow arrow in images); the oedema, and slightly enlarged ventricle observed in the *api5* crispant; and the severe oedema, disorganisation of myocytes and smaller chamber size typical of the *lmo2* crispants (yellow arrow). *hspb7* crispant larval hearts outwardly appeared no different to the Cas9 controls. The scale bar shown in the upper left-hand image represents 50 μm.

supporting the validity of our screening approach in zebrafish crispants.

At 2 dpf the most robust *api5* crispant phenotypes were observed after injection of g#1,2,3, followed by g#1 alone (**Supplementary Figure S6**), although by 4 dpf there was little indication of any gross morphological impact other than a 40% incidence of very mild pericardial oedema (the size of the oedemas was not significantly increased) in the g#1-injected animals (**Figure 3**). Histology (**Figure 4A** and **Supplementary Figure S7**) suggested a slight enlargement of the heart chambers with myocardial wall thinning, although this varied between individual animals. Chamber enlargement was, however supported by a small but significant increase in end-diastolic and end-systolic ventricle dimensions and volume in the *api5* crispants (**Figure 4B**), which also resulted in a small, but significant, increase in stroke volume (although this was not evident from the video tracking-based analysis of cardiovascular function. See below). Confocal assessment of *cmlc2::DsRed2-nuc* animals (**Figure 4C** and **Supplementary Figure S8**) revealed that *api5* crispants exhibited no evidence of an impact on cardiomyocyte number (estimated at 73 ± 4.2 vs 70 ± 3.06 in the Cas9 controls. Mean, ± SEM, n = 10) and no obvious abnormal cardiomyocyte organisation or ultrastructure was observed. The apparent mild impact of *api5* mutation was also reflected in the absence of any significant effects on cardiovascular function after video tracking-based assessment (**Figure 5** and **Supplementary Videos**).

The most robust *hspb7* crispant phenotypes at 2 dpf occurred after injection of g#1,2,3, followed by g#3 alone (**Supplementary Figure S6**), and at 4 dpf there were widespread developmental abnormalities across multiple tissues compared with the Cas9 controls (**Figure 3**). These abnormalities were particularly prevalent in the g#1,2,3-injected animals and included a 60% incidence of bent (predominantly pectoral) fins, a 45% incidence of a compressed/reduced size or malformed forebrain, and a 55% occurrence of malformed branchial arches or upper and lower jaw structures. In addition, there was a high incidence of pericardial oedema (60–80% of crispants, with both injection groups showing significantly increased oedema size) and in 20% of g#1,2,3 injected animals, misshapen, poorly-defined and small heart chambers. Histology (**Figure 4A** and **Supplementary Figure S7**), however, did not reveal any clear ultrastructural abnormalities. A significant reduction in the end-diastolic and end-systolic long axis ventricle diameters was, however, detected along with a significant reduction in end-systolic volume suggesting a reduction in ventricle size (**Figure 4B**). Analysis of cardiomyocyte organisation in *cmlc2::DsRed2-nuc* animals (**Figure 4C** and **Supplementary Figure S8**) also revealed some evidence of disorganised distribution of cardiomyocytes in the myocardium, and a small decrease in the numbers of cells present after *hspb7* mutation (estimated at 64 ± 3.06 vs 79 ± 2.78 in the Cas9 controls. Mean, ± SEM, n = 10). Interestingly, despite the high incidence of pericardial oedema and evidence of an impact on ventricle size and myocardial structure observed in the *hspb7* crispants, the impact on cardiovascular function in these animals was mild (**Figure 5** and **Supplementary Videos**). A small reduction in SSV in the g#1,2,3-injected animals was detected suggesting (along with blood pooling observed at 2 dpf) a small reduction in pumping efficiency (Note, however, that no impact was seen on stroke volume when ventricular dimensions were used for its calculation).

Assessment of *lmo2* crispants at 2 dpf revealed the most prominent phenotypes after injection of g#1,2,3, followed by g#2 alone (**Supplementary Figure S6**). The high mortality exhibited in the g#1,2,3-injected animals (76% in the first run), however, supported the use of g#2 for the second confirmatory run. At 4 dpf, there was a 100% incidence of heart, craniofacial, neural tube, jaw, swim bladder and yolk ball abnormalities and a high incidence of other non-cardiovascular abnormalities across all *lmo2* treatments (**Figure 3**). The hearts of all 4 dpf *lmo2* crispants exhibited elevated pericardial oedema (both in frequency and size), reduced heart size, lack of chamber definition and an abnormal heart shape. In addition to these cardiac specific effects, somites were poorly defined, fins small and bent, optic and otic vesicles were small and malformed, fore and midbrain boundaries were not present, brain sizes were reduced, and jaws were heavily malformed in terms of shape and size (in some individuals the presence of the jaw could not be determined). Additionally, swim bladder, liver and foregut structures could not be determined by visual inspection. The yolk ball was also excessive and the presence of yolk oedema was determined in 50% of the g#2 crispants. Histological analysis further supported the cardiac phenotype in the crispants, with observation of cardiac hypoplasia, chamber malformation and pericardial distension (**Figure 4A** and **Supplementary Figure S7**). In addition, there was altered cardiomyocyte shape in the g#1,2,3, and a pyknotic nucleus structure evident in g#2-injected larvae.

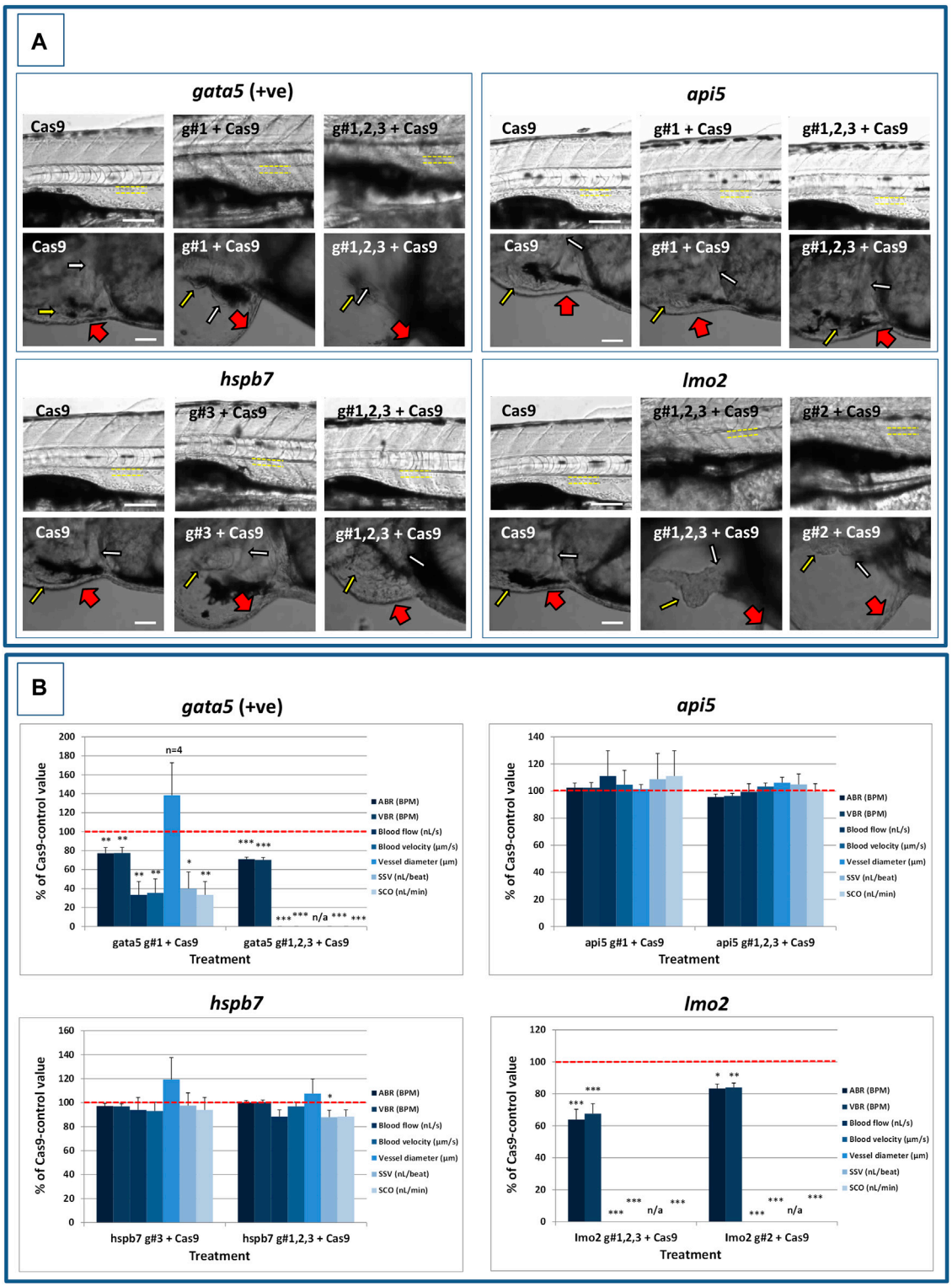

FIGURE 5 | Results of the analysis of cardiovascular function in 4 dpf *gata5* (positive control), *api5*, *hspb7* and *lmo2* zebrafish crispants versus the Cas9-injected control animals. **(A)**: Images of example Cas9 control larvae alongside larvae treated with the two gRNAs + Cas9 mixtures giving the most robust phenotypes (as assessed at 2 dpf). Images are shown for *gata5* crispants in the top left; for *api5* in the top right; for *hspb7* in the bottom left; and for *lmo2* in the bottom right. In each case the top row shows the trunk vasculature with the position of the dorsal aorta outlined in yellow dashed lines, where blood flow and vessel diameter measurements were taken. The lower row of images shows the heart from the same animals, with the atrium highlighted by a small white arrow, and the ventricle by a small yellow arrow.

(*Continued*)

FIGURE 5 | The large red arrows show the position of the pericardial membrane and the extent of pericardial oedema. Most Cas9 control animals exhibited normal morphology and function in contrast with many of the crispants. **(B)**: Cardiovascular functional endpoints quantified in the same groups of animals, with data shown for *gata5* crispants in the top left; for *api5* in the top right; for *hspb7* in the bottom left; and for *lmo2* in the bottom right. Note: the complete absence of blood flow measured in all of the *gata5* g#1,2,3, and in 6/10 of the g#1-injected animals; and the absence of effective blood flow in the *lmo2* g#1,2,3 and g#2-injected animals due to the absence of erythrocytes, meaning flow was not visible. Vessel diameter measurements were not possible in animals lacking blood flow (indicated by n/a). Data are shown as the mean % change versus the Cas9-control group (100% indicated by the red dashed line), ± SEM, $n = 19–20$ for the Cas9 and right-hand crispant treatment for each gene (data combined from two runs) and 10 for the left-hand treatment group for each gene where only one run was undertaken. *signifies a statistically significant difference versus the Cas9 control at $p < 0.05$, ** at $p < 0.01$, and *** at $p < 0.001$ (T-test or Mann Whitney U-tests for the combined guide injected groups, or 1-way ANOVA and Tukey's HSD tests or Kruskal–Wallis and Dunn's tests, for the single guide injected groups in which runs 1 and 2 were combined). The scale bar shown in the upper left-hand image of each panel represents 100 μm. The scale bar shown in the lower left-hand image of each panel represents 50 μm as a higher magnification camera mount was used in this case.

The severe impact of *lmo2* mutation was also reflected in significantly smaller ventricle end-diastolic and systolic dimensions, along with significantly reduced stroke volume, cardiac output and ejection fraction (**Figure 4B**). Confocal assessment of *cmlc2::DsRed2-nuc* crispants (**Figure 4C** and **Supplementary Figure S8**) revealed lower cardiomyocyte numbers with frequent misshapen nuclei (estimated at 43 ± 2.59 vs 79 ± 2.78 in the Cas9 controls. Mean, ± SEM, n = 10), along with an apparent breakdown in the uniformity of cell and DsRed2 distribution across the myocardium. The clear structural impact on the heart of *lmo2* crispants was reflected in the functional assessment (**Figure 5** and **Supplementary Videos**), with both crispant groups showing significantly reduced cardiovascular functionality compared with the Cas9 injection controls. It was also notable that the *lmo2* crispants lacked visible circulating erythrocytes, which is consistent with the key role of this gene in haematopoiesis and which also meant that blood flow and associated cardiovascular parameters were effectively zero.

DISCUSSION

Selection of novel drug targets generally relies on accumulated experimental evidence to support the hypothesis that target modulation affects disease pathophysiology. The use of databases and bioinformatics tools is pivotal in this process, enabling mining and integration of multiple sources of evidence linking candidate targets to disease(s) (Paananen and Fortino, 2020). Furthermore, the exponential increase in omics data generation during recent years has helped bring new insights into target discovery and validation, enabling systematic and unbiased evaluation of therapeutic efficacy and safety, as well as mechanism of action. Crucially, it is recognised that the demonstration of genetic linkage to a disease phenotype provides more confidence in target validation and a lower likelihood of drug failure due to a lack of efficacy (Cook et al., 2014). In the present study we have evaluated candidate disease genes identified in a WES study of heart failure patients *via* the use of bioinformatic tools and integrative omics data analysis. The candidate targets were assessed in terms of tissue and cell type expression, expression dysregulation and genetic association to cardiovascular disease, as well as potential mechanism of action *via* network-based methods for gene function prediction. From this, three genes were identified as having a plausible link to human cardiovascular disease prevalence and prioritised for further study. CRISPR/Cas9-mediated mutagenesis followed by morphological and functional phenotyping in zebrafish crispants was then used to reveal the role of these genes in the development and pathophysiology of the cardiovascular system *in vivo*.

Using CRISPR/Cas9-mediated multi-site mutation in zebrafish crispants resulted in the effective mutation of all 4 genes that were targeted. Adopting multi-site strategies to induce gene mutation, as used here, rapidly achieve high proportions of null alleles in F0 knockouts. Such approaches, however, can also increase off-target mutations, increase double strand breaks and are not suitable for inducing site specific mutations, where precise knockins and the creation of stable genetically modified lines may be more appropriate. Despite this, such strategies are highly beneficial for rapidly generating high-efficiency gene mutation (Kroll et al., 2021; Quick et al., 2021). This advantage is amplified when coupled with high throughput initial candidate gene identification and prioritisation, creating a potentially powerful approach for rapidly providing *in vivo* gene function data to support candidate selection as a strategy for accelerating early target validation within the wider drug discovery process. Furthermore, the inclusion of automation technology, for example, for the delivery of gRNAs/Cas9 (Zhao et al., 2018) or for the microscopic assessment of resultant phenotypes (Early et al., 2018), would only serve to increase throughput and, therefore, the utility of this approach. Supporting our approach, the positive control *gata5* crispants exhibited an expected severe and consistent impact on cardiovascular development and function at 4 dpf. Our data are consistent with the known link between *GATA5* variants and multiple human cardiovascular pathologies including familial dilated cardiomyopathy (Zhang et al., 2015) and congenital ventricular-septal defects (Wei et al., 2013). These data are also in line with previous work in zebrafish including demonstration of prominent defects in myocardial differentiation and the formation of ectopic beating myocardial tissue after loss and gain of function, respectively (Reiter et al., 1999). Here, the impact of *gata5* mutation was also evident beyond the cardiovascular system impacting various structures including the somites, fins, eyes and brain. This extracardiac impact is supported by the spatiotemporal expression of g*ata5* in developing mice (Chen et al., 2009), and by previous work in zebrafish demonstrating the central role of *gata5* in endodermal morphogenesis more broadly (Reiter et al., 2001).

The first candidate gene assessed was *API5*, which encodes human apoptosis inhibitor-5 protein (Bong et al., 2020). Published evidence for a role for *API5* in human cardiovascular disease is limited to reports of a potential involvement in vascular endothelial cell apoptosis (Lu et al., 2016; Mao et al., 2020). Our *in silico* data also suggested a

relatively strong association with myocardial infarction and various cardiomyopathies. *In vivo* mutation of zebrafish *api5* resulted in mild pericardial oedema and evidence of an increase in ventricle size. The latter is of particular interest given the observation of an association between *api5* downregulation and hypertrophic and dilated cardiomyopathies from the *in silico* data analysis. In the case of the former, histological analysis did not support myocardial thickening in 4 dpf zebrafish, although the absence of any clear change in cardiomyocyte number in *cmlc2::DsRed2-nuc api5*-crispants suggested that the change in ventricle size may be driven more by cardiac hypertrophy, rather than hyperplasia. Analysis of the cardiovascular phenotype in older animals would help to further clarify the mechanism(s) at play. Although published data on the function of *api5* in zebrafish are limited, it is modestly upregulated in adult zebrafish hearts following hypoxic insult (Marques et al., 2008) perhaps supporting a cardio-protective role against tissue injury. As our data suggest that *api5* does not play a critical role in early cardiovascular development, this may further support a role for *api5* in organ-system protection under conditions of physiological stress, or as a consequence of tissue injury.

HSPB7 encodes small heat shock protein 7, and although highly expressed in the developing and adult mammalian heart, its cardiac function remains obscure (Mercer et al., 2018). *HSPB7* gene variants have been implicated in a range of human cardiovascular diseases including heart failure (Cappola et al., 2010; Aung et al., 2019) and dilated cardiomyopathy (Villard et al., 2011; Esslinger et al., 2017). Our *in silico* analysis supported an association of *HSPB7* with various human cardiovascular pathologies, most notably downregulation associated with various cardiomyopathies, heart failure and atrial fibrillation, and upregulation associated with dilated cardiomyopathy. A central involvement in cardiovascular development and disease is certainly supported by knockout studies in mice. Wu et al. (2017), found that *Hspb7* played a critical role in development, with knockout proving embryo-lethal by around stage E12.5. Further studies on cardiac pathology in embryonic mice revealed that mutants exhibited smaller left ventricles, cardinal vein enlargement and the presence of abnormal actin bundles. Liao et al. (2017) used an inducible-conditional knockout approach to overcome the embryo-lethal effect of *Hspb7* knockout in adult mice. These authors further revealed a critical non-developmental cardiac functional role of *Hspb7* reporting disrupted myofibrillar organisation and cardiomyocyte membrane integrity, combined with abnormal cardiac conductivity, heart arrhythmia and sudden death, likely due to a reported disruption of intercalated disc structure. Here, 4 dpf *hspb7* crispant zebrafish exhibited widespread morphological abnormalities, which included a 20% occurrence of malformed or small hearts. Furthermore, a reduction in ventricle size was also detected along with some evidence of disorganised cardiomyocyte distribution, which was reminiscent of the results previously reported in *Hspb7* knockout mice. Our data are also in broad agreement with a previous study into the role of *hspb7* in zebrafish cardiovascular development using morpholino-mediated knockdown (Rosenfeld et al., 2013). These authors reported that loss of *hspb7* function resulted in disrupted heart tube looping and ventricular cardiomyocyte development. The latter effect, specifically seen in the ventricle, was reported to be driven by reduced cardiomyocyte size, rather than number and no abnormalities of cellular ultrastructure were observed. In a more recent study, Mercer et al. (2018) used TALENs to generate a frameshift near the N-terminus of zebrafish *hspb7* and reported normal cardiovascular development, including timely cardiac jogging and looping. This is in contrast to the morpholino-based knockdown work in zebrafish, previous studies in knockout mice, and the data supporting a role for *hspb7* in cardiac development generated here. In this respect, it should be noted that a crispant knockout approach generates a diversity of null alleles, which can be a drawback in disease modelling where a precise mutation needs to be duplicated. However, as our experimental objective was to reveal the consequences of the absence of the encoded protein, this approach can be advantageous in avoiding genetic compensation mechanisms, which can be observed in stable zebrafish knockout lines (El-Brolosy et al., 2019). Indeed, some aspects of the reported TALEN-based frame shift mutation point towards possible gene compensation, as the expression of *hspb5* was strongly upregulated (Mercer et al., 2018). Interestingly, despite the lack of a clear morphological phenotype in the *hspb7* mutants, these animals exhibited a reduced capacity for exercise-induced cardiovascular stress, and histopathological analysis suggested an underlying pathology manifested as cardiomegaly and mild multi-focal cardiac fibrosis (Mercer et al., 2018). This further suggests that a greater functional impact of *hspb7* may be observable under conditions of cardiovascular stress, something that could be tested through the use of an inducible-conditional knockout zebrafish and forced swimming assessment in adult animals.

LMO2 is highly conserved amongst vertebrate lineages, and encodes the Lim-domain only 2 nuclear transcriptional co-regulator crucial in early embryonic erythropoiesis and angiogenic remodelling (Chambers and Rabbitts, 2015). Beyond highlighting its well-established role in haematopoiesis and vascular development (Meng et al., 2016), our *in silico* data supported an association between *LMO2* variants and cardiomegaly and cardiomyopathy, although comparative expression data were less conclusive. CRISPR/Cas9-mediated knockout in 4 dpf zebrafish here resulted in an expected absence of circulating erythrocytes, as well as widespread morphological abnormalities affecting multiple body structures. Amongst these, *lmo2* crispants uniformly exhibited reduced heart sizes, a lack of chamber definition and an abnormal heart shape. The abnormal cardiac phenotype was reinforced by clear reductions in ventricular dimensions, reduced cardiomyocyte number and disorganisation of cell distribution through the myocardium, as well significant impacts on multiple cardiovascular functional parameters. Although the role of *LMO2* in erythropoiesis is well documented, published data on cardiac-specific impacts of *LMO2* loss of function are more limited. Deletion of *Lmo2* in

mice is embryo-lethal, with the complete failure of yolk sac erythropoiesis leading to death by around stage E10.5 (Nam and Rabbitts, 2006). Compared to wild type littermates, *Lmo2* knockout mice were reported to show no evidence of circulating erythroid cells, a small yolk sac, progressive pericardial oedema, growth retardation, significantly shortened anteroposterior axis and fewer somite pairs. Furthermore, although developing major organs were described as smaller, neurulation appeared normal, cardiac contraction was noted and there was no obvious impact on cardiac morphology (Warren et al., 1994). Knockout of *lmo2* has also previously been reported in zebrafish and appeared to result in a less severe phenotype than that observed in mice. Matrone et al. (2021) reported CRISPR/Cas9-mediated *lmo2* mutation that resulted in a 4-nucleotide insertion in exon 2 and a downstream stop codon. The resultant phenotype was described as showing mild body bending, reduced skin pigmentation, fewer circulating red blood cells, mild pericardial oedema, and mild cephalomegaly at 72 hpf. Weiss et al. (2012) also reported severe head oedema and impaired optic fissure closure in 2 dpf *lmo2* mutants isolated from an ENU-mutagenesis screen. The reason for this apparent difference in severity vs. our *lmo2* crispants is not clear, however, the complete absence of visible erythrocytes in 29/30 crispants assessed for cardiovascular function (1 animal had around 10 visible erythrocytes in the dorsal aorta) does support the extremely effective loss of *lmo2* function. Moreover, in our g#2 injected animals, an absence of blood flow was apparent in all resultant crispants. Additionally, 73% of these animals showed pericardial oedema, 82% misshapen hearts, and 11% a lack of heart chamber definition at 2 dpf suggesting the observed cardiac phenotype was initiated at a relatively early stage of development. Although it is unknown if *lmo2* is expressed in cardiomyocytes or endocardial cells themselves, it is well known that fluid forces can profoundly affect cardiac structural development. Reviewed by Sidhwani and Yelon (2019), blood flow has, for example, been shown to impact endothelial cell number and polarity, cardiac chamber morphology, cardiomyocyte shape, size and myofibril maturation, as well as endocardial cell development and morphology, atrioventricular valve formation and ventricular trabeculation. Consequently the absence of circulating erythrocytes in our *lmo2* cripsants could have significantly affected the structure and function of the developing heart. At this point, we also cannot exclude the possibility of off-target effects contributing to the observed phenotype at 4dpf, particularly in the g#1,2,3 crispants. Although off-target effects are potentially more likely in this group due to the targeting of 3 sites on *lmo2*, the demonstration of a consistent phenotype across 3 separate gRNA injection groups at 2 dpf, and between the g#1,2,3 and g#2 injected animals at 4 dpf does support the notion that *lmo2* gene function was specifically impaired. Although beyond the scope of the current study's focus on demonstrating a higher throughput work flow for supporting early stage target validation, undertaking rescue experiments would be a good strategy to provide further confidence in the genotype-phenotype link, as part of follow up work on triaged genes of particular interest.

Regarding the wider developmental impact of *lmo2* deletion in our crispants, although data in zebrafish are limited, it has been reported that in embryonic mice there is consistent expression of *Lmo2* in multiple non-haematopoietic/vascular tissues in early-mid gestation including brain, eyes, somites, liver, limb buds, tail buds and developing limbs. Furthermore, the organisation of expression in an anterior/posterior pattern was interpreted as a likely involvement in some major patterning activities during early development (Calero-Nieto et al., 2013), perhaps hinting at a wider developmental role for this gene. As suggested with *hspb7*, this is a case where the generation of an inducible-conditional knockout model may help to delineate the role of *lmo2* outside that of early development.

In conclusion, using a novel combination of *in silico* analysis of clinical data with *in vivo* assessment of CRISPR/Cas9-mediated mutation in zebrafish crispants we have generated data to strongly support the role of *api5*, *hspb7* and *lmo2* (and *gata5*) in vertebrate cardiovascular development and function, and by inference, the potential effect of loss of gene function on subsequent organ system pathophysiology. The approach we used allowed rapid screening of the impact of gene mutation on embryo-larval development and organ system function. The provision of such data greatly facilitates early target validation by providing *in vivo* data to support the selection and prioritisation of candidate genes for further investigations. These further investigations could include the creation of loss of function models in mouse, or ultimately the creation of models with disease-relevant readouts in which to test the efficacy of new chemical entities. Although the approach presented here provides *in vivo* data on gene function within just a few days, the assessment of phenotypes in early zebrafish larvae has some limitations. For example, delineation of the developmental and adult roles of candidate genes is more difficult, and embryo-lethal phenotypes would preclude the assessment of gene function at later life stages. In this respect, the generation of conditional inducible knockouts in older zebrafish would be a highly valuable next step and, if combined with the use of precise genome editing tools such as base- or prime-editing to generate specific mutant alleles, would result in a more directly translatable model of adult human heart failure. Finally, assessing organ system functionality at rest may also be relatively insensitive, whereas the use of experimental paradigms, in which cardiovascular stress is applied, may prove more revealing when relating the loss of gene function to real clinical outcomes.

DATA AVAILABILITY STATEMENT

The original contributions presented in the study are included in the article/**Supplementary Materials**, further inquiries can be directed to the corresponding authors.

ETHICS STATEMENT

All animal work was carried out in accordance with the EU Directive for the protection of animals used for scientific

purposes (2010/63/EU) and UK Animals Scientific Procedures Act (ASPA) 1986. Experimental procedures were carried out under personal and project licenses granted by the UK Home Office under ASPA, and ethically approved by the Animal Welfare and Ethical Review Body at the University of Exeter.

AUTHOR CONTRIBUTIONS

SR, MB-Y, and MJH conceived the project and developed the concept. SR, MB-Y, MJH, SS, CRT, and MJW obtained the funding. AW, EM, and MB undertook the in silico work. MJW, YO, JSB, MJH, SS, CRT, and MB-Y designed the zebrafish experiments. MJW, YO, JSB, and AT undertook the zebrafish experiments and analysed the resultant data. Data interpretation and manuscript production was undertaken by all authors.

FUNDING

This work was supported by AstraZeneca, a Royal Society short Industry Fellowship (SIF\R2\192004) awarded to MW and the University of Exeter College of Life and Environmental Sciences. In addition, research in the Scholpp lab is supported by the BBSRC (Research Grant, BB/S016295/1) and by the Living Systems Institute, University of Exeter.

ACKNOWLEDGMENTS

The authors would like to thank the staff in the Aquatic Resources Centre at the University of Exeter, for the supply and maintenance of the zebrafish. In addition, the *cmlc2::DsRed2-nuc* fish were generously provided by Geoff Burns, Boston Children's Hospital and Harvard Medical School. The authors would also like to thank Keith Cheng and Alex Yu-Shun Lin, at Pennsylvania State University College of Medicine, for their advice on the histological analysis.

SUPPLEMENTARY MATERIAL

The Supplementary Material for this article can be found online at: https://www.frontiersin.org/articles/10.3389/fphar.2022.827686/full#supplementary-material

REFERENCES

Aung, N., Vargas, J. D., Yang, C., Cabrera, C. P., Warren, H. R., Fung, K., et al. (2019). Genome-Wide Analysis of Left Ventricular Image-Derived Phenotypes Identifies Fourteen Loci Associated with Cardiac Morphogenesis and Heart Failure Development. *Circulation* 140 (16), 1318–1330. doi:10.1161/circulationaha.119.041161

Ball, J. S., Stedman, D. B., Hillegass, J. M., Zhang, C. X., Panzica-Kelly, J., Coburn, A., et al. (2014). Fishing for Teratogens: a Consortium Effort for a Harmonized Zebrafish Developmental Toxicology Assay. *Toxicol. Sci.* 139 (1), 210–219. doi:10.1093/toxsci/kfu017

Bong, S. M., Bae, S. H., Song, B., Gwak, H., Yang, S. W., Kim, S., et al. (2020). Regulation of mRNA export through API5 and Nuclear FGF2 Interaction. *Nucleic Acids Res.* 48 (11), 6340–6352. doi:10.1093/nar/gkaa335

Burger, A., Lindsay, H., Felker, A., Hess, C., Anders, C., Chiavacci, E., et al. (2016). Maximizing Mutagenesis with Solubilized CRISPR-Cas9 Ribonucleoprotein Complexes. *Development* 143 (11), 2025–2037. doi:10.1242/dev.134809

Calero-Nieto, F. J., Joshi, A., Bonadies, N., Kinston, S., Chan, W. I., Gudgin, E., et al. (2013). HOX-mediated LMO2 Expression in Embryonic Mesoderm Is Recapitulated in Acute Leukaemias. *Oncogene* 32 (48), 5471–5480. doi:10.1038/onc.2013.175

Cappola, T. P., Li, M., He, J., Ky, B., Gilmore, J., Qu, L., et al. (2010). Common Variants in HSPB7 and FRMD4B Associated with Advanced Heart Failure. *Circ. Cardiovasc. Genet.* 3 (2), 147–154. doi:10.1161/circgenetics.109.898395

Chambers, J., and Rabbitts, T. H. (2015). LMO2 at 25 years: a Paradigm of Chromosomal Translocation Proteins. *Open Biol.* 5 (6), 150062. doi:10.1098/rsob.150062

Chen, B., Yates, E., Huang, Y., Kogut, P., Ma, L., Turner, J. R., et al. (2009). Alternative Promoter and GATA5 Transcripts in Mouse. *Am. J. Physiol. Gastrointest. Liver Physiol.* 297 (6), G1214–G1222. doi:10.1152/ajpgi.00165.2009

Cook, D., Brown, D., Alexander, R., March, R., Morgan, P., Satterthwaite, G., et al. (2014). Lessons Learned from the Fate of AstraZeneca's Drug Pipeline: a Five-Dimensional Framework. *Nat. Rev. Drug Discov.* 13 (6), 419–431. doi:10.1038/nrd4309

Copper, J. E., Budgeon, L. R., Foutz, C. A., van Rossum, D. B., Vanselow, D. J., Hubley, M. J., et al. (2018). Comparative Analysis of Fixation and Embedding Techniques for Optimized Histological Preparation of Zebrafish. *Comp. Biochem. Physiol. C Toxicol. Pharmacol.* 208, 38–46. doi:10.1016/j.cbpc.2017.11.003

Early, J. J., Cole, K. L., Williamson, J. M., Swire, M., Kamadurai, H., Muskavitch, M., et al. (2018). An Automated High-Resolution *In Vivo* Screen in Zebrafish to Identify Chemical Regulators of Myelination. *Elife* 7. doi:10.7554/eLife.35136

El-Brolosy, M. A., Kontarakis, Z., Rossi, A., Kuenne, C., Günther, S., Fukuda, N., et al. (2019). Genetic Compensation Triggered by Mutant mRNA Degradation. *Nature* 568 (7751), 193–197. doi:10.1038/s41586-019-1064-z

Esslinger, U., Garnier, S., Korniat, A., Proust, C., Kararigas, G., Müller-Nurasyid, M., et al. (2017). Exome-wide Association Study Reveals Novel Susceptibility Genes to Sporadic Dilated Cardiomyopathy. *PLoS One* 12 (3), e0172995. doi:10.1371/journal.pone.0172995

Gu, J. Y., Xu, J. H., Yu, H., and Yang, Y. Q. (2012). Novel GATA5 Loss-Of-Function Mutations Underlie Familial Atrial Fibrillation. *Clinics (Sao Paulo)* 67 (12), 1393–1399. doi:10.6061/clinics/2012(12)08

Gustafson, A. L., Stedman, D. B., Ball, J., Hillegass, J. M., Flood, A., Zhang, C. X., et al. (2012). Inter-laboratory Assessment of a Harmonized Zebrafish Developmental Toxicology Assay - Progress Report on Phase I. *Reprod. Toxicol.* 33 (2), 155–164. doi:10.1016/j.reprotox.2011.12.004

Gut, P., Reischauer, S., Stainier, D. Y. R., and Arnaout, R. (2017). Little Fish, Big Data: Zebrafish as a Model for Cardiovascular and Metabolic Disease. *Physiol. Rev.* 97 (3), 889–938. doi:10.1152/physrev.00038.2016

Jiang, J. Q., Li, R. G., Wang, J., Liu, X. Y., Xu, Y. J., Fang, W. Y., et al. (2013). Prevalence and Spectrum of GATA5 Mutations Associated with Congenital Heart Disease. *Int. J. Cardiol.* 165 (3), 570–573. doi:10.1016/j.ijcard.2012.09.039

Kjekshus, J., Apetrei, E., Barrios, V., Böhm, M., Cleland, J. G., Cornel, J. H., et al. (2007). Rosuvastatin in Older Patients with Systolic Heart Failure. *N. Engl. J. Med.* 357 (22), 2248–2261. doi:10.1056/NEJMoa0706201

Konstam, M. A., Kramer, D. G., Patel, A. R., Maron, M. S., and Udelson, J. E. (2011). Left Ventricular Remodeling in Heart Failure: Current Concepts in Clinical Significance and Assessment. *JACC Cardiovasc. Imaging* 4 (1), 98–108. doi:10.1016/j.jcmg.2010.10.008

Kroll, F., Powell, G. T., Ghosh, M., Gestri, G., Antinucci, P., Hearn, T. J., et al. (2021). A Simple and Effective F0 Knockout Method for Rapid Screening of Behaviour and Other Complex Phenotypes. *Elife* 10. doi:10.7554/eLife.59683

Liao, W. C., Juo, L. Y., Shih, Y. L., Chen, Y. H., and Yan, Y. T. (2017). HSPB7 Prevents Cardiac Conduction System Defect through Maintaining Intercalated Disc Integrity. *Plos Genet.* 13 (8), e1006984. doi:10.1371/journal.pgen.1006984

Lu, W., Huang, S. Y., Su, L., Zhao, B. X., and Miao, J. Y. (2016). Long Noncoding RNA LOC100129973 Suppresses Apoptosis by Targeting miR-4707-5p and miR-4767 in Vascular Endothelial Cells. *Sci. Rep.* 6, 21620. doi:10.1038/srep21620

Mably, J. D., Mohideen, M. A., Burns, C. G., Chen, J. N., and Fishman, M. C. (2003). Heart of Glass Regulates the Concentric Growth of the Heart in Zebrafish. *Curr. Biol.* 13 (24), 2138–2147. doi:10.1016/j.cub.2003.11.055

MacRae, C. A., and Peterson, R. T. (2015). Zebrafish as Tools for Drug Discovery. *Nat. Rev. Drug Discov.* 14 (10), 721–731. doi:10.1038/nrd4627

Mao, H. Y., Liu, L. N., and Hu, Y. M. (2020). Mesenchymal Stem Cells-Derived Exosomal miRNA-28-3p Promotes Apoptosis of Pulmonary Endothelial Cells in Pulmonary Embolism. *Eur. Rev. Med. Pharmacol. Sci.* 24 (20), 10619–10631. doi:10.26355/eurrev_202010_23420

Marques, I. J., Leito, J. T., Spaink, H. P., Testerink, J., Jaspers, R. T., Witte, F., et al. (2008). Transcriptome Analysis of the Response to Chronic Constant Hypoxia in Zebrafish Hearts. *J. Comp. Physiol. B* 178 (1), 77–92. doi:10.1007/s00360-007-0201-4

Matrone, G., Xia, B., Chen, K., Denvir, M. A., Baker, A. H., and Cooke, J. P. (2021). Fli1+ Cells Transcriptional Analysis Reveals an Lmo2-Prdm16 axis in Angiogenesis. *Proc. Natl. Acad. Sci. USA* 118 (31), e2008559118. doi:10.1073/pnas.2008559118

Meeker, N. D., Hutchinson, S. A., Ho, L., and Trede, N. S. (2007). Method for Isolation of PCR-Ready Genomic DNA from Zebrafish Tissues. *Biotechniques* 43 (5), 610612614–614. doi:10.2144/000112619

Meng, S., Matrone, G., Lv, J., Chen, K., Wong, W. T., and Cooke, J. P. (2016). LIM Domain Only 2 Regulates Endothelial Proliferation, Angiogenesis, and Tissue Regeneration. *J. Am. Heart Assoc.* 5 (10). doi:10.1161/jaha.116.004117

Mercer, E. J., Lin, Y. F., Cohen-Gould, L., and Evans, T. (2018). Hspb7 Is a Cardioprotective Chaperone Facilitating Sarcomeric Proteostasis. *Dev. Biol.* 435 (1), 41–55. doi:10.1016/j.ydbio.2018.01.005

Nam, C. H., and Rabbitts, T. H. (2006). The Role of LMO2 in Development and in T Cell Leukemia after Chromosomal Translocation or Retroviral Insertion. *Mol. Ther.* 13 (1), 15–25. doi:10.1016/j.ymthe.2005.09.010

Paananen, J., and Fortino, V. (2020). An Omics Perspective on Drug Target Discovery Platforms. *Brief Bioinform* 21 (6), 1937–1953. doi:10.1093/bib/bbz122

Parker, T., Libourel, P. A., Hetheridge, M. J., Cumming, R. I., Sutcliffe, T. P., Goonesinghe, A. C., et al. (2014). A Multi-Endpoint *In Vivo* Larval Zebrafish (*Danio rerio*) Model for the Assessment of Integrated Cardiovascular Function. *J. Pharmacol. Toxicol. Methods* 69 (1), 30–38. doi:10.1016/j.vascn.2013.10.002

Pfeffer, M. A., Swedberg, K., Granger, C. B., Held, P., McMurray, J. J., Michelson, E. L., et al. (2003). Effects of Candesartan on Mortality and Morbidity in Patients with Chronic Heart Failure: the CHARM-Overall Programme. *Lancet* 362 (9386), 759–766. doi:10.1016/s0140-6736(03)14282-1

Povysil, G., Chazara, O., Carss, K. J., Deevi, S. V. V., Wang, Q., Armisen, J., et al. (2021). Assessing the Role of Rare Genetic Variation in Patients with Heart Failure. *JAMA Cardiol.* 6, 379. doi:10.1001/jamacardio.2020.6500

Quick, R. E., Buck, L. D., Parab, S., Tolbert, Z. R., and Matsuoka, R. L. (2021). Highly Efficient Synthetic CRISPR RNA/Cas9-Based Mutagenesis for Rapid Cardiovascular Phenotypic Screening in F0 Zebrafish. *Front Cel Dev Biol* 9, 735598. doi:10.3389/fcell.2021.735598

Reiter, J. F., Alexander, J., Rodaway, A., Yelon, D., Patient, R., Holder, N., et al. (1999). Gata5 Is Required for the Development of the Heart and Endoderm in Zebrafish. *Genes Dev.* 13 (22), 2983–2995. doi:10.1101/gad.13.22.2983

Reiter, J. F., Kikuchi, Y., and Stainier, D. Y. (2001). Multiple Roles for Gata5 in Zebrafish Endoderm Formation. *Development* 128 (1), 125–135. doi:10.1242/dev.128.1.125

Rosenfeld, G. E., Mercer, E. J., Mason, C. E., and Evans, T. (2013). Small Heat Shock Proteins Hspb7 and Hspb12 Regulate Early Steps of Cardiac Morphogenesis. *Dev. Biol.* 381 (2), 389–400. doi:10.1016/j.ydbio.2013.06.025

Sabaliauskas, N. A., Foutz, C. A., Mest, J. R., Budgeon, L. R., Sidor, A. T., Gershenson, J. A., et al. (2006). High-throughput Zebrafish Histology. *Methods* 39 (3), 246–254. doi:10.1016/j.ymeth.2006.03.001

Senni, M., Paulus, W. J., Gavazzi, A., Fraser, A. G., Díez, J., Solomon, S. D., et al. (2014). New Strategies for Heart Failure with Preserved Ejection Fraction: the Importance of Targeted Therapies for Heart Failure Phenotypes. *Eur. Heart J.* 35 (40), 2797–2815. doi:10.1093/eurheartj/ehu204

Sidhwani, P., and Yelon, D. (2019). Fluid Forces Shape the Embryonic Heart: Insights from Zebrafish. *Curr. Top. Dev. Biol.* 132, 395–416. doi:10.1016/bs.ctdb.2018.12.009

Suwinski, P., Ong, C., Ling, M. H. T., Poh, Y. M., Khan, A. M., and Ong, H. S. (2019). Advancing Personalized Medicine through the Application of Whole Exome Sequencing and Big Data Analytics. *Front. Genet.* 10 (49), 49. doi:10.3389/fgene.2019.00049

Villard, E., Perret, C., Gary, F., Proust, C., Dilanian, G., Hengstenberg, C., et al. (2011). A Genome-wide Association Study Identifies Two Loci Associated with Heart Failure Due to Dilated Cardiomyopathy. *Eur. Heart J.* 32 (9), 1065–1076. doi:10.1093/eurheartj/ehr105

Warren, A. J., Colledge, W. H., Carlton, M. B., Evans, M. J., Smith, A. J., and Rabbitts, T. H. (1994). The Oncogenic Cysteine-Rich LIM Domain Protein Rbtn2 Is Essential for Erythroid Development. *Cell* 78 (1), 45–57. doi:10.1016/0092-8674(94)90571-1

Wei, D., Bao, H., Zhou, N., Zheng, G. F., Liu, X. Y., and Yang, Y. Q. (2013). GATA5 Loss-Of-Function Mutation Responsible for the Congenital Ventriculoseptal Defect. *Pediatr. Cardiol.* 34 (3), 504–511. doi:10.1007/s00246-012-0482-6

Weiss, O., Kaufman, R., Michaeli, N., and Inbal, A. (2012). Abnormal Vasculature Interferes with Optic Fissure Closure in Lmo2 Mutant Zebrafish Embryos. *Dev. Biol.* 369 (2), 191–198. doi:10.1016/j.ydbio.2012.06.029

Wu, R. S., LamII, Clay, H., Duong, D. N., Deo, R. C., and Coughlin, S. R. (2018). A Rapid Method for Directed Gene Knockout for Screening in G0 Zebrafish. *Dev. Cel* 46 (1), 112–e4. doi:10.1016/j.devcel.2018.06.003

Wu, T., Mu, Y., Bogomolovas, J., Fang, X., Veevers, J., Nowak, R. B., et al. (2017). HSPB7 Is Indispensable for Heart Development by Modulating Actin Filament Assembly. *Proc. Natl. Acad. Sci. U S A.* 114 (45), 11956–11961. doi:10.1073/pnas.1713763114

Yalcin, H. C., Amindari, A., Butcher, J. T., Althani, A., and Yacoub, M. (2017). Heart Function and Hemodynamic Analysis for Zebrafish Embryos. *Dev. Dyn.* 246 (11), 868–880. doi:10.1002/dvdy.24497

Zhang, X. L., Dai, N., Tang, K., Chen, Y. Q., Chen, W., Wang, J., et al. (2015). GATA5 Loss-Of-Function Mutation in Familial Dilated Cardiomyopathy. *Int. J. Mol. Med.* 35 (3), 763–770. doi:10.3892/ijmm.2014.2050

Zhao, Y., Sun, H., Sha, X., Gu, L., Zhan, Z., and Li, W. J. (2018). A Review of Automated Microinjection of Zebrafish Embryos. *Micromachines (Basel)* 10 (1), 7. doi:10.3390/mi10010007

Conflict of Interest: Authors SR, MB-Y, AW, and EM are employees of AstraZeneca PLC.

The remaining authors declare that the research was conducted in the absence of any commercial or financial relationships that could be construed as a potential conflict of interest.

Publisher's Note: All claims expressed in this article are solely those of the authors and do not necessarily represent those of their affiliated organizations, or those of the publisher, the editors and the reviewers. Any product that may be evaluated in this article, or claim that may be made by its manufacturer, is not guaranteed or endorsed by the publisher.

frontiers | Frontiers in Pharmacology

ORIGINAL RESEARCH
published: 02 June 2022
doi: 10.3389/fphar.2022.853936

Sex-Specific Effects of Acute Ethanol Exposure on Locomotory Activity and Exploratory Behavior in Adult Zebrafish (*Danio rerio*)

Laura E. Vossen[1]*, *Ronja Brunberg*[2], *Pontus Rådén*[2], *Svante Winberg*[3,4] and *Erika Roman*[1,2]

[1]Division of Anatomy and Physiology, Department of Anatomy, Physiology and Biochemistry, Swedish University of Agricultural Sciences, Uppsala, Sweden, [2]Neuropharmacology, Addiction and Behavior, Department of Pharmaceutical Biosciences, Uppsala University, Uppsala, Sweden, [3]Behavioral Neuroendocrinology, Department of Neuroscience, Uppsala University, Uppsala, Sweden, [4]Behavioral Neuroendocrinology, Department of Medical Cell Biology, Uppsala University, Uppsala, Sweden

OPEN ACCESS

Edited by:
Anna Siebel,
Universidade Comunitária da Região de Chapecó, Brazil

Reviewed by:
Ruey-Kuang Cheng,
Institute of Molecular and Cell Biology (A*STAR), Singapore
Ricieri Mocelin,
Universidade Federal da Fronteira Sul, Brazil
Anoosha Attaran,
Western University, Canada

***Correspondence:**
Laura E. Vossen
laura.vossen@slu.se

Specialty section:
This article was submitted to Neuropharmacology, a section of the journal Frontiers in Pharmacology

Received: 13 January 2022
Accepted: 03 May 2022
Published: 02 June 2022

Citation:
Vossen LE, Brunberg R, Rådén P, Winberg S and Roman E (2022) Sex-Specific Effects of Acute Ethanol Exposure on Locomotory Activity and Exploratory Behavior in Adult Zebrafish (Danio rerio). Front. Pharmacol. 13:853936. doi: 10.3389/fphar.2022.853936

The zebrafish (*Danio rerio*) is an established model organism in pharmacology and biomedicine, including in research on alcohol use disorders and alcohol-related disease. In the past 2 decades, zebrafish has been used to study the complex effects of ethanol on the vertebrate brain and behavior in both acute, chronic and developmental exposure paradigms. Sex differences in the neurobehavioral response to ethanol are well documented for humans and rodents, yet no consensus has been reached for zebrafish. Here, we show for the first time that male zebrafish of the AB strain display more severe behavioral impairments than females for equal exposure concentrations. Adult zebrafish were immersed in 0, 1 or 2% (v/v) ethanol for 30 min, after which behavior was individually assessed in the zebrafish Multivariate Concentric Square Field™ (zMCSF) arena. Males exposed to 2% ethanol showed clear signs of sedation, including reduced activity, increased shelter seeking and reduced exploration of shallow zones. The 1% male group displayed effects in the same direction but of smaller magnitude; this group also explored the shallow areas less, but did not show a general reduction in activity nor an increase in shelter seeking. By contrast, 1 and 2% exposed females showed no alterations in explorative behavior. Females exposed to 2% ethanol did not display a general reduction in activity, rather activity gradually increased from hypoactivity to hyperactivity over the course of the test. This mixed stimulatory/depressant effect was only quantifiable when locomotory variables were analyzed over time and was not apparent from averages of the whole 30-min test, which may explain why previous studies failed to detect sex-specific effects on locomotion. Our results emphasize the importance of explicitly including sex and time as factors in pharmacological studies of zebrafish behavior. We hypothesize that the lower sensitivity of female zebrafish to ethanol may be explained by their greater body

Abbreviations: CENT, Center zone of the zMCSF; CIRC, Central circle zone of the zMCSF; CORN, Corner zone of the zMCSF; CORR1, Corridor 1 zone of the zMCSF; CORR2, Corridor 2 zone of the zMCSF; CORRS, Corridor 1, corner and corridor 2 of the zMCSF; DCR, Dark corner roof zone of the zMCSF; MCSF, Multivariate Concentric Square Field™; NTDT, Novel Tank Diving Test; PCA, Principal Component Analysis; RAMP, Inclined ramp of the zMCSF; REST, The part of the zMCSF not designated to any other zone; START, Start zone of the zMCSF; zMCSF, Zebrafish Multivariate Concentric Square Field™.

weight and associated larger distribution volume for ethanol, which may render lower brain ethanol concentrations in females.

Keywords: alcohol, swimming kinematics, exploration, anxiety-like behavior, sex differences, multivariate concentric square field (MCSF), risk taking, shelter seeking behaviour

1 INTRODUCTION

Alcohol use disorders (AUDs) and alcohol-related disease have a severe negative impact on individual health and social functioning, and on society. It is estimated that worldwide, 3 million deaths every year occur as a result of the harmful use of alcohol (Poznyak and Rekve, 2018). Alcohol (ethanol, EtOH) has both acute and chronic effects on the brain and on behavior, which to a large extent has been characterized using rodents as model organisms (Bell et al., 2017). Ethanol has a highly complex mechanism of action (Koob et al., 1998; Abrahao et al., 2017), therefore much remains to be investigated. In recent years, the zebrafish has gained popularity as a model organism in biomedical research owing to its short developmental time, ease of maintenance, high egg production, external fertilization and possibilities for gene editing tools (Liu et al., 2019). Given the increasing use of zebrafish it is important to translate and confirm results from rodents to zebrafish.

Ethanol can be administered to zebrafish via the holding water for studies of both acute (Gerlai et al., 2000) and chronic effects (Gerlai et al., 2006; Gerlai et al., 2009) as well as developmental ethanol exposure (Carvan et al., 2004; Lockwood et al., 2004). The most commonly used doses are immersion treatments with 0.25, 0.5 and 1.0% (v/v) ethanol for one hour, which result in blood and brain ethanol concentrations that are comparable to human drinkers after mild to moderate acute ethanol consumption (Dlugos and Rabin, 2003; Echevarria et al., 2011; Rosemberg et al., 2012). In agreement with mammals (Pohorecky, 1977; Calabrese and Baldwin, 2003), acute ethanol exposure alters zebrafish locomotory behavior in a biphasic dose-dependent manner; low concentrations (0.25 and 0.5% for 60 min) increase locomotory activity while higher concentrations (1% for 60 min) result in reduced activity (Gerlai et al., 2000; Gerlai, 2003), suggesting a sedative effect (but see (Gerlai et al., 2006; Mathur and Guo, 2011)). Moreover, increases in risk-taking behavior have been reported for the 0.5 and 1% dose (60 min immersion duration), including a reduced avoidance reaction (Gerlai et al., 2006; Gerlai et al., 2009), reduced diving response (Gerlai et al., 2008; Mathur and Guo, 2011), reduced scototaxis (Gebauer et al., 2011; Mathur and Guo, 2011) and reduced shoaling behavior (Gerlai et al., 2009). Finally, considerable differences in the behavioral responses to ethanol have been found between zebrafish strains (Gerlai et al., 2008; Gerlai et al., 2009; Pannia et al., 2014), emphasizing the importance of genetic differences.

Although zebrafish males and females can be difficult to distinguish from one another morphologically, it is well recognized that the sexes display behavioral differences in locomotory activity, exploration, boldness and aggression (Dahlbom et al., 2011; Dahlbom et al., 2012; Mustafa et al., 2019; Genario et al., 2020; Dos Santos et al., 2021; Souza et al., 2021). The sexes also differ markedly in responses to various toxicants and pollutants (reviewed in (Genario et al., 2020)), although for the case of ethanol no consensus has been reached. While most acute exposure studies used a population containing both sexes, and in many cases even reported an equal sex ratio, results from both sexes were often pooled in the statistical analysis (but see (Dlugos et al., 2011; Clayman et al., 2017; Goodman and Wong, 2020; Souza et al., 2021)). One exception is a study by Dlugos *et al.* (2011) who reported a greater increase in nearest neighbor distance in groups of wild-type females compared to males after exposure to 0.5% ethanol for 2 h, while males showed a greater increase at the 1% (v/v) dose (Dlugos et al., 2011). In addition, a recent study by Souza et al. (2021) found that the behavior of short-fin zebrafish females towards a novel object was affected by low concentrations (0.25 and 0.5% (v/v) for one hour) where male behavior was unaffected. We asked the question, to what extend the sex differences reported extrapolate to other behavioral contexts and zebrafish strains, in particular to the widely used AB strain. We wanted to include several proxies for ethanol-induced effects on activity, exploration, shelter seeking and risk-taking behavior while avoiding carry-over and test order effects between different behavioral tests. We therefore chose to use the recently developed zebrafish version of a multivariate test arena used in over 40 rodent studies, the Multivariate Concentric Square Field™(MCSF) (Bikovski et al., 2020; Vossen et al., 2022).

The zebrafish MCSF (zMCSF) arena consists of a central square area surrounded by semi-sheltered corridors, a dark corner roof (DCR), and an inclined ramp (Vossen et al., 2022). These areas differ in illumination and elevation, are sheltered or exposed to different degrees, and the arena cannot be overseen from any of these areas. This design offers the animal a free choice between several alternative locations of different quality in terms of risk and safety, while also providing an incentive for exploration. This generates a behavioral profile of an individual within a single behavioral test. In a previous study, we repeatedly tested male and female AB and wild-caught zebrafish in this arena, and cross-validated the results with the novel tank diving test (Vossen et al., 2022). This revealed no major sex differences in exploratory behavior, except for a higher locomotory activity in AB males compared to females. However, we detected large differences between strains. AB zebrafish avoided the risky area (inclined ramp), and often left one or more zones unexplored. Wild zebrafish swam faster than AB and spent more time on the ramp, but avoided the center of the arena. The zMCSF was largely resilient to repeated testing. These results led us to conclude that the zMCSF can distinguish between different magnitudes and types of risk taking and shelter seeking, which may also render a more fine-grained analysis of the changes in behaviors induced by acute ethanol exposure (Vossen et al., 2022).

The aim of the current study was to investigate whether acute ethanol exposure differentially affected behavioral profiles of male and female AB zebrafish in the zMCSF. In previous studies, the effect of 1% (v/v) acute ethanol exposure on locomotory activity was inconsistent even within the AB strain (Gerlai et al., 2008; Mathur and Guo, 2011; Tran and Gerlai, 2013) and AB appeared to be more tolerant than other strains (Gerlai et al., 2008). We therefore chose to include one widely used dose (1% v/v) and one higher dose (2% v/v) as suggested by Gerlai and coworkers (Gerlai et al., 2008). Regarding the choice of immersion duration, two zebrafish studies have reported that brain and blood ethanol content reached a steady-state concentration within 15–20 min (Dlugos and Rabin, 2003; Echevarria et al., 2011) while another study saw a small but significant increase from 15 to 30 min (Rosemberg et al., 2012). Hence, we chose an immersion duration of 30 min.

2 MATERIALS AND METHODS

Experiments took place at the Department of Neuroscience, located at the Biomedical Center of Uppsala University, Sweden in October and November 2017. Ethical approval for the use of animals was given by the Uppsala Regional Animal Ethical Committee (permit C55/13), following the guidelines of the Swedish Legislation on Animal Experimentation (Animal Welfare Act SFS 1998:56) and the European Union Directive on the Protection of Animals Used for Scientific Purposes (Directive 2010/63/EU).

2.1 Animals and Housing

A total of 51 adult zebrafish (23 females and 28 males, 19 months old) of the AB strain were used in this study. Animals were obtained from SciLifeLab (Evolutionary Biology Center, Uppsala University), a local zebrafish facility that regularly obtains AB strain zebrafish from the Zebrafish International Resource Center (ZIRC at the University of Oregon Eugene). Animals were kept in mixed-sex groups in a stand-alone system (Aquaneering, San Diego, 117 United States) in 2.8L tanks supplied with recirculating copper-free Uppsala municipal tap water (10% daily exchange). Temperature was maintained at 27 ± 1.5 °C and the photoperiod was 14L:10D (lights on at 07:00 a.m.). Animals were fed twice a day with flakes (tropical energy food, Aquatic 120 Nature, Roeslare, Belgium) and *Artemia* brine shrimp (Argentemia Platinum Grade 0, Argent 121 Aquaculture, Redmond, United States). All animals were naïve to behavioral testing.

2.2 Ethanol Exposure

One week before the start of behavioral testing, subjects were randomly placed into one of three 2.8L rack system tanks (Aquaneering, San Diego, United States); tank 1 (9 females, 9 males), tank 2 (10 females, 10 males) or tank 3 (9 males, 9 females). The sex of each individual was determined by visual examination (in brief, extrusion of belly, ovipositor and color of the anal fin (Gupta and Mullins, 2010)). The housing tanks were kept in the rack system for 7 days prior to behavioral testing, to ensure a stable dominance hierarchy within each dose group. Immediately prior to behavioral testing, each fish was individually immersed for 30 min into a 1.75L trapezoidal tank containing 1.0L rack system water mixed with 0, 1 or 2% (v/v) ethanol (≥99.5%, VWR, Sweden). Exposure started no earlier than 30 min after morning feeding. Immediately following ethanol (or control) treatment, an individual zebrafish was transferred to the zMCSF arena using a small net, and its behavior was video recorded for 30 min.

2.3 The Zebrafish Multivariate Concentric Square Field™ (zMCSF)

The multivariate concentric square field is a behavioral test arena that was originally developed for rodents (Bikovski et al., 2020; Meyerson et al., 2006). We recently translated the MCSF test to zebrafish and quantified strain and sex differences as well as the effect of repeated testing (Vossen et al., 2022). All behavioral tests took place in a separate room located inside the aquarium room. The experimenter was not present or visible during video recordings. The zMCSF is a square tank (30 × 30 × 25.8 cm) containing three objects; a roof, a corridor and a ramp, which are placed around the walls thereby surrounding a central open area (**Figure 1**). The arena is filled with 8L pre-heated copper-free Uppsala municipal tap water (23 ± 2°C) creating a water depth of 10 cm. The water inside the arena is exchanged fully between trials. An infrared backlight (Noldus, Wageningen, Netherlands) is placed under the zMCSF arena and an infrared camera (JVC SuperLoLux, Yokohama, Japan) on the ceiling records the movement of the fish through the arena. Two photographic lights (Walimex daylight 1,000, the Hague, Netherlands) provide ambient lighting of 0.46 Lux (Lux meter, Fisher Scientific LTD., Uppsala, Sweden). The arena is divided (virtually) into 13 zones (**Figure 1**): the area where the animal is released into the arena (START), a dark corner with a roof (DCR), a semi-sheltered area consisting of two corridors (CORR1 and CORR2) and a corner (CORN), an inclined ramp leading from high to low water depth (RAMP1-4), a central square consisting of an central circle (CIRC) and the remnant of the central square (CENT) and finally the remaining floor area that does not belong to any of the other zones (REST). From previous work on the zMCSF we derived that zebrafish seek shelter in the DCR (and to some extend CORR1, CORN and CORR2), while the RAMP zones (especially RAMP4) comprise high risk zones for AB zebrafish (Vossen et al., 2022).

2.4 Video Tracking and Data Extraction

Videos were recorded and video tracked with Ethovision XT12 software (Noldus, Wageningen, the Netherlands). Behavioral recording started 2 s after the animal was detected in the arena and ended 30 min later. All trials were manually assessed for possible tracking errors. We extracted six variables from the tracks using Ethovision XT15 (Noldus, Wageningen, Netherlands). For the whole arena we extracted duration in arena, total distance moved (cm) and average velocity (cm s^{-1}). For each zone, we extracted the cumulative duration (s) in zone, frequency of zone visits and latency (s) until first entry into zone. For the

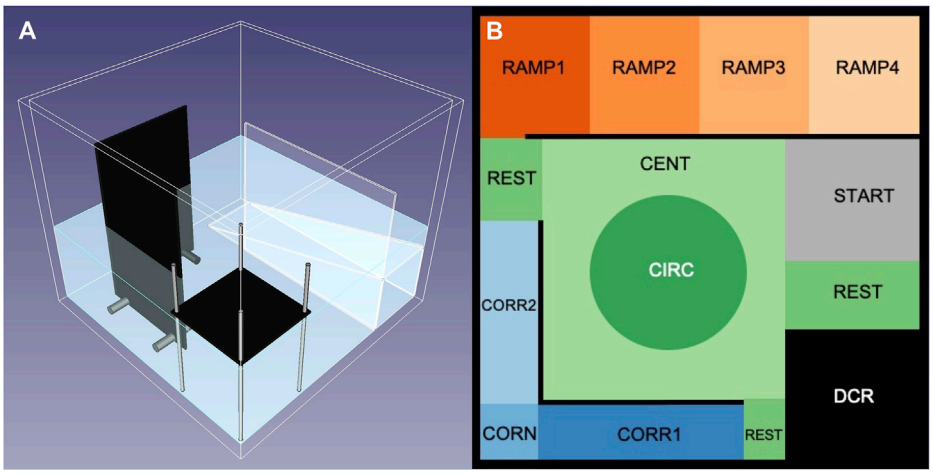

FIGURE 1 | The zMCSF testing arena, which contains a dark corner roof (DCR), two walls building a corridor and corner (CORR1, CORN, CORR2), and an inclined ramp creating decreasing water depth (RAMP1-4), all of which surround a central open area (CENT and CIRC). For exact measurements, see blueprints provided in (Vossen et al., 2022). **(A)** 3D model of the zMCSF arena. **(B)** Virtual division of zones in the arena, as seen by the ceiling mounted camera and used for video tracking with Ethovision XT15 (Noldus, Wageningen, the Netherlands). Images reprinted from (Vossen et al., 2022). Abbreviations: CENT, center; CIRC, central circle; CORN, corner; CORR, corridor; DCR, dark corner roof; REST, the part of the arena not designated to any other zone.

REST zone only the duration (s) in this zone could be extracted. From these variables, we computed an additional five ethologically relevant variables (Vossen et al., 2022). Total activity was defined as the sum of all zone frequencies (zone entries). Duration per visit (s) was computed as the total duration in zone divided by the frequency of visits to that zone. Frequency (%) was calculated as the frequency of visits to that zone divided by total activity. Using the latency (s) variable, we derived the number of zones entered by the fish, and if the fish had explored all zones (yes or no). Finally, these same variables were extracted from Ethovision over time, with one minute per time bin, which was labeled the 'minute bins dataset'.

2.5 Statistical Analyses

All statistical analyses were carried out in R statistical computing software version 4.0.2 (R_Core_Team, 2020) with added packages "lme4" (Bates et al., 2015), "emmeans" (Lenth, 2020) "bestNormalize" (Peterson and Cavanaugh, 2019; Peterson, 2021) and "ggplot2" (Wickham, 2016). We first explored the data by conducting a principal component analysis (PCA) on each dataset, using the "prcomp" function with scaling and centering of variables.

2.5.1 Statistical Analysis of Locomotory Activity

To evaluate the effect of ethanol dose (hereafter Dose) and the sex of the individual (hereafter Sex) on total distance moved (cm) and mean velocity (cm s^{-1}) over the whole trial, we computed two two-way ANOVAs with main effects of Dose and Sex plus the interaction effect. Total activity was modelled with a generalized linear model (GLM) with a negative binomial error distribution, using the same explanatory variables. Post-hoc pairwise comparisons with Bonferroni correction for multiple testing were computed using the "emmeans" function.

Since these three activity variables followed a linear pattern over time, this allowed for regression analyses on the minute bin dataset using mixed-effect modeling which allows for inclusion of repeated measurements on the same individuals. Distance moved (cm) per minute and velocity (cm s^{-1}) per minute were analyzed with two linear mixed-effect models (LMMs) with fixed effects of Dose and Sex and Minute and a random intercept of Individual. The "emtrends" function was used to compare the slopes of the different Dose/Sex groups. Total activity per minute was modelled using a generalized linear mixed-effects model (function "glmer.nb") incorporating the same explanatory variables as for distance moved (cm) and velocity (cm s^{-1}) per minute.

2.5.2 Statistical Analysis of Exploratory Behavior, Risk Taking and Shelter Seeking

To evaluate exploratory behavior, we constructed a Poisson GLM with the number of zones explored as a response variable and Dose, Sex and their interaction as explanatory variables. In addition, a binomial GLM with the same explanatory variables was performed on the binary variable indicating whether all zones had been visited.

Risk taking and shelter seeking were evaluated using zone-specific variables total duration (s), average duration per visit (s) and latency (s). A linear mixed-effects model (LMM) was constructed with fixed effects of Zone, Dose and Sex and their interactions and a random intercept of Individual. We applied a log transformation on duration and duration per visit (log (y+1)). Latency was transformed using an ordered quantile normalization ("orderNorm" function (Peterson and Cavanaugh, 2019)), a rank-based procedure, suggested by the "bestNormalize" function (Peterson, 2021). For count variables frequency and frequency (%) we computed a negative binomial generalized linear mixed-effects model (GLMM), with the same fixed and random effects, after a Poisson GLMM proved to suffer from overdispersion. For all models, we computed post-hoc

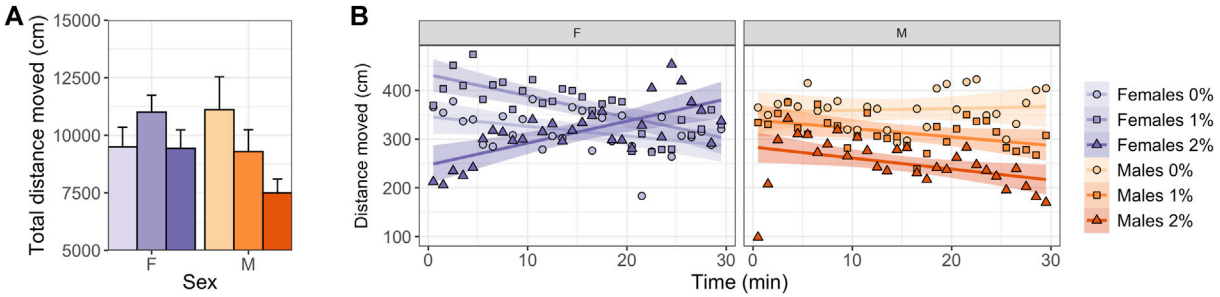

FIGURE 2 | Locomotory activity in the zMCSF of male and female AB zebrafish acutely exposed to 0, 1 or 2% (v/v) ethanol for 30 min. **(A)** Total distance moved over the 30-min trial (in cm; mean ± SEM per group) and **(B)** distance moved per minute (in cm; mean per group) by female (F; purple colors) and male (M; orange colors) zebrafish exposed to 0% (controls; light shades), 1% ethanol (medium dark shades) or 2% ethanol (dark shades). Lines indicate the linear regression line and confidence intervals (shaded) per Dose/Sex group.

TABLE 1 | Results of the linear mixed-effects model of Distance moved (cm) per minute, with fixed effects of Minute, Dose and Sex and all interactions, and a random intercept of individual.

Response	Explanatory	Test statistic	df	p-value	
Distance moved (cm)	Dose	F = 2.483	2, 61	0.087	-
	Sex	F = 0.714	1, 61	0.398	-
	Minute	F = 8.180	1, 1,473	0.004	**
	Dose × Sex	F = 2.151	2, 61	0.116	-
	Dose × Min	F = 10.648	1, 61	<0.001	***
	Sex × Min	F = 0.193	1, 1,473	0.660	-
	Dose × Sex × Min	F = 18.788	2, 1,473	<0.001	***

comparisons with Bonferroni correction and we tested only for effects within each Zone between all Dose/Sex groups.

The response variables did not show a linear pattern over time (i.e. per minute), therefore the minute bins dataset could not be analyzed using (G)LMMs. However, we provide the reader with detailed graphs of duration (s) and frequency in zone per Dose/Sex group for visual analysis.

3 RESULTS

3.1 Principal Component Analysis (PCA)

Individual principal component scores largely overlapped between groups (**Supplementary Figure S1A**). Only the 2% male group stood out, having a relatively low score on PC1 and PC2 score, indicative of a longer duration in DCR and low activity. The loading plot showed a clear separation of the variables from each zone (**Supplementary Figure S1B**).

3.2 Locomotory Activity

Males exposed to 2% ethanol showed a reduction in total distance moved (ANOVA, $t_{2,45} = 2.755$, $p = 0.025$; **Figure 2A**, **Supplementary Table S1, S2**) and mean velocity compared to control males (ANOVA, $t_{2,45} = 2.764$, $p = 0.025$; **Supplementary Table S1, S2**). No dose differences were observed in females over the entire 30-min test (**Figure 2A**, **Supplementary Table S1, S2**).

TABLE 2 | Post-hoc pair-wise comparisons between Dose/Sex groups in average Distance moved (cm) per minute, averaged over all Minutes.

	Contrast	t ratio	df	p-value	
Females	0–1%	−1.085	2, 45	0.851	-
	0–2%	0.041	2, 45	1.000	-
	1–2%	1.089	2, 45	0.846	-
Males	0–1%	1.422	2, 45	0.486	-
	0–2%	2.755	2, 45	0.025	*
	1–2%	1.405	2, 45	0.501	-
Sex difference	0%	−1.198	2, 45	0.237	-
	1%	1.294	2, 45	0.202	-
	2%	1.380	2, 45	0.174	-

TABLE 3 | Post-hoc pair-wise comparisons of the slope in Distance moved over time, per Sex/Dose group.

	Contrast	t ratio	df	p-value	
Females	0–1%	1.885	2, 1,473	0.144	-
	0–2%	−4.960	2, 1,473	<0.001	***
	1–2%	−6.781	2, 1,473	<0.001	***
Males	0–1%	2.798	2, 1,473	0.014	*
	0–2%	2.802	2, 1,473	0.014	*
	1–2%	0.076	2, 1,473	0.997	-
Sex difference	0%	−3.070	2, 45	0.013	*
	1%	−2.200	2, 45	0.068	-
	2%	6.780	2, 45	<0.001	***

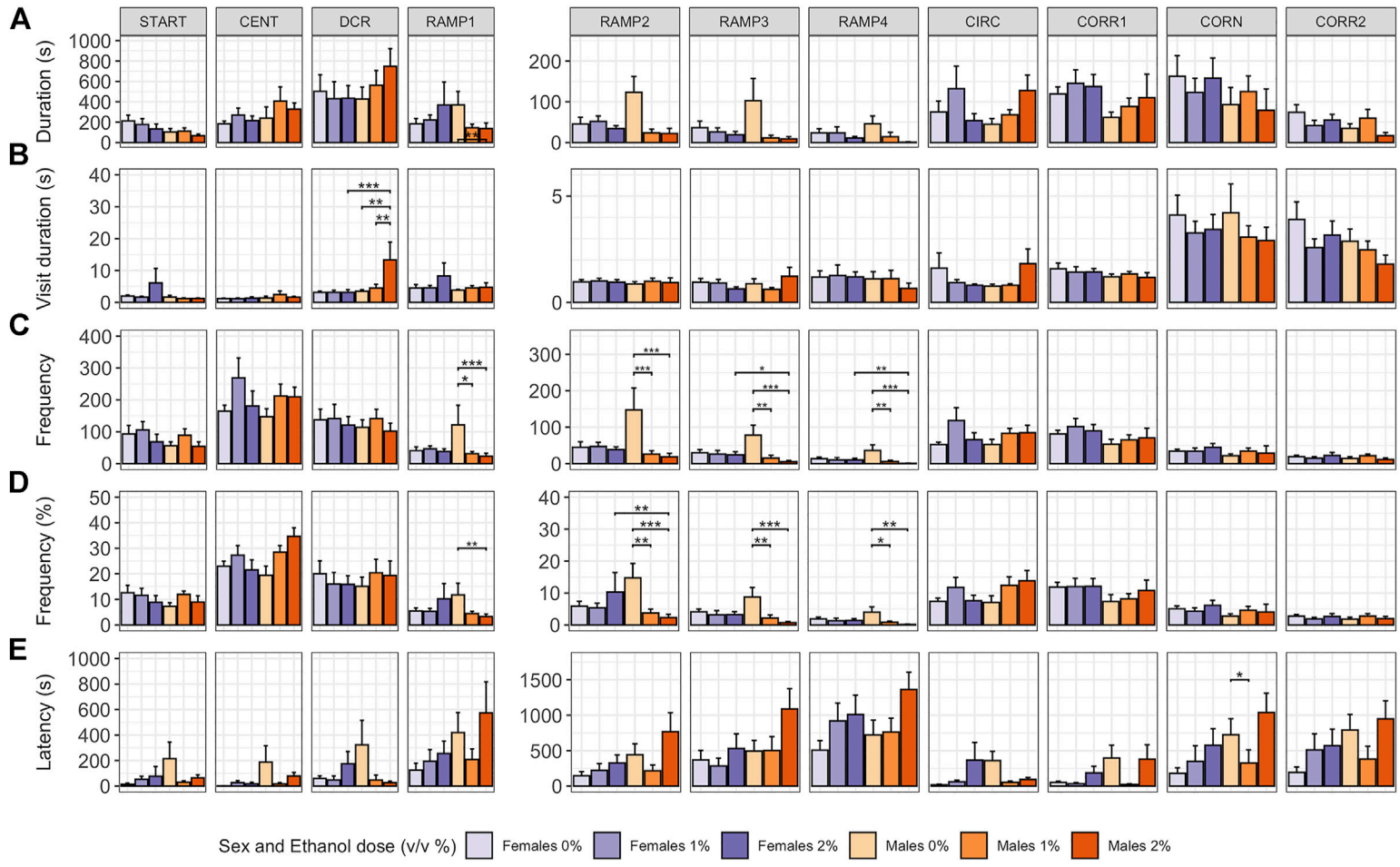

FIGURE 3 | Exploration of the zMCSF arena by male and female AB zebrafish acutely exposed to 0, 1 or 2% (v/v) ethanol for 30 min. Within each graph, the data is presented per Dose/Sex group. The different zones are presented in different columns. Rows contain different response variables: **(A)** Duration in zone (s), **(B)** Duration per visit in zone (s), **(C)** Frequency of zone entries, **(D)** Frequency of zone entries (as percentage of the total number of zone entries) and **(E)** Latency (s) until first entry into a zone. Colors indicate Dose/Sex group as follows: females (purple colors) and males (orange colors) zebrafish exposed to 0% (controls; light shades), 1% ethanol (medium dark shades) or 2% ethanol (dark shades). Bars represent mean ± SEM over the 30-min trial. Stars indicate significant differences (*$p < 0.05$, **$p < 0.01$, ***$p < 0.001$).

Regression analyses over time revealed sex-specific effects of Dose on activity patterns (**Tables 1**, **2**, **3** and **Figure 2B**). Both 1% and 2% males showed a more negative slope in distance moved over time compared to control males (LMM contrasts; males 0 vs 1%: $t_{2,1473} = 3.256$, $p = 0.014$; $t_{2,1473} = 3.344$, $p = 0.014$; **Table 3** and **Figure 2B**). While control and 1% females showed a decrease in distance moved over time, 2% females had a positive slope in distance moved over time (LMM contrast; females 0 vs 2%: $t_{2,1473} = -4.960$, $p < 0.001$; 1 vs 2%: $t_{2,1473} = -6.781$, $p < 0.001$; **Table 3** and **Figure 2B**). Finally, the slope of males and females differed significantly for the control dose (LMM contrast; $t_{2,45} = -3.070$, $p = 0.013$) and 2% dose (LMM contrast, $t_{2,45} = 6.780$, $p < 0.001$), but not for the 1% dose (LMM contrast; $t_{2,45} = -2.200$, $p = 0.068$; **Table 3** and **Figure 2B**). The patterns in velocity and total activity were highly similar to distance moved (**Supplementary Table S2**).

3.2.1 Exploratory Behavior, Risk Taking and Shelter Seeking

In males, ethanol dose influenced whether or not a fish explored all zones of the zMCSF (Poisson GLM, $\chi^2_{2,48} = 7.492$, $p = 0.024$; **Supplementary Table S2**). While for 1% males 9 out of 10 animals explored all zones, in 2% males, only 3 out of 9 animals explored all zones (**Supplementary Table S1**). Both ethanol dose and the sex of the fish influenced how long and how often animals visited the zones of the zMCSF, as indicated by significant three-way interactions between Zone, Dose and Sex for variables duration in zone, frequency in zone and percentage frequency in zone (**Supplementary Table S1, S2**). Compared to control males, 2% males spent shorter durations in RAMP1-4 (LMM contrasts; $t_{22,309} = 3.215$, $p = 0.022$; $t_{22,309} = 3.612$, $p = 0.005$; $t_{22,309} = 3.599$, $p = 0.006$; $t_{22,309} = 3.186$, $p = 0.024$; **Figure 3A** and **Supplementary Table S1**) and a longer duration per visit in the DCR (LMM contrast, $t_{22,392} = -3.974$, $p = 0.001$; **Figure 3B** and **Supplementary Table S1**). Graphical analysis of duration and frequency in zone over time revealed that the long visits to the DCR by the 2% males were particularly pronounced in the last 10 minutes of the test, a time at which control males explored RAMP1-4 (**Supplementary Figure S2**). While the 1% males also entered RAMP1-4 less often (LMM contrasts; $t_{22,309} = 3.288$, $p = 0.015$; $t_{22,309} = 4.195$, $p < 0.001$; $t_{22,309} = 3.872$, $p = 0.002$; $t_{22,309} = 3.968$, $p = 0.001$; **Figures 3C,D** and **Supplementary Table S1**), they did not pay long visits to the DCR (LMM contrast, $t_{22,392} = -0.345$, $p = 1.000$; **Figure 3B** and **Supplementary Table S1**).

In contrast to males, in females pairwise comparisons between control, 1% and 2% doses did not reveal any significant differences in zone-related variables (**Figure 3** and **Supplementary Table S1**). Control females furthermore did not differ from control males for any zone or variable (**Figure 3** and **Supplementary Table S1**). Although all female groups paid shorter visits to the DCR than all male groups (LMM contrast, $t_{10,383} = -3.372$, $p = 0.001$), this effect was driven by the long visits to the DCR by the 2% males.

4 DISCUSSION

In the present study, we exposed male and female zebrafish to control, 1% or 2% ethanol (v/v) for 30 min, after which we behaviorally phenotyped animals in the zMCSF test that we recently described (Vossen et al., 2022). Ethanol treatment differentially affected the behavior of female and male AB zebrafish. The strongest effects of the acute ethanol exposure were seen in the 2% male group, which showed a significant reduction in locomotory activity throughout the entire test, reduced risk taking, as indicated by spending less time on the inclined ramp and increased shelter seeking by longer duration per visit to the DCR. The 1% male group displayed effects in the same direction but of smaller magnitude; this group also explored the inclined ramp less, while no general reduction in activity nor an increased duration per visit to the DCR could be detected. Females exposed to 2% ethanol showed signs of lower activity during the first 10 minutes of the test, but gradually increased their activity over the test and became more active than both control and 1% females in the last 10 minutes. Explorative behavior was unaffected in 2% females. The 1% exposed females showed no alterations in any of the measured behaviors.

4.1 Sex Differences in the Response to Acute Ethanol Exposure

The observed effects of both the 1% and 2% dose on males may be best interpreted as sedative effects, which likely arise from the well-established motor suppressing and intoxicating effect of high ethanol doses (Koob et al., 1998). Although a reduced time on the ramp and longer visits to the DCR are usually interpreted as lower risk-taking and increased shelter seeking, respectively (Meyerson et al., 2013; Vossen et al., 2022), an alternative explanation is that the sedated males moved to the DCR to rest, thereby inevitably reducing the time spent on ramp. Indeed, we previously found that the majority of AB zebrafish choose the DCR as their "home base" (Vossen et al., 2022), i.e. a location in which the animal spends a disproportional amount of time and from which it makes round trips in different directions, which is often the preferred area for rest or sleep (Eilam and Golani, 1989; Stewart et al., 2010).

The mixed stimulatory/depressant effects on locomotory activity found in 2% females, with initial low activity followed by hyperactivity, show a striking resemblance to that of female mice exposed to an intermediate dose (Matchett and Erickson, 1977). While a low dose (0.5 or 1.0 g/kg i. p.) had mild stimulatory effects and a high dose (4.0 g/kg i. p.) produced a general reduction in activity, an intermediate dose (2.0 g/kg i. p.) produced first sedative followed by stimulatory effects on spontaneous locomotory behavior (Matchett and Erickson, 1977). It is possible that zebrafish females quickly eliminated the high ethanol dose from the blood (by ventilation or enzymatic oxidation, or both), whereby the lower concentration at the end of the test produced the stimulatory effect on locomotion. To test this hypothesis, more data on the rate of ethanol elimination in male and female zebrafish are needed. Hence, it seems that 2% ethanol was an intermediate dose for female zebrafish while it

constituted a high (sedative) dose for males. In other words, the dose-response curve of female zebrafish was shifted towards the right compared to males, making females the less affected sex in this strain and possibly, in this species. To further map the dose-response curve of both sexes, we suggest to behaviorally test female AB zebrafish at doses above 2% to capture at what dose sedative effects occur. In males, concentrations below 1% may convey at what concentration stimulatory and mixed stimulatory/depressant effects occur. It may also be necessary to increase the test duration to be able to estimate recovery periods for all doses.

The sex differences observed in AB zebrafish may be partially explained by the larger standardized weight of females compared to males (Fulton's condition factor (Fulton, 1902)). In a recent study using AB zebrafish from the same supplier (Vossen et al., 2020), we found females to have a 27% larger standardized weight (L.E. Vossen, unpublished data). This might well translate into a larger aqueous volume which renders a larger distribution volume for ethanol in females, reducing blood alcohol concentrations (Smith et al., 2013). Alternative explanations, such as a sex differences in absorption (Klockhoff et al., 2002), metabolizing enzymes present in the liver and stomach (Frezza et al., 1990; Baraona et al., 2001), an interaction effect with sex hormones (Dettling et al., 2008) or actual sex differences in the sensitivity of the brain at equal blood alcohol concentrations (Miller et al., 2009), as evident from human studies, should certainly not be excluded. An important recent discovery concerns the role of a brain metabolic pathway of ethanol in producing behavioral effects typical of intoxication (Jin et al., 2021).

4.2 Lack of Sex Differences in Control Animals

We observed few sex differences in unexposed AB strain females and males in the zMCSF, in line with our earlier study (Vossen et al., 2022). At baseline, control males increased their activity over time while control females showed a slight decrease, but we found no sex differences in activity or exploration over the whole trial. In conventional behavioral tests, female zebrafish often display a more "shy" or "reactive" stress coping style than males. Although there are considerable differences between strains and tests, females tend to show increased levels of thigmotaxis and shelter seeking (Dahlbom et al., 2011; Mustafa et al., 2019), a stronger diving response (Mustafa et al., 2019), lower activity in a novel environment (Mustafa et al., 2019) and more hesitation towards a novel object (Souza et al., 2021) compared to males. The absence of a sex difference in control animals in the zMCSF may be explained by the design of this arena (Vossen et al., 2022). Since males often display a higher activity in conventional tests, this may "drive" them into the center of the open field, the top zone of a novel tank diving arena, or the white compartment of a light/dark test, simply because there are no other zones to move in. In the zMCSF, the risky areas only comprise a small part of the arena, therefore a move into this area may be a more active choice for exploration versus shelter seeking. Hence the zMCSF may allow for a clearer separation between locomotory and explorative activity. Indeed, a study on acute ethanol exposure in male Wistar rats using the MCSF arena showed motor stimulative effects at a low ethanol dose (0.5 g/kg i. p.) and sedative effects at dose (1.5 g/kg i. p.) not commonly reported to induce sedation in conventional behavioral tests (Karlsson and Roman, 2016).

4.3 On the Use of the AB Strain

Our results stand in contrast to a study by Souza *et al.* (2021), where a different strain of zebrafish (short-fin zebrafish from a local pet store in Brazil) was exposed to 0, 0.25, 0.5 or 1.0% (v/v) ethanol for one hour, and subsequently tested in a novel object test (Souza et al., 2021). Both sexes showed a reduction in locomotory activity in response to the 1.0% dose. While control females spent less time in the center of the arena than control males, 0.25% exposed females spent equal time in the center as males. Compared to males exposed to the same dose, 0.5% exposed females swam faster towards and kept a greater distance to, the novel object and spent more time in the peripheral zone. The results were interpreted as an anxiolytic effect of 0.5% ethanol in females, that was absent in males (Souza et al., 2021). One explanation for the discrepancy between the studies may lie in the use of different strains. It has been noted before that AB zebrafish in general show aberrant behavior (Gerlai et al., 2008; Gorissen et al., 2015; Vossen et al., 2020) and more specifically, display a distinct response to ethanol in comparison to other strains, both in terms of behavior and monoamine neurotransmitter release (Gerlai et al., 2008; Gerlai et al., 2009). Nonetheless, most mutant strains are derived from the AB strain, which makes the characterization of the pharmacological responses in this specific strain important. Furthermore, it seems that results obtained on AB zebrafish are coherent within this strain. For example, similar sex-specific effects as found herein were detected in AB zebrafish exposed to environmental concentrations (μg L^{-1} range) of the anxiolytic benzodiazepine oxazepam (Vossen et al., 2020). AB males showed a dose-dependent increase in duration in the bottom of a diving arena and an associated decrease in velocity, indicative of a sedative effect, while AB females were largely unaffected at all concentrations (Vossen et al., 2020).

4.4 Conclusions

We found significant sex differences in the effect of acute ethanol exposure (1 or 2% (v/v) for 30 min) on adult zebrafish behavior in a complex test arena, the zMCSF. Females were more tolerant, showing mixed depressive/stimulatory effects on locomotory behavior for the 2% dose. Males displayed clear signs of sedation as indicated by reduced activity and exploration and retreat to the sheltered area under the 2% dose, and to a lesser extend under 1% exposure. Our findings emphasize the importance of explicitly including effects of sex (Souza et al., 2021) and time course (Tran and Gerlai, 2013; Pannia et al., 2014) in analyses of behavioral experiments on adult zebrafish. The use of the zMCSF test may have enabled a clearer distinction between locomotory activity and risk-taking/shelter seeking behavior. However, further pharmacological validation of the zMCSF test is needed.

DATA AVAILABILITY STATEMENT

The data generated for this study can be found on figshare with the identifier https://doi.org/10.6084/m9.figshare.18258962.

ETHICS STATEMENT

The animal study was reviewed and approved by the Uppsala Regional Animal Ethical Committee (permit C55/13), following the guidelines of the Swedish Legislation on Animal Experimentation (Animal Welfare Act SFS1998:56) and the European Union Directive on the Protection of Animals Used for Scientific Purposes (Directive 2010/63/EU).

AUTHOR CONTRIBUTIONS

ER conceptualized and designed the study and supervised RB and PR. SW provided supervision and resources. RB and PR performed the experiments. LV validated, curated and visualized the data, conducted the statistical analyses and wrote the first draft of the manuscript. All authors contributed to manuscript revision, read, and approved the submitted version.

FUNDING

This work was supported by grants from the Torvald and Britta Gahlins Foundation, the Carl Tryggers Foundation (CTS 20:352) and the Facias Foundation (all to ER).

ACKNOWLEDGMENTS

The authors thank MSc Nikita Tjernström, Dr Arshi Mustafa, and the staff of the Technical Service at BMC and the Uppsala University Behavioral Facility (UUBF), Disciplinary Domain of Medicine and Pharmacy, Uppsala University.

SUPPLEMENTARY MATERIAL

The Supplementary Material for this article can be found online at: https://www.frontiersin.org/articles/10.3389/fphar.2022.853936/full#supplementary-material

REFERENCES

Abrahao, K. P., Salinas, A. G., and Lovinger, D. M. (2017). Alcohol and the Brain: Neuronal Molecular Targets, Synapses, and Circuits. *Neuron* 96, 1223–1238. doi:10.1016/j.neuron.2017.10.032

Baraona, E., Abittan, C. S., Dohmen, K., Moretti, M., Pozzato, G., Chayes, Z. W., et al. (2001). Gender Differences in Pharmacokinetics of Alcohol. *Alcohol Clin. Exp. Res.* 25, 502–507. doi:10.1111/j.1530-0277.2001.tb02242.x

Bates, D., Mächler, M., Bolker, B., and Walker, S. (2015). Fitting Linear Mixed-Effects Models Using Lme4. *J. Stat. Softw.* 67, 1–48. doi:10.18637/jss.v067.i01

Bell, R. L., Hauser, S. R., Liang, T., Sari, Y., Maldonado-Devincci, A., and Rodd, Z. A. (2017). Rat Animal Models for Screening Medications to Treat Alcohol Use Disorders. *Neuropharmacology* 122, 201–243. doi:10.1016/j.neuropharm.2017.02.004

Bikovski, L., Robinson, L., Konradsson-Geuken, A., Kullander, K., Viereckel, T., Winberg, S., et al. (2020). Lessons, Insights and Newly Developed Tools Emerging from Behavioral Phenotyping Core Facilities. *J. Neurosci. Methods* 334, 108597. doi:10.1016/j.jneumeth.2020.108597

Calabrese, E. J., and Baldwin, L. A. (2003). Ethanol and Hormesis. *Crit. Rev. Toxicol.* 33, 407–424. doi:10.1080/713611043

Carvan, M. J., 3rd, Loucks, E., Weber, D. N., and Williams, F. E. (2004). Ethanol Effects on the Developing Zebrafish: Neurobehavior and Skeletal Morphogenesis. *Neurotoxicol Teratol.* 26, 757–768. doi:10.1016/j.ntt.2004.06.016

Clayman, C. L., Malloy, E. J., Kearns, D. N., and Connaughton, V. P. (2017). Differential Behavioral Effects of Ethanol Pre-exposure in Male and Female Zebrafish (*Danio rerio*). *Behav. Brain Res.* 335, 174–184. doi:10.1016/j.bbr.2017.08.007

Dahlbom, S. J., Backström, T., Lundstedt-Enkel, K., and Winberg, S. (2012). Aggression and Monoamines: Effects of Sex and Social Rank in Zebrafish (*Danio rerio*). *Behav. Brain Res.* 228, 333–338. doi:10.1016/j.bbr.2011.12.011

Dahlbom, S. J., Lagman, D., Lundstedt-Enkel, K., Sundström, L. F., and Winberg, S. (2011). Boldness Predicts Social Status in Zebrafish (*Danio rerio*). *PLoS One* 6, e23565. doi:10.1371/journal.pone.0023565

Dettling, A., Skopp, G., Graw, M., and Haffner, H. T. (2008). The Influence of Sex Hormones on the Elimination Kinetics of Ethanol. *Forensic Sci. Int.* 177, 85–89. doi:10.1016/j.forsciint.2007.11.002

Dlugos, C. A., Brown, S. J., and Rabin, R. A. (2011). Gender Differences in Ethanol-Induced Behavioral Sensitivity in Zebrafish. *Alcohol* 45, 11–18. doi:10.1016/j.alcohol.2010.08.018

Dlugos, C. A., and Rabin, R. A. (2003). Ethanol Effects on Three Strains of Zebrafish: Model System for Genetic Investigations. *Pharmacol. Biochem. Behav.* 74, 471–480. doi:10.1016/s0091-3057(02)01026-2

Dos Santos, B. E., Giacomini, A. C. V. V., Marcon, L., Demin, K. A., Strekalova, T., de Abreu, M. S., et al. (2021). Sex Differences Shape Zebrafish Performance in a Battery of Anxiety Tests and in Response to Acute Scopolamine Treatment. *Neurosci. Lett.* 759, 135993. doi:10.1016/j.neulet.2021.135993

Echevarria, D. J., Toms, C. N., and Jouandot, D. J. (2011). Alcohol-induced Behavior Change in Zebrafish Models. *Rev. Neurosci.* 22, 85–93. doi:10.1515/RNS.2011.010

Eilam, D., and Golani, I. (1989). Home Base Behavior of Rats (Rattus norvegicus) Exploring a Novel Environment. *Behav. Brain Res.* 34, 199–211. doi:10.1016/s0166-4328(89)80102-0

Frezza, M., Di Padova, C., Pozzato, G., Terpin, M., Baraona, E., and Lieber, C. S. (1990). High Blood Alcohol Levels in Women. The Role of Decreased Gastric Alcohol Dehydrogenase Activity and First-Pass Metabolism. *N. Engl. J. Med.* 322, 95–99. doi:10.1056/NEJM199001113220205

Fulton, T. W. (1902).*The Rate of Growth of Fishes, Annual Report of the Fishery Board for Scotland*. Edinburgh: Neill and Co.

Gebauer, D. L., Pagnussat, N., Piato, A. L., Schaefer, I. C., Bonan, C. D., and Lara, D. R. (2011). Effects of Anxiolytics in Zebrafish: Similarities and Differences between Benzodiazepines, Buspirone and Ethanol. *Pharmacol. Biochem. Behav.* 99, 480–486. doi:10.1016/j.pbb.2011.04.021

Genario, R., de Abreu, M. S., Giacomini, A. C. V. V., Demin, K. A., and Kalueff, A. V. (2020). Sex Differences in Behavior and Neuropharmacology of Zebrafish. *Eur. J. Neurosci.* 52, 2586–2603. doi:10.1111/ejn.14438

Gerlai, R., Ahmad, F., and Prajapati, S. (2008). Differences in Acute Alcohol-Induced Behavioral Responses Among Zebrafish Populations. *Alcohol Clin. Exp. Res.* 32, 1763–1773. doi:10.1111/j.1530-0277.2008.00761.x

Gerlai, R., Chatterjee, D., Pereira, T., Sawashima, T., and Krishnannair, R. (2009). Acute and Chronic Alcohol Dose: Population Differences in Behavior and Neurochemistry of Zebrafish. *Genes Brain Behav.* 8, 586–599. doi:10.1111/j.1601-183X.2009.00488.x

Gerlai, R., Lahav, M., Guo, S., and Rosenthal, A. (2000). Drinks like a Fish: Zebra Fish (*Danio rerio*) as a Behavior Genetic Model to Study Alcohol Effects. *Pharmacol. Biochem. Behav.* 67, 773–782. doi:10.1016/s0091-3057(00)00422-6

Gerlai, R., Lee, V., and Blaser, R. (2006). Effects of Acute and Chronic Ethanol Exposure on the Behavior of Adult Zebrafish (*Danio rerio*). *Pharmacol. Biochem. Behav.* 85, 752–761. doi:10.1016/j.pbb.2006.11.010

Gerlai, R. (2003). Zebra Fish: An Uncharted Behavior Genetic Model. *Behav. Genet.* 33, 461–468. doi:10.1023/a:1025762314250

Goodman, A. C., and Wong, R. Y. (2020). Differential Effects of Ethanol on Behavior and GABAA Receptor Expression in Adult Zebrafish (*Danio rerio*) with Alternative Stress Coping Styles. *Sci. Rep.* 10, 13076. doi:10.1038/s41598-020-69980-2

Gorissen, M., Manuel, R., Pelgrim, T. N., Mes, W., de Wolf, M. J., Zethof, J., et al. (2015). Differences in Inhibitory Avoidance, Cortisol and Brain Gene Expression in TL and AB Zebrafish. *Genes Brain Behav.* 14, 428–438. doi:10.1111/gbb.12220

Gupta, T., and Mullins, M. C. (2010). Dissection of Organs from the Adult Zebrafish. *J. Vis. Exp.* 2010, 1717. doi:10.3791/1717

Jin, S., Cao, Q., Yang, F., Zhu, H., Xu, S., Chen, Q., et al. (2021). Brain Ethanol Metabolism by Astrocytic ALDH2 Drives the Behavioural Effects of Ethanol Intoxication. *Nat. Metab.* 3, 337–351. doi:10.1038/s42255-021-00357-z

Karlsson, O., and Roman, E. (2016). Dose-dependent Effects of Alcohol Administration on Behavioral Profiles in the MCSF Test. *Alcohol* 50, 51–56. doi:10.1016/j.alcohol.2015.10.003

Klockhoff, H., Näslund, I., and Jones, A. W. (2002). Faster Absorption of Ethanol and Higher Peak Concentration in Women after Gastric Bypass Surgery. *Br. J. Clin. Pharmacol.* 54, 587–591. doi:10.1046/j.1365-2125.2002.01698.x

Koob, G. F., Roberts, A. J., Schulteis, G., Parsons, L. H., Heyser, C. J., Hyytiä, P., et al. (1998). Neurocircuitry Targets in Ethanol Reward and Dependence. *Alcohol Clin. Exp. Res.* 22, 3–9. doi:10.1111/j.1530-0277.1998.tb03611.x

Lenth, R. (2020). Emmeans: Estimated Marginal Means, Aka Least-Squares Means. *Am. Statistician* 34 (4), 216–221. Available at: https://github.com/rvlenth/emmeans

Liu, K., Petree, C., Requena, T., Varshney, P., and Varshney, G. K. (2019). Expanding the CRISPR Toolbox in Zebrafish for Studying Development and Disease. *Front. Cell Dev. Biol.* 7, 13. doi:10.3389/fcell.2019.00013

Lockwood, B., Bjerke, S., Kobayashi, K., and Guo, S. (2004). Acute Effects of Alcohol on Larval Zebrafish: a Genetic System for Large-Scale Screening. *Pharmacol. Biochem. Behav.* 77, 647–654. doi:10.1016/j.pbb.2004.01.003

Matchett, J. A., and Erickson, C. K. (1977). Alteration of Ethanol-Induced Changes in Locomotor Activity by Adrenergic Blockers in Mice. *Psychopharmacol. Berl.* 52, 201–206. doi:10.1007/BF00439111

Mathur, P., and Guo, S. (2011). Differences of Acute versus Chronic Ethanol Exposure on Anxiety-like Behavioral Responses in Zebrafish. *Behav. Brain Res.* 219, 234–239. doi:10.1016/j.bbr.2011.01.019

Meyerson, B. J., Augustsson, H., Berg, M., and Roman, E. (2006). The Concentric Square Field: A Multivariate Test Arena for Analysis of Explorative Strategies. *Behav. Brain Res.* 168, 100–113. doi:10.1016/j.bbr.2005.10.020

Meyerson, B. J., Jurek, B., and Roman, E. (2013). A Rank-Order Procedure Applied to an Ethoexperimental Behavior Model-The Multivariate Concentric Square Field^{TM}(MCSF) Test. *Jbbs* 03, 350–361. doi:10.4236/jbbs.2013.34035

Miller, M. A., Weafer, J., and Fillmore, M. T. (2009). Gender Differences in Alcohol Impairment of Simulated Driving Performance and Driving-Related Skills. *Alcohol Alcohol* 44, 586–593. doi:10.1093/alcalc/agp051

Mustafa, A., Roman, E., and Winberg, S. (2019). Boldness in Male and Female Zebrafish (*Danio rerio*) Is Dependent on Strain and Test. *Front. Behav. Neurosci.* 13, 248. doi:10.3389/fnbeh.2019.00248

Pannia, E., Tran, S., Rampersad, M., and Gerlai, R. (2014). Acute Ethanol Exposure Induces Behavioural Differences in Two Zebrafish (*Danio rerio*) Strains: a Time Course Analysis. *Behav. Brain Res.* 259, 174–185. doi:10.1016/j.bbr.2013.11.006

Peterson, R. A., and Cavanaugh, J. E. (2019). Ordered Quantile Normalization: a Semiparametric Transformation Built for the Cross-Validation Era. *J. Appl. Statistics* 47 (13-15), 1–16. doi:10.1080/02664763.2019.1630372

Peterson, R. A. (2021). Finding Optimal Normalizing Transformations via bestNormalize. *R J.* 13, 310–329. doi:10.32614/rj-2021-041

Pohorecky, L. A. (1977). Biphasic Action of Ethanol. *Biobehav. Rev.* 1, 231–240. doi:10.1016/0147-7552(77)90025-0

Poznyak, V., and Rekve, D. (2018). "*Global Status Report on Alcohol and Health 2018*. Geneva: World Health Organization," 450.

R Core Team (2020). *A Language and Environment for Statistical Computing*. Vienna, Austria: R Foundation for Statistical Computing.

Rosemberg, D. B., Braga, M. M., Rico, E. P., Loss, C. M., Córdova, S. D., Mussulini, B. H., et al. (2012). Behavioral Effects of Taurine Pretreatment in Zebrafish Acutely Exposed to Ethanol. *Neuropharmacology* 63, 613–623. doi:10.1016/j.neuropharm.2012.05.009

Smith, D. L., Jr., Barry, R. J., Powell, M. L., Nagy, T. R., D'Abramo, L. R., and Watts, S. A. (2013). Dietary Protein Source Influence on Body Size and Composition in Growing Zebrafish. *Zebrafish* 10, 439–446. doi:10.1089/zeb.2012.0864

Souza, T. P., Franscescon, F., Stefanello, F. V., Müller, T. E., Santos, L. W., and Rosemberg, D. B. (2021). Acute Effects of Ethanol on Behavioral Responses of Male and Female Zebrafish in the Open Field Test with the Influence of a Non-familiar Object. *Behav. Process.* 191, 104474. doi:10.1016/j.beproc.2021.104474

Stewart, A., Cachat, J., Wong, K., Gaikwad, S., Gilder, T., DiLeo, J., et al. (2010). Homebase Behavior of Zebrafish in Novelty-Based Paradigms. *Behav. Process.* 85, 198–203. doi:10.1016/j.beproc.2010.07.009

Tran, S., and Gerlai, R. (2013). Time-course of Behavioural Changes Induced by Ethanol in Zebrafish (*Danio rerio*). *Behav. Brain Res.* 252, 204–213. doi:10.1016/j.bbr.2013.05.065

Vossen, L. E., Červený, D., Sen Sarma, O., Thörnqvist, P. O., Jutfelt, F., Fick, J., et al. (2020). Low Concentrations of the Benzodiazepine Drug Oxazepam Induce Anxiolytic Effects in Wild-Caught but Not in Laboratory Zebrafish. *Sci. Total Environ.* 703, 134701. doi:10.1016/j.scitotenv.2019.134701

Vossen, L. E., Brunberg, R., Rådén, P., Winberg, S., and Roman, E. (2022). The Zebrafish Multivariate Concentric Square Field: A Standardized Test for Behavioral Profiling of Zebrafish (*Danio rerio*). *Front. Behav. Neurosci.* 16. 744533. doi:10.3389/fnbeh.2022.744533

Wickham, H. (2016). *ggplot2: Elegant Graphics for Data Analysis*. New York: Springer-Verlag.

Conflict of Interest: The authors declare that the research was conducted in the absence of any commercial or financial relationships that could be construed as a potential conflict of interest.

Publisher's Note: All claims expressed in this article are solely those of the authors and do not necessarily represent those of their affiliated organizations, or those of the publisher, the editors and the reviewers. Any product that may be evaluated in this article, or claim that may be made by its manufacturer, is not guaranteed or endorsed by the publisher.

frontiers | Frontiers in Pharmacology

ORIGINAL RESEARCH
published: 09 June 2022
doi: 10.3389/fphar.2022.841423

High Affinity Decynium-22 Binding to Brain Membrane Homogenates and Reduced Dorsal Camouflaging after Acute Exposure to it in Zebrafish

Georgianna G. Gould[1,2]*, *Priscilla A. Barba-Escobedo*[1,3], *Rebecca E. Horton*[1,2] and *Lynette C. Daws*[1,2,4]

[1]Center for Biomedical Neuroscience, University of Texas Health Science Center at San Antonio, San Antonio, TX, United States, [2]Department of Cellular and Integrative Physiology, University of Texas Health Science Center at San Antonio, San Antonio, TX, United States, [3]Department of Endodontics, University of Texas Health Science Center at San Antonio, San Antonio, TX, United States, [4]Department of Pharmacology, University of Texas Health Science Center at San Antonio, San Antonio, TX, United States

Organic cation transporters (OCTs) are expressed in the mammalian brain, kidney, liver, placenta, and intestines, where they facilitate the transport of cations and other substrates between extracellular fluids and cells. Despite increasing reliance on ectothermic vertebrates as alternative toxicology models, properties of their OCT homologs transporting many drugs and toxins remain poorly characterized. Recently, in zebrafish (*Danio rerio*), two proteins with functional similarities to human OCTs were shown to be highly expressed in the liver, kidney, eye, and brain. This study is the first to characterize *in vivo* uptake to the brain and the high-affinity brain membrane binding of the mammalian OCT blocker 1-1′-diethyl-2,2′cyanine iodide (decynium-22 or D-22) in zebrafish. Membrane saturation binding of [^{3}H] D-22 in pooled zebrafish whole brain *versus* mouse hippocampal homogenates revealed a high-affinity binding site with a K_D of 5 ± 2.5 nM and Bmax of 1974 ± 410 fmol/mg protein in the zebrafish brain, and a K_D of 3.3 ± 2.3 and Bmax of 704 ± 182 fmol/mg protein in mouse hippocampus. The binding of [^{3}H] D-22 to brain membrane homogenates was partially blocked by the neurotoxic cation 1-methyl-4-phenylpyridinium (MPP+), a known OCT substrate. To determine if D-22 bath exposures reach the brain, zebrafish were exposed to 25 nM [^{3}H] D-22 for 10 min, and 736 ± 68 ng/g wet weight [^{3}H] D-22 was bound. Acute behavioral effects of D-22 in zebrafish were characterized in two anxiety-relevant tests. In the first cohort of zebrafish, 12.5, 25, or 50 mg/L D-22 had no effect on their height in the dive tank or entries and time spent in white arms of a light/dark plus maze. By contrast, 25 mg/L buspirone increased zebrafish dive tank top-dwelling ($p < 0.05$), an anticipated anxiolytic effect. However, a second cohort of zebrafish treated with 50 mg/L D-22 made more white arm entries, and females spent more time in white than controls. Based on these findings, it appears that D-22 bath treatments reach the zebrafish brain and have partial anxiolytic properties, reducing anti-predator dorsal camouflaging, without increasing vertical exploration. High-affinity binding of [^{3}H] D-22 in zebrafish

OPEN ACCESS

Edited by:
Anna Siebel,
Universidade Comunitária da Região de Chapecó, Brazil

Reviewed by:
Maria Marchese,
Stella Maris Foundation (IRCCS), Italy
Declan Ali,
University of Alberta, Canada

***Correspondence:**
Georgianna G. Gould
gouldg@uthscsa.edu

Specialty section:
This article was submitted to Experimental Pharmacology and Drug Discovery, a section of the journal Frontiers in Pharmacology

Received: *22 December 2021*
Accepted: *29 March 2022*
Published: *09 June 2022*

Citation:
Gould GG, Barba-Escobedo PA, Horton RE and Daws LC (2022) High Affinity Decynium-22 Binding to Brain Membrane Homogenates and Reduced Dorsal Camouflaging after Acute Exposure to it in Zebrafish. Front. Pharmacol. 13:841423. doi: 10.3389/fphar.2022.841423

brain and mouse brain was similar, with nanomolar affinity, possibly at conserved OCT site(s).

Keywords: anxiety, black–white plus maze, *Danio rerio* (zebrafish), dive tank, SLC22A, pseudoisocyanine, uptake 2 transporters, predator avoidance

INTRODUCTION

Organic cation transporters (OCTs) are transmembrane proteins of the solute carrier family SLC22A responsible for bi-directional facilitated sodium-independent electrogenic transport of compounds that are mono or multivalent cations at physiological pH. They are blocked by hydrophobic polyamines and steroid hormones (Koepsell et al., 2007; Hill et al., 2011; Sala-Rabanal et al., 2013). In mammals, there are three isoforms: OCT1 is richly expressed in the liver, kidneys, and gut; OCT2 is widely found in the brain, kidneys, and to a lesser extent, in other peripheral organs; and OCT3 is predominant in the heart, lungs, adipose tissue, placenta, and brain, and also occurs in other peripheral organs (Koepsell et al., 2007; Nies et al., 2011; Koepsell, 2020; Samodelov et al., 2020; Sweet, 2021). Substrates of mammalian OCTs include the biogenic amines serotonin, norepinephrine, dopamine, and histamine; antioxidants; vitamins such as choline and thiamine; metabolites such as guanidine or putrescine; xenobiotic compounds including drugs such as metformin; and cationic neurotoxins such as the 1-methyl-4-phenyl-1,2,3,6-tetrahydropyridine (MPTP) cation, 1-methyl-4-phenyl pyridinium (MPP+), or paraquat cations that are used to model Parkinson's disease in rodents (Cui et al., 2009; Rappold et al., 2011; Nies et al., 2011; Bönisch, 2021; Yee and Giacomini, 2021). The pseudoisocyanine 1-1′-diethyl-2,2′cyanine iodide (decynium-22 or D-22) blocks human and mouse OCTs at low nM concentrations, and because of this property, D-22 is a useful pharmacological tool in the studies of OCT functions (Hayer et al., 1999; Hayer-Zillgen et al., 2002; Fraser-Spears et al., 2019; ; Bönisch, 2021).

Human gene polymorphisms affecting the expression or function of OCTs are associated with substance abuse (Aoyama et al., 2006; Bousman et al., 2009; Bergen et al., 2014), resistance to drugs such as metformin (Nies et al., 2009; Becker et al., 2010; Chen et al., 2010; Chen et al., 2015), and a more rapid progression of Parkinson's disease (Becker et al., 2011). Developmental language delays, hypotonia, and motor speech disorders were evident in two cases of chromosome 6q deletions that impacted OCT2 and OCT3 genes (Peter et al., 2017). Given this, gene polymorphisms impacting OCT expression or function may contribute to psychiatric disorders such as depression, anxiety, and autism spectrum disorders, but testing this hypothesis requires further clinical investigations (Daws et al., 2013; Gasser and Daws, 2017; Daws, 2021). In humans and rodents, OCTs have lower affinity for monoamine transmitters than sodium-dependent serotonin (SLC6A4), norepinephrine (SLC6A2), or dopamine (SLC6A3) transporters (Fraser-Spears et al., 2019). SLC6A transporters are the primary mediators of monoamine clearance, so they are called "uptake 1," while in most circumstances, OCTs play an auxiliary role in monoamine clearance and are referred to as "uptake 2" (Daws et al., 2013; Gasser, 2021). However, OCTs have a greater capacity to clear monoamines at high concentrations or if SLC6A transporters are compromised (Daws, 2009).

Rodent studies show that OCTs modulate monoamine availability in the brain to shape mood and behaviors. However, OCT effects on anxiety have been equivocal. For example, OCT3 knockout mice were more active and exhibited less anxiety in some tests (Wultsch et al., 2009), but were more stressed, anxious, and less sensitive to psychostimulants in others (Vialou et al., 2008). OCT3 knockout males had lower social interaction preferences than wild types (Garbarino et al., 2019), which may stem from early developmental dysregulation of serotonin neurotransmission (Karahoda et al., 2020). Systemic D-22 treatment blocked the serotonin uptake and produced antidepressant-like effects independent of the serotonin transporter (Baganz et al., 2008; Horton et al., 2013). Co-administration of D-22 with monoamine reuptake inhibitors enhanced antidepressant effects in wild-type mice (Krause-Heuer et al., 2017; Bowman et al., 2020). Since acute effects of D-22 on anxiety-relevant behaviors were not well characterized, one goal of this study was to use zebrafish to look for such effects. We used two different tests, dive tank and light–dark plus maze with established protocols to assess acute D-22 effects on anxiety-based behaviors (Gould, 2010a; Sackerman et al., 2010; Connors et al., 2014).

OCTs have similar structure and function in bacteria, plants, and animals (Koepsell et al., 2007). Two OCT orthologs were recently discovered and characterized in zebrafish (*Danio rerio*): drOCT1 on chromosome 20 and drOCT2 on chromosome 17; they are most syntenic with human OCT1, OCT2, and OCT3 which occur as a gene cluster on chromosome 6 (Mihaljevic et al., 2016). The expression of drOCT1 was high in liver and kidneys, while drOCT2 was high in eyes, and sex dependent expression in muscle, gonads, and gills. Brain drOCT expression in males was higher than that in females. Furthermore, the same group found many similarities in functional properties among human OCTs and zebrafish drOCT1 through homology modeling and transfection of drOCT1 into human embryonic kidney (HEK293T) cells for fluorescent substrate uptake saturation and concentration-dependent inhibition assays (Mihaljević et al., 2017). However, neither ligand-binding properties of D-22 in zebrafish nor if bath exposures to D-22 can even reach the brain were previously reported. Since pharmacological profile differences occur even among mouse, rat, and human OCTs for substrates and blockers (Maier et al., 2021), the second goal of this study was to characterize the high-affinity binding properties of radiolabeled D-22 in zebrafish whole-brain membrane homogenates that could underlie any acute changes in their anxiety behaviors.

MATERIALS AND METHODS

Animals

All procedures involving live zebrafish were approved under protocol #090124 by the University of Texas Health Science Center at San Antonio Institutional Animal Care and Use Committee in accord with the National Institutes of Health guidelines (http://oacu.od.nih.gov/ARAC). A hundred zebrafish (*Danio rerio*) 4–6 months old with a mean ± SEM weight of 0.285 ± 0.016 g were obtained in 2009 from Aquatic Eco-Systems Inc (Apopka, FL, United States). Subsequently, 48 zebrafish weighing 0.171 ± 0.013 g were obtained for additional behavior tests from Carolina Biological Supply Co. (Burlington, NC, United States). Fish were housed in mixed-sex groups of six to eight for 2–3 months in the original 2009 studies, and one week for a more recent study to acclimate before use in 3 L tanks of a benchtop flow through aquatic habitat (Aquatic Eco-Systems, Apopka, FL, United States) filled with 25–27°C deionized water (Nanopure, Barstead, Dubuque, IA, United States) supplemented with 200 mg/L "Instant Ocean" salts (Aquarium Systems, Mentor, OH, United States), pH = 7.2–7.6. Light/dark cycles were 14:10 h (lights on at 700 h and off at 2,100 h). Fish were fed "Top Fin" tropical flakes once per day (Pacific Coast Distributing, Phoenix, AZ, United States).

Six constitutive serotonin transporter knockout heterozygous six-month-old male mice weighing 26 ± 2 g came from an in-house breeding colony established by the founders generously provided by Dr. Dennis Murphy (NIMH) in 1999 (Bengel et al., 1998). The mice on a congenic C57BL/6J background were littermates derived from heterozygous mating and were raised and housed together in same-sex groups from weaning until use in radioligand binding experiments. The mice were housed in a temperature- and humidity-controlled vivarium under a 12-h light/dark cycle (lights on at 600 h) with *ad libitum* access to rodent diet (Teklad 7,912 irradiated, Envigo) and water (reverse osmosis, acidified to pH 2.5–3 with HCl). Their use for tissue was IACUC-approved under protocol #020014.

Acute Drug Treatments of Zebrafish for Behavior Testing

Initially, 45 zebrafish, a mixed assortment of males and females, were randomly assigned to seven different compound exposure groups. All compounds were from Sigma Aldrich (St. Louis, MO, United States). Fish were individually bath-exposed for 5 min to drugs dissolved in 20 ml solutions in 50-ml glass beakers. Dimethyl sulfoxide (1%) was used as a control or vehicle for all treatments. The anti-anxiety drug buspirone, a serotonin 5-HT_{1A} receptor partial agonist, was used at 25 mg/L as a positive control since it had anxiolytic effects in zebrafish dive tank tests (Bencan et al., 2009). D-22 was tested at 12.5, 25, and 50 mg/L. In addition, the mammalian stress hormone corticosterone (CORT) was administered at 25 mg/L. This corticosterone treatment was included because in vitro it has been shown to block mammalian OCTs (Gasser, 2021). Red food dye (five drops, red #40 and #3, H.E.B, San Antonio, TX, United States) was used as a color control for the D-22 (50 mg/L) solution since it had the same wavelength and similar amplitude in the spectrophotometer (DU-600, Beckman, Brea, CA, United States) absorption spectrum.

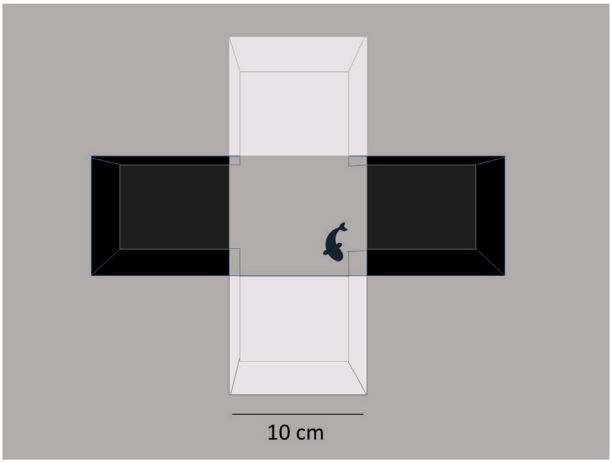

FIGURE 1 | Light/dark plus maze. The aquatic cross maze is set up with a 3 × 3 box configuration at the intersection of the maze. Fish explore the environment under bright light (800 lumens from a 60 W bulb), and the behavior is video-recorded for 5 min. Treatment-blind observers collect data on time spent in different areas of the maze.

In a follow-up experiment, 24 females and males were used. Sex of these fish was visually determined by a combination of early morning inspection for female genital papilla as described by Yossa et al. (2013) and male yellow or golden-colored pectoral fin breeding tubercles as described by McMillan et al. (2015) before assigning D-22 (50 mg/L) or vehicle treatments to 12 of each sex. These characteristics are consistent with descriptive colorations used to determine sex in the initial study as per Paull et al. (2008). After 5 min bath exposures to treatments or controls for all experiments, zebrafish were placed in 100 ml habitat water for 5 min to rinse and were given drugs to approach maximal physiological efficacy before a series of two anxiety-relevant tests of response to a novel environment.

Novel Environment Test 1: Height in Dive Tank Water Column

A 4-L triangular acrylic tank (Aquascene 1, TopFin, Phoenix, AZ) was filled 18 cm deep with 3.5 L of home tank water. Lines dividing it into thirds were drawn in advance on the outside with a permanent marker. The tank sat on a black countertop, with a 24 cm × 22 cm whiteboard against its back wall to enhance contrast. After drug exposure and 5 min in holding, each zebrafish was placed in a dive tank, observed, and digitally recorded (HP Photosmart R742, OfficeMax, United States) for 5 min to measure the time spent in the top 2/3 *vs.* the bottom 1/3 of the tank, as previously described by Sackerman et al. (2010). In the initial study, Bartlett's test ($p = 0.7$) showed standard deviations among groups that were similar so the group means were compared by the one-way analysis of variance (ANOVA) with Dunnett's multiple comparisons used for *post hoc* analysis of significant effects. In the follow-up study, a two-way (sex × treatment) ANOVA with Sidak's *post hoc* analysis for significant outcomes was performed using GraphPad Prism nine.

Novel Environment Test 2: Light-Dark Plus Maze Arm Preference

After dive tank tests, fish were tested in the aquatic light–dark plus maze that was performed as described by Gould (2010a). Briefly, a clear acrylic cross maze (Noldus, Leesburg, VA, United States) was used in a 30 cm^2 × 30 cm^2 plus configuration. Opposite arms were covered with black polyethylene and the other two with white polyethylene 10 cm^2 squares (**Figure 1**). The gray background of the copy stand (Kaiser RS1, B&H Photo, New York, NY) showed through the middle 10 cm^2 section of the maze. The maze was filled to a depth of 4 cm. A 60-W incandescent desk lamp (800 lumens) was mounted on the copy stand behind the digital camera (HP Photosmart R742) above the maze for testing. Each zebrafish was placed in the center of the maze to start, and the total number of line crosses, the percent of the total entries into the white arms, and the total time spent in the white arms were observed from 5-min video recordings. For the first experiment, Bartlett's test was performed to determine if standard deviations differed among groups, and if they did not, one-way ANOVA was performed, but if they did, then Welch's ANOVA was performed, with Dunnett's multiple comparisons for the *post hoc* analysis of significant effects. For the follow-up experiment, two-way (sex × treatment) ANOVA was performed with Sidak's *post hoc* test for significant findings using Prism nine. After behavior tests, each fish was weighed and euthanized by submersion in ice water for 5 min and subsequent decapitation to effect.

Uptake of [^{3}H] D-22 from Bath Water Into Zebrafish Muscle, Viscera, and Brain

A total of six adult zebrafish, three males and females each, were individually exposed to 25 nM [^{3}H] D-22 (25 Ci/mmol, ARC, Boston, MA (11.4 μg/L)) in 25 ml habitat water in a 50-ml beaker for 10 min. Fish were removed from the radioligand bath with forceps, anesthetized and rinsed with a 30 s dip in ice water, and euthanized by decapitation on an ice-chilled glass Petri dish with a scalpel. From each fish, [^{3}H] D-22 labeled zebrafish brain, visceral organs (heart, gastrointestinal tract, gall bladder, spleen, and liver), and a segment of the skinned lateral muscle were removed as described by Gupta and Mullins (2010), and then weighed and placed in 1.5 ml microcentrifuge tubes containing 200 ml scintillation cocktail (Ecolume, Fisher Scientific, United States). Labeled brains and muscles were mechanically homogenized with a teflon pestle and transferred to 8 ml scintillation vials (Beckman Mini Poly-Q, Fisher Scientific, United States), to which 4 ml of scintillation cocktail was added. Tissue homogenates in vials were vortexed, then mixed on an orbital shaker overnight. The [^{3}H] label (DPM) was measured on a Packard 1900 TR liquid scintillation counter (Packard Instrument Co., Downers Grove, IL) with efficiency of 40%.

Saturation Binding of [^{3}H] D-22 in Zebrafish and Serotonin Transporter-Deficient Mice

Saturation assays were performed to determine the specific binding of D-22 to uptake 2 sites in mouse hippocampus and zebrafish whole brain. Heterozygous serotonin transporter knockout mice were used because their hippocampal OCT3 expression was upregulated *vs*. the wild-type mice (Baganz et al., 2008). A 50 mM Tris HCl, 120 mM NaCl, 5 mM KCl buffer, pH 7.4 at 25°C was used. Hippocampi from two mice were combined to produce one membrane homogenate, and 12 zebrafish whole brains from males and females were combined to produce the other membrane homogenate in 25 ml buffer each. Both were homogenized separately at 26,000 rpm for 1 min with a Polytron tissue homogenizer (Brinkman Instruments, Westbury, NY, United States). Homogenates were centrifuged for 10 min at 36,000 × g at 4°C using a JA 25.50 rotor (Avanti J-E, Beckman Coulter, Indianapolis, IN, United States). The supernatant was discarded, and the pellet was resuspended in 25 ml buffer on ice using a Potter Elvehjem 10-ml glass and teflon homogenizer. The homogenate was centrifuged again for 10 min at 36,000 × g. These final pellets were resuspended to obtain an approximate protein concentration of 1 mg/ml, determined using the Bradford reagent (Sigma, St. Louis, MO), and colorimetric detection was performed at 595 nm using a plate reader (Spectra Max 190, Molecular Devices, San Jose, CA, United States).

For the incubations, a 100-μL homogenate was added to a tube containing 150 μL buffer with [^{3}H] D-22 at eight concentrations ranging from 0.1 to 14 nM [^{3}H] D-22 since concentrations exceeding this range are not pharmacologically relevant (Horton et al., 2013). To block any potential D-22 binding to uptake 1 transporters in mice or fish (Gould et al., 2007), 25 nM each of sertraline and mazindol were added to the buffer. To define the non-specific binding of [^{3}H] D-22, 25 μM MPP+ and 25 μM cold D-22 were added to the second and third groups of tubes, respectively. Each condition was reproduced in duplicate tubes. The solutions were incubated at room temperature on an orbital mixer for 60 min, and incubation was terminated by the addition of 4 ml of buffer, pH 7.4 at 4°C. Labeled homogenates were captured by filtration under vacuum on glass fiber filters pre-soaked in 0.5% polyethyleneimine (Sigma) with a Brandel tissue harvester (Gaithersburg, MD). Filters were washed twice more with 4 ml of buffer. Radioactivity trapped by the filters was measured on a scintillation counter (Packard Instrument Co., Downers Grove, IL) with 40% efficiency. Non-linear and linear curve fits were performed with Delta Graph (V5, Red Rock Software, Salt Lake City, UT, United States) and confirmed using Prism (V5 for Mac OS 10, Graph Pad, LaJolla, CA, United States).

RESULTS

Zebrafish Anxiety-Relevant Behaviors in Novel Environments After Acute D-22 Treatment: Initial Study

Dive Tank: Initially, the behavior of zebrafish exposed to red food dye matching the wavelength with a similar intensity to the 50 mg/L D-22 solution was compared with habitat water controls. There was no difference in top dwelling between these two groups [t (13) = 1.221, $p = 0.24$], so the data were pooled into a single control group of

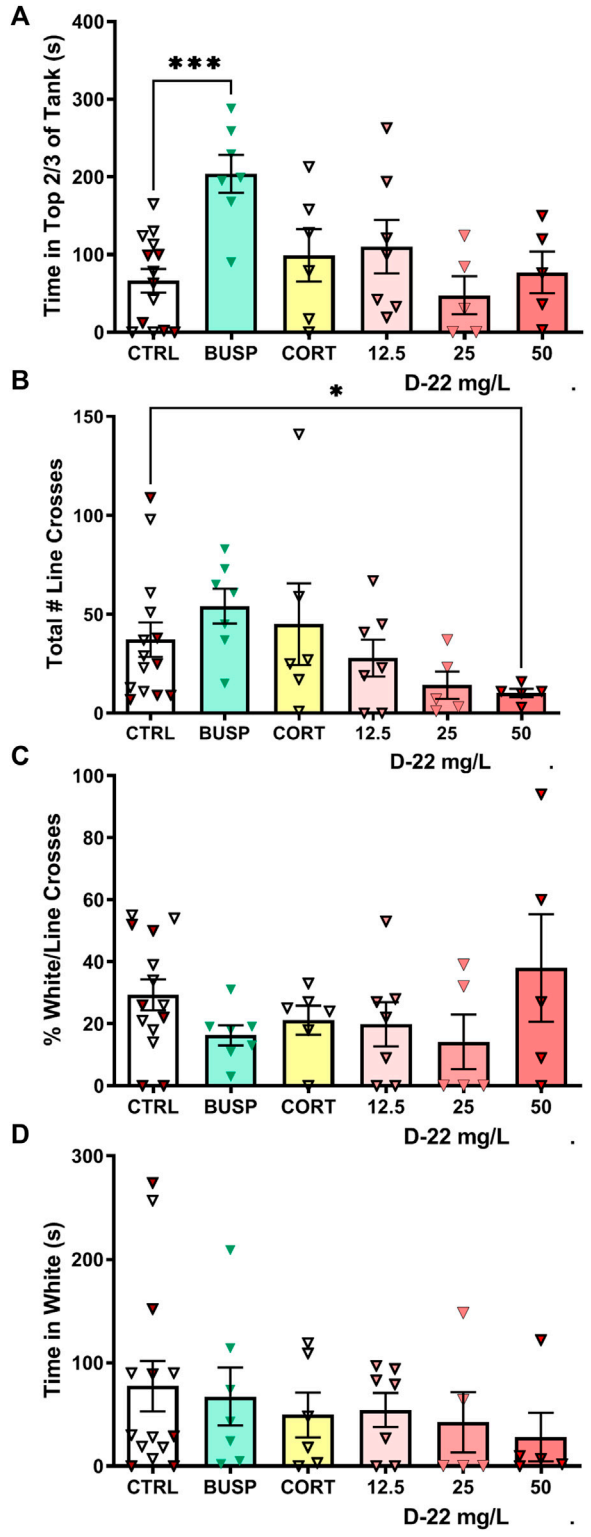

FIGURE 2 | Acute effects of D-22 on behaviors in novel environment-based anxiety tests. A total of 45 zebrafish were tested with sample sizes ranging from 5 to 15 fish with both males and females in every group. **(A)** Only the anti-anxiety drug buspirone increased the amount of time zebrafish spent at the top of the dive tank. **(B)** D-22 at 50 mg/L reduced the number of line crosses made by zebrafish exploring the light/dark plus maze. **(C)** There were no effects of D-22 or any other treatment on the percentage of white box entries/total entries. **(D)** There was no effect of D-22 or any other treatment on the time spent in white boxes. In all figures, for controls (CTRL), the filled symbols are the food color controls and open symbols are uncolored control solutions. CORT = corticosterone at 25 mg/L. Mean and S.E.M. are shown.

15 fish. The time in the top 2/3 of the dive tank for this control group was compared with the average times for five to seven fish treated with buspirone, corticosterone, or three concentrations of D-22 treatments. Only the zebrafish treated with 25 mg/L buspirone spent more time in the top 2/3 of the tank [F (5, 39) = 4.786, p = 0.0017, Dunnett's p = 0.0004], as shown in **Figure 2A**.

Light–Dark Plus Maze: The red food dye-control group did not differ from the habitat water-control group in number of line crosses into different boxes [t (13) = 0.1836, p = 0.86], percentage white of total line crosses [t (13) = 0.9615, p = 0.3538], and time in white arms [t (13) = 0.4692, p = 0.6467], so these control groups were pooled. The standard deviations for line crosses differed among the groups (Bartlett's p = 0.004), so Welch's ANOVA was used. The total number of line crosses (entries into center, white, or black boxes) in the light–dark maze was reduced only in the 50 mg/L D-22 treatment group [W (5.000, 14.49) = 6.130, p = 0.003, Dunnett's p = 0.04], as shown in **Figure 2B**. The percentage of white/total line crosses also had different standard deviations among groups (Bartlett's p = 0.03), but the means did not differ between treatments [W (5.000, 14.11) = 1.288, p = 0.323], as shown in **Figure 2C**. For time spent in white boxes, the standard deviations among groups were similar (Bartlett's p = 0.4657), and there were no significant differences among groups [F (5, 39) = 0.4940, p = 0.7787], as shown in **Figure 2D**.

Follow-Up Study: Acute D-22 50 mg/L Treatment in Females *Versus* Males

Dive Tank: There was no significant interaction [F (1,44) = 2.485, p = 0.1221], effect of sex [F (1,44) = 1.961, p = 0.1684], or effect of acute D-22 treatment [F (1,44) = 0.3468, p = 0.5589] on time spent in the top 2/3 of the dive tank in the follow-up study, as shown in **Figure 3A**.

Light–Dark Plus Maze

The total number of line crosses or box entries did not differ by sex [F (1, 44) = 0.7577, p = 0.3888] or D-22 treatment [F (1, 44) = 1.381, p = 0.2463], and there was no significant interaction [F (1, 44) = 0.000, p = 0.9999], as shown in **Figure 3B**. However, there was a significant effect of acute D-22 treatment [F (1, 44) = 14.61, p < 0.0004] to increase the percentage of white/total line crosses or entries by both female [t (12) = 2.894, p < 0.0118] and male [t (12) = 2.511, p < 0.0313] zebrafish relative to their controls, as shown in **Figure 3C**. There was no significant interaction [F (1, 44) = 0.0730, p = 0.7882] or sex effect [F (1, 44) = 0.4829, p = 0.4908] on the percentage of white/total line crosses. Female D-22-treated zebrafish

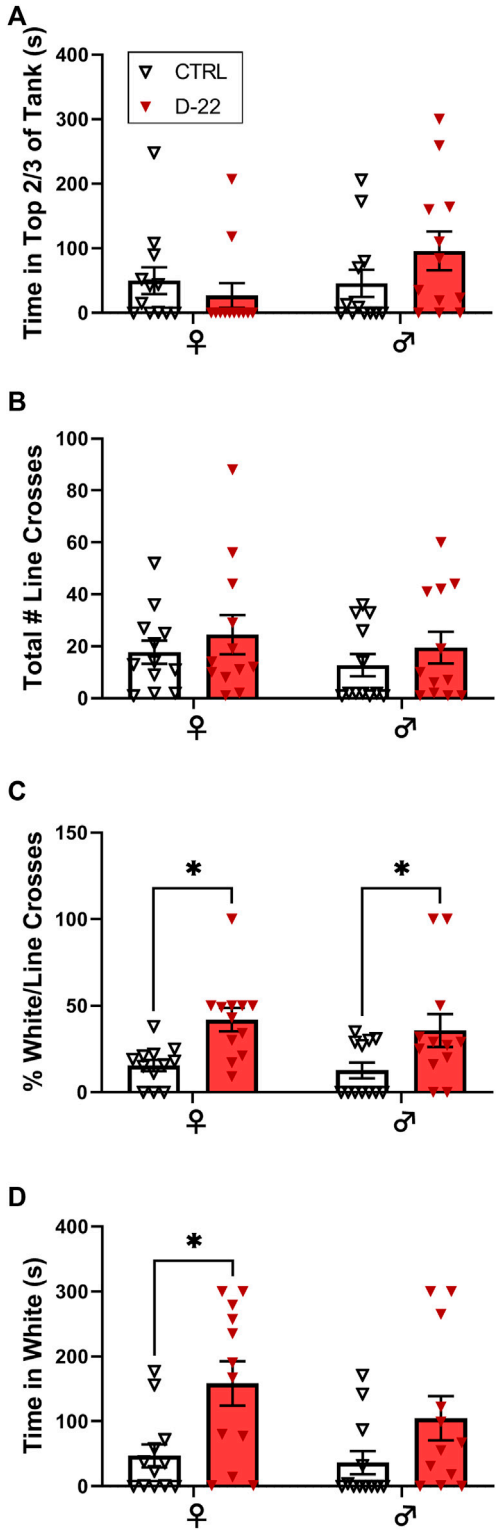

FIGURE 3 | Acute effects of D-22 (50 mg/L) on female *versus* male zebrafish in anxiety tests. A total of 48 zebrafish, 12 each of males and females, were treated with D-22 or a vehicle control for 5 min, washed for 5 min, and tested in a battery of anxiety-relevant behaviors. **(A)** There (*Continued*) was no effect of D-22 treatment or sex on top dwelling in the dive tank. **(B)** There was no effect of D-22 treatment or sex on exploration of the maze as measured by line crossings in the light–dark plus maze. **(C)** Exposure to D-22 increased the percentage of white/total line crosses for female and male zebrafish (*$p < 0.05$). **(D)** D-22 treatment increased the time female zebrafish spent in white arms of the maze (*$p < 0.05$). Mean and S.E.M. are shown.

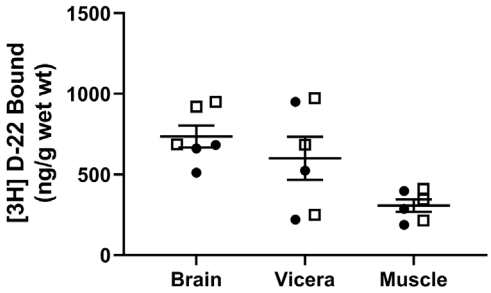

FIGURE 4 | [^{3}H] D-22 uptake from bath solution into zebrafish. After 10 min of *in vivo* bath exposure, zebrafish muscle had a lower D-22 content by wet weight than in either the brain or viscera. Males are shown as open boxes and females are closed circles. Mean and S.E.M. are shown.

also spent significantly more time in white arms than in controls [F (1, 44) = 10.99, $p < 0.0018$, t (12) = 2.904, $p < 0.0114$], while males did not [t (12) = 1.783, $p = 0.1563$], as shown in **Figure 3D**. There was no interaction [F (1, 44) = 0.6288, $p = 0.430$] or sex effect [F (1,44) = 1.391, $p = 0.2445$] on the time spent in white arms.

[^{3}H] D-22 Uptake Into Zebrafish Tissues from Water

Zebrafish exposed to 25 nM [^{3}H] D-22 for 10 min took up 736 ± 68 ng/g wet weight in the brain, 601 ± 134 ng/g in the viscera, and 308 ± 38 ng/g in the muscle ($n = 6$), as shown in **Figure 4**. This demonstrates [^{3}H] D-22 occupancy following acute bath exposure in zebrafish brain and gut are comparable and roughly double that found in muscle. This occupancy in the brain and gut is similar to zebrafish [^{3}H] citalopram uptake from a 3-min bath exposure (Sackerman et al., 2010). The outcome demonstrates that [^{3}H] D-22 or a metabolite that remains radiolabeled can cross the blood–brain barrier to occupy binding sites in the zebrafish brain. A prior study showed that blood–brain barrier properties in healthy adult zebrafish are comparable with those of higher mammals (Jeong et al., 2008). This finding supports the idea that bath exposures of zebrafish, paralleling systemic administration of D-22 to animals for behavioral studies is likely to occupy OCTs in the brain.

Saturation Binding of [^{3}H] D-22 in Zebrafish and Mouse Brain Homogenates

Total binding of [^{3}H] D-22 had maximal binding (Bmax) = 1,656 ± 2,839 fmol/mg protein in zebrafish whole-brain membrane homogenates pooled from females and males, and

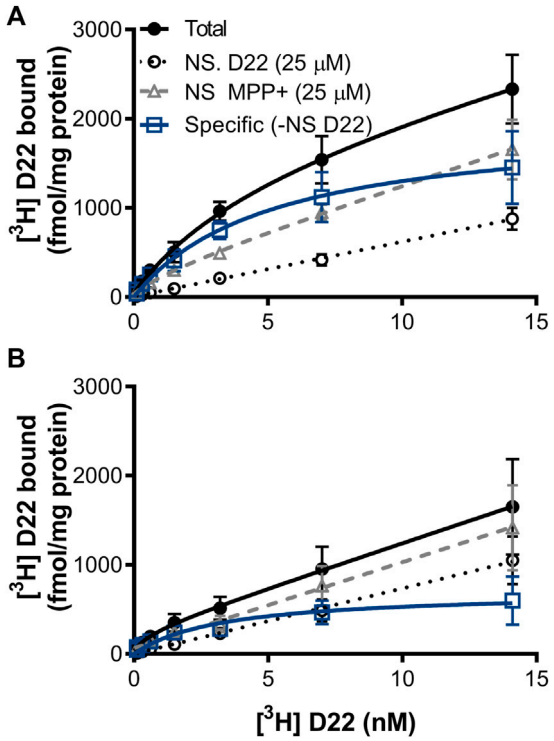

FIGURE 5 | [^{3}H] D-22 saturation in **(A)** zebrafish whole-brain *versus* **(B)** mouse hippocampus. A single high-affinity binding site for [^{3}H] D-22 with a K_D of 5 ± 2.5 nM and Bmax of 1974 ± 410 fmol/mg protein was found in whole zebrafish brain, and a K_D of 3.3 ± 2.3 and Bmax of 704 ± 182 fmol/mg protein in mouse hippocampus, respectively, with non-specific defined by 25 μM D-22. Binding of [^{3}H] D-22 was partially blocked by MPP+, $n = 3$. Mean and S.E.M. are shown.

222.7 ± 406.2 fmol/mg protein in mouse hippocampus. For total binding, the dissociation constant (K_D) = 4.853 ± 10.59 nM in the zebrafish brain and 0.7030 ± 5.175 nM in mice. Specific [^{3}H] D-22 binding, with non-specific binding defined by 25 μM D-22 plotted by linear regression and subtracted from total, had a Bmax = 1974 ± 409.7 fmol/mg protein and K_D = 5.172 ± 2.514 nM in zebrafish. In mice, specific [^{3}H] D-22 binding had a Bmax = 704.3 ± 182.0 fmol/mg protein and K_D = 3.307 ± 2.308 nM. The binding of [^{3}H] D-22 was partially blocked by MPP+, with a curve fit Bmax = 265.9 ± 676.1 fmol/mg protein and K_D = 2.124 ± 10.77 nM in zebrafish but with an ambiguous curve fit in mouse hippocampus, $n = 3$ independent experiments, as shown in **Figure 5**.

DISCUSSION

The main behavioral finding from this study is that acute exposure to D-22 at 50 mg/L increased zebrafish exploration of plus maze arms with a white background. Initially, acute bath exposure to the high-affinity mammalian OCT inhibitor D-22 reduced zebrafish box entries, the index of exploration, in the light–dark plus maze at the aforementioned dose with no other behavioral effects. For this reason, we decided not to test any higher doses of D-22 for this study. In the follow-up male vs. female experiment with the 50 mg/L D-22 dose, the percentage of white/total entries of both sexes and the amount of time spent by females in white arms was higher than those of the untreated controls (**Figures 3C,D**). Treatment with the mammalian stress hormone corticosterone at 25 mg/L was without effect, which may be consistent if the binding properties of zebrafish drOCT1 or drOCT2 are similar to those of mouse OCT3, as corticosterone has a lower affinity for murine OCT3 than D-22 (Koepsell et al., 2007). Our findings support the hypothesis that D-22 has anxiolytic properties relative to vehicle control treatment on zebrafish exploratory behavior in novel environments. Increased time spent in white arms after D-22 50 mg/L treatment may be indicative of an anxiolytic effect, perhaps because of reduced concern about predators from above (i.e. reduced dorsal camouflaging).

Anxiety behavior tests in zebrafish are based on predator avoidance strategies such as dwelling lower in the water column or staying on dark backgrounds (Córdova et al., 2016; Crane and Ferrari, 2017). Over the course of evolution, countershading, or dark dorsal coloration and light ventral coloration, may have been selected for in fish because it facilitates predator avoidance by background camouflage (Kelley et al., 2017). In zebrafish, countershading is under the control of melanocortin receptor 1 and a series of genes regulating agouti-signaling proteins that bind to it (Cal et al., 2019; Liang et al., 2021). Countershading is somewhat dynamic in zebrafish since within two days, fish can increase the dark pigmentation on their dorsum by the recruitment of melanosome into dorsal melanophores in response to visual exposure to a dark background or floor (Hatamoto and Shingyoji, 2008). Norepinephrine signaling, associated with the fight or flight response, is a driver of dynamic pigment shifts that zebrafish undergo to blend into their backgrounds (Xu and Xie, 2011). Taken together, it appears that substantial evolutionary pressure from predators from above may have driven zebrafish countershading and camouflaging into dark backgrounds.

By contrast, the height in the water column of the dive tank was not affected by 50 mg/L D-22. This response is akin to exploration of the middle of an open field test by rodents. Dwelling at the bottom of the tank is considered a thigmotaxic response consistent with predator avoidance. Among the experiments for this study, only the treatment with the anti-anxiety drug buspirone increased zebrafish exploration of the upper part of a dive tank, as had previously been reported to occur (Bencan et al., 2009). In other studies, drugs such as citalopram and desipramine also increase dwelling in the top 2/3 of the dive tank, while other drugs increasing time in the white arms of the plus maze, such as chlordiazepoxide, did not increase dwelling in the top of the dive tank (Sackerman et al., 2010). D-22 is therefore not the only drug with anxiolytic effects in rodents that yields different responses in the zebrafish dive tank versus plus maze.

The lack of sex-specific effects of D-22 on these behaviors is of interest, since in male zebrafish, drOCT1 and to a lesser extent drOCT2 are more highly expressed in the brain than in females

(Mihaljevic et al., 2016). We observed that sex differences in mouse OCT3 (in males) vs. the plasma membrane monoamine transporter (PMAT in females) contribute more to enhanced properties of amphetamine, without knowing if differential expression of these transporters corresponds with sex in mouse brain (Clauss et al., 2021). This highlights the importance of comparing expression of uptake 2 transporters in future rodent and zebrafish studies to advance our understanding of sex-specific effects of OCTs. However, sex determination in zebrafish is a very different process than what occurs in mammals; for example, females are the heterogametic sex and chromosome 4 harbors the sex-determining gene (Aharon and Marlow, 2021). Also female zebrafish have a male-appearing phenotype if reared in warm temperatures (Hosseini et al., 2019). These kind of differences may confound efforts to effectively translate zebrafish findings to mammalian and human responses.

To complicate matters further, it appears that the mammalian expression of OCT2 and OCT3, but not OCT1, may be under epistatic control in many tissues such that only maternal coding genes are expressed (Liu et al., 2022). The control element, Antisense to Igf2r RNA Noncoding (Air), is paternally expressed and as a result, genotypes and OCT2 and OCT3 expression phenotypes in most tissues may not match in heterozygous knockout mice, since only one parental allele is active (Yotova et al., 2008). One exception to this imprinting pattern in mice may be the neurons wherein at least Igf2r was shown to be bi-allelically expressed (Yamasaki et al., 2005). Initially, maternal imprinting of mouse OCT2 and OCT3 along with insulin-like growth factor 2 receptor (Igf2R) was thought to be restricted to the mouse placenta during pregnancy (Zwart et al., 2001; Sleutels et al., 2002; Nagano et al., 2008). Recently, evidence has emerged that in mice, cattle, and in some tissue types, human OCT2 and OCT3 have mono-allelic expression (Yotova et al., 2008; Peter et al., 2017; Liu et al., 2022). Given this, future studies should consider imprinting and confirming the protein level expression of OCT2 and OCT3, and also look into the potential epistatic expression of drOCTs.

We also demonstrated with a bath exposure to [^{3}H] D-22 that the drug penetrates the viscera, muscles, and brain of zebrafish in the same time frame that behavioral effects was measured. The mode of administration may affect the outcome of novel environment-based behavior tests in fish. For example, in a recent study, zebrafish were microinjected with D-22 at 0.01–10 μg/g in a salt solution vehicle, and this was found to have anxiogenic properties, increasing dark background preference, or "scotaxis" with a u-shaped curve on risk assessment based on freezing behavior (Maximino, 2021). Further studies on dosing and mode of administration that take into account the amount of D-22 reaching the brain and behavioral effects are needed to clarify its role in anxiety-related behaviors.

Characterization of high-affinity binding sites for D-22 in zebrafish or mouse brains was based on D-22 concentrations found in the brain with acute treatments that produced antidepressant-like behavioral effects in mice (Baganz et al., 2008; Horton et al., 2013). Hence the *in vitro* assays on brain membrane homogenates utilized a maximal concentration of 14 nM [^{3}H] D-22, and bath exposures used 25 nM. Our goal was to capture a single high-affinity binding site most likely responsible for the beneficial behavior effects observed with 0.01–0.1 mg/kg. We did not want to use doses of D-22 approaching equivalents of 10 mg/kg because it has a sedating effect on mice (Horton et al., 2013). In the present study, 50 mg/L D-22 initially appeared to slow the exploration of the light/dark plus maze in a few fish, but did not interfere with the exploration as evidenced by box entries in the light–dark plus maze that matched controls in the follow-up study. We found that with the aid of monoamine blockers, a putative high-affinity binding site appeared to reach a specific binding plateau in the zebrafish more clearly than in the mouse saturation assays.

The pharmacological properties of zebrafish drOCT1 were assessed in concentration-dependent inhibition assays with many drugs, hormones, and xenobiotics (Mihaljević et al., 2017). D-22 was not tested in these assays for its affinity with drOCT1. *In vivo*, we now know that drOCT1 and drOCT2 and other organic cation transporters that D-22 may bind to, occur in the brain with some capacity to affect behavior after acute treatment (Mihaljevic et al., 2016). Paralleling this, although D-22 had a slightly greater affinity for human OCT3 than OCT2 or plasma membrane monoamine transporters *in vitro* (Hayer-Zillgen et al., 2002; Fraser-Spears et al., 2019), its behavioral effects on these transporters *in vivo* may involve collective inhibition of OCTs. Furthermore, D-22 may bind to other transporters or receptors which may also help mediate its behavioral effects. For example, D-22 also blocks the plasma membrane monoamine transporter (PMAT) with high affinity (Duan and Wang, 2010), and a modest affinity of D-22 for adrenergic receptors has also been reported (Russ et al., 1996). Since OCTs transport many xenobiotics, including neurotoxins and drugs, their role in exposure-induced neurodegenerative disorders could be more safely studied at high throughput in zebrafish (Gould, 2010b; Lin et al., 2021). However, binding sites in the zebrafish brain for D-22 are even less well described, so further study in this area is warranted.

DATA AVAILABILITY STATEMENT

The raw data supporting the conclusions of this article will be made available by the authors upon reasonable request, without undue reservation.

ETHICS STATEMENT

The animal study was reviewed and approved by the Institutional Animal Care and Use Committee of the University of Texas Health Science Center at San Antonio.

AUTHOR CONTRIBUTIONS

GG wrote the manuscript, performed statistical analyses, behavior tests, and radioligand binding studies. PB-E

performed behavior test methods and collected behavior test data as a treatment-blind observer from video recordings. RH performed protein assays and contributed to writing the methods. LD provided the research environment, edited the manuscript, and wrote and edited grants supporting the work.

FUNDING

This study was funded by pilot grant sub-awards (to GG) from the Southwest Center for Occupational and Environmental Health, Houston, TX supported by the National Institute for Occupational and Environmental Health (NIOSH)/Centers for Disease Control and Prevention (CDC, T42CCT610417) and the Nathan Shock Center Biology of Aging Research Development Core (P30AG013319), the Morrison Trust and the National Institute of Mental Health grants R03MH086708 (to GG) and R01MH64489 (to LD). These funding agencies did not have any vested interest in the study outcomes or in the decision to publish these research findings.

ACKNOWLEDGMENTS

We are grateful for the exceptional technical assistance from James C. Groh for behavior data collection, Stephen R. Alvarado and William A. Owens for aquatic habitat assembly, Wouter Koek for statistical consultation, and Robert Westphalen for assistance with radioligand binding data analysis.

REFERENCES

Aharon, D., and Marlow, F. L. (2021). Sexual Determination in Zebrafish. *Cell Mol Life Sci* 79 (1), 8. doi:10.1007/s00018-021-04066-4

Aoyama, N., Takahashi, N., Kitaichi, K., Ishihara, R., Saito, S., Maeno, N., et al. (2006). Association between Gene Polymorphisms of SLC22A3 and Methamphetamine Use Disorder. *Alcohol. Clin. Exp. Res.* 30 (10), 1644–1649. doi:10.1111/j.1530-0277.2006.00215.x

Baganz, N. L., Horton, R. E., Calderon, A. S., Owens, W. A., Munn, J. L., Watts, L. T., et al. (2008). Organic Cation Transporter 3: Keeping the Brake on Extracellular Serotonin in Serotonin-Transporter-Deficient Mice. *Proc. Natl. Acad. Sci. U S A.* 105 (48), 18976–18981. doi:10.1073/pnas.0800466105

Becker, M. L., Visser, L. E., van Schaik, R. H., Hofman, A., Uitterlinden, A. G., and Stricker, B. H. (2010). Interaction between Polymorphisms in the OCT1 and MATE1 Transporter and Metformin Response. *Pharmacogenet Genomics* 20 (1), 38–44. doi:10.1097/FPC.0b013e328333bb11

Becker, M. L., Visser, L. E., van Schaik, R. H., Hofman, A., Uitterlinden, A. G., and Stricker, B. H. (2011). OCT1 Polymorphism Is Associated with Response and Survival Time in Anti-parkinsonian Drug Users. *Neurogenetics* 12 (1), 79–82. doi:10.1007/s10048-010-0254-5

Bencan, Z., Sledge, D., and Levin, E. D. (2009). Buspirone, Chlordiazepoxide and Diazepam Effects in a Zebrafish Model of Anxiety. *Pharmacol. Biochem. Behav.* 94 (1), 75–80. doi:10.1016/j.pbb.2009.07.009

Bengel, D., Murphy, D. L., Andrews, A. M., Wichems, C. H., Feltner, D., Heils, A., et al. (1998). Altered Brain Serotonin Homeostasis and Locomotor Insensitivity to 3, 4-methylenedioxymethamphetamine ("Ecstasy") in Serotonin Transporter-Deficient Mice. *Mol. Pharmacol.* 53 (4), 649–655. doi:10.1124/mol.53.4.649

Bergen, A. W., Javitz, H. S., Krasnow, R., Michel, M., Nishita, D., Conti, D. V., et al. (2014). Organic Cation Transporter Variation and Response to Smoking Cessation Therapies. *Nicotine Tob. Res.* 16 (12), 1638–1646. doi:10.1093/ntr/ntu161

Bönisch, H. (2021). Substrates and Inhibitors of Organic Cation Transporters (OCTs) and Plasma Membrane Monoamine Transporter (PMAT) and Therapeutic Implications. *Handb. Exp. Pharmacol.* 266, 119–167. doi:10.1007/164_2021_516

Bousman, C. A., Glatt, S. J., Everall, I. P., and Tsuang, M. T. (2009). Genetic Association Studies of Methamphetamine Use Disorders: A Systematic Review and Synthesis. *Am. J. Med. Genet. B Neuropsychiatr. Genet.* 150B (8), 1025–1049. doi:10.1002/ajmg.b.30936

Bowman, M. A., Mitchell, N. C., Owens, W. A., Horton, R. E., Koek, W., and Daws, L. C. (2020). Primary Lab of Origin LCD. Effect of Concurrent Organic Cation Transporter Blockade on Norepinephrine Clearance Inhibiting- and Antidepressant-Like Actions of Desipramine and Venlafaxine. *Eur. J. Pharmacol.* 883, 173285. doi:10.1016/j.ejphar.2020.173285

Cal, L., Suarez-Bregua, P., Braasch, I., Irion, U., Kelsh, R., Cerdá-Reverter, J. M., et al. (2019). Loss-of-function Mutations in the Melanocortin 1 Receptor Cause Disruption of Dorso-Ventral Countershading in Teleost Fish. *Pigment Cel Melanoma Res* 32 (6), 817–828. doi:10.1111/pcmr.12806

Chen, E. C., Liang, X., Yee, S. W., Geier, E. G., Stocker, S. L., Chen, L., et al. (2015). Targeted Disruption of Organic Cation Transporter 3 Attenuates the Pharmacologic Response to Metformin. *Mol. Pharmacol.* 88 (1), 75–83. doi:10.1124/mol.114.096776

Chen, L., Takizawa, M., Chen, E., Schlessinger, A., Segenthelar, J., Choi, J. H., et al. (2010). Genetic Polymorphisms in Organic Cation Transporter 1 (OCT1) in Chinese and Japanese Populations Exhibit Altered Function. *J. Pharmacol. Exp. Ther.* 335 (1), 42–50. doi:10.1124/jpet.110.170159

Clauss, N. J., Koek, W., and Daws, L. C. (2021). Role of Organic Cation Transporter 3 and Plasma Membrane Monoamine Transporter in the Rewarding Properties and Locomotor Sensitizing Effects of Amphetamine in Male andFemale Mice. *Int. J. Mol. Sci.* 22 (24), 13420. doi:10.3390/ijms222413420

Connors, K. A., Valenti, T. W., Lawless, K., Sackerman, J., Onaivi, E. S., Brooks, B. W., et al. (2014). Similar Anxiolytic Effects of Agonists Targeting Serotonin 5-HT1A or Cannabinoid CB Receptors on Zebrafish Behavior in Novel Environments. *Aquat. Toxicol.* 151, 105–113. doi:10.1016/j.aquatox.2013.12.005

Córdova, S. D., Dos Santos, T. G., and de Oliveira, D. L. (2016). Water Column Depth and Light Intensity Modulate the Zebrafish Preference Response in the Black/white Test. *Neurosci. Lett.* 619, 131–136. doi:10.1016/j.neulet.2016.03.008

Crane, A. L., and Ferrari, M. C. O. (2017). Patterns of Predator Neophobia: a Meta-Analytic Review. *Proc. Biol. Sci.* 284 (1861), 28420170583. doi:10.1098/rspb.2017.0583

Cui, M., Aras, R., Christian, W. V., Rappold, P. M., Hatwar, M., Panza, J., et al. (2009). The Organic Cation Transporter-3 Is a Pivotal Modulator of Neurodegeneration in the Nigrostriatal Dopaminergic Pathway. *Proc. Natl. Acad. Sci. U S A.* 106 (19), 8043–8048. doi:10.1073/pnas.0900358106

Daws, L. C., Koek, W., and Mitchell, N. C. (2013). Revisiting Serotonin Reuptake Inhibitors and the Therapeutic Potential of "uptake-2" in Psychiatric Disorders. *ACS Chem. Neurosci.* 4 (1), 16–21. doi:10.1021/cn3001872

Daws, L. C. (2021). Organic Cation Transporters in Psychiatric Disorders. *Handb Exp. Pharmacol.* 266, 215–239. doi:10.1007/164_2021_473

Daws, L. C. (2009). Unfaithful Neurotransmitter Transporters: Focus on Serotonin Uptake and Implications for Antidepressant Efficacy. *Pharmacol. Ther.* 121 (1), 89–99. doi:10.1016/j.pharmthera.2008.10.004

Duan, H., and Wang, J. (2010). Selective Transport of Monoamine Neurotransmitters by Human Plasma Membrane Monoamine Transporter and Organic Cation Transporter 3. *J. Pharmacol. Exp. Ther.* 335 (3), 743–753. doi:10.1124/jpet.110.170142

Fraser-Spears, R., Krause-Heuer, A. M., Basiouny, M., Mayer, F. P., Manishimwe, R., Wyatt, N. A., et al. (2019). Comparative Analysis of Novel Decynium-22 Analogs to Inhibit Transport by the Low-Affinity, High-Capacity Monoamine Transporters, Organic Cation Transporters 2 and 3, and Plasma Membrane Monoamine Transporter. *Eur. J. Pharmacol.* 842, 351–364. doi:10.1016/j.ejphar.2018.10.028

Garbarino, V. R., Santos, T. A., Nelson, A. R., Zhang, W. Q., Smolik, C. M., Javors, M. A., et al. (2019). Prenatal Metformin Exposure or Organic Cation Transporter 3 Knock-Out Curbs Social Interaction Preference in Male Mice. *Pharmacol. Res.* 140, 21–32. doi:10.1016/j.phrs.2018.11.013

Gasser, P. J., and Daws, L. C. (2017). Extending the Family: Roles for Uptake2 Transporters in Regulation of Monoaminergic Signaling. *J. Chem. Neuroanat.* 83-84, 107–108. doi:10.1016/j.jchemneu.2017.07.009

Gasser, P. J. (2021). Organic Cation Transporters in Brain Catecholamine Homeostasis. *Handb Exp. Pharmacol.* 266, 187–197. doi:10.1007/164_2021_470

Gould, G. G., Brooks, B. W., and Frazer, A. (2007). [(3)H] Citalopram Binding to Serotonin Transporter Sites in Minnow Brains. *Basic Clin. Pharmacol. Toxicol.* 101 (3), 203–210. doi:10.1111/j.1742-7843.2007.00100.x

Gould, G. G. (2010a). "Aquatic Light/Dark Plus Maze Novel Environment for Assessing Anxious versus Exploratory Behavior in Zebrafish (*Danio rerio*) and Other Small Teleost Fish," in *Zebrafish Neurobehavioral Protocols*. Editors A.V. Kalueff and J. M Cachat (NY: Humana Press), 99–108. doi:10.1007/978-1-60761-953-6_8

Gould, G. G. (2010b). "Zebrafish Biogenic Amine Transporters and Behavior in Novel Environments: Targets of Reuptake Inhibitors and Pesticide Action as Tools for Neurotoxicology Research," in *Zebrafish Models in Neurobehavioral Research*. Editors A.V. Kalueff and J.M. Cachat (NY: Humana Press), 181–209. doi:10.1007/978-1-60761-922-2_8

Gupta, T., and Mullins, M. C. (2010). Dissection of Organs from the Adult Zebrafish. *J. Vis. Exp.* 4 (37), 1717. doi:10.3791/1717

Hatamoto, K., and Shingyoji, C. (2008). Cyclical Training Enhances the Melanophore Responses of Zebrafish to Background Colours. *Pigment Cel Melanoma Res* 21 (3), 397–406. doi:10.1111/j.1755-148X.2008.00445.x

Hayer, M., Bönisch, H., and Brüss, M. (1999). Molecular Cloning, Functional Characterization and Genomic Organization of Four Alternatively Spliced Isoforms of the Human Organic Cation Transporter 1 (hOCT1/SLC22A1). *Ann. Hum. Genet.* 63 (Pt 6), 473–482. doi:10.1017/S0003480099007770

Hayer-Zillgen, M., Brüss, M., and Bönisch, H. (2002). Expression and Pharmacological Profile of the Human Organic Cation Transporters hOCT1, hOCT2 and hOCT3. *Br. J. Pharmacol.* 136 (6), 829–836. doi:10.1038/sj.bjp.0704785

Hill, J. E., Makky, K., Shrestha, L., Hillard, C. J., and Gasser, P. J. (2011). Natural and Synthetic Corticosteroids Inhibit Uptake 2-mediated Transport in CNS Neurons. *Physiol. Behav.* 104 (2), 306–311. doi:10.1016/j.physbeh.2010.11.012

Horton, R. E., Apple, D. M., Owens, W. A., Baganz, N. L., Cano, S., Mitchell, N. C., et al. (2013). Decynium-22 Enhances SSRI-Induced Antidepressant-like Effects in Mice: Uncovering Novel Targets to Treat Depression. *J. Neurosci.* 33 (25), 10534–10543. doi:10.1523/JNEUROSCI.5687-11.2013

Hosseini, S., Ha, N. T., Simianer, H., Falker-Gieske, C., Brenig, B., Franke, A., et al. (2019). Genetic Mechanism Underlying Sexual Plasticity and its Association with Colour Patterning in Zebrafish (*Danio rerio*). *BMC Genomics* 20 (1), 341. doi:10.1186/s12864-019-5722-1

Jeong, J. Y., Kwon, H. B., Ahn, J. C., Kang, D., Kwon, S. H., Park, J. A., et al. (2008). Functional and Developmental Analysis of the Blood-Brain Barrier in Zebrafish. *Brain Res. Bull.* 75 (5), 619–628. doi:10.1016/j.brainresbull.2007.10.043

Karahoda, R., Horackova, H., Kastner, P., Matthios, A., Cerveny, L., Kucera, R., et al. (2020). Serotonin Homeostasis in the Materno-Foetal Interface at Term: Role of Transporters (SERT/SLC6A4 and OCT3/SLC22A3) and Monoamine Oxidase A (MAO-A) in Uptake and Degradation of Serotonin by Human and Rat Term Placenta. *Acta Physiol. (Oxf)* 229 (4), e13478. doi:10.1111/apha.13478

Kelley, J. L., Taylor, I., Hart, N. S., and Partridge, J. C. (2017). Aquatic Prey Use Countershading Camouflage to Match the Visual Background. *Behav. Ecol.* 28 (5), 1314–1322. doi:10.1093/beheco/arx093

Koepsell, H., Lips, K., and Volk, C. (2007). Polyspecific Organic Cation Transporters: Structure, Function, Physiological Roles, and Biopharmaceutical Implications. *Pharm. Res.* 24 (7), 1227–1251. doi:10.1007/s11095-007-9254-z

Koepsell, H. (2020). Organic Cation Transporters in Health and Disease. *Pharmacol. Rev.* 72 (1), 253–319. doi:10.1124/pr.118.015578

Krause-Heuer, A. M., Fraser-Spears, R., Dobrowolski, J. C., Ashford, M. E., Wyatt, N. A., Roberts, M. P., et al. (2017). Evaluation of the Antidepressant Therapeutic Potential of Isocyanine and Pseudoisocyanine Analogues of the Organic Cation Decynium-22. *Eur. J. Med. Chem.* 137, 476–487. doi:10.1016/j.ejmech.2017.06.011

Liang, Y., Grauvogl, M., Meyer, A., and Kratochwil, C. F. (2021). Functional Conservation and Divergence of Color-Pattern-Related agouti Family Genes in Teleost Fishes. *J. Exp. Zool B Mol. Dev. Evol.* 336 (5), 443–450. doi:10.1002/jez.b.23041

Lin, W., Yan, Y., Ping, S., Li, P., Li, D., Hu, J., et al. (2021). Metformin-Induced Epigenetic Toxicity in Zebrafish: Experimental and Molecular Dynamics Simulation Studies. *Environ. Sci. Technol.* 55 (3), 1672–1681. doi:10.1021/acs.est.0c06052

Liu, X., Huo, H., Jin, L., Dong, Y., Li, D., Zhang, C., et al. (2022). Genomic Imprinting of the IGF2R/AIR Locus Is Conserved between Bovines and Mice. *Theriogenology* 180, 121–129. doi:10.1016/j.theriogenology.2021.12.013

Maier, J., Niello, M., Rudin, D., Daws, L. C., and Sitte, H. H. (2021). The Interaction of Organic Cation Transporters 1-3 and PMAT with Psychoactive Substances. *Handb Exp. Pharmacol.* 266, 199–214. doi:10.1007/164_2021_469

Maximino, C. (2021). Decynium-22 Affects Behavior in the Zebrafish Light/dark Test. *nab* 3 (1), e21. doi:10.35430/nab.2021.e21

McMillan, S. C., Géraudie, J., and Akimenko, M. A. (2015). Pectoral Fin Breeding Tubercle Clusters: a Method to Determine Zebrafish Sex. *Zebrafish* 12 (1), 121–123. doi:10.1089/zeb.2014.1060

Mihaljević, I., Popović, M., Žaja, R., Maraković, N., Šinko, G., and Smital, T. (2017). Interaction between the Zebrafish (*Danio rerio*) Organic Cation Transporter 1 (Oct1) and Endo- and Xenobiotics. *Aquat. Toxicol.* 187, 18–28. doi:10.1016/j.aquatox.2017.03.012

Mihaljevic, I., Popovic, M., Zaja, R., and Smital, T. (2016). Phylogenetic, Syntenic, and Tissue Expression Analysis of Slc22 Genes in Zebrafish (*Danio rerio*). *BMC Genomics* 17 (1), 626. doi:10.1186/s12864-016-2981-y

Nagano, T., Mitchell, J. A., Sanz, L. A., Pauler, F. M., Ferguson-Smith, A. C., Feil, R., et al. (2008). The Air Noncoding RNA Epigenetically Silences Transcription by Targeting G9a to Chromatin. *Science* 322 (5908), 1717–1720. doi:10.1126/science.1163802

Nies, A. T., Koepsell, H., Damme, K., and Schwab, M. (2011). Organic Cation Transporters (OCTs, MATEs), *in vitro* and *in vivo* Evidence for the Importance in Drug Therapy. *Handb. Exp. Pharmacol.* 2011 (201), 105–167. doi:10.1007/978-3-642-14541-4_3

Nies, A. T., Koepsell, H., Winter, S., Burk, O., Klein, K., Kerb, R., et al. (2009). Expression of Organic Cation Transporters OCT1 (SLC22A1) and OCT3 (SLC22A3) Is Affected by Genetic Factors and Cholestasis in Human Liver. *Hepatology* 50 (4), 1227–1240. doi:10.1002/hep.23103

Paull, G. C., Van Look, K. J., Santos, E. M., Filby, A. L., Gray, D. M., Nash, J. P., et al. (2008). Variability in Measures of Reproductive success in Laboratory-Kept Colonies of Zebrafish and Implications for Studies Addressing Population-Level Effects of Environmental Chemicals. *Aquat. Toxicol.* 87 (2), 115–126. doi:10.1016/j.aquatox.2008.01.008

Peter, B., Lancaster, H., Vose, C., Fares, A., Schrauwen, I., and Huentelman, M. (2017). Two Unrelated Children with Overlapping 6q25.3 Deletions, Motor Speech Disorders, and Language Delays. *Am. J. Med. Genet. A.* 173 (10), 2659–2669. doi:10.1002/ajmg.a.38385

Rappold, P. M., Cui, M., Chesser, A. S., Tibbett, J., Grima, J. C., Duan, L., et al. (2011). Paraquat Neurotoxicity Is Mediated by the Dopamine Transporter and Organic Cation Transporter-3. *Proc. Natl. Acad. Sci. U S A.* 108 (51), 20766–20771. doi:10.1073/pnas.1115141108

Russ, H., Friedgen, B., Königs, B., Schumacher, C., Graefe, K. H., and Schömig, E. (1996). Pharmacokinetic and Alpha 1-adrenoceptor Antagonistic Properties of Two Cyanine-type Inhibitors of Extraneuronal Monoamine Transport. *Naunyn Schmiedebergs Arch. Pharmacol.* 354 (3), 268–274. doi:10.1007/BF00171057

Sackerman, J., Donegan, J. J., Cunningham, C. S., Nguyen, N. N., Lawless, K., Long, A., et al. (2010). Zebrafish Behavior in Novel Environments: Effects of Acute Exposure to Anxiolytic Compounds and Choice of *Danio rerio* Line. *Int. J. Comp. Psychol.* 23 (1), 43–61. https://escholarship.org/uc/item/82h78048.

Sala-Rabanal, M., Li, D. C., Dake, G. R., Kurata, H. T., Inyushin, M., Skatchkov, S. N., et al. (2013). Polyamine Transport by the Polyspecific Organic Cation

Transporters OCT1, OCT2, and OCT3. *Mol. Pharm.* 10 (4), 1450–1458. doi:10.1021/mp400024d

Samodelov, S. L., Kullak-Ublick, G. A., Gai, Z., and Visentin, M. (2020). Organic Cation Transporters in Human Physiology, Pharmacology, and Toxicology. *Int. J. Mol. Sci.* 21 (21), 7890. doi:10.3390/ijms21217890

Sleutels, F., Zwart, R., and Barlow, D. P. (2002). The Non-coding Air RNA Is Required for Silencing Autosomal Imprinted Genes. *Nature* 415 (6873), 810–813. doi:10.1038/415810a

Sweet, D. H. (2021). *Organic cation transporter expression and function in the CNS. In Organic Cation Transporters in the Central Nervous System*. Cham: Springer, 41–80.

Vialou, V., Balasse, L., Callebert, J., Launay, J. M., Giros, B., and Gautron, S. (2008). Altered Aminergic Neurotransmission in the Brain of Organic Cation Transporter 3-deficient Mice. *J. Neurochem.* 106 (3), 1471–1482. doi:10.1111/j.1471-4159.2008.05506.x

Wultsch, T., Grimberg, G., Schmitt, A., Painsipp, E., Wetzstein, H., Breitenkamp, A. F., et al. (2009). Decreased Anxiety in Mice Lacking the Organic Cation Transporter 3. *J. Neural Transm. (Vienna)* 116 (6), 689–697. doi:10.1007/s00702-009-0205-1

Xu, J., and Xie, F. K. (2011). A- and β-adrenoceptors of Zebrafish in Melanosome Movement: a Comparative Study between Embryo and Adult Melanophores. *Biochem. Biophys. Res. Commun.* 405 (2), 250–255. doi:10.1016/j.bbrc.2011.01.020

Yamasaki, Y., Kayashima, T., Soejima, H., Kinoshita, A., Yoshiura, K., Matsumoto, N., et al. (2005). Neuron-specific Relaxation of Igf2r Imprinting Is Associated with Neuron-specific Histone Modifications and Lack of its Antisense Transcript Air. *Hum. Mol. Genet.* 14 (17), 2511–2520. doi:10.1093/hmg/ddi255

Yee, S. W., and Giacomini, K. M. (2021). Emerging Roles of the Human Solute Carrier 22 Family. *Drug Metab. Dispos.* doi:10.1124/dmd.121.000702

Yossa, R., Sarker, P. K., Proulx, E., Saxena, V., Ekker, M., and Vandenberg, G. W. (2013). A Practical Approach for Sexing Zebrafish, *Danio rerio*. *J. Appl. Aquac.* 25 (2), 148–153. doi:10.1080/10454438.2013.792170

Yotova, I. Y., Vlatkovic, I. M., Pauler, F. M., Warczok, K. E., Ambros, P. F., Oshimura, M., et al. (2008). Identification of the Human Homolog of the Imprinted Mouse Air Non-coding RNA. *Genomics* 92 (6), 464–473. doi:10.1016/j.ygeno.2008.08.004

Zwart, R., Sleutels, F., Wutz, A., Schinkel, A. H., and Barlow, D. P. (2001). Bidirectional Action of the Igf2r Imprint Control Element on Upstream and Downstream Imprinted Genes. *Genes Dev.* 15 (18), 2361–2366. doi:10.1101/gad.206201

Conflict of Interest: The authors declare that the research was conducted in the absence of any commercial or financial relationships that could be construed as a potential conflict of interest.

Publisher's Note: All claims expressed in this article are solely those of the authors and do not necessarily represent those of their affiliated organizations, or those of the publisher, the editors, and the reviewers. Any product that may be evaluated in this article, or claim that may be made by its manufacturer, is not guaranteed or endorsed by the publisher.

Advantages of publishing in Frontiers

OPEN ACCESS
Articles are free to read for greatest visibility and readership

FAST PUBLICATION
Around 90 days from submission to decision

HIGH QUALITY PEER-REVIEW
Rigorous, collaborative, and constructive peer-review

TRANSPARENT PEER-REVIEW
Editors and reviewers acknowledged by name on published articles

Frontiers
Avenue du Tribunal-Fédéral 34
1005 Lausanne | Switzerland

Visit us: www.frontiersin.org
Contact us: frontiersin.org/about/contact

REPRODUCIBILITY OF RESEARCH
Support open data and methods to enhance research reproducibility

DIGITAL PUBLISHING
Articles designed for optimal readership across devices

FOLLOW US
@frontiersin

IMPACT METRICS
Advanced article metrics track visibility across digital media

EXTENSIVE PROMOTION
Marketing and promotion of impactful research

LOOP RESEARCH NETWORK
Our network increases your article's readership